Laurentide Ice Sheet dynamics across multiple glacial-interglacial cycles from Quaternary stratigraphic records in the western Hudson Bay Lowland, central Canada

By

Tyler James Hodder

A thesis

presented to the University of Waterloo

in fulfillment of the

thesis requirement for the degree of

Doctor of Philosophy

in

Earth Sciences

Waterloo, Ontario, Canada, 2026

© Tyler James Hodder 2026

Examining Committee Membership

The following served on the Examining Committee for this thesis. The decision of the Examining Committee is by majority vote.

External Examiner	Dr. Alberto Reyes Associate Professor Department of Earth and Atmospheric Sciences University of Alberta
Supervisor(s)	Dr. Martin Ross Associate Professor Department of Earth and Environmental Sciences University of Waterloo
	Dr. Olav Lian Adjunct Professor Department of Earth and Environmental Sciences University of Waterloo Professor Department of Geoscience University of the Fraser Valley
Internal Member	Dr. John Johnston Associate Professor, teaching stream Department of Earth and Environmental Sciences University of Waterloo
	Dr. Eric Grunsky Adjunct Professor Department of Earth and Environmental Sciences University of Waterloo
Internal-external Member	Dr. Roland Hall Professor Department of Biology University of Waterloo

Author's Declaration

This thesis consists of material all of which I authored or co-authored: see Statement of Contributions included in the thesis. This is a true copy of the thesis, including any required final revisions, as accepted by my examiners.

I understand that my thesis may be made electronically available to the public.

Statement of Contributions

Tyler Hodder was the sole author for Chapters 1 and 7 which were written under the supervision of Dr. Martin Ross and were not written for publication. This thesis consists in part of five manuscripts written for publication. Exceptions to sole authorship of material are as follows:

The research presented in Chapter 2 is published in *Quaternary Research* (Hodder et al., 2023). A large portion of this work was conceptualized and conducted by the author of this thesis with critical design and recommendations by the second author (Michelle Gauthier) and third author (Martin Ross, thesis supervisor). The fourth author (Olav Lian, co-supervisor) was instrumental in the application of optical dating and assisted with geological interpretations within this study. As lead author, I was responsible for writing and revising the manuscript and all co-authors contributed throughout the writing and publishing process.

Citation:
Hodder, T.J., Gauthier, M.S., Ross, M. and Lian, O. 2023. Was there a nonglacial episode in the western Hudson Bay Lowland during Marine Isotope Stage 3? Quaternary Research, 116: 148–168. doi:10.1017/qua.2023.35.

The research presented in Chapter 3 is published in *Canadian Journal of Earth Sciences* (Hodder et al., 2024a) and the supporting datasets are published within two government open-access publications (Dalton et al. 2022; Hodder et al., 2024b) that are not included within this thesis. This study was conceptualized by the author of this thesis with recommendations by the second author (Michelle Gauthier), third author (Martin Ross, thesis supervisor) and fourth author (Samuel Kelley). The fifth author (Olav Lian, co-supervisor) was involved with the application of optical dating and assisted with geological interpretations within this study. The sixth (April Dalton) and seventh author (Sarah Finkelstein) conducted the pollen analysis of intertill organic-bearing sediments and paleo-ecological interpretations. As lead author, I was responsible for writing and revising the manuscript and all co-authors contributed their expertise throughout the writing, editing and publishing process.

Citations:

Dalton, A.S., Finkelstein, S.F., Hodder, T.J. and Gauthier, M.S. 2022. Palynological analyses of subtill sediments from four sites in the western Hudson Bay Lowland region (parts of NTS 53O; 54A, C, D). Manitoba Geological Survey, Open File OF2022-1, 13 p.

Hodder, T.J., Gauthier, M.S., Ross, M., Kelley, S.E., Lian, O.B., Dalton, A.S. and Finkelstein, S.A. 2024a. Unravelling the fragmented sediment-landscape assemblage in an area of thick Quaternary sediment, western Hudson Bay Lowland, Canada. Canadian Journal of Earth Sciences 61(11): 1156–1183. doi:10.1139/cjes-2024-0018.

Hodder, T.J., Gauthier, M.S., Kelley, S.E. and Ross, M. 2024b. Quaternary site, till composition and ice-flow indicator datasets in the Kaskattama highland area, northeastern Manitoba (parts of NTS 53N, O, 54B, C). Manitoba Geological Survey, Open File OF2024-1, 20 p., 9 appendices.

The research presented in Chapter 4 has been submitted to the *Canadian Journal of Earth Sciences* and the supporting datasets are published within two government open-access publications (Dalton et al., 2024; Hodder and Gauthier, 2025a) that are not included within the text of this thesis. This study was conceptualized by the author of this thesis with recommendations by the second author (Michelle Gauthier) and third author (thesis supervisor Martin Ross). The fourth (April Dalton) and seventh (Sarah Finkelstein) authors conducted the pollen analysis of intertill organic-bearing sediments and interpretations. The fifth (Maria Schaarschmidt) and sixth (Olav Lian, co-supervisor) authors were instrumental in the application of optical stimulated luminescence (OSL) and assisted with geological interpretations within this study. The eighth author (Eric Grunsky) assisted with till-matrix geochemistry interpretations. The ninth author (Anne Jennings) analyzed a subset of pollen samples for the presence of foraminifera to assist with depositional environment interpretations. As lead author, I was responsible for writing the manuscript, while co-authors contributed their expertise throughout the writing process

Citations:

Dalton, A.S., Finkelstein, S.F., Hodder, T.J. and Gauthier, M.S. 2024. Palynological analyses of subtill sediments from eleven sites in the western Hudson Bay Lowland region of Manitoba (parts of NTS 54B, 54C, 54E, 54F). Manitoba Geological Survey Open File OF2024-5, 6 p.

Hodder, T.J. and Gauthier, M.S. 2025a. Quaternary site, till composition and ice-flow indicator data for the Little Churchill to Churchill rivers area, northeastern Manitoba (part of NTS 54E). Manitoba Geological Survey Open File OF2025-1, 5 p., 6 appendices.

Hodder, T.J., Gauthier, M.S., Ross, M, Dalton, A.S., Schaarschmidt, M., Lian, O.B., Finkelstein, S.A., Grunsky, E., Jennings, A.E. *In review*. Laurentide Ice Sheet dynamics across multiple glacial-interglacial cycles from Quaternary stratigraphic records in central Canada. Canadian Journal of Earth Sciences.

The research presented in Chapter 5 has not yet been submitted to an academic journal. This study was conceptualized by the author of this thesis and Manitoba Geological Survey colleague Michelle Gauthier, with recommendations from the thesis supervisor (Martin Ross). Olav Lian and Maria Schaarschmidt completed the optical dating of sediments and assisted with geological interpretations. April Dalton and Sarah Finkelstein completed the pollen analysis of intertill sediments and provided interpretations of the dataset, while Anne Jennings examined a select number of subsamples for the presence of foraminifera. The supporting datasets are published within three government open-access publications (Dalton et al., 2022, 2024; Hodder and Gauthier, 2025b) that are not included within the text of this thesis. As lead author, I was responsible for writing the manuscript, while co-authors contributed their expertise throughout the writing process.

Citations:

Dalton, A.S., Finkelstein, S.F., Hodder, T.J. and Gauthier, M.S. 2022. Palynological analyses of subtill sediments from four sites in the western Hudson Bay Lowland region (parts of NTS 53O; 54A, C, D). Manitoba Geological Survey, Open File OF2022-1, 13 p.

Dalton, A.S., Finkelstein, S.F., Hodder, T.J. and Gauthier, M.S. 2024. Palynological analyses of subtill sediments from eleven sites in the western Hudson Bay Lowland region of Manitoba (parts of NTS 54B, 54C, 54E, 54F). Manitoba Geological Survey, Open File OF2024-5, 6 p.

Hodder, T.J. and Gauthier, M.S. 2025b. Quaternary site, till composition and ice-flow indicator datasets in the Nelson River Estuary–Black Duck River area, northeastern Manitoba (parts of NTS 54A, B, C, F). Manitoba Geological Survey, Open File OF2025-2, 6 p., 8 appendices.

The research presented in Chapter 6 has not yet been submitted to an academic journal. This chapter provides an updated synthesis of the Quaternary stratigraphic framework for the western Hudson Bay Lowland based on correlations between the areas examined in Chapters 2–5 and related investigations in the Gillam area (Gauthier et al., 2024, 2025). This new stratigraphic framework is used to discuss the evolution of the Laurentide Ice Sheet across the past two glaciations. The majority of this research has been conducted by the author of thesis but draws on recent stratigraphic findings from the Hudson Bay Lowland, which includes contributions from all co-authors listed above in Chapters 2–5 and below.

Citations:

Gauthier, M.S., Hodder, T.J., Dalton, A.S., Lian, O.B., Schaarschmidt, M., Ross, M., and Väliranta, M. 2024. Preservation of probable MIS 7 deglacial and nonglacial deposits near the edge of the Hudson Bay Lowland in Manitoba, Canada. Canadian Journal of Earth Sciences, 61(11): 1184–1211. doi:10.1139/cjes-2024-0019.

Gauthier, M.S., Hodder, T.J., Hathaway, J., Ross, M., Schaarschmidt, M., Lian, O.B., Finkelstein, S.A. and Kelley, S.E., 2025. Extending the western Hudson Bay Lowland Quaternary stratigraphy, in Manitoba Canada, to at least Marine Isotope Stage 10. Canadian Journal of Earth Sciences, *in press*. doi:10.1139/cjes-2025-0027.

Abstract

Understanding the terrestrial Quaternary stratigraphic record is necessary to reconstruct regional- to continental-scale paleo-ice sheet fluctuations and compare how these events relate to oxygen isotope proxies derived from marine sediments, sea level change, and contemporary ice sheets. Regions that contain an extensive stratigraphic record beyond the last glacial maximum are key to understanding the long-term behaviour of ice sheets and provide field-based constraints for ice-sheet reconstructions and modelling. The Hudson Bay Lowland (HBL) is one of these key regions situated in central Canada that contains a fragmented stratigraphic record of at least the last four Laurentide Ice Sheet (LIS) glaciations. The main objectives of this thesis are to 1) reconstruct the spatio-temporal evolution of the LIS from the Quaternary stratigraphic record of three relatively understudied regions of the western HBL and 2) determine the timing and climate conditions that persisted during ice-free periods across multiple glacial-interglacial cycles.

To better understand the fragmented stratigraphic record that is dominated by glacial sediments (till), this thesis developed a hybrid lithostratigraphy-allostratigraphy approach that relies on multi-parameter characterization of tills to establish sediment provenance and the ice-flow direction that deposited the sediment. This included detailed study of 70 sections, the collection of 193 stratigraphic ice-flow indicators (154 till fabrics and 39 lodged clasts) and analysis of 393 till samples. Once the till framework was established, the relative age of each nonglacial bed was then determined using the bounding surfaces of designated till units. At least 18 units have been identified this way and correlated across the western HBL. The nonglacial beds were further characterized to assess the timing of sediment deposition using radiocarbon and optical dating methods and paleo-environmental conditions that existed using pollen and foraminifera analysis. Lastly, stratigraphic frameworks presented herein did not rely on geochronology constraints to anchor correlations and the age of identified interglacial beds can be further tested to confirm the age of interglacial beds.

The new stratigraphic framework for the western HBL provides important field-based constraints for LIS reconstructions. This includes evidence that there was asynchronous growth of the two major

domes of the LIS during the last two glaciations, with accelerated early growth of the Quebec–Labrador Dome relative to the Keewatin Dome. In each glaciation, the Keewatin Dome becomes more active relatively later in glaciation and persists until deglaciation. During the last glaciation, ice-flowing from the Keewatin Dome likely did not occur until MIS 2 and this S-trending ice-flow transitions into late-glacial SW-trending ice-streams. During the penultimate glaciation (~MIS 6), till deposition by S- to SW-trending ice was extensive and one of the main ice-flow events across the western HBL when the Keewatin Dome was likely situated in northern mainland Nunavut. Furthermore, during deglaciation the Keewatin Dome or an ice divide was likely situated in the western HBL.

There is widespread evidence across the western HBL that sediments belonging to at least three pre-Holocene interglacial periods exists, which provides an important archive to understanding past climatic conditions in central Canada. For two of these interglacials there is evidence of marine inundation which likely occurred during Termination II (~130 ka) and Termination III (~243 ka). In the Churchill River region, the marine limits for both marine incursions are higher compared to the Tyrrell Sea (Holocene) marine limit, providing important field-based constraints for LIS modelling. Importantly, new age estimations from the uppermost intertill nonglacial sediments, combined with consideration of the paleobotanical datasets in the western HBL stratigraphic record, suggest that the region was last deglaciated during MIS 5e. This implies that the HBL, and likely Hudson Bay, remained glaciated during MIS 3.

The presence of weathered bedrock within the western HBL indicates that glacial erosion of bedrock was negligible in places during the Quaternary Period. Relict landscapes across northeastern Manitoba, such as preserved streamlined landform flowsets that are situated outside the margins of late-glacial ice streams, provide evidence of limited erosion following initial glacial advance into the area.

The results of this thesis have provided an updated Quaternary stratigraphic framework for the western HBL, a key region for understanding the long-term evolution of the LIS. The Quaternary stratigraphic record is highly fragmented, which reflects patchy erosion and deposition over multiple

glacial-interglacial cycles of the region. The new stratigraphic frameworks developed provide an increased understanding of the growth, evolution and retreat of the LIS during the past two glaciations and insights into pre-Illinoian glaciations, which are essential to improving reconstruction and modelling of the ice sheet throughout the Middle and Late Pleistocene.

Acknowledgements

The field of Quaternary geology first piqued my interest when I took Martin Ross' 4th year class way back in 2010. Little did I know at the time that it would send me on the trajectory to where I am today. I want to sincerely thank Martin for his support and encouragement throughout this journey from BSc thesis to MSc thesis and finally during the writing of this PhD thesis.

Michelle Gauthier is thanked for her mentorship and guidance during the examination of countless sections across the Hudson Bay Lowland and excellent discussions back in the office. I thoroughly enjoyed our time in the field as we navigated sections far too steep and interglacial sediments that were far too saturated. Olav Lian is thanked for joining as a co-supervisor and providing valuable insight into the interpretation of Quaternary depositional environments. Olav's insight and expertise was essential for the application of optical dating. Maria Schaarschmidt is thanked for the grueling amount of lab work undertaken at the University of Fraser Valley and with the interpretation of optical data. April Dalton and Sarah Finkelstein are thanked for stimulating discussions regarding the Hudson Bay Lowland region and genuine interest to characterize subtill nonglacial deposits to advance our understanding of the stratigraphic record. Anne Jennings is thanked for analyzing suspected marine sediments for presence of foraminifera. Harvey Thorleifson is thanked for providing a copy of the original Operation Winisk notes and stimulating discussion about the Quaternary stratigraphy of the Hudson Bay Lowland. Eric Grunsky is thanked for excellent discussion and guidance regarding statistical analyses incorporated within this thesis.

I would not have been able to pursue this research without the support of the Manitoba Geological Survey and I thank the organization for their support throughout this thesis and for fieldwork funding. In particular, my supervisor Michelle Nicolas and colleague Michelle Gauthier were instrumental in supporting me to pursue this thesis. These studies would not have been possible without the fieldwork assistance provided by colleagues Sam Kelley, Marc Rinne, Christian Böhm and Michelle Gauthier. Lastly, thanks to my wife Coryn for her unwavering support throughout the process. It has certainly been a busy time in our lives!

Dedication

This thesis is dedicated to my wife Coryn Hodder and our children Hazel Belle and Theo Tyrrell. We hope that you both grow up to explore and question the world around you.

Table of Contents

Examining Committee Membership ii

Author's Declaration iii

Statement of Contributions iv

Abstract viii

Acknowledgements xi

Dedication xii

List of Figures xx

List of Tables xxv

Chapter 1 Introduction 1

1.1 Western Hudson Bay Lowland 1

1.1.1 Quaternary stratigraphy 2

1.1.2 Timing of ice-free periods 5

1.1.3 Glacial dynamics prior to the last glacial maximum 7

1.2 Methodology overview 8

1.2.1 Field data collection 8

1.2.2 Geochronology of intertill nonglacial sediments 11

1.2.3 Till characterization 12

1.2.4 Stratigraphic approach 15

1.3 Thesis objectives 19

1.4 Thesis format 19

Chapter 2 Was there a nonglacial episode in the western Hudson Bay Lowland during Marine Isotope Stage 3? 22
2.1 Overview 22
2.2 Introduction 23
2.3 Methods 25
2.3.1 Field data 25
2.3.2 Optical dating 26
2.3.3 Radiocarbon dating 29
2.4 Results 30
2.4.1 Assessing the geochronological constraints 30
2.4.2 New optical ages 31
2.4.3 Stratigraphy and age constraints 35
2.5 Discussion 45
2.5.1 Optical dating 45
2.5.2 Resolving the age of the Black Duck River nonglacial sediments 47
2.5.3 Hudson Bay Lowland evidence for MIS 3 deglaciation? 48
2.6 Conclusions 49
2.7 References 51
Chapter 3 Unravelling the fragmented sediment-landform assemblage in an area of thick Quaternary sediment, western Hudson Bay Lowland, Canada 58
3.1 Overview 58
3.2 Introduction 59

3.3 Regional setting 63
3.3.1 Bedrock geology 63
3.3.2 Surficial ice-flow record 65
3.3.3 Intertill nonglacial sediments 65
3.4 Methods 66
3.4.1 Field data 66
3.4.2 Till provenance 69
3.4.3 Pollen analysis 72
3.4.4 Geochronology 73
3.4.5 Stratigraphic approach 75
3.5 Results 76
3.5.1 Stratigraphy 76
3.5.2 Till-matrix geochemistry 95
3.6 Discussion 97
3.6.1 The stratigraphic mosaic and Implications for correlations 99
3.6.2 Stratigraphic evidence for a preserved advance-phase streamlined-sediment-landform flowset 101
3.6.3 Repeated northwest-trending ice advances from the Quebec-Labrador dome 103
3.7 Conclusion 105
3.8 References 107
Chapter 4 Laurentide Ice Sheet dynamics across multiple glacial-interglacial cycles from Quaternary stratigraphic records in central Canada 118

4.1 Overview 118
4.2 Introduction 119
4.3 Regional setting 122
4.3.1 Bedrock geology and clast provenance 122
4.4 Methods 125
4.4.1 Field data 125
4.4.2 Till provenance 127
4.4.3 Stratigraphic approach 129
4.4.4 Geochronology 130
4.4.5 Paleo-environmental analysis 131
4.4.6 X-ray diffraction (XRD) analysis 133
4.5 Results and interpretations 134
4.5.1 Quaternary stratigraphy 134
4.5.2 Till-matrix geochemistry 165
4.5.3 Optical ages 169
4.6 Discussion 171
4.6.1 Reconciling the timing of marine incursions and interglacial sedimentation 173
4.7 Glacial dynamics 176
4.7.1 Glaciation I: ~MIS 5–1 176
4.7.2 Glaciation II: ~MIS 6 178
4.7.3 Glaciation(s) III: ~MIS 8 or older 180
4.8 Conclusions 182

4.9 References 184

Chapter 5 Glacial-interglacial cycles: insights from the stratigraphic record of western Hudson Bay Lowland 195

5.1 Overview 195

5.2 Introduction 196

5.3 Regional setting 199

5.3.1 Bedrock geology and clast provenance 199

5.4 Methods 202

5.4.1 Field Data 202

5.4.2 Till provenance 205

5.4.3 Stratigraphic approach 207

5.4.4 Paleoenvironmental characterization 207

5.4.5 Geochronology 209

5.5 Results and interpretations 211

5.5.1 Quaternary stratigraphy 211

5.5.2 Till geochemistry 239

5.6 Discussion 242

5.6.1 Glacial dynamics 244

5.6.2 Reconciling the timing and correlation of nonglacial deposits 246

5.6.3 Correlation of nonglacial beds across the Hudson Bay Lowland 251

5.7 Conclusions 252

5.8 References 254

Chapter 6 Long-term evolution of the Laurentide Ice Sheet: insights from stratigraphic records of western Hudson Bay Lowland, central Canada 264
6.1 Overview 264
6.2 Introduction 265
6.3 Stratigraphic correlations and nomenclature 266
6.4 Western Hudson Bay Lowland Glaciations 268
6.4.1 HBL Glacial Stage I (~MIS 5–1) 268
6.4.2 HBL Glacial Stage II (~MIS 6) 272
6.4.3 HBL Glacial Stage(s) III (~MIS 8 or older glaciations) 274
6.5 Laurentide Ice Sheet evolution across the last two glaciations 277
6.5.1 Initial ice-sheet growth and evolution 277
6.5.2 Late-glacial dynamics in the HBL 278
6.6 Conclusions 279
6.7 Future work 280
6.8 References 281
Chapter 7 Main contributions and future work 287
7.1 Western Hudson Bay Lowland Quaternary Stratigraphy advances 287
7.2 Laurentide Ice Sheet reconstructions 288
7.3 Previous interglacials 290
7.3.1 Marine Isotope Stage 3 292
7.4 Future work 294
References 296

Appendix A Supplemental materials for Chapter 2 305

Appendix B Supplemental materials for Chapter 3 315

Appendix C Supplemental materials for Chapter 4 327

Appendix D Supplemental materials for Chapter 5 366

Appendix E Supplemental materials for Chapter 7 404

List of Figures

Figure 1.1: Location of the study area in the western Hudson Bay Lowland (A) in context to the Laurentide Ice Sheet and Keewatin (K) and Quebec-Labrador (Q-L) domes at 22 cal ka bp (B) as defined in Dalton et al. (2023) 2
Figure 1.2: Previous stratigraphic frameworks for the western HBL region 4
Figure 1.3: The LR04 benthic delta ^{18}O stack for the last 350 ka (Lisiecki and Raymo, 2005) 5
Figure 1.4: Geochronology data for Quaternary intertill nonglacial deposits in the western Hudson Bay Lowland region of central Canada that have been interpreted to support deglaciation of the region during Marine Isotope Stage 3 7
Figure 1.5: Examples of ice-flow data collected 10
Figure 1.6: Regional bedrock geology of central Canada. 14
Figure 1.7: An example of tills in the Kaskattama highland study area characterized by similar sediment facies, but that were deposited by different ice-flow directions 17
Figure 2.1: Geochronology data for Quaternary intertill nonglacial deposits in the western Hudson Bay Lowland region of central Canada 24
Figure 2.2: Luminescence decay curve (main graph) showing the 'natural' signal, and a dose-response curve (inset) for sample 112-19-605-OSL-004, which are typical of those of this sample and of the others samples 28
Figure 2.3: Radial plots (Galbraith 2010) showing the distribution of De values for each sample and estimations of representative De values (weighted mean) used for dating, using either the CAM or the MAM (solid line that intersects the curved axis) 34
Figure 2.4: Quaternary stratigraphy and sediment photos of site 15 37
Figure 2.5: Quaternary stratigraphy and sediment photos of site 20 39
Figure 2.6: Quaternary stratigraphy and sediment photos of site 23 41
Figure 2.7: Quaternary stratigraphy at site 3 and 4 in the on the Nelson River at Hudson Bay 43
Figure 3.1: Location of the study area in western Hudson Bay Lowland, Canada. 61
Figure 3.2: Streamlined landform flowsets and examples of streamlined landforms in the study area 62

Figure 3.3: Regional bedrock geology of central Canada and examples of clasts observed in the study area 64
Figure 3.4: Example of surficial sampling methods and tills observed in the study area 67
Figure 3.5: Optical data for sample 112-19-630-OSL025 74
Figure 3.6: Spatial distribution of interpreted stratigraphic units with age constraints and ice-flow data plotted 78
Figure 3.7: Quaternary stratigraphy exposed at Section 19-628 on Twin Creeks and examples of sediments exposed 79
Figure 3.8: Tukey box plots showing the proportion of undifferentiated greenstone and greywacke clasts (eastern source) in the 2–8 mm size-fraction of till. The recovery of distinctive oolitic jasper clasts (eastern source) and Dubawnt Supergroup clasts (northwestern source) is displayed at the bottom of the box plots for each stratigraphic unit 80
Figure 3.9: Quaternary stratigraphy exposed along an unnamed tributary to the Echoing River and examples of diamicton exposed at sections. 81
Figure 3.10: Example of organic-bearing nonglacial sediments from Unit 2 82
Figure 3.11: Pollen analysis for site 16-416 85
Figure 3.12: Quaternary stratigraphy exposed at Section 16-430 on an unnamed tributary to the Echoing River and with examples of Unit 3 and 6 exposed here 87
Figure 3.13: Detrital hornblende $^{40}Ar/^{39}Ar$ ages determined for selected till units displayed as stacked histograms (100 Ma bins) with a consistent scale on the y-axis for each plot 88
Figure 3.14: Example of Unit 5 sorted sediments 91
Figure 3.15: Principal component analysis results and clast-lithology examples 96
Figure 3.16: Quaternary stratigraphic framework for the Kaskattama highland region 98
Figure 3.17: Summary of Quaternary stratigraphic relationships in the Kaskattama highland area: a) the stratigraphy at each local-scale site is shown highlighting the fragmented nature of the stratigraphic record 100
Figure 4.1: Location of the study area in the Churchill to Little Churchill rivers region of western Hudson Bay Lowland, Canada 120

Figure 4.2: Simplified bedrock geology of central Canada with examples of distinct erratics observed and a clast-lithology count 124
Figure 4.3: Example of field till-till contacts observed and associated till fabrics at section 21-805. 126
Figure 4.4: Summary of Quaternary stratigraphic relationships interpreted for sections investigated on the Churchill River 135
Figure 4.5: Interpreted occurrence of weathered bedrock at the base of section 21-806 (A) and plot (B) of the whole rock geochemical data of this material and data from the unweathered Chipewyan granite on an A-CN-K diagram (Fedo et al., 1995)..... 136
Figure 4.6: Summary of Quaternary stratigraphic relationships interpreted for sections investigated on the Little Churchill River 138
Figure 4.7: Examples of Unit 1 sediment..... 139
Figure 4.8: Quaternary stratigraphy exposed at section 21-807 on the Churchill River..... 141
Figure 4.9: Quaternary stratigraphy exposed at section 21-806 on the Little Churchill River..... 143
Figure 4.10: Tukey box plots displaying till compositional data for each identified unit..... 144
Figure 4.11: Quaternary stratigraphy of Unit 4 sediments at section 21-832 (34–40 m depth bgs) 145
Figure 4.12: Pollen analysis for Unit 4 sediments at sections 21-806, 21-807 and 21-832 150
Figure 4.13: Intertill sorted sediments interpreted to have been deposited in a marine environment (Unit 4a) at section 21-807 151
Figure 4.14: Intertill organic-rich sediment and paleosol development at section 21-806..... 152
Figure 4.15: Uppermost Quaternary stratigraphy exposed at section 21-828 (0–16 m bgs) 159
Figure 4.16: Quaternary stratigraphy exposed at section 21-827 on the Little Churchill River..... 164
Figure 4.17: A) Till-matrix geochemistry (<63 µm size-fraction) k-means cluster analysis results plotted on PC2 vs. PC1; B) Till-matrix geochemistry (<63 µm size-fraction) k-means cluster analysis results plotted a biplot of till granitoid vs. undifferentiated greenstone and greywacke clasts; and C) k-means cluster analysis results according to sampled till unit. 168
Figure 4.18: Quaternary stratigraphic framework of the Churchill to Little Churchill rivers area with interpreted glacial and interglacial intervals..... 172
Figure 5.1: Location of study area in the western Hudson Bay Lowland 197

Figure 5.2: Simplified bedrock geology of central Canada and examples of rock types identified within the study area..... 200
Figure 5.3: Examples of tills identified within the study area and the nature of till-till contacts observed..... 203
Figure 5.4: Summary of Quaternary stratigraphic relationships interpreted for sections investigated in the Kaskattama River (A), Machichi River (B) and Nelson River Estuary (C) areas 214
Figure 5.5: Quaternary stratigraphy exposed at section 19-607 on the Kaskattama River with photos of identified till units 218
Figure 5.6: Till-matrix grainsize proportions for identified till units..... 219
Figure 5.7: Till clast-lithology proportions for identified till units..... 220
Figure 5.7: Till detrital hornblende ages grouped according to identified till unit displayed on kernel density estimation plots..... 221
Figure 5.9: Quaternary stratigraphy exposed at section 20-704 on the Machichi River with photos of identified till units 223
Figure 5.10: Unit 5a marine sediments exposed along the Machichi River (A–C) and examples of foraminifera specimens identified within these sediments (D–G). 226
Figure 5.11: Upper stratigraphy exposed at section 19-613 with photos of sediments..... 229
Figure 5.12: Pollen data for site 112-19-601 (1 sample) and 112-19-613 (14 samples) 230
Figure 5.13: Unit 9 intertill sorted sediments 234
Figure 5.14: Principal component analysis classified according to each area studied and stratigraphic unit 241
Figure 5.15: Quaternary stratigraphic framework for the Nelson River Estuary to Kaskattama River region of the western Hudson Bay Lowland 243
Figure 6.1: Location of sections investigated in the western Hudson Bay Lowland, central Canada (A) and the context of the study area to the Laurentide Ice Sheet at 22 cal. ka (B)..... 266
Figure 6.2: Quaternary stratigraphy correlations across the western Hudson Bay Lowland 269
Figure 6.3: Ice-flow phase reconstructions during HBL Glacial Stage I based on the new Quaternary stratigraphic framework, paleo–ice-flow indicators and till provenance. 270

Figure 6.4: Ice-flow phase reconstructions during HBL Glacial Stage II based on the new Quaternary stratigraphic framework, paleo–ice-flow indicators and till provenance 273
Figure 6.5: Ice flow phase reconstructions during HBL Glacial Stage III based on the new Quaternary stratigraphic framework, paleo–ice-flow indicators and till provenance. 276
Figure 7.1: Inventory of interpreted interglacial deposits 293

List of Tables

Table 2.1: Optical age sample water content, radioisotopes concentrations, sample depths, and calculated dose rates. 29
Table 2.2: Number of aliquots measured (N), overdispersion values (OD), equivalent dose values (D_e), optical ages, and dose recovery (DR) ratios 33
Table 3.1: Optical dating sample water content, radioisotope concentrations, depths and calculated dose rates. 74
Table 3.2: Ice-flow data for each stratigraphic unit. 77
Table 3.3: Number of aliquots measured (N), overdispersion values (OD), equivalent dose values (D_e), optical ages, and dose recovery (DR) ratios. 85
Table 4.1: Summary of pollen and foraminifera analysis. 132
Table 4.2: Geochemistry and calculated weathering indices of interpreted weathered bedrock at section 21-826 and the Chipewyan granite. 136
Table 4.3: Radiocarbon ages and shell $\delta^{13}C$ values. 150
Table 4.4: Number of aliquots measured (n), overdispersion values (OD), equivalent dose values (D_e), optical ages, and dose recovery (DR) ratios. 170
Table 5.1: Summary of pollen and foraminifera analysis of intertill sorted sediments. 208
Table 5.2: Number of aliquots measured (n), overdispersion values (OD), equivalent dose values (D_e), optical ages, and dose recovery (DR) ratios. 216
Table 5.3: Radiocarbon data 228

Chapter 1

Introduction

1.1 Western Hudson Bay Lowland

The near inner core regions of the Laurentide Ice Sheet (LIS) have experienced prolonged ice-cover, shifting ice divide(s), and varying basal thermal conditions that have resulted in the extensive preservation of evidence of previous ice-flow events in the erosional and depositional record (Gauthier et al., 2019; McMartin et al., 2021). The record of former ice divide positions is integral to understanding the history of former ice sheets and evidence of ice-flow reversals attests to the dynamic nature of the core regions of the LIS during the late Pleistocene (Veillette et al., 1999; McMartin and Henderson, 2004; Hodder et al., 2016; Rice et al., 2019). In addition, the timing of ice retreat in these regions provides important constraints for the margins of the LIS, which is a topic of significant debate for interstadial periods of the last glaciation (Dalton et al., 2019; Miller and Andrews, 2019). One of the best regions to understand the growth and demise of previous glaciations of the LIS is the western Hudson Bay Lowland (HBL) region of central Canada (Figure 1.1) since the stratigraphic record here spans at least the last three glacial-interglacial cycles (Nielsen et al., 1986; Dredge and McMartin, 2011), thus representing an important sedimentary record to reconstruct the dynamics of Middle to Late Pleistocene glaciations.

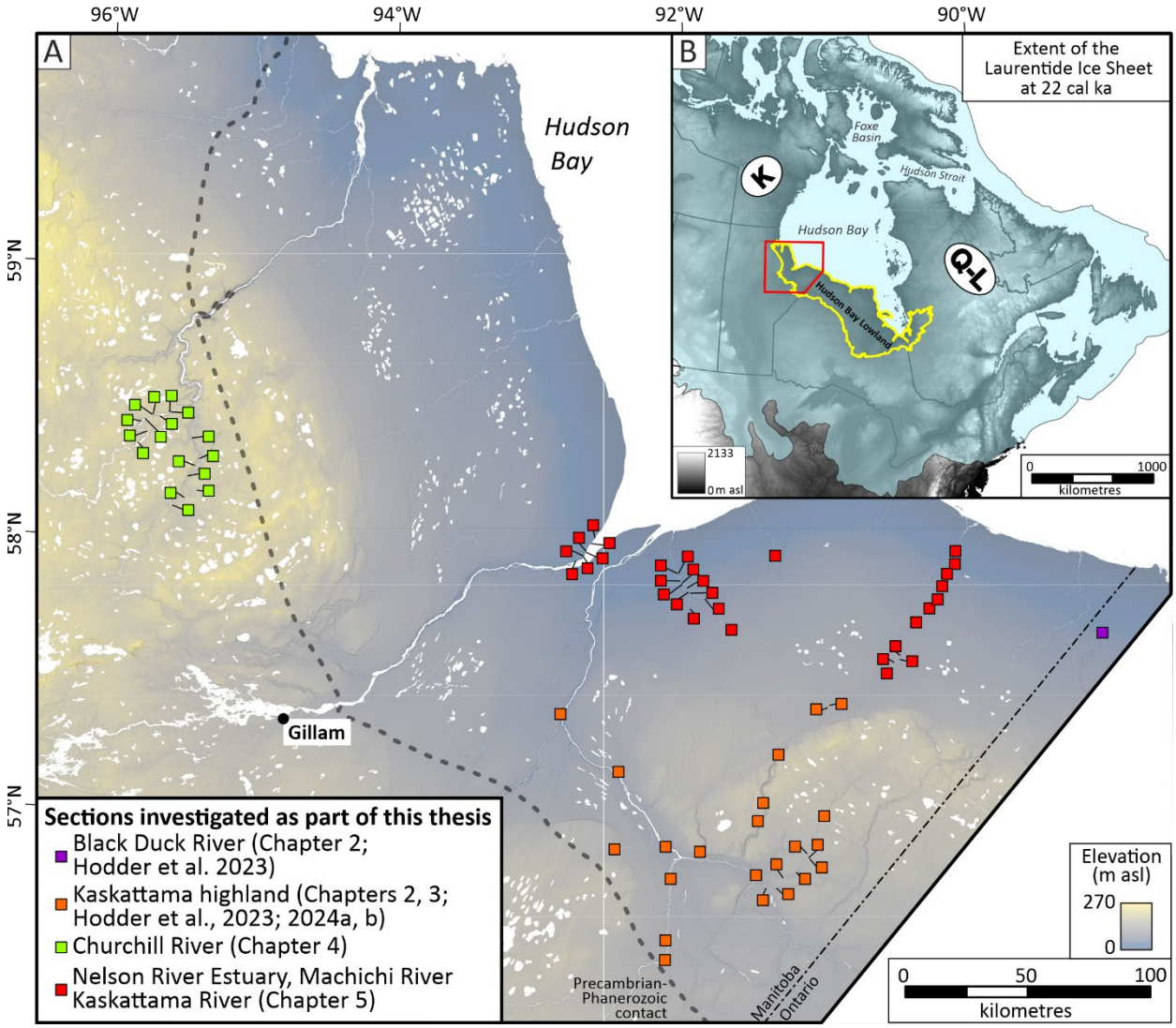

Figure 1.1: Location of the study area in the western Hudson Bay Lowland (A) in context to the Laurentide Ice Sheet and Keewatin (K) and Quebec-Labrador (Q-L) domes at 22 cal ka bp (B) as defined in Dalton et al. (2023).

1.1.1 Quaternary stratigraphy

The western HBL region of Canada contains an extensive archive of Quaternary sediments that record the growth and decay of the LIS, as well as paleo-environmental conditions that prevailed during previous non-glacial periods (Figure 1.2; Nielsen et al., 1986; Dredge et al., 1990; Roy, 1998; Dredge and McMartin, 2011). The stratigraphic record has previously been interpreted to contain four tills and two interglacial units that were deposited during the Sangamonian interglacial (~128–116 ka; Stirling et al., 1998) and a previous interglaciation (Figure 1.2). The region was over-ridden by ice that flowed from both major domes of the LIS, with the Keewatin Dome to the northwest and Quebec-Labrador Dome to

the east (Figure 1.1), providing unique insight into the relative strength of ice-flow events from each dome throughout glaciations (Shilts, 1980; Nielsen et al., 1986; Roy, 1998; Gauthier et al., 2019). The spatio-temporal waxing and waning of ice flowing from each of these domes has left a complex ice-flow record in northeast Manitoba that spans a 295° azimuth, with stratigraphic ice-flow indicators in the western HBL ranging from NW-trending (310°) to ESE-trending (105°) (Gauthier et al., 2019). Distinctive erratics derived from central mainland Nunavut and eastern Hudson Bay observed in the western HBL and Hudson Bay attest to continental-scale dispersal from both core regions of the LIS (Shilts, 1980; Henderson, 1990; Prest et al., 2000; Dredge and McMartin, 2011).

Deciphering the complex ice-flow record in this region is hindered by the occurrence of both NW- and SE-trending ice-flow events (Nielsen et al., 1986; Thorleifson et al., 1992; Gauthier et al., 2019). Previous sediment provenance interpretations have typically assumed continuous, curvilinear glacial pathways (e.g., Shilts, 1980). This approach has led to problems and inconsistencies whereby reconstructed ice-flow trajectories are either oversimplified or follow some unlikely pathways with abrupt directional changes to fit the evidence (Shilts, 1980). Similarly, stratigraphic units have been correlated across long distances assuming a relatively continuous depositional record (Nielsen et al., 1986; Thorleifson et al., 1992). For example, the first intertill nonglacial beds encountered in the subsurface are typically correlated as the same unit across the entire HBL (McDonald, 1969; Nielsen et al., 1986; Dredge and McMartin, 2011), and till deposits have been correlated across the entire HBL (960 km; McDonald, 1969). Recently, glacial landscapes have been interpreted as a fragmented non-coeval landscape, which attest to a more complex surficial record (Kleman et al., 1997; Stea and Finck, 2001; Ross et al. 2009). This is evident in the glacial landscape of northeast Manitoba which is highly fragmented (Trommelen et al., 2012; Gauthier et al., 2019) and the composition of glacial sediments, which consists of a spatial mosaic with variable intensities of overprinting and inheritance (Trommelen et al., 2013). The complex ice-flow history and heterogeneous till composition in northeast Manitoba requires that reliable till provenance parameters be combined with stratigraphic observations to decipher the glacial history of the region.

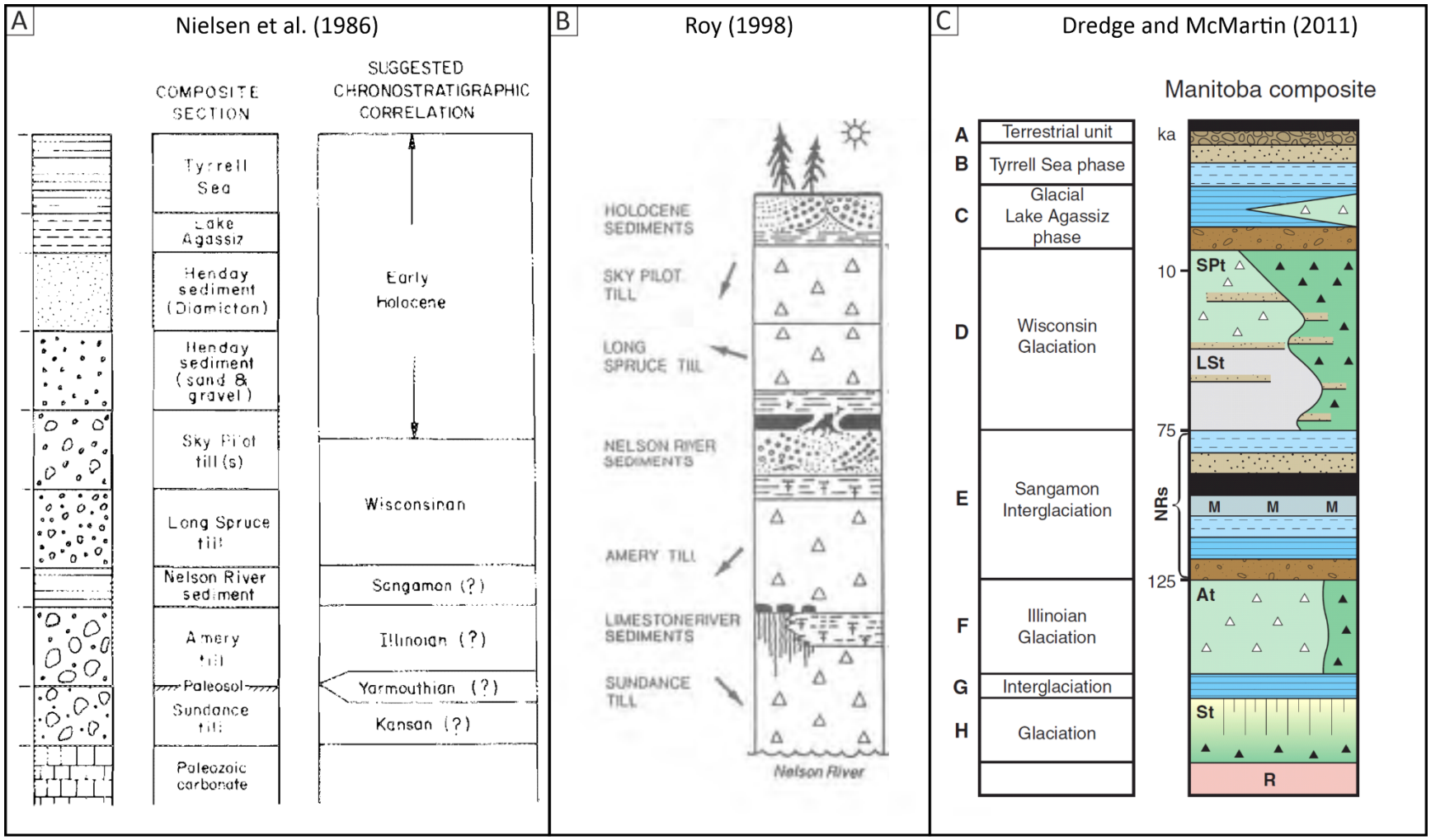

Figure 1.2: Previous stratigraphic frameworks for the western HBL region (modified from Nielsen et al., 1986; Roy, 1998; Dredge and McMartin, 2011).

1.1.2 Timing of ice-free periods

Intertill organic-bearing sediments have long been recognized throughout the HBL region of central Canada (e.g., Bell, 1880; Tyrrell, 1913; McDonald, 1969; Skinner, 1973; Netterville, 1974; Dredge et al., 1990). The preservation of these sediments within the stratigraphic record provides an archive of the timing of ice-free conditions and paleo-environmental conditions during these time periods. The majority of intertill nonglacial deposits in the western HBL do not have age determinations. This is largely due to the difficulty in dating sediments that were deposited beyond the limit of radiocarbon dating (~50–60 ka; Trumbore, 2000). Attempts to date these deposits using other geochronology methods have been limited to thermoluminescence (Forman et al., 1987; Berger and Nielsen, 1990) and optical stimulated luminescence (Roy, 1998; Dalton et al., 2016).

Marine Isotope Stage (MIS) 3 (57–29 ka) is an interstadial period of relatively reduced global ice volume during the last glacial cycle (Figure 1.3; Lisiecki and Raymo, 2005). During this time period, core regions of the Fennoscandian Ice Sheet were likely deglaciated (Kleman et al., 2021; Mangerud et al., 2023) and the extent of the LIS is debated (Dalton et al., 2019; Miller and Andrews, 2019). The interpretation of radiocarbon ages near the limit of this geochronometer has been one factor fueling a prolonged debate about whether the HBL was deglaciated during MIS 3 (Shilts, 1982; Andrews et al., 1983; Dredge and Thorleifson, 1987; Dalton et al., 2016, 2019; Miller and Andrews, 2019). The configuration of the LIS during this time period is important for global ice sheet modelling (Gowan et al., 2021), since the North American ice sheet complex was responsible for the equivalence of up to ~85 m eustatic sea level equivalence at peak glacial conditions during the last glacial cycle (Stokes et al., 2012).

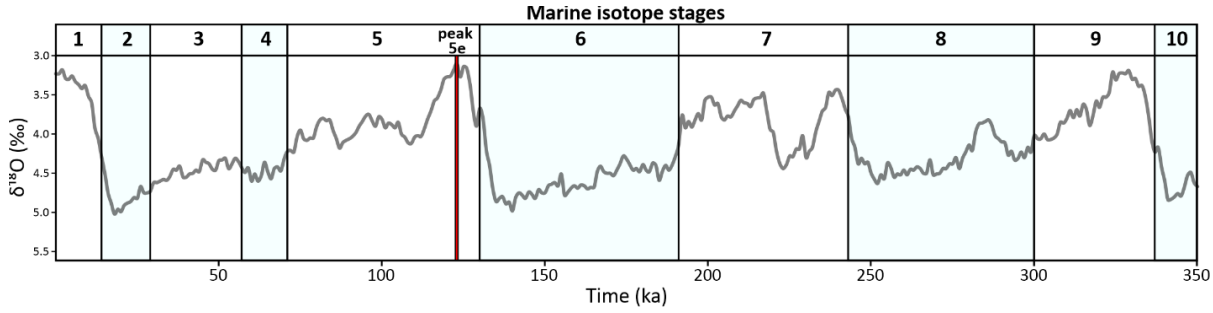

Figure 1.3: The LR04 benthic delta ^{18}O stack for the last 350 ka (Lisiecki and Raymo, 2005). Marine Isotope Stages are numbered and the shaded blue areas show relatively cold stages (even numbers).

Recent studies have interpreted MIS 3-aged nonglacial sediments in the HBL using radiocarbon and optical dating methods (Dalton et al., 2016, 2018). This evidence has been used to imply a significantly reduced LIS during MIS 3 compared to previous reconstructions, and possibly a deglaciated Hudson Bay (Dalton et al., 2019). This interpretation has been questioned suggesting that the evidence in support of a deglaciated HBL is minimal, and that many of the MIS 3 ages obtained are in contradiction with older age estimates from the same stratigraphic unit (Miller and Andrews, 2019). Miller and Andrews (2019) also argue that other far-field LIS proxies need to be considered, such as the timing of Heinrich events in the Atlantic Ocean. In the western HBL, evidence that supports MIS 3 deglaciation is limited to thermoluminescence ages (32–46 ka) from sorted intertill sediments at four sites along the Nelson River (sections 1–4, Figure 1.4; Berger and Nielsen, 1990), near-finite radiocarbon ages from wood at a site on the Black Duck River (section 6, Figure 1.4; Dalton et al., 2016) and optical ages from interpreted marine sediments exposed along the Severn River (section 7, Figure 1.4; Dalton et al., 2016). The configuration of the LIS during MIS 3, especially in the HBL region, is integral to calibrating global paleo-ice sheet (and sea level) models (Pico et al., 2019; Gowan et al., 2021) and needs to be reconciled.

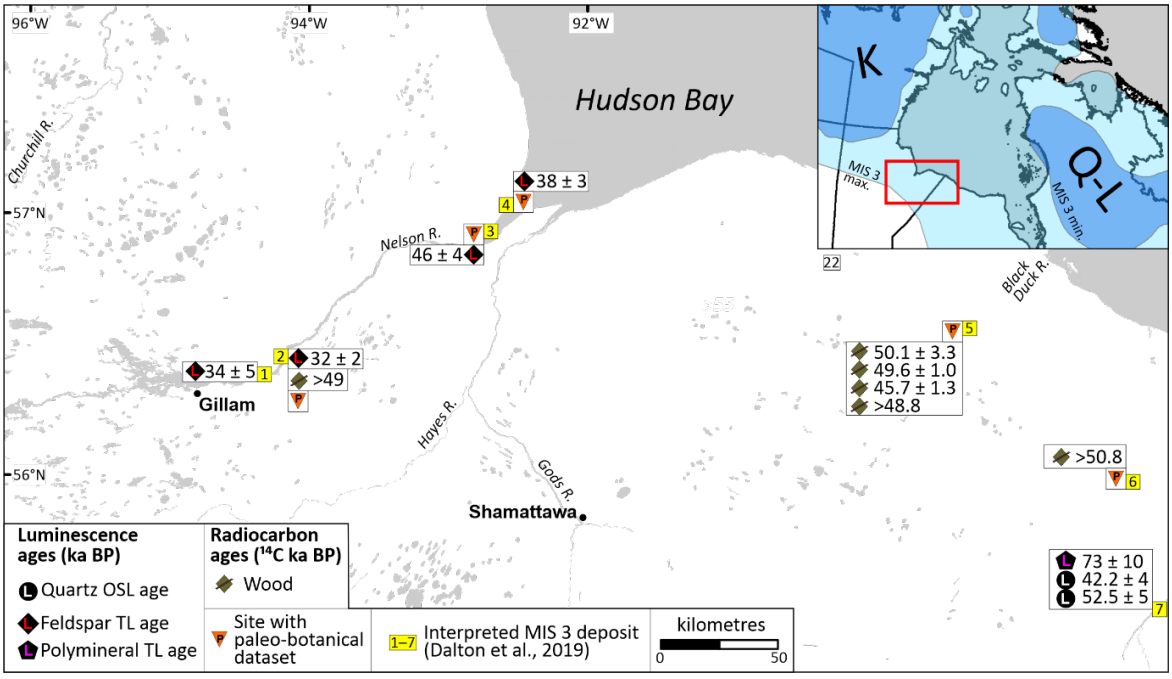

Figure 1.4: Geochronology data for Quaternary intertill nonglacial deposits in the western Hudson Bay Lowland region of central Canada that have been interpreted to support deglaciation of the region during Marine Isotope Stage 3 (sites 1–7; Dalton et al., 2019). The inset map shows the location of the study area in central Canada, relative to deglacial position of the Keewatin (K) and Quebec-Labrador (Q-L) domes of the Laurentide ice sheet and the Batchelor et al. (2019) minimum and maximum reconstruction limits for the LIS during MIS 3 at 45 ka.

1.1.3 Glacial dynamics prior to the last glacial maximum

Reconstructions of the LIS during the Late Pleistocene are relatively well constrained from the last glacial maximum (LGM) during MIS 2 to MIS 1 deglaciation (~25ka–6 ka BP), largely from mapping and dating of ice-marginal features (Dalton et al., 2023). The extent and dynamics of the LIS prior to LGM are much less certain, but minimum and maximum extents throughout the last glaciation have been proposed based on the available datasets which provide insight into ice sheet growth and decay (Stokes et al., 2012; Dalton et al., 2022b). Similarly, ice margins have been proposed for the entire Pleistocene and into the Pliocene for the LIS (Batchelor et al., 2019); however, there are minimal field-based constrains for the LIS within this reconstruction and the majority that do exist are from sites situated close to the past ice sheet margin limits (Batchelor et al., 2019). Furthermore,

these data do not provide insight into past ice sheet dynamics such as ice-flow directions, sediment dispersal trends or growth patterns from the interior regions of the LIS. To better understand the long-term dynamics of the LIS, areas containing thick sequences of Quaternary-aged sediments need to be better understood by documenting temporal ice-flow changes, sediment provenance evolution and the relationship of glacial events to ice-free periods (interglaciations and/or interstadials).

A recent study in northeast Manitoba combined field-based erosional indicators, streamlined landforms and stratigraphic ice-flow data to provide a coupled reconstruction of the ice-flow history across thin and thick drift regions (Gauthier et al., 2019). Gauthier et al. (2019) identified at least 10 ice-flow phases across western HBL, which is more than double what had previously been recognized in the western HBL (c.f. Figure 1.2). The timing of these ice flow phases is largely unknown and was limited to stratigraphic relationships with intertill nonglacial sediments of unknown age. Gauthier et al. (2019) did not extensively incorporate till provenance data in their analysis and the abundant NW-SE oriented ice-flow indicators in western HBL had to be interpreted as bidirectional. Deciphering between NW- and SE-trending ice-flows was highlighted as a significant hurdle to reconstructing the ice-flow history in northeast Manitoba (Gauthier et al., 2019).

1.2 Methodology overview

1.2.1 Field data collection

Helicopter-supported fieldwork was conducted to access natural exposures of Quaternary sediments along active waterways or meltwater corridors and to document the sediments at surface. At each section, the presence and nature of contacts between different sediment facies were first determined. Intertill sorted sediments were thoroughly investigated to determine if there was any organic material within the sediment, such as shells, peat or wood. Glacial sediments (till) were tentatively subdivided in the field at each section based on colour, matrix grain-size, degree of compactness and sedimentary structures. Surficial stations investigated the sediments in the near-surface (<1.2 m bgs) through hand-dug pits and/or Dutch-auger holes. Surface till samples were

collected from C-horizon material in hand-dug pits or from mudboils. Mudboils were the preferred sampling sites, as these permafrost features bring unweathered till to the surface (McMartin and McClenaghan, 2001). At sections, till samples were collected at all qualitative facies change in the field (colour, texture or compaction change) and also every 1–4 m even when obvious stratigraphic changes could not be seen, in order to fully quantify the changes in till composition with depth. A field duplicate was collected after every twentieth sample.

Ice-flow indicators measured include till fabrics of elongated clasts, and in-situ lodged cobble- to boulder-sized clasts that had parallel striations on their upper surfaces (Figure 1.5). Till clast-fabrics measurements were conducted on three vertical faces carved into the till to create a 'box', after the section was cleared of slumped material. The trend and plunge of the A-axis from at least 30 clasts were measured, each with an A:B axis ratio >1.5 (Figure 1.5a). A non-magnetic knitting needle was used to extrapolate the plunge of the A-axis out of the till face, allowing for increased accuracy of measurements. Care was taken to ensure that the dip of the A-axis was less than 70°. Clasts with a B-axis of less than ~40° were measured, since the B-axis orientation affects A-axis fabric strength (Holmes, 1941). Clasts in contact with other clasts or clasts that were adjacent to large boulders that would not have allowed free rotation were not measured (Andrews, 1969). The modality of each fabric was assessed visually (Hicock et al., 1996) and eigenvalues and eigenvectors calculated (Mark, 1973; Benn, 1994). All ice-flow-orientation interpretations using clast-fabrics are initially considered bi-directional, since the imbrication of clasts up-ice is not consistent in the western HBL (Gauthier et al., 2019). Lodged, in-situ, cobble- to boulder-sized clasts with parallel striae on their upper surface are also considered an indicator of paleo-ice direction (McMartin and Paulen, 2009) and were measured where encountered in section (Figure 1.5b–d).

Till samples collected in the field were first split at the Manitoba Geological Survey warehouse to archive unprocessed samples. The colour of the till-matrix was determined on moist samples under laboratory light conditions using standard Munsell nomenclature. Till samples were then sieved at the Saskatchewan Research Council to obtain the silt and clay (<63 μm) size-fraction for analyses of the till-matrix geochemistry and the granule- to medium-pebble (2–8 mm) size fraction for clast-lithology counts.

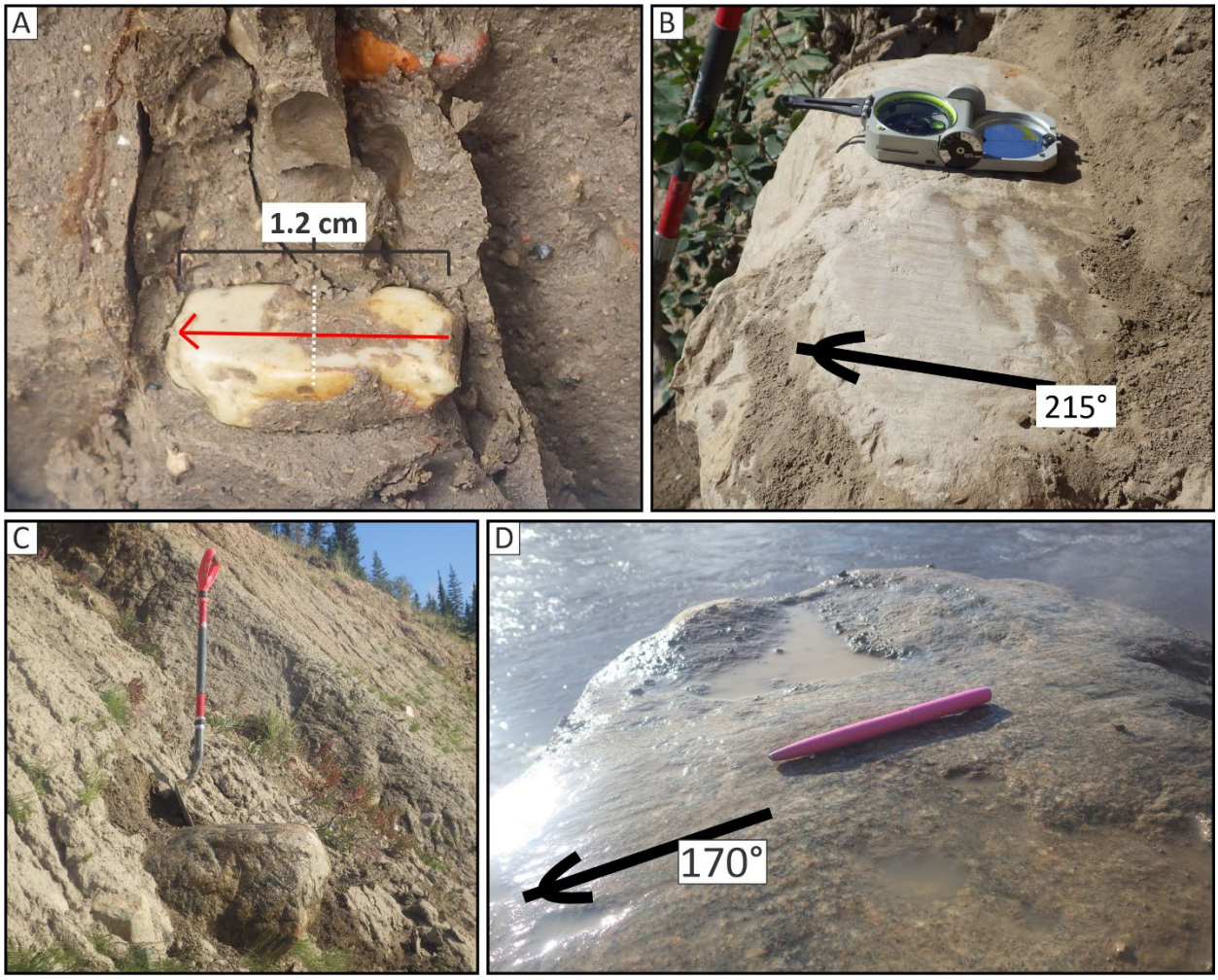

Figure 1.5: Examples of ice-flow data collected: a) clast measured during clast-fabric analysis, the a-axis and dip direction are highlighted by the red arrow and the b-axis is highlighted by the dashed white line; b) lodged boulder with parallel striations on its upper surface indicating 215° ice-flow; c) section view of a lodged boulder within till; and d) view of the flat, striated and grooved upper surface of the boulder shown in c.

1.2.2 Geochronology of intertill nonglacial sediments

1.2.2.1 Radiocarbon

The timing of MIS 3 (57–29 ka; Lisiecki and Raymo, 2005) is partly within the range of radiocarbon age determination (upper limit at ~50–60 ka; Trumbore 2000), but ages obtained near the upper limit of this geochronology method need to be treated cautiously as a small amount of contamination by modern carbon can create erroneously younger ages (e.g., Briner et al., 2025). For example, the amount of original ^{14}C used for age estimation in samples >40 ka is <1% of the initial total and is thus extremely sensitive to contamination during burial, sampling or laboratory processing (Pigati et al., 2007). When calculating radiocarbon ages (e.g., Stuiver and Polach, 1977), one percent modern carbon contamination of a sample that would normally have yielded a non-finite age (>50 ka) would come out at about 36.6 ka. In the context of the MIS 3 problem, this has major implications because a fossil from the last interglaciation would be erroneously assigned to MIS 3, supporting a reduced LIS volume and ice-free Hudson Bay. Buried carbonate shells often behave as open systems and are prone to post-depositional contamination by exchange with younger carbon in porewater (e.g., Briner et al., 2025), and finite ages between 35–50 ka are usually best considered as minimum age estimates (Miller and Andrews, 2019). Similarly, peat and bulk organics are susceptible to the introduction of contamination post burial by modern day rootlets and should be interpreted cautiously. Contamination by 'old carbon' also needs to be considered, such as lignite derived from Cretaceous shales (Clayton and Moran, 1982). Wood is the optimal material near the upper limit of radiocarbon dating to limit potential contamination (Dalton et al., 2016); thus, wood was the targeted material in intertill sorted sediments to attempt radiocarbon age determination. If intertill sediments encountered contained shells, but no wood, then shells were submitted for radiocarbon age determination.

1.2.2.2 Optical ages

The western HBL stratigraphy contains sediments deposited during the last interglacial (MIS 5e; Nielsen et al., 1986), as well as possible MIS 3 aged sediments (Dalton et al., 2019). To obtain ages for sediments that may be older or near the upper limit of radiocarbon age determination (~50–60

ka; Trumbore, 2000) or do not contain organic material, optical dating methods were incorporated (Rhodes, 2011). Sediments targeted in this study are intertill sediments that are moderately- to well-sorted, bedded sand that is interpreted to have been deposited in low energy lacustrine, marine or fluvial environments that should be conducive to sufficient light exposure prior to burial. Luminescence ages from quartz grains were used to avoid the deleterious effect of anomalous fading from alkali feldspars on optical age estimations (Rhodes, 2011). Ideally, sampled sediments were from stratigraphic intervals that also contained in-situ organic material, which allowed for paleo-environmental criteria to be examined as supporting evidence. Luminescence methods are experimental in nature and are dependent on the optical properties of the minerals investigated in a study area.

1.2.3 Till characterization

To improve the current stratigraphic framework of the western HBL region, this thesis uses multiple parameters to constrain till provenance. The identification of till units is reliant on field-based sedimentology and ice-flow data, coupled with analytical results to determine ice-flow direction.

1.2.3.1 Till clast-lithology composition

The till clast-lithology of the granule- to medium-pebble (2–8 mm) size-fraction was determined using a 10x optical microscope to help identify the dominant till provenance (bedrock source). Clast-lithology counts initially separated the 2–4 and 4–8 mm size-fraction into lithological classes that were dependent on lithologies observed within a study area (minor variations between field areas). Clast-lithology data is reported as a count proportion (ct. %), to allow for comparison with previous datasets published in northeast Manitoba (e.g., Trommelen et al., 2013; Trommelen and Ross, 2014).

1.2.3.2 Till-matrix geochemistry

The till matrix silt and clay size-fraction (<63 μm) was submitted to Activation Laboratories Ltd. (Actlabs) for determination of sediment geochemistry. The geochemistry of till sampled from 2016–2017 was analyzed after both a partial (Aqua Regia) and near-total (4-acid) digestion of the till

matrix (<63 µm). The geochemistry of till sampled from 2019–2021 was analyzed after both a partial (Aqua Regia) and total (lithium metaborate/tetraborate fusion) digestion of the till-matrix (<63 µm). Additionally, for the 2019–2021 analysis years an internal reference standard (OREAS 46) was inserted after every 20 samples in similar sample containers to create an internal blind reference standard for QA/QC purposes. The elemental values were then determined by ICP-MS and ICP-OES and reported as a proportion (ppb, ppm, wt. %). These geochemical data are published in Hodder et al. (2024b) and Hodder and Gauthier (2025a, b).

1.2.3.3 Detrital hornblende $^{40}Ar/^{39}Ar$ ages

The application of detrital hornblende$^{40}Ar/^{39}Ar$ ages to assist provenance interpretations has been used at the southern margin of the LIS (Roy et al., 2007), within the Quebec-Labrador region of the LIS (Roy et al., 2009), and in marine sediments associated with glacial transport (Hemmings et al., 2000; Hemmings and Hajdas, 2003). The $^{40}Ar/^{39}Ar$ age of hornblende grains records time elapsed since the last metamorphic event that exceeded the closure temperature of the mineral, which for hornblende grains is approximately 510°C (Schaen et al., 2021). Thus, hornblende grains record the last major orogenic event that a region experienced. The Canadian Shield is Precambrian in age and classified into geological provinces based on the tectonic history of these regions. Three geological provinces are important to this study for the application of the detrital hornblende $^{40}Ar/^{39}Ar$ ages: the Superior, Western Churchill and Trans Hudson Orogen provinces, which have approximate $^{40}Ar/^{39}Ar$ ages of >2.6, 1.8–2.0 and 1.7–1.9 Ga, respectively (Roy et al., 2007). The study area is well positioned to use the age of these geological provinces to discriminate between an eastern and northwestern provenance for hornblende grains (Figure 1.6). In particular, hornblende grains with a $^{40}Ar/^{39}Ar$ age that is >2.6 Ga (Superior Province) are an important indicator of eastern or southeastern provenance, since there is no documentation of N-trending ice-flow in the study area (Gauthier et al., 2019). The application of detrital hornblende $^{40}Ar/^{39}Ar$ ages to assist with provenance has not been used in the HBL prior to this study and one problem that this parameter helps address is deciphering between NW- and SE- trending ice-flow directions. Detrital hornblende grains were hand-picked from till mineral separates using a binocular microscope. A total of 14–16

grains were analyzed for selected till samples at the Ar-Ar lab at the Manitoba Isotope Research Facility after irradiation.

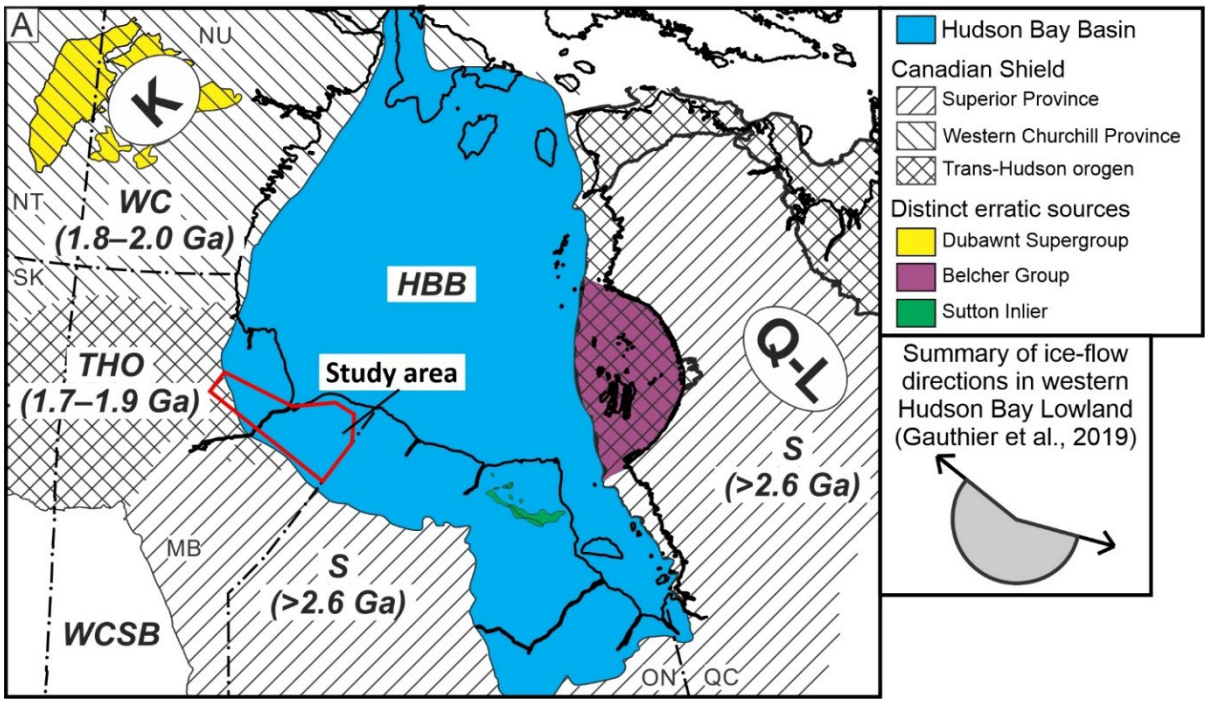

Figure 1.6: Regional bedrock geology of central Canada. Bedrock geology is modified from Wheeler et al. (1996) and the tectonic age of geological provinces is derived from Roy et al. (2007). The location of the Keewatin (K) and Quebec-Labrador (Q-L) domes of the Laurentide Ice Sheet are their positions during deglaciation from Dalton et al. (2020).

1.2.3.4 Statistical analysis of till compositional data

This thesis incorporates a wide variety of data to characterize till. While this allows for thorough documentation of the composition, understanding the relationships within and between these data can prove difficult using only univariate or bivariate plots and manual interpretation. For instance, we may be interested in determining whether there is a relationship between some of these compositional characteristics, and if there is one, then to quantify how strong it is and what it can tell us about sediment transport processes or other processes? To help answer these questions and better understand the relationships between variables in the data, multivariate analysis methods were incorporated. Multivariate analysis reduces the number of variables needed to explain the

variance within the dataset and can allow for an easier recognition of important trends and relationships within a dataset or across multiple datasets (Grunsky, 2010).

Statistical analysis first used exploratory data analysis techniques using Q-Q, scatter and box plots to understand the structure of the datasets and assess if there are outliers. In sedimentology, sediments samples are often separated by grain-size fractions, which are then analyzed in different ways (e.g., <63 µm size-fraction geochemistry or 2–8 mm size-fraction clast lithology counts). These variables are reported as a proportion (ct. %, wt. %, ppm, ppb, etc.) subject to a constant sum and restricted to the positive number space. Datasets restricted to the real positive number space can lead to misleading results using statistical measures such as correlation and covariance (Grunsky, 2010). To overcome these issues, Atchison (1986) introduced the use of log ratios to project the dataset into the entire (positive and negative) real number space. At the analysis stage, geochemical data with a common unit of measure were processed using a centred log-ratio transformation to create an open dataset (Davis, 2002). Statistical analysis did not combine datasets determined by different digestion methods. This thesis uses a combination of principal component analysis (PCA; Atchison, 1984; Davis 2002) and k-means cluster analysis (McQueen, 1967; Davis, 2002) to process till-matrix geochemistry data, an unsupervised classification technique that has been previously used to investigate till provenance trends in northeast Manitoba (Wang, 2018).

1.2.4 Stratigraphic approach

The nomenclature referring to North American glacial and interglacial stages has evolved through time. Prior to 1950, the nomenclature consisted of four glacial and three interglacial stages within the Pleistocene Series that were established at the southern margin of these glaciations in the United States (Flint, 1963). Flint (1963) reconciled the terminology for the Wisconsinan Stage which represents the entirety of the last glacial cycle, and this definition is still used in the same capacity today (Cohen and Gibbard, 2019). Subsequent detailed stratigraphic investigations of the pre-Wisconsinan sediments, supported by age dating of volcanic beds and paleomagnetic measurements, indicated that the pre-Wisconsinan stratigraphic framework was an immense oversimplification (Boellstorff, 1978; Hallberg, 1986; Roy et al., 2004). The penultimate glaciation is

referred to as the Illinoian Stage, but Early- to Mid- Pleistocene glacial stages are referred to as 'pre-Illinoian A' through to 'pre-Illinoian K' (Cohen and Gibbard, 2019). There are many challenges with defining the last interglacial period (Sangamonian Stage) in North America, which are discussed in detail by Ovtos (2015). For this study, we assign sediments/units that are interpreted to have been deposited during the penultimate ice-free period and have a climatic signature similar to the present day to the Sangamonian Stage. There are currently no defined stages for sediments deposited during interglacial stages prior to the Sangamonian Stage (Cohen and Gibbard, 2019).

Within the western HBL, there are consistent observations of diamicton with similar qualitative properties that have contrasting ice-flow data (e.g., Figure 1.7). These diamictons, interpreted as till, are at the same relative stratigraphic position. In some instances, these tills have considerable variation within compositional data, which allows them to be distinguished and designated as distinct lithofacies or unit. Yet, in other instances, these tills are indistinguishable with compositional data. Previous lithostratigraphic studies have considered till deposits to be laterally continuous and used qualitative criteria to designate till units. As such, designated till units have mis-matched ice-flow and compositional data (Nielsen et al., 1986). This inhibits reconstruction of the ice-flow history of the region, as well as defining dispersal patterns within till. This thesis places a stronger emphasis on ice-flow data combined with extensive provenance analysis to determine stratigraphic units.

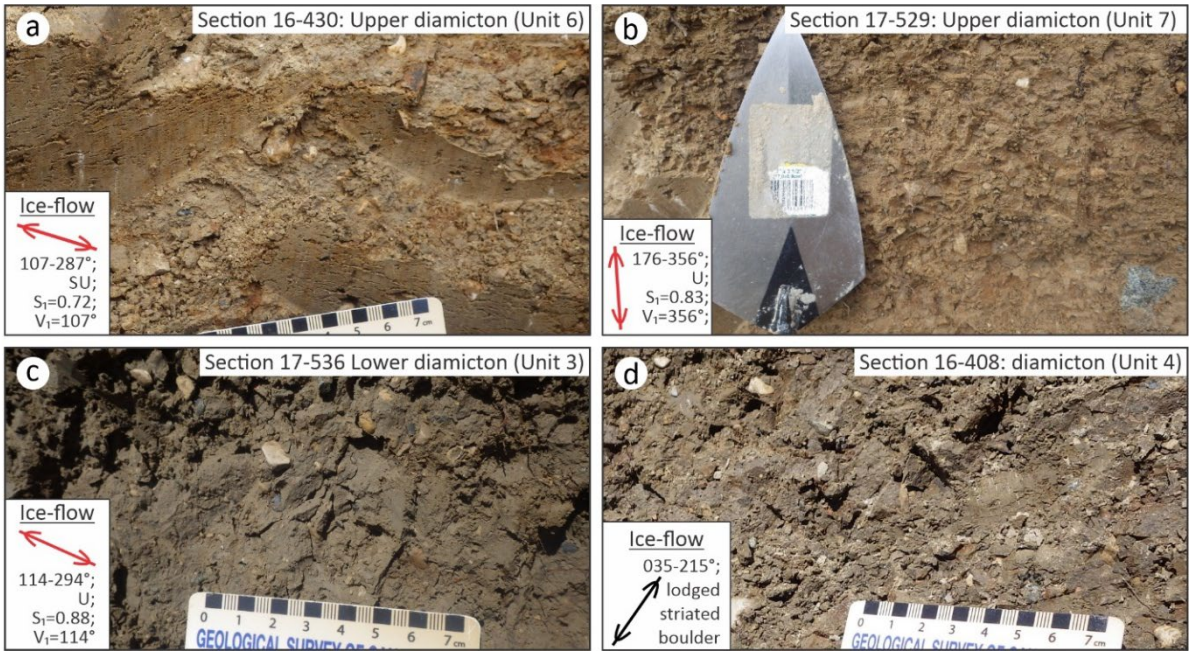

Figure 1.7: An example of tills in the Kaskattama highland study area characterized by similar sediment facies, but that were deposited by different ice-flow directions. The tills in a and b have similar texture and color, but a different fabric. Similarly, tills in c and d have similar facies, but contrasting fabric. Abbreviations: SU, spread unimodal modality; U, unimodal modality; S_1, principal eigenvalue; V_1, principal eigenvector.

A hybrid-stratigraphic approach is used that incorporates both lithostratigraphy and allostratigraphy principles to define informal stratigraphic units. The North American Stratigraphic Code (North American Commission on Stratigraphic Nomenclature, 2021) recommends defining informal units when the extent and significance of units beyond the study area are still undetermined and/or when units are defined using innovative techniques. To build a stratigraphic framework of informally defined till units, a multi-parameter lithostratigraphy approach was taken that incorporates sedimentology observations (relative consolidation, colour, sedimentary structures, clast fabric and other ice-flow indicators) and laboratory analytical data (till provenance). The approach started in the field where till beds may be recognized at a section based on facies characteristics, their upper and lower boundaries, as well as their general stratigraphic position. This allowed for preliminary

facies- or litho-correlations of units with similar characteristics and stratigraphic positions at a local scale. It is important to note here that this initial field-based correlation between sections incorporated ice-flow indicator data for each identified till unit. These field-based observations were then verified by detailed provenance analysis to confirm the direction of ice-flow that deposited the sediment. After till units were defined using a lithostratigraphic approach, an allostratigraphic approach was used to identify the relative age of intertill sorted sediment packages using the bounding surfaces of the enclosing till units. The use of an allostratigraphic approach to identify the relative age of intertill sorted sediments was necessary due to the fragmented nature of the stratigraphic record in the region, where the uppermost intertill nonglacial sediments encountered at a section may not necessarily be related to the penultimate deglaciation of the region (e.g., Dube-Loubert et al., 2013; Gauthier et al., 2024, 2025b). The stratigraphy was first developed at local scales, and correlations were progressively extended across each study area to produce regional stratigraphic frameworks. Lastly, stratigraphic frameworks established within each study area are compared and an updated stratigraphic framework for the western HBL is proposed (Chapter 6).

1.3 Thesis objectives

The thesis aims to improve our understanding of the evolution of the LIS in a complex region that provides constraints for both the Keewatin and Quebec-Labrador domes over multiple glaciations by investigating three understudied or unstudied areas that contain some of the richest Quaternary stratigraphic records of central Canada. This is accomplished by collecting detailed field-based observations and combining these observations with till analytical and nonglacial sediment geochronology data to establish the Quaternary stratigraphy in selected areas of study. In particular, this study aims to determine the ice-flow direction that deposited till units by using multiple parameters to firmly establish provenance. The relationship(s) of identified till units to intertill nonglacial sediments is then assessed using allostratigraphic principles to establish the Quaternary stratigraphy. The depositional age of intertill nonglacial units is further explored using radiocarbon and optical age methods to elucidate the timing of nonglacial periods. This multi-parameter methodology across a wide region of the western HBL provides insight into past LIS glacial dynamics through multiple glacial cycles. In particular, objectives of this thesis are:

1. Establish Quaternary stratigraphic frameworks for three unstudied or understudied regions of the western Hudson Bay Lowland using field-based sedimentological and ice-flow datasets that are supplemented with laboratory-based datasets (till composition, geochronology);
2. Evaluate if the western Hudson Bay Lowland was ice-free during MIS 3 and provide age estimations and paleo-climate interpretations for recognized interglacial units; and
3. Discuss the implications of the new stratigraphic frameworks for understanding the evolution of the Laurentide Ice Sheet across multiple glaciations.

1.4 Thesis format

This thesis is comprised of five journal manuscripts (Chapters 2–6) with an introductory chapter (Chapter 1) and a concluding chapter (Chapter 7) summarizing the findings of the thesis.

Chapter 2 presents a review of available geochronology data for intertill nonglacial deposits in the western HBL and discusses the robustness of these previous age determinations. This study also highlights the fragmented nature of the stratigraphic record and the importance of understanding the entire depositional sequence to make robust correlations and interpretations of intertill nonglacial sediments. Furthermore, this study targeted the uppermost intertill nonglacial sediments in the regional stratigraphic record at three sites to determine the optical age of the sediment. These new optical ages, combined with a review of previous geochronology data and considerations of far-field ice sheet constraints, is used to argue against the notion of a deglaciated western Hudson Bay Lowland during MIS 3. Chapter 2 is published in *Quaternary Research* (Hodder et al., 2023).

Chapter 3 investigates the Quaternary stratigraphy in and around the Kaskattama highland region of the western HBL (Figure 1.1a). A key aspect of this work is developing a methodology that can be used to better understand Quaternary stratigraphic records in thick drift regions that have experienced a complex ice-flow history, such as the HBL. This chapter establishes a hybrid lithostratigraphic-allostratigraphy approach that relies on multi-parameter characterization of glacial sediments (till). In particular, it was noted that documenting the ice-flow direction that deposited till beds needs to be an integral part of field-based stratigraphic studies in the HBL. The bounding surfaces of till units is then used to determine the relative age of the intertill nonglacial deposits. This study reinforces concepts introduced in Chapter 2 and provides additional caution regarding the correlation of intertill nonglacial sediments. The constructed stratigraphic framework for the region is then discussed to provide insight into past glacial dynamics. Chapter 3 is published in *Canadian Journal of Earth Sciences* (Hodder et al., 2024a).

Chapter 4 builds off methodologies developed in Chapter 3 to investigate the Quaternary stratigraphy in the Churchill to Little Churchill rivers area of the western HBL (Figure 1.1a). This region of the western HBL is unique due to the thick (up to 50 m) exposures of Quaternary sediment that overlie Precambrian bedrock. This study details 16 identified stratigraphic units within the area and discusses the implications of this record for initial LIS growth and glacial dynamics across the last three glaciations. In particular, the Churchill to Little Churchill rivers area contains an important

record of MIS 6 glaciation and deglaciation. Chapter 4 is currently in review with the *Canadian Journal of Earth Sciences*.

Chapter 5 investigates the Quaternary stratigraphy of three remote understudied or unstudied regions of the western HBL: the Nelson River Estuary, Machichi River and Kaskattama River (Figure 1.1a). This study highlights how the hybrid lithostratigraphy-allostratigraphy approach can be effectively applied to unstudied areas of the HBL and 13 stratigraphic units are recognized. The study provides additional insight into glacial dynamics of the western HBL and supports some findings presented in chapters 3 and 4 regarding temporal evolution of the LIS across multiple glaciations. At the time of writing, Chapter 5 has not yet been submitted to an academic journal.

Chapter 6 provides a correlation of the stratigraphic frameworks presented in chapters 3–5 and a recently published revision of the stratigraphic record in the Gillam area (Gauthier et al., 2025b) to provide an updated stratigraphic framework for the western HBL. This chapter then compares and contrasts the last two glaciations in the western HBL. At the time of writing, Chapter 6 has not yet been submitted to an academic journal.

Chapter 7 summarizes the main contributions presented in chapters 2–6. This chapter also highlights regions for future stratigraphic study and future work that could build upon research presented in this thesis.

Chapter 2

Was there a nonglacial episode in the western Hudson Bay Lowland during Marine Isotope Stage 3?

2.1 Overview

Establishing the timing of glacial and nonglacial intervals in the core regions of the Laurentide Ice Sheet (LIS) is essential to constrain ice sheet configuration at times of globally reduced ice volume, such as during Marine Isotope Stage (MIS) 3 (~57–29 ka). Hudson Bay Lowland (HBL) deglaciation, at the centre of the LIS, has been inferred at MIS 3 based on near-infinite wood radiocarbon ages and limited luminescence ages. To better constrain the age of the penultimate deglaciation of the western HBL, this study initially identified the youngest intertill nonglacial sediments, based on extensive fieldwork and till characterization. Next, vetted radiocarbon ages were combined with revised stratigraphy to show that five previously-identified 'MIS 3' sites were likely deposited during an earlier ice-free period. Finally, new optical ages targeting the youngest intertill nonglacial bed at three localities yielded ages ranging 146–166 ka; all older than MIS 3. These ages indicate that the penultimate deglaciation of the western HBL likely occurred during MIS 5e. This interpretation better explains accompanying paleobotanical datasets that indicate vegetation similar to present interglacial conditions. Currently no firm evidence exists in the terrestrial stratigraphic record for the deglaciation of the western HBL during MIS 3.

2.2 Introduction

The Laurentide Ice Sheet (LIS) repeatedly waxed and waned over the North American continent during the Quaternary period. Considerable progress has been made in understanding ice sheet configuration and evolution during and after the Last Glacial Maximum (LGM; e.g., Dalton et al., 2020). Yet, large uncertainties persist, especially for earlier stages of the late Pleistocene glaciation. Knowing the extent of former ice sheets at different times is critical for understanding long-term behavior of ice sheets, and this requires evidence from the geological record. For instance, mapping of ice margin positions provides critical domain boundaries in ice sheet models, which are used to get insights into past ice sheet evolution that in turn affect the global ice volume budget (e.g., Pico et al., 2018; Gowan et al., 2021). One key time period that requires robust field-based evidence to reconstruct ice margins is the Marine Isotope Stage (MIS) 3 interstadial, spanning the time interval of ~57–29 ka (Lisiecki and Raymo, 2005). During this interstadial, the extent and volume of the LIS was restricted compared to the MIS 4 (71–57 ka) and MIS 2 (29–14 ka) stadials (Stokes et al., 2012; Dalton et al., 2019, Gowan et al., 2021; Dalton et al., 2021), but the exact configuration of the LIS geometry during this time period is uncertain with large differences between estimated minima and maxima extents (Dredge and Thorleifson, 1987; Batchelor et al., 2019; Gowan et al., 2021). Hence, there is a need for robust geochronological constraints that are supported by detailed lithostratigraphic and palaeoecological studies to elucidate the LIS geometry during MIS 3, as well as other periods of relatively reduced ice volume.

Data from the Hudson Bay Lowland (HBL), which is situated approximately in the geographic centre of the LIS between two major ice dispersal centres (Figure 2.1), has long been used to argue for or against MIS 3 deglaciation in central Canada (Andrews et al., 1983; Dredge and Thorleifson, 1987; Dalton et al., 2019; Miller and Andrews, 2019). Initial interpretations, using relative dating methods, assumed that a mapped subtill nonglacial stratigraphic bed (Bell Sea sediments; Shilts, 1982; Andrews et al., 1983) was deposited during the last interglacial period around MIS 5e (~115–130 ka, peak highstand at 123 ka; Lisiecki and Raymo, 2005). The first direct dating of intertill sorted sediments in the western HBL using thermoluminescence (TL) age determination resulted in four MIS 3 ages and one MIS 5 age (Berger and Nielsen, 1991); however, the MIS 3 ages conflicted with a

nonfinite radiocarbon age from wood within the same stratigraphic bed (Figure 2.1, Site 2; Dredge et al., 1990). More recently, a deglaciated HBL during MIS 3 has been interpreted using newer optical and near-finite radiocarbon ages (Dalton et al., 2016, 2019), but this was contested by Miller and Andrews (2019). The latter argued that only two radiocarbon ages from the HBL provided in Dalton et al. (2019) could plausibly be considered as finite radiocarbon ages, compared to a significant amount of nonfinite radiocarbon ages. Furthermore, they argue that the timing of Heinrich events H4 (~38 ka) and H5 (~46 ka) provide firm evidence for an extensive LIS during this time interval, which is further supported in the terrestrial record of northeastern Canada (Edwards et al., 2022). Recent studies of the marine record in the Labrador Sea provide further support for an extensive LIS during MIS 3 (Parker et al., 2022).

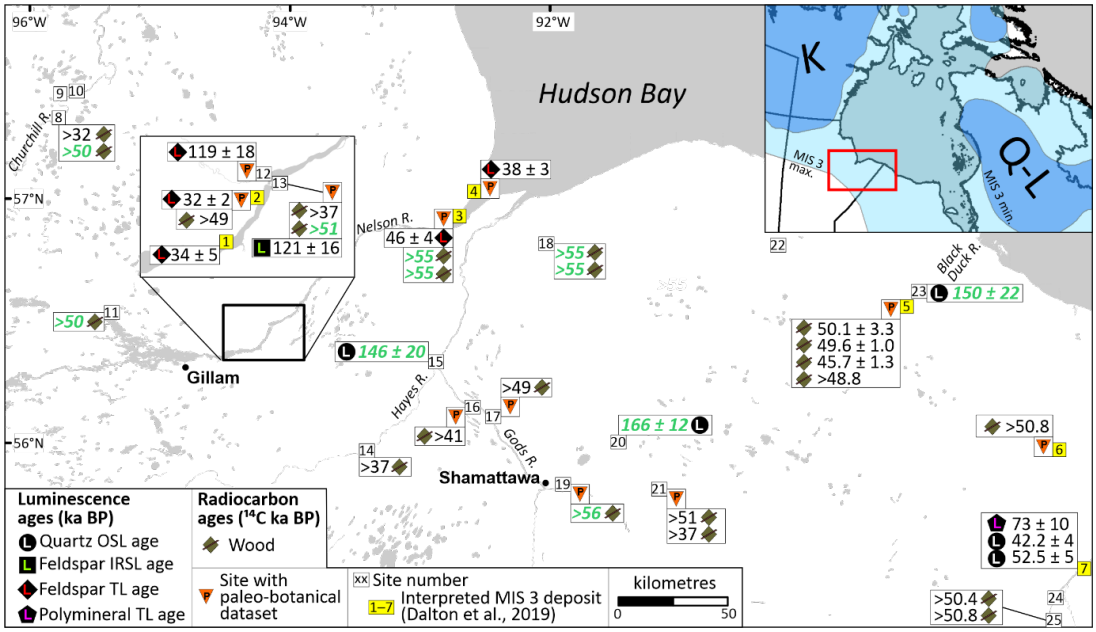

Figure 2.1: Geochronology data for Quaternary intertill nonglacial deposits in the western Hudson Bay Lowland region of central Canada. New ages from this study are green, bolded and italicized. Sites 1–7 were interpreted as possible MIS 3-aged deposits (Dalton et al., 2019), and readers are referred to Appendix A, Supplemental material 1 for additional details about site-specific geochronology data and references. Some sites are shown without data, due to vetting of potentially unreliable radiocarbon ages. The inset map shows the location of the study area in central Canada, relative to deglacial position of the Keewatin (K) and Quebec-Labrador (Q-L) domes of the Laurentide ice sheet and the Batchelor et al. (2019) minimum and maximum reconstruction limits for the LIS during MIS 3 at 45 ka.

The western HBL is a key region in the heart of the LIS, with an extensive pre-LGM stratigraphic record (Nielsen et al., 1986; Dredge et al., 1990; Dalton et al., 2018). The stratigraphic record is fragmented (Gauthier et al., 2019), and contains organic-bearing sediment deposited during at least two different ice-free interstadials and/or interglacial periods (Nielsen et al., 1986; Dredge and McMartin, 2011). As such, detailed stratigraphic studies are necessary to identify the youngest intertill nonglacial sorted sediment bed(s) in the region. Based on extensive stratigraphic work in the western HBL (Gauthier et al. 2019 and references therein; Hodder and Gauthier, 2019; Gauthier et al., 2021; Hodder and Gauthier, 2021; Gauthier et al., 2022), we document a series of new ages, from both optical and radiocarbon dating methods, on the uppermost intertill organic-bearing and sorted sediments in the western HBL. We show that key stratigraphic beds, including some that were previously assigned to MIS 3, can now be more confidently assigned to MIS 5e.

2.3 Methods

2.3.1 Field data

Sediment exposures investigated were first cleared of slumped detritus, exposing a continuous section with no gap, and then described in detail. This includes describing the grain-size, structure, colour, thickness, lateral variations, composition (clast-lithology and geochemistry) and ice-flow data of identified stratigraphic beds. Ice-flow data were obtained from studied sections by measuring the long-axes orientation, or fabric, of clasts within till. Elongate clasts, defined by a minimum 1.5 ratio of the a-axis (longest) to the b-axis (middle), will, in most cases, rotate within the till matrix and orient parallel to the direction of shear that the overriding glacier exerts on the till (Holmes, 1941; Hicock et al., 1996). A minimum of 30 elongated clasts were measured at each of the nine clast-fabric sites and the dataset is provided in Appendix A, Supplemental material 2.

This work highlights three new sites where the stratigraphically youngest intertill nonglacial bed was identified through regional mapping and the sediment was suitable for optical dating (Figure 2.1: sites 15, 20, 23). It also includes revision of two known sites, with the support of new stratigraphy

correlations and radiocarbon ages from wood, where nonglacial beds were previously assigned to MIS 3 (Figure 2.1: sites 3, 4).

2.3.2 Optical dating

At sites 15, 20 and 23 (Figure 2.1), the stratigraphically youngest intertill sorted sediments were sampled for optical age determination. Optical dating samples were collected by inserting opaque plastic tubes (~20 cm long and 5 cm in diameter) into the sediment faces, extracting them, and then sealing each end to preserve water content. Sample tubes were opened under appropriate laboratory lighting and the light-exposed material at the ends of the tubes was removed and discarded. Bulk sediment extracted from the middle of the tubes was treated with HCl acid to remove any carbonates, and then by concentrated H_2O_2 to remove any disseminated organic matter. Sediment in the 180–250 µm diameter size range was then extracted by wet-sieving, and the quartz fraction separated by density separation in lithium metatungstate. Quartz grains were then etched with concentrated HF acid to remove the outer alpha affected surfaces of the grains and to dissolve any remaining feldspar (e.g., Wintle, 1997). Aliquots consisted of 50–100 quartz grains mounted on aluminum disks using silicon oil as an adhesive.

Equivalent dose (D_e) values were found using the single-aliquot regenerative-dose (SAR) method (Murray and Wintle 2000, 2003). Irradiations and luminescence measurements were made using a Risø TL/OSL DA-20 reader. Laboratory irradiations were applied using a calibrated $^{90}Sr/^{90}Y$ beta-source on the reader that delivered ~4.7 Gy·min^{-1} to the sample grains. Aliquots were stimulated by exposing them to 56 mW·cm^{-2} of blue (470 ± 20 nm) light for 100 s while being held at 125 °C (Murray and Wintle, 2003). Ultraviolet emissions (~350 nm) were detected by an Electron Tubes Ltd. 9235QB photomultiplier tube placed behind a 7.5-mm-thick Hoya U-340 optical filter. An infrared 'wash' (exposure to ~130 mW·cm^{-2} of 870 ± 40 nm light for 100 s while at 50 °C) was administered prior to stimulation with blue light in order to reduce or eliminate the signal from any contaminating feldspar (Olley et al., 2004; Wintle and Murray, 2006). Aliquots were accepted for SAR analysis if their natural signals showed a clear 'fast' component. Dose-response data were generated by giving the aliquots various laboratory doses, up to ~400 Gy, and one of the doses was repeated to test the

effectiveness of the chosen test dose to correct for sensitivity change incurred during the SAR cycles. A preheat temperature and duration of 220 °C for 10 s was chosen, which is about midway in the range of typical values (160–300 °C, Wintle and Murray, 2006) used by most practitioners for quartz. The preheat treatment administered after the test dose involved heating the aliquot to 160 °C at a rate of 5 °C/s and then turning off the heat. A 'zero dose' measurement was also included to measure the degree of thermal transfer (recuperation). For each aliquot, the luminescence measured over the last 20 s of 100 s of stimulation was subtracted from that recorded over the first 0.4 s of stimulation, and this was divided by that measured after the test dose. These data were plotted as a function of laboratory dose and were best-fitted with saturating exponential+linear curves. The luminescence intensity measured from a preheated aliquot of prepared grains that had received no laboratory dose (the 'natural') was interpolated onto its dose response curve, and a D_e value was measured off the dose axis; a representative example is show in Figure 2.2. Standard SAR quality control tests were applied, and these included assuring that the intensities of the recuperation signals were less than 5% of those of the natural signals, and that recycling ratios were no more than ±10% of unity (Wintle and Murray 2006). Finally, the efficacy of the chosen SAR protocol was tested for each sample by means of dose recovery tests (Wintle and Murray, 2006). For these, 15 aliquots were bleached by natural sunlight for 30 minutes, then given a laboratory dose approximately equal to the samples' D_e, and then the same SAR protocol was applied to see if that dose could be recovered.

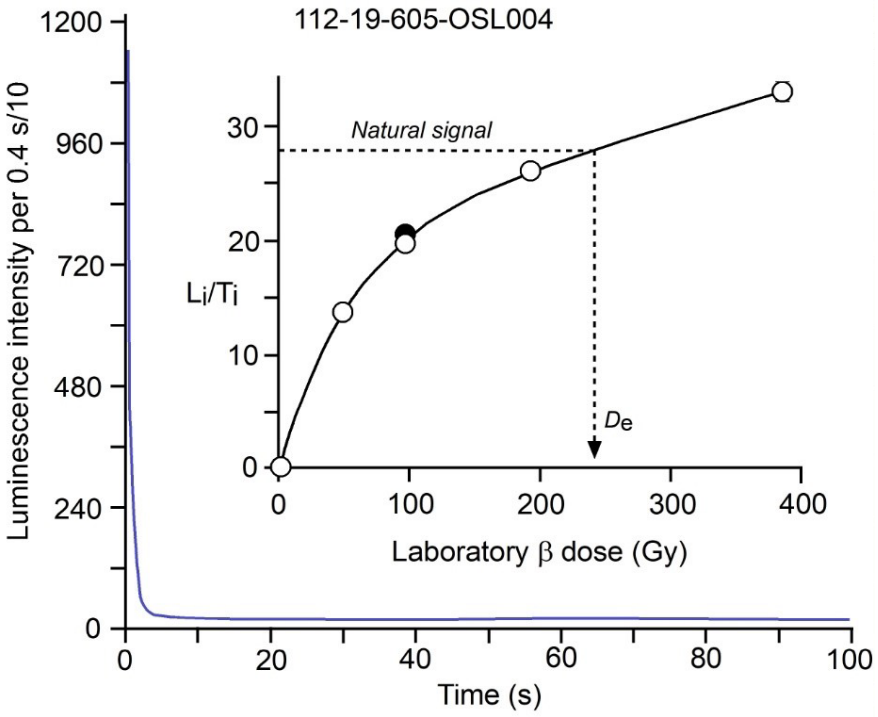

Figure 2.2: Luminescence decay curve (main graph) showing the 'natural' signal, and a dose-response curve (inset) for sample 112-19-605-OSL-004, which are typical of those of this sample and of the others samples. Note that the initial part of the luminescence decay is dominated by the desired 'fast' signal component. In each case, the final 20 s of the signal was subtracted from the initial 0.4 s, and this value (Li) was divided by that measured from a subsequent test dose (Ti) to produce the normalized (i.e., sensitivity corrected) signal, which is plotted on the vertical axis of the dose response curve graph. Note that the dose response is best fitted by an exponential+linear function. The equivalent dose (De) is estimated by interpolation of the natural signal onto the dose response curve as shown.

Environmental dose rates (Table 2.1) were determined by drying and milling a representative fraction of the bulk sediment used for dating and analyzing for U, Th, and K by neutron activation analysis (Table 2.1). As all our samples consisted of well-drained sand, the as-collected water content was used in the dose rate calculations, with a ±10% uncertainty (1σ) that is intended to account for moisture fluctuation over time. Dose rates were calculated using standard formulae (Aitken, 1985; Berger, 1988; Lian et al., 1995) and the dose-rate scaling and conversion factors of

Guerrin et al. (2011) and Brennan (2003), respectively. The contribution from cosmic ray radiation (Table 2.1) was estimated using present burial depths and the relationship of Prescott and Hutton (1994).

Table 2.1: Optical age sample water content, radioisotopes concentrations, sample depths, and calculated dose rates.

Site	Sample ID	Δ^w [1]	K (%)	U ($\mu g \cdot g^{-1}$)	Th ($\mu g \cdot g^{-1}$)	d [2] (m)	$\dot{D}_C$ (Gy/ka) [3]	$\dot{D}_T$ (Gy/ka) [3]
15	112-19-629-024	0.063	1.16 ± 0.06	0.577 ± 0.120	2.62 ± 0.14	17.7	0.023 ± 0.002	1.37 ± 0.06
20	112-16-407-019	0.101	1.44 ± 0.08	1.06 ± 0.09	4.31 ± 0.22	12.3	0.030 ± 0.003	1.77 ± 0.08
23	112-19-605-004	0.178	1.22 ± 0.07	1.06 ± 0.12	4.08 ± 0.21	3.9	0.110 ± 0.010	1.53 ± 0.07

[1] Δ^w = water content (mass water/mass dry sediment). For the dose rate calculations each Δ^w value included an uncertainty of ±10% (1σ) to account for fluctuations in water content over time

[2] d = sample depth beneath the ground surface

[3] $\dot{D}_C$ = cosmic ray dose rate; $\dot{D}_T$ = total dose rate (that due to cosmic rays plus that due to β and γ radiation)

2.3.3 Radiocarbon dating

Radiocarbon ages determined by accelerator mass spectrometry (AMS) were obtained from detrital wood (n=8) and carbonate shell material (n=5). Wood specimens were physically pre-treated prior to analysis at the A.E. Lalonde AMS laboratory or Keck Carbon Cycle AMS Laboratory at the University of California by removing the outer layer of the specimen and then chemically pre-treated with an acid-alkali-acid wash. Carbonate shell specimens were physically pre-treated prior to analysis at the A.E. Lalonde AMS laboratory by removing porous or recrystallized areas with a Dremel bit and then chemically pre-treated by etching with 0.2N HCl to remove the outer 20–30% (Crann et al., 2017). Radiocarbon ages are interpreted as minimum limiting ages for the stratigraphic beds they were sampled from.

2.3.3.1 Vetting of radiocarbon ages

Given the geochronological inconsistencies in the western HBL, we first vetted all new and previous radiocarbon ages for intertill sediments across the study area (Figure 2.1; Appendix A, Supplemental

material 1), building off Dalton et al. (2019). This vetting needs to be completed prior to interpretation to remove unreliable ages. Wood is the best material to attempt radiocarbon-age determination when the material is near the upper limit of this geochronometer (e.g., Dalton et al., 2016; Bayliss and Marshall, 2019), and all vetted radiocarbon constraints for the western HBL are from wood (Figure 2.1). Like others (e.g., Young et al. 2021), we removed all ages from bulk organic samples (n=6) because this material can more easily be contaminated by inclusion of older carbon (old detrital fragments) and/or by younger carbon (modern day rootlets). For example, site 6 (Figure 2.1) was included as a potential MIS 3 site in Dalton et al. (2019) based on an untreated bulk organic age of 37 ± 1.6 ^{14}C ka BP (WAT-1378). Yet, there are another four nonfinite ages from pre-treated bulk organics collected during this initial study and a nonfinite AMS age from wood [>50.8 ^{14}C ka BP; (ISGS A1658)] at the same site (Appendix A, Supplemental material 1). Given that only one of the six ages is finite, and the source material is the least reliable of the group, this site should not be used to support MIS 3 deglaciation. We also removed the finite shell ages that are >40 ka (n=4) because shell material is susceptible to some isotopic exchange with the surrounding environment (e.g., Ramsey, 2008). This issue is not always minimized with physical and acid etching pre-treatment (method used in this study) and more advanced pre-treatment procedures are necessary to gain confidence in shell radiocarbon ages (e.g., Douka et al., 2010).

2.4 Results

2.4.1 Assessing the geochronological constraints

Ideally, multiple lines of geochronological evidence should be used to support any MIS 3 age determination without dispute, considered to span ~57–29 ka. The vetted compilation of new and existing radiocarbon ages on sub-till wood shows only 1 out of 14 sites has finite radiocarbon ages; that one site also contains wood with a nonfinite radiocarbon age, indicating that these sediments are potentially older than MIS 3 (site 5, Figure 2.1; Appendix A, Supplemental material 1). Sediments with MIS 3 TL ages at sites 2 and 3 also contained wood with conflicting nonfinite radiocarbon ages (Figure 2.1; Appendix A, Supplemental material 1). Finding nonfinite radiocarbon-age wood at two different sites decreases the likelihood of 'transported' wood (i.e., reworked older wood). As

pointed out by Roy (1998), site 1–4 TL ages are likely underestimations due to the now better-understood effect of anomalous fading on the luminescence signal of feldspars. Berger and Nielsen (1991) used long-term storage of their laboratory irradiated samples, some at an elevated temperature, in an attempt to reduce the effect of anomalous fading of the TL signal, but it has been found that this treatment is, at least for some samples, not sufficient (cf. Spooner 1992, 1993). Roy (1998) also questions these TL ages on the basis of the range of glow curve temperatures from which the TL signal used to build dose response curves is determined. Roy (1998) notes that inclusion of the 'unstable' 270 °C TL peak could have resulted in the calculated TL age being too young. This might be the case as others have found that the infrared-stimulated luminescence (IRSL) signal associated with the 270 °C TL peak is thermally unstable, but are not certain that this is also the case for the TL signal from this peak (Duller and Bøtter-Jensen, 1993). Another point of concern are the dose rates reported by Berger and Nielsen (1991) for their samples, which are up to a factor of two higher than those reported by Roy (1998) for sediments extracted from the same stratigraphic bed. Indeed, one of our samples (not part of this study) collected from the same stratigraphic bed as the apparent MIS 3 age of Berger and Nielsen (1991) has radioisotope concentrations close to those of Roy (1998). These values are much lower than those presented in Berger and Nielsen (1991). If a dose rate that is the average of those of Roy (1998) are applied to the equivalent dose values of Berger and Nielsen (1991), the ages will almost double in magnitude, and they would increase even more if corrected for anomalous fading. For these reasons, we believe that the previously reported TL ages of Berger and Nielsen (1991) are likely to be underestimations of the true depositional age and we suggest that the ages should be removed from the MIS-3 age dataset.

2.4.2 New optical ages

Three samples were collected for optical age determination (sites 15, 20, 23; Figure 2.1). For each sample, all the aliquots passed the SAR quality control tests, but for some (5 to 10 aliquots per sample) their natural signals plotted beyond the last data point of their respective dose-response curves, and these were excluded from further analysis. The D_e values from accepted aliquots were

plotted on radial plots (Galbraith, 2010) (Figure 2.3), and overdispersion (OD) values were calculated (Table 2.2). Overdispersion is the variation between individual aliquot D_e values above and beyond that associated with analytical uncertainties. It has been demonstrated that for samples consisting of quartz grains that were mostly likely fully bleached, OD values from small multigrain aliquots (less than 100 grains per aliquot) are, on average, about 20% (Galbraith et al. 1999; Lian and Roberts 2006; Jacobs and Roberts 2007), although for some of these samples OD values are higher than 30% (Arnold and Roberts 2009). The convention therefore has been to use a weighted mean D_e found using the central age model (CAM) (Galbraith et al. 1999) for the age calculation for samples for which OD is 20% or less (Jacobs and Roberts, 2007). For samples with OD higher than 20%, that are assumed to consist of grains that have been heterogeneously bleached prior to deposition, the minimum age model (MAM) is appropriate. In that case, the MAM D_e would give an approximation of true depositional age of a sample if a significant number of grains had been fully bleached, or it would give an age closer to the true age than that derived using the CAM if this is not the case. Experiments have shown that, for some samples, OD measured from D_e values derived from large aliquots (~80 grains) is less than that derived from small aliquots (<10 grains), and much less than that derived from aliquots that contain single grains (Galbraith et al., 2005; Arnold and Roberts 2009). These variations are likely due to averaging of various single grain signals in multigrain aliquots. These observations, together with the fact that the sedimentology at our sample sites indicates that heterogeneous bleaching was highly probable prior to deposition and burial, suggest that the variation in D_e values of the individual grains in our samples could be higher that that suggested by our multigrain OD values. As such, we have provided ages using both CAM and MAM (Table 2), but we suggest that the MAM ages should be used for our stratigraphic interpretations due to the nature of the depositional environments. The ages derived using the MAM are 146 ± 20 ka (1σ, site 15, sample 112-19-629-024), 166 ± 12 ka (1σ, site 20, sample 112-16-407-019) and 150 ± 22 ka (1σ, site 23, sample 112-19-605-004). Results of the dose recovery experiments (Table 2.2) suggest that the chosen SAR protocol was sufficient for producing accurate D_e and age values. In consideration of the inferred depositional environments for the units from which our optical dating samples were collected, these MAM ages should be considered as upper limits. But because all

three ages are statistically consistent (within 1σ of each other), the true age probably lies somewhere within the range indicated by their analytical uncertainties.

Table 2.2: Number of aliquots measured (N), overdispersion values (OD), equivalent dose values (D_e), optical ages, and dose recovery (DR) ratios

Site	Sample	N[1]	OD (%)	D_e (Gy) – C[2]	D_e (Gy) – M[3]	Age (ka) - C	Age (ka) - M	DR ratios[4]
15	112-19-629-024	31/36	32 ± 5	278 ± 17	201 ± 26	202 ± 15	146 ± 20	0.96 ± 0.05
20	112-16-407-019	32/37	15 ± 3	304 ± 10	294 ± 17	172 ± 8	166 ± 12	1.12 ± 0.03
23	112-19-605-004	25/34	28 ± 5	292 ± 18	229 ± 33	191 ± 15	150 ± 22	0.99 ± 0.02

[1]N = numbers of aliquots accepted/number of aliquots measured

[2]C = Determined using the central age model (CAM), ± 1σ

[3]M = Determined using the three-parameter minimum age model (MAM), ± 1σ

[4]DR = dose recovery ratio (given dose/recovered dose)

Note: equivalent dose and OD values calculated using the software of Liang and Forman, 2019

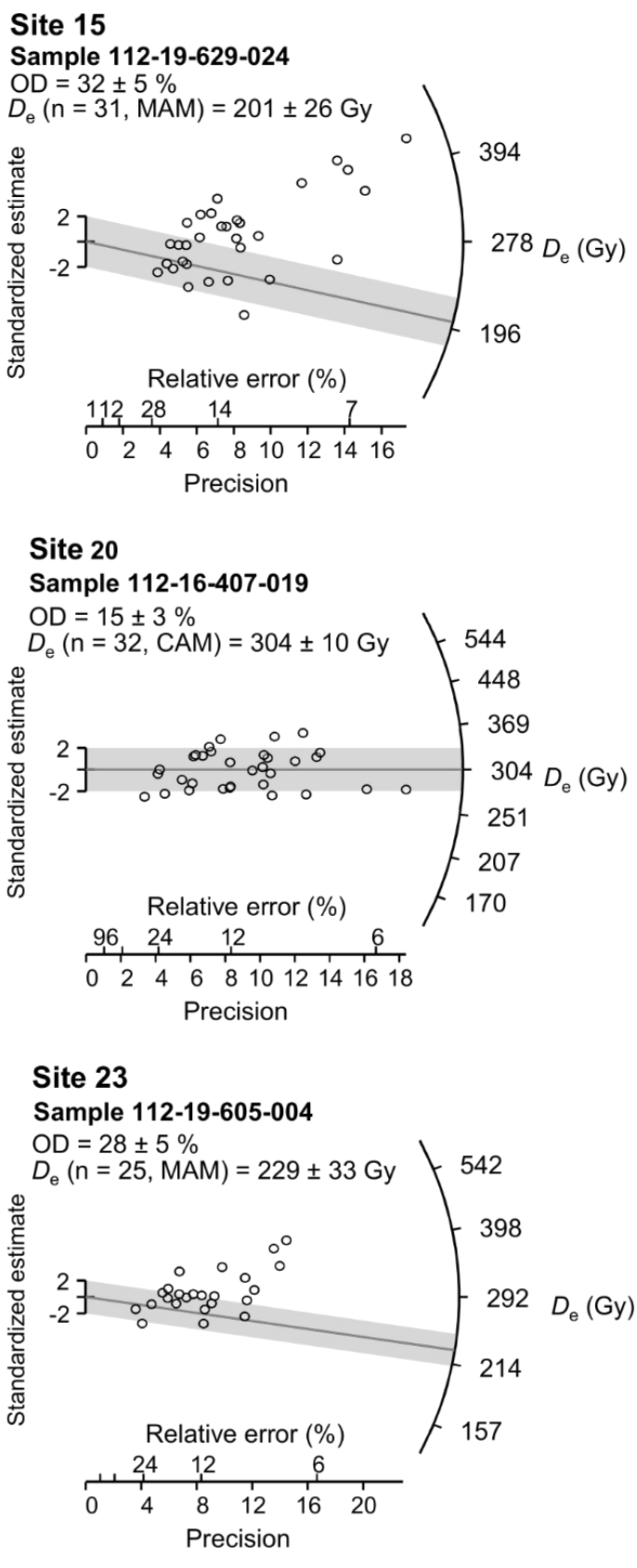

Figure 2.3: Radial plots (Galbraith 2010) showing the distribution of De values for each sample and estimations of representative De values (weighted mean) used for dating, using either the CAM or the MAM (solid line that intersects the curved axis). Values that plot in the shaded zones fall within 2σ of the weighted mean value.

2.4.3 Stratigraphy and age constraints

Three sections are highlighted herein that contain sediment suitable for optical dating and which our till-stratigraphic framework has identified as lying directly under an advance-phase till from the last glaciation. Two other sections then show the impact till stratigraphy can have on understanding the relative age of intertill nonglacial sediments.

2.4.3.1 Site 15

The exposed stratigraphy at site 15 consists of five beds (Figure 2.4). The youngest, uppermost bed (Bed A) consists of horizontally bedded sand and gravel with minor clay (Figure 2.4). Shell fragments were observed throughout the upper sediments and paired whole valves of *Hiatella arctica* occur between 4 and 5 m depth, which are indicative of deposition within a marine environment. The horizontal bedding and grain-size variations in Bed A are interpreted to represent postglacial marine transgression at this site. A 7.8 m thick layer of brown, massive, matrix-supported diamicton (Bed B, Figure 2.4) sharply underlies Bed A. The diamicton contains 10–15% clasts and has a sandy-silt matrix (27% sand, 56% silt and 13% clay). The diamicton has a crumbly appearance with minor oxidation rind developed on joint surfaces. A 0.6 m thick layer of matrix-supported, massive, sandy gravel (Bed C) sharply underlies Bed B. The gravel is poorly sorted and contains 40% clasts that are granule- to large pebble-sized. The lower 0.2 m of this gravel contains rip-up clasts of diamicton. This gravel is interpreted as a glaciofluvial or fluvial deposit based on the poorly sorted nature of the sediments. A 1.6 m thick layer of well sorted sand sharply underlies the gravel (Bed D). The sand is horizontally bedded, with bedding defined by textural differences between alternating beds of very fine sand and beds of medium- to coarse-grained sand (Bed D). Shell fragments were observed in the upper 0.1 m of the bedded sands. The sands were likely deposited in a shallow marine environment, based on the rhythmic bedding, the low elevation (41 m asl), the position beneath postglacial Tyrrell Sea sediments and the proximity to the modern shoreline (~90 km). More than 6.0 m of dark greyish-brown, massive, matrix-supported diamicton (Bed E; Figure 2.4) sharply underlies Bed D sand. The diamicton contains 15% clasts and has a clayey sandy-silt matrix (25% sand, 54% silt and 21% clay). The diamicton has a blocky appearance with oxidation rind on the joint surfaces, and is relatively denser compared to the upper diamicton (Figure 2.4). The massive structure, texture, typical glacigenic shape of the clasts (bullet-shaped, faceted and striated), the

modality and strength of the pebble fabric and lateral continuity indicate that Bed B and D diamicton are subglacial traction tills (Evans et al., 2006). The stratigraphy at site 15 is interpreted to consist of postglacial marine sediments that are underlain by two till beds separated by intertill sorted sediments. The interpretation of a marine depositional environment for Bed D requires that Hudson Bay was ice-free and that relative sea level was higher than the present day. The age of the bedded, well sorted sand (Bed D) was determined to be 146 ± 20 ka (Figure 2.3, 2.4; Table 2.2).

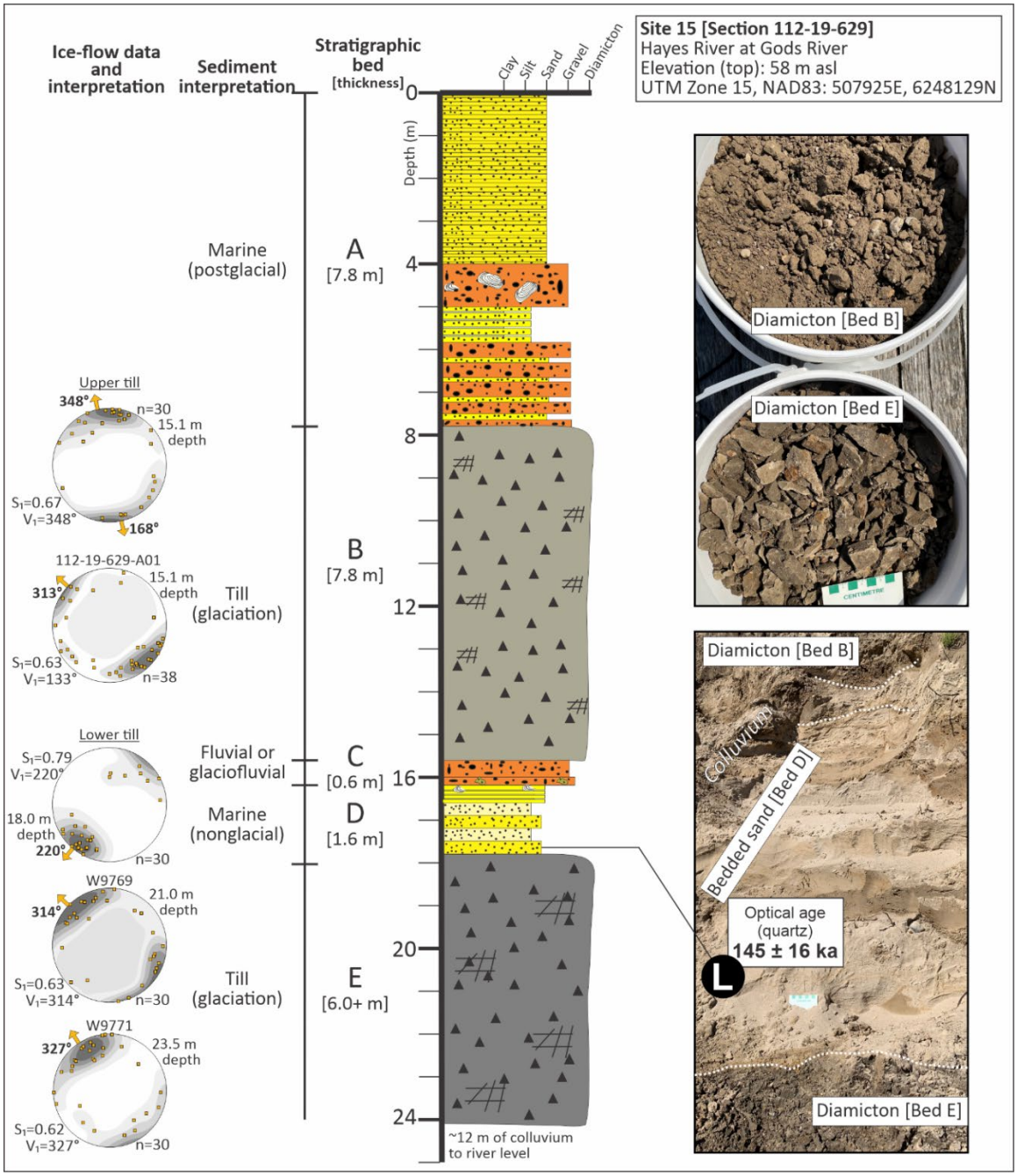

Figure 2.4: Quaternary stratigraphy and sediment photos of site 15. Till fabric data is plotted on equal area, lower hemisphere projection stereonets and the principal eigenvalue (S_1) and eigenvector (V_1) is provided. Contours were generated using the Kamb method. The sample location for optical age determination is shown by the black circle with an 'L'.

2.4.3.2 Site 20

The exposed stratigraphy at site 20 consists of four beds (Figure 2.5). The uppermost stratigraphic bed (Bed A) consists of 1.0 m of massive, moderately- to well-sorted sand that is interpreted to have been deposited in a postglacial subaqueous environment, which was likely Lake Agassiz, since this site is above the local Holocene marine limit (~145 m asl; Gauthier et al., 2020) and the region was inundated by Lake Agassiz following deglaciation. Bed A sharply overlies 9.0 m of dark yellowish brown, massive, matrix-supported diamicton (Bed B). The diamicton contains 10% clasts and has a sandy clayey-silt matrix (21% sand, 51% silt and 28% clay). Bed B is in sharp contact with 1.4 m of grey, massive, matrix-supported diamicton that contains rip-up mud clasts (Bed C). The diamicton contains 10% clasts and has a silty-clay matrix (5% sand, 35% silt and 60% clay). The massive structure, texture, glacigenic shape of the clasts (bullet-shaped, faceted and striated), the modality and strength of the pebble fabric and lateral continuity indicate that Bed B and C diamicton are subglacial traction tills (Evans et al., 2006). Considering the fine-grained texture of Bed C, and mud rip-up clasts, it is interpreted that the ice that deposited this bed likely advanced over fine-grained sediments. Tills B and C were likely deposited during the same ice-flow event, based on the similar ice-flow direction interpreted from till fabrics (Figure 2.5). Underlying these two tills is 3.8+ m of well-sorted sand (Bed D). Within the upper 1.0 m of this bed, there is convolute bedding and dewatering structures at places laterally along the contact (Figure 2.5). These structures could have formed syn-depositional in a subaqueous environment or from post-depositional dewatering. Beyond 1.0 m depth into this bed, the sand is cross-bedded to ripple cross-laminated sand. This thick sequence of cross-bedded sands indicates unidirectional bedload transport within a low flow regime. No evidence was observed for settling from a suspension cloud. The stratigraphy at site 20 is interpreted to consist of well sorted, cross-bedded sand deposited during a nonglacial period that is overlain by glacial and postglacial sediments. The optical age of the rippled sands (Bed D) was determined to be 166 ± 12 ka (Figures 2.3, 2.5; Table 2.2). This optical age had a low overdispersion (15 ± 3%) and a unimodal aliquot *De* population, which supports that the quartz grains were likely well bleached prior to burial. However, it is nevertheless possible that more than one age population exists and are masked as our aliquots consist of 50–100 grains.

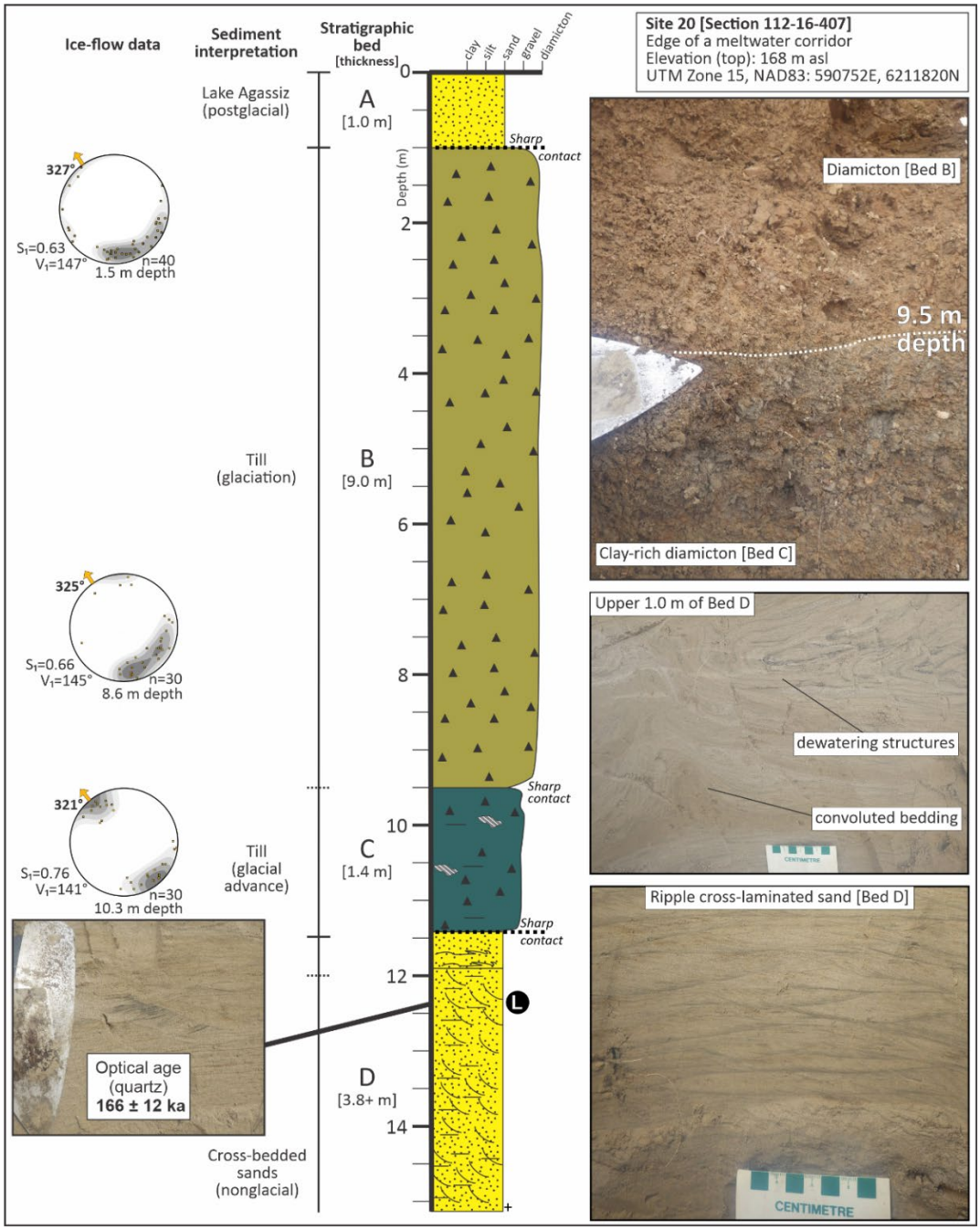

Figure 2.5: Quaternary stratigraphy and sediment photos of site 20. Till fabric data is plotted on equal area, lower hemisphere projection stereonets and the principal eigenvalue (S_1) and eigenvector (V_1) is provided. Contours were generated using the Kamb method. The sample location for optical age determination is shown by the black circle with an 'L'.

2.4.3.3 Site 23

The exposed stratigraphy at site 23 consists of four beds (Figure 2.6). The youngest, uppermost bed (Bed A) consists of 1.5 m of horizontally bedded sand and gravel. Bed A is interpreted to have been deposited in a post-glacial marine environment based on the sediment texture and regional setting, since this site is situated below the local Holocene marine limit (~145 m asl; Gauthier et al., 2020) and the top of the section is 26 m above the modern sea level elevation. Bed A sharply overlies 1.4 m of brown to dark greyish brown, massive, matrix-supported diamicton (Bed B). The diamicton contains 5% clasts and has a sandy clayey-silt matrix (24% sand, 51% silt and 25% clay). The diamicton has a minor blocky structure with oxidation rind on the joint surfaces. This diamicton, like the others described at sites 15 and 20, has all the main characteristics of a subglacial traction till. Bed B sharply overlies massive silt and massive to horizontally-bedded fine-sand to silty fine-sand that contains disseminated organic material (Bed C). The presence of organic material requires terrestrial input into the depositional environment. Thus, the sediments that were targeted for optical dating were likely transported within a fluvial environment prior to deposition, which should be favourable to sufficient light exposure prior to burial. Bed C sharply overlies 3.3+ m of poorly sorted, matrix-supported sandy gravel (Bed D). Bed D gravel contains granule- to small cobble-sized clasts and rare shell fragments and is interpreted to have been deposited in a subaqueous environment. The subtill sediments (Bed C and D) indicate an overall fining upwards sequence, possibly deposited in a fluvial environment. The stratigraphy at site 23 is interpreted to consist of nonglacial sediments that are overlain by glacial and postglacial sediments. The optical age of the organic-bearing fine sand (Bed C) was determined to be 150 ± 22 ka (Figures 2.3, 2.6; Table 2.2).

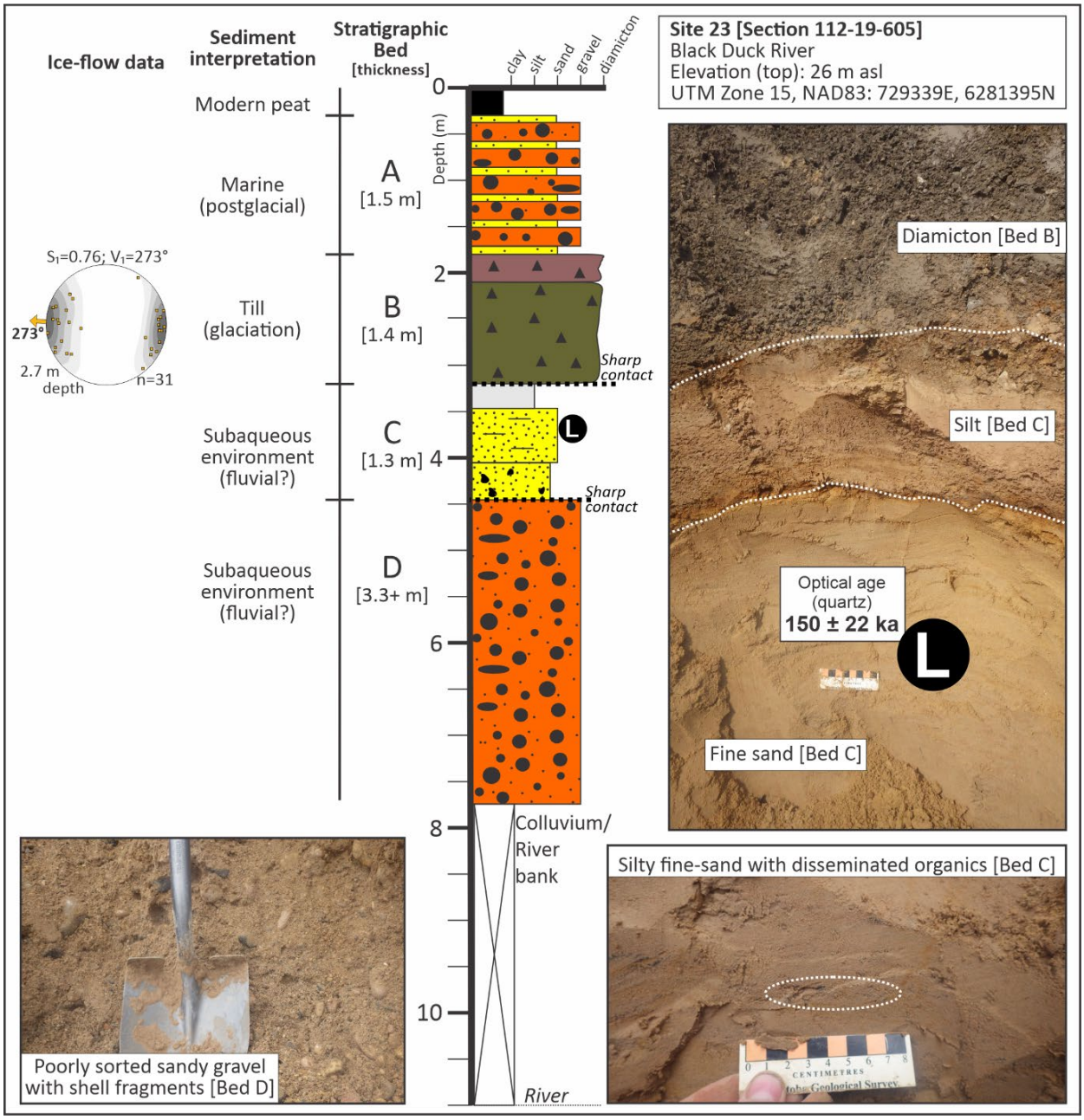

Figure 2.6: Quaternary stratigraphy and sediment photos of site 23. Till fabric data is plotted on equal area, lower hemisphere projection stereonet and the principal eigenvalue (S_1) and eigenvector (V_1) is provided. Contours were generated using the Kamb method. The sample location for optical age determination is shown by the black circle with an 'L'.

2.4.3.4 Till stratigraphy as an important tool

Sites 3 and 4 (Figure 2.7) are located ~10–12 km apart, and the stratigraphy at both sites was previously interpreted to contain one correlative intertill nonglacial bed (Dredge and Nielsen, 1985, Dredge et al., 1990; Dredge and McMartin, 2011). At site 3, the Bed C gravel is discontinuous across the exposure and pinches out to a till-till contact between Bed B and D in places. Bed C gravel contains an in-situ peat bed with large (>10 cm) wood fragments that yielded a nonfinite radiocarbon age (>55 ^{14}C ka BP, UOC-10974). Similarly, a detrital wood fragment from the gravel underlying the peat bed yielded a nonfinite radiocarbon age (>55 ^{14}C ka BP, UOC-10975). Paleobotanical data from these sediments indicate a northern boreal forest to forest-tundra environment, which is similar to the present day for that area (Dredge et al., 1990). Hence, these uppermost intertill nonglacial sediments are interpreted to have been deposited during the last interglacial period (MIS 5e; Dredge et al., 1990); leading us to reject the MIS 3 TL age at site 3 (46 ± 4 ka, Berger and Nielsen, 1991) when conditions must have been colder based on the global sea level record (Lisiecki and Raymo, 2005).

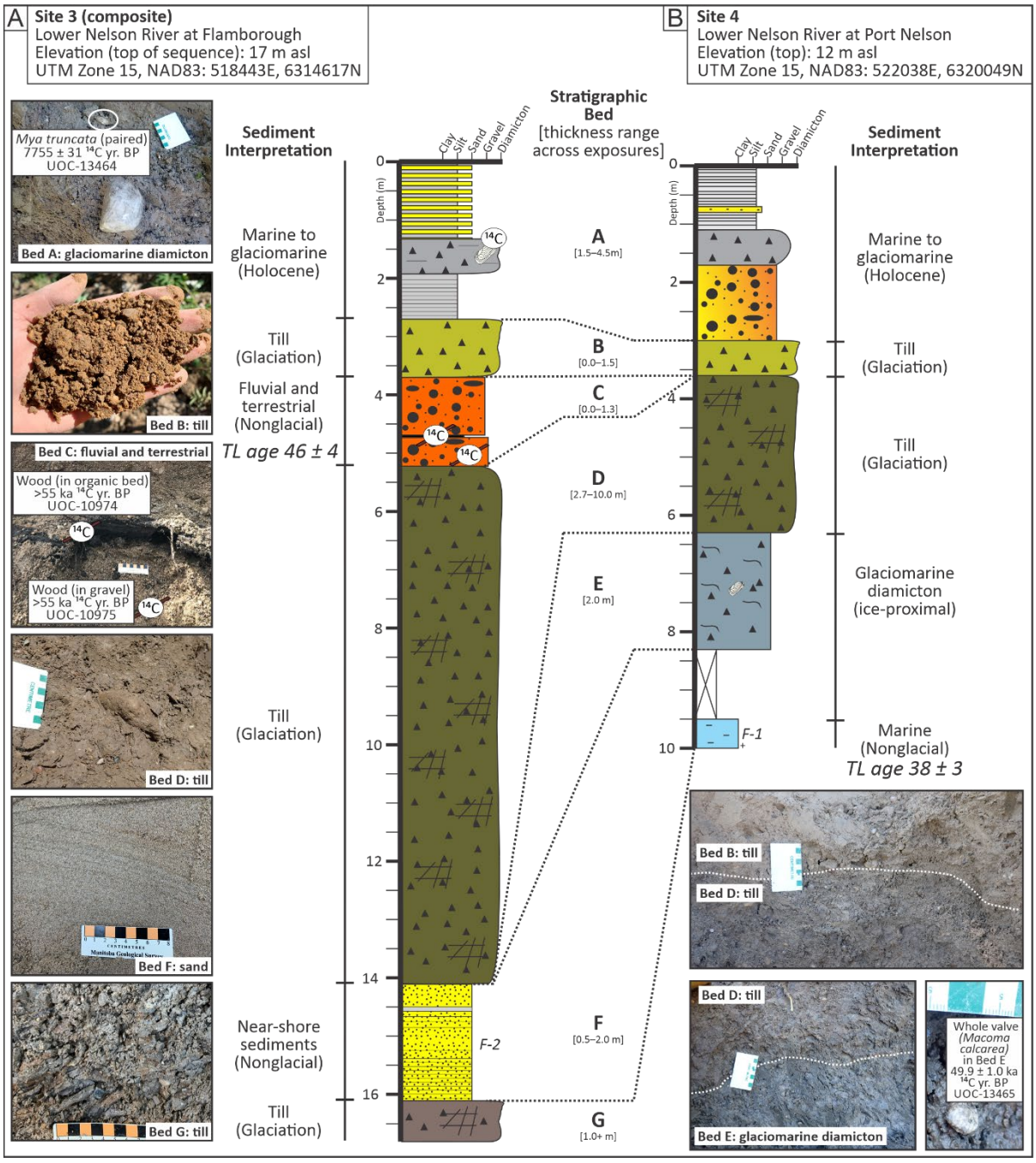

Figure 2.7: Quaternary stratigraphy at site 3 and 4 in the on the Nelson River at Hudson Bay. The stratigraphic beds identified have been interpreted based on qualitative and quantitative observations. The thermoluminescence (TL) age estimations for stratigraphic beds (Berger and Nielsen, 1991) are interpreted to be age underestimations.

Bed C is missing between beds B and D at site 4 (Figure 2.7). However, site 4 does expose nonglacial sediments below Bed D that have a TL age of 38 ± 3 ka (Berger and Nielsen, 1991; Figure 2.1). Bed E consists of a clay-rich diamicton that contains whole valves of *Macoma calcarea* (Figure 2.4), interpreted as a glaciomarine deposit. Underlying Bed E is massive, blue clay (Bed F-1), interpreted as a marine deposit. Owing to the principles of superposition and relative age, and perhaps ignoring the differences between till beds B and D, Bed C at site 3 was originally correlated to Bed F-1 at site 4 (Dredge et al., 1990; Dredge and McMartin, 2011).

At site 3, we documented a newly-discovered second, lower, intertill nonglacial bed which indicates that there are actually two intertill nonglacial beds exposed in the stratigraphic record at site 3 (Bed F-2, Figure 2.7). This lowermost intertill nonglacial bed consists of well sorted, horizontally bedded sands (Bed F-2). To support correlations between sites 3 and 4, we examined the tills in addition to the sorted sediments. The upper till (Bed B) is significantly less dense, sandier, and has a higher proportion of carbonate detritus compared to the middle till (Bed D), enabling stratigraphic correlation between these two sites (Appendix A, Supplemental material 3). These differences, together with the knowledge that Bed C was deposited between the two tills, shows that the subtill marine sediments at site 4 are correlated to the second, older nonglacial unit at site 3 (Bed F, Figure 2.7). Thus while Bed C was deposited during MIS 5e, based on nonfinite radiocarbon ages, regional stratigraphy and pollen data, the Bed F intertill sediments are even older (pre-MIS 5).

The reassessment of the stratigraphy at site 3 and 4 indicates that the previously reported MIS 3 TL age from Bed F at site 4 (38 ± 3 ka), like the other TL ages in the region, is underestimated (Figure 2.1). Furthermore, the stratigraphic evidence confirms that the near-finite radiocarbon age (49.9 ± 1.0 ka ^{14}C yr. BP, UOC-13465) from a *Macoma calcarea* whole valve in Bed E is not accurate, and supports our approach of removing near-finite shell ^{14}C ages from the dataset. The stratigraphy here also highlights the importance of studying till beds, since the first bed of nonglacial sorted sediments encountered below till may not relate to the most recent ice-free period (i.e., site 4).

2.5 Discussion

2.5.1 Optical dating

Doses of up to 400 Gy were needed to be applied in the SAR sequences to interpolate the natural quartz luminescence signals from a sufficient number of aliquots onto their dose response curves. The high doses resolved a dose response that was best fit with a saturating exponential that includes a linear component (Figure 2.2). An exponential+linear dose response has been observed for quartz in many other studies, but the reason for its existence and its efficacy for dating remains uncertain. Some workers have found that for samples expected to have ages >100 ka and that exhibit exponential+linear dose responses, standard SAR protocols perform well and yield ages consistent with independent information (e.g., Murray et al., 2008; Pawley et al., 2008, 2010), while there have been other studies that show that it produces ages that are too young when compared to independent information (see review by Lowick and Preusser, 2011). For many of these studies, however, reliable independent age information is lacking. A detailed study that examined the effectiveness of the SAR protocol for dating fine grain quartz samples with exponential+linear dose responses has found that it performs well (e.g., Lowick and Preusser, 2011); it is therefore possible that the usefulness of the exponential+linear signal in quartz for dating is sample dependent. Nonetheless, it is clear that more work needs to be undertaken to better understand the underlying physical processes; until that is done, ages found from samples with exponential+linear dose responses should be considered with some caution (e.g., Li et al. 2015).

This study targeted intertill sorted sediment beds that were identified using a regional till stratigraphic framework to have been deposited during the penultimate deglaciation of the region. At face value, two of our optical ages are within 1σ of MIS 5e, which is an expected ice-free period in the HBL considering this was a period of time with significantly reduced global ice volume (Lisiecki and Raymo, 2005). The third age (166 ± 12 ka) is not within 1σ of MIS 5e, but, based on the stratigraphy at this site these sediments could have been deposited during the deglaciation phase of MIS 6. Furthermore, terrestrial glaciation is not always synchronous with marine isotope stages (Gibbard and Hughes, 2021) and it is therefore possible that the timing of glaciation in the HBL was

slightly out of phase with the timing of climate shifts recorded in the marine record. It is likely that any overestimation of our optical ages is due to the inclusion of a sufficient amount of grains whose signals were not adequately reset prior to burial.

K-feldspar is also routinely used for optical dating, and its upper age limit is usually higher than that for quartz, but it was not used in this study because its dose response was expected to be nonlinear in the region of our samples' natural luminescence signals, and it therefore would not be possible to correct them for anomalous fading (Huntley and Lamothe, 2001). The post-IR IR (pIR-IR) signal from K-feldspar, which usually fades less (in some cases negligibly), was also not investigated as its signal resets (bleaches) relatively slowly, and it was therefore anticipated that this would be a problem for the fluvial and lakeshore sedimentary environments sampled here. Another option for dating quartz in this region would be to investigate the thermally transferred optically stimulated luminescence (TT-OSL) signal, which has been observed to maintain a dose response defined by a single saturating exponential, even at high doses (e.g., Neudorf et al. 2019), but like the pIR-IR signal from feldspar, the TT-OSL signal from quartz bleaches much more slowly than the standard quartz signal used for dating (Jacobs et al. 2011; Neudorf et al. 2019) and it would therefore be expected to be of limited use for the sedimentary environments studied here; eolian units would need to be identified. Dating aliquots that consist of single grains of quartz would be an advantage as D_e populations would be easier to identify using the MAM, or the finite mixture model (FMM) which is suited to analysis of D_e values derived from single grain aliquots, but can present serious problems when applied to multi-grain aliquots (Arnold and Roberts 2009). However, routine SAR dating of single grains from the samples studied here is not practical as the sensitivity of the quartz in the region is variable which would require that thousands of grains be analyzed. Moreover, the depositional age of the samples requires high-dose irradiations and therefore exceedingly long machine time. Nevertheless, single grain dating of a few key strata in the region, including some where reliable independent age information is available, should be considered in future research.

2.5.2 Resolving the age of the Black Duck River nonglacial sediments

The organic-bearing nonglacial sediments at site 5 (Figure 2.1) are described to be near the surface and overlain by ~1.5 m of gravel that is interpreted to have been deposited in a postglacial marine environment (Dalton et al., 2016). Three of the four radiocarbon ages on wood from the organic-bearing nonglacial sediments are near-infinite (45.7 ± 1.3 ^{14}C ka BP [ISGS-A1656], 49.6 ± 1.0 ^{14}C ka BP [UOC-0587], 50.1 ± 3.3 ^{14}C ka BP [ISGS-A1995]), which led to the interpretation that these sediments were deposited during MIS 3 (Dalton et al., 2016, 2019). Dalton et al. (2016) considered these ages reliable, based on the repeatability of the radiocarbon ages from different laboratories, and stratigraphic-age agreement. Importantly though, the paleobotanical data from the site 5 organic-bearing bed indicate a paleoenvironment dominated by boreal and peatland taxa, which is similar to vegetation currently present in the region (Dalton et al., 2022). Quantitative paleoenvironmental reconstruction of these sediments indicate the mean summer temperature varied between 9.4–14.5°C compared to the present day 11°C, and a total precipitation similar to the present day (467 mm; Dalton et al., 2022). This evidence of climatic conditions similar to the present day supports deposition during an interglacial period, such as MIS 5e, since it is difficult to reconcile a climate reconstruction similar to the present day with the LIS still covering large areas of North America in the most restrictive reconstructions for MIS 3 (e.g., Batchelor et al., 2019; Gowan et al., 2021). As such, it seems likely that the nonfinite radiocarbon age is more reliable than those near-finite from the same strata, and that deposition at site 5 occurred during MIS 5e.

This study attempted to obtain an optical age from the nonglacial sediments at the Black Duck River site 5, to test the accuracy of the near-finite radiocarbon ages from wood; however, the exact site could not be accurately located in the field based on published location information. While the stratigraphy at site 23 on the Black Duck River (Figure 2.6) in this study is different from site 5, considering that both of these sections contain near-surface interglacial deposits and are situated within ~1 km of each other, we interpret that the organic-bearing Bed C at site 23 is likely correlated to the organic-bearing nonglacial bed at site 5 studied by Dalton et al. (2016). Owing to the susceptibility of near-infinite radiocarbon ages to modern contamination (e.g., Reyes et al., 2020), the presence of one nonfinite radiocarbon age, and paleoenvironment information consistent with a

climate warmer than that expected during MIS 3, we consider our site 23 to have more reliable stratigraphy and chronological data than site 5 (Dalton et al., 2016). Thus, we suggest that the optical age at site 23 (150 ± 22 ka), within 1σ error of MIS 5e, more accurately dates the deposition of interglacial sediments situated on the Black Duck River and is in better agreement with pollen profile from this bed at site 5.

2.5.3 Hudson Bay Lowland evidence for MIS 3 deglaciation?

Vetting of previous radiocarbon ages, together with new optical and radiocarbon ages, has led to removal of sites 1–6 from the MIS 3 age dataset in the western HBL (Figure 2.1 inset). That leaves site 7, where two MIS 3 optical ages were obtained from quartz grains (42.2 ± 4 and 52.5 ± 5 ka; Dalton et al., 2016), as well as an older TL age of 73 ± 10 ka (Forman et al., 1987), from subtill sediments interpreted to be marine. A third MIS 3 optical age provided in Dalton et al. (2016) is from the Drowning River near James Bay (~540 km to the southeast of site 7). At this site, the quartz optical age of 42.9 ± 3.7 ka is incompatible at 1σ error with two nonfinite AMS radiocarbon ages on wood (>48.4 ^{14}C ka BP [ISGS 2463] and >51.7 ^{14}C ka BP [ISGS A2425]; Dalton et al., 2016). The inconsistency between the optical ages and nonfinite radiocarbon ages at this site raises questions about the accuracy of the optical ages in Dalton et al. (2016). Furthermore, Gao et al. (2020) report new chronology data from a site just 16 km away from the Dalton et al. (2016) Drowning River site, with an optical age from feldspar that is much older than MIS 3 (118 ± 13 ka); correlation of the two subtill units is unclear. The optical age provided by Gao et al. (2020) is likely a lower limit, as an age of this magnitude is expected to have a dose response that is nonlinear and such ages cannot be corrected for anomalous fading using the method of Huntley and Lamothe (2001). However, Gao et al. (2020) do not provide representative dose-response curves necessary to fully evaluate the efficacy of their fading correction procedure. As such, site 7 will require additional investigation to confirm the sediments there are indeed MIS 3. For now, it remains the only site with a MIS 3 age in western HBL – compared to the high number of sites with nonfinite radiocarbon ages or older optical ages (Figure 2.1).

Our new minimum limiting radiocarbon and optical ages for the stratigraphically-youngest intertill nonglacial sediments in the western HBL indicate that these sediments were likely deposited during MIS 5e to late MIS 6. Hence, we find there is insufficient stratigraphic and geochronological evidence for models and reconstructions (e.g., Carlson et al., 2018; Gowan et al., 2021) to consider the western HBL region ice free during MIS 3. Additional work is needed to pinpoint the southern margin of the LIS in central Canada during this time period.

As pointed out by Miller and Andrews (2019), the timing and provenance of large iceberg discharge events into the North Atlantic, which are recorded by Heinrich layers (e.g., Hemmings, 2004), can provide an important proxy for ice extent and needs to be reconciled with HBL age constraints. Heinrich events H4 (~38 ka) and H5 (~45 ka), which occurred during MIS 3, have a similar provenance signature to Heinrich event H2 (~24 ka), which has long been associated to the Hudson Strait Ice Stream, and a catchment zone extending deep into Hudson Bay and perhaps beyond (e.g., Hemming, 2004; Ross et al., 2011; Miller and Andrews, 2019). As pointed out by Roy et al. (2009), some uncertainties persist about the exact provenance of the sediment, but an ice sheet over Hudson Bay during MIS 3 feeding a long, topographically controlled Hudson Strait Ice Stream remains the most plausible model for the source of Heinrich layers H4 and H5. Configuration of a 'big' ice sheet is also in agreement with the interpretation that the Hudson Strait Ice stream was stable at the ice shelf during H4 and H5 (Rashid et al., 2019). Heinrich events thus provide additional independent support for a glaciation of Hudson Bay and the western HBL during MIS 3.

2.6 Conclusions

New age determinations from the uppermost intertill nonglacial sediments, combined with consideration of the paleobotanical datasets in the western HBL stratigraphic record, suggest that the region was last deglaciated during MIS 5e. New radiocarbon ages and vetting of the radiocarbon age dataset, together with the new optical ages and detailed stratigraphic correlations herein, have removed six sites from the HBL 'MIS 3' dataset, and leave just one potential MIS 3 site that has conflicting age assignments.

The Quaternary stratigraphy of the HBL is highly fragmented, which hampers correlations and also indicates that previous investigations of the region have provided an oversimplified stratigraphic framework. This complex stratigraphic record, including detailed lithostratigraphy of enclosing glacial units, needs to be considered alongside geochronology results to provide robust reconstructions of late Quaternary nonglacial events. This study suggests that the LIS southern margin did not retreat north or northeast of the western HBL and that Hudson Bay remained glaciated during MIS 3. Future studies to determine the maximal or minimal extent of the LIS during MIS 3 should continue reconstruction of the stratigraphic record south of the western HBL.

2.7 References

Aitken, M.J., 1985. Thermoluminescence Dating. Academic Press, New York.

Andrews, J.T., Shilts, W.W., Miller, G.H., 1983. Multiple deglaciations of the Hudson Bay Lowlands, Canada, since deposition of the Missinaibi (last interglacial?) Formation. Quaternary Research 19, 18–37.

Arnold, L.J., Roberts, R.G., 2009. Stochastic modelling of multi-grain equivalent dose (*De*) distributions: Implications for OSL dating of sediment mixtures. Quaternary Geochronology 4, 204–230.

Bayliss, A., Marshall, P., 2019: Confessions of a serial polygamist: the reality of radiocarbon reproducibility in archaeological samples; Radiocarbon, v. 61, no. 5, p. 1143-1158, 10.1017/RDC.2019.55.

Berger, G.W., 1988. Dating Quaternary events by luminescence. In: Easterbrook, D.J. (Ed.), Quaternary Sediments. Geological Society of America Special Paper 227, pp. 13–50.

Berger, G.W., Nielsen, E., 1991. Evidence from thermoluminescence dating for Middle Wisconsinan deglaciation in the Hudson Bay Lowland of Manitoba. Canadian Journal of Earth Sciences 28, 240–249.

Brennan, B., 2003. Beta doses to spherical grains. Radiation Measurements 37, 299–303.

Carlson, A.E., Tarasov, L., Pico, T., 2018. Rapid Laurentide ice-sheet advance towards southern last glacial maximum limit during marine isotope stage 3. Quaternary Science Reviews 196, 118–123.

Crann, C.A., Murseli, S., St-Jean, G., Zhao, X., Clark, I.D., Kieser, W.E., 2017. First status report on radiocarbon sample preparation techniques at the A.E. Lalonde AMS laboratory (Ottawa, Canada). Radiocarbon 59(3), 695–704, doi:10.1017/RDC.2016.55

Dalton, A.S., Finkelstein, S.A., Barnett, P.J., Forman, S.L,. 2016. Constraining the Late Pleistocene history of the Laurentide Ice Sheet by dating the Missinaibi Formation, Hudson Bay Lowlands, Canada. Quaternary Science Reviews 146, 288–299.

Dalton, A. S., Finkelstein, S. A., Barnett, P. J., Väliranta, M., Forman, S.L. 2018. Late Pleistocene chronology, palaeoecology and stratigraphy at a suite of sites along the Albany River, Hudson Bay Lowlands, Canada. Palaeogeography, Palaeoclimatology, Palaeoecology 492, 50–63.

Dalton, A.S., Finkelstein, S.A., Forman, S.L., Barnett, P.J., Pico, T., Mitrovica, J.X., 2019. Was the Laurentide Ice Sheet significantly reduced during Marine Isotope Stage 3?. Geology 47, 111–114.

Dalton, A.S., Finkelstein, S.F., Hodder, T.J., Gauthier, M.S., 2022. Palynological analyses of subtill sediments from four sites in the western Hudson Bay Lowland region (parts of NTS 53O; 54A, C, D). Open File OF2022-1. Manitoba Geological Survey, Winnipeg.

Dalton, A.S., Stokes, C.R., Batchelor, C.L., 2021. Evolution of the Laurentide and Innuitian ice sheets prior to the Last Glacial Maximum (115 to 25 ka). Earth Science Reviews, 103875, https://doi.org/10.1016/j.earscirev.2021.103875.

Dalton, A.S. et al. 2020. An updated radiocarbon-based ice margin chronology for the last deglaciation of the North American Ice Sheet Complex. Quaternary Science Reviews 234, 106223, https://doi.org/10.1016/j.quascirev.2020.106223.

Douka, K., Hedges, R.E.M., Higham, T.F.G., 2010. Improved AMS ^{14}C dating of shell carbonates using high-precision x-ray diffraction and a novel density separation protocols (CarDS). Radiocarbon 52(2-3), 735–751.

Dredge, L.A., McMartin, I., 2011. Glacial stratigraphy of northern and central Manitoba. Bullet 600. Geological Survey of Canada, Ottawa.

Dredge, L.A., Morgan, A.V., Nielsen, E., 1990. Sangamon and pre-Sangamon interglaciations in the Hudson Bay Lowlands of Manitoba. Geographie physique et Quaternaire 44, 319–336.

Dredge, L.A., Nielsen, E., 1985. Glacial and interglacial deposits in the Hudson Bay lowlands: a summary of sites in Manitoba. Current Research Paper 85-1A. Geological Survey of Canada, Ottawa.

Dredge, L.A., Thorleifson, L.H., 1987. The Middle Wisconsinan history of the Laurentide Ice Sheet. Geographie physique et Quaternaire 41, 215–235.

Dube-Loubert, H., Roy, M., Allard, G., Veillette, J.J., 2013. Glacial and nonglacial events in the eastern James Bay lowlands, Canada. Canadian Journal of Earth Science 50, 379–396.

Duller, G.A.T., Bøtter-Jensen, L.1993. Luminescence from potassium feldspars stimulated by infrared and green light. Radiation Protection Dosimetry 47, 683–688.

Edwards, G.H., Blackburn, T., Piccione, G., Tulaczyk, S., Miller, G.H., Sikes, C. 2022. Terrestrial evidence for ocean forcing of Heinrich events and subglacial hydrologic connectivity of the Laurentide Ice Sheet. Science Advances 8, 42, eabp9329, doi:10.1126/sciadv.abp9329.

Evans, D.J.A., Phillip, E.R., Hiemstra, J.F., Auton, C.A., 2006. Subglacial till: Formation, sedimentary characteristics and classification. Earth Science Reviews 78, 115-176.

Gao, C., Huot, S., McDonald, A.M., Crabtree, D.C., Turton, C.L., 2020. Subtill nonglacial deposits and their climatic implications for the Last Interglacial (MIS 5e), Hudson Bay Lowlands, Canada. Quaternary Science Reviews 248, 106590.

Galbraith, R.F., 2010. On plotting OSL equivalent doses. Ancient TL 28, 1–9.

Galbraith, R.F.. Roberts, R.G., 2012. Statistical aspects of equivalent dose and error calculation and display in OSL dating: An overview and some recommendations. Quaternary Geochronology 11, 1–27.

Galbraith, R.F., Roberts, R.G., Laslett, G.M., Yoshida, H., Olley, J.M., 1999. Optical dating of single and multiple grains of quartz from Jinmium rock shelter, northern Australia: Part I, Experimental design and statistical models. Archaeometry 41, 339–364.

Gauthier, M.S., Hodder, T.J., Ross, M., Kelley, S.E., Rochester, A., McCausland, P., 2019. The subglacial mosaic of the Laurentide Ice Sheet; a study of the interior region of southwestern Hudson Bay. Quaternary Science Reviews 214, 1–27.

Gauthier, M.S., Hodder, T.J., Lian, O.B., Finkelstein, S.A., Dalton, A.S., Paulen, R.C. 2021. Stratigraphic, paleoenvironmental and geochronological investigations of intertill nonglacial deposits in northeastern Manitoba (parts of NTS 54B–F, K, L, 64A, H, I). *Report of Activities 2021*, 71–76, Manitoba Geological Survey, Winnipeg.

Gauthier, M.S., Kelley, S.E. and Hodder, T.J., 2020. Lake Agassiz drainage bracketed Holocene Hudson Bay Ice Saddle collapse. Earth and Planetary Science Letters 544, 116372.

Gauthier, M.S., Hodder, T.J., Ross, M. 2022. Quaternary stratigraphy and ice-flow indicator data for the Gillam region, Manitoba (parts of NTS 54C, D; 64A). *Geological Paper 2022-2*, Manitoba Geological Survey, Winnipeg.

Gibbard, P.L., Hughes, P.D., 2021. Terrestrial stratigraphical division in the Quaternary and its correlation. Journal of the Geological Society 178, jgs2020-134.

Gowan, E.J., Zhang, X., Khosravi, S., Rovere, A., Stocchi, P., Hughes, A.L.C., Gyllencreutz, R., Mangerud, J., Svendsen, J.-I., Lohmann, G. 2021. A new global ice sheet reconstruction for the past 80 000 years. Nature Communications 12:1199.

Guérin, G.N. Mercier, G. Adamiec. 2011. Dose-rate conversion factors: update. Ancient, TL 29, 5– 8.

Hodder, T.J., Gauthier, M.S. 2019. Quaternary stratigraphy and till sampling in the Machichi–Kettle rivers area, far northeastern Manitoba (parts of NTS 54A–C). *Report of Activities 2019*, 83–89, Manitoba Geological Survey, Winnipeg.

Hodder, T.J., Gauthier, M.S. 2021. Quaternary stratigraphy in the Churchill to Little Churchill rivers area of northeastern Manitoba (part of NTS 54E). *Report of Activities 2021*, 84–87, Manitoba Geological Survey, Winnipeg.

Hicock, S.R., Goff, J.R., Lian, O.B., Little, E.C. 1996. On the interpretation of subglacial till fabric. Journal of Sedimentary Research 66, 928–934.

Holmes, C.D. 1941. Till fabric. Bulletin of the Geological Society of America 52, 1299–1354.

Hemming, S.R., 2004. Heinrich events: massive late Pleistocene detritus layers of the North Atlantic and their global climate imprint. Review of Geophysics 42, RG1005, Paper number 2003RG000128.

Huntley, D.J., Lamothe, M., 2001. Ubiquity of anomalous fading in K-feldspars and the measurement and correction for it in optical dating. Canadian Journal of Earth Sciences 38, 1093-1106.

Jacobs, Z., Roberts, R.G., 2007. Advances in optically stimulated luminescence dating of individual grains of quartz from archeological deposits. Evolutionary Anthropology 16, 210–223.

Knight, J., 2010. Basin-scale patterns of subglacial sediment mobility: Implications for glaciological inversion modelling; Sedimentary Geology 232, 145–160.

Li, B, Roberts, R.G., Jacobs, Z., Li, S.-H., 2015. Potential of establishing a 'global standardised growth curve' (gSGC) for optical dating of quartz from sediments. Quaternary Geochronology 27, 91–104.

Lian, O.B., Hu, J., Huntley, D.J., Hicock, S.R., 1995. Optical dating studies of Quaternary organic-rich sediments from southwestern British Columbia and northwestern Washington State. Canadian Journal of Earth Sciences 32, 1194–1207.

Lian, O.B., Roberts, R.G., 2006. Dating the Quaternary: progress in luminescence dating of sediments. Quaternary Science Reviews 25, 2449–2468.

Liang, P., Forman, S. 2019. LDAC: an Excel-based program for luminescence equivalent dose and burial age calculations. Ancient TL 37, 21–40.

Lisiecki, L.E., Raymo, M.E., 2005. A Pliocene-Pleistocene stack of 57 globally distributed benthic d18O records. Paleoceanography 20, PA1003.

Lowick, S.E., Preusser, F. 2011. Investigating age underestimation in the high dose region of optically stimulated luminescence using fine grain quartz. Quaternary Geochronology 6, 33–41.

Miller, G.H., Andrews, J.T., 2019. Hudson Bay was not deglaciated during MIS-3. Quaternary Science Reviews 225, 105944.

Murray, A.S., Buylaert, J.-P., Henriksen, M., Svendsen, J.-I., Mangerud, J., 2008. Testing the reliability of quartz OSL ages beyond the Eemian. Radiation Measurements 43, 776–780.

Murray, A.S., Wintle, A.G., 2000. Luminescence dating of quartz using an improved single-aliquot regenerative-dose protocol. Radiation Measurements 32, 57–73.

Murray, A.S., Wintle, A.G., 2003. The single aliquot regenerative dose protocol: potential for improvements in reliability. Radiation Measurements 37, 377–381.

Neudorf, C.M., Lian, O.B., McIntosh, P.D., Gingerich, T.B., Augustinus, P.C., 2019. Investigation into the OSL and TT-OSL signal characteristics of ancient (>100 ka) Tasmanian aeolian quartz and its utility as a geochronometer for understanding long-term climate-driven landscape change. Quaternary Geochronology 53, 101005.

Nielsen, E., Morgan, A.V., Morgan, A., Mott, R.J., Rutter, N.W., Causse, C., 1986. Stratigraphy, paleoecology and glacial history of the Gillam area, Manitoba. Canadian Journal of Earth Sciences 23, 1641–1661.

Olley, J.M., Pietsch, T., Roberts, R.G., 2004. Optical dating of Holocene sediments from a variety of geomorphic settings using single grains of quartz. Geomorphology 60, 337–358.

Parker, R.L., Foster, G.L., Gutjahr, M., Wilson, P.A., Littler, K.L., Cooper, M.J., Michalik, A., Milton, J.A., Crocket, K.C., Bailey, I. 2022. Laurentide Ice Sheet extent over the last 130 thousand years traced by the Pb isotope signature of weathering inputs to the Labrador Sea, Quaternary Science Reviews 287, 107564.

Pawley, S.M, Toms, P., Armitage, S.J., Rose, J. 2010. Quartz luminescence dating of Anglian Stage (MIS 12) fluvial sediments: Comparison of SAR age estimates to the terrace chronology of the Middle Thames valley, UK. Quaternary Geochronology 5, 569–582.

Pawley, S.M., Bailey, R.M., Rose, J., Moorlock, B.S.P., Hamblin, R.J.O., Booth, S.J., Lee, J.R., 2008. Age limits on Middle Pleistocene glacial sediments from OSL dating, north Norfolk, UK. Quaternary Science Reviews 27, 1363–1377.

Pico, T., Birch, L., Weisenberg, J., Mitrovica, J. X. 2018. Refining the Laurentide Ice Sheet at Marine Isotope Stage 3: A data-based approach combining glacial isostatic simulations with a dynamic ice model. Quaternary Science Reviews 195, 171–179.

Prescott, J.R., Hutton, J.T., 1994. Cosmic ray contributions to dose rates for luminescence and ESR dating: large depths and long-term time variations. Radiation Measurements 23, 497–500.

Ramsey, C.B. 2008. Radiocarbon dating: revolutions in understanding. Archaeometry 50(2), 249–275.

Rashid, H., Piper, D.J.W., Drapeau, J., Marin, C., Smith, M.E. 2019. Sedimentology and history of sediment sources to the NW Labrador Sea during the past glacial cycle; Quaternary Science Reviews 221, 105880.

Reyes, A.V., Dillman, T., Kennedy, K., Froese, D., Beaudoin, A.B., Paulen, R.C. 2020. Legacy radiocarbon ages and the MIS 3 dating game: a cautionary tale from re-dating of pre-LGM sites in western Canada. Geological Society of America Abstracts with Programs, v. 52, no. 6, 10.1130/abs/2020AM-360064.

Ross, M., Lajeunesse, P. and Kosar, K. 2011. The subglacial record of northern Hudson Bay: insights into the Hudson Strait Ice Stream catchment. Boreas 40, 73–91.

Roy, M. 1998. Pleistocene stratigraphy of the lower Nelson River area- implications for the evolution of the Hudson Bay lowland of Manitoba, Canada. M.Sc. thesis, University of Quebec, Montreal, 220 pp.

Roy, M., Hemmings, S., Parent, M. 2009. Sediment sources of northern Quebec and Labrador glacial deposits and the northeastern sector of the Laurentide Ice Sheet during ice-rafting events of the last glacial cycle. Quaternary Science Reviews 28, 3236–3245.

Shilts, W.W. 1982. Quaternary evolution of the Hudson/James Bay region. Le Naturaliste Canadien 109, 309–332.

Spooner, N.A. 1993. The validity of optical dating based on feldspar. Ph.D. thesis, University of Oxford, 207 p.

Spooner, N.A. 1992. Optical dating: Preliminary results on the anomalous fading of luminescence from feldspars. Quaternary Science Reviews 11, 139–145.

Stokes, C. R., Tarasov, L., Dyke, A. S. 2012. Dynamics of the North American Ice Sheet Complex during its inception and build-up to the Last Glacial Maximum. Quaternary Science Reviews 50, 86–104.

Trommelen, M.S., Ross, M., Campbell, J.E. 2013. Inherited clast dispersal patterns: implications for paleoglaciology of the southeast Keewatin Sector of the Laurentide Ice Sheet. Boreas 42, 693–713.

Tylmann, K., Piotrowski, J.A., Wysota, W. 2012. The ice/bed interface mosaic: deforming spots intervening with stable areas under the fringe of the Scandinavian Ice Sheet at Samplawa, Poland. Boreas 42, 428–441.

Wintle, A.G. 1997. Luminescence dating: laboratory procedures and protocols. Radiation Measurements 27, 769–817.

Wintle, A.G., Murray, A.S., 2006. A review of quartz optically stimulated luminescence characteristics and their relevance in single-aliquot regeneration dating protocol. Radiation Measurements 41, 369–391.

Young, J.M., Reyes, A.V. and Froese, D.G. 2021. Assessing the ages of the Moorhead and Emerson phases of glacial Lake Agassiz and their temporal connection to the Younger Dryas cold reversal. Quaternary Science Reviews 251, 106714.

Chapter 3

Unravelling the fragmented sediment-landform assemblage in an area of thick Quaternary sediment, western Hudson Bay Lowland, Canada

3.1 Overview

Laurentide Ice Sheet (LIS) reconstructions beyond the last glacial maximum (LGM) are difficult due to the incomplete stratigraphic record that has largely been overprinted by the most recent glaciation. The Hudson Bay Lowland (HBL) is a key region to understanding the long-term evolution of the LIS, as it contains an extensive pre-LGM stratigraphic record of glacial and nonglacial events across three or more glacial-interglacial cycles. This study uses a hybrid lithostratigraphy-allostratigraphy approach to decipher the palimpsest stratigraphic record in the Kaskattama highland region of the western HBL, Manitoba, Canada. We identify five glacial (till) units and three nonglacial (sorted sediment) units that were deposited during at least three glacial-interglacial cycles, which are constrained by radiocarbon and optical age datasets. The provenance of till units is identified using clast-lithology, detrital hornblende $^{40}Ar/^{39}Ar$ ages and supported by matrix geochemistry. The new stratigraphic framework for this western Hudson Bay Lowland region indicates that the ice emanating from the Quebec-Labrador Dome advanced into the region at the start of the last two glaciations, suggesting accelerated early growth of the Quebec–Labrador Dome relative to the Keewatin Dome.

3.2 Introduction

Regions of thick Quaternary sediment cover, such as the western Hudson Bay Lowland (HBL), provide an important sedimentary record of ice-sheet changes over time. The Quaternary stratigraphic record can enable an understanding of ice-sheet growth and decay over multiple glacial-interglacial cycles, beyond what can be gleaned from the surficial landscape, and provide important insights into past interglacial climates (Nielsen et al., 1986; Dredge et al., 1990; Gao et al., 2012; Hodder et al., 2016; Norris et al., 2018; Möller et al., 2019; Evans et al., 2021). At the surface, interior regions of paleo-ice sheets consist of fragmented patches of differently-oriented streamlined landforms and outcrop-scale ice-flow indicators, with palimpsest sediment dispersal patterns (Dyke et al., 1982; Prest, 1990; McMartin and Henderson, 2004; Veillette, 2004; Gauthier et al., 2019; Rice et al., 2019; McMartin et al., 2021). Such complex landscape records present many challenges yet provide an opportunity to better understand the long-term behavior of ice sheets (Dalton et al., 2022a). To advance reconstructions of pre-LGM ice sheet dynamics, beyond what can be understood from the landscape record, the palimpsest stratigraphic record in the relatively rare regions that contain these records needs to be deciphered.

The Laurentide Ice Sheet (LIS) overran the western HBL during the last glaciation, with ice emanating from both the Keewatin and Quebec-Labrador (Q-L) domes (Shilts, 1980; Prest, 1990), and either a separate 'Hudson dome' (Dyke et al., 1982) or late deglacial Hudson Bay Ice Saddle (Dyke and Dredge, 1989). How these competing ice centres interacted is mainly understood from the last glacial maximum (LGM) through to deglaciation (Dalton et al., 2023), but less so for glacial events prior to that (Kleman et al., 2010; Batchelor et al., 2019). The Quaternary stratigraphy of the HBL is the net result of erosion and deposition that spans at least three glacial-interglacial cycles (Nielsen et al., 1986; Thorleifson et al., 1992; Dredge and McMartin, 2011). Regional reconstructions of the relative ice-flow history have identified evidence for ice flowing towards the northwest and/or west (Quebec-Labrador dome) during both pre-LGM growth and a previous glacial cycle (Gauthier et al., 2019). Understanding the extent, relative timing, and number of northwest-oriented ice-flow phases in the western HBL is important because they must have occurred at times when the Keewatin dome was smaller or situated further to the west compared to its deglaciation position.

The geomorphic record of the western HBL is composed of a complex and fragmented landscape (Gauthier et al., 2019). This is exemplified in the study area, where two streamlined-landform flowsets are aligned at near perpendicular angles and situated within 5 km of each other (Figures 3.1, 3.2), but do not crosscut (Gauthier et al., 2019). The larger flowset represents SSW-trending ice-flow and is interpreted to have been formed during deglacial ice streaming by the Hayes Lobe (Figures 3.1, 3.2; Dredge and Cowan, 1989; Margold et al., 2018; Gauthier et al., 2019). Here, we focus on the isolated Kaskattama flowset that occurs on a relatively flat-topped hill, informally referred to as the "Kaskattama highland", but the timing and direction of the NW-SE oriented Kaskattama flowset is unknown (Figures 3.1, 3.2; Gauthier et al., 2019). The 'highland' contains thick Quaternary-aged sediments (Hodder, 2018; Hodder and Gauthier 2021), and forms a raised (~130 m above the surrounding lowland; Figure 3.1) and isolated landscape whose surface geomorphology does not fit with the surrounding deglacial ice-flow events. Unravelling this poorly understood part of the Quaternary stratigraphic record in the western HBL will help advance regional ice-sheet reconstructions and understanding. In order to do this, new stratigraphic strategies that take into account the fragmented nature of the sediment-landform assemblages (as described in Gauthier et al., 2019) were developed.

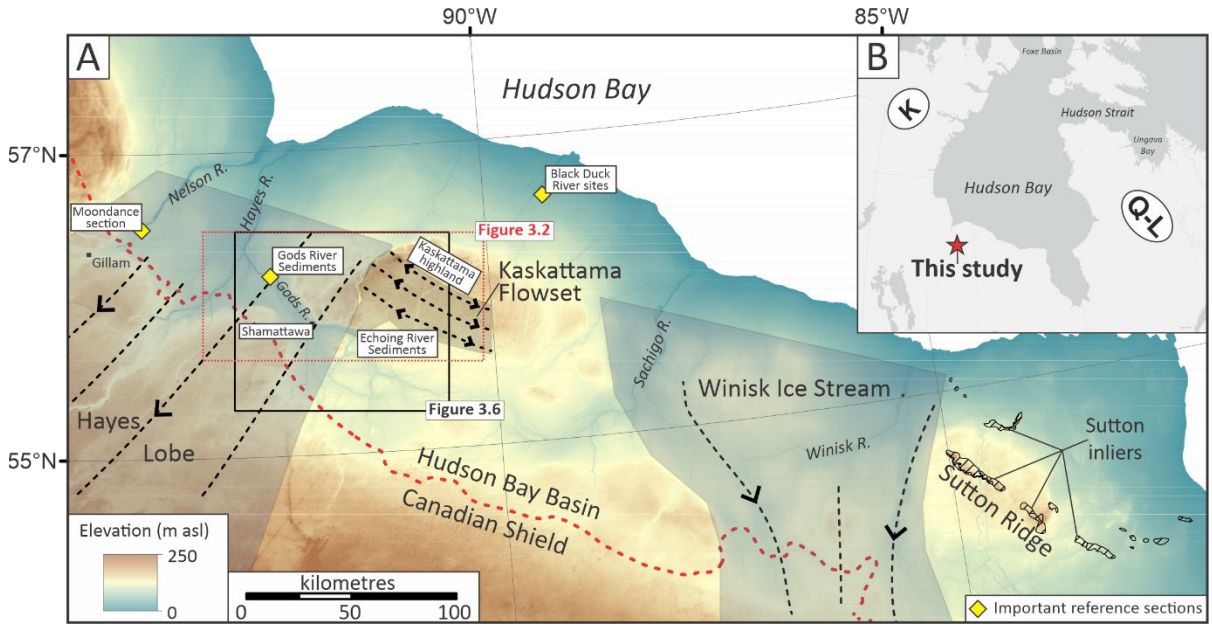

Figure 3.1: Location of the study area in western Hudson Bay Lowland, Canada. The Kaskattama streamlined-landform flowset (Flowset F of Gauthier et al., 2019) and the larger imprints of the deglacial Hayes Lobe (Flowest K of Gauthier et al., 2019) and Winisk Ice Stream (modified from Margold et al., 2018) are overlain on the topography. The inset map (b) shows the interpreted location of the Keewatin (K) and Quebec-Labrador (Q-L) domes of the Laurentide Ice Sheet during MIS 2 deglaciation (Dalton et al., 2023). Background hillshade image was generated using Canadian Digital Surface Model (Natural Resources Canada, 2012).

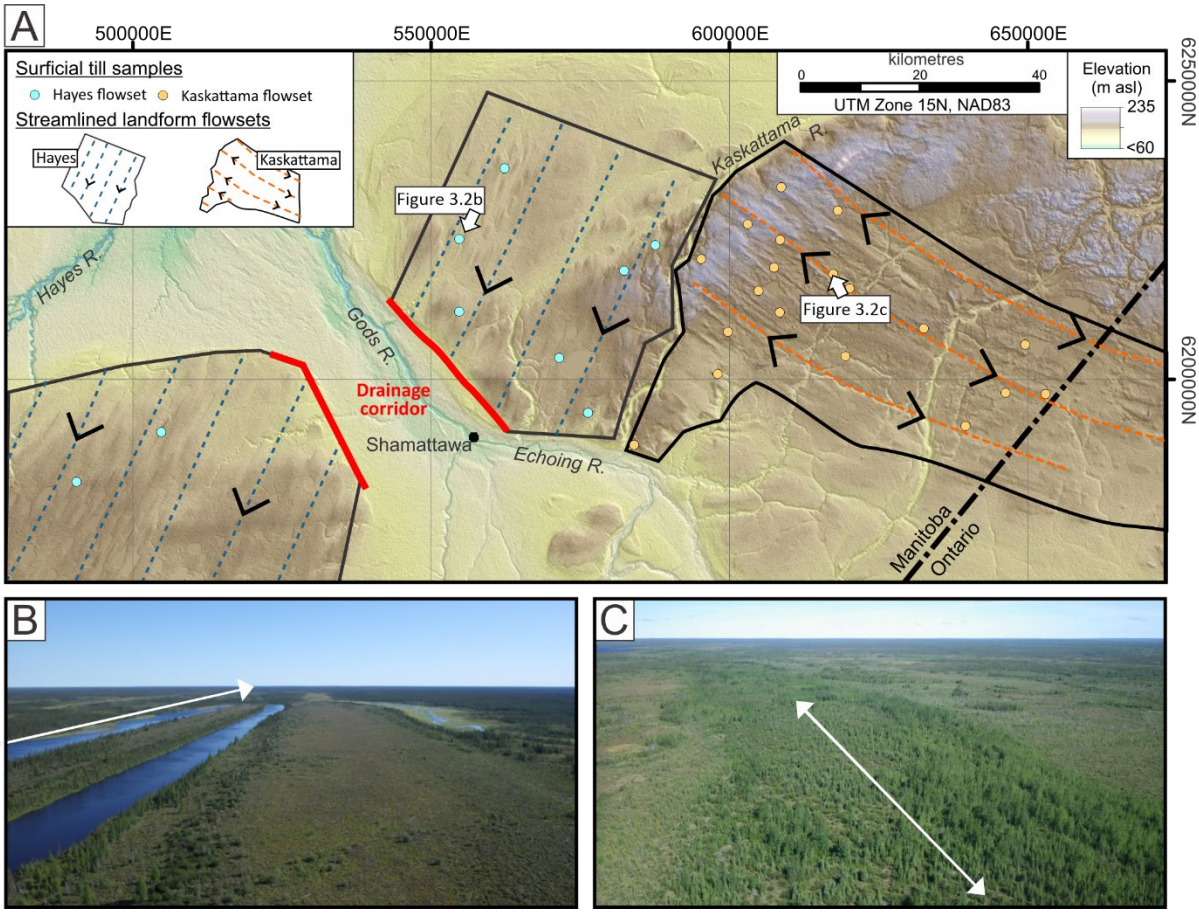

Figure 3.2: Streamlined landform flowsets and examples of streamlined landforms in the study area: a) footprint of the Hayes and Kaskattama flowsets (modified from Gauthier et al., 2019) and location of surficial till samples collected from each flowset; b) oblique aerial view of streamlined landforms in the Hayes flowset; and c) oblique aerial view of a streamlined landform in the Kaskattama flowset. The location and orientation of the photos in panels b and c is shown in panel a. Background hillshade image was generated using Canadian Digital Surface Model (Natural Resources Canada, 2012).

3.3 Regional setting

Quaternary sediment cover is extensive in the study area and the only known bedrock outcrops are carbonates within the bed of the Gods River, near the First Nation community of Shamattawa (Figure 3.1). The Gods River has incised through 15 to 30 m of Quaternary sediments at this location, but less is known about the thickness of Quaternary sediments elsewhere in the study area and throughout most of the western HBL region (Hodder and Gauthier, 2021). Near Shamattawa, a prominent drainage corridor formed during the Holocene when this area was an eastern outlet for Lake Agassiz (Dredge, 1983). Here, the bottom of this drainage corridor is at an elevation of ~80–84 m asl and the Hayes Flowset on either side of the corridor is at an elevation of ~125–144 m asl, indicating that ~45 to 60 m of the stratigraphic record was eroded (Figure 3.2). The limit of postglacial marine transgression around the highland is ~145 m asl (Gauthier et al., 2020), and the geomorphic record below this limit is partially or completely covered by marine sediments.

3.3.1 Bedrock geology

The study area is primarily underlain by carbonate Paleozoic rocks (limestone and dolomite) of the Hudson Bay Basin (HBB; Manitoba Geological Survey, 2022), which unconformably overlie the Precambrian Canadian Shield surround the HBB (Figure 3.3a). Rocks of the Precambrian Canadian Shield are composed primarily of granite and gneiss with scattered greenstone belts.

In northern Manitoba, distinctive erratics indicative of continental-scale dispersal includes both northwestern- and eastern-sourced lithologies. Distinctive erratics from the Dubawnt Supergroup have been transported towards the southeast over 800 km (Figure 3.3a; Rainbird, 2003). Examples include transported clasts of the Pitz Formation (Figure 3.3b; purple to mauve-coloured volcanic rocks with distinctive chalky sanidine phenocrysts) and Christopher Island Formation (red volcanic rocks with phlogopite phenocrysts). Eastern erratics that have been transported towards the west, a minimum of 650 km, include the Belcher Group (Figure 3.3a) greywacke with hemispherical calcareous concretions (Figure 3.3c) that are sourced from the Omarolluk Formation (“Omars”; Prest, 1990; Prest et al., 2000; Jackson, 2013) and oolitic jasper derived from the Kipalu Formation

(Figure 3.3d). Oolitic jasper can also be sourced the Sutton Inlier situated 400 km to the southeast, where metabasalt also outcrops (Figure 3.3a; Stott et al., 2010).

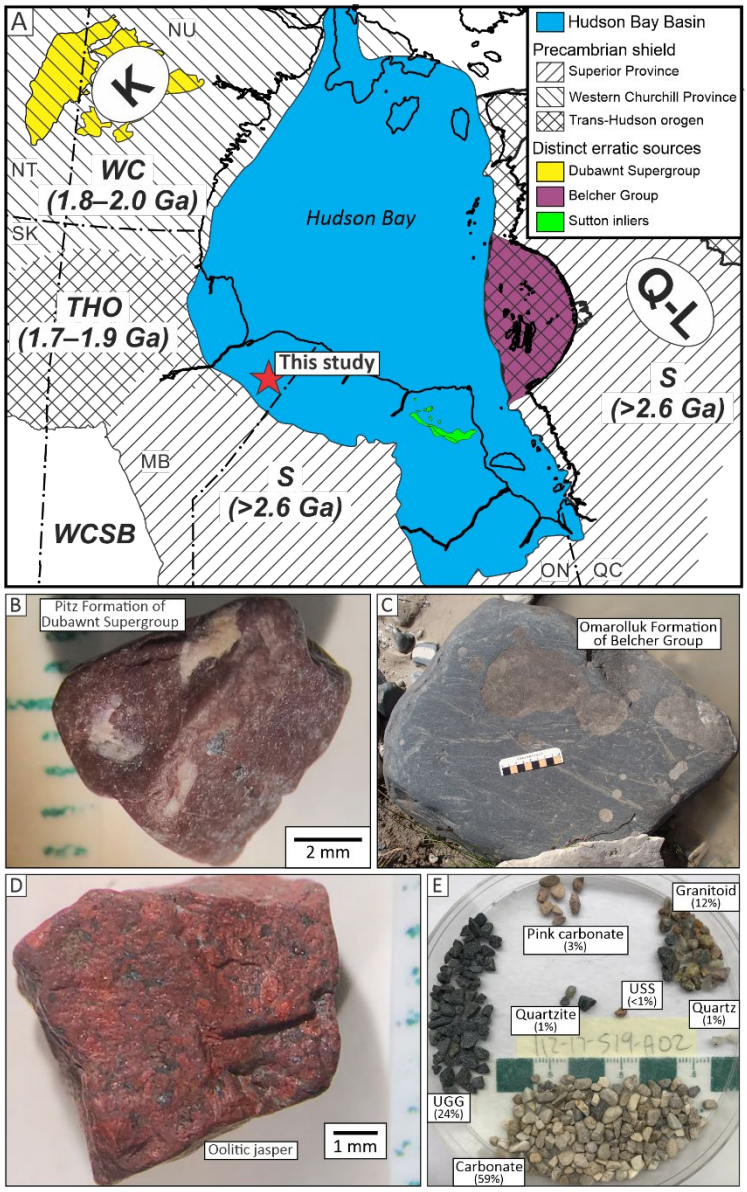

Figure 3.3: Regional bedrock geology of central Canada and examples of clasts observed in the study area: a) bedrock geology modified from Wheeler et al. (1996) and tectonic age of geological provinces, which is derived from Roy et al. (2007a). The location of the Keewatin (K) and Quebec-Labrador (Q-L) domes of the Laurentide Ice Sheet is their position during deglaciation from Dalton et al. (2020); b) pebble-sized example of the Pitz Formation of the Dubawnt Supergroup recovered from Unit 7 till at Section 17-540; c) boulder-size example of the Omarolluk Formation observed along the creek shoreline at the base of Section 17-536; d) pebble-sized example of oolitic jasper from a surficial till sample within the Kaskattama flowset (Unit 6); and e) example of clast lithologies in the 2–4 mm size fraction from Unit 6 at Section 19-519. Abbreviations: WC, Western Churchill; THO, Trans-Hudson Orogen; S, Superior; HBB, Hudson Bay Basin; WCSB, Western Canada Sedimentary Basin; UGG, undifferentiated greywacke and greenstone; USS, undifferentiated sandstone and siltstone.

3.3.2 Surficial ice-flow record

Streamlined landforms from two separate ice-flow events overlie parts of the study area – grouped and named as the Hayes and Kaskattama flowsets (Figure 3.2; flowsets F and K, respectively, of Gauthier et al., 2019). The SSW-trending Hayes flowset (204–207° in the study area) is a large (400 by 300 km) flowset that extends beyond the study area to the southwest and is interpreted to have been formed by the Hayes Lobe ice stream (Dredge and Cowan, 1989; Margold et al., 2018; Gauthier et al., 2019, 2022). The Kaskattama flowset is smaller (85 x 60 km) and is oriented NW-SE, extending across the Kaskattama highland at a mean elevation of 165 metres above sea level (asl). It is characterized by curvilinear glacially streamlined landforms (Figure 3.2) with orientations varying from about 110-290° on the east side of the Kaskattama highland to 125-305° at the northwest edge the Kaskattama highland. Streamlined-landform elongation ratios are between 4.5:1 and 10:1. The Kaskattama flowset is an isochronous event flowset (Greenwood and Clark 2009; Gauthier et al., 2019). This is because the flowset has high parallel conformity but is isolated from the surrounding geomorphology. It is transversely crosscut by meltwater corridors parallel to the Hayes Lobe (Figure 3.2), which indicates that the event occurred prior to the formation of the Hayes flowset (Gauthier et al., 2019). The boundary between the two streamlined-landform flowsets is one of the meltwater corridors, and individual landforms do not meet or crosscut. The terrain on the north edge of the Kaskattama highland is hummocky and lacks streamlined landforms at the 30-m resolution of available elevation models (Shuttle Radar Topography Mission; United States Geological Survey, 2014).

3.3.3 Intertill nonglacial sediments

There is an exceptional, yet fragmented, depositional record of intertill nonglacial deposits in the western HBL (McDonald, 1969; Netterville, 1974; Shilts, 1984; Nielsen et al., 1986; Dredge et al., 1990; Dalton et al., 2016), deposited during at least two pre-Holocene interglaciations (Dredge and McMartin, 2011). Two previously-studied organic-bearing interglacial beds are located in the study area, along tributaries of the Echoing River (McDonald, 1969; Dredge and Nielsen, 1985; Dredge et al., 1990) and along Gods River (Netterville, 1974; Klassen, 1986; Mesich et al., 2023). These

sediments, named after their rivers, both contain wood that have nonfinite radiocarbon ages and paleoenvironment records indicating climate conditions similar to the present day (Dredge et al., 1990). The age of these subtill interglacial beds is unknown but based on stratigraphic relationships they are presumed to be ~Marine Isotope Stage 5 (MIS 5; Dredge et al., 1990, Dredge and McMartin 2011). Furthermore, preliminary stratigraphic investigations along the Gods River indicate at least two separate subtill interglacial beds are preserved in the stratigraphic record exposed (Mesich et al., 2023).

3.4 Methods

3.4.1 Field data

To investigate the stratigraphic record of the Kaskattama highland and surrounding area, helicopter-supported fieldwork was undertaken in 2016, 2017 and 2019. Surficial sediments were characterized from hand-excavated pits and/or using a Dutch auger (Figure 3.4a, b), while sub-surface sediments were described from natural sections exposed along rivers and meltwater corridors. Sections were first cleared to remove colluvium, then the in-situ sediments were described over a 1–2 m wide interval based on their texture, colour, relative consolidation, clast content, sedimentary structure and nature of lower contact. Thick colluvium inhibited a thorough assessment of the lateral continuity of most identified sedimentary packages. Samples of surficial diamicton interpreted to be subglacial till were collected from the C-horizon. At sections, till samples were collected above and below all facies changes in the field (colour, texture or change in compaction) and from every 1–4 m even when visible stratigraphic changes could not be observed. Stratigraphic observations are summarized on stratigraphic columns using standard lithofacies codes (Evans and Benn, 2021). Detailed sediment descriptions, coordinates and photos for all sections cited in the text (e.g., Section 16-416) are provided in Hodder et al. (2024) and key sections not presented within the manuscript are provided in Appendix B, Supplemental material 1.

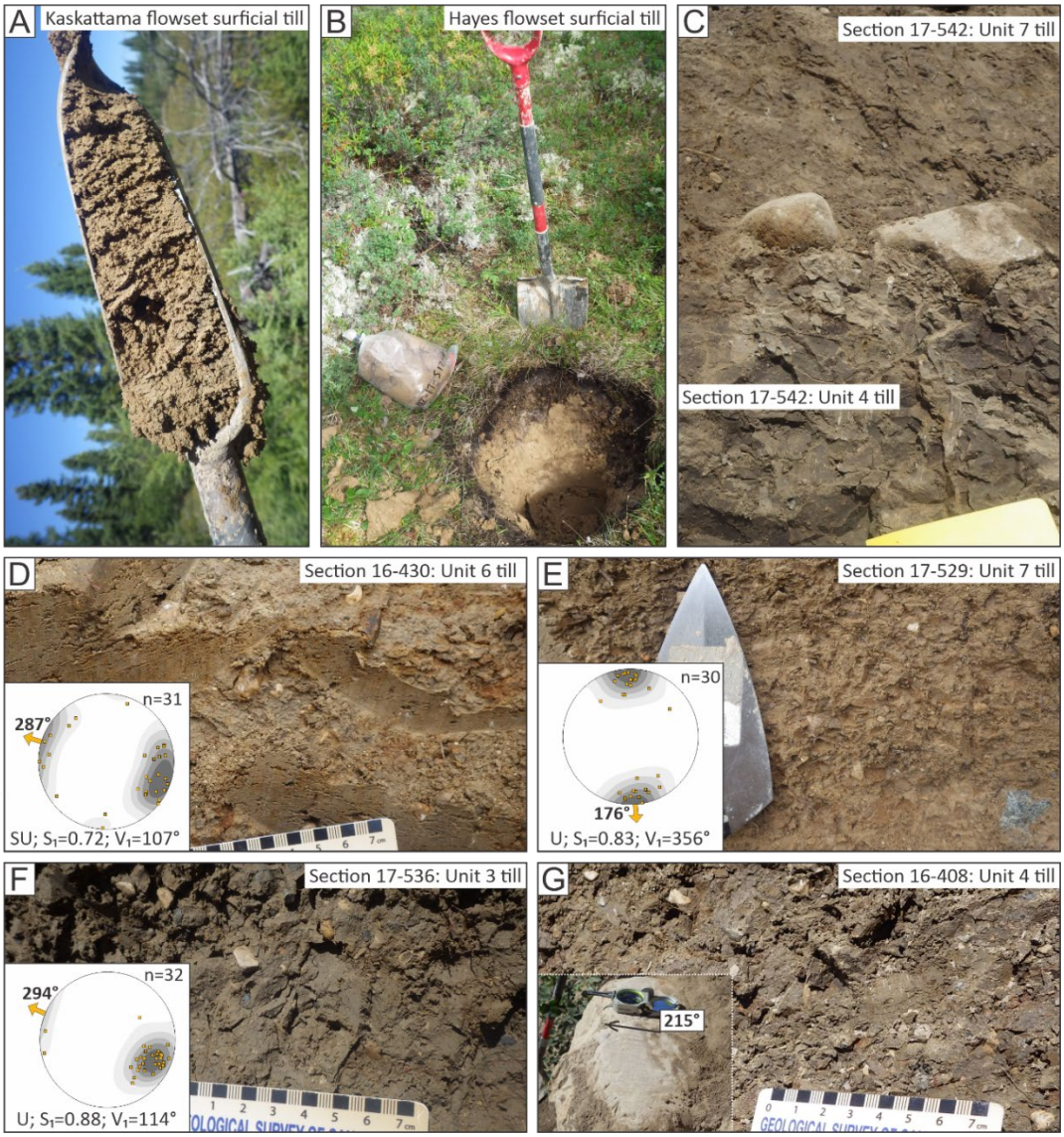

Figure 3.4: Example of surficial sampling methods and tills observed in the study area: a) yellowish brown surficial till sampled with a dutch auger from a streamlined landform in the Kaskattama flowset; b) light yellow brown surficial till sampled with a hand-dug pit from a streamlined landform in the Hayes flowset; c) boulder pavement separating Unit 7 from Unit 4 till at Section 17-542; d) yellowish brown diamicton with NW-trending till fabric (Unit 6); e) yellowish brown diamicton with south-trending till fabric (Unit 7); f) dense, dark greyish brown diamicton with NW-trending till fabric (Unit 3); g) dense, dark greyish brown diamicton with a southwest-trending ice-flow indicator (Unit 4) as demonstrated by the lodged boulder with parallel striations on the upper surface shown within the inset photo. Abbreviations: SU, spread unimodal; U, unimodal; S_1, principal eigenvalue; V_1, principal eigenvector.

To characterize the ice-flow direction during till formation, indicators of ice flow were measured from sections investigated. Till beds observed in the study area are generally massive and no glaciotectonic features were observed to supplement or contradict ice-flow interpretations. Ice-flow data includes clast fabrics (e.g., Figure 3.4d–f), as well as the orientations of the youngest parallel striations on the upper surfaces of in situ, lodged, cobble- to boulder-sized clasts, which are considered a good indicator of paleo-ice flow direction (Figure 3.4g; McMartin and Paulen, 2009; Stokes et al., 2008). Clast fabrics provide information on the direction of shear during till deposition (e.g., Hicock et al., 1996; Lian and Hicock 2000) and determining this direction was the sole purpose of measuring clast fabrics. Clast-fabrics measurements were conducted on three vertical faces of a 'box' carved into the section. At each fabric site, the trend and plunge of stone a-axes were measured from at least 30 clasts where the a:b axis ratio was >1.5, the a-axis dip was <70° and the b-axis dip was <60°. At one site only 20 clasts were measured due to a field time constraint. A non-magnetic knitting needle was used to extrapolate the plunge of the a-axis out of the till face, allowing for increased accuracy of measurements. We did not measure clasts if they were in contact with other clasts or smaller clasts that were adjacent to larger clasts, which could restrict their rotation and alignment as passive markers of strain (Andrews and Smith, 1969; Evans et al., 2016, 2018). The modality of each fabric was assessed visually (Hicock et al., 1996) and eigenvectors and eigenvalues were calculated (Mark, 1973; Benn, 1994) using Rockware StereoStat v1.6.1. This was a necessary step to identify spread-bimodal or multi-modal fabrics where no ice-flow direction could be confidently interpreted. All ice-flow-orientation interpretations based on clast-fabrics were initially considered bi-directional, since the up-ice plunge is not consistent (Andrews and Smith, 1969; Saarnisto and Peltoniemi, 1984; Larsen and Piotrowski, 2003; Gauthier et al., 2019). In these cases, other factors such as regional ice-flow history and/or provenance of clasts within the till may provide an indication of ice-flow direction (e.g., Catto, 1998). Existing studies in the western HBL do not document north-, northeast- or east-trending ice-flow (Gauthier et al., 2019), so all similarly-oriented clast fabrics are interpreted to have formed during south, southwest or west-trending ice flow, respectively. The final interpretation is further supported by till provenance analysis.

3.4.2 Till provenance

In northern Manitoba both northwest- and southeast-trending ice-flow is documented in the stratigraphic and erosional ice-flow records (Gauthier et al., 2019). This makes the interpretation of ice-flow indicator data, such as clast fabrics from till and the NW-SE oriented Kaskattama flowset, complicated. Till-provenance analysis is used in this study to complement the ice-flow orientation data for each identified stratigraphic bed. Provenance analysis is a group of techniques that are used together to investigate the composition of sediment to infer their bedrock source(s). It is thus used to solve an 'inverse problem', whereby the composition of sediment allows one to determine the nature of the bedrock source area (e.g., Lipp et al. 2021). A common approach for poorly-sorted sediment like tills is to investigate the lithology of the coarse fractions, typically referred to as 'clast lithology counts' (e.g., Shilts, 1980). This is often complemented with an analysis of sand-sized indicator minerals and matrix geochemistry (e.g., McClenaghan et al., 2022). To discriminate amongst possible bedrock sources, dating the formation or metamorphic age of mineral grains (e.g., zircon or hornblende) is another approach that has been applied on both glacial erratics (e.g., Doornbos et al. 2009) and smaller detrital grains in tills (e.g. Roy et al. 2007a; Kassab et al. 2017) or ice-rafted debris layers (Hemming 2004; Roy et al., 2007b). In this study, till clast-lithology counts and detrital hornblende $^{40}Ar/^{39}Ar$ ages are used together to constrain the bedrock sources of till detritus. Matrix geochemistry is used to further support these interpretations.

3.4.2.1 Clast lithology counts

The clast lithology types identified within the 2–8 mm size-fraction of till were first sorted into 16 detailed classes and then grouped into three simplified classes reflective of the regional bedrock geology: Hudson Bay Basin, granitoid and undifferentiated greenstone and greywacke (UGG; Hodder et al., 2024). Interestingly, there is a background concentration of ~10% granitoid clasts within till sampled across the Hudson Bay Basin, as noted by Shilts (1980). Hence, they are not an effective indicator to delineate dispersal patterns at low concentrations. To resolve the NW-SE direction problem, we focus on the UGG class (e.g., Figure 3.3e). The source of these indiscriminate fine-grained, dark grey rock fragments is presumed to be the Belcher Group to the east, or Sutton inliers

to the southeast (Figure 3.3a; Shilts, 1980; Thorleifson et al., 1993). Thus, tills with elevated UGG concentration are interpreted to have been derived from the east and deposited by ice flowing from the Q-L sector of LIS. Similarly, oolitic jasper clasts are found in trace concentrations in till in the study area (e.g., Figure 3.3d) and have a presumed eastern to southeastern provenance (Figure 3.3a, Belcher Group and Sutton inlier). Dubawnt Supergroup erratics, sourced to the northwest of the study area, are found in trace concentrations in till within the study area (Figure 3.3b). An average of 377 clasts were counted for each till sample, ranging from 224–540 clasts per sample. Two surficial till samples have anomalous proportions of Precambrian clasts (62.7 and 79.4 ct. %; Appendix B; Supplemental material 3) and were removed from the dataset prior to analysis. The potential significance of these results is discussed in Hodder et al. (2024).

3.4.2.2 Detrital hornblende $^{40}Ar/^{39}Ar$ age determination

The $^{40}Ar/^{39}Ar$ age of hornblende grains records time elapsed since they were last subject to temperatures exceeding the closure temperature of the mineral, which for hornblende grains is approximately 510°C (Schaen et al., 2021). The Canadian Shield is Precambrian in age and categorized into geological provinces based on the tectonic history of these regions (e.g., Hoffman, 1989). Three geological provinces are important to this study in terms of the detrital hornblende $^{40}Ar/^{39}Ar$ ages: Superior, Western Churchill and Trans Hudson Orogen provinces (S, WC, THO; Figure 3.3a), which have approximate hornblende $^{40}Ar/^{39}Ar$ ages of >2.6, 1.8–2.0 and 1.7–1.9 Ga, respectively (Roy et al., 2007a). Given the location of the study area relative to these bedrock provinces, hornblende grains with a $^{40}Ar/^{39}Ar$ age that is >2.6 Ga (Superior Province) would indicate an eastern to southeastern provenance, since there is no evidence of east- or northeast-trending ice-flow in the stratigraphic record of the western HBL (Gauthier et al., 2019). Four samples were chosen from select stratigraphic units as well as a fifth sample from a till with a well-constrained northwestern provenance near the town of Gillam (Moondance section on Figure 3.1). This reference ‘Sundance Till’ has NW-SE trending till fabrics with SE-trending striations on bedrock at base of the unit and contains elevated granitoid-clast concentrations, indicating a northwestern provenance for the sediment (Nielsen et al., 1986; Roy, 1998; Hodder et al. 2017). Detrital

hornblende grains were handpicked from till mineral separates for $^{40}Ar/^{39}Ar$ age determination. A total of 14–16 grains were analyzed for each sample at the Ar-Ar lab at the Manitoba Isotope Research Facility. The complete $^{40}Ar/^{39}Ar$ age dataset from this study is provided in Appendix B, Supplemental material 2.

3.4.2.3 Matrix geochemistry

The <63 µm size-fraction of till samples were separated by sieving, and then digested in a four acid ($HF:HNO_3:HClO_4:HCl$) mixture. Following this near-total digestion, samples were analyzed by ICP-MS for 58 elements at Activation Laboratories Ltd. Exploratory data analysis of the near-total digestion dataset indicated significant variation between the 2016 and 2017 dataset (Appendix B, Supplemental material 3) that could not be explained by geological field variability; during the 2017 survey we increased the density of sampling but did not expand beyond the spatial bounds of the 2016 survey. The variability between analysis years is likely due to differences in the strength of the 4-acid digestion used. To perform statistical analysis of the dataset for both years together, the 2017 dataset was levelled to 2016 data. A linear regression-based leveling approach was used (as described in Grunsky 2010), correcting the 2017 data with respect to the 2016 data following an assumption about incomplete digestion. Leveling was performed using a linear regression equation derived from the comparison of every 5th percentile (e.g. 5th, 10th, 15th up to the 95th). The limited number (n=8) of till samples collected during the 2019 field season were analyzed using a stronger lithium metaborate fusion digestion and were excluded from analysis.

Compositional data, like till-matrix-geochemistry datasets, pose challenges due to its high dimensionality, hindering relationship identification and data interpretation (Grunsky 2010). To investigate if the till-matrix geochemistry supports till-provenance interpretations, and if it could be used to elucidate differences between tills deposited by similar ice-flow orientations, principal component analysis (PCA) was applied to the dataset. PCA addresses the high dimensionality problem by transforming the original variables into a set of orthogonal dimensions (principal components). These components are ordered by their importance in explaining variance in the data. Focusing on the first few principal components enables concise data summarization without losing

too much information (Jolliffe and Cadima, 2016). PCA facilitates the detection of relationships and correlations not readily apparent in the initial dataset, which may reveal patterns of geological significance. Recently, PCA has seen increased use in analyzing sediment geochemical datasets for process discovery and exploration of specific elements or minerals associated with ore deposits (Chen et al. 2019; Bronac de Vazelhes et al. 2021), or for regional bedrock provenance analysis (McMartin et al. 2016; Lipp et al. 2021, Rice et al. 2024), which is how PCA is applied in this study. The levelled dataset was first investigated using exploratory data analysis (probability plots, histograms) and investigated for outliers (Appendix B; Supplemental material 3). The dataset was then transformed using a centred log ratio transformation to avoid the effects of data closure (Grunsky, 2010), i.e., variables that sum to a constant 100 percent. PCA was applied to this transformed dataset using ioGAS^{TM} software. To maintain acceptable degrees of freedom within the dataset of 109 samples, PCA was restricted to major elements (Ca, Mg, Na, Al, Fe, K, Mn), Rb, Zr and the sum of light rare earth elements (LREE = La, Ce, Pr, Nd, Sm, Eu). There are thus about 11 times more samples than selected variables, which should help properly condition the covariance matrix.

3.4.3 Pollen analysis

Fossil pollen grains have routinely been used to reconstruct paleoclimate during past non-glacial intervals in the western HBL (Netterville, 1974; Nielsen et al., 1986; Dredge et al., 1990; Roy, 1998). Such information can be valuable for understanding local and regional vegetation during past interstadial/interglacials and the environments (climate) inferred from them. For this study, pollen analysis was conducted on a previously undocumented organic-bearing unit. Three samples were taken from the subtill organic-bearing sediments exposed at Section 16-416 at 20- to 30-cm intervals, consistent with the sampling intervals at the Echoing River tributary section (Dredge et al., 1990). From each sample, a 1-cm^3 subsample was used for pollen analysis. Pollen was concentrated using standard palynological techniques involving acid digestions (Faegri and Iversen, 1975), supplemented with the use of sodium polytungstate as a dense floatation medium to remove mineral sediments that remained after standard pollen preparation (Zabenskie, 2006; Campbell et al., 2016). Ceramic palynospheres were added to the preparation to estimate pollen concentration

(Kitaba and Nakagawa, 2017). Pollen samples were processed at the Paleoecology Laboratory at the University of Toronto.

In each sample, a minimum of 150 herb, arboreal and shrub pollen grains were counted using a compound microscope at 400x magnification and identified using the pollen key for the Great Lakes region (McAndrews et al., 1973). Stratigraphic plots were made in R package 'rioja' (Juggins, 2015; Juggins et al., 2015). Quantitative paleoclimate reconstructions were undertaken using the modern analogue technique (Overpeck et al., 1985) while using a previously published modern-day dataset for North America (4882 sites, see: Whitmore et al., 2005; Dalton et al., 2017). Statistical tests on the modern-day pollen database show strong significant relationships with total annual precipitation and mean summer temperature (June, July, August); therefore these were the variables targeted for paleoclimate reconstruction. Raw pollen counts and additional details about the modern analogue technique are available in Dalton et al. (2022b). To provide additional context on local soil development, we estimated organic matter content for each pollen interval using loss-on-ignition by combusting sediment at 550°C for 4 hours and measuring the mass lost (Heiri et al., 2001).

3.4.4 Geochronology

The optical age of the stratigraphically-youngest intertill sorted sediments has previously been determined for two sites in the study area (Hodder et al., 2023). This study used the same methodology to investigate a stratigraphically older nonglacial unit in the record and the sample properties are provided in Table 3.1. Sorted sand from this unit were sampled for optical age determination by inserting an opaque plastic tube (~20 cm long and 5 cm diameter) into the sediment face, extracting the tube, and then sealing each end to preserve water content. Samples were prepared using standard laboratory methods and 180–250 μm diameter quartz grains were isolated for dating. Equivalent dose (D_e) values were determined using multi-grain aliquots (50-100 grains per aliquot) and the single-aliquot regenerative dose (SAR) method (Murray and Wintle 2000, 2003). Representative D_e values used for dating were calculated using the central age model (CAM) and minimum age model (MAM) (Figure 3.5b; Galbraith et al. 1999). Additional details regarding the optical dating methodology can be found in Hodder et al. (2023).

Table 3.1: Optical dating sample water content, radioisotope concentrations, depths and calculated dose rates.

Site	Sample ID	d^a (m)	Δw [b]	K (%)	U (mg·g^{-1})	Th (mg·g^{-1})	$\dot{D}_C$ (Gy/ka)[c]	$\dot{D}_T$ (Gy/ka)[c]	Source
19-629	112-19-629-024	17.7	0.063	1.16 ± 0.06	0.577 ± 0.120	2.62 ± 0.14	0.023 ± 0.002	1.37 ± 0.06	Hodder et al. (2023)
16-407	112-16-407-019	12.3	0.101	1.44 ± 0.08	1.06 ± 0.09	4.31 ± 0.22	0.030 ± 0.003	1.77 ± 0.08	Hodder et al. (2023)
19-630	112-19-630-OSL025	6.7	0.034	0.89 ± 0.05	0.41 ± 0.05	1.90 ± 0.1	0.073 ± 0.007	1.13 ± 0.05	This study

[a] d = sample depth beneath the ground surface.
[b] Δw = water content (mass water/mass dry sediment). For the dose-rate calculations, each Δw value included an uncertainty of ±10% (1σ) to account for fluctuations in water content over time.
[c] $\dot{D}C$ = cosmic ray dose rate; $\dot{D}$ T = total dose rate (that due to cosmic rays plus that due to β and γ radiation).

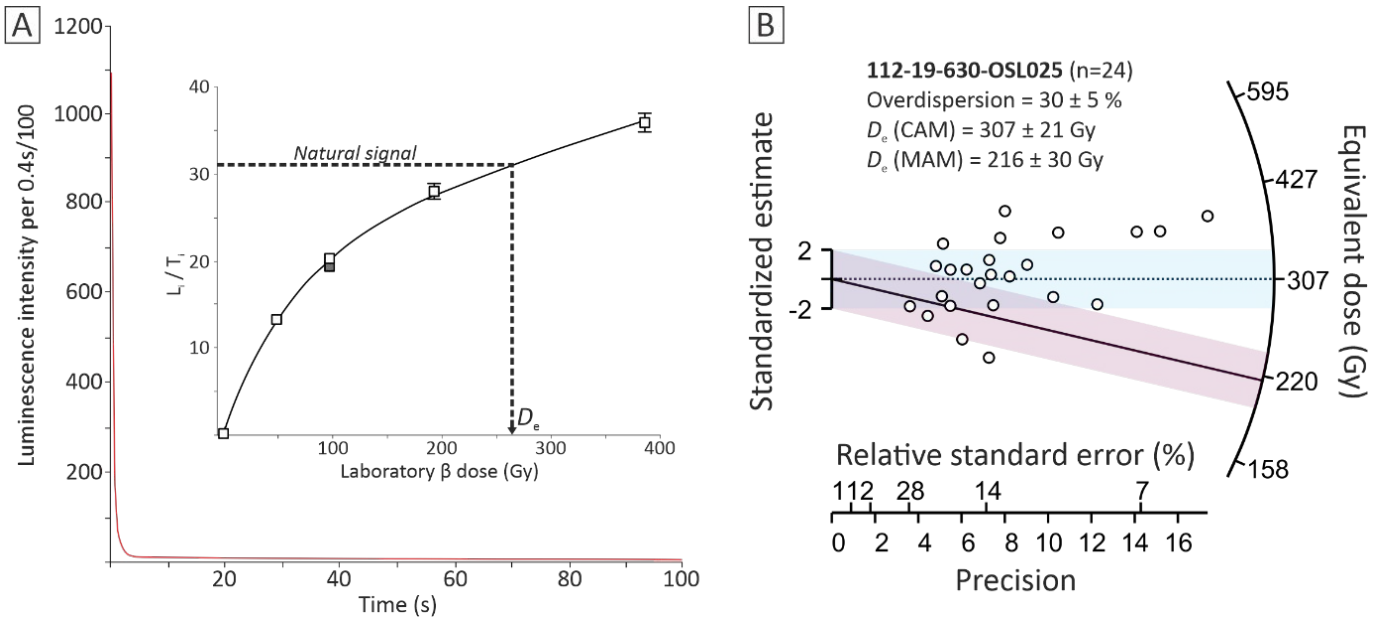

Figure 3.5: Optical data for sample 112-19-630-OSL025: A) luminescence decay curve (main graph) showing the "natural" signal and dose response curve (inset). These curves are typical for aliquots measured for this sample. Note, that the initial part of the decay curve is dominated by the desired 'fast' component and in this example the maximum signal intensity measured was 114 200 counts per 0.4s. In each case, the final 20 s of the signal was subtracted from the initial 0.4 s and this value (L_i) was divided by the value measured from a subsequent test dose (T_i) to produce the sensitivity-corrected signal (L_i/T_i), which is plotted on the y-axis of the dose response curve; and B) radial plot showing the distribution of the equivalent dose values (D_e) values and estimations of representative D_e values used for age determination that were calculated using either the central age model (CAM; dashed line, blue shading) or minimum age model (MAM; solid line, purple shading). Values plotted within the shaded regions fall within 2σ of the weighted mean values.

3.4.5 Stratigraphic approach

A hybrid-stratigraphic approach was used that incorporates both lithostratigraphy and allostratigraphy principles to define informal stratigraphic units. The North American Stratigraphic Code (North American Commission on Stratigraphic Nomenclature, 2021) recommends defining informal units when the extent and significance of units beyond the study area are still undetermined and/or when units are defined using innovative techniques. To build a stratigraphic framework of informally defined till units, a multi-parameter lithostratigraphy approach was taken that incorporates sedimentology observations (relative consolidation, colour, sedimentary structures, clast fabric and other ice-flow indicators) and laboratory analytical data (till provenance). The approach started in the field where till beds may be recognized at a section based on facies characteristics, their upper and lower boundaries, as well as their general stratigraphic position. This allowed for preliminary facies or litho-correlations of units with similar characteristics and stratigraphic positions at a local scale. It is important to note here that this initial field-based correlation between sections incorporates ice-flow indicator data for each identified till unit. These field-based observations were verified by detailed provenance analysis (clast lithology counts and detrital hornblende $^{40}Ar/^{39}Ar$ data) to confirm the direction of ice-flow that deposited the sediment. After till units were defined using a lithostratigraphic approach, an allostratigraphic approach was used to identify the relative age of intertill sorted sediment packages using the bounding surfaces of the enclosing till units. Use of an allostratigraphic approach to identify the relative age of intertill sorted sediments was necessary due to the fragmented nature of the stratigraphic record in the region, where the uppermost intertill nonglacial sediments encountered at a section may not necessarily be related to the penultimate deglaciation of the region (e.g., Dube-Loubert et al., 2013). The stratigraphy was first developed at local scales, and correlations were progressively extended across the study area to provide a regional stratigraphic framework.

3.5 Results

3.5.1 Stratigraphy

Below we discuss our stratigraphic findings at 22 sites (Figure 3.6a; Hodder et al., 2024), beginning with the stratigraphically oldest recognized depositional event. The regional ice-flow data, geochronology and spatial location of each identified stratigraphic unit are plotted in Figure 3.6b–h. Eight stratigraphic units are recognized and described below and placed in a chronostratigraphic context based on age constraints from intertill sorted sediment units.

3.5.1.1 Unit 1: Lower till(s) deposited by SW ice flow

Unit 1 occurs at seven sections (Figure 3.6b) and is best exposed at Section 19-628 (Figure 3.7). Unit 1 consists of a massive, matrix-supported diamicton that contains striated, bullet-shaped and faceted clasts. The matrix is blue-grey, greenish-grey, dark greyish-brown, brown or reddish brown in colour. The diamicton is highly consolidated and strongly jointed, with oxidation rinds developed on joint surfaces. The massive structure, clast shape, lodged in situ cobbles with striated upper surfaces and lateral continuity indicate that Unit 1 diamicton is a subglacial traction till (Evans et al., 2006; Evans 2018). Ice-flow data from Unit 1 includes lodged cobbles and spread-unimodal till fabrics that are interpreted to have formed by SW-trending (229–246°) ice-flow (Table 3.2; Figure 3.6b). Unit 1 till has decreased UGG clast concentrations relative to other tills (Figure 3.8) and no oolitic jasper or Dubawnt clasts. The lower contact of Unit 1 was not observed at any section. The upper contact of Unit 1 is unconformable or transitional and it underlies the sorted heterogeneous sediments of Unit 2 (six occurrences) or postglacial sediments of Unit 8 (one occurrence). In the latter case, the section is located near Shamattawa within the post-glacial drainage corridor (Figure 3.2).

Table 3.2: Ice-flow data for each stratigraphic unit.

Unit	Section ID	Ice flow indicator	n	Modality[1]	V_1 (azi °)	S_1	Interpreted ice-flow direction (azi °)
1	19-628	a-axis clast fabric	30	SU	229	0.70	229
1	19-628	striated lodged cobble	-	-	-	-	235
1	19-628	striated lodged cobble	-	-	-	-	230
1	17-531	a-axis clast fabric	30	SU	66	0.56	246
3	16-430	a-axis clast fabric	30	SU	102	0.73	282
3	17-515	a-axis clast fabric	30	SU	130	0.48	298
3	17-530	a-axis clast fabric	32	U	114	0.71	294
3	17-536	a-axis clast fabric	32	U	114	0.88	294
3	17-536	striated lodged cobble	-	-		-	284
3	19-629	a-axis clast fabric	30	SU	314	0.63	314
3	19-629	a-axis clast fabric	30	SU	327	0.58	327
3	19-628	a-axis clast fabric	35	SU	112	0.60	282
4	16-412	a-axis clast fabric	30	U	237	0.75	237
4	16-412	a-axis clast fabric	33	SU	244	0.57	244
4	16-412	striated lodged boulder	-	-	-	-	220
4	16-412	striated lodged boulder	-	-	-	-	226
4	17-519	a-axis clast fabric	33	SU	1	0.80	181
4	17-529	a-axis clast fabric	31	SU	193	0.58	193
4	16-408	striated lodged boulder	-	-	-	-	215
4	16-416	a-axis clast fabric	32	SU	270	0.56	270
4	16-416	a-axis clast fabric	30	SU	5	0.70	185
4	16-416	striated lodged cobble	-	-	-	-	276
4	17-531	a-axis clast fabric	30	SB	320	0.47	245/325-145
4	17-540	striated lodged boulder	-	-		-	178
4	17-542	striated lodged cobble	-	-		-	175
4	19-629	a-axis clast fabric	30	SU	220	0.79	220
6	16-430	a-axis clast fabric	31	SU	107	0.72	287
6	17-515	a-axis clast fabric	32	SU	124	0.68	304
6	17-519	a-axis clast fabric	33	SU	153	0.53	333
6	17-536	a-axis clast fabric	32	SU	201	0.64	201
6	16-407	a-axis clast fabric	40	SU	147	0.63	327
6	16-407	a-axis clast fabric	30	SU	145	0.66	325
6	16-407	a-axis clast fabric	30	U	141	0.76	321
6	19-629	a-axis clast fabric	38	SU	133	0.63	313
6	19-629	a-axis clast fabric	30	SU	348	0.67	348
7	17-529	a-axis clast fabric	30	U	356	0.83	176
7	17-530	a-axis clast fabric	30	SU	198	0.77	198
7	16-416	a-axis clast fabric	30	SU	178	0.80	178
7	17-540	a-axis clast fabric	20	SU	60	0.53	240
7	17-540	striated lodged boulder	-	-	-	-	195
7	17-542	striated lodged boulder	-	-	-	-	185
7	17-542	striated lodged boulder	-	-	-	-	197

Abbreviations: S_1, principal eigenvalue; V_1, principal eigenvector; U, unimodal; SU, spread unimodal; SB, spread bimodal

[1]As defined by Hicock et al. (1996)

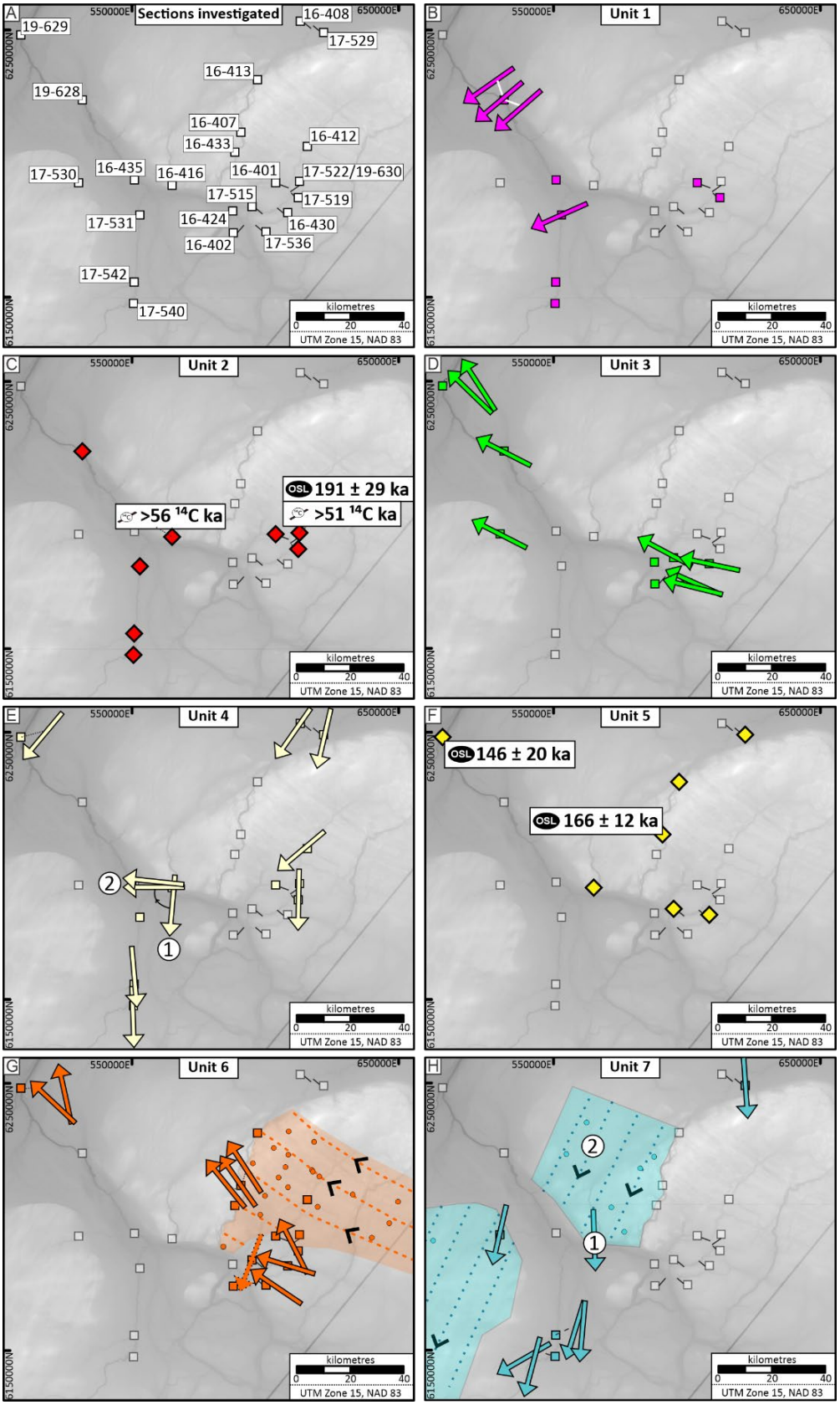

Figure 3.6: Spatial distribution of interpreted stratigraphic units with age constraints and ice-flow data plotted. Coloured squares represent till units and the arrows plot the ice-flow data for the respective till unit (Table 3.2). Coloured diamonds represent intertill nonglacial units. Geochronology data for nonglacial units includes optical ages (Table 3.3) and nonfinite radiocarbon ages (Hodder et al., 2023).

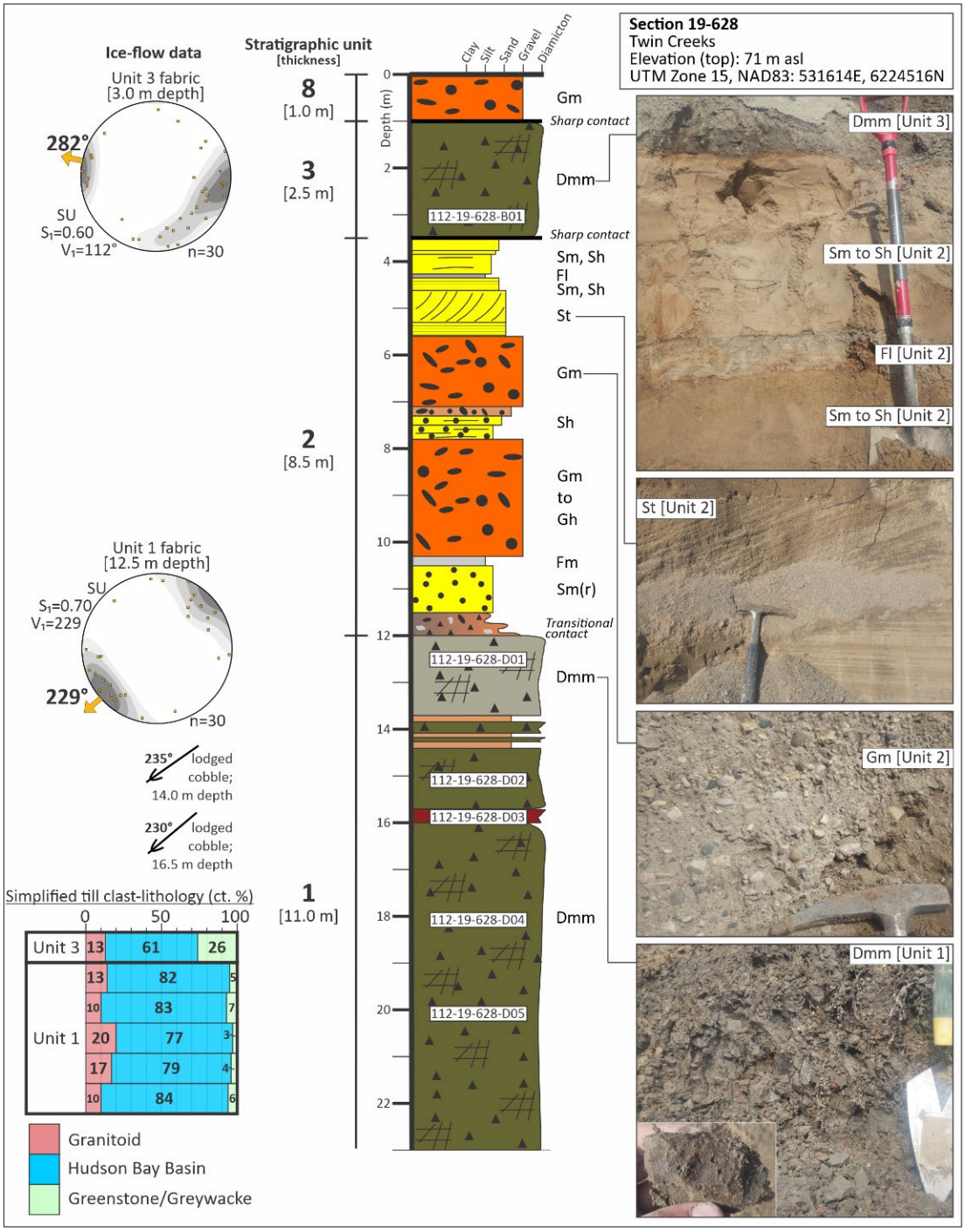

Figure 3.7: Quaternary stratigraphy exposed at Section 19-628 on Twin Creeks and examples of sediments exposed. Till sample numbers and till fabric sites are labelled within the white boxes on the stratigraphic column. Till clast-fabric data is plotted on equal area, lower hemisphere projection stereonets. The value of the principal eigenvalue (S_1) and direction of the principal eigenvector (V_1) are provided, and an interpretation of the ice-flow direction is indicated (orange arrow). Abbreviations: SU, spread unimodal; S_1, principal eigenvalue; V_1, principal eigenvector. Simplified till clast-lithology data is provided as an inset box for each till sample shown on the stratigraphic column with the lowermost sample plotted at the bottom.

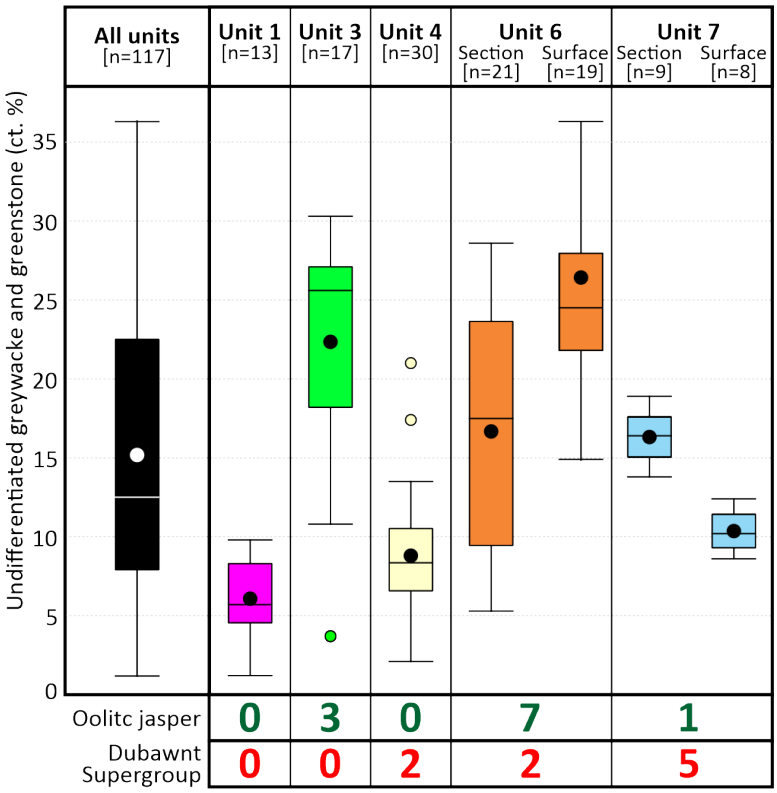

Figure 3.8: Tukey box plots showing the proportion of undifferentiated greenstone and greywacke clasts (eastern source) in the 2–8 mm size-fraction of till. The recovery of distinctive oolitic jasper clasts (eastern source) and Dubawnt Supergroup clasts (northwestern source) is displayed at the bottom of the box plots for each stratigraphic unit. Till samples have been classified according to the stratigraphic unit that they were sampled from.

3.5.1.2 Unit 2: Heterogeneous sediments of MIS 7-age

Unit 2 is recognized at eight sections (Figure 3.6c) and is best exposed at Section 17-522/19-630 (Figures 3.9, 3.10a, b); this includes the previously published “Echoing River Section” (Dredge et al., 1990). Unit 2 consists of several contrasting lithofacies and is defined by its bounding surfaces (allostratigraphy). Unit 2 is defined by its upper bounding surface with Unit 3 till (one occurrence) or Unit 4 till (seven occurrences) and lower bounding surface with Unit 1 till (six occurrences). Unit 2 ranges in thickness from 0.1 m to 8.5 m and consists of bedded clay, silt, sand and gravel. Three of the occurrences (16-416, 17-522 and 17-531) are organic bearing (wood and/or peat; Figure 3.9). Each section has a unique exposure of sediment lithofacies, and lateral variations across and between exposures are common. This includes the transition from organic-bearing sediment (Figure 3.10a) to organic-barren sediment (Figure 3.10b) or pinching out laterally into a till-till

contact/unconformity (Figure 3.10d). The thickness of Unit 2 changes over short distances and in many cases is the uppermost occurrence of intertill nonglacial sediments at a section (e.g., Figure 3.9). Sediments correlated to Unit 2 are situated at elevations between 69–114 m asl.

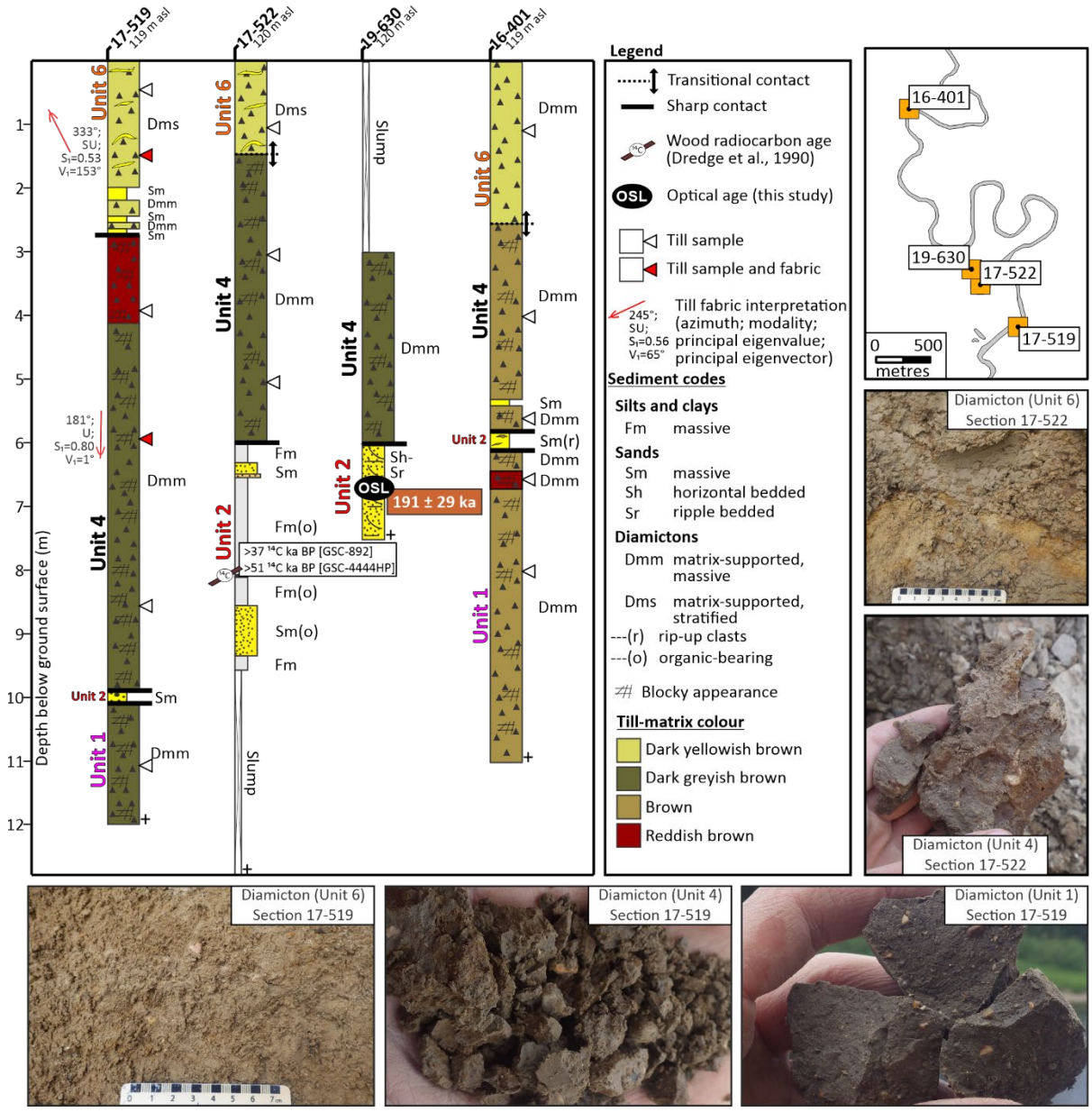

Figure 3.9: Quaternary stratigraphy exposed along an unnamed tributary to the Echoing River and examples of diamicton exposed at sections.

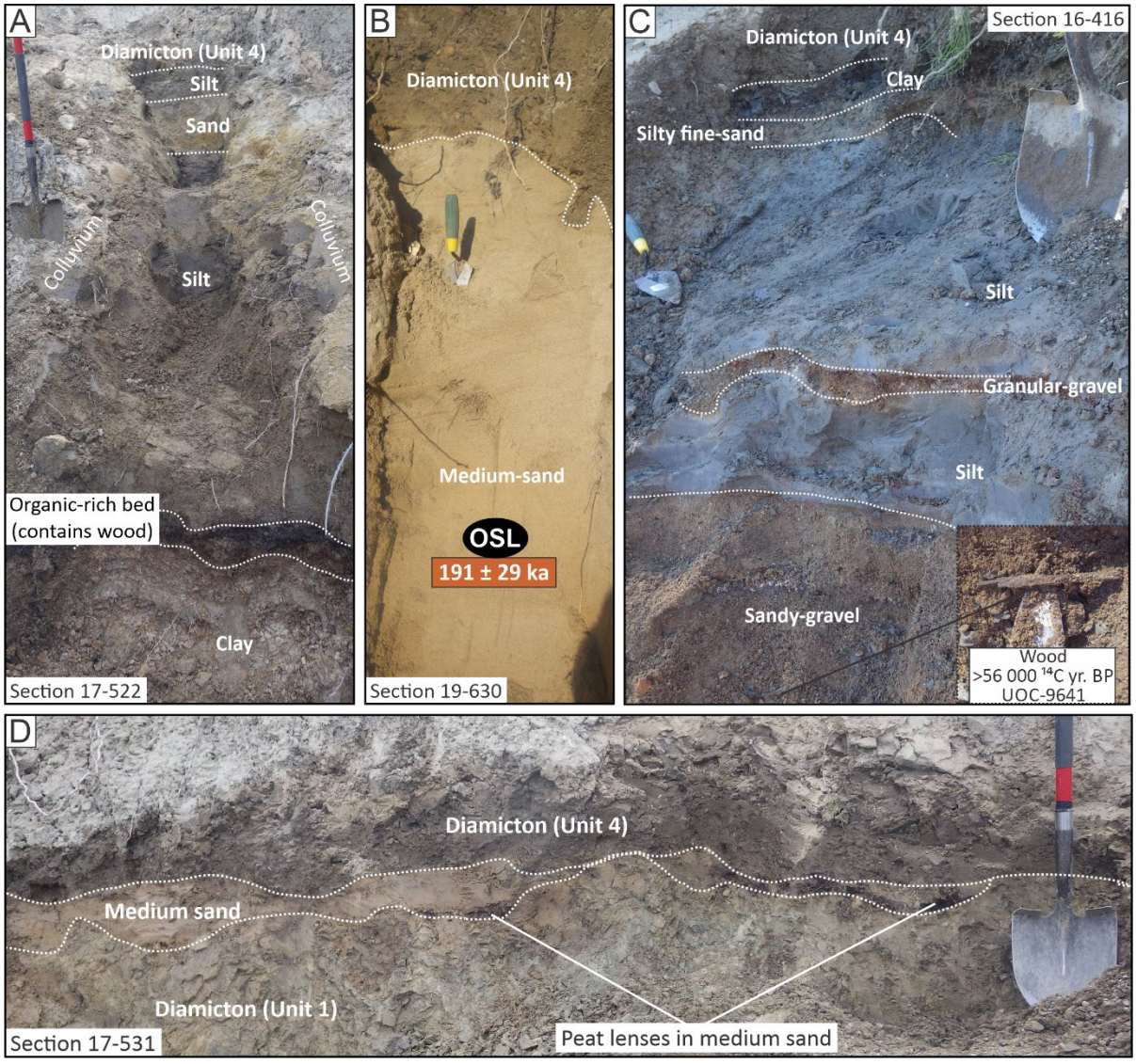

Figure 3.10: Example of organic-bearing nonglacial sediments from Unit 2: a) bedded clay, sand, silt and wood-bearing facies at Section 17-522; b) bedded medium sand at Section 19-630 and location where an OSL age of 191 ± 29 ka was determined; c) bedded clay, silty, sand and gravel at Section 16-416 with a photo of detrital wood recovered from the gravel that has a nonfinite radiocarbon age; d) laterally discontinuous intertill medium sand with peat lenses at Section 17-531.

The pollen record from Unit 2 was investigated at Section 16-416. Only two of the three examined samples contained sufficient pollen concentrations and unidentified grains (> 5000 pollen grains/cm^3 and <10% broken/unidentified) for further analysis. These two intervals contained pollen groups typical of a boreal peatland environment akin to what exists there today (Figure 3.11). Notably, pollen was composed of arboreal (*Picea*, *Pinus*, *Salix*) and wetland (Cyperaceae, *Sphagnum*) components, along with grass (Poaceae) pollen, fern (Polypodiaceae) spores and the algal aquatic indicator, *Pediastrum.* Loss-on-ignition analysis confirms a highly minerogenic component (organic content was 4–6%). Quantitative paleoclimate reconstruction using the modern-analogue technique indicates deposition during a mean summer temperature of 13.4–13.9°C, which is indistinguishable from present-day mean summer temperature of 13.4°C (Figure 3.11). Reconstructed mean annual precipitation ranged from 537 mm to 689 mm, which is similar or slightly higher than present-day values for the area (474 mm). Detrital wood collected from sandy gravel sediments at Section 16-416 yielded a nonfinite radiocarbon age (>56 ka ^{14}C BP; UOC-9641; Hodder et al., 2023).

Pollen and paleoenvironmental data at section 17-522 (Figure 3.9, Figure 3.10a) were previously published as the "Echoing River Section" (Dredge et al., 1990). The lowermost clay in this section was possibly deposited in a marine or glaciomarine environment. This interpretation is based on relatively elevated boron and vanadium values of the sediment and the recovery of trace foraminifera; however these microfossils may be allochthonous (Dredge et al., 1990). Only 0.15 m of this bed was accessible when the site was revisited, and excessive colluvium prohibited further investigation. The overlying clay, silt, sand, and peat (Figure 3.10a) contained freshwater gastropods and ostracods, which indicate deposition in a terrestrial or freshwater environment (Dredge et al., 1990). Similar to Section 16-416, pollen at Section 17-522 was largely composed of arboreal (*Picea*, *Pinus*) and wetland (Cyperaceae, *Sphagnum*) components. The pollen profile indicates an overall warming trend from an open tundra to boreal forest-type environment. The occurrence of trees in the area is corroborated by the recovery of spruce wood from the organic-rich bed (Dredge et al., 1990). The insect fauna investigated from the organic-rich bed indicates boreal conditions close to the tree line (Dredge et al., 1990). Wood at this site yielded nonfinite radiocarbon ages (>31 ^{14}C ka BP [GSC-892]; >51 ^{14}C ka BP [GSC-4444HP]; Dredge et al., 1990). At a location 160 m to the north

along the same Section 17-522 exposure, Unit 2 sorted sediments consist of >1.5 m of well-sorted medium sand that is weakly horizontally bedded to cross-bedded (Figure 3.10b). The optical age of the well-sorted, sub-horizontally bedded medium sands were determined to be 191 ± 29 ka [MAM, 1σ (sample 112-19-630-OSL025); Table 3.3] or 272 ± 22 ka [CAM, 1σ (sample 112-19-630-OSL025); Table 3.3]. This sand sample has a relatively high overdispersion (OD) value of 30 ± 5 % and therefore most likely consists of grains that have been heterogeneously bleached prior to deposition. In this case the MAM D_e would give an approximation of true depositional age of a sample if a significant number of grains had been fully bleached, or it would give an age closer to the true age than that derived using the CAM if this is not the case. For these reasons we interpret that MAM age of 191 ± 29 ka [1σ (112-19-630-OSL025)] to be closer to the depositional age of the sediments. Nonetheless, the CAM and MAM ages for this sediment bracket the MIS 7 interglacial period (243–191 ka; Lisiecki and Raymo, 2005). These observations suggest that Unit 2 sediments were deposited during the MIS 7 interglacial period in marine, fluvial, lacustrine and/or eolian environments during an overall warming trend from an open tundra to boreal forest-type environment.

Table 3.3: Number of aliquots measured (N), overdispersion values (OD), equivalent dose values (D_e), optical ages, and dose recovery (DR) ratios.

Site	Sample ID	N[a]	OD (%)	D_e (Gy) – C[b]	D_e (Gy) – M[c]	Age (ka) - C	Age (ka) - M	DR ratios[d]	Source
19-629	112-19-629-024	31/36	32 ± 5	278 ± 17	201 ± 26	202 ± 15	146 ± 20	0.96 ± 0.05	Hodder et al. (2023)
16-407	112-16-407-019	32/37	15 ± 3	304 ± 10	294 ± 17	172 ± 8	166 ± 12	1.12 ± 0.03	Hodder et al. (2023)
19-630	112-19-630-OSL025	24/24	30 ± 5	307 ± 21	216 ± 30	272 ± 22	191 ± 29	--	This study

Note: OD and D_e values calculated using the software of Liang and Forman (2019).
[a]N = number of aliquots accepted/number of aliquots measured.
[b]C determined using the central age model (CAM).
[c]M determined using the three-parameter minimum age model (MAM).
[d]DR = dose-recovery ratio (given dose/recovered dose).

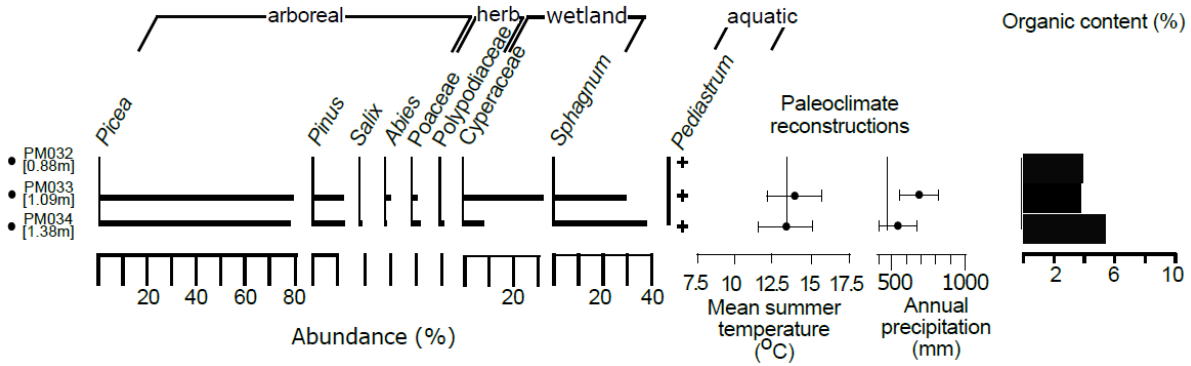

Figure 3.11: Pollen analysis for site 16-416 (Appendix B, Supplemental material 1, Figure SA2); only taxa appearing at >1% abundance is plotted.

3.5.1.3 Unit 3: Lower till deposited by NW-trending ice-flow

Unit 3 is documented at eight sections (Figure 3.6d) and is best exposed at sections 16-430 (Figure 3.12) and 17-515. Unit 3 consists of a massive, matrix-supported diamicton that contains striated, bullet-shaped and faceted clasts. The matrix is greyish brown, dark greyish brown to brown in colour. The diamicton is highly consolidated and strongly jointed with oxidation rinds developed on joint surfaces. The massive structure, clast shape, lodged in-situ cobbles with striated upper surfaces and lateral continuity indicate that Unit 3 diamicton is a subglacial traction till (Evans et al., 2006; Evans 2018). Unit 3 has elevated UGG clast concentrations (eastern provenance) relative to other tills (Figure 3.8). Three oolitic jasper clasts (eastern provenance) and no northern provenance Dubawnt clasts were counted (Figure 3.8). The detrital hornblende $^{40}Ar/^{39}Ar$ ages are predominantly 2.6–2.7 Ga, with 10 of 15 grains falling in this range (Superior Province, Figure 3.13c). Together, these parameters provide supporting evidence for an eastern provenance for sediments in this unit, which is reflected in the interpretation of ice-flow data collected. Ice-flow data collected from Unit 3 includes a lodged cobble and unimodal to spread unimodal clast fabrics that are interpreted to have formed by WNW- to NNW-trending ice-flow (282–327°; Table 3.2; Figure 3.6d). The lower contact of Unit 3 was only observed at one section (Section 19-628; Figure 3.7), where the till unconformably overlies the sorted heterogeneous sediments of Unit 2. The upper contact of Unit 3 occurs with intertill sorted sediments of Unit 5 (three occurrences), Unit 6 till (two occurrences), Unit 7 till (one occurrence) and Unit 8 post-glacial sediments (two occurrences). Sediments correlated to Unit 3 are spatially restricted to the south and west of the Kaskattama highland study area (Figure 3.6d). Furthermore, the till unit appears to be discontinuous laterally along the southern edge of the Kaskattama highland (Figure SA1, Appendix B, Supplemental material 1).

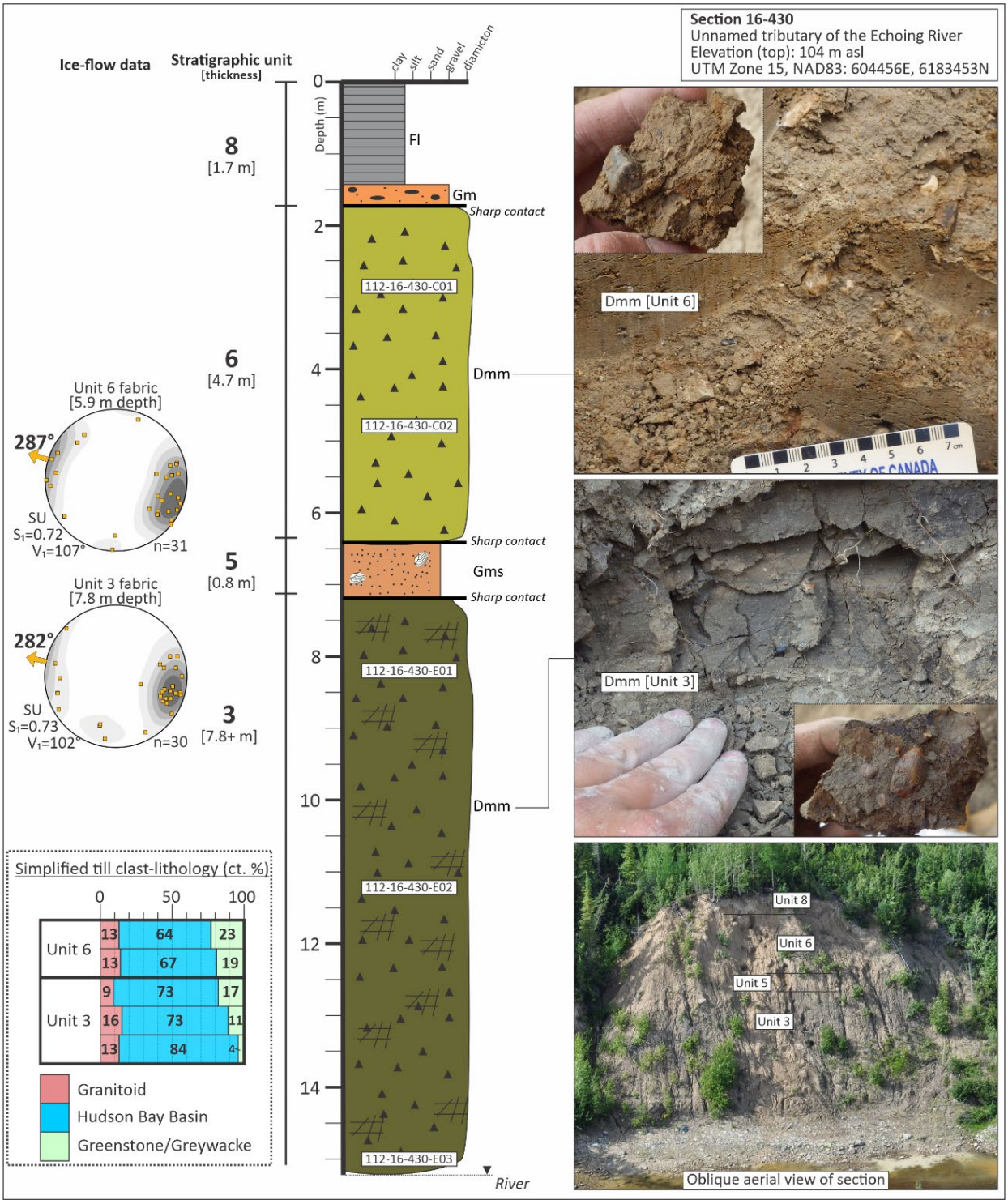

Figure 3.12: Quaternary stratigraphy exposed at Section 16-430 on an unnamed tributary to the Echoing River and with examples of Unit 3 and 6 exposed here. Till sample numbers are labelled within the white boxes. Till clast-fabric data is plotted on equal area, lower hemisphere projection stereonets. The value of the principal eigenvalue (S_1) and direction of the principal eigenvector (V_1) are provided, and an interpretation of the ice-flow direction is indicated (orange arrow).

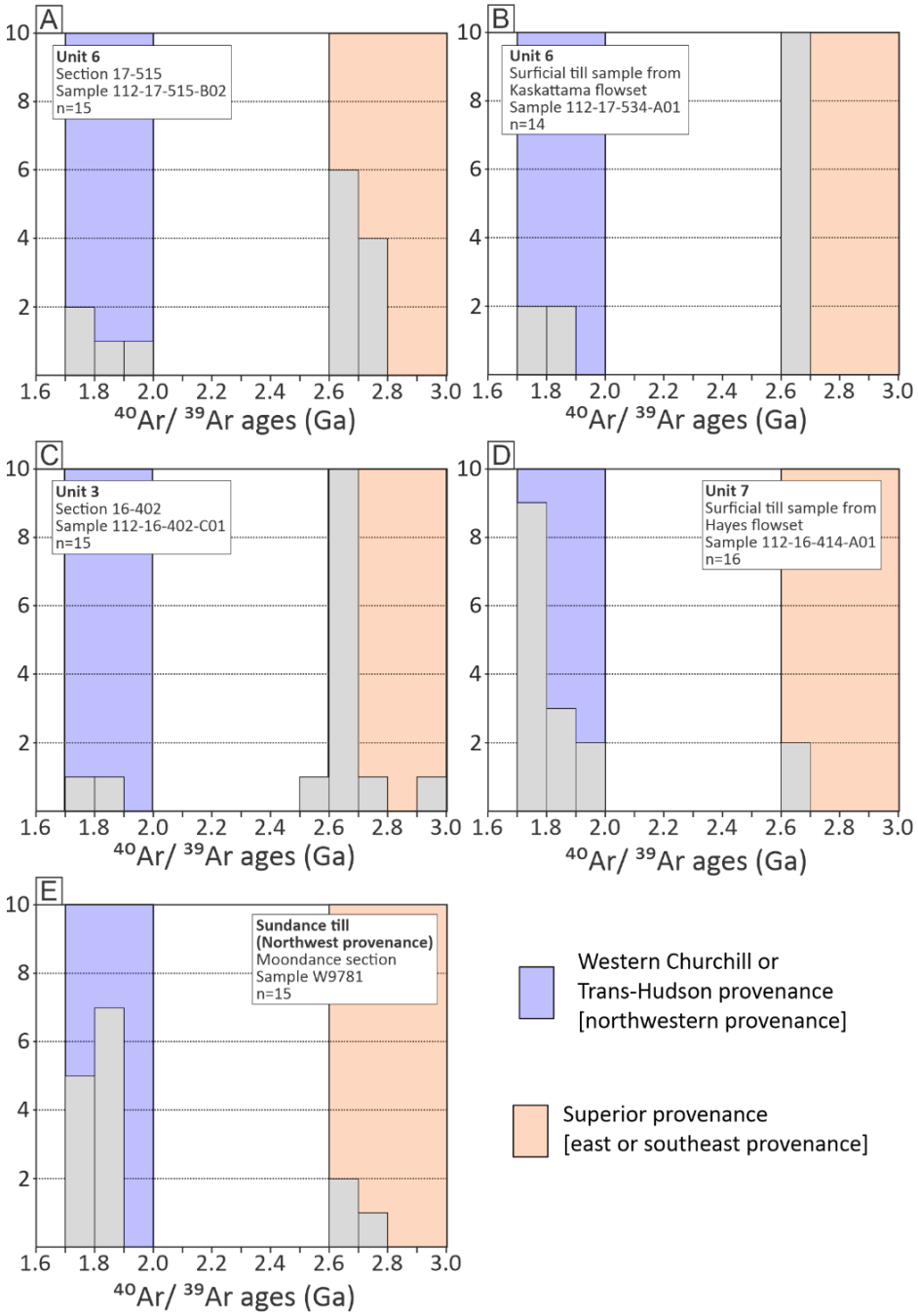

Figure 3.13: Detrital hornblende $^{40}Ar/^{39}Ar$ ages determined for selected till units displayed as stacked histograms (100 Ma bins) with a consistent scale on the y-axis for each plot: a), Unit 6 till at Section 17-515, b) Unit 6 till sampled at surface from a streamlined landform in the Kaskattama flowset, c) Unit 3 till at Section 16-402, d) Unit 7 till sampled at surface from a streamlined landform in the Hayes flowset; and e) Sundance till at the Moondance section (documented northwestern provenance).

3.5.1.4 Unit 4: Lower till deposited by S- to SW- to W-trending ice-flow

Unit 4 is recognized at eleven sections (Figure 3.6e) and is best exposed at Section 16-416 (Figure SA2, Appendix B, Supplemental material 1). Unit 4 consists of a massive, highly consolidated, matrix-supported diamicton that contains striated, bullet-shaped and faceted clasts (e.g., Figures 3.4c, g, 3.9). The matrix is dark greyish brown to reddish brown to light brownish grey. The diamicton is highly consolidated and strongly jointed with oxidation rinds developed on joint surface. The massive structure, high level of consolidation, clast-shape, lodged in-situ cobbles and boulders with striated upper surfaces and lateral continuity indicate that Unit 4 diamicton is a subglacial traction till (Evans et al., 2006; Evans 2018). Ice-flow data collected from Unit 4 including unimodal to spread unimodal clast fabrics that are interpreted to have formed by S- to WSW-trending (175–244°) ice-flow (Table 3.2; Figure 3.6e). One section (Section 16-416) shows an up-unit switch from S- to W-trending ice-flow (Table 3.2; Figure 3.6e). Unit 4 has decreased UGG clast concentrations (eastern provenance) relative to other tills, with no oolitic jasper clasts (eastern provenance) and two Dubawnt clasts (northwestern provenance; Figure 3.8). The lower contact of Unit 4 was observed at seven sections, where it is in sharp contact with sorted intertill sediments of Unit 2 (e.g., Figure 3.9). The upper contact of Unit 4 is in sharp or transitional contact with Unit 5 intertill sorted sediments (two occurrences), Unit 6 till (four occurrences), Unit 7 till (two occurrence) and Unit 8 post-glacial sediments (two occurrences). Sediments correlated to Unit 4 occur across the entire study area (Figure 3.6e).

3.5.1.5 Unit 5: Heterogeneous sediments of MIS 5–6 age

Unit 5 is identified at seven sections (Figure 3.6f) and is best exposed at Section 16-407 (Figure 3.14a; Figure SA3, Appendix B, Supplemental material 1). Like Unit 2, this unit consists of highly variable lithofacies and is thus defined based on its relationship to bounding units. Unit 5 is defined by its upper bounding surface with Unit 6 till (five occurrences) or Unit 7 till (two occurrences) and lower bounding surface with Unit 3 till (two occurrences) or Unit 4 till (three occurrences). At two sites no lower bounding surface was observed due to excessive colluvium. Unit 5 ranges in thickness from 0.5 m to more than 3.8 m and consists of clay, silt, sand and gravel and no organics were observed within the sediment except for abraded shell fragments (Figure 3.14). Sand facies are often ripple cross laminated (e.g., Figure 3.14a) or horizontally bedded (e.g., Figure 3.14b). Each

section exposes a unique sequence of sediment facies, and lateral variations in an exposure were commonly observed. This includes pinching out laterally into a till-till contact unconformity across a single exposure. The thickness of Unit 5 therefore changes over short distances. The optical age of Unit 5 sediment has been determined previously at sections 19-629 and 16-407 to be 146 ± 20 [MAM, 1σ (sample 112-19-629-024); Table 3.3] and 166 ± 12 ka [MAM, 1σ (sample 112-16-407-019); Table 3.3], respectively (Hodder et al., 2023). Sediments correlated to Unit 5 are situated at elevations between 40–157 m asl.



Figure 3.14: Example of Unit 5 sorted sediments: a) ripple cross-laminated sand at Section 16-407; b) intertill bedded sand at Section 19-629; c) intertill sandy gravel at section 16-430; d) intertill bedded sand, silt and clay that underlain by massive silt at Section 17-515. Note, the overlying till matrix colour transitions upward from grey to yellowish brown due to incorporation of the underlying sediments near the contact; e) intertill massive blue-grey clay at Section 16-416; and f) intertill massive silt with a blocky appearance that contains minor oxidation rind along joint surfaces at Section 17-529.

3.5.1.6 Unit 6: Upper till deposited by NW-trending ice-flow

Unit 6 is recognized at twelve sections (Figure 3.6g) and is best exposed at Section 16-407 (Figure SA3, Appendix B, Supplemental material 1; Hodder et al, 2023). Unit 6 consists of massive to stratified, matrix-supported diamicton that contains striated, bullet-shaped and faceted clasts. The matrix is dark yellowish brown to light olive brown. The diamicton is over-consolidated but significantly less than the underlying Unit 1, 3 and 4 tills (where observed). The diamicton is not jointed to weakly jointed with minor oxidation rinds on joint surfaces. The massive to stratified structure, clast-shape and lateral continuity that Unit 6 diamicton is a subglacial traction till (Evans et al., 2006; Evans 2018). Unit 6 has elevated UGG clast concentrations (eastern provenance) relative to other tills and contains seven oolitic jasper clasts (eastern provenance) and two Dubawnt clasts (northern provenance; Figure 3.8). The detrital hornblende $^{40}Ar/^{39}Ar$ ages of a surface and subsurface sample from Unit 6 both have predominantly 2.6–2.7 Ga (Superior Province) distributions (Figure 3.13). Together, these parameters point to an eastern provenance for the till, which is reflected in the interpretation of ice-flow data for this unit (Figure 3.6g). The majority of ice-flow data collected from Unit 6 in section indicates deposition by WNW- to NNW-trending ice-flow as interpreted from spread unimodal to unimodal till fabrics (287–333°; Table 3.2; Figure 3.6g). One spread unimodal till fabric in Unit 6 is oriented perpendicular to this orientation (201°) and is interpreted as a transverse fabric, i.e. perpendicular to ice flow, since the qualitative (sedimentology) and quantitative (clast count) properties of this till are similar to Unit 6 till at adjacent sections nearby. The streamlined landforms of the Kaskattama flowset, which trend towards the 290° on the east side of the Kaskattama highland and 305° at the northwest edge the Kaskattama highland (Figures 3.2, 3.6g) are interpreted to be the surficial geomorphic expression of Unit 6. This sediment-landform relationship is evident at some sections where Unit 6 extends to the surface within the footprint of the Kaskattama flowset and is not overlain by postglacial sediments (e.g., Section 16-413). Furthermore, till collected from streamlined landforms of the Kaskattama flowset is qualitatively similar to that of Unit 6 in section (e.g., Figure 3.4a) and has similar till UGG clast content (Figure 3.8).

The lower contact of Unit 6 was observed at 11 sections, and it separates Unit 6 from underlying Unit 3 till (two occurrences), Unit 4 till (four occurrences) and intertill sediments of Unit 5 (five occurrences). At Section 16-407 (Figure SA3, Appendix B, Supplemental material 1), there is a lower clay-rich facies of the till with rip-up clasts of mud, suggesting that ice may have advanced over fine-grained sediments (Hodder et al., 2023). Similarly, underlying Unit 6 at Section 17-519 is bedded sand, silt and clay (Figure 3.14d; Figure SA4, Appendix B, Supplemental material 1). The lower 30–40 cm of the diamicton has the same colour as the underlying silt implying incorporation of the underlying silt into the matrix (Figure 3.14d), supporting the interpretation that Unit 6 till formed during an advance over fine-grained sediments. Unit 6 till is at the surface (five occurrences) or overlain by postglacial sediments of Unit 8 (seven occurrences). Unit 6 till was encountered on the Kaskattama highland, south of Kaskattama highland underlying post-glacial sediments and at one section at the junction of the Gods and Hayes rivers (Figure 3.6g).

3.5.1.7 Unit 7: Upper till deposited by S- to SW-trending ice-flow

Unit 7 is interpreted at five sections (Figure 3.6h) and is best exposed at Section 17-542 (Figure SA5, Appendix B, Supplemental material 1). Unit 7 consists of massive to stratified, matrix-supported diamicton that contains striated, bullet-shaped and faceted clasts. The matrix is brown to dark yellowish brown to olive brown. The diamicton is over-consolidated but significantly less consolidated relative to the underlying Unit 1, 3 and 4 tills (where observed) and in places has a boulder pavement at its lower contact (e.g., Figure 3.4c). The massive structure, clast-shape and lateral continuity indicate that Unit 7 diamicton is a subglacial traction till (Evans et al., 2006; Evans 2018). Ice-flow data collected from Unit 7 includes lodged boulders and unimodal to spread unimodal till fabrics that are interpreted to have formed by S- to WSW-trending ice-flow (176–240°; Table 3.2; Figure 3.6h). The streamlined landforms of the Hayes flowset are oriented 204–207° in the study area (Figure 3.2) and are interpreted to be the surficial geomorphology expression of Unit 7 based on similarities between clast fabric direction and streamlined landforms, stratigraphic position and qualitative similarities between the surficial till and till described in section. Sections 16-416 and 17-529 have strong S-trending fabrics (176° and 178°; Table 3.2), and Section 16-416 is

overlain by the Hayes streamlined-landform flowset (Figure 3.6h). As such, formation of the south-trending clast fabric occurred prior to the late-glacial SSW-trending ice-flow that formed flowset. Unit 7 has average UGG clast concentrations (eastern provenance) relative to other tills and contains one oolitic jasper clasts (eastern provenance) and five Dubawnt clasts (northern provenance; Figure 3.8). The five Dubawnt clasts counted amount to 55% (n=5/9) of the total count in the dataset, yet Unit 7 samples represent only 15% of the sample population. The detrital hornblende $^{40}Ar/^{39}Ar$ age distribution from one sample is predominantly 1.7–2.0 Ga (Figure 3.13; Western Churchill or Trans-Hudson orogen, Figure 3.3). This $^{40}Ar/^{39}Ar$ age distribution is similar to the Sundance Till situated to the west of the study area near the town of Gillam (Figure 3.1), which has a well-documented northwestern provenance (Figure 3.13). Together, these provenance parameters indicate a northwestern provenance for Unit 7. This contrasts with the orientation of the surficial flowset indicative of SW ice flow and till fabrics indicative of S and SW ice flows. Considering these ice-flow directions, the NW provenance indicators in Unit 7 could be inherited from older tills deposited by SE-trending ice-flow or could indicate long-distance transport from mainland Nunavut by the Hayes Lobe. The lower contact of Unit 7 was observed at all five sections, with Unit 3 till (one occurrences), Unit 4 till (two occurrences) and intertill sediments of Unit 5 (one occurrences). The upper contact of Unit 7 is overlain by postglacial sediments of Unit 8 (three occurrences), or the unit ends at the surface of the section (one occurrence) and could not be accessed for observation at one section. Unit 7 till is spatially restricted to the Hayes flowset or in areas overlain by Unit 8 postglacial sediments in close proximity to the flowset.

3.5.1.8 Unit 8: Postglacial sediments of MIS 1-age

Unit 8 consists of massive to bedded clay, silt, sand and gravel that was deposited during the Holocene Epoch (MIS 1) following retreat of LIS from northeastern Manitoba. These sediments were deposited in glaciolacustrine, marine or fluvial environments and have collectively been grouped into one stratigraphic unit that is representative of ‘post-glacial sediments’. A detailed investigation of the post-glacial history of this region is beyond the scope of this manuscript; however, some

aspects of the postglacial history of this region are discussed in Dredge (1983) and Gauthier et al. (2020).

3.5.2 Till-matrix geochemistry

Principal component (PC) 1, 2 and 3 account for 40%, 19% and 15% of the observed variance within the dataset, respectively (Figure 3.15a). Exploratory examination of PC biplots indicated that stratigraphic units, identified independent of the matrix geochemical data, were best differentiated using PC1 and PC3 (Figure 3.15b) and the biplot of PC1 and PC2 is provided in Appendix B, Supplemental material 4. Samples with positive PC1 values are representative of a relative Shield-rich provenance signature (Al-Fe-Rb; e.g., Figure 3.15c). Samples with negative PC1 values and positive PC3 values are representative of a relative Paleozoic-rich provenance signature (Ca-Mg-Mn; e.g., Figure 3.15d). Samples with negative PC3 values are representative of a relative UGG-rich provenance signature (Na-Zr; e.g., Figure 3.15c, e).

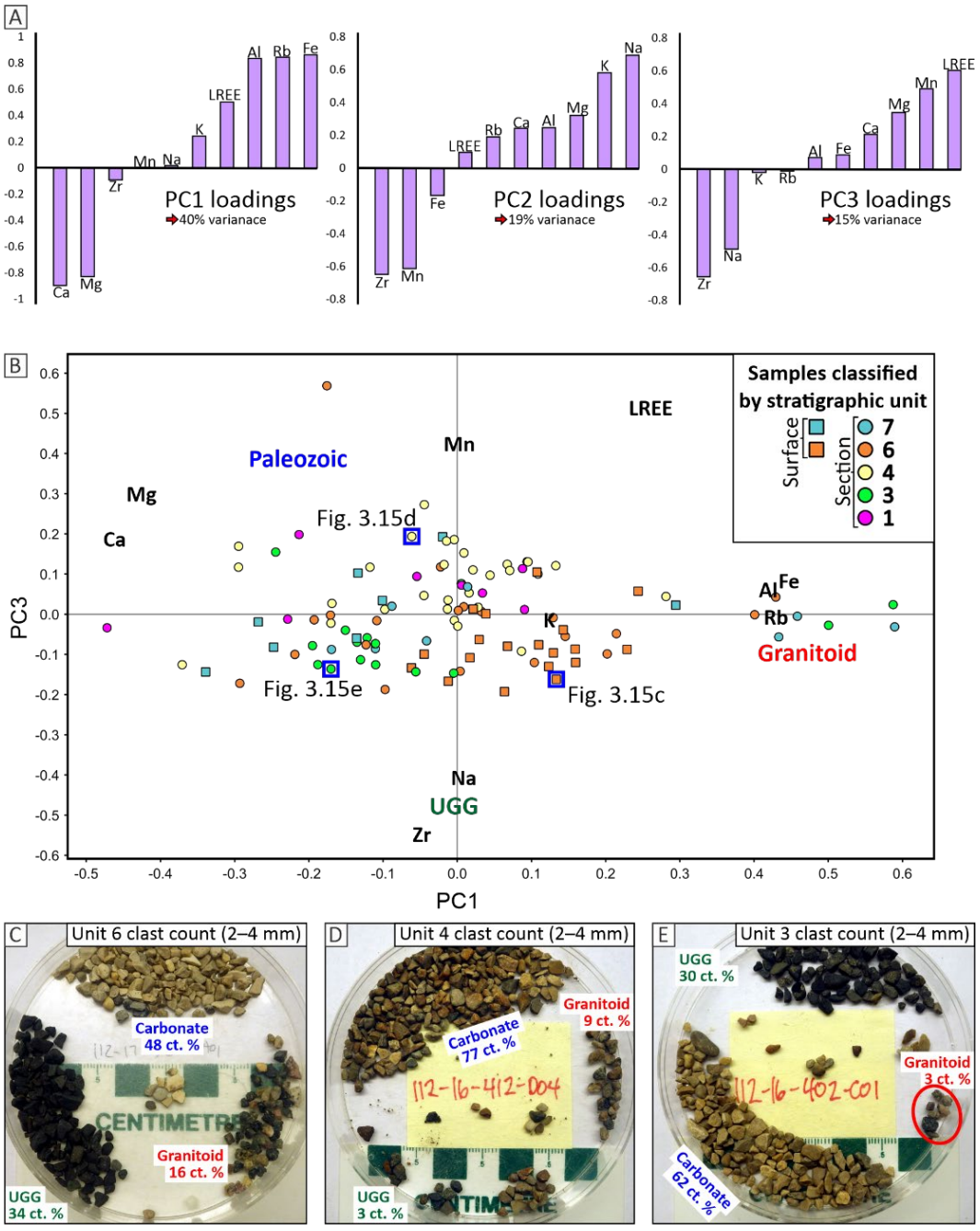

Figure 3.15: Principal component analysis results and clast-lithology examples: a) PC1, 2 and 3 elemental loadings; b) biplot of PC3 vs. PC1. Samples have been coloured according to the stratigraphic unit they were sampled from. Surficial and subsurface (section) samples are differentiated by shape; c–e) examples of sorted clasts in the 2–4 mm size-fraction for three units. Note, these samples are highlighted on the PC3 vs. PC1 biplot.

3.6 Discussion

This study incorporated a hybrid stratigraphic approach that identified till units using principles of lithostratigraphy. We then used principles of allostratigraphy and examined the bounding surfaces of identified till units with intertill sorted sediments. This was a necessary approach since the stratigraphy is dominated by glacial sediments (till) and intertill sorted sediments that are heterogeneous and variably preserved (or deposited) in the stratigraphic record. This approach assembled a stratigraphic framework for the region consisting of eight units (Figure 3.16). The units are: Unit 1, a till deposited by SW-trending ice-flow; Unit 2, nonglacial sediments of likely MIS 7 age; Unit 3, a till deposited by NW-trending ice-flow; Unit 4, a till deposited by S- to W-trending ice-flow; Unit 5 nonglacial sediments of early MIS 5 or late MIS 6 age; Unit 6 a till deposited by NW-trending ice-flow; Unit 7, a till deposited by S- to SW-trending ice-flow; and Unit 8, sorted sediment of MIS 1 age.

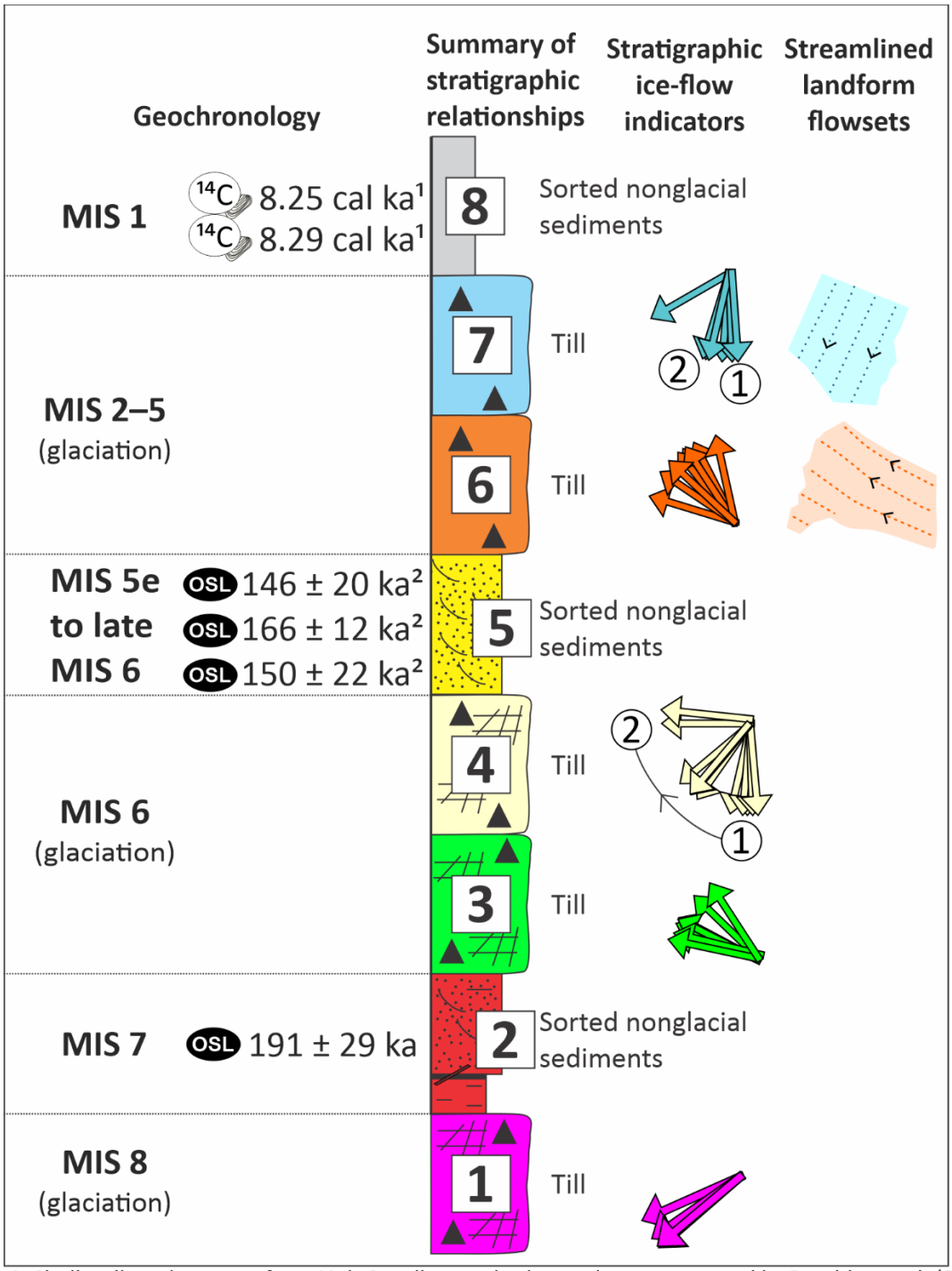

1. Shell radiocarbon ages from Unit 8 sediments in the study area reported in Gauthier et al. (2020).
2. OSL ages from Unit 5 sediments in the study area reported in Hodder et al. (2023).

Figure 3.16: Quaternary stratigraphic framework for the Kaskattama highland region.

3.6.1 The stratigraphic mosaic and Implications for correlations

Deciphering the fragmented record from the Kaskattama highland, especially identifying till units, is challenging because the stratigraphic framework relies on 22 sections and is not complete at any one location in the study area (Figure 3.17a), which is a common theme in regions of thick till-dominated sequences (e.g., Möller et al., 2019). This highly fragmented record highlights either patchy deposition of till, patchy erosion of till, or likely a combination of both processes. This work shows that till units in the region can be indistinguishable based on certain properties (e.g. texture, color, compaction) yet have contrasting till fabrics and unique provenance indicators, which provide compelling evidence they were transported and deposited by ice flowing in different directions (Figure 3.4d vs 3.4e and 3.4f vs 3.4g). “Similar tills”, such as Unit 3 and 4, can be in the same relative-stratigraphic position (underlying nonglacial Unit 5) and spatially close (Figure 3.17a; Figure SA1, Appendix B, Supplemental material 1), but be deposited by ice flowing in near-perpendicular directions. To differentiate these similar till units, our approach relied upon the till clast-fabrics coupled with till provenance data to determine the ice-flow direction at time of till deposition, and the dominant bedrock source regions of the sediment particles. This is an important distinction, because previous stratigraphic work in the western HBL did not define tills by ice-flow direction, but instead the ice-flow data was considered an attribute of the lithostratigraphic units. In some cases, that led to identified till units containing mismatched ice-flow indicators (e.g., Long Spruce till of Nielsen et al., 1986). To accurately construct a Quaternary stratigraphic framework in similar areas, the multi-parameter characterization of till units, using parameters such as clast fabric, colour, relative degree of compaction, clast lithology and till-matrix geochemistry, is necessary and an emphasis needs to be placed on collecting extensive ice-flow indicator datasets.

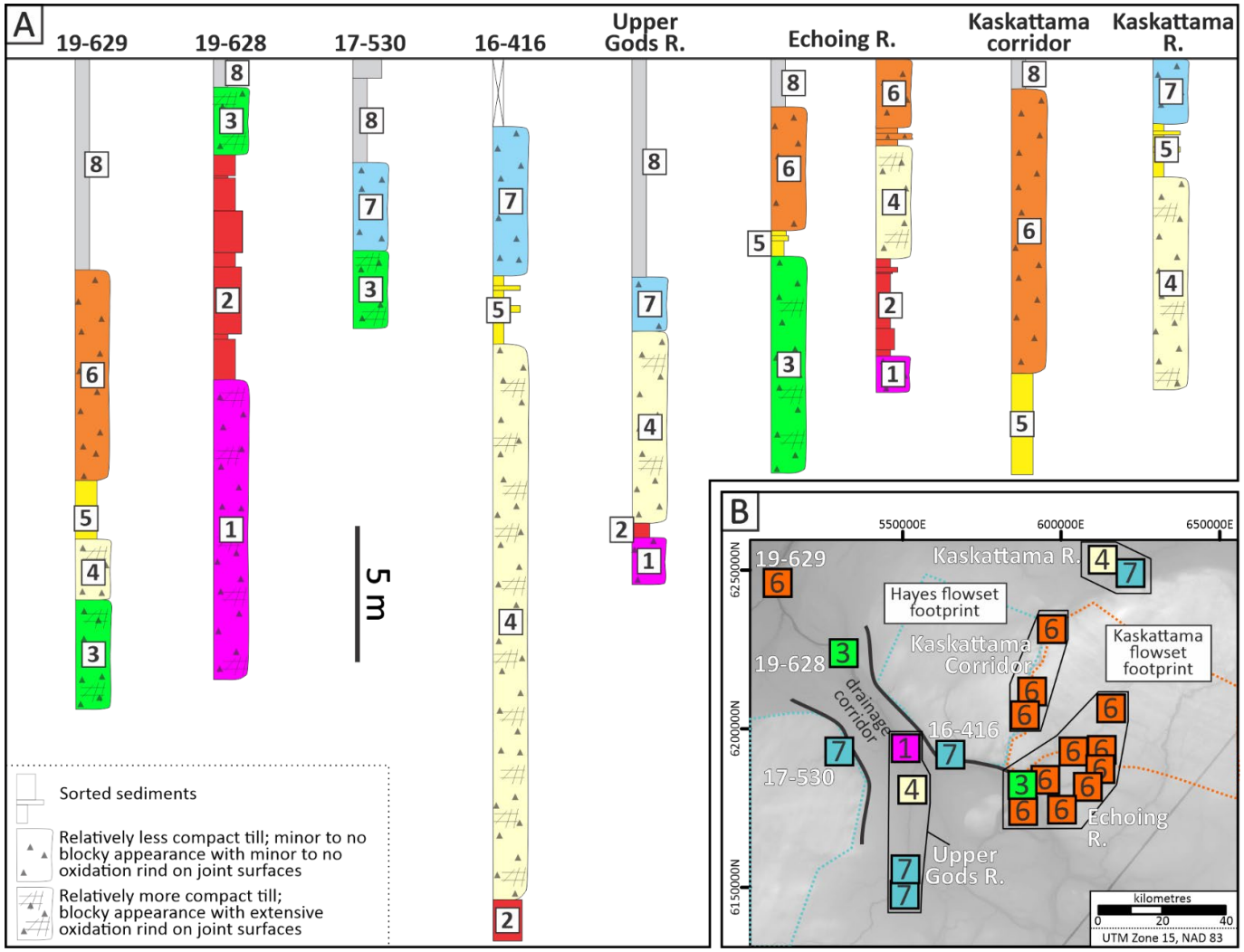

Figure 3.17: Summary of Quaternary stratigraphic relationships in the Kaskattama highland area: a) the stratigraphy at each local-scale site is shown highlighting the fragmented nature of the stratigraphic record. Note, some locations are a stratigraphic composite of multiple sections (compare with Figure 3-6); b) the uppermost till unit exposed at each section investigated is shown. Note, the location of a drainage corridor which has eroded up to 60 m of sediments from the stratigraphic record exposing relatively old till units overlain by post-glacial sediments.

Understanding the till stratigraphy is also a necessary step to establish the relative age of intertill sorted sediment units using an allostratigraphic approach. If we examine the current stratigraphic architecture of the study area, Holocene-aged postglacial sediments (Unit 8) overlie till correlated to five separate units deposited during at least three separate glaciations (Figure 3.17b). Age constraints on the intertill sediments (Unit 2 and 5) suggest that these tills were deposited during MIS 2–5, 6 and 8 or older (Figure 3.16). Previously, Unit 2 sediments at section 17-519 were interpreted to be MIS 5 in age (Dredge and McMartin 2011) based on the paleobotanical reconstructions that indicate deposition during an interglacial climate and because the interglacial bed was the first subtill occurrence of organic-bearing sediments. This new stratigraphic framework and optical age estimation suggests that these sediments were likely deposited during MIS 7 (191 ± 29 ka, MAM, 1σ (112-19-630-OSL025)]. This means that, as in other HBL stratigraphic studies, the uppermost sorted sediments underlying glacial sediments (till) may not have been deposited during the penultimate ice-free period (e.g., Dube-Loubert et al., 2013; Gauthier et al., *submitted*), and therefore cannot be used to 'anchor' a stratigraphic framework or used as 'marker' beds for correlating between stratigraphic observations.

It must be noted that the optical age estimations from Unit 2 and 5 slightly overlap at 1σ error (Table 3.3) and this reflects the difficulties in dating nonglacial deposits >100 ka. Nonetheless, this study has documented two distinct intertill nonglacial sorted sediment units separated by till(s) indicating a glacial event(s). The simplest interpretation based on our new Quaternary stratigraphic framework, existing age constraints and comparison to the marine oxygen isotope record is that Unit 2 was deposited during MIS 7 and Unit 5 was deposited during MIS 5–6. The age of intertill sorted sediment units presented in the stratigraphic framework herein can readily be tested as geochronology methods improve since unit correlations did not rely on the estimated ages determined.

3.6.2 Stratigraphic evidence for a preserved advance-phase streamlined-sediment-landform flowset

Using ice-flow data, till provenance and stratigraphic relationships we show that the enigmatic Kaskattama streamlined-landform flowset is a part of stratigraphic Unit 6 that extends off the

Kaskattama highland, and the flowset was formed by ice flowing towards the northwest (Figure 3.6g). At several sections investigated (e.g., 16-416 and 17-519), the stratigraphy indicates that this ice-flow event advanced over a fine-grained substrate and incorporated these sediments into the overlying till, including mud rip-up clasts. This ice-flow phase is currently interpreted as an advance-phase event because it requires an ice sheet configuration that is consistent with other reconstructions that put a Q-L ice divide east of James Bay in the early build-up phase and MIS 4 (e.g., Veillette et al., 1999). The timing of this ice-flow event is constrained by the optical age estimations of the underlying intertill sorted sediments (Unit 5) of 146 ± 20 ka [MAM, 1σ (112-19-629-024)] and 166 ± 12 ka [MAM, 1σ (112-16-407-019)]. A third optical age of 150 ± 22 ka [MAM, 1σ (112-19-605-004)] was determined from correlative subtill sediments at a site near the Manitoba-Ontario border (Hodder et al., 2023; Black Duck River site on Figure 3.1). Here, 1.4 m of till with a W-trending (273°) till fabric is underlain by massive silt and massive to horizontally-bedded fine-sand to silty fine-sand that contains disseminated organics (Hodder et al., 2023). These sediments were correlated to the Black Duck River Section of Dalton et al. (2016), where the pollen signature indicates deposition during climatic conditions similar to the current interglacial period (Dalton et al., 2022b). As such, Unit 6 till advanced over sorted sediments (Unit 5) interpreted to have been deposited during the MIS 5 interglacial period or MIS 6 deglaciation, and records an initial advance of ice emanating from the Q-L dome into the western HBL at the start of the last glacial cycle (Figure 3.16). This glacial advance likely occurred during MIS 4 or late MIS 5, based on global sea level considerations and modelling of the LIS (Stokes et al., 2012; Gowan et al., 2021) and other regional field-based studies (e.g., Veillette et al. 1999).

The presence of till and streamlined landforms at the surface, interpreted to have been deposited at the start of the most recent glaciation, implies that this region experienced extensive landscape preservation throughout the vast majority of the last glaciation, possibly under cold-based conditions, a phenomena observed in other inter-ice stream localities (Kleman et al., 1994; Hättestrand and Stroeven, 2002; Kleman and Glasser, 2007; Ross et al., 2009, 2011). The Kaskattama highland rises ~130 m above the flat-lying HBL and the highland is flanked by deglacial ice streams to the east (Winisk ice stream) and west (Hayes lobe). The interpretation of the Kaskattama flowset as

an advance-phase till supports the concept that the highland was likely a large inter-ice stream sticky spot during deglacial ice streaming in the region (Stokes et al., 2007; Gauthier et al., 2019). This work now conclusively shows that these fragmented landscape patches, or glacial terrain zones (c.f. Trommelen et al., 2012), can be of different ages and represent spatiotemporal variations within the subglacial bed mosaic (c.f. Gauthier et al., 2019) and that this needs to be considered when reconstructing the depositional record over multiple glacial cycles.

3.6.3 Repeated northwest-trending ice advances from the Quebec-Labrador dome

This study shows that two episodes of NW-trending ice-flow advanced over the study area at a similar trajectory during different glacial cycles (Unit 3 and Unit 6; Figure 3.16). This new stratigraphic framework places the oldest NW-trending ice-flow event at the start of MIS 6. Importantly, this framework is supported by regional-scale correlations in the western HBL (Gauthier et al., 2019) and recent stratigraphic observations in the Churchill River area (Hodder and Gauthier, 2023). Within the central HBL, a relatively old till deposited by NW-trending ice-flow referred to as the Rocksand Till is recognized (Thorleifson et al., 1992). The timing of deposition of the Rocksand Till was interpreted to be either at the start of last glacial cycle (late MIS 5) or MIS 6 glaciation and this interpretation was dependent on the accuracy of available thermoluminescence (TL) ages of overlying sediment at the time (Thorleifson et al., 1992). The TL ages incorporated by Thorleifson et al. (1992) from Manitoba are now interpreted as age underestimations and it is likely that these sediments were deposited during MIS 5 instead of MIS 3 based on new geochronology constraints (Hodder et al., 2023), therefore placing the Rocksand Till in MIS 6. This alternative framework presented in Thorleifson et al. (1992) would also re-assign the Missinaibi Formation, including the Bell Sea sediments, to the MIS 7 interglacial period. This reinterpretation has significant implications for the relative age framework proposed using amino acid racemization data for the HBL (Andrews et al., 1983), since this framework assumed the Bell Sea Sediments were deposited during MIS 5e. Furthermore, the Rocksand till is tentatively correlated to Unit 3 in the Kaskattama highland area based on stratigraphic position, clast fabric orientations and UGG clast content, which extends this northwesterly ice-flow event into the western HBL. Therefore, we suggest that this ice-flow event

should no longer be used to constrain the growth of the LIS during the last glacial cycle (e.g., Kleman et al., 2010; Dalton et al., 2022a), but instead is an important regional-scale ice-flow event to be considered in reconstructions of the MIS 6 glaciation.

3.6.3.1 Same ice-flow direction, different till provenance signature

Despite the similar ice-flow directions for Unit 3 and Unit 6, the provenance signature of the tills deposited by these ice-flow events is different and best exemplified by their till-matrix geochemistry (Figure 3.15b). Unit 6 till has a relatively high granitoid provenance signature compared to Unit 3, which is more calcareous. The nearest igneous and metamorphic rocks to the east/southeast are part of the Superior Province, which implies a higher proportion of more distally derived detritus within Unit 6 till. Interpreting the cause of the different provenance signature between these ice-flow events is difficult since the principles of overprinting and inheritance (e.g., Trommelen et al., 2013) need to be considered, as well as the overall evolution of sediment transport and deposition in the HBL. For example, one interpretation is that the Q-L dome was situated further to the east during deposition of Unit 6 relative to Unit 3, which would have led to increased erosion and transportation of detritus derived from the Superior Province into the western HBL. Alternatively, the Q-L dome could have been situated in the same position during these ice-flow events, but Unit 3 has a more local bedrock signature, possibly since it was deposited earlier in time when there was potentially more bedrock exposed or because it eroded a more Paleozoic-rich (local signature) till that was previously deposited. Relating these far-field observations to evolution of the Q-L dome are difficult without direct comparison to reconstructions from the core region of the Q-L dome, which are generally restricted to the erosional record and identified ice-flow events that are largely attributed to the last glacial cycle (e.g., Veillette et al., 1999).

3.7 Conclusion

This study constructed a stratigraphic framework for the Kaskattama highland region of the western HBL that consists of five glacial (till) units that were deposited across at least three separate glaciations along with three nonglacial (organic-bearing sorted sediments) units that were deposited during separate interglacial periods and supported by radiocarbon and optical age constraints. Importantly, we acknowledge that the stratigraphic record is highly fragmented, which is similarly expressed in the fragmented surficial streamlined landform record. To produce a stratigraphic framework in this geological setting a hybrid stratigraphic approach that incorporated principles of lithostratigraphy and allostratigraphy with an emphasis on supporting ice-flow datasets was incorporated. To determine the flow direction of ice (NW versus SE) that deposited till units, an extensive characterization of the sediment provenance was undertaken that included till-clast lithology counts, matrix geochemistry and detrital hornblende $^{40}Ar/^{39}Ar$ ages to provide a more robust bedrock provenance interpretation. The application of optical dating and paleobotanical analyses to interglacial units have provided important age and climatic brackets for the timing of glacial events. Nevertheless, more work needs to be done to assess the utility of optical dating of quartz from HBL (Hodder et al. 2023; Gauthier et al. submitted). This is especially so for samples, like the one discussed here, where calculated ages are greater than 150 ka. The magnitude of the optical ages requires extensive machine time, and therefore limits the number of ages that can be provided for any one unit. Nevertheless, dating of more samples at key units should be done to better understand both variations in luminescence signals and calculated ages, possibly alongside other geochronology methods.

This stratigraphic record provides important constraints to the growth of ice sheets and glacial dynamics within the interior region of North America. At the start of the last glaciation, NW-trending ice advanced into the western HBL and is currently exposed at surface (Kaskattama flowset). During late glacial streaming, this ‘patch’ of the subglacial bed deposited during the advance of the ice sheet was preserved as a large ‘sticky spot’ flanked laterally on both sides by ice streams. The existence of this patch requires extensive landscape preservation for the majority of the glaciation, implying persistent cold-based conditions. Interestingly, this study showed that there is an older

NW-trending ice-flow event in the stratigraphic record that also advanced over sorted sediments. This till unit is tentatively correlated to the Rocksand Till documented in the central HBL and recent geochronology studies now support this as a likely early MIS 6 ice-flow event. This indicates that the growth of the ice sheet during the start of the last two glaciations was likely similar with an accelerated growth of the Quebec–Labrador dome early in the glaciation relative to the Keewatin dome.

3.8 References

Andrews, J.T. and Smith, D.I. 1969. Statistical analysis of till fabric: methodology, local and regional variability (with particular reference to the north Yorkshire till cliffs). Quarterly Journal of the Geological Society 125(1-4), 503–542. DOI: 10.1144/gsjgs.125.1.0503.

Andrews, J.T., Shilts, W.W. and Miller, G.H. 1983. Multiple deglaciations of the Hudson Bay Lowlands, Canada, since deposition of the Missinaibi (last interglacial?) Formation. Quaternary Research 19, 18–37.

Batchelor, C.L., Margold, M., Krapp, M., Murton, D.K., Dalton, A.S., Gibbard, P.L., Stokes, C.R., Murton, J.B. and Manica, A., 2019. The configuration of Northern Hemisphere ice sheets through the Quaternary. Nature Communications 10:3713.

Benn, D.I. 1994. Fabric shape and the interpretation of sedimentary fabric data. Journal of Sedimentary Research 64, 910–915.

Bronac de Vazelhes, V., Beaudoin, G., McMartin, I., Côté-Mantha, O. and Boulianne-Verschelden, N. 2021. Assessment of the Amaruq gold deposit signature in glacial sediments using multivariate geochemical data analysis and indicator minerals. Journal of Geochemical Exploration 228, Article 106800.

Campbell, J.F.E., Fletcher, W.J., Hughes, P.D. and Shuttleworth, E.L. 2016. A comparison of pollen extraction methods confirms dense-media separation as a reliable method of pollen preparation. Journal of Quaternary Science 31, 631–640.

Catto, N.R. 1998. Comparative study of striations and basal till clast fabrics, Malpeque -Bedeque region, Prince Edward Island, Canada. Boreas 27, 259–274.

Chen, Y., Zhang, L., and Zhao, B. 2019. Identification of the anomaly component using BEMD combined with PCA from element concentrations in the Tengchong tin belt, SW China. Geoscience Frontiers 10 (4), 1561–1576.

Dalton, A.S., Dulfer, H., Margold, M., Heyman, J., Clague, J., Froese, D., Gauthier, M.S., Hughes, A.L.C., Jennings, C. E., Norris, S.L. and Stoker, B.J. 2023. Deglaciation of the North American Ice Sheet Complex in calendar years based on a new comprehensive database of chronological data: NADI-1. Quaternary Science Reviews 321, Article 108345.

Dalton, A.S., Finkelstein, S.A., Hodder, T.J. and Gauthier, M.S. 2022b. Palynological analyses of subtill sediments from four sites in the western Hudson Bay Lowland region (parts of NTS 53O; 54A, C, D). Manitoba Geological Survey Open File OF2022-1, 13 p.

Dalton, A.S., Finkelstein, S.A., Barnett, P.J. and Forman, S.L. 2016. Constraining the Late Pleistocene history of the Laurentide Ice Sheet by dating the Missinaibi Formation, Hudson Bay Lowlands, Canada. Quaternary Science Reviews 146, 288–299.

Dalton, A.S., Finkelstein, S.A., Hodder, T.J. and Gauthier, M.S. 2022b. Palynological analyses of subtill sediments from four sites in the western Hudson Bay Lowland region (parts of NTS 53O; 54A, C, D). Manitoba Geological Survey Open File OF2022-1, 13 p.

Dalton, A.S., Stokes, C.R. and Batchelor, C.L. 2022a. Evolution of the Laurentide and Innuitian ice sheets prior to the Last Glacial Maximum (115 ka to 25 ka). Earth Science Reviews 224, 103875.

Dalton, A.S., Väliranta, M., Barnett, P.J. and Finkelstein, S.A. 2017. Pollen and macrofossil-inferred paleoclimate at the Ridge Site, Hudson Bay Lowlands, Canada: Evidence for a dry climate and significant recession of the Laurentide Ice Sheet during Marine Isotope Stage 3. Boreas 46, 388-401.

Doornbos, C., Heaman, L.M., Doupé, J.P., England, J., Simonetti, A., and Lajeunesse, P. 2009. The first integrated use of in situ U–Pb geochronology and geochemical analyses to determine long-distance transport of glacial erratics from mainland Canada into the western Arctic Archipelago. Canadian Journal of Earth Sciences 46, 101–122.

Dredge, L.A. 1983: Character and development of northern Lake Agassiz and its relation to Keewatin and Hudsonian ice regimes; *in* Glacial Lake Agassiz, J.T. Teller and L. Clayton (eds.), Geological Association of Canada, Special Paper 26, 117–131.

Dredge, L.A. and Cowan, W.R. 1989. Quaternary geology of the southwestern Canadian Shield; *in* Quaternary Geology of Canada and Greenland. R.J. Fulton (ed.). Geological Survey of Canada, Geology of Canada Series, no 1, 214–248.

Dredge, L.A. and McMartin, I. 2011. Glacial stratigraphy of northern and central Manitoba, Geological Survey of Canada Bulletin 600, 27 p.

Dredge, L.A., Morgan, A.V. and Nielsen, E. 1990. Sangamon and pre-Sangamon interglaciations in the Hudson Bay Lowlands of Manitoba. Géographie Physique et Quaternaire 44 (3), 319–336.

Dube-Loubert, H., Roy, M., Allard, G. and Veillette, J.J. 2013: Glacial and nonglacial events in the eastern James Bay lowlands, Canada. Canadian Journal of Earth Sciences 50, 379–396.

Dyke, A.S. and Dredge, L.A. 1989. Quaternary geology of the northwestern Canadian Shield; *in* Quaternary Geology of Canada and Greenland. R.J. Fulton (ed.). Geological Survey of Canada, Geology of Canada Series, no 1, 189-214.

Dyke, A.S., Dredge, L.A. and Vincent, J.S. 1982. Configuration and dynamics of the Laurentide Ice Sheet during the Late Wisconsinan Maximum; Geographie physique et Quaternaire 36 (1-2), 5–14.

Evans 2018. Till: A glacial process sedimentology. Wiley-Blackwell, Chichester.

Evans, D.J.A. and Benn, D.I. 2021. A practical guide to the study of glacial sediments. 2nd edition. Quaternary Research Association, London.

Evans, D.J.A., Phillips, E.R., Hiemstra, J.F. and Auton, C.A. 2006. Subglacial till: Formation, sedimentary characteristics and classification. Earth Science Reviews 78, no. 1-2, 115–176.

Evans, D.J.A., Smith, I.R., Gosse, J.C. and Galloway, J.M. 2021. Glacial landforms and sediments (landsystem) of the Smoking Hills area, Northwest Territories, Canada: Implications for regional Pliocene – Pleistocene Laurentide Ice Sheet dynamics. Quaternary Science Reviews 262, Article 106958.

Evans, D.J.A., Roberts, D.H., Evans, S.C. 2016. Multiple subglacial till deposition: A modern exemplar for Quaternary palaeoglaciology. Quaternary Science Reviews 145, 183–203.

Evans, D.J.A., Roberts, D.H., Hiemstra, J.F., Nye, K.M., Wright, H., Steer, A. 2018. Submarginal debris transport and till formation in active temperate glacier systems: The southeast Iceland type locality. Quaternary Science Reviews 195, 72–108.

Faegri, K. and Iversen, J. 1975. Textbook of Pollen Analysis, 3rd Edition ed. Munksgaard, Copenhagen and Denmark.

Galbraith, R.F., Roberts, R.G., Laslett, G.M., Yoshida, H., Olley, J.M., 1999. Optical dating of single and multiple grains of quartz from Jinmium rock shelter, northern Australia: Part I, Experimental design and statistical models. Archaeometry 41, 339–364.

Gao, C., McAndrews, J.H., Wang, X., Menzies, J., Turton, C.L., Wood, B.D., Pei, J. and Kodors, C... 2012. Glaciation of North America in the James Bay Lowland, Canada, 3.5 Ma. Geology 40, 975–978.

Gauthier, M.S., Breckenridge, A. and Hodder, T.J. 2022. Patterns of ice recession and ice stream activity for the MIS 2 Laurentide Ice Sheet in Manitoba, Canada. Boreas 51 (2), 274–298, DOI:10.1111/bor.12571

Gauthier, M. S., Hodder, T. J., Ross, M., Kelley, S. E., Rochester, A. and McCausland, P. 2019. The subglacial mosaic of the Laurentide Ice Sheet; a study of the interior region of southwestern Hudson Bay. Quaternary Science Reviews 214, 1–27, DOI: 10.1016/j.quascirev.2019.04.015.

Gauthier, M.S., Kelley, S.E. and Hodder, T.J. 2020. Lake Agassiz drainage bracketed Holocene Hudson Bay Ice Saddle collapse; Earth and Planetary Science Letters, 544, DOI: 10.1016/j.epsl.2020.116372.

Gauthier, M.S., Breckenridge, A. and Hodder, T.J. 2022: Patterns of ice recession and ice stream activity for the MIS 2 Laurentide Ice Sheet in Manitoba, Canada Boreas 51 (2), 274–298.

Gauthier, M. S., Hodder, T. J., Dalton, A. S., Lian, O. B., Schaarschmidt, M., Ross, M. and Väliranta, M. *submitted*: Preservation of probable MIS 7 deglacial and nonglacial deposits near the edge of the Hudson Bay Lowland in Manitoba, Canada. Canadian Journal of Earth Sciences.

Gowan, E.J., Zhang, X., Khosravi, S., Rovere, A., Stocchi, P., Hughes, A.L.C., Gyllencreutz, R., Mangerud, J., Svendsen, J.-I. and Lohmann, G. 2021. A new global ice sheet reconstruction for the past 80 000 years. Nature Communications 12, 1199, DOI: 10.1038/s41467-021-21469-w.

Greenwood, S. L. and Clark, C. D. 2009. Reconstructing the last Irish Ice Sheet 1: changing flow geometries and ice flow dynamics deciphered from the glacial landform record. Quaternary Science Reviews 28, 3085–3100.

Grunsky, E. 2010. The interpretation of geochemical survey data. Geochemistry, Exploration, Environment, Analysis 10, 27–74.

Hättestrand, C. and Stroeven, A. 2002: A relict landscape in the centre of Fennoscandian glaciation: Geomorphological evidence of minimal Quaternary glacial erosion. Geomorphology 44, 127–143.

Heiri, O., Lotter, A. F. and Lemcke, G. 2001. Loss on ignition as a method for estimating organic and carbonate content in sediments: reproducibility and comparability of results. Journal of Paleolimnology 25 (1), 101–110.

Hemming, S.R. 2004. Heinrich events: massive late Pleistocene detritus layers of the North Atlantic and their global climate imprint. Review of Geophysics 42 (1), Paper number 2003RG000128, DOI: 10.1029/2003RG000128.

Hicock, S.R., Goff, J.R., Lian, O.B. and Little, E.C. 1996. On the interpretation of subglacial till fabric. Journal of Sedimentary Research 66 (5), 928–934.

Hodder, T.J., 2018. Till composition of the Kaskattama Kimberlite No. 1 drillcore, Kaskattama highland region, northeastern Manitoba (part of NTS 54B7); *in* Report of Activities 2018. Manitoba Growth Enterprise and Trade, Manitoba Geological Survey, pp. 166–174.

Hodder, T.J. and Gauthier, M.S. 2021. Quaternary stratigraphic and depth to bedrock data compilation for northeastern Manitoba; *in* Report of Activities 2021. Manitoba Agriculture and Resource Development, Manitoba Geological Survey, pp. 66–70.

Hodder, T.J. and Gauthier, M.S. 2023. Indicator mineral and gold grain data from till sampled in the Churchill to Little Churchill rivers area, northeastern Manitoba. Manitoba Economic Development, Investment and Trade, Manitoba Geological Survey Open File OF2023-1, 19 p.

Hodder, T.J., Gauthier, M.S., Kelley, S.E. and Ross, M. 2024. Quaternary site, till composition and ice-flow indicator datasets in the Kaskattama highland area, northeastern Manitoba (parts of NTS 53N, O, 54B, C). Manitoba Geological Survey Open File OF2024-1, 20 p.

Hodder, T.J., Gauthier, M.S., Ross, M., Lian, O. 2023. Was there a nonglacial episode in the western Hudson Bay Lowland during Marine Isotope Stage 3? Quaternary Research 116, 148–168, DOI: 10.1017/qua.2023.35

Hodder, T. J., Gauthier, M. S. and Nielsen, E. 2017. Quaternary stratigraphy and till composition along the Hayes, Gods, Nelson, Fox, Stupart, Yakaw, Angling and Pennycutaway rivers, northeast Manitoba (parts of NTS 53N, 54C, 54D, 54F). Manitoba Growth, Enterprise and Trade, Manitoba Geological Survey Open File OF2017-4, 20 p.

Hodder, T.J., Ross, M. and Menzies, J. 2016. Sedimentary record of ice divide migration and ice streams in the Keewatin core region of the Laurentide Ice Sheet. Sedimentary Geology 338, 97–114, DOI: 10.1016/j.sedgeo.2016.01.001.

Hoffman, P. H. 1989. Precambrian geology and tectonic history; *in* The Geology of North America—An Overview, edited by A. W. Bally and A. R. Palmer, Decade North Am. Geol., vol. A, pp. 447–512, Geological Society of America, Boulder, Colorado

Jackson, G.D. 2013. Geology, Belcher Islands, Nunavut. Geological Survey of Canada, Open File 4923, 149 p.

Jolliffe, I. T., and Cadima, J. 2016. Principal component analysis: A review and recent developments. Philosophical Transactions of the Royal Society A: Mathematical, Physical and Engineering Sciences 374: 20150202, DOI: 10.1098/rsta.2015.0202

Juggins, S., 2015. rioja: Analysis of Quaternary Science Data. R package version (0.9-5). <http://cran.r-project.org/package=rioja>

Juggins, S., Simpson, G. L. and Telford, R. J. 2015. Taxon selection using statistical learning techniques to improve transfer function prediction. The Holocene 25 (1), 130–136, DOI: 10.1177/095968361455638.

Kassab, C., Brickles, S., Licht, K., and Monaghan, G. 2017. Exploring the use of zircon geochronology as an indicator of Laurentide Ice Sheet till provenance, Indiana, USA. Quaternary Research, 88(3), 525-536, DOI:10.1017/qua.2017.71

Kitaba, I., and Nakagawa, T. 2017. Black ceramic spheres as marker grains for microfossil analyses, with improved chemical, physical, and optical properties. Quaternary International 455, 166–169.

Klassen, R.W. 1986: Surficial geology of north-central Manitoba. Geological Survey of Canada Memoir 419, 57 p.

Kleman, J. and Glasser, N. F. 2007. The subglacial thermal organization (STO) of ice sheets. Quaternary Science Reviews 26, 585–597.

Kleman, J., Borgström, I. and Hättestrand, C. 1994. Evidence for a relict glacial landscape in Quebec-Labrador. Palaeogeography, Palaeoclimatology, Palaeoecology, 111 (3-4), 217–228.

Kleman, J., Jansson, K.N., De Angelis, H., Stroeven, A., Hättestrand, C., Alm, G., Glasser, N.F., 2010. North American Ice Sheet build-up during the last glacial cycle, 115-21 kyr. Quaternary Science Reviews 29, 2036-2051.

Larsen, N.K. and Piotrowski, J.A. 2003. Fabric pattern in a basal till succession and its significance for reconstructing subglacial processes. Journal of Sedimentary Research 73 (5), 725–734, DOI: 10.1306/021303730725

Lian, O.B. and Hicock, S.R. 2000. Thermal conditions beneath parts of the last Cordilleran Ice Sheet near its centre as inferred from subglacial till, associated sediments, and bedrock. Quaternary International 68-71, 147–162.

Lipp, A.G., Roberts, G.G., Whittaker, A.C., Gowing, C.J.B., & Fernandes, V.M. 2021. Source region geochemistry from unmixing downstream sedimentary elemental compositions. Geochemistry, Geophysics, Geosystems 22, e2021GC009838, DOI: 10.1029/2021GC009838.

Lisiecki, L.E., Raymo, M.E., 2005. A Pliocene-Pleistocene stack of 57 globally distributed benthic d18O records. Paleoceanography 20, PA1003.

Manitoba Geological Survey 2022. Bedrock geology of Manitoba. Manitoba Geological Survey Open File OF2022-2, scale 1:1 000 000.

Margold, M., Stokes, C.R., and Clark, C.D., 2018. Reconciling records of ice streaming and ice margin retreat to produce a palaeogeographic reconstruction of the deglaciation of the Laurentide Ice Sheet. Quaternary Science Reviews 189, 1–30.

Mark, D.M. 1973. Analysis of axial orientation data, including till fabrics. Geological Society of America Bulletin 84, 1369–1374.

McAndrews, J.H., Berti, A.A. and Norris, G. 1973. Key to the Quaternary Pollen and Spores of the Great Lakes Region. Royal Ontario Museum, Toronto, Canada, 74 p.

McClenaghan, M.B., Spirito, W.A., Day, S.J.A., McCurdy, M.W., McNeil, R.J. and Adcock, S.W. 2022. Overview of surficial geochemistry and indicator mineral surveys and case studies from the Geological Survey of Canada's GEM Program. Geochemistry: Exploration, Environment, Analysis 22 (1), geochem2021-070, DOI: 10.1144/geochem2021-070.

McDonald, B.C. 1969. Glacial and interglacial stratigraphy, Hudson Bay Lowland; *in* Earth Science Symposium on Hudson Bay. P.J. Hood (ed.). Geological Survey of Canada Paper 68-83, p. 78–99.

McMartin, I., Godbout, P.-M., Campbell, J. E., Tremblay, T. and Behnia, P. 2021. A new map of glacigenic features and glacial landsystems in central mainland Nunavut, Canada. Boreas 50(1), 51–75, DOI: 10.1111/bor.12479

McMartin, I., Dredge, L.A., Grunksy, E., Pehrsson, S.J., 2016. Till Geochemistry in West-Central Manitoba: Interpretation of Provenance and Mineralization Based on Glacial History and Multivariate Data Analysis. Economic Geology 111, 1001–1020.

McMartin, I. and Henderson, P. 2004. Evidence from Keewatin (central Nunavut) for paleo-ice divide migration. Géographie physique et Quaternaire 58(2-3), 163–186.

McMartin, I. and Paulen, R.C. 2009. Ice-flow indicators and the importance of ice-flow mapping for drift prospecting; *in* Application of Till and Stream Sediment Heavy Mineral and Geochemical Methods to Mineral Exploration in Western and Northern Canada, R.C. Paulen and I. McMartin (ed.), Geological Association of Canada, GAC Short Course Notes 18, 15–34.

Mesich, N., Gauthier, M.S., Hodder, T.J., Hathaway, J., Schaarschmidt, M., Lian, O.B. and Ross, M. 2023. Quaternary stratigraphic investigations along the Gods and Yakaw rivers, northeastern Manitoba (parts of NTS 54C2, 7); *in* Report of Activities 2023. Manitoba Economic Development, Investment, Trade and Natural Resources, Manitoba Geological Survey, pp. 120–123.

Möller, P., Benediktsson, Í.Ö., Anjar, J., Bennike, O., Bernhardson, M., Funder, S., Håkansson, L.M., Lemdahl, G., Licciardi, J.M., Murray, A.S. and Seidenkrantz, M.-S., 2019. Glacial history and palaeo-environmental change of southern Taimyr Peninsula, Arctic Russia, during the Middle and Late Pleistocene. Earth-Science Reviews 196, Article 102832.

Murray, A.S., and Wintle, A.G. 2000. Luminescence dating of quartz using an improved single-aliquot regenerative-dose protocol. Radiation Measurements 32, 57–73.

Murray, A.S., and Wintle, A.G. 2003. The single aliquot regenerative dose protocol: potential for improvements in reliability. Radiation Measurements 37, 377–381.

Natural Resources Canada 2012: Canadian Digital Surface Model; Natural Resources Canada, URL <http://geogratis.gc.ca/api/en/nrcan-rncan/ess-sst/34f13db8-434b-4a37-ae38-03643433fbbb.html> [September 2015].

Netterville, J. A. 1974. Quaternary stratigraphy of the lower Gods River region, Hudson Bay lowlands, Manitoba. Master of Science thesis, The University of Calgary, Calgary, Alberta, Canada, 79 p.

Nielsen, E., Morgan, A.V., Morgan, A., Mott, R.J., Rutter, N.W. and Causse, C. 1986. Stratigraphy, paleoecology and glacial history of the Gillam area, Manitoba. Canadian Journal of Earth Sciences 23, 1641-1661.

Norris, S.L., Evans, D.J.A., Cofaigh, C.O., 2018. Geomorphology and till architecture of terrestrial palaeo-ice streams of the southwest Laurentide Ice Sheet: A borehole stratigraphic approach. Quaternary Science Reviews 186, 186-214.

North American Commission on Stratigraphic Nomenclature 2021. Stratigraphy 18 (3), 153–204.

Overpeck, J.T., Webb, T. and Prentice, I.C. 1985. Quantitative Interpretation of Fossil Pollen Spectra: Dissimilarity Coefficients and the Method of Modern Analogs. Quaternary Research 23, 87–108.

Prest, V.K., 1990. Laurentide Ice-Flow Patterns: A Historical Review, and Implications of the Dispersal of Belcher Islands Erratics. Géographie physique et Quaternaire 44, 113–136.

Prest, V.K., Donaldson, J.A., Mooers, H.D., 2000. The Omar story: The role of Omars in assessing glacial history of west-central North America. Géographie Physique et Quaternaire 54, 257–270.

Rainbird, R.H., Hadlari, T., Aspler, L.B., Donaldson, J.A., LeCheminant, A.N., Peterson, T.D. 2003. Sequence stratigraphy and evolution of the Paleoproterozoic intracontinental Baker Lake and Thelon basins, western Churchill Province, Nunavut, Canada. Precambrian Research 125, 21–53.

Rice, J.M., Ross, M., Paulen, R.C., Kelley, S.E., Briner, J.P., Neudorf, C.A. and Lian, O.B. 2019. Refining the ice flow chronology and subglacial dynamics across the migrating Labrador Divide of the Laurentide Ice Sheet with age constraints on deglaciation. Journal of Quaternary Science 34 (7), 519–535.

Rice, J.M., Ross, M., Campbell, H.E., Paulen, R.C., McClenaghan, M.B. 2024. Net evolution of subglacial sediment transport in the Quebec–Labrador sector of the Laurentide Ice Sheet. Canadian Journal of Earth Sciences 61, 524–542.

Ross, M., Campbell, J.E., Parent, M., Adams, R.S., 2009. Paleo-ice streams and the subglacial landscape mosaic of the North American mid-continental prairies. Boreas 38, 421–439.

Ross, M., Lajeunesse, P., Kosar, K., 2011. The subglacial record of northern Hudson Bay: insights into the Hudson Strait Ice Stream catchment. Boreas 40, 73–91.

Roy, M. 1998. Pleistocene stratigraphy of the lower Nelson River area—implications for the evolution of the Hudson Bay lowland of Manitoba, Canada. Master of Science thesis, University of Quebec, Montreal, Canada, 220 p.

Roy, M., Clark, P.U., Duncan, R.A. and Hemming, S.R. 2007a. Insights into the late Cenozoic configuration of the Laurentide Ice Sheet from $^{40}Ar/^{39}Ar$ dating of glacially transported minerals in midcontinent tills. Geochemistry, Geophysics, Geosystems 8 (9), DOI: 10.1029/2006GC001572.

Roy, M., van de Flierdt, T., Hemming, S.R. and Goldstein, S.L. 2007b. $^{40}Ar/^{39}Ar$ ages of hornblende grains and bulk Sm/Nd isotopes of circum-Antarctic glacio-marine sediments: Implications for sediment provenance in the Southern Ocean. Chemical Geology 244, 507–519.

Saarnisto, M. and Peltoniemi, H. 1984. Glacial stratigraphy and compositional properties of till in Kainuu, eastern Finland. Fennia–- International Journal of Geography, 162(2).

Schaen, A.J., Jicha, B.R., Hodges, K.V., Vermeesch, P., Stelten, M.E., Mercer, C.M., et al. 2021. Interpreting and reporting $^{40}Ar/^{39}Ar$ geochronologic data. GSA Bulletin, 133 (3-4), 461–487.

Shilts, W.W. 1980. Flow patterns in the central North American ice sheet. Nature 286, 213–218.

Shilts, W.W. 1984. Quaternary Events – Hudson Bay Lowland and southern District of Keewatin; *in*: Quaternary stratigraphy of Canada – a Canadian contribution to IGCP project 24. Fulton, R.J. (Ed.), Geological Survey of Canada Paper 84-10, pp. 117–126.

Stokes, C.R., Clark, C.D., Lian, O.B., Tulaczyk, S. 2007. Ice stream sticky spots: A review of their identification and influence beneath contemporary and palaeo-ice streams. Earth Science Reviews 81, 217–249.

Stokes, C.R., Lian, O.B., Tulaczyk, S, and Clark, C.D. 2008. Superimposition of ribbed moraines on a palaeo-ice stream bed: implications for ice stream dynamics and shutdown. Earth Surface Processes and Landforms, 33: 593-609.

Stokes, C. R., Tarasov, L., Dyke, A. S. 2012. Dynamics of the North American Ice Sheet Complex during its inception and build-up to the Last Glacial Maximum. Quaternary Science Reviews 50, 86–104.

Stott, G.M., Buse, S., Davis, D.W. and Hamilton, M.A. 2010. The Sutton inliers—a Paleoproterozoic succession in the Hudson Bay Lowland; in Summary of Field Work and Other Activities 2010, Ontario Geological Survey, Open File Report 6260, 19-1–19-14.

Thorleifson, L.H., Wyatt, P.H., Shilts, W.W. and Nielsen, E. 1992. Hudson Bay Lowland Quaternary Stratigraphy: evidence for early Wisconsinan glaciation centred in Quebec. Geological Society of America Special Papers 270, 207–222.

Thorleifson, L. H., Wyatt, P. H. and Warman, T. A. 1993: Quaternary stratigraphy of the Severn and Winisk drainage basins, northern Ontario, Geological Survey of Canada, Bulletin 442, 65 p.

Trommelen, M.S., Ross, M. and Campbell, J.E. 2012: Glacial terrain zone analysis of a fragmented paleoglaciological record, southeast Keewatin sector of the Laurentide Ice Sheet. Quaternary Science Reviews 40, 1–20.

Trommelen, M.S., Ross, M., Campbell, J.E., 2013. Inherited clast dispersal patterns: implications for paleoglaciology of the southeast Keewatin Sector of the Laurentide Ice Sheet. Boreas 42, 693-713.

United States Geological Survey 2014: USGS EROS archive – digital elevation – Shuttle Radar Topography Mission (SRTM) 1 arc-second global. U.S. Geological Survey, 30 m cell, zipped hgt format; <https://doi.org/10.5066/F7PR7TFT [data files for 30 m cell data available on the Web] >, [September 2020].

Veillette, J.J. 2004. Ice-flow chronology and palimpsest, long-distance dispersal of indicator clasts, north of the St. Lawrence River valley, Quebec. Géographie physique et Quaternaire 58(2-3), 187–216.

Veillette, J.J., Dyke, A.S. and Roy, M. 1999. Ice-flow evolution of the Labrador Sector of the Laurentide Ice Sheet: a review, with new evidence from northern Quebec. Quaternary Science Reviews 18, 993–1019.

Wheeler, J.O., Hoffman, P.F., Card, K.D., Davidson, A., Sanford, B.V., Okulitch, A.V. and Roest, W.R. 1996. Geological Map of Canada, Geological Survey of Canada Map 1860A, DOI: 10.4095/208175.

Whitmore, J., Gajewski, K., Sawada, M., Williams, J.W., Shuman, B., Bartlein, P.J., Minckley, T., Viau, A.E., Webb III, T., Anderson, P.M. and Brubaker, L.B. 2005. North American and Greenland modern pollen data for multi-scale paleoecological and paleoclimatic applications. Quaternary Science Reviews 24, 1828–1848, DOI: 10.1016/j.quascirev.2005.03.005.

Zabenskie, S. 2006. Postglacial Climatic Change on Boothia Peninsula, Nunavut, Canada. Master of Science thesis, University of Ottawa, Ottawa, Ontario, Canada, 98 p.

Chapter 4

Laurentide Ice Sheet dynamics across multiple glacial-interglacial cycles from Quaternary stratigraphic records in central Canada

4.1 Overview

Quaternary terrestrial stratigraphic records are key to understanding the long-term behaviour of past ice sheets beyond the most recent glaciation. Glacial sediments provide important information on ice-flow direction and dispersal patterns, while intertill organic-bearing sediments provide insight into climatic conditions during past ice-free periods. The Hudson Bay Lowland (HBL) is situated near the geographic centre of glaciated North America and contains amongst the best preserved and laterally extensive Quaternary stratigraphic successions that were deposited over at least three glacial-interglacial cycles. This unique geological setting that contains an extensive pre-last glacial maximum geological record is ideal for understanding the growth of and decay of the Laurentide Ice Sheet and assessing the relative size of the Keewatin and Quebec-Labrador domes. Here, we investigate a remote region of the western HBL and construct the first stratigraphic framework of the region using a hybrid lithostratigraphic-allostratigraphic approach. The stratigraphic framework consists of Holocene-aged sediments that are underlain by nine glacial (till) units, three proglacial units and three interglacial units. Stratigraphic and geochronologic constraints indicate that the study area was likely inundated by marine waters following terminations II (~130 ka) and III (~243 ka) and both of these marine incursions reached a greater elevation compared to the Holocene (Termination I) marine limit in the region. These marine inundations were then followed by fluvial and/or lacustrine deposition during interglacials. The glacial record indicates a predominance of ice-flowing from the Quebec-Labrador dome and/or from a dome situated in Hudson Bay during glaciations. This field-base record is important for constraining the long-term behaviour of the LIS and provides important limits for ice-sheet modelling of North American glaciations.

4.2 Introduction

The Quaternary Period (last 2.58 Ma) is characterized by repeated growth and decay of large continental ice sheets, which had a direct impact on global sea level (Lisiecki and Raymo, 2005; Ehlers and Gibbard, 2007). In particular, the Laurentide Ice Sheet (LIS) over North America was likely responsible for most of the sea level fluctuations during the Late Pleistocene (129–11.7 ka; Gowan et al., 2021). Despite the importance of the LIS on global ice volume and reciprocal sea level fluctuations, the long-term evolution of this ice sheet prior to the last glacial maximum (LGM), defined by Greenland Stadial 3 (27.3–23.4 ka; Hughes and Gibbard, 2015), remains poorly-constrained by field-based data with limited stratigraphic or chronological supporting evidence in central Canada (Batchelor et al., 2019; Dalton et al., 2022). A particular concern is that reconstructions prior to the Late Pleistocene are, by necessity, heavily reliant on data and inferences from the most recent glaciation (e.g., Batchelor et al., 2019) and it is unclear if these comparisons are reasonable since LIS dynamics during this glaciation appear to be unique. For example, the last glaciation was likely the first time that glaciers crossed into southwestern Alberta and coalesced with the Cordilleran Ice sheet (Young et al., 1994). Furthermore, there appears to be significant variations in glaciations globally during the middle Pleistocene, which reinforces the importance of terrestrial stratigraphic records for understanding continental glaciations (Gibbard and Hughes, 2021). A better understanding of key regions with thick Quaternary sediments that extend beyond the most recent glaciation are essential to advance pre-LGM reconstructions of the LIS.

The western Hudson Bay Lowland (HBL) is one of these key regions, containing a stratigraphic record that spans at least the last three glacial-interglacial cycles (Nielsen et al., 1986; Dredge and McMartin, 2011; Hodder et al., 2024; Gauthier et al., 2025). At the LGM, the western HBL was situated at the geographic centre of the LIS and significantly closer to the position of the Keewatin dome (~700 km) compared to the Quebec-Labrador (Q-L) dome (~1 600 km; Dalton et al., 2023; Figure 4.1b). Interestingly, field-based research confirms that ice first advanced into the western HBL from the more distant eastern dome (Q-L) at the start of the last glacial cycle (Hodder et al., 2024). However, the magnitude of this initial Late Pleistocene glaciation is unknown, and even less is known about the MIS 6 ice-sheet growth in central Canada, which is also interpreted to have

emanated from the Q-L dome during initial ice-sheet growth (Gauthier et al., 2019; Hodder et al., 2024). To test the limit of these ice advances and further our understanding of LIS dynamics beyond the LGM, the Quaternary stratigraphic record along the Churchill and Little Churchill rivers of central Canada (herein referred to as the study area) was investigated (Figure 4.1A).

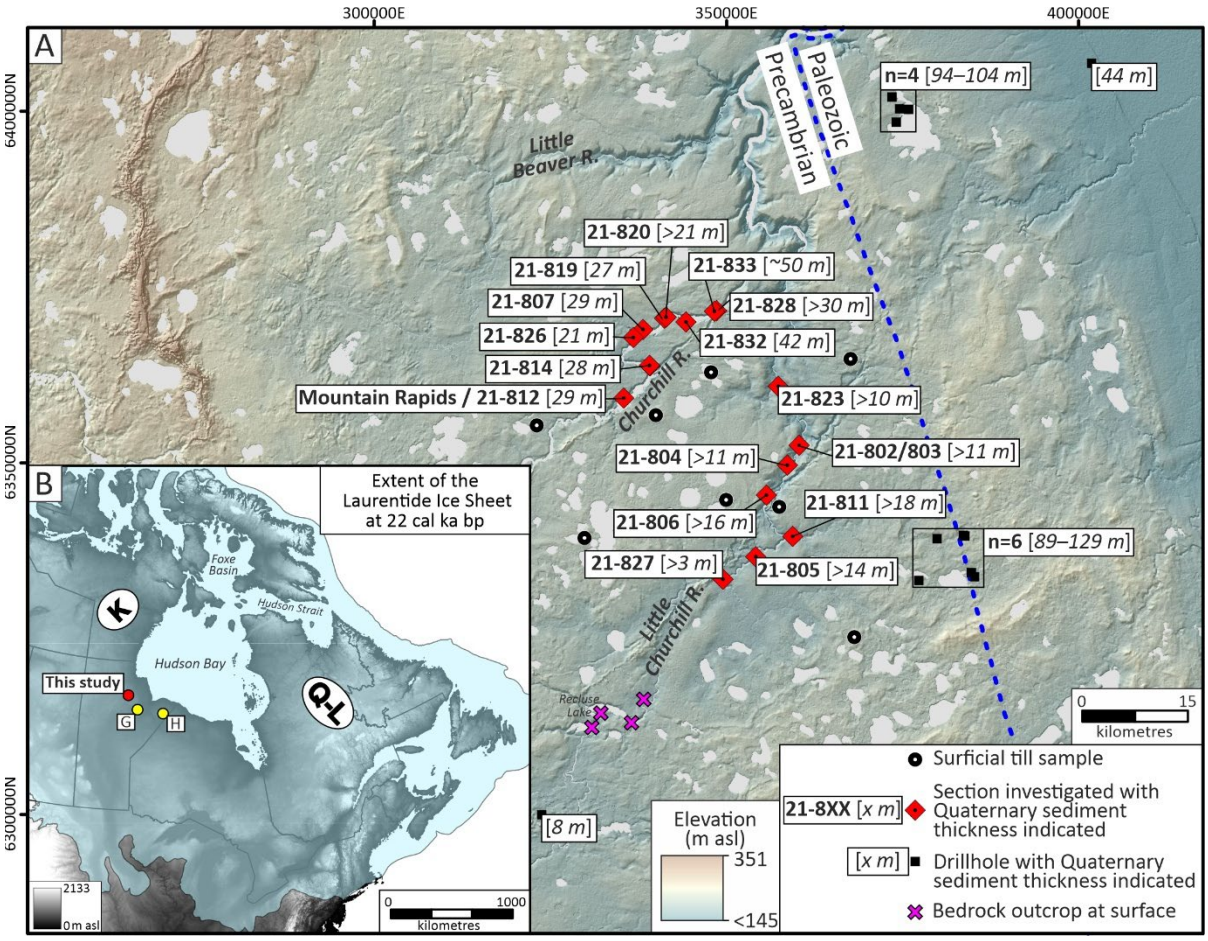

Figure 4.1: Location of the study area in the Churchill to Little Churchill rivers region of western Hudson Bay Lowland, Canada: A) sections and surficial stations visited and measurements of depth to bedrock where available; and B) location of the study area (red circle) in context to the reconstructed Laurentide ice sheet at 22 cal ka bp, with the interpreted location of the Keewatin (K) and Quebec-Labrador (Q-L) domes of the Laurentide Ice Sheet during MIS 2 deglaciation (Dalton et al., 2023). Quaternary stratigraphic studies discussed in the text are shown by the yellow circle: G, Gillam (Nielsen et al., 1986; Gauthier et al., 2025) and H, Kaskattama highland (Hodder et al., 2024). Background hillshade image was generated using Canadian Digital Surface Model (Natural Resources Canada, 2012). Coordinates in A) are in a UTM Zone 15N projection using NAD83 Datum.

The study area has undergone little geological study, despite initial exploration of the area by Bell (1880) who noted the thick bluffs of Quaternary sediments exposed along the rivers. Dredge and Nixon (1992) investigated one section on the Churchill River and three sections on the Little Churchill River. The Churchill River section, named Mountain Rapids (Figure 4.1a), contains two intertill sorted sediment beds and four till units (Dredge and Nielsen, 1985; Dredge et al., 1990; Dredge and Nixon, 1992; Dredge and McMartin, 2011). The uppermost intertill sorted sediment unit contains detrital wood with a nonfinite age (>32 ^{14}C ka BP, GSC-3074) and small peat balls (Dredge et al., 1990). Detrital organic nodules, peaty fragments and diamictic inclusions from this bed contained different fossil pollen assemblages; however, the assemblages are all associated with northern boreal to tundra environments (Dredge et al., 1990). The lowermost intertill sorted sediments contain planar- to cross-bedded sand and gravel beds that indicate a paleo-current towards the east. A paleo-current towards the east implies that the paleo-Churchill River was draining toward Hudson Bay, which can only happen after full deglaciation of the region and subsequent isostatic uplift to conditions similar to today; hence, these sediments were interpreted to have been deposited during an interglacial episode (Dredge et al., 1990). Interestingly, the tills are all calcareous and contain shell fragments despite the site being situated on the Precambrian Shield, which suggested an eastern till provenance (Dredge et al., 1990). Despite the nonfinite wood radiocarbon age and stratigraphic position situated ~10 m above the lowermost interglacial bed, the uppermost intertill sorted sediments were interpreted to have not been deposited during an interglacial period (Dredge et al., 1990). This study provides a glimpse into the exceptional stratigraphic record of the study area, yet elicits many questions, such as how many interglacial periods are preserved in the stratigraphic record? If all the tills have an eastern provenance, then what does this imply about long-term behavior of the LIS?

To provide insight into these important questions, this study produces the first Quaternary stratigraphic framework for the region and discusses the implications of this record for understanding long-term glacial dynamics of the LIS and climatic conditions during past interglacial periods. We first outline our methodology, which includes field sampling strategies, laboratory analyses and statistical approach. To aid in the organization of this thesis chapter, we then present

the results and interpretation under the same heading. We then explore the implications of this work in the “Discussion”.

4.3 Regional setting

The known thickness of Quaternary sediments in the region is highly variable (0–129 m; Figure 4.1). Sediments are exposed along deeply-incised fluvial valleys resulting from glacioisostatic adjustment. Sections investigated on the Churchill River are 21–50 m thick and expose Quaternary sediment and bedrock at the base of sections investigated, or bedrock outcrops in the river nearby. Sections investigated on the Little Churchill River expose 3–18 m of Quaternary sediment and no exposures of bedrock were observed from the ground or air.

4.3.1 Bedrock geology and clast provenance

The buried boundary between the Precambrian bedrock and Paleozoic bedrock of the Hudson Bay Basin (HBB) is situated 17–39 km to the east of sections investigated as part of this study (Figure 4.1; Figure 4.2a). The HBB of northeastern Manitoba is composed predominantly of carbonate (limestone or dolostone) rocks (Manitoba Geological Survey, 2024). There are no distinctive characteristics within the carbonate rocks of the HBB that allow individual formations to be identified within clast counts; however, since the study area is underlain by Precambrian bedrock, any detritus derived from the HBB had to be transported towards the west, southwest or northwest into the study area at some point in time (Figure 4.2). The Precambrian bedrock directly underlying the study area is granite of the Chipewyan-Wathaman Batholith that formed during the Trans-Hudson orogen (Martins et al., 2022). There is a background concentration (~10%) of granitoid clasts within till sampled across the HBL, as first noted by Shilts (1980). Hence, they are not an effective indicator to delineate dispersal patterns at low concentrations. However, the proportion of granitoid clasts relative to HBB clasts can be used as one parameter to effectively differentiate the ice-flow direction that deposited tills. Second, the proportion of undifferentiated greenstone and greywacke (UGG) clasts within till can be used as one parameter to delineate a distal eastern provenance (Shilts, 1980). The primary source of UGG clasts (indiscriminate fine-grained, dark grey rock fragments) is the Belcher Group that is situated a minimum of 900 km to the east, or Sutton inliers

that are situated a minimum of 700 km to the southeast (Shilts, 1980; Thorleifson et al., 1993; Hodder et al., 2024). The nearest greenstone belt to the study area is within the North Knife to Seal River area, ≥100 km to the north-northwest (Manitoba Geological Survey, 2024). Based on regional dispersal patterns, UGG clasts are not sourced from there (Gauthier et al., 2019). As such, tills with elevated proportions of UGG clasts are interpreted to have been derived from the east and deposited by ice flowing from the Q-L sector of LIS across the HBL. Distinctive erratics encountered in northeastern Manitoba include both northwestern- and eastern-sourced lithologies. Distinct northwestern erratics have been transported towards the southeast over 700 km from the Dubawnt Supergroup (Rainbird, 2003; Figure 4.2a). Examples include transported clasts of the Pitz Formation (purple to mauve-coloured volcanic rocks with distinctive chalky sanidine phenocrysts; Figure 4.2d) and Christopher Island Formation (red volcanic rocks with phlogopite phenocrysts). Erratics of eastern provenance have been transported a minimum of 900 km from the Belcher Group located in southeastern Hudson Bay (Jackson, 2013; McDonald and Partin, 2024; Figure 4.2a). Clasts from the Belcher Group include greywacke with hemispherical calcareous concretions (Figure 4.2b) that are sourced from the Omarolluk Formation (‘Omars’; Prest, 1990; Prest et al., 2000), porphyritic rocks that are sourced from Eskimo and Flaherty formations and granular iron formation derived from the Kipalu Formation (e.g., McDonald and Partin, 2024). Granular iron formation clasts can also be sourced from the Sutton Inlier (Figure 4.2a) situated 700 km to the southeast (Stott et al., 2010).

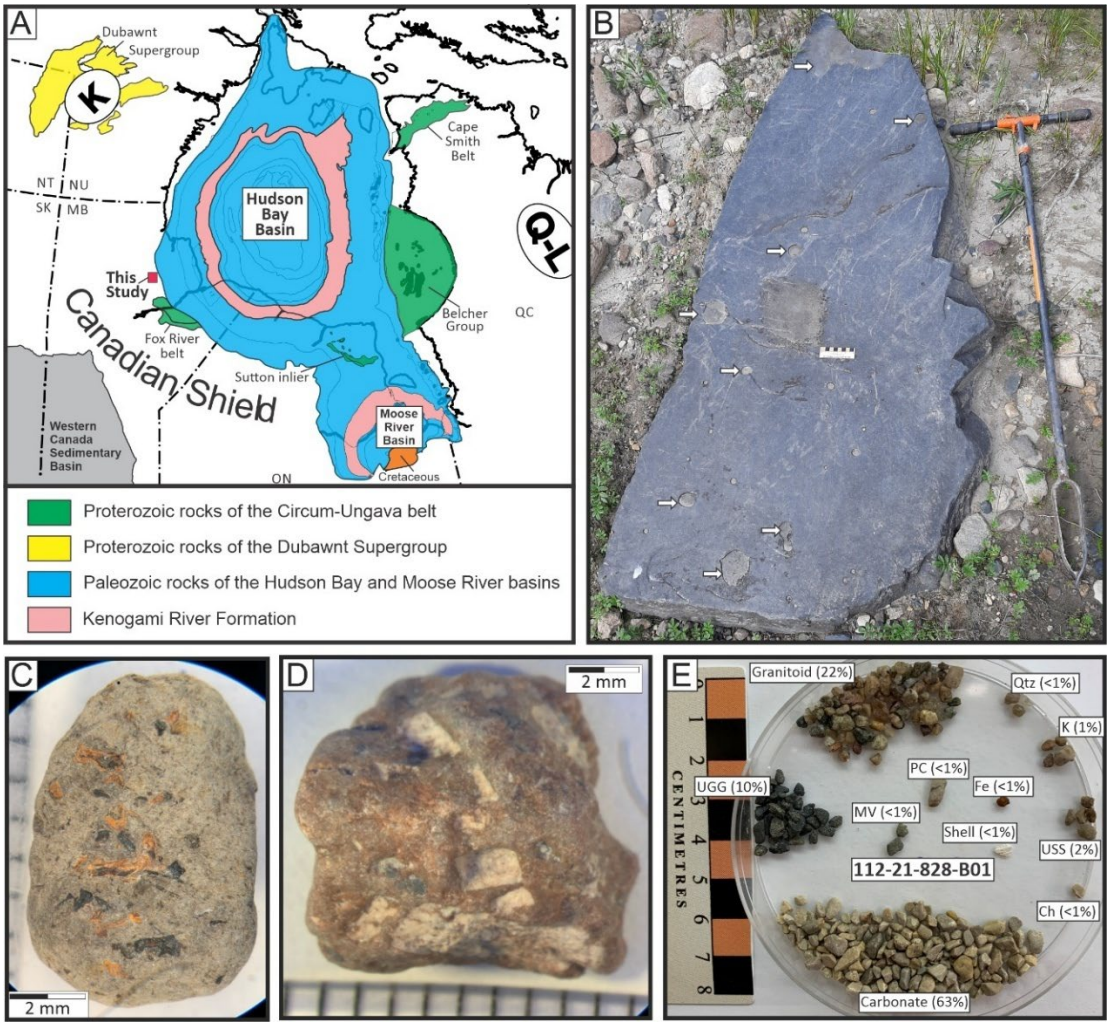

Figure 4.2: Simplified bedrock geology of central Canada with examples of distinct erratics observed and a clast-lithology count: A) bedrock geology modified from Wheeler et al. (1996). The location of the Keewatin (K) and Quebec-Labrador domes of the Laurentide ice sheet is their position during MIS 2 deglaciation from Dalton et al. (2023); B) example of an Omarolluk Formation boulder observed along the shoreline of the Little Churchill River with some concretions highlighted by the white arrows. The Dutch auger shown is 1.2 m in length; C) pebble-sized example of a grey siltstone clast with fish scales recovered from a black-coloured till at section 21-833; D) pebble-sized example of the Pitz Formation of the Dubawnt Supergroup recovered from Unit 8 till (sample 112-21-805-F02); and E) example of clast lithologies in the 2–4 mm size fraction of Unit 13 till (sample 112-21-828-B01). Abbreviations: UGG, undifferentiated greywacke and greenstone; MV, metavolcanic; Qtz, quartz; K, fine-grained light green to red sandstone and siltstone interpreted to be sourced from the Kenogami River Formation; PC, pink carbonate interpreted to be sourced from the Kenogami River Formation; Fe, ironstone; USS, undifferentiated siltstone and sandstone; Ch, chert.

4.4 Methods

4.4.1 Field data

To investigate the Quaternary stratigraphy of the study area, helicopter-supported fieldwork was undertaken in 2021. Surficial sediments were described from hand-excavated pits and/or using a Dutch auger, while sub-surface sediments were described from natural sections exposed along rivers or creeks. Sections were first cleared to remove colluvium, then the in-situ sediments were described over a 1–2 m wide interval based on their texture, colour, relative consolidation, clast content, sedimentary structure and nature of contacts. The degree of diamicton consolidation was determined qualitatively based on relative observations between beds and is used to differentiate between overconsolidated and highly overconsolidated diamicton (e.g., Figure 4.3). Overconsolidated diamicton beds do not have a blocky appearance, or they have a minor blocky appearance with no or minor oxidation rind developed on joint surfaces (Figure 4.3a), whereas highly overconsolidated and indurated diamicton have a blocky appearance with moderate to extensive oxidation rind developed on joint surfaces (Figure 4.3b). Thick colluvium inhibited a thorough assessment of the lateral continuity of most identified beds. At sections, till samples were collected above and below all facies changes in the field (colour, texture or relative consolidation) and every 1–5 m when visible stratigraphic changes could not be observed. Till-matrix colour was determined with moist subsamples under standard laboratory light conditions post-fieldwork and is expressed using standard Munsell colours (Munsell Color–X-Rite, 2015). Stratigraphic observations are summarized on stratigraphic columns herein and detailed stratigraphic descriptions, sediment photos and datasets are available in Hodder and Gauthier (2025). Lithofacies codes modified from Möller et al. (2019b) are used to simplify certain figures; a key to these codes is provided in Appendix C, Supplemental material 1, Table S1-1.

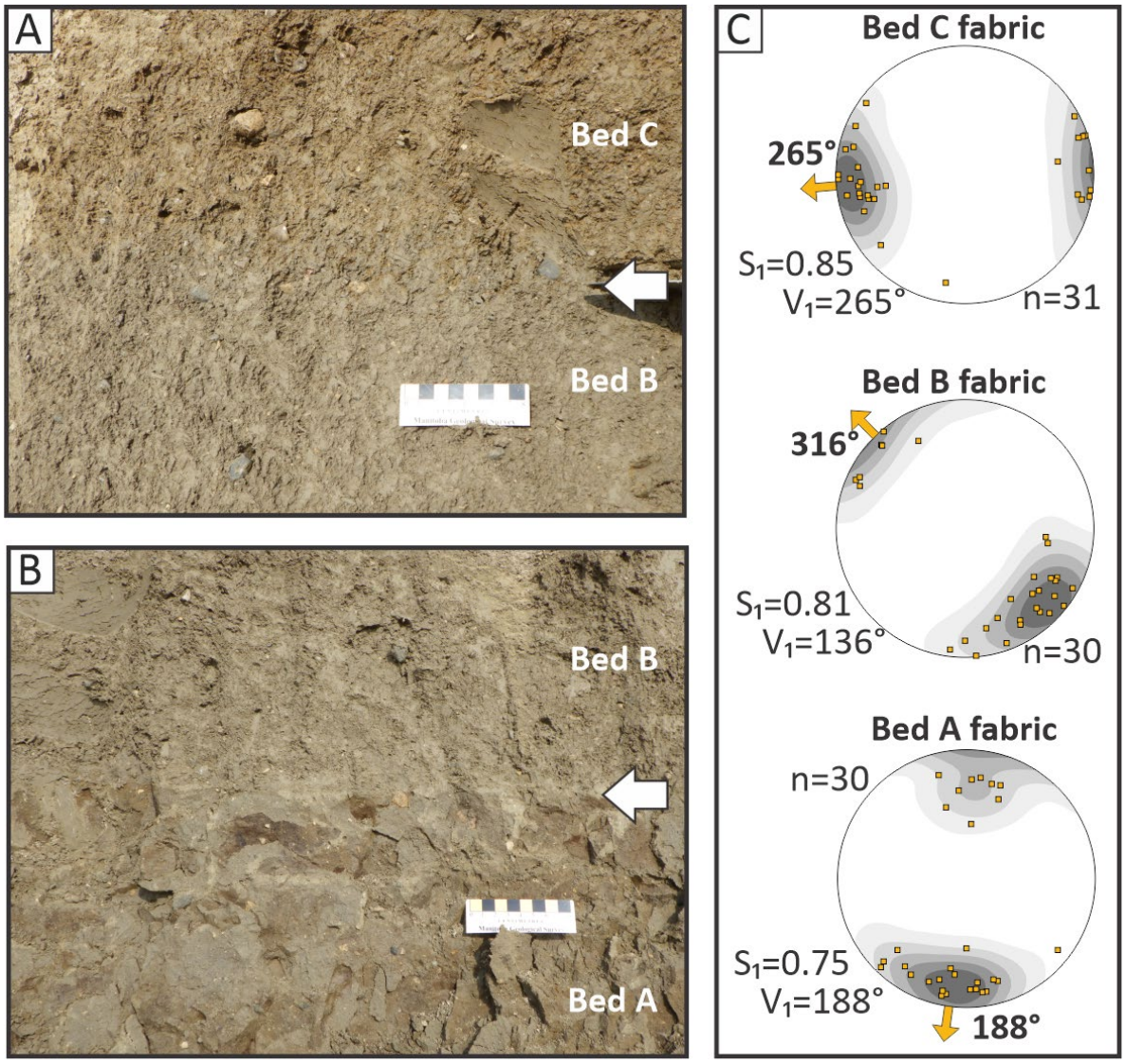

Figure 4.3: Example of field till-till contacts observed and associated till fabrics at section 21-805: A) example of a till-till contact between two overconsolidated diamicton beds that is defined by a sharp change in matrix colour; B) example of a till-till contact between an overconsolidated diamicton (Bed B) and a highly overconsolidated diamicton (Bed A) where the contact is defined by the relative change in consolidation observed; C) till fabrics from each associated bed that supports the interpretations that these beds were deposited by different ice-flow events.

Identified till beds were further investigated to determine ice-flow direction during till deposition. Ice-flow indicators measured include clast fabrics and the orientation of parallel striations on the upper surfaces of in-situ, lodged, cobble- to boulder-sized clasts, which are considered a good indicator of paleo-ice flow direction (McMartin and Paulen, 2009). Clast fabrics provide information on the preferred orientation of elongated clasts, which often gives direction of shear during till deposition, which in turns provides insights into paleo-ice flow direction (e.g., Hicock et al., 1996; Lian and Hicock, 2000). Attaining this preferred orientation was the sole reason for measuring clast fabrics. Clast-fabrics measurements were conducted on three vertical faces of a 'box' carved into the section. At each fabric site, the trend and plunge of 28–40 clasts (average of 31 clasts) were measured where the a:b axis ratio was >1.5, and the a- and b-axis plunge was <60°. A non-magnetic knitting needle was used to extrapolate the plunge of the a-axis out of the till face, allowing for increased accuracy of measurements. Clasts that were in contact with other clasts or smaller clasts that were adjacent to larger clasts, which could restrict rotation of clasts (Andrews and Smith, 1969), were not measured. A total of 73 stratigraphic ice-flow indicators were measured (64 clast fabrics and 9 lodged clasts) and at least one ice-flow indicator was obtained for each identified till bed. The eigenvectors and eigenvalues for each clast fabric were calculated (Mark, 1973; Benn, 1994) and the data was plotted on equal area, lower hemisphere projection stereonets using Rockware StereoStat V1.6.1. All ice-flow-orientation interpretations were initially considered bi-directional, since the imbrication of clasts up-ice is not consistent (Andrews and Smith, 1969; Saarnisto and Peltoniemi, 1984; Larsen and Piotrowski, 2003; Gauthier et al., 2019). In these cases, the provenance of the till needs to be considered to determine the ice-flow direction (Catto, 1998). Till beds observed in the study area are generally massive and no glaciotectonic structures were observed that could support or contradict ice-flow interpretations.

4.4.2 Till provenance

Northeastern Manitoba has been over-ridden by ice sheets moving in a wide range of direction ranging from northeast to north-northwest (045–340°; Gauthier et al., 2019). Thus, to differentiate the direction that deposited tills with measured northwest-southeast and southwest-northeast ice-

flow orientations, the provenance of the till needs to be assessed. This study uses till clast-lithology counts and matrix geochemistry datasets to determine provenance, which supports interpreted ice-flow directions.

4.4.2.1 Clast lithology

The clast lithologies identified within the 2–8 mm size-fraction of till were first sorted into 22 detailed classes and then grouped into three simplified classes reflective of the regional bedrock geology: HBB, UGG and granitoid (Hodder and Gauthier, 2025). Furthermore, the trace concentrations (≤1 ct. %) of distinctive eastern and north erratics were categorized separately. Lastly, clasts that could not be confidently tied to a regional bedrock geology class, primarily quartz grains, were classified as 'Other' (≤8 ct. %). An average of 519 clasts were counted for each till sample, ranging from 319–1058 clasts per sample, totaling 58 132 clasts.

4.4.2.2 Matrix geochemistry

The <63 µm size-fraction of till samples (the matrix) was separated by sieving and then an aliquot was subjected to a total digestion using lithium metaborate/tetraborate fusion followed by dissolution in 5% HNO_3. Major and trace elements were then determined by inductively coupled plasma mass spectrometry and inductively coupled plasma optical emission spectrometry at Activation Laboratories (Ancaster, Canada; Hodder and Gauthier, 2025).

Till-matrix geochemistry datasets sum to a constant (e.g., 100 wt. %) and are thus susceptible to effects of closure when applying statistical analyses (Grunsky, 2010). To avoid this, the dataset was transformed using a centred log ratio (CLR) transformation (Aitchison, 1986). Following this, the CLR-transformed data was analyzed using a combination of principal component analysis (PCA) and k-means clustering. To maintain acceptable degrees of freedom within the dataset of 111 samples, PCA was restricted to: Si, Al, Fe, Mn, Mg, Ca, Na, K, Ti, P, ∑LREE and ∑HREE, whereby ∑LREE=La+Ce+Pr+Nd+Sm+Eu+Gd and ∑HREE=Y+Tb+Dy+Ho+Er+Tm+Yb+Lu as defined in Van Gosen et al. (2017). There are thus about 9 times more samples than selected variables, which should help properly condition the covariance matrix. The number of clusters chosen for k-means cluster

analysis was based on a scree plot of the sum of squares distances from cluster centres and is provided in Appendix C, Supplemental material 3. Statistical analysis was completed using ioGAS™ software.

4.4.3 Stratigraphic approach

The Quaternary stratigraphic record of the HBL, like many formerly glaciated regions, is highly fragmented (e.g., Nielsen et al., 1986; Thorleifson et al., 1993; Möller et al., 2019b; Hodder et al., 2024). Deciphering this record requires an innovative approach that employs multiple parameters to characterize both glacial and nonglacial sediments. This study incorporates both lithostratigraphy and allostratigraphy principles to define informal regional stratigraphic units. The North American Stratigraphic Code (North American Commission on Stratigraphic Nomenclature, 2021) recommends defining informal units when the extent and significance of units beyond the study area are still undetermined and/or when units are defined using innovative techniques. Till units are defined using a multi-parameter lithostratigraphy approach that incorporates sedimentology observations (relative consolidation, colour, sedimentary structures, and ice-flow indicators) and compositional data (clast-lithology) to confirm the direction that ice was flowing from when the sediment was deposited. It must be noted that most tills cannot be differentiated using only till composition since the principles of inheritance and overprinting (Stea and Finck, 2001) have a large impact on till composition (Gauthier et al. 2025). After till units were defined using a lithostratigraphic approach, an allostratigraphic approach is used to identify the relative age of intertill sorted sediment packages using the bounding surfaces of the enclosing till units. The use of an allostratigraphic approach to identify the relative age of intertill sorted sediments is a necessary approach since the till-dominated stratigraphic record has been produced through deposition and erosion that varied spatio-temporally, which has led to a highly fragmented stratigraphic record (Gauthier et al., 2019; Hodder et al., 2024). This is clearly exemplified by the preservation of near-surface (<7 m depth) sediments deposited during the MIS 7 interglacial period at multiple localities in the western HBL that lack a MIS 5e depositional record (Gauthier et al., 2024, 2025; Hodder et al., 2024), which highlights that interglacial beds cannot be used to ‘anchor’ any stratigraphic interpretations. Some

intertill sorted sediment units are broken down further with a letter modifier, e.g., Unit 11a, where an interpretation of the depositional environment of the sediment was attainable. Similarly, one till unit is broken down further with a letter modifier based on ice-flow data. The stratigraphy is first established at each section, and then correlations are progressively interpreted across both rivers investigated to provide a regional stratigraphic framework.

4.4.4 Geochronology

4.4.4.1 Radiocarbon dating and $\delta^{13}C$ values

Radiocarbon ages determined by accelerator mass spectrometry (AMS) were obtained from one detrital wood specimen and two carbonate shell specimens at the A.E. Lalonde AMS laboratory (Ottawa, Canada). The wood specimen was physically pre-treated prior to analysis by removing the outer layer of the specimen and then chemically pre-treated with an acid-alkali-acid wash. Carbonate shell specimens were physically pre-treated prior to analysis by removing porous or recrystallized areas with a Dremel bit and then chemically pre-treated by etching with 0.2N HCl to remove the outer 20–30% (Crann et al., 2017). Radiocarbon ages are interpreted as minimum limiting ages for the stratigraphic beds they were sampled from. The $\delta^{13}C$ values of three shell specimens were determined at the Ján Veizer Stable Isotope Laboratory (Ottawa, Canada), to help establish if the shell belonged to a freshwater or marine organism (McConnaughey and Gillikin, 2008; Gauthier, 2023).

4.4.4.2 Optical dating

Optical ages using quartz grains have recently been determined at localities in the western HBL (Hodder et al., 2023, 2024; Gauthier et al., 2024, 2025). This study used the same methodology to investigate the age of identified nonglacial beds in the study area. Analyses were done at the Luminescence Dating Laboratory at University of the Fraser Valley. Sorted sand from these units were sampled for optical age determination by inserting an opaque plastic tube (~20 cm long and 5 cm diameter) into the sediment face, extracting the tube, and then sealing each end of the packed tube tightly to preserve water content and mixing of sediment during transport. Samples were

prepared using standard laboratory methods and 180–250 µm diameter quartz grains were concentrated for dating. Equivalent dose (D_e) values were determined using multi-grain aliquots (50–100 grains per aliquot) and the single-aliquot regenerative dose (SAR) method (Murray and Wintle 2000, 2003). Aliquot D_e values were screened for outliers using the interquartile range method (e.g., Medialdea et al., 2014). Representative D_e values used for dating were calculated using the central age model (CAM) and the minimum age model (MAM) (Galbraith et al. 1999). Additional details regarding the optical dating methodology can be found in Hodder et al. (2023).

4.4.5 Paleo-environmental analysis

Ten samples (1 cm^3) for pollen analyses were taken from subtill sediments across six exposures (Table 4.1). Pollen was processed using standard palynological techniques involving acid digestions (Faegri and Iversen, 1975) at the Paleoecology Laboratory at the University of Toronto. Sodium polytungstate was used to remove any residual mineral sediments (Zabenskie, 2006; Campbell et al., 2016). Palynospheres were added to the preparation to estimate pollen concentration (Kitaba and Nakagawa, 2017). We identified (McAndrews et al., 1973) and counted a minimum of 150 pollen grains (types: herb, arboreal and shrub) in each sample using a compound microscope at 400x magnification. Stratigraphic plots were made in R package 'rioja' (Juggins, 2015; Juggins et al., 2015). Quantitative paleoclimate plots were constructed using the modern analogue technique (Overpeck et al., 1985) using a previously published modern-day dataset for North America (4882 sites, see: Whitmore et al., 2005; Dalton et al., 2017). Raw pollen counts and additional details about the modern analogue technique are available in Dalton et al. (2024). At four of these sites a subsample was screened for the presence of foraminifera at the micropaleontology lab at University of Colorado, Boulder and genera were identified (Table 4.1).

Table 4.1: Summary of pollen and foraminifera analysis.

Stratigraphic unit	Sample_ID	Sample interval (m depth)	Sample medium	Are pollen data of sufficient quality for paleoclimate reconstruction? [a]	Reconstructed mean annual precipitation (mm)	Reconstructed mean summer temperature (°C)	Foraminifera Preservation (genera noted) [b]
1	112-21-805-G01	13.00–13.80	silty fine-sand	No; PP	--	--	Barren
	112-21-826-PM1	16.70–18.40	detrital organics in sandy gravel	No; LC and PP	--	--	NAC
4a	112-21-807-PM1	15.80–15.90	silt	Yes	508 ± 169	12.1 ± 1.8	Poorly preserved (*Elphidium, Buccella, Cassidulina, Islandiella*)
	112-21-807-PM2	17.80–17.90	silt	No; LC and PP	--	--	Well presereved (*Elphidium*, *Cassidulina*)
	112-21-807-PM3	18.10–18.20	silt	No; PP	--	--	Well preserved (*Elphidium, Buccella, Cassidulina, Islandiella*)
4b	112-21-806-PM1	10.10–10.20	organic-rich sediment	Yes	771 ± 169	9.0 ± 1.8	NAC
	112-21-832-PM1	34.80–34.90	fine sand	No; LC and PP	--	--	NAC
	112-21-832-PM2	36.00–36.10	silty fine-sand	Yes	800 ± 169	14.3 ± 1.8	NAC
	112-21-832-PM3	36.20–36.25	bedded sand and clay	No; LC and PP	--	--	NAC
11b	112-21-812-PM1	4.20–4.30	organic nodules	No; LC and PP	--	--	NAC

[a] LC, low concentration (<5000 grain per cm^3); PP, poor preservation (>10% broken)

[b] NAC, no analysis completed

4.4.6 X-ray diffraction (XRD) analysis

XRD analysis was carried out using a Malvern Panalytical Aeris at the Groundwater Geochemistry Remediation Laboratory at the University of Waterloo. Sample preparation involved powdering of the bulk sample with a mortar and pestle. For uniformity of particle size a Wig-L-Bug grinding mill was also used, with Stainless steel vial, 1/2" diameter x 1" long, with stainless steel ball, 1/4" diameter. The machine was run for 5 min for each vial. Powdered samples were mounted onto back-loaded steel sample holders. The HighScore software was used to plot and interpret the XRD data. The technique utilizes the Rietveld method for phase identification and quantification (Rietveld, 1969).

4.5 Results and interpretations

4.5.1 Quaternary stratigraphy

The Quaternary stratigraphic framework for the study area is derived from observations across 16 sections together with 73 measured ice-flow indicators and 111 analysed till samples. Using a hybrid allostratigraphic-lithostratigraphic approach, a total of 16 stratigraphic units are recognized and no single section contains all identified units. The stratigraphic framework includes one occurrence of weathered bedrock, nine glacial (till) units and seven sorted sediment units. The spatial location of each identified stratigraphic unit including accompanying ice-flow data and photos of sediments described is provided in Appendix C, Supplemental material 2.

4.5.1.1 Weathered bedrock

Along the Churchill River, Precambrian bedrock is exposed either at the base of sections investigated, along the river shoreline or visibly outcropping in the river. At section 21-826 (Figure 4.4), the lowermost 0.7 m of geologic material overlying bedrock consists of grey, silver and orange clay with sand-sized quartz grains (Figure 4.5a). To investigate this material further, the whole rock geochemistry was determined and compared to available data from the Chipewyan granite using weathering indices (Table 4.2). A plot of these data on an A-CN-K diagram shows that this material lies on a predictable weathering trend for granitic parent material (Fedo et al., 1995; Figure 4.5b). The chemical index of alteration (Nesbitt and Young, 1982) and plagioclase index of alteration (Fedo et al., 1995) values suggest that this material is highly altered compared to the Chipewyan granite (Table 4.2). The XRD analysis indicates that the material is primarily composed of kaolinite (48.8%), followed by quartz (18.0 %) microcline (16.2%), albite (16.5%) and biotite (0.5%). Kaolinite is a by-product formed during the weathering of feldspars by hydrolysis and this mineral assemblage is typically what would be expected from weathering of granite (e.g., Middelburg et al., 1988); therefore, this unique material is interpreted to be weathered bedrock. Additional occurrences of weathered bedrock have been documented in northeastern Manitoba, 130 km north-northwest of section 21-826 along the North Knife River, where kaolinite was the dominant clay mineral (Dredge and Nixon, 1992).

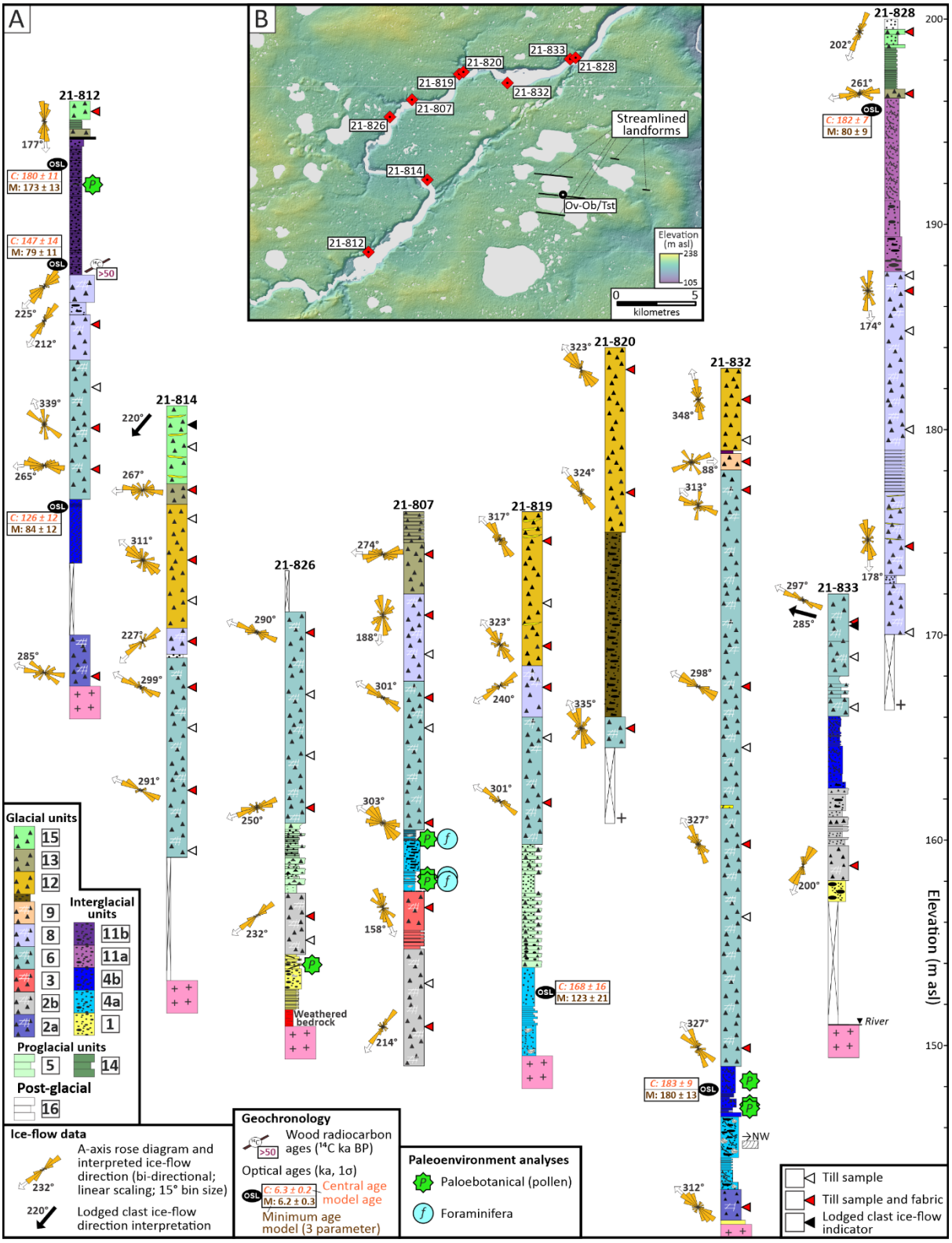

Figure 4.4: Summary of Quaternary stratigraphic relationships interpreted for sections investigated on the Churchill River: A) stratigraphic interpretations of sections investigated. The sections shown are not presented to scale laterally but are displayed according to the correct elevation; B) detailed location of each section investigated and mapped west-trending streamlined landforms. The location of a surficial till sample is indicated by the black and white circle.

Table 4.2: Geochemistry and calculated weathering indices of interpreted weathered bedrock at section 21-826 and the Chipewyan granite.

Sample	Al_2O_3 (wt. %)	CaO (wt. %)	Na_2O (wt. %)	K_2O (wt. %)	CIA[a]	PIA[b]
21-826	15.70	0.27	0.21	6.64	66	91
Chipewyan granite (in-situ)[c]	15.62	2.11	3.39	5.93	50	48
Chipewyan granite (in-situ)[c]	13.95	1.67	3.12	4.77	51	50

a. Chemical index of alteration (Nesbitt and Young, 1982): [Al_2O_3 / (Al_2O_3+CaO Na_2O+K_2O)] * 100, data in molecular proportions

b. Plagioclase index of alteration (Fedo et al., 1995): [(Al_2O_3-K_2O) / (Al_2O_3+CaO+Na_2O-K_2O)] * 100, data in molecular proportions

c. Geochemical data for the Chipewyan granite was sampled from the northeastern shoreline of Southern Indian Lake (Martins et al., 2019)

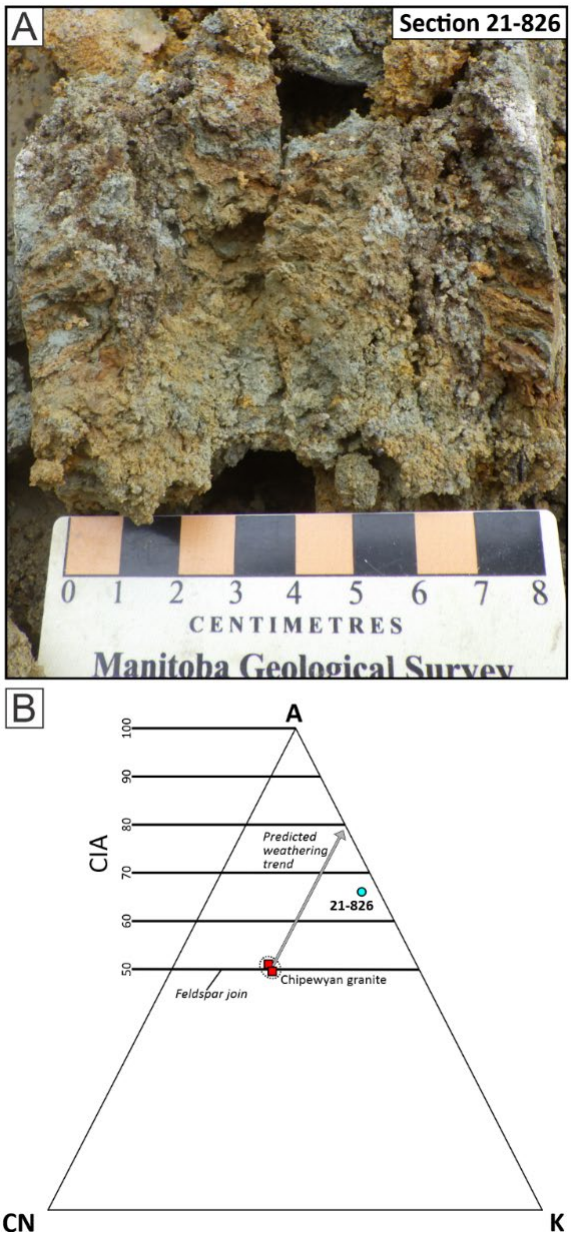

Figure 4.5: Interpreted occurrence of weathered bedrock at the base of section 21-806 (A) and plot (B) of the whole rock geochemical data of this material and data from the unweathered Chipewyan granite on an A-CN-K diagram (Fedo et al., 1995).

4.5.1.2 Unit 1: Interglacial sorted sediments

The lowermost unit, Unit 1, consists of different sediment facies at each section investigated. It is recognized by its upper bounding surface (allostratigraphy) with Unit 2 till (two occurrences) or Unit 3 till (one occurrence; Figures 4.4, 4.6) and its lower bounding surface with weathered bedrock, bedrock or not determined (bottom of section). At section 21-833, Unit 1 consists of >3.5 m of clast- to matrix-supported gravel, with subrounded to rounded granule- to boulder-sized clasts of mixed lithologies (Figure 4.7a). At section 21-805, Unit 1 consists of >2.5 m of fine sand to silty fine sand (Figure 4.7b). The upper 0.9 m consists of yellow-brown fine sand with horizontal to undulatory bedding and minor faulting in places. The lower 1.6+ m is orange and grey silty fine-sand with 3–5 cm thick beds that are defined by variations in the texture. At section 21-832, the lowermost 0.2 m of sediment overlying bedrock consists of poorly sorted, greenish-grey silt and clay with minor (<5%) pebble-sized clasts. At section 21-826, 1.7 m of bedded clay, silt, sand and gravel is exposed. These sediments are poorly sorted with weakly defined planar bedding planes. The sediment contains abraded shell fragments, flattened pieces of wood and rounded detrital peat 'clasts' that are up to 4–5 cm in diameter (e.g., Figure 4.7c). The presence of detrital wood and peat clasts suggests deposition during an interglacial episode or the erosion of a nearby interglacial deposit. Two of these sites were investigated for paleoenvironmental analysis (21-826 and 21-805). Neither site had adequate pollen preservation for statistical analyses or paleoclimate reconstruction (Table 4.1). However, numerous conifer grains including *Picea* (spruce), and *Pinus* (pine) were observed in these samples, along with small amounts of *Betula* (birch) and *Salix* (willow). Also noted were Poaceae (grasses) and Asteraceae (flowering plants) along with a strong wetland component of sedge and moss (Cyperaceae and *Sphagnum*). The interpretation of such small numbers of pollen grains should be treated with caution. However, broadly, these palynomorphs suggest a regional boreal forest and local wetland conditions, not dissimilar to the conditions in the region today. The sediments at section 21-805 were screened for foraminifera, but none were found.

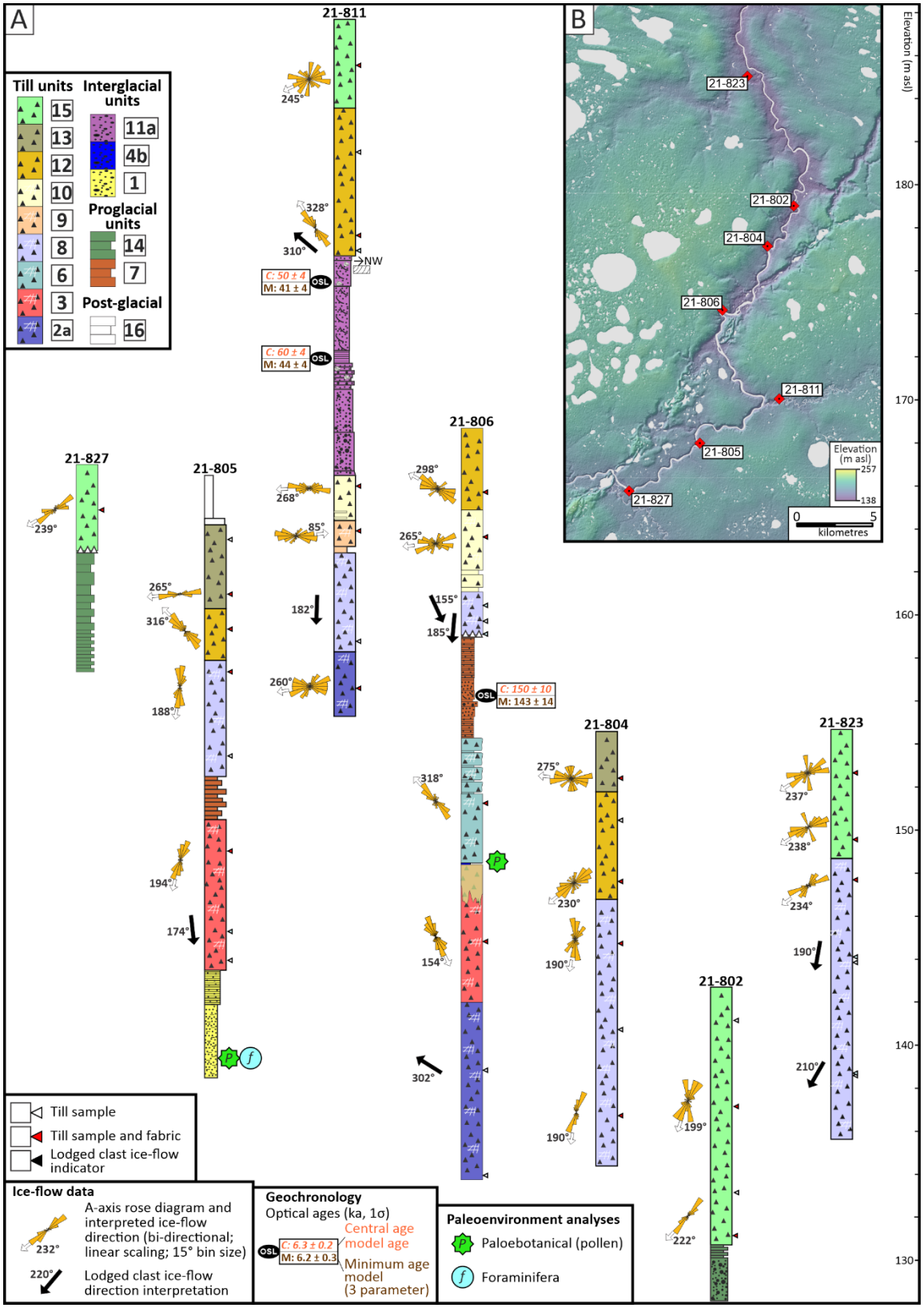

Figure 4.6: Summary of Quaternary stratigraphic relationships interpreted for sections investigated on the Little Churchill River: A) stratigraphic interpretations of sections investigated. The sections shown are not presented to scale laterally but are displayed according to the correct elevation; B) detailed location of each section investigated along the Little Churchill River.



Figure 4.7: Examples of Unit 1 sediment: A) clast- to matrix-supported gravel at section 21-833; B) bedded fine sand to silty fine sand at section 21-805. A raft of the underlying sand within Unit 3 is highlighted; and C) rounded detrital peat 'clast' at section 21-826 that was analyzed for pollen composition.

4.5.1.3 Unit 2: Till(s) deposited by SW- and NW-trending ice-flow and minor intertill sorted sediment beds

Unit 2 consists of a massive, matrix-supported diamicton that contains striated, bullet-shaped and faceted clasts that is 1.5 to >6.6 m thick and is best exposed at sections 21-807 (Figure 4.8) and 21-806 (Figure 4.9). The diamicton is highly overconsolidated and strongly jointed with oxidation rind developed on joint surfaces. The matrix colour is olive brown, dark grey, dark greyish brown or black (Appendix C, Supplemental material 1, Table S1-2) and is predominantly silt (23–41 wt. % sand, 44–47 wt. % silt and 14–33 wt. % clay; Appendix C, Supplemental material 1, Figure S1-3). The massive structure, clast shape, lodged in-situ clasts with striated upper surfaces and lateral continuity indicate that Unit 2 diamicton is a subglacial traction till (Evans et al., 2006; Evans, 2018). Unit 2 till contains a high proportion of HBB clasts (Figure 4.10); thus, the direction of Unit 2 clast fabrics are interpreted to have formed by SW- to SSW-trending (200–232°, n=3) and W- to NW-trending (260–312°, n=4) ice-flow phases (Figures 4.4, 4.6, Appendix C, Supplemental material 1, Table S1-3). Most occurences of till with a black-coloured matrix occur within Unit 2 (n=3/4; Appendix C, Supplemental material 1, Table S1-2). These tills contain black shale to siltstone clasts, often with fish scales (e.g., Figure 4.2c); however, the bedrock source of these clasts is unknown in the region (Dredge and Nixon, 1992). No stratigraphic relationships were discovered to determine a relative age between ice-flow events within Unit 2 and a letter modifier is used to distinguish tills deposited W- to NW-trending (Unit 2a) and SW- to SSW-trending (Unit 2b). Overlying Unit 2b till at section 21-833 is 2.9 m of interbedded sand, gravel and diamicton. The diamicton beds are qualitatively similar to the underlying Unit 2b diamicton. Similarly, Unit 2b till at section 21-807 is overlain by 0.9 m of interbedded diamicton and sand (Figure 4.8) and the diamicton beds have a similar matrix colour compared to the Unit 2b diamicton. These two occurrences of bedded sorted sediment and diamicton has been grouped with Unit 2b and are interpreted to have been deposited in a proglacial environment possibly during a deglaciation event.

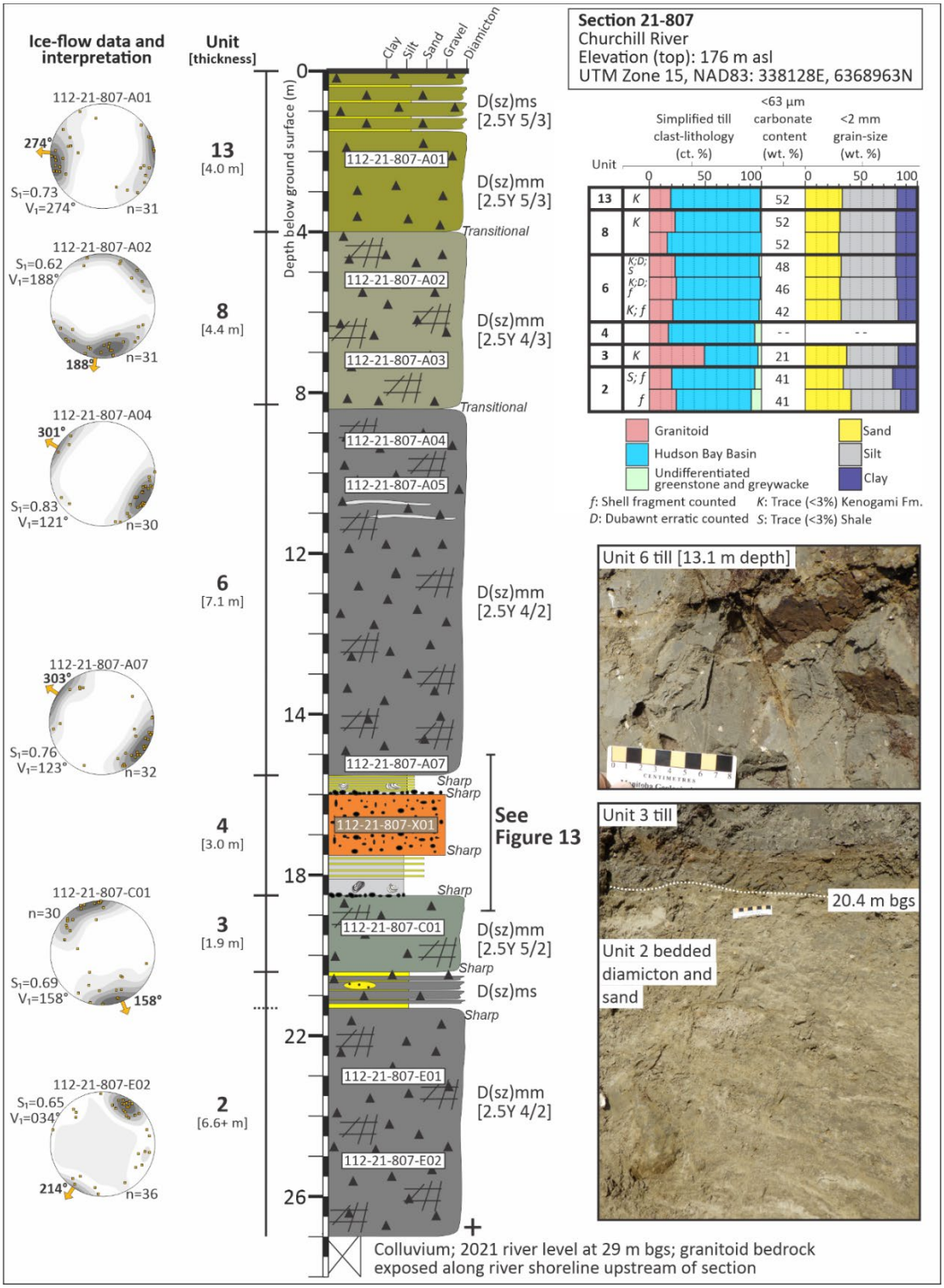

Figure 4.8: Quaternary stratigraphy exposed at section 21-807 on the Churchill River. Till sample numbers are labelled within the white boxes and a gravel sample within the brown box. Simplified clast-lithology counts, <63 µm carbonate values and matrix texture data are provided for these samples in the top right panel. Till clast-fabric data are plotted on equal area, lower hemisphere projection stereonets. The value of the principal eigenvalue (S1) and direction of the principal eigenvector (V1) are provided, and an interpretation of the ice-flow direction is indicated (orange arrow). Please refer to Appendix C, Supplemental 1, Table S1-1 for a translation of the lithofacies codes used.

The lower contact of Unit 2 till is Unit 1 (three occurences), bedrock (one occurrence) or not observed due to excessive colluvium (three occurrences). The upper contact of Unit 2 till occurs with Unit 3 (two occurrences), Unit 4 (three occurrences), Unit 5 (one occurrence) or Unit 8 (one occurrence).

4.5.1.4 Unit 3: Till deposited by SSE- to SSW-trending ice-flow and minor intertill sorted sediments

Unit 3 consists of massive, matrix-supported diamicton that contains striated, bullet-shaped and faceted clasts that is 1.9 to 3.5 m thick and is best exposed at section 21-807 (Figure 4.8). The diamicton is highly overconsolidated and strongly jointed and/or fissile, with oxidation rind developed on joint surfaces. The matrix colour is greyish brown, dark grey, dark olive grey or grey (Appendix C, Supplemental material 1, Table S1-2) and is predominantly silt (ranges 37–41 wt. % sand, 41–47 wt. % silt and 15–18 wt. % clay; Appendix C, Supplemental material 1, Figure S1-3). The massive structure, clast-shape (bullet-shaped, faceted and striated), lodged in-situ clasts with striated upper surfaces and lateral continuity indicate that Unit 3 diamicton is a subglacial traction till (Evans et al., 2006; Evans, 2018). Unit 3 till contains abundant granitoid clasts relative to the dataset (Figure 4.10); which is in agreement with ice-flow data that indicates till deposition by SSE- to SSW-trending (154–194°) ice flow (Appendix C, Supplemental material 1, Table S1-3). A relative age-relationship at section 21-805 indicates a minor clockwise rotation in ice-flow direction during deposition of Unit 3 till (Figure 4.6). The lower contact of Unit 3 till is Unit 1 (one occurrence) or Unit 2 (two occurrences). The upper contact of Unit 3 till occurs with Unit 4 (two occurrences) or Unit 7 (one occurrence).

4.5.1.5 Unit 4: Interglacial sorted sediments and paleosol development in till

Unit 4 sorted sediments are identified at six sections, defined by its sharp upper bounding surface with Unit 5 (one occurrence) or Unit 6 (five occurrences) and lower bounding surface with Unit 3 (two occurrences), Unit 2 (three occurrences) or bedrock (one occurrence; Figure 4.4, 4.6). Unit four consists of bedded silt, sand and gravel and is best exposed at sections 21-832 (Figure 4.11), 21-807 (Figure 4.13) and 21-806 (Figure 4.9, 4.14), which are described in detail below. The different depositional environments recognized within Unit 4 sediments are distinguished herein using a letter modifier, Unit 4a (marine) and Unit 4b (terrestrial).

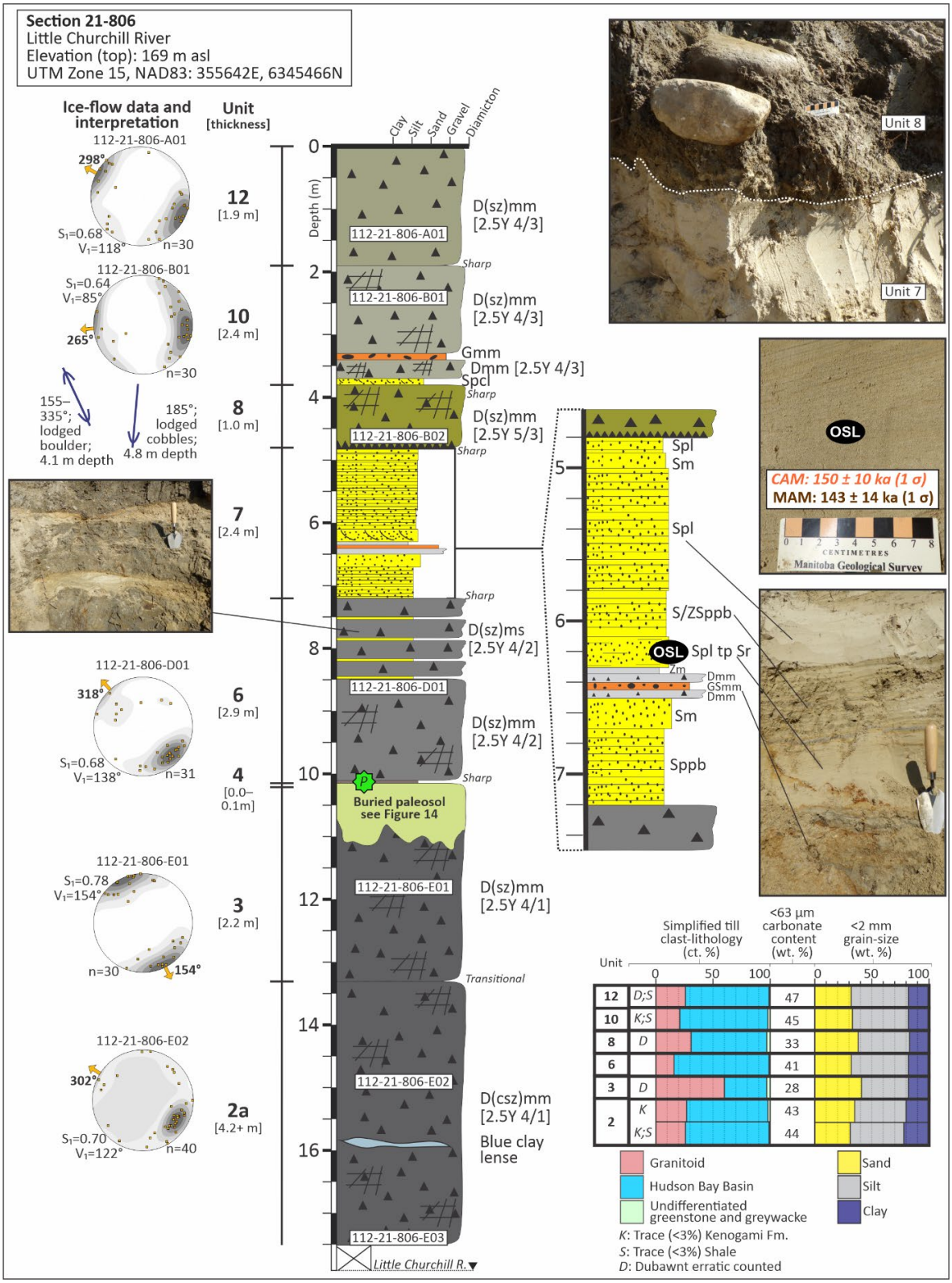

Figure 4.9: Quaternary stratigraphy exposed at section 21-806 on the Little Churchill River. Till sample numbers are labelled within the white boxes. Simplified clast-lithology counts, <63 µm carbonate values and matrix texture data are provided for these samples in the bottom right panel. Till clast-fabric data are plotted on equal area, lower hemisphere projection stereonets. The value of the principal eigenvalue (S_1) and direction of the principal eigenvector (V_1) are provided, and an interpretation of the ice-flow direction is indicated (orange arrow). Please refer to Appendix C, Supplemental material 1, Table S1-1 for a translation of the lithofacies codes used.

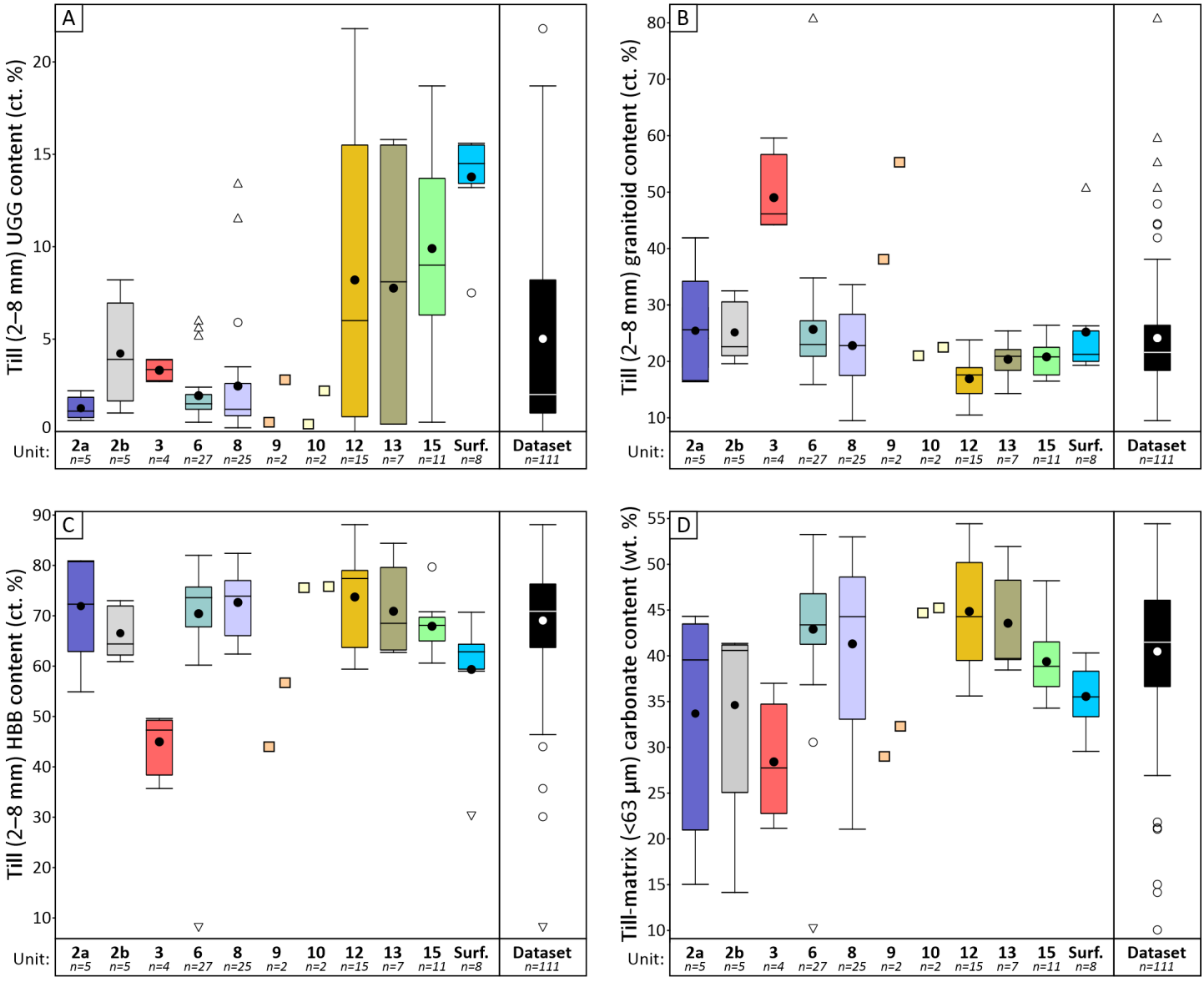

Figure 4.10: Tukey box plots displaying till compositional data for each identified unit: A) proportion of undifferentiated greywacke and greenstone (UGG) clasts in the 2–8 mm size fraction (ct. %); B) proportion of granitoid clasts in the 2–8 mm size fraction (ct. %); C) proportion of Hudson Bay Basin (HBB) clasts in the 2–8 mm size fraction (ct. %); and D) carbonate content of the till matrix (<63 µm size-fraction).

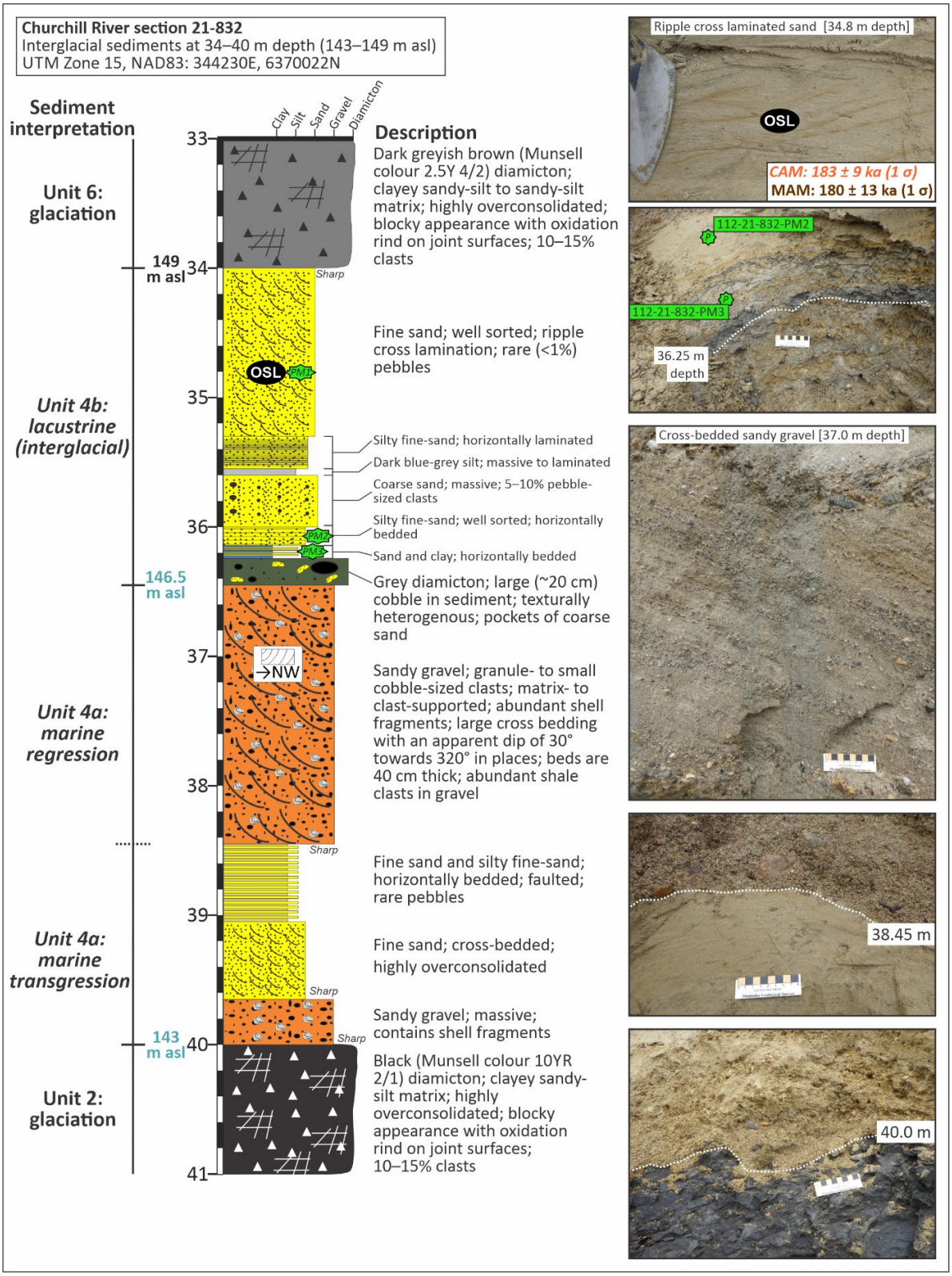

Figure 4.11: Quaternary stratigraphy of Unit 4 sediments at section 21-832 (34–40 m depth bgs). Please refer to Figure 4.4 for an interpretation of the entire stratigraphy exposed at this section or Hodder and Gauthier (2025) for a detailed description and stratigraphic column.

At section 21-832, a thick (6 m) package of intertill sorted sediments is situated between Unit 2 and Unit 6 tills at an elevation of 143–149 m asl (Figure 4.4, 4.11). The lowermost lithofacies is in sharp contact with the underlying Unit 2 till and consists of massive, sandy gravel that contains shell fragments. Overlying this sandy gravel is 0.6 m of cross-bedded fine sand that is overlain by 0.6 m of horizontally bedded fine sand and silty fine sand with rare pebbles. The bedded sand is in sharp contact with overlying sandy gravel (Figure 4.11). The sandy gravel is matrix- to clast-supported and contains granule- to small cobble-sized clasts with abundant shell fragments. The gravel contains thick (40 cm) cross-beds in places along the exposure with an apparent dip of 30° towards 320° (Figure 4.11). A shell fragment from this gravel has a $\delta^{13}C$ value of 0.5 ‰. This value is within the present-day range for marine specimens sampled in Manitoba, where individual marine specimens (n=7) have $\delta^{13}C$ values of 0.10–1.82 ‰ and bulk shell samples (n=33) have $\delta^{13}C$ values of -1.32–3.2 ‰ (Gauthier, 2023). However, some present-day freshwater shells are also within range of these $\delta^{13}C$ values (Gauthier, 2022), so it is possible that shell is from a freshwater organism. This package of sediments from 143.0–146.5 m asl at section 21-832, is interpreted to have been deposited during a marine transgression and regression cycle following deglaciation of the area. This interpretation is based on the sequence of lithofacies observed and abundant likely-marine shell fragments within the sediment. Following regression of the marine waters, an additional 2.5 m of sorted sediment was deposited (Unit 4b). This package of sediment consists of 0.2 m of diamicton that is texturally heterogenous with pockets of coarse sand that is overlain by 0.25 m of horizontally bedded clay, silty fine-sand and fine sand, which is overlain by coarse sand (0.4 m thick) with 5–10% pebble-sized clasts (Figure 4.11). The sand is in sharp contact with overlying grey silt (0.05 m thick), horizontally bedded silt fine sand (0.25 m thick) and well sorted, ripple cross laminated fine sand (1.3 m thick; Figure 4.11). This package of sediments from 146.5–149.0 m asl is interpreted to have been deposited in a terrestrial environment, possibly a nearshore lacustrine setting, based on sedimentary structures and sequence of lithofacies observed. Three samples from this upper sedimentary sequence were analyzed for pollen (Figure 4.11), and one contained sufficient preservation for a complete a paleo-climate reconstruction (sample 112-21-832-PM2; see Figure 4.12). This sample indicates that the mean summer temperature was similar to the present day (14.3 °C), but average annual precipitation may have been higher (~800 mm). Pollen was poorly

preserved and/or of insufficient concentration in the other two samples from this unit (-PM1 and -PM3; Figure 4.11). However, some additional inferences can still be made including that typical boreal tree pollen (*Picea*, *Pinus*, *Betula, Alnus, Salix*) was identified throughout, along with 5 *Abies* (fir) grains at -PM2 (Figure 4.11). The presence of *Abies* is somewhat notable, since it is more common to temperate forests where precipitation is slightly higher (Burns and Honkala, 1990). However, it is also noted in places in the HBL and surrounding boreal area (Riley, 2003). Wetland indicators (Cyperaceae and *Sphagnum*) suggest the presence of water-logged conditions similar to today. Thus, broadly, the pollen data suggest conditions similar to present-day interglacial period (Figure 4.12).

At section 21-807, a thick (3.0 m) package of intertill sorted sediments is situated at an elevation of 157.5–160.5 m asl (Figures 4.4, 4.8, 4.13). The lowermost sediments consist of massive silt with minor sand lenses that are in sharp contact with a clast lag developed on the underlying till (Figure 4.13). The silt contains in-situ whole valves of shells that are very brittle and soft, prohibiting sampling. The sediment is highly overconsolidated and has a blocky appearance. This massive silt transitions upwards into rhythmites of silt and fine to medium sand. The sand beds are 1–3 cm thick and the silt beds are 5–10 cm thick. This bedded sand and silt is in sharp contact with 1.5 m of sandy gravel. The sandy gravel is matrix-supported, poorly sorted and highly overconsolidated. At the top of the sandy gravel is a cobble layer. This cobble layer is draped by an overlying silt that is massive to laminated in places and transitions upward into silt and sand that is horizontally bedded with 1–3 cm thick beds. The silt contains large shell fragments and one of these fragments (1 cm diameter) with periostracum still attached has a $\delta^{13}C$ value of -0.8 ‰ and a near-finite radiocarbon age of 46.2 ± 1.2 ^{14}C ka BP (UOC-16664; Figure 4.13; Table 4.3). The near-finite age is interpreted as a nonfinite age based on the unreliability of radiocarbon ages from shell materials near the upper limit of method (Miller and Andrews, 2019). Three samples from the silt beds were analyzed for pollen and foraminifera (Table 4.1; Figure 4.13). The lowermost two samples do not contain a sufficient concentration and/or a proportion of unbroken pollen grains to complete a paleo-climate reconstruction (Table 4.1; Figure 4.13). However, these two samples contain well preserved foraminifera, including species of *Elphidium*, *Buccella*, *Cassidulina* and *Islandiella* (Table 4.1; e.g.,

Figure 4.13b, c, d). The upper silt sampled 0.1 m above the clast lag contains poorly preserved foraminifera with similar species to that observed at depth (Table 4.1) and this silt does contain a sufficient concentration and proportion of unbroken grains to complete a paleoenvironmental interpretation. The palynological analysis indicates that the mean summer temperature and annual precipitation was similar to the present day (12.1°C and 508 mm respectively; see Table 4.1; Figure 4.12). The intertill sediments at section 21-807 are interpreted to have been deposited in a marine environment based on the presence of foraminifera.

At section 21-806, a thin (maximum 0.1 m thick) laterally discontinuous bed of organic-rich silt separates two diamicton beds (Figure 4.9). This dark grey organic-rich silt is horizontally bedded with distinct pale yellow-coloured laminae within the silt. A pollen sample from this silt contained a sufficient proportion of unbroken grains and concentration of pollen to allow for a paleo-climate reconstruction (Table 4.1). This reconstruction indicates a lower mean summer temperature (9.0°) and higher average annual precipitation (771 mm) compared to the present day (Figure 4.12). Like the other pollen samples analyzed for this study, sample 21-806 contained typical boreal tree pollen (*Picea*, *Pinus*, *Betula, Alnus, Salix*) throughout, with smaller amounts of Poaceae, Asteraceae and wetland indicators (Cyperaceae and *Sphagnum*). A distinctive feature of this pollen sample was the relatively high percentage of *Betula* (~30%; birch), which are opportunistic, fast-growing trees that commonly surge in recently disturbed landscapes, such as early successional, or post-fire landscapes. Next, underlying this thin silt bed is till, the uppermost 0.4–0.5 m of which was oxidized (Figure 4.14a). Across most of the exposure this oxidized till was the only evidence of an-ice free period, since the organic-rich silt is laterally discontinuous and units 3 and 6 tills appear qualitatively similar in the field. The geochemistry of this oxidized zone was further characterized by sampling above and below the till-till contact every 10–20 cm from 9.9–11.1 m below ground surface (bgs). These samples are compared to 'unaltered' C-horizon till samples at 8.5 and 11.8 m bgs from the two till beds, using the till-matrix (<63 µm size-fraction) carbonate content and a base ion leach index consisting of the sum of relatively mobile elements Ca, Mg, Na and K compared to the relatively immobile element Ti (Sheldon and Tabor, 2009; Figure 4.14). Till sampled directly below this contact has decreased carbonate content and base ion leach index values. However, these

values then increase with depth through the visibly altered zone before stabilizing at 10.7 m bgs. Beyond this depth, the values decrease and are similar to the underlying unaltered till (Figure 4.14). These chemical changes are interpreted to indicate a leaching of the relatively more-mobile elements and carbonate from the upper 0.1–0.2 m of the till bed and an accumulation of these elements at depths of 0.3–0.6 m. Thus, the top of Unit 3 till at section 21-806 is interpreted to have undergone subaerial weathering resulting in the formation of the paleosol documented herein. The thin, laterally discontinuous silt bed was deposited at some point after the development of the paleosol and during possibly a somewhat cooler and wetter climate, with normal boreal disturbances, such as forest fires.

Table 4.3: Radiocarbon ages and shell $\delta^{13}C$ values.

Section	Stratigraphic unit	Laboratory ID	Material	^{14}C ka bp	$\delta^{13}C$ (‰)	Interpretation
21-812	11a	UOC-16584	wood	>50	-	nonfinite age
21-828	11a	UOC-16663	shell fragment	44..5 ± 0.9	2.0	nonfinite age; marine shell fragment
21-807	4a	UOC-16662	shell	46.2 ± 1.2	-0.8	nonfinite age; likely marine shell
21-832	4a	-	shell fragment	not analyzed	0.5	likely marine shell fragment

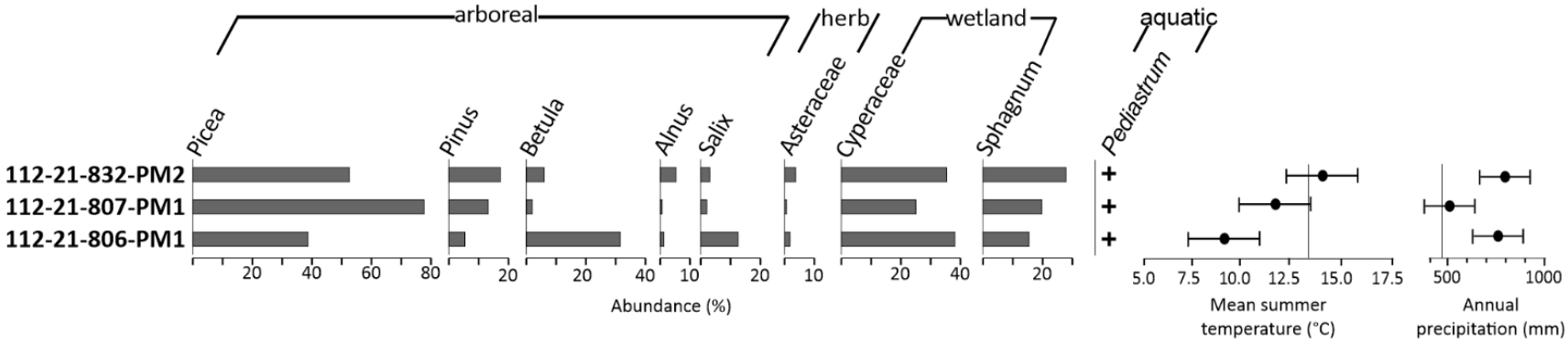

Figure 4.12: Pollen analysis for Unit 4 sediments at sections 21-806, 21-807 and 21-832. Only taxa appearing at >1% abundance is plotted. Vertical lines in the paleoclimate reconstructions represent present-day conditions in the region, which are approximately 12.7°C and 482 mm (Natural Resources Canada, 2015).

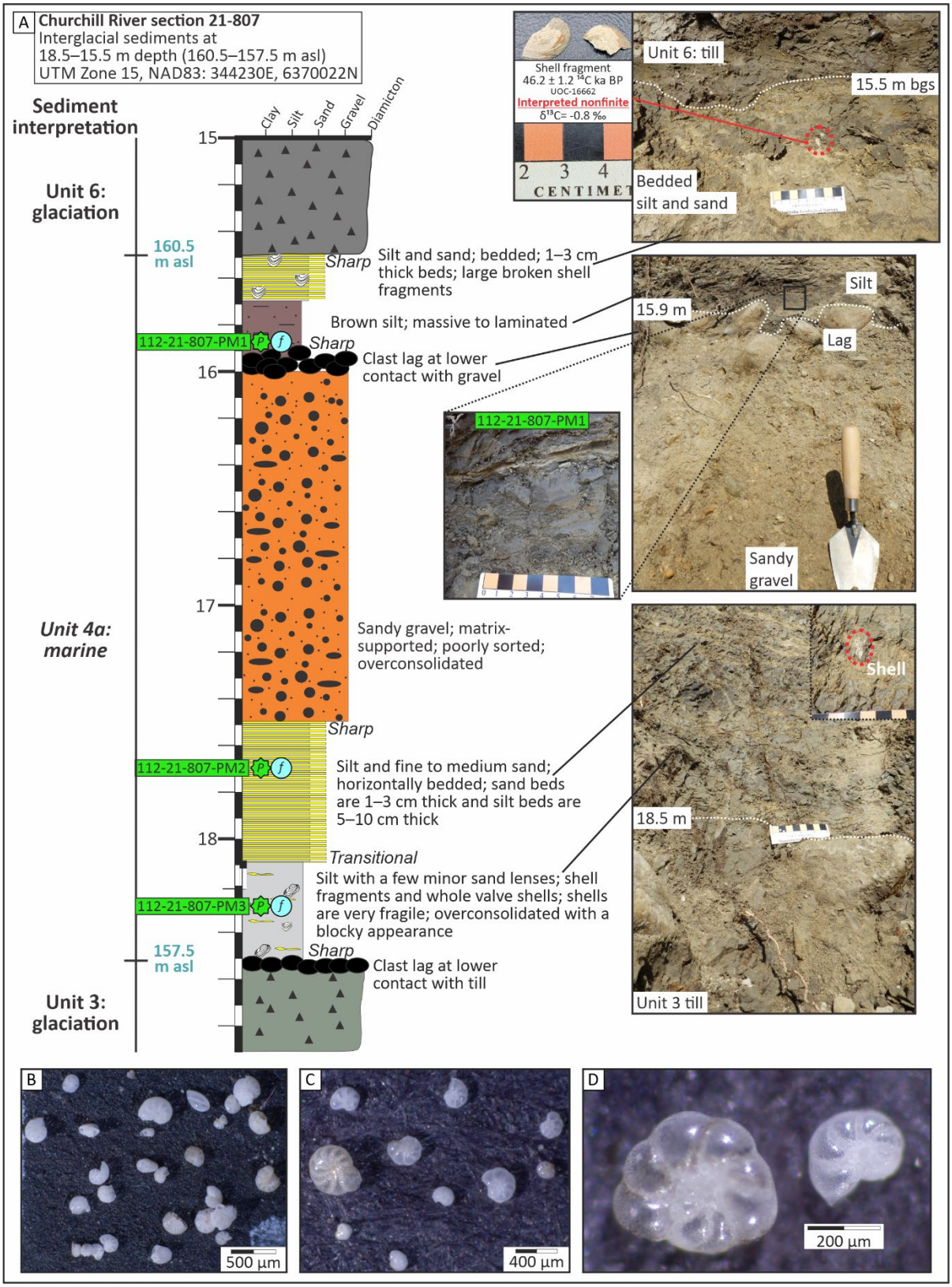

Figure 4.13: Intertill sorted sediments interpreted to have been deposited in a marine environment (Unit 4a) at section 21-807. Pollen and foraminifera sampling locations are shown as the green polygon with a 'P' and cyan circle with a '*f*', respectively (A). Example of all foraminifera identified in samples 112-21-807-PM1 (B), 112-21-807-PM2 (C) and 112-21-807-PM3 (D).

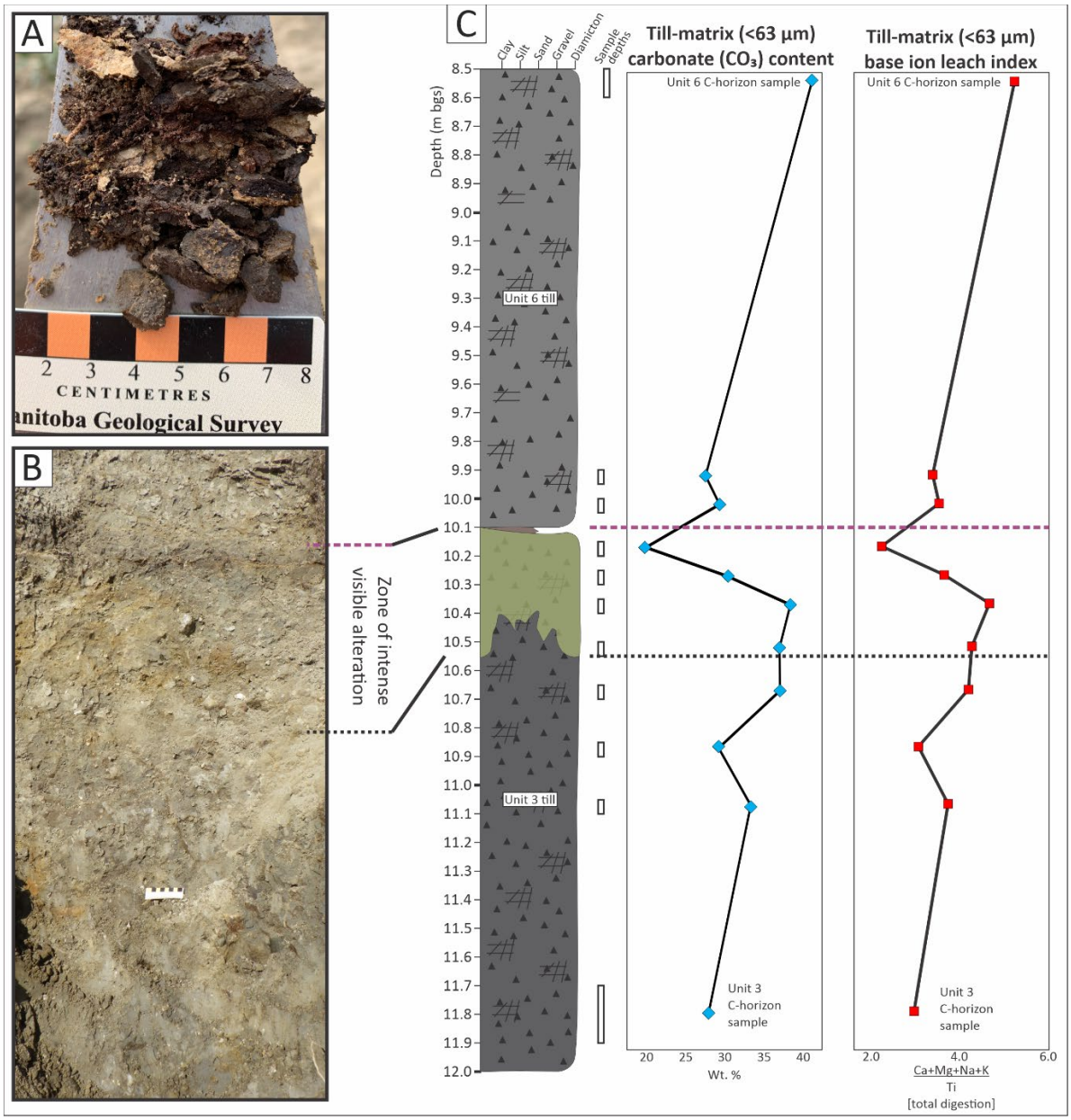

Figure 4.14: Intertill organic-rich sediment and paleosol development at section 21-806: A) organic-rich sediment sampled for pollen analysis; B) visibly altered zone at the top of Unit 3 till interpreted to be a result of early paleosol development from subaerial weathering; and C) till-matrix carbonate and base ion leach index values of Unit 6 and 3 tills with detailed sampling above and below the interpreted paleosol.

4.5.1.6 Unit 5: Proglacial bedded sorted sediments and diamicton

Unit 5 sediments are identified at two section on the Churchill River, defined by its sharp upper bounding surface with Unit 6 and lower bounding surface with Unit 5 (one occurrence) or Unit 2 (one occurrence; Figure 4.4). Unit 5 consists of horizontally to sub-horizontally bedded diamicton, silt, sand and gravel and ranges in thickness from 3.4 to 7.9 m. Individual beds range from 0.01 to 0.25 m in thickness and there is lateral variation in the thickness of beds. The beds consist of massive, matrix-supported diamicton. The matrix colour is dark greyish brown and the diamicton is qualitatively similar to the overlying Unit 6 till at each section investigated. The sand beds are typically massive but do contain horizontal to sub-horizontal bedding planes in places and contain faceted and striated pebble- to cobble-sized clasts interpreted as dropstones (e.g., Appendix C, Supplemental material 2). Unit 5 is interpreted to have been deposited in a proglacial lake that formed during advance of the ice sheet. This interpretation is based on the deposition of repeating diamicton and sorted sediment beds that contain dropstones, which require a nearby glacial source.

4.5.1.7 Unit 6: Till deposited by WSW- to NW- trending ice-flow

Unit 6 consists of massive, matrix-supported diamicton that contains striated, bullet-shaped and faceted clasts that is 2.9–29.0 m thick and is best exposed at section 21-832 (Figure 4.4). The diamicton is highly overconsolidated and strongly jointed and/or fissile, with oxidation rind developed on joint surfaces. The matrix colour is olive brown or dark greyish brown (Appendix C, Supplemental material 1, Table S1-2) and grain size ranges are 28–45 wt. % sand, 43–60 wt. % silt and 1–25 wt. % clay (Appendix C, Supplemental material 1, Figure S1-3). The massive structure, clast-shape (bullet-shaped, faceted and striated), lodged in-situ clasts with striated upper surfaces and lateral continuity indicate that Unit 6 diamicton is a subglacial traction till (Evans et al., 2006; Evans 2018). Unit 6 till contains abundant HBB clasts (Figure 4.10) and clast fabrics measured are interpreted to have been formed by W- or WSW-trending (265°, 250°) and WNW- to NNW-trending ice-flow (290–339°) (Figures 4.4, 4.6; Appendix C, Supplemental material 1, Table S1-3). At sections 21-812 and 21-826, Unit 6 till contains no sedimentological (consolidation, colour, texture) changes but there is a switch up-unit from W- or WSW-trending ice-flow to WNW- or NNW-trending ice-flow

(Figure 4.4). This relative-age relationship suggests that the area may have first experienced WSW-trending ice-flow before switching to NNW-trending ice-flow. The uppermost 1.4 m of Unit 6 at section 21-806 (Figure 4.9) contains diamicton beds that are 0.30–0.45 m in thickness that are separated by 0.01–0.03 m thick sorted sediments that contain preserved cross-bedding in places and an irregular geometry that pinches and swells laterally. These repetitive intertill sorted sediments beds are interpreted to have been deposited during episodic hydraulic decoupling at the ice-bed interface (e.g., Piotrowski et al., 2006). At section 21-832, there is a large (0.7 m wide x 1.0 m thick) raft of sand within Unit 6 till that is situated 4 m above the lower contact with Unit 4 sand. The lower contact of Unit 6 till occurs with Unit 4 (five occurences), Unit 5 (two occurences) or not observed due to excessive colluvium (two occurrences). The upper contact of Unit 6 till occurs with intertill sorted sediments of Unit 7 (one occurrence), Unit 8 (four occurrences), Unit 9 (one occurrence), Unit 12 (one occurrence) or the upper contact was not observed due to excessive colluvium (two occurrences).

4.5.1.8 Unit 7: Proglacial intertill sorted sediments

Unit 7 sediments are identified at two sections on the Little Churchill River, defined by its sharp upper bounding surface with Unit 8 till (2 occurrences; e.g., Figure 4.9) and lower bounding surface with either Unit 3 (1 occurrence) or Unit 6 (1 occurrence) tills (Figure 4.6). At section 21-806, there is 2.4 m of fine sand with minor silt and diamicton (Figure 4.9). The sand is massive, cross- or horizontally-bedded and is normal faulted in places. At section 21-805, there is 1.0 m of medium sand, silty fine sand and diamicton that contains irregular, deformed subhorizontal bedding planes. Individual beds range in thickness from 0.03–0.10 m thick. The medium sand beds are well sorted and contain cross-bedding while the silty fine-sand beds are moderately sorted with 3–5% granule to pebble-size clasts. Unit 7 sediments at both sections do not contain visible organics, and samples were not collected for pollen analysis. As such, they could have been deposited subglacially, in a proglacial environment or during an nonglacial period (interstadial or interglacial). Given that the bounding tills (Unit 6 and 8) at sections investigated are different with near perpendicular ice-flow directions indicated, these sediments may represent an ice-free period within stratigraphic record,

and the diamicton beds require a nearby glacial source, the preferred interpretation at this time is a proglacial depositional environment.

4.5.1.9 Unit 8: Till deposited by S- to SW-trending ice-flow and minor intertill sorted sediments

Unit 8 consists of massive, matrix-supported diamicton that contains striated, bullet-shaped and faceted clasts that is 1.0–17.7 m thick and is best exposed at section 21-828 (Figure 4.4). The diamicton is highly overconsolidated and strongly jointed, with oxidation rind developed on joint surfaces. The matrix colour is light olive brown, olive brown, dark olive grey, dark greyish brown, greyish brown or black (Appendix C, Supplemental material 1, Table S1-2) and grain size ranges 24–53 wt. % sand, 31–53 wt. % silt and 12–24 wt. % clay (Appendix C, Supplemental material 1, Figure S1-3). The massive structure, clast shape and other characteristics (bullet-shaped, faceted and striated), lodged in-situ clasts with striated upper surfaces and lateral continuity indicate that Unit 8 diamicton is a subglacial traction till (Evans et al., 2006; Evans, 2018). Unit 8 till contains abundant HBB clasts (Figure 4.10); thus, the Unit 8 clast fabrics are interpreted to have formed by S-trending to WSW-trending (174–240°) ice-flow (Figures 4.4, 4.6; Appendix C, Supplemental material 1, Table S1-3). Unit 8 includes one occurrence of intertill sorted sediments at section 21-828 that consists of 3.5 m of bedded diamicton, sand, and gravel (Figure 4.4). These sediments have been grouped within Unit 8, given the same orientation of fabrics measured 3 m below and 8 m and the similar till composition observed in samples above and below this bed (Hodder and Gauthier, 2025). This single occurrence of intertill sorted sediments beds is interpreted to have been deposited in either a subglacial or proglacial environment based on the presence of repetitive diamicton beds requiring a nearby glacial source; however, further stratigraphic investigations may provide additional insight into the origin of these sediments. The lower contact of Unit 8 till occurs with Unit 2 (one occurrence), Unit 6 (four occurrences), Unit 7 (two occurrences) or was not observed due to excessive colluvium (three occurrences). The upper contact of Unit 8 till occurs with intertill sorted sediments of Unit 9 (one occurrence), Unit 10 (one occurrence), Unit 11 (two occurrence), Unit 12 (four occurrence), Unit 13 (one occurrence) or Unit 15 (one occurrence).

4.5.1.10 Unit 9: Till deposited by E-trending ice-flow and minor sorted sediments

Unit 9 consists of massive, matrix-supported diamicton that is 0.8 to 1.9 m thick and is best exposed at section 21-811 (Figure 4.6, Appendix C, Supplemental material 1, Figure S1-1). The matrix colour is greyish brown or dark greyish brown (Appendix C, Supplemental material 1, Table S1-2) and grain size ranges from 38–46 wt. % sand, 40–43 wt. % silt and 14–20 wt. % clay (Appendix C, Supplemental material 1, Figure S1-3). The massive structure, clast-shape and other clast characteristics (bullet-shaped, faceted and striated), lodged in-situ clasts with striated upper surfaces and lateral continuity indicate that Unit 9 diamicton is a subglacial traction till (Evans et al., 2006; Evans, 2018). Unit 9 contains abundant granitoid clasts relative to the dataset (Figure 4.10) and clast fabric measurements are interpreted to have formed by E-trending (85–88°) ice-flow (Figures 4.4, 4.6; Appendix C, Supplemental S1, Table 1-3). At section 21-811 the lower 0.25 m of the diamicton is interbedded with moderately sorted, medium to very coarse sand, which is underlain by well sorted, horizontally bedded fine sand and silt. The sand and silt beds have variable thickness (0.15–0.90 m) and drape the lower undulating contact with Unit 8 till. This single occurrence of intertill sorted sediments has been grouped with Unit 9 till and is interpreted to have been deposited in a proglacial or subglacial environment. The lower contact of Unit 9 till occurs with Unit 6 till (one occurrence) or 8 till (two occurences). The upper contact of Unit 9 till occurs with Unit 10 (one occurrence) or Unit 12 (one occurrence).

4.5.1.11 Unit 10: Till deposited by W-trending ice-flow and minor sorted sediments

Unit 10 consists of massive, matrix-supported diamicton that contains striated, bullet-shaped and faceted clasts that is 0.9 to 1.9 m thick and is best exposed at section 21-811 (Appendix C, Supplemental material 1, Figure S1-1). The matrix colour is olive brown or dark greyish brown (Appendix C, Supplemental material 1, Table S1-2) and has a sandy-silt texture (33–34 wt. % sand, 49 wt. % silt and 17–18 wt. % clay; Appendix C, Supplemental material 1, Figure S1-3). Unit 10 till contains a high proportion of HBB clasts (Figure 4.10) and clast fabric measurements are interpreted to have formed by W-trending (265–268°) ice-flow (Figures 4.4, 4.6; Appendix C, Supplemental material 1, Table S1-3). This interpretation is supported by the stratigraphy at section 21-811

(Appendix C, Supplemental material 1, Figure S1-1), where Unit 9 and 10 tills are in sharp contact with sediments that have similarly oriented till fabrics, yet contrasting compositional and qualitative properties. The lower contact of Unit 10 till occurs with Unit 8 (one occurrence) or Unit 9 (one occurrence). The upper contact of Unit 10 till occurs with Unit 11 (one occurrence) or Unit 12 (one occurrence).

4.5.1.12 Unit 11: Interglacial sediments

Unit 11 sorted sediments are identified at three sections, defined by its sharp upper bounding surface with Unit 12 (one occurrence) or Unit 13 (two occurrences) and lower bounding surface with Unit 8 (two occurrences) or Unit 10 (one occurrence; Figures 4.4, 4.6). Unit 11 consists of bedded silt, sand and gravel and is described in detail for each section investigated.

At section 21-828, a thick (8.5 m) package of intertill sorted sediments is situated between Unit 8 and Unit 13 tills at an elevation of 188–196 m asl (Figure 4.15). The lowermost 0.4 m of this sequence is composed of poorly sorted, bouldery sandy gravel that is in contact with the underlying till. The uppermost sample from Unit 8 till (12.4–12.6 m depth) at the contact with sandy gravel contains decreased proportions of silt and clay compared to underlying till samples (Figure 4.15) and the texture is anomalous compared to all till samples collected (c.f., Appendix C, Supplemental material 1, Figure S1-3), which indicates that the upper surface of the till was winnowed upon submergence with fines removed. Above the bouldery sandy gravel is 2.3 m of clast-supported sandy gravel. The gravel contains granule- to large pebble-sized clasts and shell fragments were observed through the sediment. A large (1 cm diameter) shell fragment collected at 12.0 m depth has a $\delta^{13}C$ value of 2.0 ‰ and a near-finite radiocarbon age of 44.5 ± 0.9 ^{14}C ka BP (UOC-16663; Figure 4.8; Table 4.3). The $\delta^{13}C$ value confirms that this shell fragment is from a marine organism since freshwater shells have lower $\delta^{13}C$ values (McConnaughey and Gillikin, 2008), which in Manitoba is typically a $\delta^{13}C$ of <1.0 ‰ (Gauthier, 2022). The near-finite ^{14}C age is interpreted as a nonfinite age based on the unreliability of shell materials near the upper limit of radiocarbon dating (Miller and Andrews, 2019). Overlying the sandy gravel is 0.8 m of massive pebbly coarse sand with 2–5% clasts that are pebble-sized or larger and contains shell fragments. The upper 5.0 m of the

intertill sediments consists of coarse sand with <1% clasts. The coarse sand is weakly horizontal- to cross-bedded in places and contains shell fragments. The sequence of sediments exposed at section 21-828 is interpreted to represent a marine transgression of Hudson Bay marine waters after deglaciation and these marine sediments have been recognized by a letter modifier and designated as Unit 11a. This interpretation is based on the thick fining upwards sequence from gravel to coarse sand, presence of shell fragments throughout and $\delta^{13}C$ value of a shell fragment at 12.0 m depth indicating it was a marine organism.

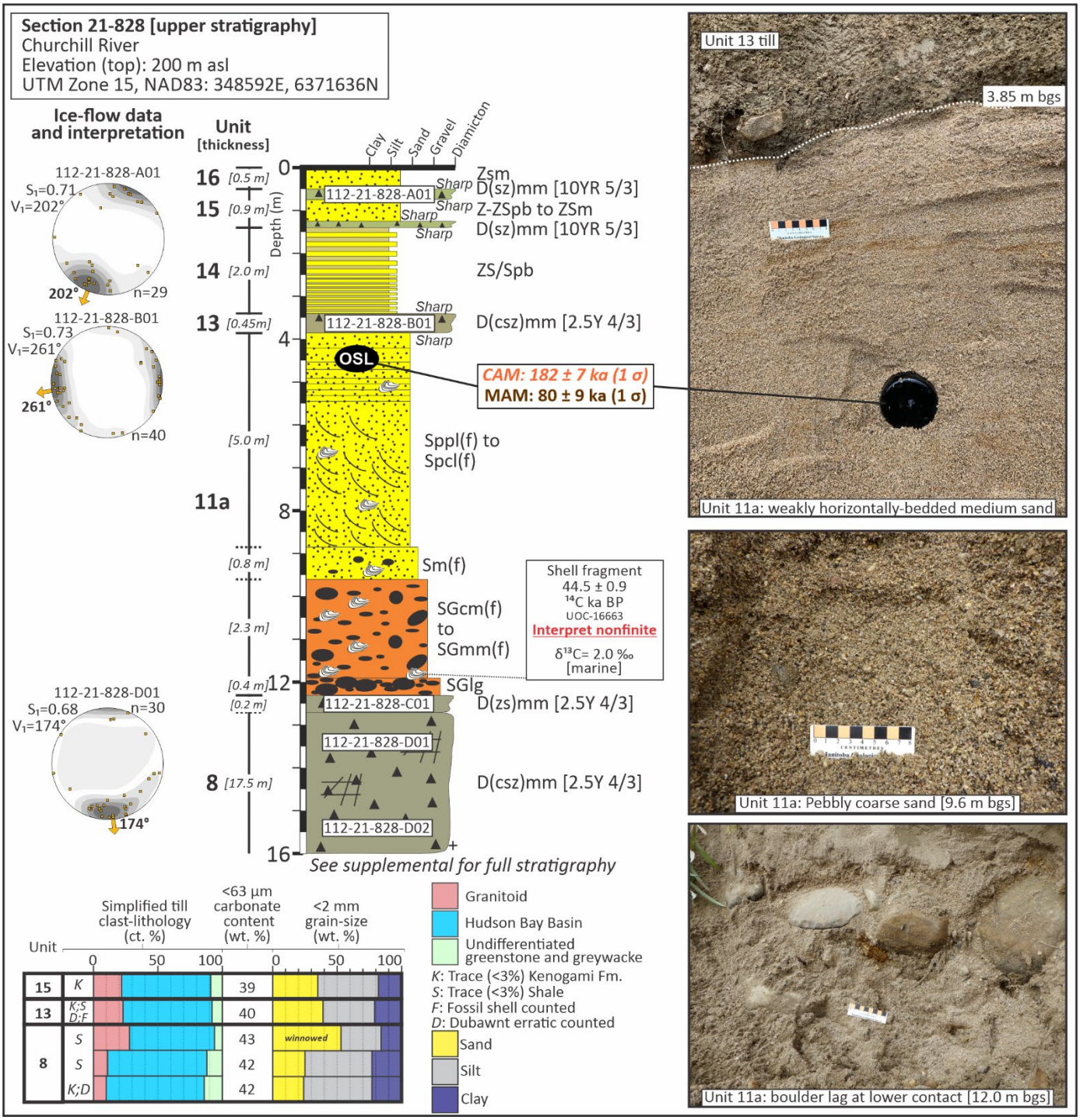

Figure 4.15: Uppermost Quaternary stratigraphy exposed at section 21-828 (0–16 m bgs). Till sample numbers are labelled within the white boxes. Simplified clast-lithology counts, <63 µm carbonate values and matrix texture data are provided for these samples in the bottom left panel. Till clast-fabric data are plotted on equal area, lower hemisphere projection stereonets. The value of the principal eigenvalue (S_1) and direction of the principal eigenvector (V_1) are provided, and an interpretation of the ice-flow direction is indicated (orange arrow). Please refer to Appendix C, Supplemental material 1, Table S1-1 for a translation of the lithofacies codes used.

At section 21-811, a thick (5.1 m) package of intertill sorted sediments is situated between Unit 12 and Unit 10 tills at an elevation of 177.5–182.5 m asl (Appendix C, Supplemental material 1, Figure S1-1). This package of sediments contains a sequence of fining-upwards sediments from clast-supported gravel to cross-bedded sand with washed till at the lower contact, similar to the sequence of lithofacies observed at section 21-828. Shell fragments were observed in the sediment from 5.5–6.2 m and 8.0–8.5 m depth and no other organics were uncovered. These sediments have been assigned to Unit 11a based on the similar sequence of sediments described at section 21-828 and is interpreted to represent a marine transgression following deglaciation of the region.

At section 21-812 (Figure 4.4; Appendix C, Supplemental material 1, Figure S1-2), a thick (6.5 m) package of intertill sediments is situated between Unit 12 and Unit 8 tills at an elevation of 188–194 m asl. The sediment consists of fine to coarse sand that is massive to horizontally bedded and is in sharp contact with the underlying Unit 8 till. Organic materials were noted throughout the sediment package including: shell fragments throughout, small pieces of wood (≤1 cm in length) and disseminated organics at 2.2–4.2 m depth, detrital organic granules (1–2 mm in diameter) at 4.2–4.3 m depth and a relatively high concentration of flattened twigs and wood fragments (≤10 cm in length) at 7.7–8.7 m depth. One flattened piece of wood (1.0 x 3.0 cm) at 7.7 m depth has a nonfinite radiocarbon age (>50 ^{14}C ka; UOC-16584; Table 4.3). The organic granules were analyzed for pollen and contained traces of Cyperaceae, *Sphagnum*, *Typha*, *Picea*, *Pinus* and *Salix*, which would suggest similar boreal wetland conditions as today in the region. However, this interpretation should be taken with caution because pollen counts were very low in this sample owing to extremely low concentrations (<5000 grains/ml) and very poor preservation (>30% broken; Table 4.1; Dalton et al., 2024). The thickness of Unit 11b at section 21-812 was noted to change laterally in the field but it was difficult to investigate laterally in 2021 due to colluvium on the section slopes. Dredge et al. (1990) noted that this stratigraphic bed is only 0.4 m thick along the same exposure, which indicates that the thickness of this stratigraphic bed changes significantly laterally. This sequence of sediments at section 21-812 is interpreted to have been deposited in a fluvial environment, possibly a floodplain, based on the sedimentary characteristics of the site, along with the abundance of peat granules and wood, which are commonly integrated into fluvial sediments.

Alternatively, the sediment could have been deposited in a nearshore lacustrine environment with detrital input from a nearby creek/river or an oxbow lake.

4.5.1.13 Unit 12: Till deposited by NW- trending ice-flow and associated glaciofluvial sediments

Unit 12 consists of massive, matrix-supported diamicton that contains striated, bullet-shaped and faceted clasts that is 1.2–9.0 m thick and is best exposed at section 21-811 (Appendix C, Supplemental material 1, Figure S1-1). The matrix colour is brown, light olive brown, olive brown or dark greyish brown (Appendix C, Supplemental material 1, Table S1-2) and is predominantly silt (22–32% sand, 50–59% silt and 18–26% clay; Appendix C, Supplemental material 1, Figure S1-3). The diamicton is overconsolidated but less than underlying tills (where observed) and has a minor blocky appearance or no blocky appearance. The massive structure, clast-shape and characteristics (bullet-shaped, faceted and striated), lodged in-situ clasts with striated upper surfaces and lateral continuity indicate that Unit 12 diamicton is a subglacial traction till (Evans et al., 2006; Evans, 2018). Unit 12 till contains high proportion of HBB clasts and a variable proportion of UGG clasts; therefore, the directions of Unit 12 clast fabrics are interpreted to have formed by WNW- to NNW-trending (298–348°) ice-flow (Figures 4.4, 4.6; Appendix C, Supplemental material 1, Table S1-3). One till fabric in Unit 12 is oriented perpendicular to this orientation (230°) and is interpreted be a transverse fabric or could represent a shift in ice-flow direction during deposition at this site (section 21-804). A similar till at the same stratigraphic position was identified at three nearby sections situated to the SW of section 21-804 (Figure 4.6). Unit 12 till at section 21-820 has a sharp lower contact with 9.0 m of gravel. The gravel is massive, poorly sorted, clast- to matrix-supported and contains subrounded to subangular granule- to large pebble-sized clasts. The clasts consist of a mixed lithology, but the majority are carbonate lithologies (Appendix C, Supplemental material 2). Thick colluvium along the river bank inhibited lateral observations of this gravel bed; however, section 21-819 is situated 300 m to the west-southwest of section 21-820 and this gravel bed is absent in the stratigraphic record at that section (Figure 4.4). This gravel bed is interpreted to have been deposited in a glaciofluvial environment based on the poor sorting, massive structure, dominant carbonate lithology which suggests a provenance toward the east, thickness of this bed

which requires a high sediment supply and geometry of the bed which is laterally discontinuous. This single occurrence of intertill sediment is grouped with Unit 12 till and is interpreted to be associated with the glacial event. The lower contact of Unit 12 till occurs with Unit 6 (one occurrence), Unit 8 (four occurences), Unit 10 (one occurrence) or Unit 11 (two occurences). The upper contact of Unit 12 occurs with Unit 13 till (three occurrences), Unit 15 till (one occurrence) or was observed to the top of the section (four occurrences).

4.5.1.14 Unit 13: Till deposited by W-trending ice-flow

Unit 13 consists of massive to stratified, matrix-supported diamicton that contains striated, bullet-shaped and faceted clasts that is 0.5 to 4.0 m thick and is best exposed at section 21-805 and 21-807 (Figure 4.8). The diamicton is overconsolidated but less consolidated relative to underlying tills (where observed) and does not have a blocky appearance. The matrix colour is brown, light olive brown or olive brown (Appendix C, Supplemental material 1, Table S1-2) and grain size ranges are 18–39 wt. % sand, 39–60 wt. % silt and 18–23 wt. % clay (Appendix C, Supplemental material 1, Figure S1-3). The massive structure, clast-shape (bullet-shaped, faceted and striated), lodged in-situ clasts with striated upper surfaces and lateral continuity indicate that Unit 13 diamicton is a subglacial traction till (Evans et al., 2006; Evans, 2018). Unit 13 till contains a high proportion of HBB clasts and a variable proportion of UGG clasts; therefore, the direction of Unit 13 clast fabrics are interpreted to have formed by W-trending (261–275°) ice-flow (Figure 4.4, 4.6; Appendix C, Supplemental material 1, Table S1-3). Unit 13 is in sharp contact with unit 12 at section 21-805 and 21-814 with high quality ice-flow indicators at both sections providing a robust stratigraphic relationship between Unit 12 and 13 tills. The upper contact of Unit 13 till occurs with Unit 14 (two occurrences), Unit 15 (one occurrence), Unit 16 (one occurrence) or was observed to the top of the section (two occurrences).

4.5.1.15 Unit 14: Proglacial intertill sorted sediments

Unit 14 sorted sediments are identified at four sections, defined by its sharp upper bounding surface with Unit 15 till (all occurrences) and lower bounding surface with Unit 13 (two occurrences) or not determined (bottom of section). Unit 14 consists of bedded clay, silt, sand and gravel and is best

exposed at section 21-827 (Figure 4.16). At section 21-827, Unit 14 consists of rhythmically bedded silt and sand and the thickness of the beds increases up-section from 0.05–0.10 m at the base of section to 0.10–0.30 m thick at the upper contact with Unit 15. The upper contact with Unit 15 is sharp and marked by the presence of a clast pavement (Figure 4.16). These sediments are interpreted to have been deposited in a proglacial lake based on the rhythmic bedding and the increased sediment input up-unit due to the advancing ice that deposited the overlying till at this site (Unit 15). A similar sequence of proglacial lacustrine sediments is interpreted at section 21-828 (Figure 4.15) and 21-812 (Appendix C, Supplemental material 1, Figure S1-2). At section 21-802/803, Unit 14 is at least 4.3 m thick and consists primarily of poorly sorted, matrix-supported sandy gravel to gravelly sand with granule- to small cobble-sized clasts. This gravel is capped by a 0.3 m thick bed of horizontally bedded fine sand, coarse sand and granules, that is in sharp contact with Unit 15 till. The gravels lack bedding and require a high energy sediment input to deposit the thick beds and it is interpreted that these sediments were deposited in a glaciofluvial or proglacial environment.

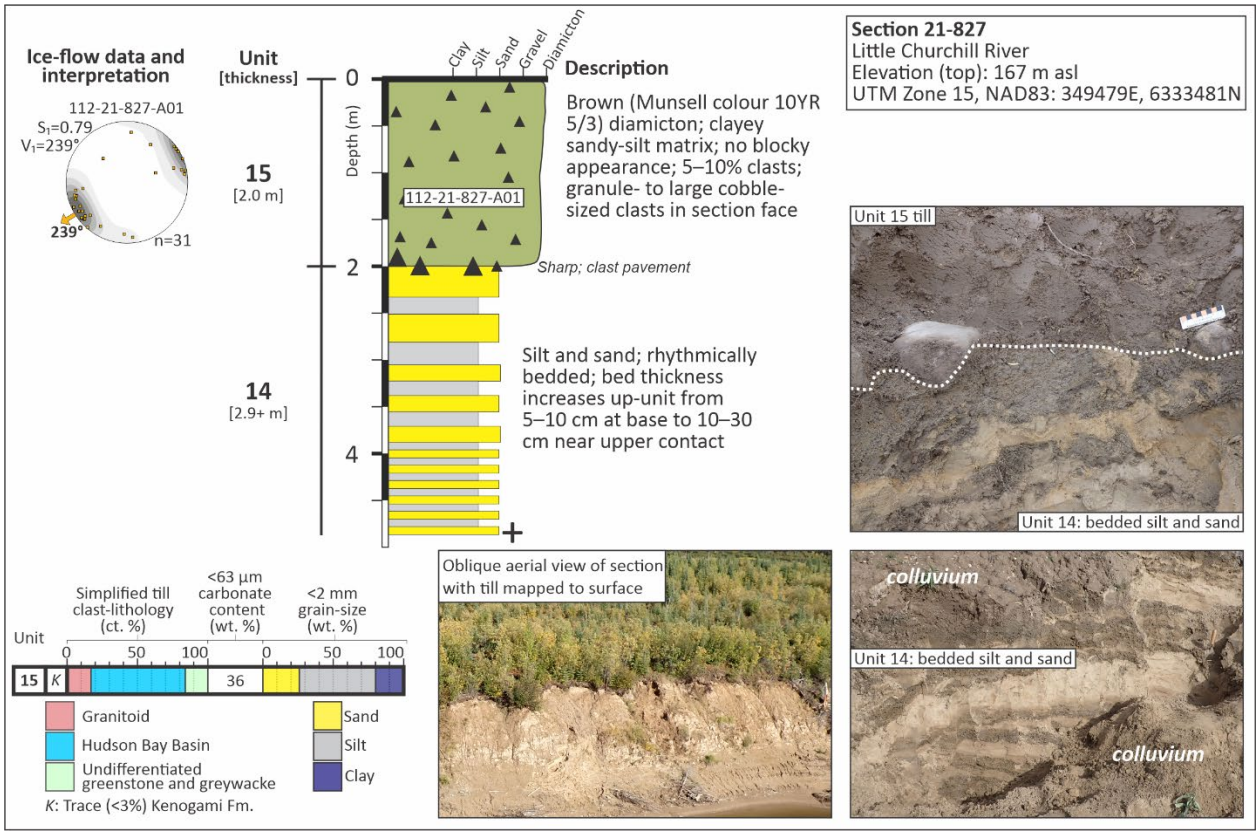

Figure 4.16: Quaternary stratigraphy exposed at section 21-827 on the Little Churchill River. Till sample numbers are labelled within the white boxes. Simplified clast-lithology counts, <63 µm carbonate values and matrix texture data are provided for these samples in the bottom left panel. Till clast-fabric data are plotted on equal area, lower hemisphere projection stereonets. The value of the principal eigenvalue (S_1) and direction of the principal eigenvector (V_1) are provided, and an interpretation of the ice-flow direction is indicated (orange arrow).

4.5.1.16 Unit 15: Till deposited by a WSW- to S-trending re-advance

Unit 15 consists of massive to stratified, matrix-supported diamicton that is 0.3 to 6.0 m thick and is best exposed at section 21-827 (Figure 4.16). The diamicton contains striated, bullet-shaped and faceted clasts, is overconsolidated but less consolidated relative to underlying tills (where observed) and does not have a blocky appearance (e.g., Figure 4.16). The matrix colour is brown or light olive brown (Appendix C, Supplemental material 1, Table S1-2) and grain size ranges are 17–35 wt. % sand, 47–64 wt. % silt and 18–24 wt. % clay (Appendix C, Supplemental material 1, Figure S1-3). The

massive structure, clast-shape (bullet-shaped, faceted and striated), lodged in-situ clasts with striated upper surfaces and lateral continuity indicate that Unit 15 diamicton is a subglacial traction till (Evans et al., 2006; Evans, 2018). Unit 15 till contains a high proportion of HBB clasts (Figure 4.10) and the direction of the Unit 15 clast fabrics are interpreted to have formed by SSW- to WSW-trending (200–245°) ice flow, with one fabric indicating a S-trending (177°) ice-flow (Figures 4.4, 4.6; Appendix C, Supplemental material 1, Table S1-3). The lower contact of Unit 15 till occurs with Unit 8 (one occurrence), Unit 12 (one occurrence), Unit 13 (one occurrence) or Unit 14 (four occurrences). The upper contact of Unit 15 occurs with Unit 16 (one occurrence) or was observed to the top of the section (six occurrences).

4.5.1.17 Unit 16: Surficial glaciofluvial and post-glacial sediments

Unit 16 consists of massive to bedded clay, silt, sand and gravel that was deposited during the Holocene Epoch (MIS 1) during and following retreat of the LIS from northeastern Manitoba. These sediments were deposited in glaciofluvial, glaciolacustrine or fluvial environments and have collectively been grouped into one stratigraphic unit for simplicity. The distribution of these surficial sediments has been mapped at a 1:250 000 scale (Dredge and Nixon, 1982). A detailed investigation of the post-glacial history of this region is beyond the scope of this manuscript; however, some aspects of the postglacial history of the study area are discussed in Gauthier et al. (2020, 2022) and Dredge and Nixon (1992).

4.5.1.18 Surficial till(s)

The surficial till is light olive brown or yellowish brown (Appendix C, Supplemental material 1, Table S1-2). Surficial till samples were collected from west or northwest-oriented streamlined landforms (n=2) or from hummocky terrain (n=6). These till samples are not linked to till units defined by sections.

4.5.2 Till-matrix geochemistry

Till beds with a black-coloured matrix contain a relatively high abundance of black to dark grey siltstone and shale clasts. These black tills were observed at four sections where it is the lowermost

exposed till bed at each site (three Unit 2 occurrences and one Unit 8 occurrence). The source of the siltstone/shale detritus is an enigma, since there is no known bedrock source in the region (Dredge and Nixon, 1992). Exploratory data analysis indicated that these black tills (n=6 samples) have a unique geochemical signature that accounts for most of the variance observed in the dataset (Appendix C, Supplemental material 3). Second, there is a single occurrence of grey till with a highly elevated proportion of granitoid clasts (81 ct. %), which is an outlier within the dataset (Figure 4.10) and has a unique geochemical signature (Appendix C, Supplemental material 3).

While these are important observations, to further understand the relationship between identified stratigraphic units and the till-matrix geochemistry, a second iteration of PCA and k-means cluster analysis was performed with these seven samples removed from the dataset. The second iteration of the statistical analysis indicated that principal component (PC) 1, 2, 3 and 4 account for 52%, 14%, 11% and 10% of the observed variance within the dataset, respectively (Appendix C, Supplemental material 3). The k-means clustering analysis indicated 6 clusters within the dataset based on the scree plot of the sum of squares distances of samples to their closest cluster center (Appendix C, Supplemental material 3). Samples were classified according to their identified cluster and were plotted on a bivariate plot of PC2 vs. PC1 (Figure 4.17a) and on a bivariate plot of till granitoid vs. UGG clast content (Figure 4.17b). Using these two bivariate plots we can gain insight into elemental assemblages and their relationship with clast provenance. For example, cluster 4 and to a less extent cluster 3 encompass samples with relatively elevated UGG clast concentrations in the dataset and these two clusters are associated with Na, K and Ti (Figure 4.17a, b). Likewise, Cluster 5 and to a less extent Cluster 6 encompass samples with relatively high granitoid concentrations, and these two clusters are associated with Fe, Si, Al and Ti (Figure 4.17a, b). Importantly, this multivariate analysis reinforces provenance interpretations that were established with till clast counts providing a second parameter to confirm sediment provenance. For example, till clast counts indicated that starting with Unit 12 and continuing with units 13, 15 and surficial till samples, there is a provenance shift represented by an influx of UGG clasts (Figure 4.10). This same relationship is observed with a higher proportion of matrix-geochemistry cluster 4 within Units 12, 13 and 15 and surficial till samples (Figure 4.17c). Unit 9 and 10 are interpreted to have been deposited by ice-flowing in near opposite

directions and this is reflected within the till-matrix geochemical dataset (Figure 4.17), which supports interpretations made using ice-flow data and till clast-lithology counts that these two tills are compositionally distinct.

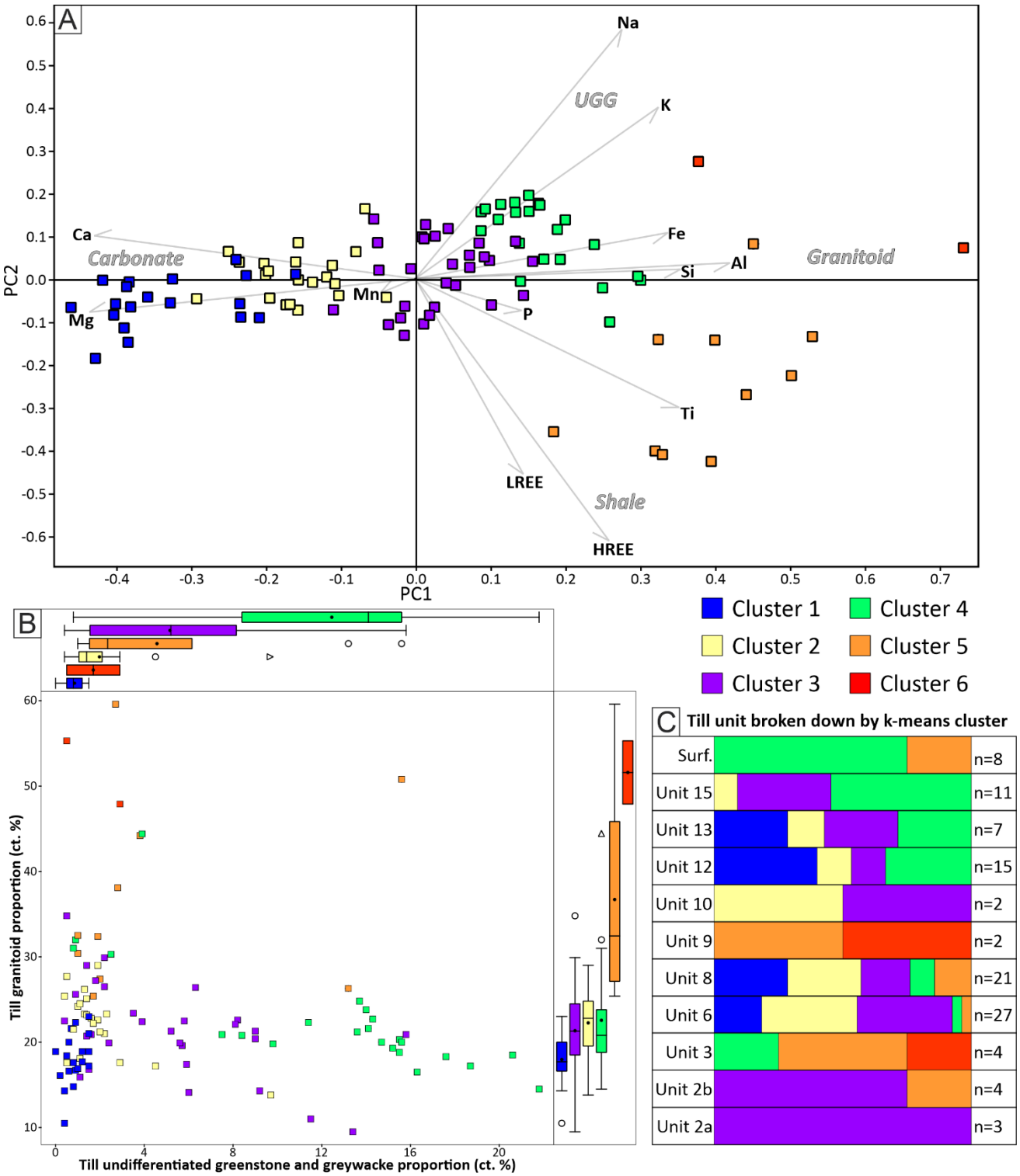

Figure 4.17: A) Till-matrix geochemistry (<63 µm size-fraction) k-means cluster analysis results plotted on PC2 vs. PC1; B) Till-matrix geochemistry (<63 µm size-fraction) k-means cluster analysis results plotted a biplot of till granitoid vs. undifferentiated greenstone and greywacke clasts; and C) k-means cluster analysis results according to sampled till unit.

Ultimately though, this analysis highlights the difficulties in identifying stratigraphic units with a strictly compositionally-based approach (Figure 4.17c). In thick sediment terrains, such as this study area, till provenance analysis is complicated by principles of inheritance and overprinting (Stea and Finck, 2001), where successive differently oriented ice-flow events cannibalize previously deposited till leading to a complicated mixed provenance signature that varies spatially within any given stratigraphic bed (e.g., distance from lower contact). Thus, the result is a stratigraphy whereby till units are rarely discernible using only till compositional datasets, but compositional analysis may bring key insights into the degree of mixing due to inheritance and overprinting. In this study, a simple k-means clustering approach was used, which has its own limitations.

4.5.3 Optical ages

The optical age of sorted sediments sampled from units 4, 7 and 11 were determined (Table 4.4). For all of the samples luminescence signals were dominated by the thermally-stable 'fast component' desirable for dating (Appendix C, Supplemental material 4, Figure S3-3) and passed the selection criteria built into the SAR protocol and the suitability of the chosen SAR protocol was checked using dose recovery tests (Appendix C, Supplemental material 4). Radial plots showing the distribution of accepted aliquot D_e values for each sample are provided in Appendix C, Supplemental material 4. The new stratigraphic framework interprets units 1, 4 and 11 to be interglacial, and Unit 7 as possibly a proglacial deposit. No optical dating was attempted on Unit 1 sediments since quartz grains within these sediments are likely saturated and thus beyond the limit of this dating method. For Unit 4, a surprisingly young MAM age of 123 ± 21 ka was obtained for Unit 4a (nearshore marine facies) and conflicting MAM ages of 84 ± 12 ka and 184 ± 13 ka for Unit 4b (fluvial or nearshore lacustrine facies). For Unit 7, a single MAM age of 143 ± 14 ka was obtained. For Unit 11, MAM ages range from 41 ± 4 to 80 ± 9 ka for Unit 11a (possibly nearshore marine facies) and conflicting ages of 79 ± 11 and 173 ± 12 ka for Unit 11b at section 21-812 (fluvial or nearshore lacustrine facies).

Table 4.4: Number of aliquots measured (n), overdispersion values (OD), equivalent dose values (D_e), optical ages, and dose recovery (DR) ratios.

Section_ID	Unit	Interpreted depositional environment	Lab ID	n[a]	OD (%)	D_e (Gy) – C[b]	D_e (Gy) – M[c]	Age (ka) - C	Age (ka) - M	DR ratios[d]
112-21-832	4a	nearshore marine	HBL21-14	21/36	12 ± 4	328 ± 13	321 ± 21	183 ± 9	180 ± 13	0.99 ± 0.03
112-21-819	4a	nearshore marine	HBL21-11	24/48	30 ± 6	261 ± 19	190 ± 30	168 ± 16	123 ± 21	--
112-21-812	4b	fluvial or lacustrine	HBL22-5	26/45	33 ± 6	240 ± 18	161 ± 21	126 ± 12	84 ± 12	--
112-21-806	7	proglacial lacustrine	HBL21-6	24/58	17 ± 4	271 ± 13	258 ± 22	150 ± 10	143 ± 14	1.12 ± 0.04
112-21-828	11a	nearshore marine	HBL21-13	29/51	49 ± 8	259 ± 27	124 ± 13	182 ± 17	80 ± 9	0.80 ± 0.06
112-21-811	11a	nearshore marine	HBL21-7	29/34	22 ± 3	99 ± 4	79 ± 7	50 ± 4	41 ± 4	0.93 ± 0.02
112-21-811	11a	nearshore marine	HBL21-8	37/42	31 ± 4	96 ± 5	68 ± 6	60 ± 4	44 ± 4	0.93 ± 0.03
112-21-812	11b	fluvial or lacustrine	HBL21-10	30/83	40 ± 7	262 ± 22	141 ± 18	147 ± 14	79 ± 11	0.99 ± 0.03
112-21-812	11b	fluvial or lacustrine	HBL21-9[e]	20/44	0 ± 3	293 ± 7	291 ± 14	174 ± 10	173 ± 12	0.98 ± 0.04

[a]N = numbers of aliquots accepted/number of aliquots measured

[b]C = Determined using the central age model (CAM)

[c]M = Determined using the three-parameter minimum age model (MAM)

[d]DR = dose recovery ratio (given dose/recovered dose)

[e]Sample HBL21-9 age with one outlier removed, refer to Appendix C, supplemental material 4

Note: equivalent dose and OD values calculated using the software of Liang and Forman, 2019

4.6 Discussion

The fragmented Quaternary stratigraphic record of the study area, deciphered using a hybrid lithostratigraphy-allostratigraphy framework, contains 16 units (Figure 4.18). This newly-developed local stratigraphic framework consists of Holocene-aged sediments that are underlain by nine glacial (till) units, three proglacial units and three pre-Holocene interglacial units. In addition to these Quaternary-aged sediments, one occurrence of weathered material derived from Precambrian granite was recognized that could predate the Quaternary Period. We first discuss the chronological framework and then present an overview of glacial and interglacial dynamics from the Late Pleistocene (Glaciation I: MIS 5-1), the penultimate glacial cycle (Glaciation II: MIS 6) and earlier ice-flow phases (Glaciation(s) III: MIS 8 and earlier).

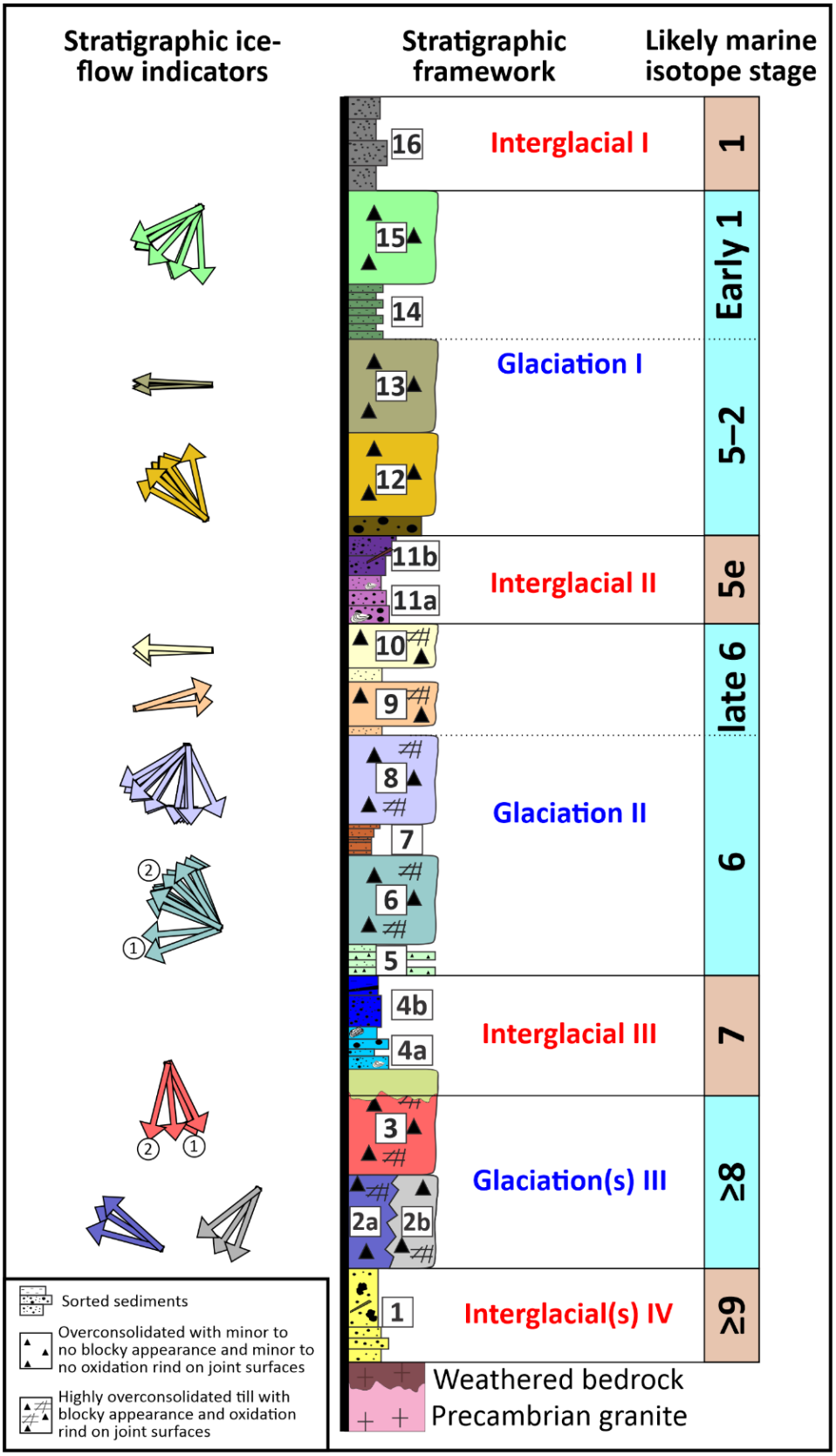

Figure 4.18: Quaternary stratigraphic framework of the Churchill to Little Churchill rivers area with interpreted glacial and interglacial intervals.

4.6.1 Reconciling the timing of marine incursions and interglacial sedimentation

In the current study, radiocarbon dating attempts on wood obtained from intertill sorted sediments all yielded infinite ages, and we therefore anchor most of our chronological framework on quartz optical dating. The optical dating samples analysed had dose responses that are best fit with a saturated exponential plus a linear component (SEPL). A SEPL dose response has been observed for quartz in many optical dating studies worldwide (e.g., Buylaert et al., 2007; Murray et al., 2007; Murray et al., 2008; Pawley et al., 2008, 2010; Lowick et al., 2010; Arnold et al., 2016). Studies with independent age controls have indicated the SEPL dose response can produce small age underestimations of 10–15% for MIS 5-aged deposits (Murray et al., 2007). Yet, other studies have indicated that the SEPL dose response can produce significant age underestimations (Timar et al., 2010). In this case, Timar et al. (2010) interpreted that extrapolation from the linear portion of the curve resulted in age underestimation for samples >70 ka (D_e values of ~200 Gy). The magnitude of this underestimation was ~50% for a modelled age consistent with MIS 9 (~337–300 ka). Similarly, studies of loess deposits in China suggest limiting samples with SEPL dose responses to ages <50–40 ka (D_e values of ~120–150 Gy) and that older optical ages should be regarded as minimum ages citing potential age underestimations (Buylaert et al., 2007; Buylaert et al., 2008). Despite these challenges associated with dating older deposits with SEPL dose responses, Murray et al. (2008) indicated the D_e extrapolation from the linear portion of the SEPL dose response produced accurate ages for an intertill MIS 7-aged (~247–191 ka) deposit, while Pawley et al. (2008, 2010) produced optical ages as old as 450 ka (MIS 12) from samples with SEPL dose responses that were consistent with independent age information. These high age values were in part enabled by low environmental dose rates at their sites. It should be noted, however, that in most of these studies independent chronological information is uncertain. In our previous work in the HBL, east of this study within the Hudson Bay Basin, we have found that optical ages derived from quartz samples with SEPL dose responses are consistent with independent palaeobotanical and stratigraphic information (Hodder et al., 2023, 2024; Gauthier et al., 2024, 2025). Moreover, a detailed technical study by Lowick and Preusser (2011) could find no issues with using SEPL dose reponses to dertemine optical ages from their quartz samples.

Considering all these results together it seems that the efficacy of optical dating of quartz with SEPL dose responses may be sample dependent, influenced by local bedrock geology (quartz luminescence characteristics). Until the mechanism that results in SEPL dose responses is determined, and a reason(s) why it apparently can be applied successfully for some samples but apparently not for others, ages derived from it should be interpreted with caution (e.g., Li et al., 2015) and together with other information. As with the work of Pawley et al. (2008, 2010), this study had to apply laboratory doses of up to 528 Gy to construct dose response curves that natural signals could be interpolated onto to find a D_e (i.e., the linear part of the SEPL curve). Calculated D_e values were all >200 Gy, except for the sample collected from Unit 11a (Table 4.4). For the reasons mentioned above, our ages should be considered minimum values (underestimations), assuming that the samples investigated were sufficiently bleached prior to burial. It is possible that these samples were partially bleached before burial, given the interpreted depositional environments in this study (e.g., fluvial), then signal-inherited grains within aliquots could increase the calculated D_e values. In consideration of depositional environment, we have therefore chosen to use the MAM D_e values and interpret the resultant ages as minimum limiting ages for each unit. The CAM ages are provided in Table 4.4 and are discussed alongside MAM ages for some units. We then compare these optical ages for each interglacial unit identified with the marine $\delta^{18}O$ record to identify time periods of significantly reduced global ice volume and focus on terminations (transitions from glacial to interglacial stages), since these relatively abrupt changes are necessary to have significant marine transgression into the western HBL. Furthermore, sediment with a pollen signature that indicates a climatic signature similar to the present day presumably requires reduced North American ice sheets with $\delta^{18}O$ values similar to the present day providing supporting evidence for interglacial interpretations.

Unit 11a sediments are situated at 178–196 m asl and are interpreted to have been deposited during a marine transgression (e.g., Figure 4.15). For reference, following MIS 2 deglaciation of northern Manitoba the local marine limit was 140–150 m asl in the Churchill River area (Gauthier et al., 2020) and was up to ~170–180 m asl at Caribou Lake (~110 km north of this study) in northeastern Manitoba (McMartin et al., 2022). Thus, in order to deposit marine sediments at 178–

196 m asl it requires a significantly depressed landscape following deglaciation coupled with relatively high eustatic sea level that is comparable to Termination I (~14 ka, MIS 2 to 1 transition). The MAM optical ages from these marine sediments (Unit 11a) indicate a minimum depositional age in the range of ~41–81 ka, while the fluvial sediments of Unit 11b have MAM optical ages of ~79 and 173 ka and contain wood with a nonfinite ^{14}C age. Considering the scant evidence for an ice-free Hudson Bay during MIS 3 (Miller and Andrews, 2019; Hodder et al., 2023), we have interpreted that Unit 11 sediments were likely deposited during MIS 5 (Figure 4.18), with Unit 11a likely deposited during termination II (~130 ka; MIS 6 to 5 transition).

Unit 4a sediments are situated at 143–161 m asl and are interpreted to have been deposited in a marine environment (Figure 4.13). Similar to Unit 11a, in order to deposit marine sediments at this elevation it requires a significantly depressed landscape and sea level that is close to that observed during Termination I (MIS 2 to 1 transition). Since this period of marine inundation is interpreted to have occurred prior to Termination II (130 ka, MIS 6–5 transition) that deposited Unit 11a, the most likely timing of deposition for Unit 4a is during Termination III (243 ka, MIS 8–7 transition; Lisiecki and Raymo, 2005). The stratigraphy at section 21-832 (Figure 4.11) indicates that following regression of marine waters, there was an interglacial climate similar to the present day (Unit 4b). This provides supporting evidence that Unit 4 was deposited during an interglacial period. The MAM optical ages indicate a minimum depositional age of ~123 ± 21 (HBL21-11) and 180 ± 13 ka (HBL21-14) at two sites investigated, which overlap at 2σ. Note, the CAM optical for sample HBL21-11 is 168 ± 16 ka, which is within 1σ error of the CAM and MAM age for sample HBL21-14 and the overdispersion for HBL21-11 is higher (30 ± 6 %) compared to HBL21-14 (12 ± 4 %). This suggest that the HBL 21-14 is possibly a more robust age estimation for Unit 4a. Considering the stratigraphic relationships identified, and interpreting the optical ages as minimum limiting, our current interpretation is that Unit 4 was deposited during the MIS 7 interglacial period (Figure 4.18).

There are currently no geochronological constraints for Unit 1 sediments other than they were likely deposited during or before MIS 9 since they are separated from Unit 4 interglacial sediments by at least one, and possibly three glacial episode(s) (Figure 4.18). Unit 1 sediments are defined by their upper bounding surfaces with Unit 2 or 3 tills and could have been deposited during the same

interglacial episode or possibly during different interglacial episodes since correlations between sections are uncertain. For example, Unit 1 sediments are underlain by weathered bedrock at section 21-826, a surface which could potentially predate the Quaternary Period. Additional stratigraphic and geochronological studies (e.g., cosmogenic burial, electron spin resonance and/or single-aliquot quartz optical dating) are necessary to understand the significance of these older nonglacial deposits and confirm age assignments for units 4 and 11.

The hybrid lithostratigraphic-allostratigraphic framework constructed in this study did not use any geochronology data to anchor interpretations. This is necessary since at many sections visited, the youngest interglacial sediments are missing and the shallowest interglacial unit at depth belongs to a much older interglacial (e.g., sections 21-805, 21-807, 21-832; Figures 4.4, 4.6). This fragmented stratigraphic record with missing interglacial intervals has now, in places, been documented at numerous localities across the western HBL (Gauthier et al., 2024, 2025; Hodder et al., 2024) and needs to be considered for any further investigations across the HBL. Age constraints produced during this study were restricted to quartz optical ages, which provided large age brackets and conflicting ages for each identified interglacial bed. Additional geochronological studies incorporating complementary age dating techniques and/or the application of single-grain optical dating would be beneficial to assess the ages assigned to interglacial beds identified and is recommended as geochronological methods improve.

4.7 Glacial dynamics

4.7.1 Glaciation I: ~MIS 5–1

The majority of glacial sediment deposition during the last glacial cycle is interpreted to have happened during advance of the ice sheet (Unit 12; Figures 4.4, 4.6). The exact timing of this ice advance is unknown but likely occurred during late MIS 5 based on numerical modelling (Stokes et al., 2012). Along the Churchill River, this early NW-trending ice-flow eroded a ‘channel’ within the landscape and deposited till (Figure 4.4). At the periphery of this mapped ice-flow event, there are preserved interglacial sediments near the surface, at a higher elevation (Figure 4.4). The

preservation of interglacial sediments at a higher elevation than the younger till is a result of these locations escaping erosion by the advancing icesheet, possibly due to being situated outside the margins of an ice stream and/or protected by cold-based ice. Following this initial NW-trending ice flow phase, the study area was overrun by W-trending ice-flow as evidenced by stacked tills in the stratigraphic record (Unit 13, e.g., Figure 4.4). Both tills deposited by NW- and W-trending ice-flow contain detritus sourced from eastern Hudson Bay that cannot be entirely sourced from underlying tills, and it is interpreted that these ice-flow events emanated from the Q-L dome. Hodder et al. (2024) recognized the preservation of a NW-trending streamlined-landform flowset at surface 250 km to the southeast of this study ('H' on Figure 4.1b) that is interpreted to have been deposited during advance of the LIS at the start of the last glaciation. We correlate this flowset to the NW-trending advance observed in the study area, based on stratigraphic position and similar till qualitative and quantitative properties (namely calcareous-rich, overconsolidated but less than underlying tills, no blocky appearance). In Quebec, a relatively early and extensive NW-trending ice-flow phase has long been recognized and hypothesized to be concurrent with inception of the LIS in the Quebec highlands north of the St. Lawrence River (Veillette et al., 1999; Veillette, 2004). Furthermore, a W-trending ice-flow, likely related to a pre-LGM ice-flow phase is also recognized (Veillette et al., 1999). These observations agree with the stratigraphic record documented herein regarding the initial growth and evolution of the Q-L dome of the LIS. These observations suggest that LIS ice-sheet growth during that last glacial cycle was not dominated by rapidly south-trending ice sheet expansion as depicted by modelling efforts (Geng et al., 2025).

Following the deposition of these 'advance' tills (c.f., Boulton, 1996), the stratigraphic record contains proglacial sediments (Unit 14) that are overlain by till (Unit 15) indicating that the ice margin retreated and then re-advanced. The timing of this retreat and advance is unknown, but the most likely timing is when paleo-ice streams were active across the area during deglaciation of the region. During this time there is evidence of ice margin retreat and advance in the Hudson Bay region (Dalton et al., 2023) and in northeastern Manitoba, which is evidenced by buried proglacial sediment within the Quinn Lake ice stream (Trommelen, 2015). Unit 15 ice-flow indicators are aligned parallel to eskers formed during deglaciation, which is when the Etawney and Whitecap

moraines were being constructed around 8.5–9.0 cal ka (Gauthier et al., 2022), suggesting the most likely timing of this ice-flow event is during deglaciation. If this re-advance is indeed late-glacial, then this suggests that ice-flowing from the Keewatin dome, or a saddle in Hudson Bay, did not cross into the study area until late MIS 2 or early MIS 1 and was sluggish or cold-based ice prior to this and did not deposit sediment.

The geomorphic record of the study area is complex and is difficult to unravel with current elevation models (Gauthier et al., 2022). Nonetheless, there are preserved W-trending (276°) landforms at surface near Churchill River (Figure 4.4b) where this ice-flow event is recognized in the stratigraphic record as Unit 13. The preservation of these streamlined landforms at surface, cross-cut by NW-SE trending eskers, provides additional evidence that the landscape experienced very limited modification after the initial NW- and W-trending ice-flow events; possibly due to cold-based conditions that could have persisted for the majority of the last glaciation in the region. This again highlights the larger influence of the Q-L dome relative to the Keewatin dome in terms of initial MIS 5 ice sheet growth and till production in central Canada. Importantly, this has implications on sediment dispersal across this region and counter-intuitively suggests that earlier Late Pleistocene ice-flow events may be more important for sediment production and dispersal compared to Late Pleistocene ice-flow events.

4.7.2 Glaciation II: ~MIS 6

During the build-up of ice in MIS 6, there is evidence for the development of a proglacial lake (Unit 5) as the ice margin advanced against topography into the study area. The formation of a proglacial lake would require natural northeastern drainage routes into Hudson Bay to be blocked. Ice-flow-indicator relationships at several sections suggest that a W- or WSW-trending (265°, 250°) ice-flow phase followed this initial period of proglacial sedimentation (e.g., section 21-826, Figure 4.4). This early W- to WSW-trending ice-flow was followed by an extensive NW-trending ice-flow (Unit 6) with unit thickness reaching up to 29.0 m on the Churchill River (section 21-832, Figure 4.4). However, the thickness of this till unit is highly variable and is absent from some sections on the Little Churchill River (Figure 4.6). Evidence of hydraulic lifting of the ice sheet within the upper portion of Unit 6

indicates high pore water pressures were present during the latter stages of this ice-flow event. This bedded diamicton is then sharply overlain by 1.0–2.4 m of horizontally- and cross-bedded sand with minor diamicton beds (Unit 7). Unit 7 sediments are bound by tills deposited by contrasting ice-flow directions and provenance indicating that there was a significant reorganization of the LIS during this time period, and it is interpreted that these sediments were deposited in a proglacial environment during a brief retreat of the ice sheet from the study area, which indicates that there was possibly a reduction in the LIS at some point during MIS 6. There is then a sharp shift in ice-flow direction to SW- and S-trending ice-flow with minor SE-trending ice-flow indicators measured (Unit 8, Figure 4.18). Similar to Unit 6, the thickness of Unit 8 till is highly variable reaching impressive thicknesses of up to 17.7 m yet is missing in places. Along the Churchill River, these two MIS 6 ice-flow events account for the majority of the entire stratigraphic record (Figure 4.4). Considering that the MIS 6 tills are thicker compared to the MIS 5–1 tills deposited, it is interpreted that this region received increased sedimentation during MIS 6, possibly from being situated in a more ice-marginal setting for longer periods of time (Boulton, 1996).

Following these main ice-flow events, there are two relatively thin deposits (Unit 9 and 10) that likely occurred during deglaciation of the area since these tills are associated with thin packages of intertill sorted sediments. Unit 9 indicates that during the latter part of MIS 6 glaciation, ice first flowed towards the east across the study area. This stratigraphic unit is possibly correlated to northeast-trending erosional ice-flow indicators near the Seal River and streamlined landforms observed near the Manitoba-Nunavut border (Phase 4 of Gauthier et al., 2019). This ice-flow event suggests that the onset region for the Hudson Strait ice stream during late MIS 6 likely reached further into the interior of central Canada compared to the MIS 2 deglacial ice-sheet configuration and requires an ice divide situated west of the Churchill River. Interestingly, following this E-trending ice-flow, Unit 10 indicates a switch to W-trending ice-flow as evidenced by stacked tills (section 21-811; Appendix C, Supplemental material 1, Figure S1-1). This ice-flow reversal suggests that a late glacial ice divide crossed the study area during the deglaciation of MIS 6. This potential ice divide migration could have been caused by increased ice discharge along the southwestern margin of the ice sheet during this time, which would have caused a reorganization of the ice surface topography

leading to ice divide migration towards the northeast. The migration of ice divides in core regions of LIS during MIS 2 deglaciation is well documented (e.g., McMartin and Henderson, 2004; Rice et al., 2019), and it is likely similar ice dynamics were in operation during the MIS 6 deglaciation albeit with a different LIS geometry. Interestingly, the possible presence of an ice dome or divide in north-central Manitoba in late MIS 6 supports the findings of a significant marine transgression observed in the study area following deglaciation of this ice sheet from the region (Unit 11a) that was greater than the Holocene marine limit. Furthermore, if the Keewatin dome was situated in a more southern position during the latter part of MIS 6 compared to MIS 2, then this could be one factor as to why the LIS expanded further south during this glaciation compared to the last glacial cycle (e.g., Curry et al., 2011).

4.7.3 Glaciation(s) III: ~MIS 8 or older

A till with elevated proportions of Precambrian detritus that has a well-developed paleosol at its upper contact has previously been recognized in the western HBL and commonly referred to as the Sundance Till (Nielsen et al., 1986; Roy, 1998). This study has identified a relatively old till that has a compositional signature (clasts and geochemistry) indicative of a relatively elevated proportion of Precambrian detritus, with a documented paleosol (Unit 3). In the Gillam area, recent stratigraphic studies have indicated that this ice-flow event (Sundance Till) was likely deposited during the MIS 10 glaciation or earlier (Gauthier et al., 2025). Within this study area, Unit 3 till directly underlies interpreted MIS 7-aged interglacial sediments and is tentatively assigned to MIS 8 based on this relationship, but it is difficult to reconcile the exact timing of these older ice-flow events based on the sparse number of observations and limited geochronological constraints. Thus, if the upper contact is erosional, then Unit 3 till could possibly be correlated to the Sundance till (Unit G-2 of Gauthier et al., 2025) or could represent a different SE-trending ice-flow event. This is one example that highlights the persistent challenges with reconciling the timing of relatively older ice-flow events within the western HBL.

Ice-flow indicators from Unit 2 indicate till deposition by ice-flow trending towards the west to northwest (Unit 2a) and by ice-flow trending towards the southwest to south-southwest (Unit 2b).

There was no age relationship between these two ice-flow events in the stratigraphic record. Nonetheless, this stratigraphic record indicates that west- to northwest-trending ice-flow has crossed the study area during at least three separate glaciations providing evidence for the long-term influence of ice-flowing from the Q-L dome which had previously been recognized for two glaciations (Gauthier et al., 2019).

4.8 Conclusions

This study developed a stratigraphic framework for the Churchill to Little Churchill rivers region of the western HBL that consists of at least nine glacial (till) units that were deposited across at least three separate glaciations along with three pre-Holocene interglacial units recognized. This stratigraphic record provides several important findings regarding Late Quaternary glacial and nonglacial events. The main findings of this study are:

- During the most recent glaciation (MIS 5–2), NW-trending ice (Unit 12) first flowed across the study area, which was followed by W-trending ice-flow (Unit 13). Following these relatively early ice-flow events, the stratigraphic record indicates that there was no further deposition until late-glacial ice streams were active in the area. The preservation of earlier deposited tills and W-trending streamlined landforms implies that the study area was overlain by cold-based ice or sluggish ice for much of the last glacial cycle with limited sediment mobilization, which has also been documented in the Kaskattama highland area of the western HBL (Hodder et al., 2024).
- Glaciers advancing into central Canada at the start of the last glacial cycle (MIS 4 or 5) and penultimate glacial cycle (MIS 6) from the Q-L dome indicates that ice sheet growth in central Canada is not arctic-driven, which is often suggested by modelling efforts (Stokes et al., 2012; Geng et al., 2025).
- During late MIS 6, ice first flowed towards the east across the study area (Unit 9), which is interpreted to indicate that the onset region for the Hudson Strait ice stream possibly reached further into the interior of central Canada during MIS 6 deglaciation compared to the MIS 2 deglaciation and requires an ice divide situated west of the Churchill River.

This ice-divide later crossed the study area and ice flowed towards the west (Unit 10), which constrains a much different deglacial configuration of the LIS during late MIS 6 compared to late MIS 2 with an ice divide and possibly a dome situated in northern Manitoba.

- The MIS 6 deglaciation is followed by a marine highstand that reached at least 196 m above current sea level (Unit 11a), which is higher than the MIS 2 highstand in the region and lends support to the concept of a thicker MIS 6 ice sheet over the study area compared to MIS 2; which could be one factor that influenced a more southern limit of the North American glaciation during this time period.
- The study area was inundated by marine waters during Termination III (~243 ka) that reached at least 161 m above current sea level (Unit 4a) and this period of marine sedimentation was followed by an interglacial climate similar to the present day (Unit 4b); providing an important constraint for this glacial-interglacial transition.
- Lastly, there are three WNW–NNW ice-flow phases identified, and each event occurred following an interglacial period, which implies predominance of the Q-L dome during ice sheet growth across multiple glacial cycles and expands the known footprint of these ice-flow events to at least the Churchill River.

4.9 References

Aitchison, J. 1986. The statistical analysis of compositional data. Methuen Inc.

Andrews, J.T. and Smith, D.I. 1969. Statistical analysis of till fabric: methodology, local and regional variability (with particular reference to the north Yorkshire till cliffs). Quarterly Journal of the Geological Society 125(1-4): 503–542. doi:10.1144/gsjgs.125.1.0503.

Arnold, L.J., Duval, M., Demuro, M., Spooner, N.A., Santonja, M. and Pérez-Gonzàlez, A. 2016. OSL dating of individual quartz 'supergrains' from the Ancient Middle Palaeolithic site of Cuesta de la Bajada, Spain. Quaternary Geochronology, 36: 78–101. doi:10.1016/j.quageo.2016.07.003.

Batchelor, C.L., Margold, M., Krapp, M., Murton, D. K., Dalton, A.S., Gibbard, P.L., Stokes, C.R., Murton, J.B. and Manica, A. 2019. The configuration of Northern Hemisphere ice sheets through the Quaternary. Nature Communications, 10:3713. doi:10.1038/s41467-019-11601-2.

Bell, R. 1880. Report of explorations on the Churchill and Nelson rivers and around God's and Island Lakes, 1879. Geological Survey of Canada Report of Progress for 1878–1879, part C, 72 p.

Benn, D.I. 1994. Fabric shape and the interpretation of sedimentary fabric data. Journal of Sedimentary Research, 64: 910–915.

Boulton, G.S. 1996. Theory of glacial erosion, transport and deposition as a consequence of subglacial sediment deformation. Journal of Glaciology, 42(140): 43–62. doi:10.3189/S0022143000030525.

Burns, R. and Honkala, B. 1990. Silvics of North America: Vol 1. Conifers. United States Department of Agriculture (USDA), Forest Service, Agriculture Handbook 654.

Buylaert, J.P., Vandenberghe, D., Murray, A.S., Huot, S., De Corte, F. and Van den haute, P. 2007. Luminescence dating of old (470 ka) Chinese loess: A comparison of single-aliquot OSL and IRSL techniques. Quaternary Geochronology, 2: 9–14. doi:10.1016/j.quageo.2006.05.028.

Buylaert, J.P., Murray, A.S., Vandenberghe, D., Vriend, M., De Corte, F. and Van den haute, P. 2008. Optical dating of Chinese loess using sand-sized quartz: Establishing a time frame for Late Pleistocene climate changes in the western part of the Chinese Loess Plateau. Quaternary Geochronology, 3: 99–113. doi:10.1016/j.quageo.2007.05.003.

Campbell, J.F.E., Fletcher,W.J., Hughes, P.D., and Shuttleworth, E.L. 2016. A comparison of pollen extraction methods confirms dense-media separation as a reliable method of pollen preparation. Journal of Quaternary Science, **31**: 631–640. doi:10.1002/jqs.2886.

Catto, N.R. 1998. Comparative study of striations and basal till clast fabrics, Malpeque-Bedeque region, Prince Edward Island. Boreas, 27:259–274. doi:10.1111/j.1502-3885.1998.tb01420.x.

Curry, B. B., Grimley, D.A. and McKay III, E.D. 2011. Chapter 36 – Quaternary Glaciations in Illinois. *In* Quaternary Glaciations – Extent and Chronology: a closer look. Developments in Quaternary Science 15. *Edited by* J. Ehlers, P.L. Gibbard and P.D. Hughes. Elsevier, Amsterdam. pp. 467–487. doi:10.1016/B978-0-444-53447-7.00036-2.

Crann, C.A., Murseli, S., St-Jean, G., Zhao, X., Clark, I.D., Kieser, W.E., 2017. First status report on radiocarbon sample preparation techniques at the A.E. Lalonde AMS laboratory (Ottawa, Canada). Radiocarbon 59, 695–704. doi:10.1017/RDC.2016.55.

Dalton, A.S., Stokes, C.R. and Batchelor, C.L. 2022.Evolution of the Laurentide and Innuitian ice sheets prior to the Last Glacial Maximum (115 ka to 25 ka). Earth Science Reviews, 224: 103875. doi:10.1016/j.earscirev.2021.103875.

Dalton, A.S., Valiranta, M., Barnett, P.J., and Finkelstein, S.A. 2017. Pollen and macrofossil-inferred paleoclimate at the Ridge Site, Hudson Bay Lowlands, Canada: evidence for a dry climate and significant recession of the Laurentide Ice Sheet during Marine Isotope Stage 3. Boreas, 46: 388–401. doi:10.1111/bor.12218.

Dalton, A.S., Dulfer, H., Margold, M., Heyman, J., Clague, J., Froese, D., et al. 2023. Deglaciation of the North American Ice Sheet Complex in calendar years based on a new comprehensive database of chronological data: NADI-1. Quaternary Science Reviews, 321: 108345. doi:10.1016/j.quascirev.2023.108345.

Dalton, A.S., Finkelstein, S.A., Hodder, T.J. and Gauthier, M.S. 2024. Palynological analyses of subtill sediments from eleven sites in the western Hudson Bay Lowland region of Manitoba (parts of NTS 54B, 54C, 54E, 54F). Manitoba Geological Survey Open File OF2024-5, 6 p.

Dredge, L.A. and McMartin, I. 2011. Glacial stratigraphy of northern and central Manitoba. Geological Survey of Canada Bulletin 600, 27 p.

Dredge, L.A. and Nielsen, E. 1985. Glacial and interglacial deposits in the Hudson Bay lowlands: a summary of sites in Manitoba. I*n* Geological Survey of Canada Current Research Paper 85-1A: 247–257.

Dredge, L.A. and Nixon, F.M. 1982. Surficial geology, Herchmer, Manitoba. Geological Survey of Canada Preliminary Map 1-1980, scale 1:250 000.

Dredge, L.A. and Nixon, F.M. 1992. Glacial and environmental geology of northeastern Manitoba. Geological Survey of Canada Memoir 432, 80 p.

Dredge, L.A., Morgan, A.V., and Nielsen, E. 1990. Sangamon and pre-Sangamon interglaciations in the Hudson Bay Lowlands of Manitoba. Géographie Physique et Quaternaire, 44(3): 319–336. doi:10.7202/032833ar.

Ehlers, J. and Gibbard, P. L. 2007. The extent and chronology of Cenozoic global glaciation. Quaternary International, 164-165: 6–20.

Evans. 2018. Till: a glacial process sedimentology. Wiley-Blackwell, Chichester. doi: 10.1002/9781118652541

Evans, D.J.A., Phillips, E.R., Hiemstra, J.F., and Auton, C.A. 2006. Subglacial till: formation, sedimentary characteristics and classification. Earth-Science Reviews, 78(1–2): 115–176. doi:10.1016/j.earscirev.2006.04.001.

Faegri, K., and Iversen, J. 1975. Textbook of pollen analysis. 3rd ed. Munksgaard, Copenhagen and Denmark.

Fedo, C.M., Nesbitt, H.W. and Young, G.M. 1995. Unraveling the effects of potassium metasomatism in sedimentary rocks and paleosols, with implications for paleoweathering conditions and provenance. Geology, 23(10): 921–924. doi:10.1130/0091-7613(1995)023<0921:UTEOPM>2.3.CO;2

Galbraith, R.F., Roberts, R.G., Laslett, G.M., Yoshida, H., and Olley, J.M. 1999. Optical dating of single and multiple grains of quartz from Jinmium rock shelter, northern Australia: part i, experimental design and statistical models. Archaeometry, 41: 339–364. doi:10.1111/j.1475-4754.1999.tb00987.x.

Gauthier, M.S. 2022. Using radiocarbon ages on organics affected by freshwater – a geologic and archaeologic update on the freshwater reservoir ages and freshwater digest effect in Manitoba, Canada. Radiocarbon, 64(2), 253–264. doi:10.1017/RDC.2022.30.

Gauthier, M.S. 2023. Manitoba radiocarbon ages. Manitoba Geological Survey GeoFile 6-2023, 7 p.

Gauthier, M.S., Hodder, T.J., Ross, M., Kelley, S.E., Rochester, A., and McCausland, P. 2019. The subglacial mosaic of the Laurentide Ice Sheet; a study of the interior region of southwestern Hudson Bay. Quaternary Science Reviews, 214: 1–27. doi:10.1016/j.quascirev.2019.04.015.

Gauthier, M.S., Kelley, S.E., and Hodder, T.J. 2020. Lake Agassiz drainage bracketed Holocene Hudson Bay Ice Saddle collapse. Earth and Planetary Science Letters, 544: 116372. doi:10.1016/j.epsl.2020.116372.

Gauthier, M.S., Breckenridge, A., and Hodder, T.J. 2022. Patterns of ice recession and ice stream activity for the MIS 2 Laurentide Ice Sheetin Manitoba, Canada. Boreas, 51(2): 274–298. doi:10.1111/bor.12571.

Gauthier, M.S., Hodder, T.J., Dalton, A.S., Lian, O.B., Schaarschmidt, M., Ross, M., and Väliranta, M. 2024. Preservation of probable MIS 7 deglacial and nonglacial deposits near the edge of the Hudson Bay Lowland in Manitoba, Canada. Canadian Journal of Earth Sciences, 61(11): 1184–1211. doi:10.1139/cjes-2024-0019.

Gauthier, M.S., Hodder, T.J., Hathaway, J., Ross, M., Schaarschmidt, M., Lian, O.B., Finkelstein, S.A. and Kelley, S.E., 2025. Extending the western Hudson Bay Lowland Quaternary stratigraphy, in Manitoba Canada, to at least Marine Isotope Stage 10. Canadian Journal of Earth Sciences, *in press*. doi:10.1139/cjes-2025-0027.

Geng, M.S., Tarasov, L. and Dalton, A.S. 2025. A comparison of the last two glacial inceptions (MIS 7/5) via fully coupled transient ice and climate modeling. EGUsphere [preprint]. doi:10.5194/egusphere-2025-495.

Gibbard, P.L., Hughes, P.D., 2021. Terrestrial stratigraphical division in the Quaternary and its correlation. Journal of the Geological Society 178(2): jgs2020-2134. doi:10.1144/jgs2020-134.

Gowan, E.J., Zhang, X., Khosravi, S., Rovere, A., Stocchi, P., Hughes, A.L.C., et al. 2021. A new global ice sheet reconstruction for the past 80 000 years. Nature Communications, 12: 1199. doi:10.1038/s41467-021-21469-w.

Grunsky, E. 2010. The interpretation of geochemical survey data. Geochemistry, Exploration, Environment, Analysis, 10: 27–74. doi:10.1144/1467-7873/09-210.

Hicock, S.R., Goff, J.R., Lian, O.B. and Little, E.C. 1996. On the interpretation of subglacial till fabric. Journal of Sedimentary Research, 66(5): 928–934. doi:10.1306/D4268441-2B26-11D7-8648000102C1865D.

Hodder, T.J. and Gauthier, M.S. 2025. Quaternary site, till composition and ice-flow indicator data for the Little Churchill to Churchill rivers area, northeastern Manitoba (part of NTS 54E). Manitoba Geological Survey Open File OF2025-1, 5 p., 6 appendices, *in press*.

Hodder, T.J., Gauthier, M.S., Ross, M. and Lian, O.B. 2023. Was there a nonglacial episode in the western Hudson Bay Lowland during Marine Isotope Stage 3? Quaternary Research, 116: 148–161. doi:10.1017/qua.2023.35

Hodder, T.J., Gauthier, M.S., Ross, M., Kelley, S.E., Lian, O.B., Dalton, A.S. and Finkelstein, S.A. 2024. Unravelling the fragmented sediment-landform assemblage in an area of thick Quaternary sediment, western Hudson Bay Lowland, Canada. Canadian Journal of Earth Sciences, 61(11), 1156–1183. doi:10.1139/cjes-2024-0018

Hughes, P.D. and Gibbard, P.L. 2015. A stratigraphical basis for the Last Glacial Maximum (LGM). Quaternary International 383: 174–185. doi:10.1016/j.quaint.2014.06.006.

Jackson, G.D. 2013. Geology, Belcher Islands, Nunavut. Geological Survey of Canada, Open File 4923, 149p.

Juggins, S. 2015. rioja: Analysis of Quaternary science data. R package version (0.9-5). Available from http://cran.r-project.org/package=rioja [accessed November 2023].

Juggins, S., Simpson, G.L., and Telford, R.J. 2015. Taxon selection using statistical learning techniques to improve transfer function prediction. The Holocene, 25(1): 130–136, doi:10.1177/095968361455638.

Kitaba, I., and Nakagawa, T. 2017. Black ceramic spheres as marker grains for microfossil analyses, with improved chemical, physical, and optical properties. Quaternary International, 455: 166–169. doi:10.1016/j.quaint.2017.08.052.

Larsen, N.K. and Piotrowski, J.A. 2003. Fabric pattern in a basal till succession and its significance for reconstructing subglacial processes. Journal of Sedimentary Research, 73(5): 727–734. doi:10.1306/021303730725.

Li, B., Roberts, R.G., Jacobs, Z. and Li, S.-H. 2015. Potential of establishing a 'global standardised growth curve' (gSGC) for optical dating of quartz from sediments. Quaternary Geochronology, 27: 91–104. doi:10.1016/j.quageo.2015.02.011.

Lian, O.B. and Hicock, S.R. 2000. Thermal conditions beneath parts of the last Cordilleran Ice Sheet near its centre as inferred from subglacial till, associated sediments, and bedrock. Quaternary International, 68–71: 147–162. doi:10.1016/S1040-6182(00)00040-9.

Lichti-Federovich, S. and J. C. Ritchie. 1968. Recent pollen assemblages from the Western Interior of Canada. Review of Palaeobotany and Palynology. 7: 297–344. doi:10.1016/0034-6667(68)90035-3.

Lisiecki, L.E., and Raymo, M.E. 2005. A Pliocene–Pleistocene stack of 57 globally distributed benthic d18O records. Paleoceanography, 20: PA1003. doi:10.1029/2004PA001071.

Lowick, S.E., Preusser, F. and Wintle, A.G. 2010. Investigating quartz optically stimulated luminescence dose response curves at high doses. Radiation Measurements, 45: 975–984. doi:10.1016/j.radmeas.2010.07.010.

Manitoba Geological Survey, 2024. Bedrock geology of Manitoba. Manitoba Geological Survey Open File OF2024-4, scale 1:1 000 000.

Mark, D.M. 1973. Analysis of axial orientation data, including till fabrics. Geological Society of America Bulletin, 84: 1369–1374. doi:10.1130/0016-7606(1973)84%3c1369:AOAODI%3e2.0.CO;2.

Martins, T., Corrigan D. and Rayner, N. 2019. Lithogeochemical, assay and U-Pb geochronological data for the Southern Indian domain, north-central Manitoba (parts of NTS 64G1, 2, 7–10, 64H3–6). Manitoba Geological Survey Data Repository Item DRI2019001.

Martins, T., Rayner, N., Corrigan, D. and Kremer, P. 2022. Regional geology and tectonic framework of the Southern Indian domain, Trans-Hudson orogen, Manitoba. Canadian Journal of Earth Sciences, 59(6): 371–388. doi:10.1139/cjes-2020-0142.

McAndrews, J.H., Berti, A.A., and Norris, G. 1973. Key to the Quaternary pollen and spores of the Great Lakes Region. Royal Ontario Museum, Toronto, Canada, 74p.

McConnaughey, T.A. and Gillikin, D.P. 2008. Carbon isotopes in mollusk shell carbonates. Geo-Marine Letters 28: 287–299. doi:10.1007/s00367-008-0116-4.

McDonald, B. and Partin, C. 2024. Paleoproterozoic Rocks of the Belcher Islands, Nunavut: A Review of Their Remarkable Geology and Relevance to Inuit-led Conservation Efforts. Geoscience Canada 51(2): 7–42. doi:10.12789/geocanj.2024.51.207

McMartin, I., and Henderson, P. 2004. Evidence from Keewatin (central Nunavut) for paleo-ice divide migration. Geographie physique et Quaternaire, 58(2–3): 163–186. doi:10.7202/013137ar.

McMartin, I., and Paulen, R.C. 2009. Ice-flow indicators and the importance of ice-flow mapping for drift prospecting. *In* Application of till and stream sediment heavy mineral and geochemical methods to mineral exploration in Western and Northern Canada. GAC Short Course Notes 18. *Edited by* R.C. Paulen and I. McMartin. Geological Association of Canada. pp. 15–34.

McMartin, I., Gauthier, M.S. and Page, A.V. 2022. Updated postglacial marine limits along western Hudson Bay, central mainland Nunavut and northern Manitoba. Geological Survey of Canada Open File 8921, 19 p. doi:10.4095/330940.

Medialdea, A., Thomsen, K.J., Murray, A.S. and Benito, G. 2014. Reliability of equivalent-dose determination and age-models in the OSL dating of historical and modern palaeoflood sediments. Quaternary Geochronology, 22: 11–24. doi:10.1016/j.quageo.2014.01.004.

Middelburg, J.J., Van Der Wejden, C.H. and Woittiez, J.R.W. 1988. Chemical processes affecting the mobility of major, minor and trace elements during weathering of granitic rocks. Chemical Geology, 68: 253–273. doi:10.1016/0009-2541(88)90025-3.

Miller, G.H. and Andrews, J.T. 2019. Hudson Bay was not deglaciated during MIS-3. Quaternary Science Reviews, 225: 105944. doi:10.1016/j.quascirev.2019.105944.

Möller, P., Benediktsson, I.O., Anjar, J., Bennike, O., Bernhardson, M., Funder, S., Håkansson, L.M., Lemdahl, G., Licciardi, J.M., Murray, A.S. and Seidenkrantz, M. 2019a. Data set on sedimentology, palaeoecology and chronology of Middle to Late Pleistocene deposits on the Taimyr Peninsula, Arctic Russia. Data in brief, 25: 104267. doi:10.1016/j.dib.2019.104267

Möller, P., Benediktsson, I. O., Anjar, J., Bennike, O., Bernhardson, M., Funder, S., Håkansson, L. M., Lemdahl, G., Licciardi, J. M., Murray, A. S. and Seidenkrantz, M. 2019b. Glacial history and palaeo-environmental change of southern Taimyr Peninsula, Arctic Russia, during the Middle and Late Pleistocene. Earth Science Reviews, 196: 102832. doi:10.1016/j.earscirev.2019.04.004

Munsell Color–X-Rite, Incorporated. 2015. Munsell Soil Color Book, Pantone LLC, Carlstadt, New Jersey, 42 p.

Murray, A.S., and Wintle, A.G. 2000. Luminescence dating of quartz using an improved single-aliquot regenerative-dose protocol. Radiation Measurements, 32: 57–73. doi:10.1016/S1350-4487(99)00253-X.

Murray, A.S., and Wintle, A.G. 2003. The single aliquot regenerative dose protocol: potential for improvements in reliability. Radiation Measurements, 37: 377–381. doi:10.1016/S1350-4487(03)00053-2.

Murray, A.S., Svendsen, J.I., Mangerud, J. and Astakhov, V.I. 2007. Testing the accuracy of quartz OSL dating using a known-age Eemian site on the river Sula, northern Russia. Quaternary Geochronology, 2: 102–109. doi:10.1016/j.quageo.2006.04.004.

Murray, A., Buylaert, J.P., Henriksen, M., Svendsen, J.I. and Mangerud, J. 2008. Testing the reliability of quartz OSL ages beyond the Eemian. Radiation Measurements, 43: 776–780. doi:10.1016/j.radmeas.2008.01.014.

Natural Resources Canada 2015. Obtain climate estimates at your locations; Government of Canada. http://gmaps.nrcan.gc.ca/cl_p/ climatepoints.php, URL <http://gmaps.nrcan.gc.ca/cl_p/climate-points.php> [February 2016].

Nesbitt, H. W. and Young, G. M. 1982. Early Proterozoic climates and plate motions inferred from major element chemistry of lutites. Nature, 299: 715–717.

Nielsen, E., Morgan, A.V., Morgan, A., Mott, R.J., Rutter, N.W., and Causse, C. 1986. Stratigraphy, paleoecology and glacial history of the Gillam area, Manitoba. Canadian Journal of Earth Sciences, 23: 1641–1661. doi:10.1139/e86-153.

North American Commission on Stratigraphic Nomenclature. 2021. Stratigraphy 18(3): 153–204.

Overpeck, J.T., Webb, T., and Prentice, I.C. 1985. Quantitative interpretation of fossil pollen spectra: dissimilarity coefficients and the method of modern analogs. Quaternary Research, **23**: 87–108. doi:10.1016/0033-5894(85)90074-2.

Pawley, S.M., Bailey, R.M., Rose, J., Moorlock, B.S.P., Hamblin, R.J.O., Booth, S.J., Lee, J.R., 2008. Age limits on Middle Pleistocene glacial sediments from OSL dating, north Norfolk, UK. Quaternary Science Reviews 27: 1363–1377. doi:10.1016/j.quascirev.2008.02.013.

Pawley, S.M., Toms, P., Armitage, S.J., Rose, J., 2010. Quartz luminescence dating of Anglian Stage (MIS 12) fluvial sediments: Comparison of SAR age estimates to the terrace chronology of the Middle Thames valley, UK. Quaternary Geochronology 5: 569–582. doi:10.1016/j.quageo.2009.09.013.

Piotrowski, J.A., Larsen, N.K., Menzies, J. and Wysota, W. 2006. Formation of subglacial till under transient bed conditions: deposition, deformation, and basal decoupling under a Weichselian ice sheet lobe, central Poland. Sedimentology, 53: 83–106. doi:10.1111/j.1365-3091.2005.00755.x.

Prest, V.K. 1990. Laurentide ice-flow patterns: a historical review, and implications of the dispersal of Belcher Islands Erratics. Geographie physique et Quaternaire, 44: 113–136. doi:10.7202/032812ar.

Prest, V.K., Donaldson, J.A., and Mooers, H.D. 2000. The Omar story: the role of Omars in assessing glacial history of west–central North America. Geographie Physique et Quaternaire, 54: 257–270. doi:10.7202/005654ar.

Rainbird, R.H., Hadlari, T., Aspler, L.B., Donaldson, J.A., LeCheminant, A.N., and Peterson, T.D. 2003. Sequence stratigraphy and evolution of the Paleoproterozoic intracontinental Baker Lake and Thelon basins, western Churchill Province, Nunavut, Canada. Precambrian Research, 125: 21–53. doi:10.1016/S0301-9268(03)00076-7.

Rice, J.M., Ross, M., Paulen, R.C., Kelley, S.E., Briner, J.P., Neudorf, C.A. and Lian, O.B. 2019. Refining the ice flow chronology and subglacial dynamics across the migrating Labrador Divide of the Laurentide Ice Sheet with age constraints on deglaciation. Journal of Quaternary Science, 34(7): 519–535. doi:10.1002/jqs.3138.

Rietveld, H. M. 1969. A profile for nuclear and magnetic structures. Journal of applied Crystallography, 2(2): 65–71. doi:10.1107/S0021889869006558.

Riley, J.L. 2003. Flora of the Hudson Bay Lowland and its Postglacial Origins. NRC Research Press, 237 p.

Roy, M. 1998. Pleistocene stratigraphy of the lower Nelson River area—implications for the evolution of the Hudson Bay lowland of Manitoba, Canada. Master of Science thesis, University of Quebec, Montreal, Canada, 220 p.

Saarnisto, M. and Peltoniemi, H. 1984. Glacial stratigraphy and compositional properties of till in Kainuu, eastern Finland. Fennia, 162: 163–199.

Sheldon, N.D. and Tabor, N.J. 2009. Quantitative paleoenvironmental and paleoclimatic reconstruction using paleosol. Earth Science Reviews, 95: 1–52. doi:10.1016/j.earscirev.2009.03.004

Shepard, F.P. 1954: Nomenclature based on sand-silt-clay ratios. Journal of Sediment 24(3): 151–158. doi:10.1306/D4269774-2B26-11D7-8648000102C1865D.

Shilts, W.W. 1980. Flow patterns in the central North American ice sheet. Nature, 286: 213–218. doi:10.1038/286213a0.

Stea, R.R. and Finck, P.W. 2001. An evolutionary model of glacial dispersal and till genesis in Maritime Canada. *In* Drift Exploration in Glaciated Terrain. *Edited by* M. B. McClenaghan, P. T. Bobrowsky, G.E.M. Hall and S. J. Cook. The Geological Society of London, Special Publications 185: 237–265. doi:10.1144/GSL.SP.2001.185.01.11.

Stokes, C.R., Tarasov, L. and Dyke, A.S. 2012. Dynamics of the North American Ice Sheet Complex during its inception and build-up to the Last Glacial Maximum. Quaternary Science Reviews, 50: 86–104. doi:10.1016/j.quascirev.2012.07.009.

Stott, G.M., Buse, S., Davis, D.W., and Hamilton, M.A. 2010. The Sutton inliers——a Paleoproterozoic succession in the Hudson Bay Lowland. *In* Summary of Field Work and Other Activities 2010, Ontario Geological Survey, Open File Report 6260, 19-1–19-14.

Thorleifson, L.H., Wyatt, P.H. and Warman, T.A. 1993. Quaternary stratigraphy of the Severn and Winisk drainage basins, northern Ontario. Geological Survey of Canada Bulletin 442, 65 p.

Timar, A., Vandenberghe, D., Panaiotu, E.C., Pantiaotu, C.G., Necula, C., Cosma, C. and van den haute, P. 2010. Optical dating of Romanian loess using fine-grained quartz. Quaternary Geochronology, 5: 143–148. doi:10.1016/j.quageo.2009.03.003.

Trefethen, J.M. 1950. Classification of sediments. American Journal of Science, 48: 55–62.

Trommelen, M.S. 2015. Till composition and glacial history, Gauer Lake – Wishart Lake, Manitoba (NTS 64H4, 5, 12, 13). Manitoba Geological Survey Geoscientific Paper GP2014-1, 32 p.

Van Gosen, B.S., Verplanck, P.L., Seal II, R.R., Long, K.R. and Gambogi, J. 2017. Rare-earth elements. *In* Critical mineral resources of the United States—Economic and environmental geology and prospects for future supply. *Edited by* K.K. Schulz, J.H. DeYoung Jr., R.R. Seal II and D. Bradley. United States Geological Survey Professional Paper 1802: 01–031. doi:10.3133/pp1802O.

Veillette, J.J. 2004. Ice-flow chronology and palimpsest, long-distance dispersal of indicator clasts, north of the St. Lawrence River valley, Quebec. Geographie physique et Quaternaire, 58(2–3): 187–216. doi:10.7202/013138ar.

Veillette, J.J., Dyke, A.S. and Roy, M. 1999. Ice-flow evolution of the Labrador Sector of the Laurentide Ice Sheet: a review, with new evidence from northern Quebec. Quaternary Science Reviews, 18: 993–1019. doi:10.1016/S0277-3791(98)00076-6.

Wheeler, J.O., Hoffman, P.F., Card, K.D., Davidson, A., Sanford, B.V., Okulitch, A.V. and Roest, W.R. 1996. Geological Map of Canada, Geological Survey of Canada Map 1860A. doi:10.4095/208175.

Whitmore, J., Gajewski, K., Sawada, M., Williams, J.W., Shuman, B., Bartlein, P.J., et al. 2005. North American and Greenland modern pollen data for multi-scale paleoecological and paleoclimatic applications. Quaternary Science Reviews, 24: 1828–1848. doi:10.1016/j.quascirev.2005.03.005.

Young, R.R., Burns, J.A., Smith, D.G., Arnold, L.D. and Rains, R.B. 1994. A single, late Wisconsin, Laurentide glaciation, Edmonton area and southwestern Alberta. Geology, 22: 683–686. doi:10.1130/0091-7613(1994)022<0683:ASLWLG>2.3.CO;2.

Zabenskie, S. 2006. Postglacial climatic change on Boothia Peninsula, Nunavut, Canada. Master of Science thesis, University of Ottawa, Ottawa, Ontario, Canada, 98p.

Chapter 5

Glacial-interglacial cycles: insights from the stratigraphic record of western Hudson Bay Lowland

5.1 Overview

The Hudson Bay Lowland (HBL) region of central Canada contains an extensive stratigraphic record of glacial and nonglacial events that provides important insights into the growth and demise of North American ice sheets during the Quaternary. The HBL is situated at the heart of previously glaciated North America and was over-run by ice sourced from the northwest (Keewatin dome) and east (Quebec-Labrador dome) during glaciations, thus the stratigraphic record provides information on which domes were more active during different glaciations and their relative pace of growth following ice-free periods. To better understand these ice-flow events and their relation to ice-free periods, we focused on three relatively unstudied areas in the western HBL and propose a regional stratigraphic framework. The stratigraphic framework consists of eight glacial (till) units that were deposited across at least three separate glaciations along with at least three pre-Holocene interglacial units and possibly a fourth interstadial or interglacial unit recognized. The stratigraphic record likely extends to Marine Isotope Stage 9 or older, and provides important constraints for ice sheet dynamics and climatic conditions during the past three glacial-interglacial cycles. Furthermore, this study confirms that the recently developed till-focused lithostratigraphy-allostratigraphy methodology can be confidently applied to new areas of the Hudson Bay Lowland to better understand the fragmented stratigraphic record and the relative age of interglacial sediments.

5.2 Introduction

Empirical reconstructions of the Laurentide Ice Sheet (LIS) are best constrained from the last glacial maximum (LGM) during Marine Isotope Stage (MIS) 2 and MIS 1 deglaciation (~25ka–6 ka BP) largely from mapping and dating of ice-marginal features (Dyke and Prest, 1987; Dyke et al., 2002; Dalton et al., 2023). The dynamics of the LIS from the onset of the last glaciation to the LGM are less certain, but minimum and maximum extents of the LIS from ~115–25 ka have been proposed based on the available datasets which provide insight into ice sheet growth and decay patterns during the last glaciation (Dalton et al., 2022b). The ice-flow datasets within this reconstruction use the 'swarm' record proposed by Kleman et al. (2010) which is based on interpretations of streamlined landforms (a relative-age record) and the timing of these events in relation to the age of the interglacial Bell Sea sediments in the Hudson Bay Lowland (HBL); however, the age of the Bell Sea sediments lacks robust dating and may not belong to the most recent interglacial period (Thorleifson et al., 1992; Hodder et al., 2024b). Thus, additional insight about the relative timing and direction of ice-flow phases during the last glaciation can be gained by incorporating ice-flow data from the stratigraphic record in the HBL region (e.g., Gauthier et al., 2019, 2025; Hodder et al., 2024b). Furthermore, comparatively little is known about the LIS prior to the last glaciation and well-documented field-based records continue to be mostly located along the past ice sheet margin near the LGM limits (Batchelor et al., 2019), which do not provide insight into ice sheet dynamics of the interior regions. This is a limitation, especially for reconstructing ice sheet growth patterns and ice divide positions and migrations. To better understand the long-term dynamics of the LIS, interior areas of Canada with thick sequences of sediments that were deposited prior to the last glaciation (pre-Wisconsinan) need to be better understood by documenting temporal ice-flow changes, sediment provenance evolution and by establishing the relationship of these glacial events to ice-free periods (interglaciations and/or interstadials). Thus, unravelling the extensive Quaternary stratigraphic record of the HBL, which is situated in central Canada at the heart of the LIS (Figure 5.1b) and contains an extensive pre-Wisconsinan Quaternary stratigraphic record (e.g., Nielsen et al., 1986; Gauthier et al., 2025), remains integral to understanding the long-term dynamics of the LIS.

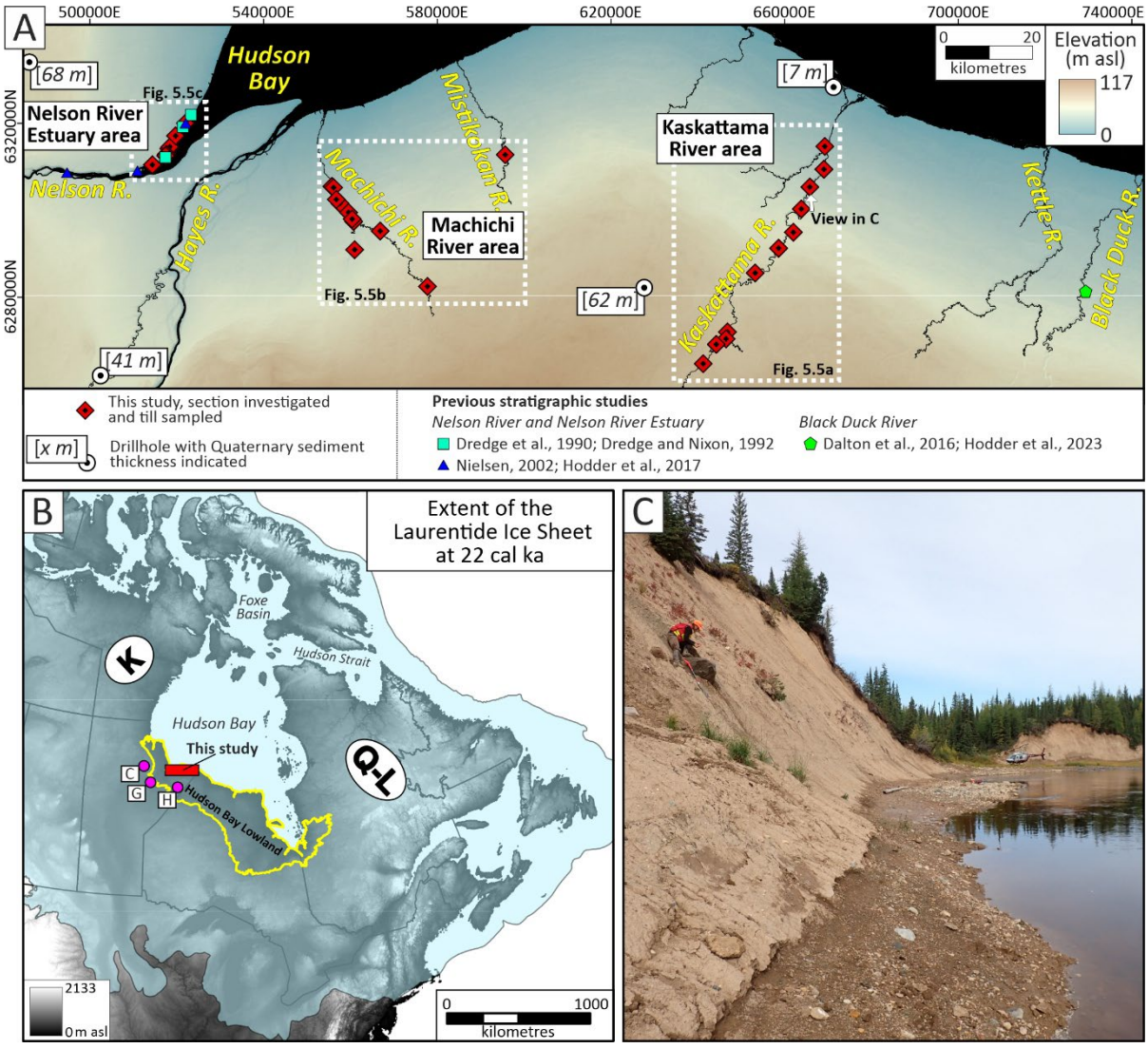

Figure 5.1: Location of study area in the western Hudson Bay Lowland: A) sections visited in the study area grouped according to their stratigraphic region (Kaskattama River, Machichi River or Nelson River Estuary); B) location of the study area in context to the Laurentide Ice Sheet at 22 cal ka bp, with the interpreted location of the Keewatin (K) and Quebec-Labrador (Q-L) domes during MIS 2 deglaciation (Dalton et al., 2023) and previous studies: C, Churchill River area (Chapter 4); G, Gillam area (Gauthier et al., 2025) and H, Kaskattama highland (Hodder et al., 2024a,b); and C) example of Quaternary sediments exposed along the Kaskattama River (section 19-626).

The HBL has long been known to contain an important archive of past glacial and nonglacial events (Tyrrell, 1916; McDonald, 1969; Skinner, 1973; Nielsen et al., 1986; Dredge et al., 1990; Thorleifson et al., 1992), but understanding the stratigraphy of the region is challenging and requires multi-parameter characterization of glacial and nonglacial beds to fully grasp the fragmented nature of the geological record (Hodder et al., 2024b). Recent studies have shown that the Quaternary stratigraphy in the western region of the HBL is significantly more complex than was previously understood (Hodder et al., 2023; Hodder et al., 2024b; Gauthier et al., 2025), which offers an opportunity to gain insight into the Quaternary record. To better understand the extent of the Quaternary stratigraphy exposed in the western HBL, this study focused on two areas that lack any previous detailed investigations (the Kaskattama River and Machichi River areas; Figure 5.1a) and one relatively understudied area that contains previously described exposures of subtill interglacial sediments (Nelson River Estuary; Figure 5.1a). Interglacial sediments exposed at the Flamborough and Port Nelson sections along the Nelson River Estuary were previously correlated to the penultimate interglacial period (Sangamonian, ~MIS 5e; Dredge and McMartin, 2011); however, preliminary investigations of the area suggested that these interglacial beds likely belong to separate interglacial periods (Hodder et al., 2023). This study places these observations into a regional context and provides the first stratigraphic framework for the region, which brings new insights into past glacial dynamics across multiple glacial cycles and climatic conditions that characterized interglacials.

5.3 Regional setting

The western HBL is a flat-lying landscape, with local relief typically <2 m, and is composed primarily of wetlands (Dredge and Dyke, 2020). This flat-lying landscape has been incised by fluvial processes during glacioisostatic adjustment which exposes sections of Quaternary sediments that are the focus of this study (e.g., Figure 5.1c). Sections investigated range in height from 5.4–19.3 m. The thickness of Quaternary sediments is largely unknown in the region and bedrock was not observed during field work. Four drillholes indicate the thicknesses of Quaternary sediments range from 7–68 m (Figure 5.1a).

5.3.1 Bedrock geology and clast provenance

The study area is underlain by Paleozoic rocks of the Hudson Bay Basin (HBB). The HBB of northeastern Manitoba is composed predominantly of carbonate (limestone or dolostone) rocks and there are only a few distinguishable bedrock units that can be useful for provenance analysis. One of these distinct bedrock units is the Kenogami River Formation (Kenogami) which contains red to light green sandstone to siltstone (e.g., Figure 5.2a). The source of pink to red carbonate clasts (e.g., Figure 5.2a) is also interpreted to be the Kenogami, similar to other regional sediment provenance studies (e.g., Gao et al., 2020; Hodder et al., 2024a).

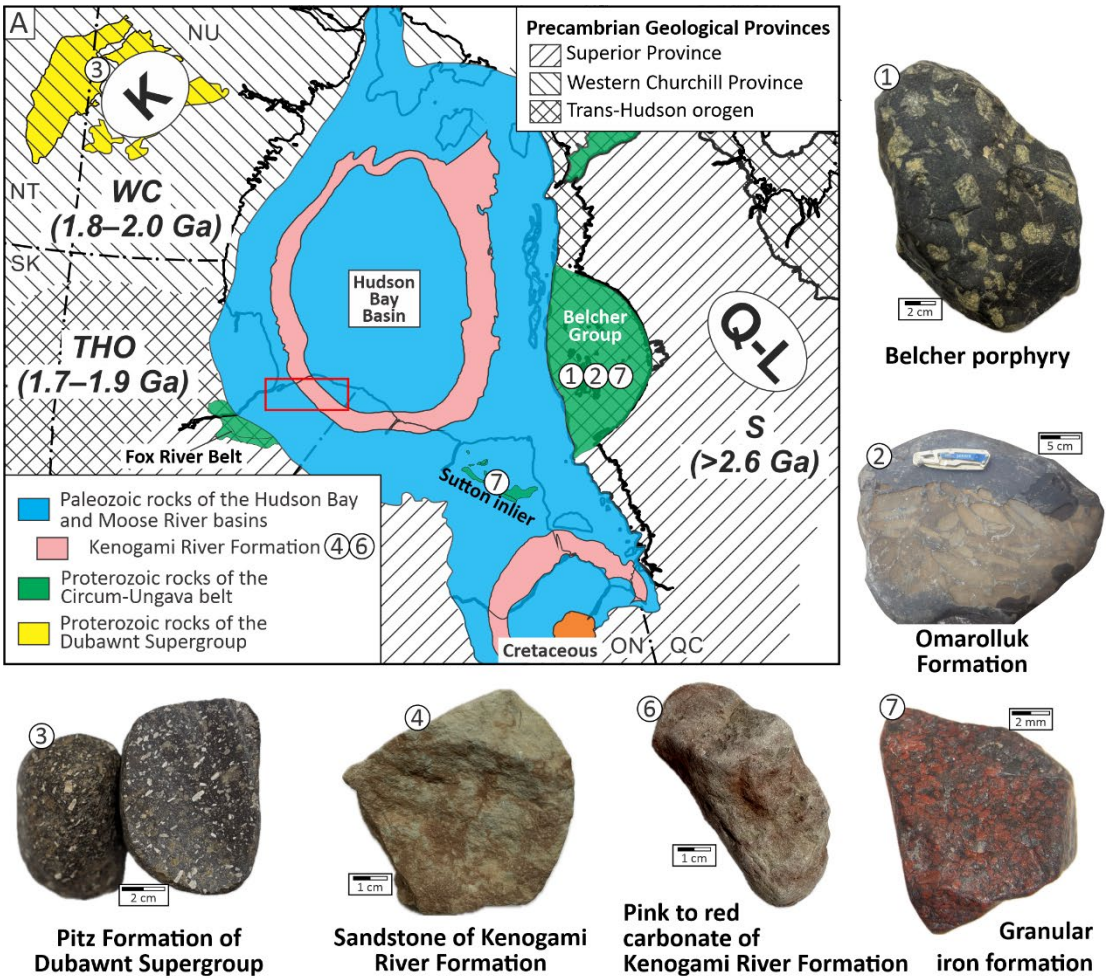

Belcher porphyry

Omarolluk Formation

Pitz Formation of Dubawnt Supergroup

Sandstone of Kenogami River Formation

Pink to red carbonate of Kenogami River Formation

Granular iron formation



Figure 5.2: Simplified bedrock geology of central Canada and examples of rock types identified within the study area: A) bedrock geology modified from Wheeler et al. (1996). The location of the Keewatin (K) and Quebec-Labrador domes of the Laurentide ice sheet is their position during MIS 2 deglaciation from Dalton et al. (2023). Examples of bedrock types identified in the field or in clast lithology counts and their bedrock source area shown by numbers 1–7; B) example of clast lithology count for one till sample showing the 4–8 mm (left) and 2–4 mm (right) sorted fractions. Abbreviations: KSS, Kenogami River Formation sandstone; KPC, pink to red carbonate interpreted to be sourced from the Kenogami River Formation; F, Paleozoic fossil; S, sulphide; UGG, undifferentiated greywacke and greenstone; Pitz, purple to red volcanic from the Pitz Formation.

Distinctive eastern-sourced rock types are derived primarily from the Belcher Group which is situated at a minimum of 575 km to the east (Figure 5.2a). Erratics identified within the study area from the Belcher Group include greywacke with hemispherical calcareous concretions (Figure 5.2a) that are sourced from the Omarolluk Formation ('Omars'; Prest, 1990; Prest et al., 2000), porphyritic rocks that are sourced from Eskimo and Flaherty formations ('Belcher porphyry') and granular iron formation derived from the Kipalu Formation (McDonald and Partin, 2024). Granular iron formation clasts can also be sourced from the Sutton Inlier (Figure 5.2a) situated 400 km to the southeast (Stott et al., 2010). Omars and Belcher porphyry clasts are not easily identifiable in the size-fraction (2–8 mm size-fraction) used for till clast lithology counts since distinctive features of these rock types are larger than the size-fraction analyzed (e.g., Figure 5.2a). As such, till provenance studies in central Canada have grouped indiscriminate dark grey rocks as 'dark erratics' (Shilts, 1980) or 'Proterozoic sources' (Thorleifson et al., 1993). Recent studies have referred to these fine-grained dark grey to grey Precambrian clasts as 'undifferentiated greenstone and greywacke' (UGG; Hodder et al., 2024b; Gauthier et al., 2025), which is the lithology classification used in this study. Similar to previous researchers (Shilts, 1980; Thorleifson et al., 1993), we assume most of these UGG clasts are from the Belcher Group or Sutton inlier with minor input from greenstone belts of the Canadian Shield. We thus hypothesize that a large decrease in the relative proportion of UGG reflects a change of provenance from Belcher/Sutton sources to a different bedrock source region.

Distinct northwestern erratics have been transported towards the southeast over 800 km from the Dubawnt Supergroup (Rainbird, 2003; Figure 5.2a). Examples include clasts of the Pitz Formation (purple to mauve-coloured volcanic rocks with distinctive chalky sanidine phenocrysts (Figure 5.2a) and Christopher Island Formation (red volcanic rocks with phlogopite phenocrysts). There is a background concentration of ~10% granitoid clasts within till sampled across the HBL, as first noted by Shilts (1980). Hence, they are not an effective indicator to delineate dispersal patterns at low concentrations. However, at higher concentrations, the proportion of granitoid clasts relative to UGG clasts can be used as one parameter to assist with establishing between northwestern and eastern sediment provenance in the western HBL.

5.4 Methods

5.4.1 Field Data

Sediments exposed along post-glacially incised fluvial valleys were investigated with helicopter support in 2019–2021. These natural sections were first cleared to remove colluvium, then the in-situ sediments were described over a 1–2 m wide interval based on their texture, colour, relative consolidation, clast content, sedimentary structure and nature of contacts. Diamicton beds were interpreted as subglacial traction till based on their typically massive structure, clast-shape and characteristics (bullet-shaped, faceted and striated), lodged in-situ clasts with striated upper surfaces and lateral continuity (e.g., Figure 5.3; Evans et al., 2006; Evans, 2018). The degree of till consolidation was determined qualitatively based on observations between beds and is used to differentiate between overconsolidated and highly overconsolidated diamicton. Overconsolidated diamicton beds do not have a blocky appearance or have a minor blocky appearance with no or minor oxidation rind developed on joint surfaces (e.g., upper till(s) in Figure 5.3d, f, g), whereas highly overconsolidated and indurated diamicton have a blocky appearance with moderate to extensive oxidation rind developed on joint surfaces (e.g., Figure 5.3a, b, c, e). Thick colluvium inhibited a thorough assessment of the lateral continuity of most identified beds. At sections, till samples were collected above and below all identified facies changes in the field (colour, texture or relative consolidation) and every 1–4 m when visible stratigraphic changes could not be observed. Till-matrix colour was determined with moist subsamples under standard laboratory light conditions post-fieldwork and is expressed using standard Munsell colours (Munsell Color–X-Rite, 2015). Stratigraphic observations are summarized on stratigraphic columns herein and detailed stratigraphic descriptions, sediment photos and datasets are available in Hodder and Gauthier (2025). Lithofacies codes modified from Möller et al. (2019) are used to simplify certain figures and a key to these codes is provided in Chapter 4 (Appendix C, Supplemental material 1, Table S1-1).

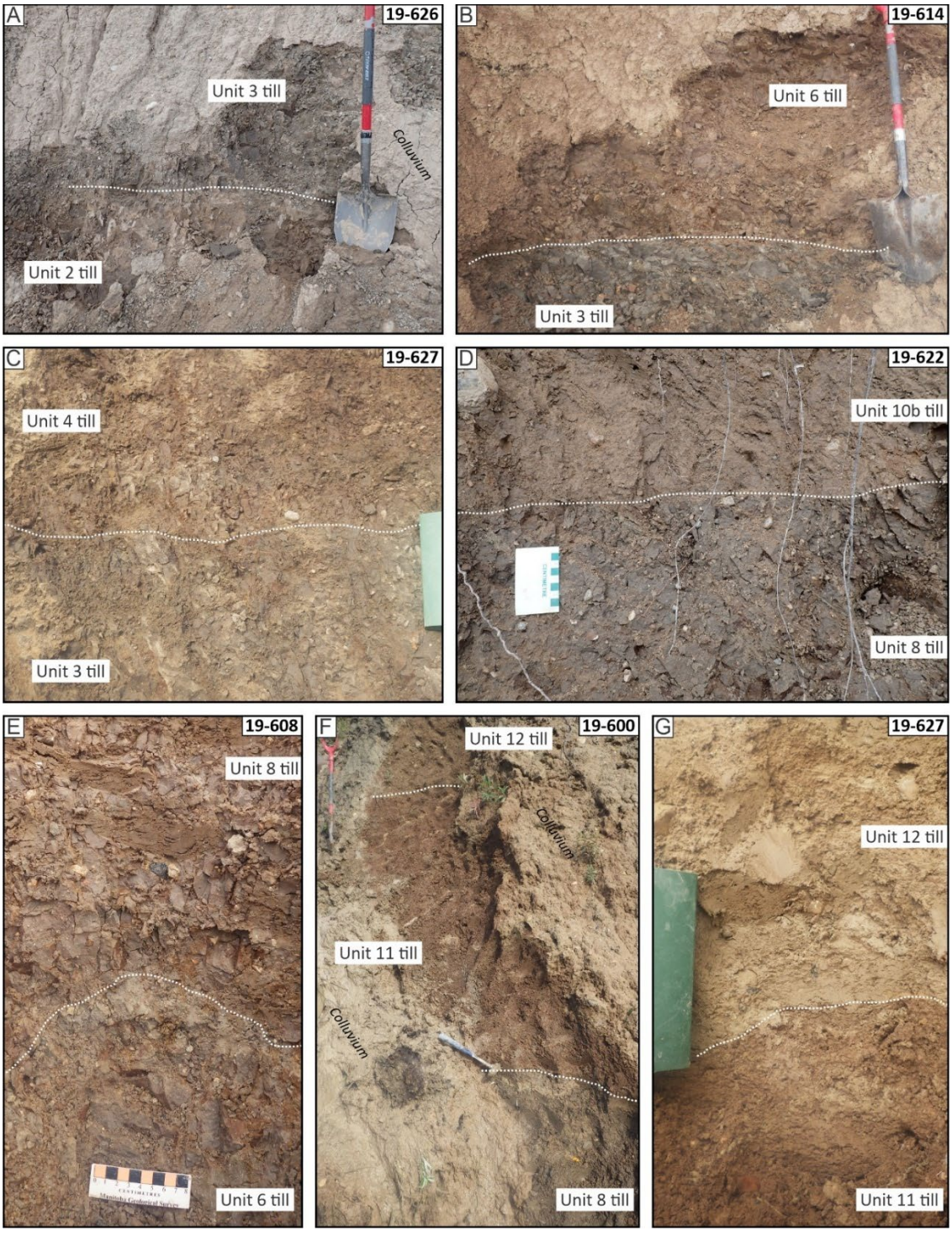

Figure 5.3: Examples of tills identified within the study area and the nature of till-till contacts observed. The blade of the shovel in panel A and B is 28 cm in length, the green notebook in panel D and F is 20 cm in length and the rock hammer in panel E is 30 cm in length.

Till beds were further investigated to determine ice-flow direction during deposition. Ice-flow indicators measured include clast fabrics and the orientation of parallel striations on the upper surfaces of in-situ, lodged, cobble- to boulder-sized clasts, which are considered a good indicator of paleo-ice flow direction (McMartin and Paulen, 2009). Clast fabrics provide information on the preferred orientation of elongated clasts, which generally gives the direction of shear during till deposition, which in turns provides insights into paleo-ice flow direction (e.g., Hicock et al., 1996; Lian and Hicock, 2000). Clast-fabrics measurements were conducted on three vertical faces of a 'box' carved into the section. At each fabric site, the trend and plunge of 28–40 clasts (average of 31 clasts) were measured where the a:b axis ratio was >1.5, and the a- and b-axis plunge was <60°. A non-magnetic knitting needle was used to extrapolate the plunge of the a-axis out of the till face, allowing for increased accuracy of measurements. Clasts that were in contact with other clasts or smaller clasts that were adjacent to larger clasts, which could restrict rotation of clasts (Andrews and Smith, 1969), were not measured. These criteria are designed for the specific purpose of obtaining the preferred orientation of matrix-supported elongated clasts and not for establishing transport and deposition processes (e.g., lodgement, deformation). A total of 77 stratigraphic ice-flow indicators were measured (Appendix D, Table S1-1; 59 clast fabrics and 18 lodged clasts). Due to time constraints in the field, not all sections and identified till beds have clast fabric data. The eigenvectors and eigenvalues for each clast fabric were calculated (Mark, 1973; Benn, 1994) and the data was plotted on equal area, lower hemisphere projection stereonets using Rockware StereoStat V1.6.1. All ice-flow-orientation interpretations were initially considered bi-directional, since the up-ice plunge of clasts is not consistent (Andrews and Smith, 1969; Saarnisto and Peltoniemi, 1984; Larsen and Piotrowski, 2003; Gauthier et al., 2019). In these cases, the provenance of the till needs to be considered to determine the ice-flow direction (Catto, 1998). Till beds observed in the study area are generally massive and no glaciotectonic features were observed that could support or contradict ice-flow interpretations.

5.4.2 Till provenance

5.4.2.1 Clast lithology counts

The clast lithologies identified within the 2–8 mm size-fraction of till were first sorted into 22 detailed classes (Hodder and Gauthier, 2025). Four classes account for ≥92 ct. % of the rock types identified within each till sample and these classes are the focus of clast provenance analysis: grey, tan or white carbonate, granitoid, UGG and Kenogami clasts (e.g., Figure 5.2b). An average of 397 clasts were counted for each till sample, ranging from 174–587 clasts per sample, totaling 65 050 clasts. The entire dataset, including photos for each sample, is available in Hodder and Gauthier (2025).

5.4.2.2 Detrital hornblende $^{40}Ar/^{39}Ar$ age determination

The $^{40}Ar/^{39}Ar$ age of hornblende grains records time elapsed since they were last subject to temperatures exceeding the closure temperature of the mineral. The closer temperature for hornblende grains is approximately 510°C (Schaen et al., 2021) and this is typically related to the last major orogenic episode that a geological province in the Canadian Shield experienced. Three geological provinces are of interest for the purpose of better understanding till provenance in the study area: Superior, Western Churchill (WC) and Trans-Hudson Orogen (THO) geological provinces of the Canadian Shield (Figure 5.2a), and these geologic provinces have approximate hornblende $^{40}Ar/^{39}Ar$ ages of >2.6, 1.8–2.0 and 1.7–1.9 Ga, respectively (e.g., Roy et al., 2007). Detrital mineral provenance studies can be complicated by a long transport history of individual grains, which needs to be considered for Quaternary-aged sediments in central Canada. For example, rocks eroded during the Trans-Hudson orogen were subsequently deposited into Proterozoic basins (e.g., upper Belcher Group; McDonald and Partin, 2025), thus, these basins can also be an eastern bedrock source of Trans Hudson-aged hornblende grains. Rocks in the HBB and previously deposited tills contain detritus eroded from different geological provinces of the Canadian Shield, which further complicates detrital provenance studies. Therefore, the detrital hornblende $^{40}Ar/^{39}Ar$ ages are one parameter, among many, used to interpret sediment provenance.

Detrital hornblende grains were handpicked from till mineral separates for $^{40}Ar/^{39}Ar$ age determination. A total of 14–15 grains were analyzed for each sample at the Ar-Ar lab at the Manitoba Isotope Research Facility. The complete $^{40}Ar/^{39}Ar$ age dataset from this study is available in Hodder and Gauthier (2025). The data for each sample is displayed on kernel density estimate plots that were generated using IsoplotR (Vermeesch, 2018), which help to identify different age populations and compare relative trends within and between identified till units.

5.4.2.3 Matrix geochemistry

The <63 µm size-fraction of till-matrix was subjected to a lithium metaborate/tetraborate fusion followed by a 5% nitric acid digestion. This method ensures dissolution of the most resistant minerals, which is more useful for provenance analysis than partial digestion. The proportion of 55 elements were then determined by inductively coupled plasma mass spectrometry and inductively coupled plasma optical emission spectrometry at Activation Laboratories (Hodder and Gauthier, 2025).

At the data analysis stage all variables were converted to a common unit (ppm). To reduce the number of variables prior to analysis, the light and heavy rare earth elements were grouped, whereby ∑LREE=La+Ce+Pr+Nd+Sm+Eu+Gd and ∑HREE=Y+Tb+Dy+Ho+Er+Tm+Yb+Lu as defined in Van Gosen et al. (2017). Next, elements with a high proportion of censored values (>60%) were removed from the dataset (Ag, As, Bi, Ge, In, Mo, Sb, W). Trace elements where the internal standard indicated poor precision (>10% relative standard deviation; Piercey, 2014) were removed prior to analysis (Be, Co, Cu, Hf, Nb, Ni, Pb, Ta, Tl, Hf, Zn, Zr). The remaining data (n=23 variables) is comprised of major elements (Si, Al, Fe, Mn, Mg, Ca, Na, K, Ti, P), trace elements (Ba, Cr, Cs, Ga, Rb, Sc, Sn, Th, U, V) and rare earth elements (∑LREE and ∑HREE). To avoid potential pitfalls of closure on the dataset (Grunsky, 2010), a centred log ratio (CLR) transformation (Aitchison, 1986) was applied prior to principal component analysis (PCA) using ioGAS™ software.

5.4.3 Stratigraphic approach

To better understand the stratigraphic architecture of the western HBL, this study uses a hybrid lithostratigraphic-allostratigraphic approach that has been previously described in Hodder et al. (2024b) and applied in the western HBL (Chapter 4; Gauthier et al., 2025; Mesich, 2025). For identified till beds with no ice-flow data, the tills were correlated to adjacent sections with clast fabric data by using sedimentological observations (matrix colour, degree of consolidation), stratigraphic relationships, and till composition (clast lithology) and texture (matrix grain-size). The till clast-lithology signature between the three stratigraphic areas can be different for similar tills identified due to variations in the local subglacial conditions (e.g., pre-existing sediment thickness) and distance from bedrock sources. For this reason, the compositional data according to stratigraphic area that the till was sampled is provided in Appendix D, Supplemental 5 in addition to the data analysis herein.

5.4.4 Paleoenvironmental characterization

Twenty-two samples (1-cm^3) for pollen analyses were taken from subtill sediments across six exposures (Table 5.1). Pollen samples were processed at the Paleoecology Laboratory at the University of Toronto using standard acid digestions (Faegri and Iversen, 1975) with an additional step of sodium polytungstate to clear any mineral sediments (Zabenskie, 2006; Campbell et al., 2016) and palynospheres to estimate pollen concentration (Kitaba and Nakagawa, 2017). At least 150 pollen grains of type herb, arboreal and shrub were identified at each sample using a compound microscope at 400x magnification and the standard identification key for this region (McAndrews et al., 1973). Stratigraphic plots showing the relative abundance of pollen groups were made in R package ‘rioja’ (Juggins, 2015; Juggins et al., 2015).

Table 5.1: Summary of pollen and foraminifera analysis of intertill sorted sediments.

Stratigraphic unit	Sample ID	Sample interval (m depth)	Sample medium	Are pollen data of sufficient quality for paleoclimate reconstruction? [a]	Reconstructed mean annual precipitation (mm)	Reconstructed mean summer temperature (°C)	Foraminifera analysis genera noted[b]
5a	112-19-608-D01	6.90–6.95	blue-grey clay	No; Barren	--	--	Barren
	112-19-608-D02	7.40–7.45	blue-grey clay	No; Barren	--	--	Barren
	112-19-608-E01	7.90–7.95	brick red silt	No; LC and PP	--	--	Bucella; Elphidium
	112-19-620-C01	8.50–8.55	blue-grey clay	No; PP	--	--	Elphidium clavatum; Islandiella norcrossi
5b	112-19-613-PM012	3.10–3.12	grey silt	Yes	539 ± 126	10.1 ± 1.6	NAC
	112-19-613-PM013	3.30–3.32	grey silt	Yes	462 ± 126	14.9 ± 1.6	NAC
	112-19-613-PM014	3.50–3.52	grey silt	Yes	593 ± 126	11.9 ± 1.6	NAC
	112-19-613-PM015	3.70–3.72	grey silt (visibly organic-bearing)	Yes	513 ± 126	12.3 ± 1.6	NAC
	112-19-613-PM016	3.90–3.92	organic rich horizon	No; PP	--	--	NAC
	112-19-613-PM017	4.10–4.12	brown silt	No; PP	--	--	NAC
	112-19-613-PM018	4.30–4.32	brown silt	Yes	481 ± 126	12.5 ± 1.6	NAC
	112-19-613-PM019	4.50–4.52	brown silt	Yes	680 ± 126	13.5 ± 1.6	NAC
	112-19-613-PM020	4.70–4.72	diamicton	No; PP	--	--	NAC
	112-19-613-PM021	4.90–4.92	sandy gravel	No; PP	--	--	NAC
	112-19-613-PM022	5.70–5.72	silt	Yes	440 ± 126	14.2 ± 1.6	NAC
	112-19-613-PM023	5.90–5.92	fine sand	No; PP	--	--	NAC
	112-19-613-PM024	6.20–6.22	poorly sorted fine sand	Yes	758 ± 126	14.6 ± 1.6	NAC
	112-19-613-PM025	6.47–6.49	organic horizon	Yes	589 ± 126	14.7 ± 1.6	NAC
5c	112-20-702-F01	6.00–6.70	glaciomarine diamicton	No; LC and PP	--	--	Elphidium albiumbilicatum
7	112-19-613-PM007	2.35–2.40	peat	No; PP	--	--	NAC
9	112-19-601-PM004	5.50–5.55	peat bed	Yes	515 ± 169	11.7 ± 1.8	NAC
	112-19-609-PM006	2.35–2.40	laminated silt and fine-sand	No; LC	--	--	NAC

[a] LC, low concentration (<5000 grain per cm^3); PP, poor preservation (>10% broken)

[b] NAC, no analysis completed

A key goal of the pollen work was to quantitatively calculate paleoclimate for the fossil intervals. We used the modern analogue technique (Overpeck et al., 1985), which estimates paleoclimate values (precipitation, temperature) based on the location of similar pollen assemblages in a large modern-day dataset (4882 sites across North America, see: Whitmore et al., 2005; Dalton et al., 2017). Raw pollen counts and additional details about the modern analogue technique are available in Dalton et al. (2022a, 2024). At five sample sites, a subsample was screened for the presence of foraminifera at the micropaleontology lab at University of Colorado, Boulder and genera identified.

5.4.5 Geochronology

5.4.5.1 Radiocarbon

Radiocarbon ages determined by accelerator mass spectrometry were obtained from five wood specimen and nine carbonate shell specimens at the A.E. Lalonde AMS laboratory (Ottawa, Canada). The wood specimens were physically pre-treated prior to analysis by removing the outer layer of the specimen and then chemically pre-treated with an acid-alkali-acid wash. Carbonate shell specimens were physically pre-treated prior to analysis by removing porous or recrystallized areas with a Dremel bit and then chemically pre-treated by etching with 0.2N HCl to remove the outer 20–30% (Crann et al., 2017). Photos of the specimens dated are provided in Hodder and Gauthier (2025).

Radiocarbon ages were calibrated using the Calib 8.2 program (see Stuiver and Reimer, 1993). Marine molluscs were calibrated using the Marine20 calibration curve (Heaton et al., 2020) with an average reservoir offset (ΔR) of -21 ± 72 for Hudson Bay (Pieńkowski et al., 2023). Wood specimens were calibrated using the IntCal20 calibration curve (Reimer et al., 2020).

5.4.5.2 Optical stimulated luminescence

Optical ages for sediment samples from the western HBL have recently been published (Hodder et al., 2023; Gauthier et al., 2024; Hodder et al., 2024b) using the same methodology as in the present study. Opaque plastic tubes (~20 cm long and 5 cm diameter) were inserted into the sediment face of the sorted sand units, extracted, and sealed on each end to preserve the water content. Samples were prepared using standard methods, including wet-sieving and density separation to isolate quartz grains of 180–250 μm in diameter, and a wash with hydrofluoric acid (50%) for 45 minutes.

Equivalent dose (D_e) values were determined using multi-grain aliquots (50–100 grains per aliquot) and the single-aliquot regenerative dose (SAR) method (Murray and Wintle 2000, 2003) and outliers were identified using the interquartile range method (Medialdea et al., 2014). Equivalent doses for each sample were estimated using the central age model (CAM) and minimum age model (MAM) (Galbraith et al. 1999). Additional details regarding the optical dating methodology can be found in Hodder et al. (2023).

5.5 Results and interpretations

5.5.1 Quaternary stratigraphy

A total of 13 stratigraphic units has been identified in this study including 8 till units, recording different ice flow phases, and as much as five non-glacial units. Simplified stratigraphic correlations are shown for the three field areas (Figure 5.4), with more detailed cross-sections provided in Appendix D, Supplemental material 2 and sediment photos of identified units in Appendix D, Supplemental material 3.

5.5.1.1 Unit 1: Marine sediments

Near the base of two sections (19-624 and 20-705) along the Machichi River (Figure 5.4b), the lower bounding surface of the lowest tills is underlain by sand and/or silty clay. The sand is medium to coarse-grained, moderate to well sorted, massive to planar-parallel or cross-bedded and contains shell fragments throughout. At section 20-705, medium to coarse sand is in sharp contact with overlying till and 20 m laterally there is massive blue-grey silty clay at the same stratigraphic position. No contact was observed between these contrasting facies, and they are thus interpreted as a lateral facies variation within a single unit. As such, Unit 1 is primarily defined based on its relative position (at the base of the sections) and by the seemingly continuous upper bounding surface separating it from the lowermost tills along the two sections. The lateral proximity of sand and silty-clay indicates a water-lain depositional environment with significant changes in energy regimes. Given the abundant shell fragments and elevation at 19–20 m above current sea level, Unit 1 sediments are interpreted to have been deposited in a marine environment.

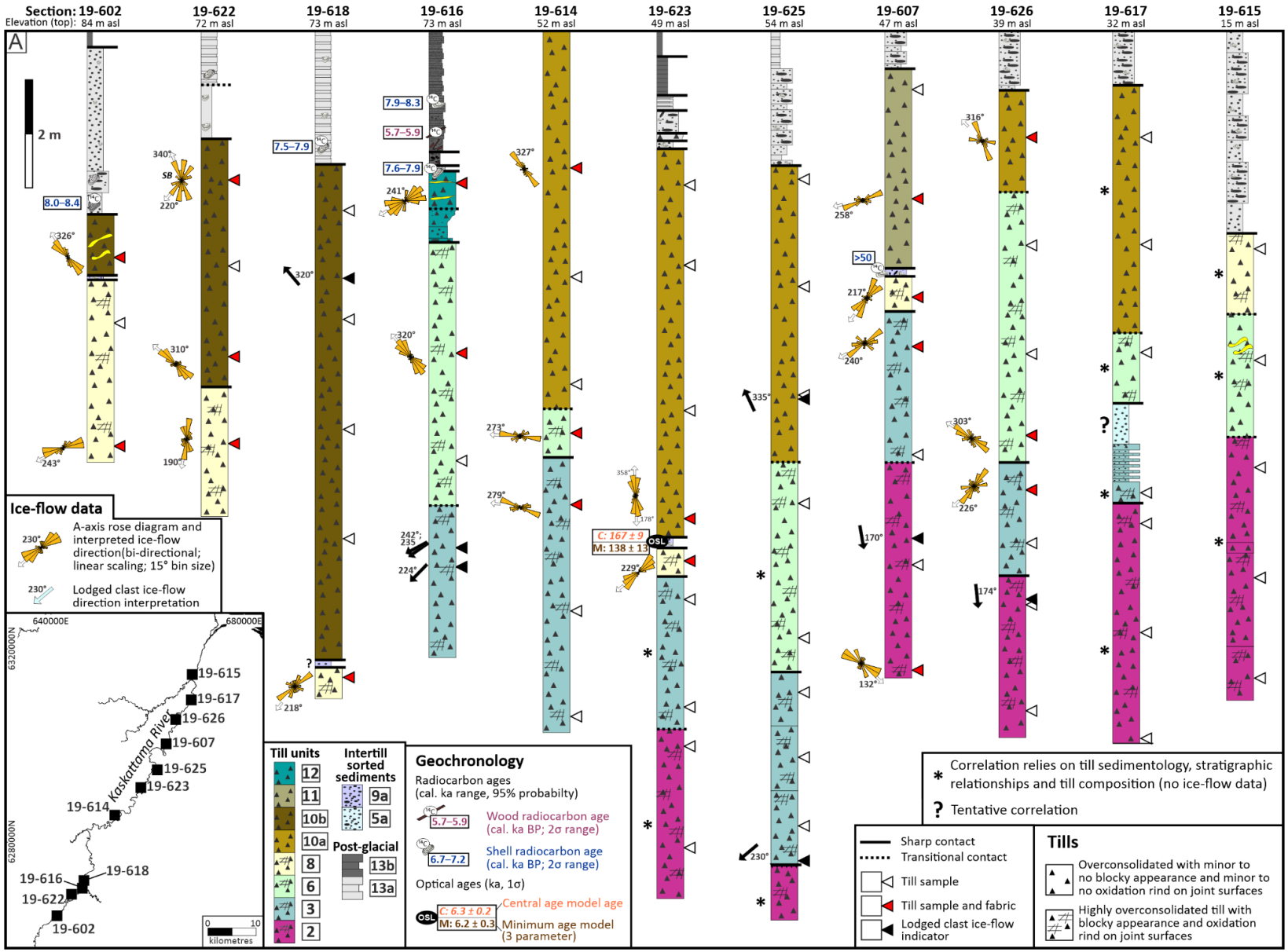
Section: 19-602
Elevation (top): 84 m asl
19-622
72 m asl
19-618
73 m asl
19-616
73 m asl
19-614
52 m asl
19-623
49 m asl
19-625
54 m asl
19-607
47 m asl
19-626
39 m asl
19-617
32 m asl
19-615
15 m asl
A
2 m
8.0–8.4
7.5–7.9
7.9–8.3
5.7–5.9
7.6–7.9
>50
C: 167 ± 9
M: 138 ± 13
OSL
Ice-flow data
A-axis rose diagram and interpreted ice-flow direction(bi-directional; linear scaling; 15° bin size)
Lodged clast ice-flow direction interpretation
640000E
680000E
6320000N
6280000N
19-615
19-617
19-626
19-607
19-625
19-623
19-614
19-616
19-618
19-622
19-602
Kaskattama River
0
10
kilometres
Till units
12
11
10b
10a
8
6
3
2
Intertill sorted sediments
9a
5a
Post-glacial
13b
13a
Geochronology
Radiocarbon ages
(cal. ka range, 95% probabilty)
5.7–5.9
Wood radiocarbon age (cal. ka BP; 2σ range)
6.7–7.2
Shell radiocarbon age (cal. ka BP; 2σ range)
Optical ages (ka, 1σ)
C: 6.3 ± 0.2
M: 6.2 ± 0.3
Central age model age
Minimum age model (3 parameter)
* Correlation relies on till sedimentology, stratigraphic relationships and till composition (no ice-flow data)
? Tentative correlation
Sharp contact
Transitional contact
Till sample
Till sample and fabric
Lodged clast ice-flow indicator
Tills
Overconsolidated with minor to no blocky appearance and minor to no oxidation rind on joint surfaces
Highly overconsolidated till with blocky appearance and oxidation rind on joint surfaces

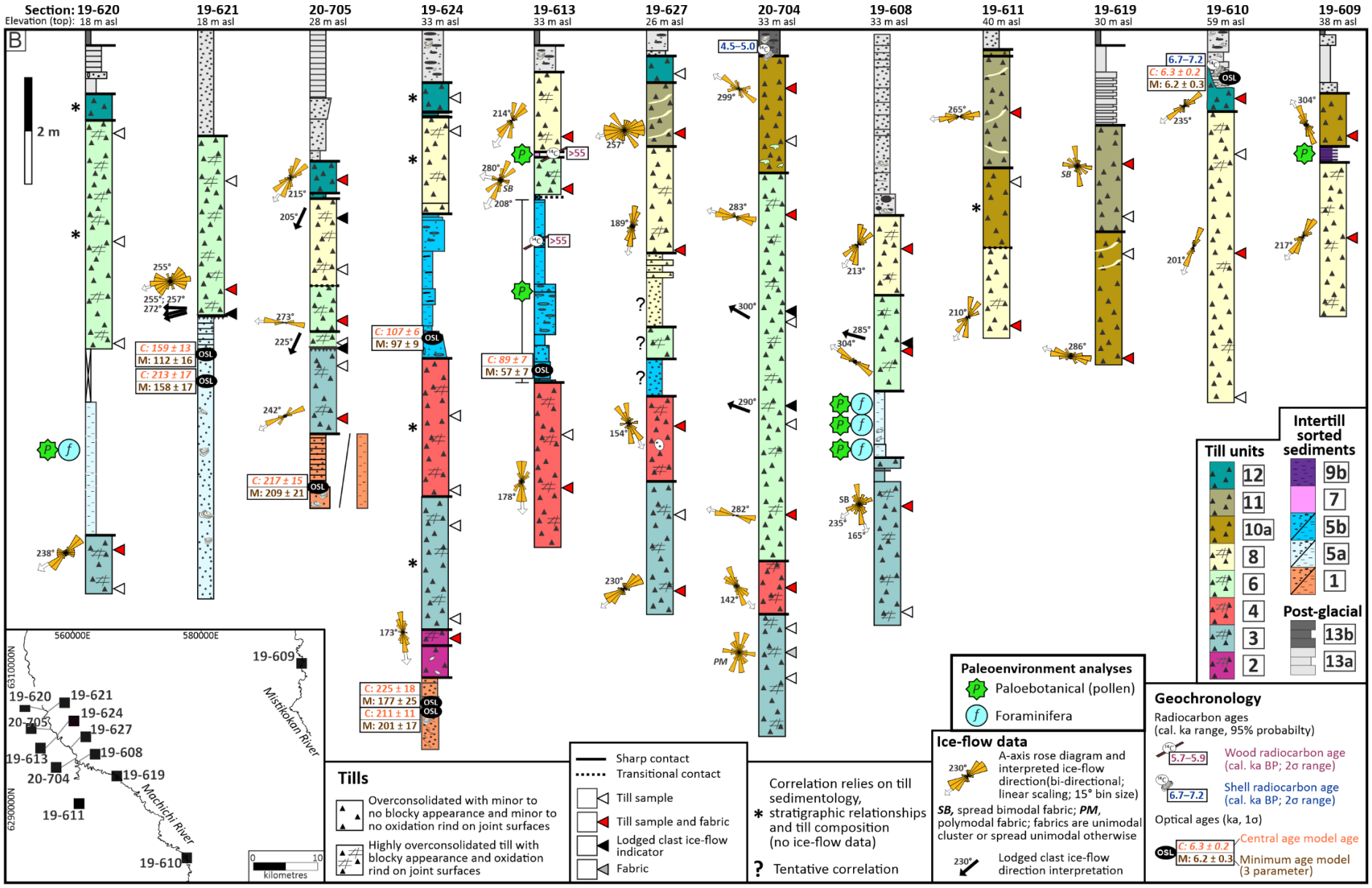
Section: 19-620
Elevation (top): 18 m asl
19-621
18 m asl
20-705
28 m asl
19-624
33 m asl
19-613
33 m asl
19-627
26 m asl
20-704
33 m asl
19-608
33 m asl
19-611
40 m asl
19-619
30 m asl
19-610
59 m asl
19-609
38 m asl
B
2 m
C: 159 ± 13
M: 112 ± 16
C: 213 ± 17
M: 158 ± 17
C: 217 ± 15
M: 209 ± 21
C: 107 ± 6
M: 97 ± 9
C: 225 ± 18
M: 177 ± 25
C: 211 ± 11
M: 201 ± 17
C: 89 ± 7
M: 57 ± 7
>55
4.5–5.0
6.7–7.2
C: 6.3 ± 0.2
M: 6.2 ± 0.3
OSL
SB
PM
560000E
580000E
6310000N
6290000N
19-620
19-621
19-624
20-705
19-627
19-608
19-613
20-704
19-619
19-611
19-610
19-609
Mistikokan River
Mochichi River
0
10
kilometres
Tills
Overconsolidated with minor to no blocky appearance and minor to no oxidation rind on joint surfaces
Highly overconsolidated till with blocky appearance and oxidation rind on joint surfaces
Sharp contact
Transitional contact
Till sample
Till sample and fabric
Lodged clast ice-flow indicator
Fabric
Correlation relies on till sedimentology, stratigraphic relationships and till composition (no ice-flow data)
Tentative correlation
Paleoenvironment analyses
Paloebotanical (pollen)
Foraminifera
Ice-flow data
A-axis rose diagram and interpreted ice-flow direction(bi-directional; linear scaling; 15° bin size)
SB, spread bimodal fabric; PM, polymodal fabric; fabrics are unimodal cluster or spread unimodal otherwise
Lodged clast ice-flow direction interpretation
Till units
12
11
10a
8
6
4
3
2
Intertill sorted sediments
9b
7
5b
5a
1
Post-glacial
13b
13a
Geochronology
Radiocarbon ages
(cal. ka range, 95% probabilty)
5.7–5.9
Wood radiocarbon age (cal. ka BP; 2σ range)
6.7–7.2
Shell radiocarbon age (cal. ka BP; 2σ range)
Optical ages (ka, 1σ)
C: 6.3 ± 0.2
M: 6.2 ± 0.3
Central age model age
Minimum age model (3 parameter)

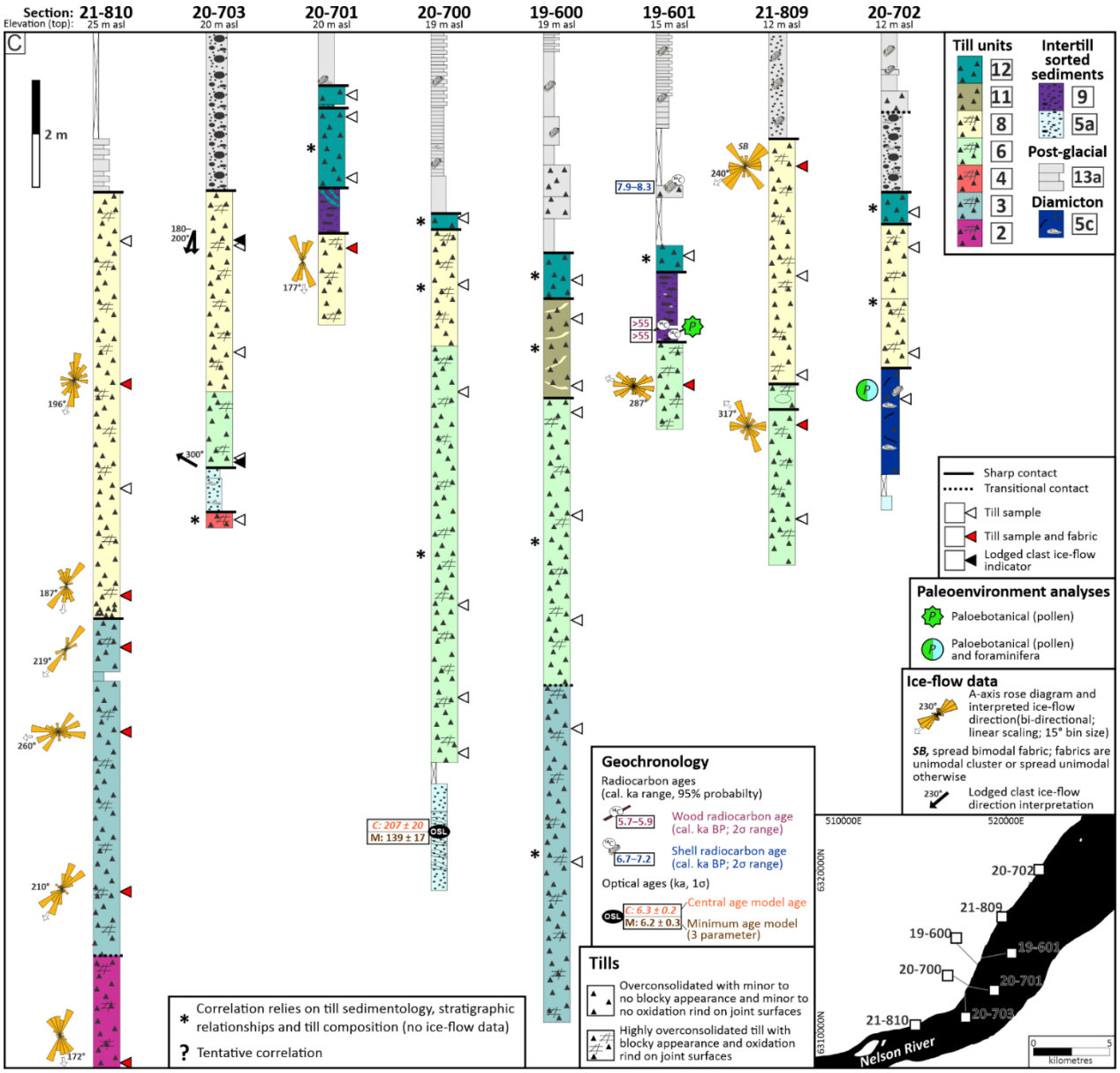

Figure 5.4: Summary of Quaternary stratigraphic relationships interpreted for sections investigated in the Kaskattama River (A), Machichi River (B) and Nelson River Estuary (C) areas. Please refer to Supplemental 1 for additional detailed stratigraphic cross-sections.

The optical ages of two Unit 1 marine beds were investigated along the Machichi River (Figure 5.4b). The optical ages of the well sorted, medium sand at section 19-624 was determined by two samples at 13.0 m depth (Table 5.2). These optical ages are 201 ± 17 ka [MAM, 1σ (sample 112-19-624-OSL018)] or 211 ± 11 ka [CAM, 1σ (sample 112-19-624-OSL018) and 179 ± 26 ka [MAM, 1σ (sample 112-19-624-OSL100)] or 225 ± 18 ka [CAM, 1σ (sample 112-19-624-OSL100)]. A second marine bed at 8.7 m depth and consisting of moderately sorted, medium to coarse sand at section 20-705 yielded an optical age of 209 ± 21 ka [MAM, 1σ (sample 112-20-705-OSL008)] or 217 ± 15 ka [CAM, 1σ (sample 112-20-705-OSL008)]. The MAM optical ages overlap at 1σ error.

Table 5.2: Number of aliquots measured (n), overdispersion values (OD), equivalent dose values (D_e), optical ages, and dose recovery (DR) ratios.

Section_ID	Stratigraphic unit	Depth (m)	Lab ID	N[1]	OD (%)	D_e (Gy) – M[3]	D_e (Gy) – C[2]	Age (ka) - M	Age (ka) - C	DR ratios[4]
112-19-610	13a	1.1	112-19-610-OSL005	23/30	11 ± 2	11.4 ± 0.3	11.5 ± 0.3	6.2 ± 0.3	6.3 ± 0.2	1.02 ± 0.02
112-19-623	9a	9.6	112-19-623-OSL015	29/49	21 ± 4	217 ± 19	263 ± 12	138 ± 13	167 ± 9	0.99 ± 0.04
112-19-613	5b	6.3	112-19-613-OSL007	26/30	33 ± 5	83 ± 10	129 ± 9	57 ± 7	89 ± 7	0.99 ± 0.02
112-19-624	5b	6	112-19-624-OSL300	24/26	18 ± 3	124 ± 10	137 ± 6	97 ± 9	107 ± 6	--
112-20-700	5a	15	112-20-700-OSL004	22/36	33 ± 6	138 ± 15	206 ± 17	139 ± 17	207 ± 20	--
112-19-621	5a	6.2	112-19-621-OSL016	23/39	31 ± 6	180 ± 25	254 ± 20	112 ± 16	159 ± 13	0.99 ± 0.04
112-19-621	5a	6.7	112-19-621-OSL012	24/24	28 ± 5	245 ± 24	329 ± 21	158 ± 17	213 ± 17	--
112-20-705	1	8.7	112-20-705-OSL008	24/39	18 ± 5	272 ± 25	282 ± 15	209 ± 21	217 ± 15	1.03 ± 0.04
112-19-624	1	13.1	112-19-624-OSL100	21/24	26 ± 5	266 ± 35	339 ± 22	177 ± 25	225 ± 18	--
112-19-624	1	13.1	112-19-624-OSL018	21/34	14 ± 5	283 ± 22	297 ± 14	201 ± 17	211 ± 11	0.98 ± 0.05

[1]N = numbers of aliquots accepted/number of aliquots measured

[2]C = Determined using the central age model (CAM)

[3]M = Determined using the three-parameter minimum age model (MAM)

[4]DR = dose recovery ratio (given dose/recovered dose)

Note: equivalent dose and OD values calculated using the software of Liang and Forman, 2019

5.5.1.2 Unit 2: Till deposited by southeast- to south-trending ice-flow

Unit 2 consists of massive, matrix-supported till that is highly overconsolidated and strongly jointed with oxidation rind developed on joint surfaces (e.g., Figure 5.3a; Figure 5.5) and is best exposed along the Kaskattama River (Figure 5.4a). The matrix colour is brown or dark greyish-brown (Appendix D, Table S1-2) and typically has a sandy-silt to clayey sandy-silt texture (Figure 5.6). Ice-flow data collected includes two lodged boulders and three clast fabrics that are interpreted to have formed by SE- to S-trending ice-flow (132–174°; Appendix D, Table S1-1). At section 19-607 (Figure 5.5), there is a switch up-unit from SE-trending ice-flow (132°) to S-trending ice-flow (170°), suggesting that there may have been a clockwise-rotation in ice-flow direction during the deposition of Unit 2 till. Unit 2 till contains a relatively high proportion of granitoid clasts and Dubawnt erratics (75th percentile of 23.0 ct. % versus 19.4 ct. % for dataset; Figure 5.7). Detrital hornblende $^{40}Ar/^{39}Ar$ ages from one sample are predominantly 1.7–2.0 Ga, with 10 of 14 grains falling in this range (Figure 5.8), which suggest contribution from the WC or THO geological provinces. Together, ice-flow data and composition provide supporting evidence for a northwestern sediment provenance. Unit 2 overlies Unit 1 (one section), or was continous to the bottom of the section (seven sections). The upper contact of Unit 2 is with Unit 3 (seven sections) or Unit 6 (one section). At section 19-625 a laterally extensive boulder pavement seperates Unit 2 and Unit 3 tills.

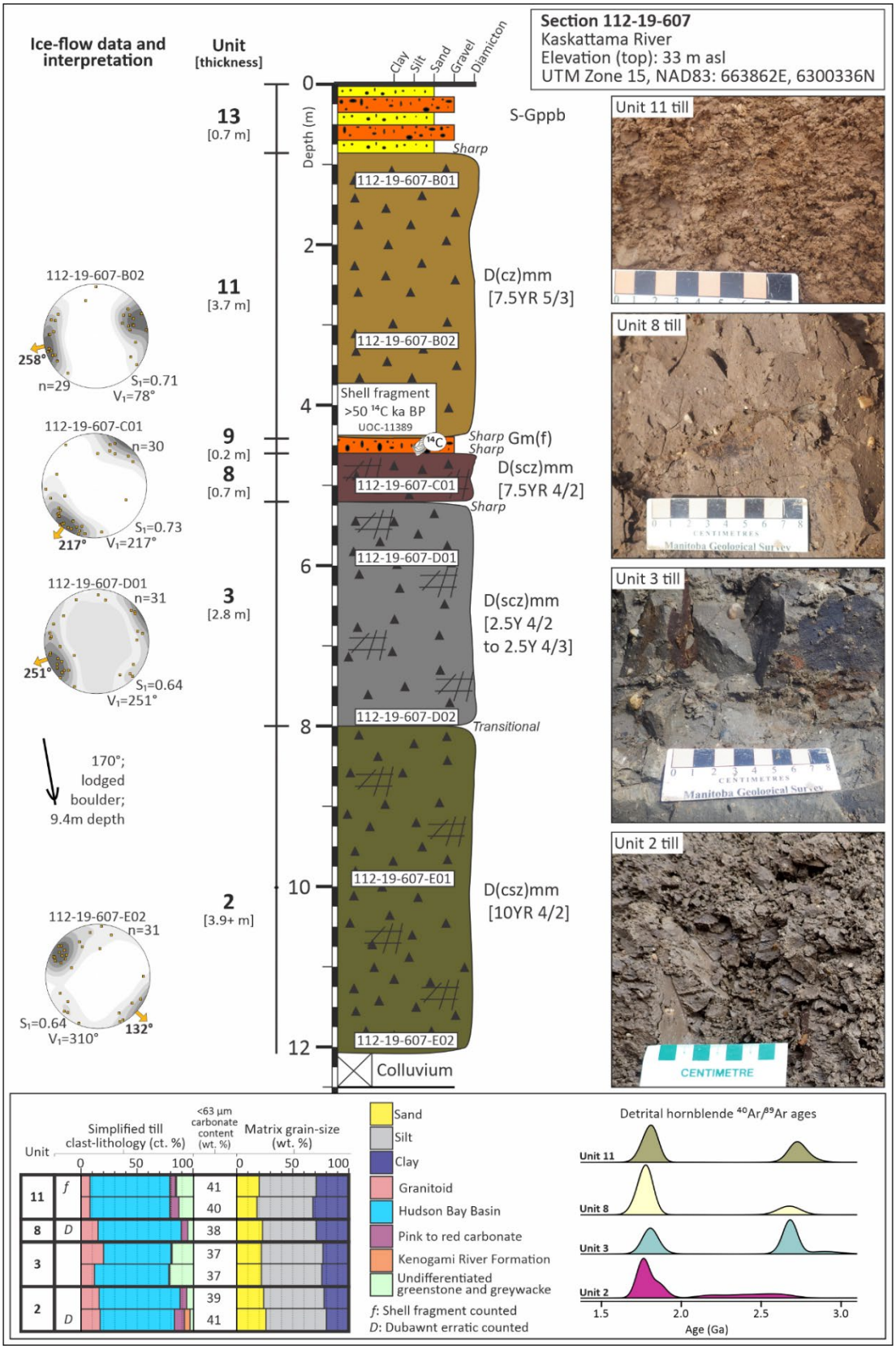

Figure 5.5: Quaternary stratigraphy exposed at section 19-607 on the Kaskattama River with photos of identified till units. Till sample numbers are labelled within the white boxes. Simplified clast-lithology counts, <63 µm carbonate values, matrix texture data and detrital hornblende $^{40}Ar/^{39}Ar$ ages are provided for these samples in the bottom panel (see Figure 5.8 for additional details). Till clast-fabric data are plotted on equal area, lower hemisphere projection stereonets. The value of the principal eigenvalue (S_1) and direction of the principal eigenvector (V_1) are provided, and an interpretation of the ice-flow direction is indicated (orange arrow).

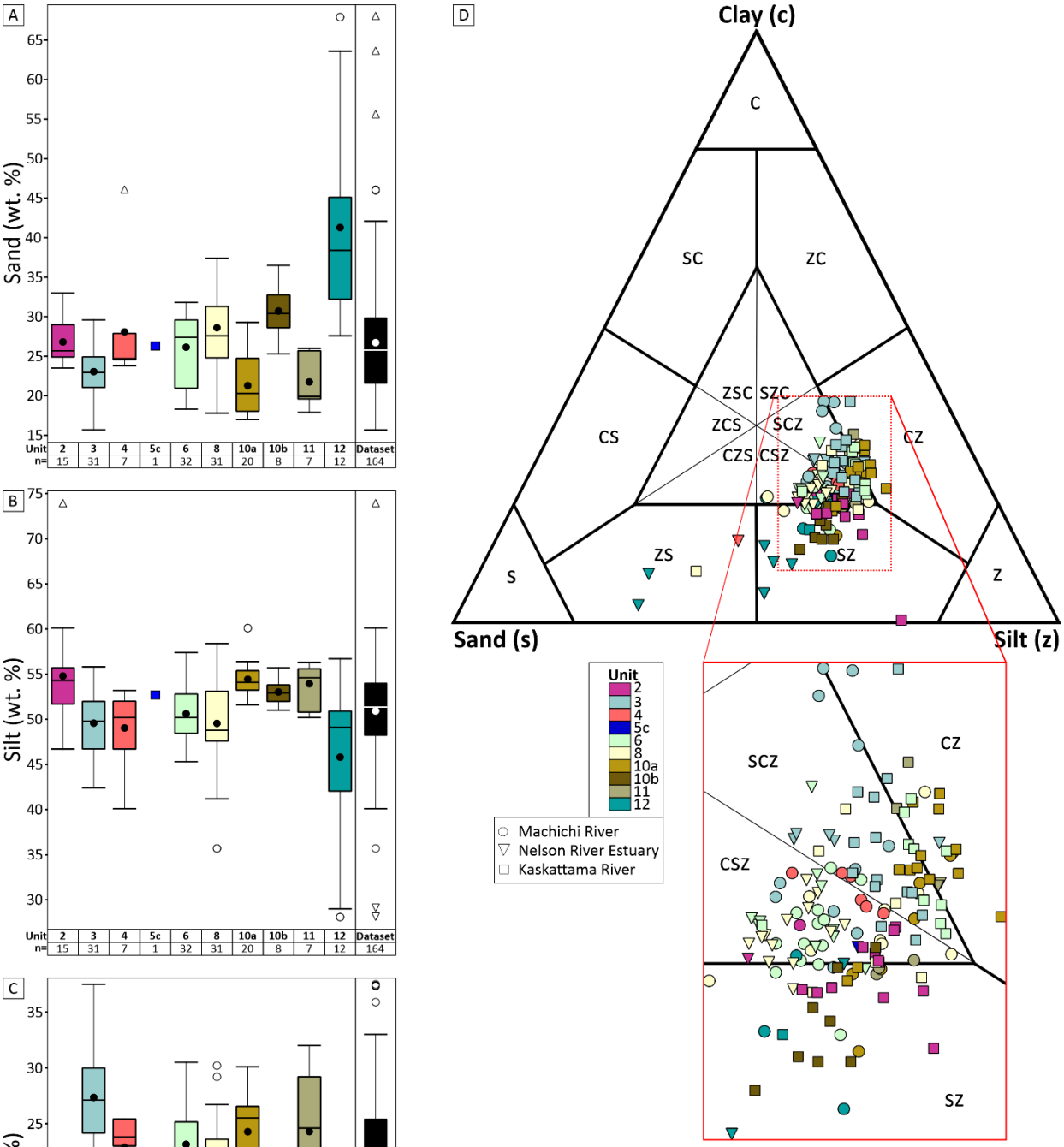

Figure 5.6: Till-matrix grainsize proportions for identified till units: A) Tukey box plot of sand (wt. %); B) Tukey box plot of silt (wt. %); C) Tukey box plot of clay (wt. %); and D) sand-silt-clay ternary plot, textural fields plotted are modified from Trefethen (1950) and Shepard (1954).

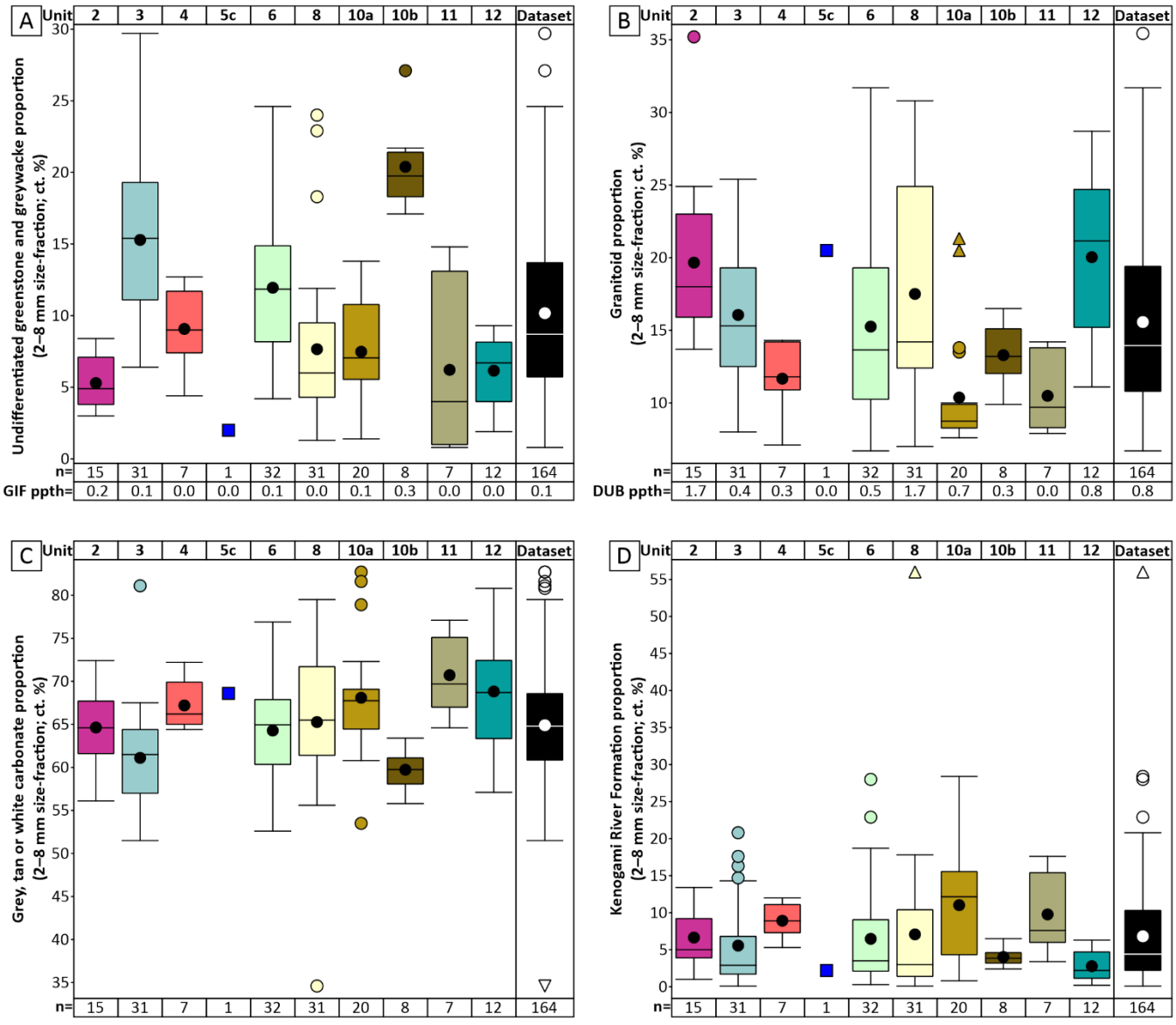

Figure 5.7: Till clast-lithology proportions for identified till units: A) undifferentiated greenstone and greywacke (UGG) clasts; B) granitoid clasts; C) carbonate clasts; and D) Kenogami River Formation clasts. Abbreviations: Dub, Dubawnt erratic; GIF, granular iron formation erratic; ppth, parts per thousand.

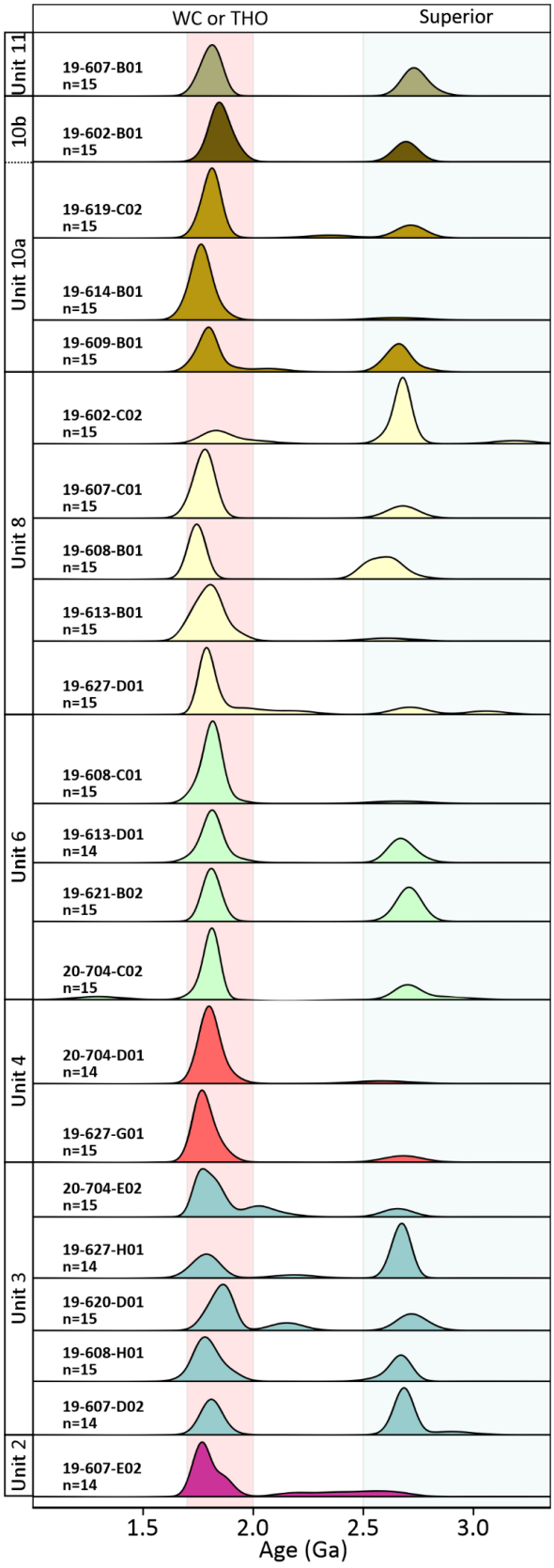

Figure 5.8: Till detrital hornblende ages grouped according to identified till unit displayed on kernel density estimation plots.

5.5.1.3 Unit 3: Till deposited by southwest-trending ice-flow

Unit 3 consists of massive, matrix-supported till that is highly overconsolidated and strongly jointed with oxidation rind developed on joint surfaces (Figure 5.3a, b, c; Figure 5.5; Figure 5.9). The matrix is mostly dark greyish-brown and typically has a distinctive grey colour in the field (Appendix D, Table S1-2; Figure 5.3a, b, c; Figure 5.5). The matrix is clayey sandy-silt to clayey silt, which places in a relatively 'clay-rich' till group for the study area (Figure 5.6). Ice-flow data includes eight lodged clasts and nine clast fabrics that indicate paleo-ice flow ranging 210–279° (Appendix D, Table S1-1). Unit 3 till contains a relatively high proportion of UGG clasts (75th percentile of 19.4 ct. % versus 13.7 ct. % for dataset; Figure 5.7). Detrital hornblende $^{40}Ar/^{39}Ar$ ages from five samples contain a variable proportion of Superior-aged grains (Figure 5.8), with two samples having a greater amount of Superior-aged grains compared to WC- or THO-aged grains. This composition is consistent with transport from a dome situated east of Hudson Bay. The majority of ice-flow indicators (n=13/17) fall within the 224–260° range, and when taken together with till provenance, suggests Unit 3 was deposited by SW- to WSW-trending ice. The lower contact of Unit 3 is with Unit 1 (one section), Unit 2 (seven sections) or was continous to the bottom of the section (seven sections). The upper contact of Unit 3 is with Unit 4 (three sections), Unit 5 (three sections), Unit 6 (six sections) or Unit 8 (three sections).

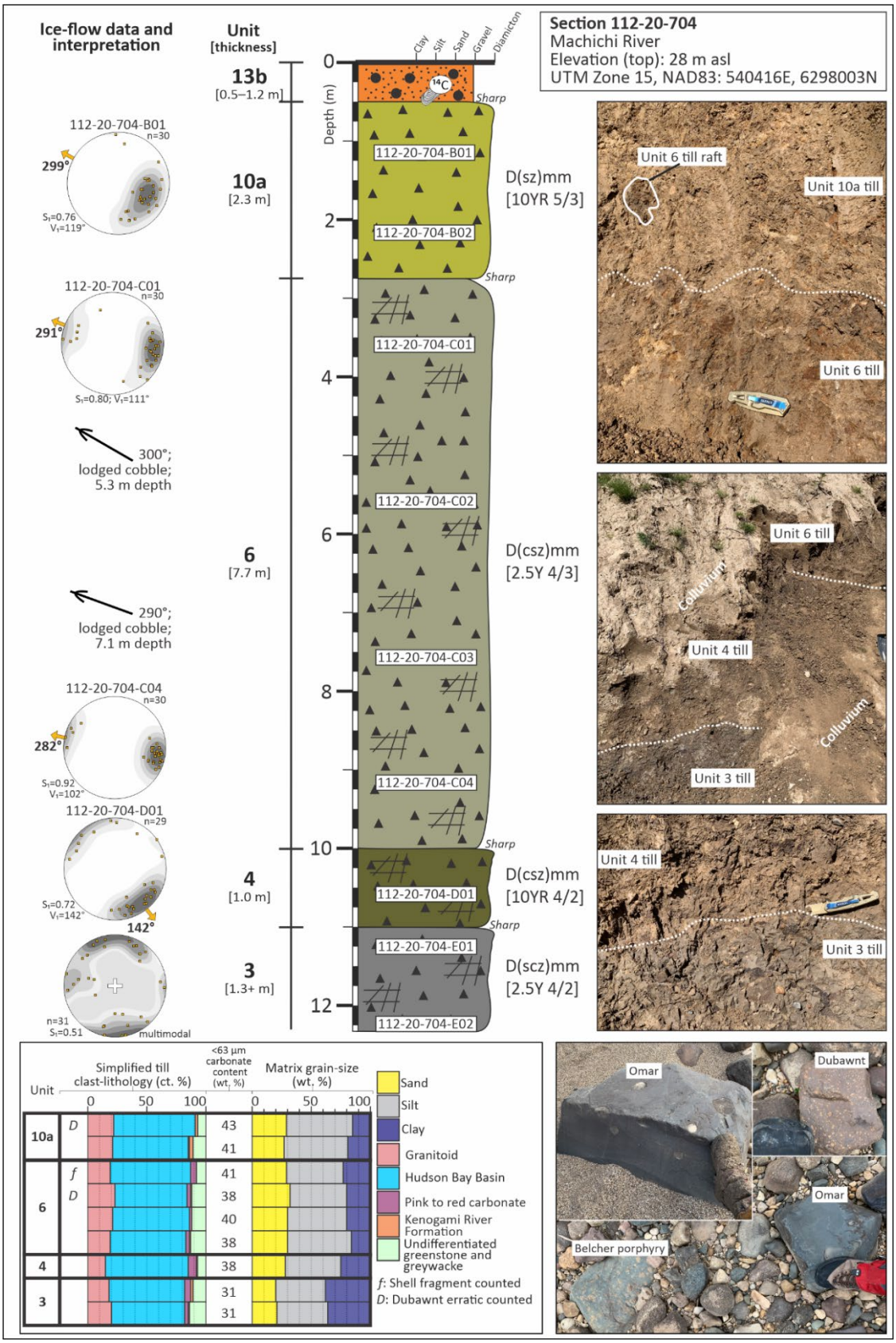

Figure 5.9: Quaternary stratigraphy exposed at section 20-704 on the Machichi River with photos of identified till units. Till sample numbers are labelled within the white boxes. Simplified clast-lithology counts, <63 µm carbonate values and matrix texture data are provided for these samples in the bottom left panel. The bottom right panel provides examples distinct erratics observed along the river shoreline (not in-situ). Till clast-fabric data are plotted on equal area, lower hemisphere projection stereonets. The value of the principal eigenvalue (S_1) and direction of the principal eigenvector (V_1) are provided, and an interpretation of the ice-flow direction is indicated (orange arrow).

5.5.1.4 Unit 4: Till deposited by south- to south-southeast trending ice-flow

Unit 4 consists of massive, matrix-supported till that contains striated, bullet-shaped and faceted clasts that is highly overconsolidated and strongly jointed with oxidation rind developed on joint surfaces. The matrix colour is brown or dark greyish brown (Appendix D, Table S1-2; Figure 5.3d) and typically has a clayey sandy-silt to sandy clayey-silt texture (Figure 5.6). Ice-flow data collected includes three clast fabrics that are interpreted to have formed by SE- to S-trending ice-flow (142–178°; Appendix D, Table S1-1). Unit 4 till contains slightly elevated proportions pf Kenogami clasts (75th percentile of 11.1 ct. % versus 10.3 ct. % for dataset; Figure 5.7). Detrital hornblende $^{40}Ar/^{39}Ar$ ages from two samples are predominantly 1.7–2.0 Ga (26/29 grains; Figure 5.8), which suggests a contribution from WC or THO geological provinces, situated to the northwest (Figure 5.2). As such, Unit 4 till was likely deposited by SE- to S-trending ice flow from a dome situated in mainland Nunavut or in Hudson Bay. The lower contact of Unit 4 till is with Unit 3 (three sections) or was continous to the bottom of the section (two sections). The upper contact of Unit 4 is with Unit 5 (four sections) or Unit 6 (one sections).

5.5.1.5 Unit 5: Marine and terrestrial sediments

Unit 5 intertill sorted sediments are recognized at eight sections and tentatively correlated at another two sections (Figure 5.4). The sorted sediment unit is defined by its upper bounding surface with Unit 6 (six sections) or Unit 8 (two sections) and lower bounding surface with Unit 3 (two section), Unit 4 (three sections) or was not determined (lowermost unit at three sections). Unit 5 consists of bedded clay, silt, sand and gravel and key sections investigated along the Machichi River and Nelson River Estuary are described in detail below.

5.5.1.5.1 Unit 5a: marine sediments

In the Machichi River area, three sections contain 1.3–5.3+ metres of blue-grey to brick red silt, clay and medium- to coarse sand (e.g., Figure 5.10), situated between 7.5 and 27.0 m asl (Figure 5.4b). The sediments do not contain visible detrital organics, but the sandy facies contain shell fragments. The fine-grained sediments at two sites (sections 19-608 and 19-620) were analyzed for the recovery of foraminifera. Two of three samples from section 19-608 were barren, but the third sample from

the lowermost red silt contain *Bucella* and *Elphidium* (Figure 5.10; Table 5.1). The lone sample from section 19-620 contained *Elphidium clavatum* and *Islandiella norcrossi*. The recovery of foraminifera along with relatively thick sequences of blue-grey coloured silt and sands with marine shell fragments all point to a marine depositional environment. This depositional event is assigned a letter modifier and designated as Unit 5a. Three additional Unit 5a occurrences on the Nelson River Estuary situated between 3 and 12 m asl that contain bedded to massive sand or clay have been correlated to Unit 5a based on stratigraphic position (Figure 5.4c). Four pollen samples from unit 5a were analyzed, but these samples were all barren of pollen grains or were extremely low concentrations, which prohibits any meaningful paleoclimate interpretation.

At the Nelson River Estuary (section 20-702; Figure 5.4c), a unique dark grey (Munsell colour 7.5YR 4/1) clayey sandy-silt diamicton that contains whole valves of *Macoma calcarea* was identified (Hodder and Gauthier, 2025). The diamicton bed is separated from overlying Unit 8 till by a sharp contact, and these two beds have a similar clast-lithology signature. This diamicton bed is interpreted to have likely been deposited during a glacial advance, whereby the till has a high inheritance of Unit 5a nonglacial sediments including whole-valve shells. If this is the case, then the bed could be assigned to Unit 6. Alternatively, this bed could have been deposited in a proglacial glaciomarine environment. Given the depositional environment uncertainties and lack of ice-flow data collected from this bed, this unique bed of diamicton has been assigned to its own unit (Unit 5c).

The ages of two Unit 5a marine beds were assessed by optical dating (Figure 5.4b, c). Two optical ages of the thick bed (>5.3 m) of well sorted, medium sand at section 19-621 was determined at 6.7 and 6.2 m depth (Table 5.2). The sand at 6.7 m depth yielded an age of 158 ± 17 ka [MAM, 1σ (112-19-621-OSL012)] or 213 ± 17 ka [CAM, 1σ (sample 112-19-621-OSL012), whereas the sand at 6.2 m depth yielded an age of 112 ± 16 ka [MAM, 1σ (112-19-621-OSL016)] or 159 ± 13 ka [CAM, 1σ (sample 112-19-621-OSL016)]. These two optical ages overlap at 2σ error. The optical age of another bed of well sorted, medium sand at section 20-700 was determined to be 139 ± 17 ka [MAM, 1σ (112-20-700-OSL004)] or 206 ± 17 ka [CAM, 1σ (sample 112-20-700-OSL004)].

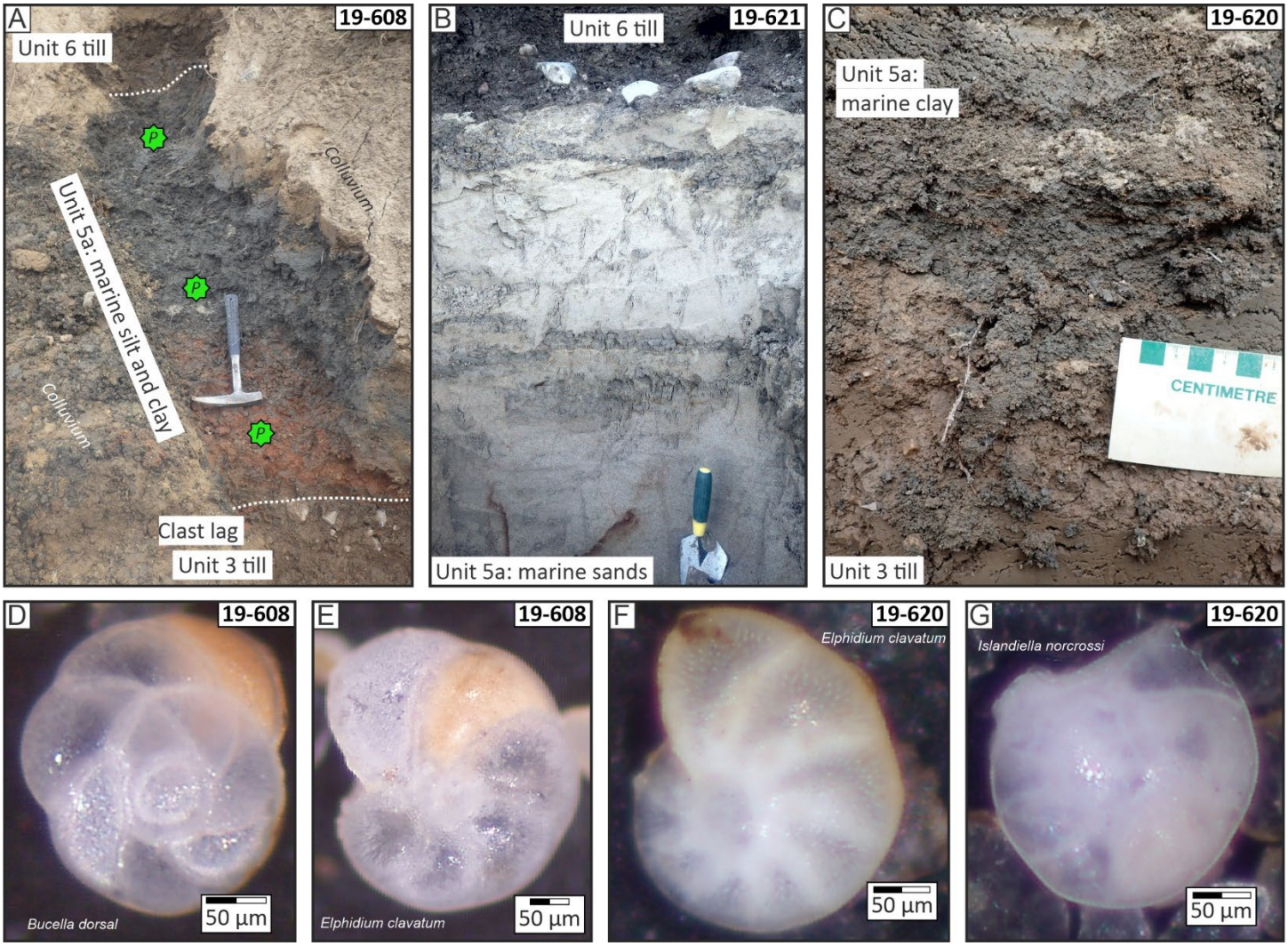

Figure 5.10: Unit 5a marine sediments exposed along the Machichi River (A–C) and examples of foraminifera specimens identified within these sediments (D–G).

5.5.1.5.2 Unit 5b: terrestrial sediments

The Machichi River area contains two sections, situated just 100 m apart, that consist of 2.7–3.3 m of organic-bearing, bedded, sand, silt and gravel; 26.3–30.0 m above the current sea level (e.g., Figure 5.11). These sediments contain wood with a nonfinite radiocarbon age (>55 ^{14}C ka BP; UOC-10978; Table 5.3) and the pollen profile of section 19-613 was investigated in detail (Table 5.1). Nine of the fourteen pollen samples spanning this interval contained sufficiently preserved pollen grains for paleoenvironmental interpretation (Figure 5.12). In terms of tree pollen, the assemblage is characterized by 40–60% *Picea*, 10–20% *Pinus* and smaller amounts of *Betula* and *Salix*. The dominant herbs identified were Poaceae and Asteraceae (both 12% or less), with smaller amounts of Amaranthaceae, Ericaceae, *Lycopodium*, *Corylus*, Cupressaceae and Polypodiaceae (low percentages). Statistically, the analogous modern-day sites are widely distributed from the boreal shield of the Canadian Prairies, into the HBL and also in northern Quebec and Labrador (Dalton et al., 2022a). Reconstructed mean summer temperature ranges widely across the sampled interval from ~15°C near the base to ~11°C in the topmost sample. Reconstructed annual precipitation is equally variable, with relatively high values (~800 mm) near the base, transitioning to slightly drier conditions (~600 mm) in the topmost sample. It is possible that the early part of the fossil record captured ambient conditions during an ice-free interval, and the transition toward cooler and drier conditions in the topmost samples represents the onset of a glacial stage. Pollen samples had highly variable Cyperaceae and *Sphagnum* counts, along with occasional *Pediastrum, Equisetum* and *Typha* which suggests the presence of local wetland waterlogged conditions. In sum, the pollen data suggests that the terrestrial sediments in unit 5b represent similar-to-present boreal peatland conditions as are in the area today (e.g., Farley-Gill, 1980). A slight shift toward increased Cyperaceae and decreased Sphagnum up the core suggests a transition from bog to fen. Aquatic indicators (*Equisetum*, *Typha* and *Pediastrum*) are occasionally present in the fossil interval, which suggest an occasional transition to a local aquatic depositional environment. The organic content, determined via loss-on-ignition, ranged from 2–25%, throughout the pollen section of 19-613.

Table 5.3: Radiocarbon data.

Section	Unit	Easting[1]	Northing[1]	Depth minimum (m bgs)	Sample elevation (m asl)[2]	Material dated	Laboratory ID	^{14}C yr BP	Calibrated age (95% prob. range)	Calibrated age (median prob.)	Interpretation
112-19-616	13b	646840	6272038	2.00	71.0	detrital wood directly above leaf litter bed	UOC-10977	5049 ± 25	5730–5899	5826	Terrestrial limiting
112-19-616	13b	646840	6272038	1.65	71.4	unidentified shell fragment	UOC-10983	7777 ± 29	7886–8303	8083	Detrital marine shell
112-20-704	13b	560416	6298003	0.40	28.0	*Macoma calcarea* (whole valve)	UOC-13467	4712 ± 28	4522–5034	4782	Fluvial terrace; marine limiting
112-19-602	13a	641256	6264744	3.35	80.7	*Mya truncata* (whole valve)	UOC-10981	7838 ± 29	7948–8345	8144	Marine limiting
112-19-610	13a	577758	6282509	1.40	57.6	*Macoma calcarea* (whole valve)	UOC-10982	6609 ± 26	6693–7154	6922	Marine limiting
112-19-616	13a	646840	6272038	2.48	70.5	*Hiatella arctica* (whole valve)	UOC-10984	7441 ± 28	7558–7935	7741	Marine limiting
112-19-618	13a	646518	6270461	2.49	70.5	*Hiatella arctica* (paired valves)	UOC-10985	7381 ± 30	7492–7888	7648	Marine limiting
112-19-601	13a	518443	6314617	2.90	12.1	*Mya truncata* (paired valves)	UOC-13464	7755 ± 31	7858–8281	8061	Marine limiting
112-19-601	9	518443	6314617	5.50	9.5	detrital wood	UOC-10974	>55 000	--	--	Nonfinite age
112-19-601	9	518443	6314617	5.84	9.2	wood in organic bed	UOC-10975	>55 000	--	--	Nonfinite age
112-19-607	9	663862	6300336	4.50	28.5	unidentified shell fragment	UOC-11389	>50 000	--	--	Nonfinite age
112-19-613	7	557686	6301533	2.35	30.7	wood in organic bed	UOC-10976	>55 000	--	--	Nonfinite age
112-20-702	5c	522038	6320049	7.4	4.6	*Macoma calcarea* (whole valve)	UOC-13465	49 928 ± 1040	--	--	Nonfinite age; marine limiting
112-19-613	5b	557686	6301533	3.90	29.1	wood in organic bed	UOC-10978	>55 000	--	--	Nonfinite age

1. Easting and northing coordinates are UTM 15N projection and NAD83 datum.

2. Elevation measurements were taken with a handheld GPS and the associated error is approximately +/- 3 metres.

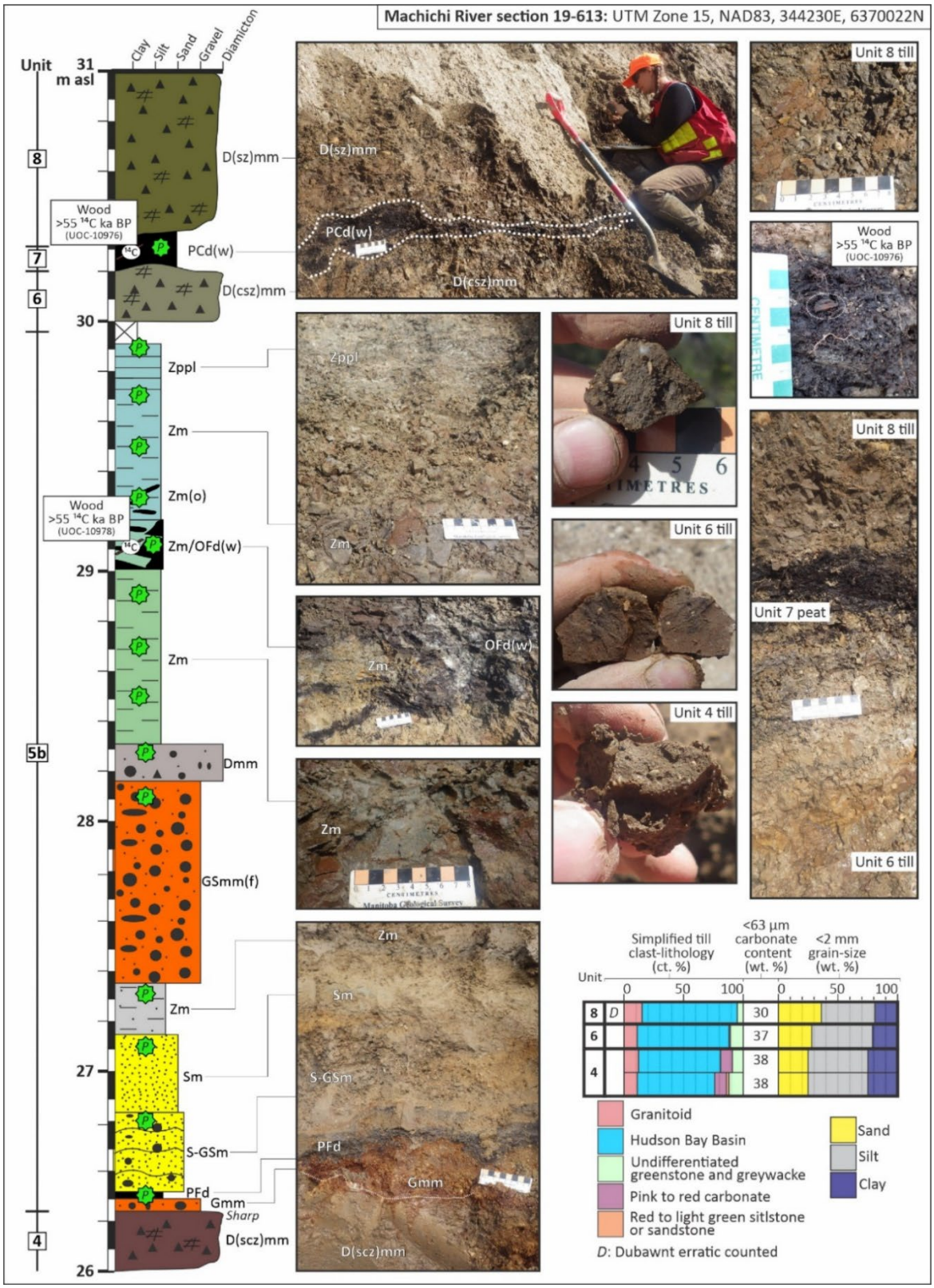

Figure 5.11: Upper stratigraphy exposed at section 19-613 with photos of sediments. Simplified clast-lithology counts, <63 µm carbonate values and matrix texture data are provided for tills identified in the bottom right panel.

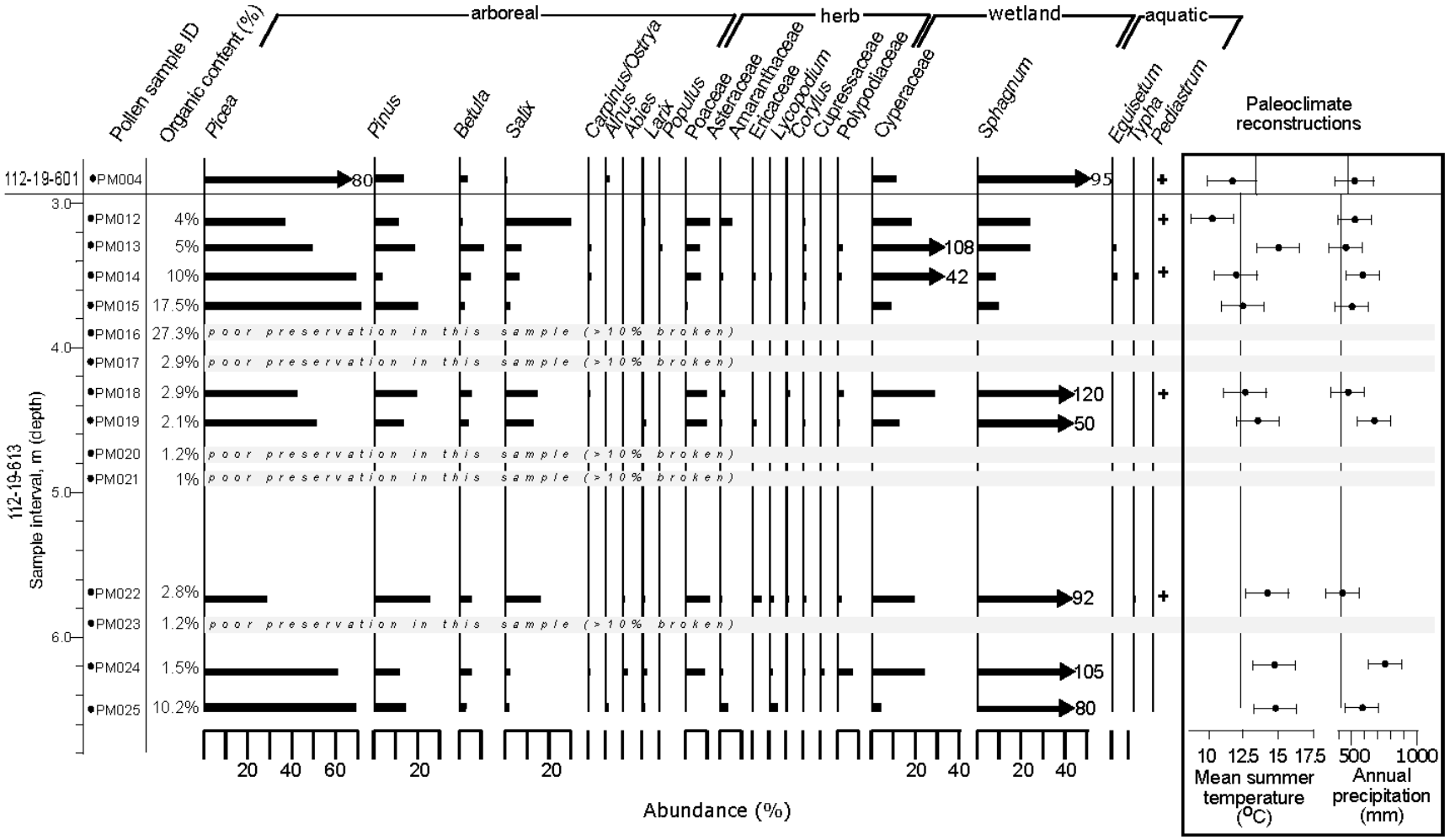

Figure 5.12: Pollen data for site 112-19-601 (1 sample) and 112-19-613 (14 samples). Only groups reaching a relative abundance of >1% are shown here. Reconstructed paleoclimate values are shown alongside the pollen data, with the vertical lines representing present-day conditions at the site. Measurements of organic content are also shown for 112-19-613 (no measurements of organic content were made for site 112-19-601).

The optical ages of Unit 5b sediments was determined at sections 19-613 and 19-624 (Table 5.2; Figure 5.4b). At section 19-613, the bed of moderately sorted, granular coarse sand yielded an optical age of 57 ± 7 ka [MAM, 1σ (112-19-613-OSL007)] or 89 ± 7 ka [CAM, 1σ (sample 112-19-613-OSL007)]. At section 19-624, the optical age of a moderately sorted, medium sand bed was determined to be 97± 9 ka [MAM, 1σ (112-19-624-OSL300)] or 107 ± 6 ka [CAM, 1σ (sample 112-19-624-OSL300)].

5.5.1.6 Unit 6: Till deposited by west- to northwest-trending ice-flow

Unit 6 consists of massive, matrix-supported till that is highly overconsolidated and strongly jointed with oxidation rind developed on joint surfaces. The matrix colour is typically olive brown or dark greyish brown (Appendix D, Table S1-2) and typically has a clayey sandy-silt to clayey-silt texture (Figure 5.6). Ice-flow data collected includes 10 clast fabrics and four lodged clasts that indicate paleo-ice-flow ranged from 255–320° (Appendix D, Table S1-1). Unit 6 till contains a relatively higher proportion of UGG clasts (75th percentile of 14.9 ct. % versus 13.7 ct. % for dataset; Figure 5.7). Detrital hornblende $^{40}Ar/^{39}Ar$ ages from four samples have a variable distribution (Figure 5.8). The majority of ice-flow indicators (n=13/14) fall within 285–320°, and when taken together with till provenance, suggests Unit 6 was deposited by WNW- to NW-trending ice-flow. The lower contact of Unit 6 is with Unit 2 (one section), Unit 3 (six sections), Unit 4 (one sections), Unit 5 (seven sections) or was continous to the bottom of the section (two sections). The upper contact of Unit 6 is with Unit 7 (one section), Unit 8 (six sections), Unit 9 (one section), Unit 10 (five sections), Unit 11 (one section), Unit 12 (two sections) or Unit 13 (one section).

5.5.1.7 Unit 7: Organic-bearing intertill sediments

Unit 7 is identified at just one section (section 19-613 along the Machichi River; Figure 5.4b, Figure 5.11) where it is defined by an upper bounding surface with Unit 8 till and a lower bounding surface with Unit 6 till. Unit 7 consists of a peat bed of variable thickness (maximum of 0.3 m) that contains wood fragments (Figure 5.11). A wood fragment recovered from within the peat yielded a nonfinite radiocarbon age (>55 ^{14}C ka BP; UOC-10976; Table 5.3). Based on LOI, the peat has about 33% organic carbon content, which is higher than sediments analyzed in Unit 5b below (maximum 27%). The peat bed was not observed at section 19-624, situated 100 m to the northwest, indicating Unit 7

pinches out laterally. The peat bed is currently lying horizontal in sharp contact with two distinct bounding tills and there was no evidence of deformation such as shear planes or overturned beds. Unit 7 peat bed is thus interpreted to represent a separate ice-free period rather than a piece of peat from underlying Unit 5b that would have been incorporated into the till. Our interpretation is based on the contrasting qualitative and quantitative properties of the till above and below, the higher organic content of the peat bed compared to interglacial sediments below and lack of any deformation signature within the peat bed.

5.5.1.8 Unit 8: Till deposited by south- to southwest-trending ice-flow

Unit 8 consists of massive, matrix-supported till that is highly overconsolidated and strongly jointed with oxidation rind developed on joint surfaces. The matrix colour is typically olive brown or dark greyish brown (Appendix D, Table S1-2) and typically has a clayey sandy-silt to clayey silt texture (Figure 5.6). Ice-flow data collected includes 15 clast fabrics and two lodged clasts that are interpreted to have formed by S- to WSW-trending ice-flow (177–243°; Appendix D, Table S1-1). Unit 8 till contains a relatively high proportion of granitoid clasts (75th percentile of 24.9 ct. % versus 19.4 ct. % for dataset; Figure 5.7) and Dubawnt erratics (Figure 5.7). Detrital hornblende $^{40}Ar/^{39}Ar$ ages from four samples primarily have a dominant WC- or THO-source signature and one sample has a dominant Superior-source age distribution *(*Figure 5.8). Together, ice-flow data and composition provide supporting evidence for a north to northeast provenance for Unit 8 till. The lower contact of Unit 8 is Unit 3 (three sections), Unit 5 (two sections), Unit 6 (seven sections), Unit 7 (one section) or was continous to the bottom of the section (seven sections). The upper contact of Unit 8 is Unit 9 (six section), Unit 10 (two sections), Unit 11 (one section), Unit 12 (five sections) or Unit 13 (six sections).

5.5.1.9 Unit 9: Marine and terrestrial sediments

Unit 9 consists of bedded clay, silt, sand and gravel that are situated at 9–80 m asl. Unit 9 sorted sediments are defined by their lower bounding surfaces with Unit 8 till (four sections) or Unit 6 till (one section) and upper bounding surfaces with Unit 10a/b (two sections), Unit 11 till (one section) or Unit 12 till (two sections). Key sections are described in detail below. Collectively, these

sediments are interpreted to have been deposited during an interglacial period based on geochronology and paleo-ecological constraints described below.

5.5.1.9.1 Unit 9a: marine sediments

Along the Kaskattama River, there are at least three occurrences of a thin (0.01–0.15 m thick) intertill bed of sandy gravel to sand that contain marine shell fragments (Figure 5.13d). At each location, the intertill sediments are bound by Unit 8 till below and Unit 10a/b or 11 till above (Figure 5.4a). These sediments are thus also correlated to Unit 9. At section 19-607, the largest marine shell fragment (~9 mm diameter) returned a nonfinite radiocarbon age (>50 ^{14}C ka BP; UOC-11389; Table 5.3). Given the sandy texture of the sediments and presence of marine shell fragments, these sediments are interpreted to have been deposited in a marine environment (Unit 9a). At section 19-623, the optical age of well sorted, fine to medium sand was determined to be 138 ± 13 ka [MAM, 1σ (sample 112-19-623-OSL015)] or 167 ± 9 ka [CAM, 1σ (sample 112-19-623-OSL015)].



Figure 5.13: Unit 9 intertill sorted sediments: A) bed of organic-rich fines overlain and underlain by sandy gravel at section 19-601; B) 0.15 m long flatten conifer wood specimen recovered from the sandy gravel underlying the organic-rich fines at section 19-601; C) grey silt and red fine-sand rhythmites at section 19-607; and D) intertill shell-bearing sandy gravels at sections 19-607 and 19-602 on the Kaskattama River. The location of pollen samples analyzed is shown by the green symbol with a 'P'.

5.5.1.9.2 Unit 9b: terrestrial sediments

At section 19-601 in the Nelson River Estuary area (Figure 5.1), Unit 9 consists of 1.54 m of intertill sorted sediments sharply overlying Unit 8 till at an elevation of 9.0–10.5 m asl (Figure 5.4c). The exposure consists of sandy gravel underlying and overlying a thin (0.02–0.06 m) bed of organic-rich fines (Figure 5.13a). The lowermost sandy gravel is poorly sorted, contains granule– to cobble–sized clasts and multiple pieces of detrital flattened wood specimens (up to 0.15 m in length). The largest piece of detrital wood was identified as coniferous (Figure 5.13b), but the species could not be determined (R.D Fecteau and Associates, 2024). The overlying sandy gravel is poorly sorted, contains granule– to large pebble-sized clasts, shell fragments and no visible wood. Wood from both the lowermost gravel and the middle organic-rich fines returned non-finite radiocarbon ages (>55 ^{14}C ka BP; UOC-10975 and UOC-10974; Table 5.3). A single pollen sample from the organic-rich bed (Figure 5.12) contains an assemblage typical of a boreal forest and peatland environment, dominated with *Picea* (80%) and smaller amounts of *Pinus*, *Betula*, *Alnus* and *Salix*. Wetland indicators Cyperaceae, *Sphagnum* are also present (Figure 5.12). The present-day pollen samples most similar to the fossil assemblage are located along the Canadian boreal forest, centered on the Hudson Bay Lowland, which suggests a depositional environment similar to today (Unit 9b). Quantitative reconstructions confirm conditions not different from present-day, with a mean annual precipitation of 515 ± 159 mm and mean summer temperature of 11.7 ± 1.8 °C. The deposition of the sediments during an interglacial climate is supported by the elevation of this bed (9.0–10.5 m above the current sea level), which requires a geological setting similar to present day with an ice-free Hudson Bay and comparable relative sea level.

Along the Mistikokan River (section 19-609, Figure 5.1, Figure 5.4b), there is an intertill sequence of grey silt and red fine-sand rhythmites (Figure 5.4b; Figure 5.13c). The rhythmites bed has a maximum thickness of 0.3 m thick and is laterally discontinuous, pinching out to a till-till contact along the exposure where Unit 10a and Unit 8 tills are in sharp contact. The rhythmites contain a pollen assemblage typical of a boreal peatland (e.g., *Picea*, *Pinus*, *Betula* and *Sphagnum*), but the concentration of pollen is too low to support a quantitative paleo-climate reconstruction.

Nonetheless, the presence of pollen suggests that the sediment at section 19-609 was not deposited subglacially and instead within a water body capable of depositing rhythmites during a period of subaerial exposure (ice-free conditions) and are thus correlated to Unit 9b.

5.5.1.10 Unit 10: Till deposited by northwest-trending ice-flow

Unit 10 consists of massive, matrix-supported till that is overconsolidated but less than underlying tills (where observed) and has a minor blocky appearance or no blocky appearance (e.g., Figure 5.3d; Figure 5.9). Ice-flow data collected from Unit 10 includes two lodged clasts and nine clast fabrics and the majority of ice-flow indicators (n=9/11) fall within a range 286–335° (Appendix D, Table S1-1) indicating deposition by WNW- to NNW-trending ice-flow flow when considered alongside provenance data. On the Kaskattama River, there is a notable difference in the composition and matrix colour of Unit 10 between sections 19-618 and 19-614, despite similar ice-flow indicators. To acknowledge this different and mappable provenance signature, Unit 10 is separated using a letter modifier based on the relative proportions of UGG and Kenogami clasts (Figure 5.7). Unit 10a contains relatively less UGG clasts (75th percentile of 10.8 ct. % versus 13.7 ct. % for dataset) and elevated proportions of Kenogami clasts (75th percentile of 16.5 ct. % versus 10.3 ct. % for dataset; Figure 5.7). In addition, Unit 10b contains elevated proportions of UGG clasts (75th percentile of 21.4 ct. % versus 13.7 ct. % for dataset) and below average proportions (75th percentile of 4.6 ct. % versus 10.3 ct. % for dataset) of Kenogami clasts (Figure 5.7). This compositional difference is also reflected in the grain-size data with Unit 10a having primarily a sandy clayey-silt to clayey-silt texture and Unit 10b having primarily a sandy-silt texture (Figure 5.6). The cause of this compositional difference is interpreted to be a result of an increased incorporation of the local bedrock (Unit 10a) compared to a more distal eastern provenance (Unit 10b) as evidenced by the proportion of UGG concentrations, possibly due to relatively thinner Quaternary sediments in places. The depth to bedrock is poorly constrained throughout the study area, but limited observations indicate a significantly thinner cover (7 m) of Quaternary sediments where the Kaskattama River drains into Hudson Bay compared to the upper Kaskattama River (62 m; Figure 5.1a). Detrital hornblende $^{40}Ar/^{39}Ar$ ages from four samples have a variable distribution, similar to

the results for Unit 6 till (Figure 5.8). Together, ice-flow data and composition provide supporting evidence for deposition by NW- to NNW- trending ice-flow that emanated from a dome situated east of James Bay. The lower contact of Unit 10 is Unit 6 (five sections), Unit 8 (two sections), Unit 9 (four sections) or was continous to the bottom of the section (one sections). The upper contact of Unit 10 is Unit 11 (two sections), Unit 13 (nine sections) or was exposed to the top of of section (one section).

5.5.1.11 Unit 11: Till deposited by west-trending ice-flow

Unit 11 consists of massive, matrix-supported till that contains mm- to cm-scale silt and sand stringers (three out of four sections) and is overconsolidated but less than underlying tills (where observed) with a minor blocky appearance or no blocky appearance (e.g., Figure 5.3e, f). The matrix is brown (Appendix D, Table S1-2) and has a distinct reddish colour in the field compared to other tills (e.g., Figure 5.3e, f) and the matrix grain-size is sandy silt to clayey silt (Figure 5.6). Ice-flow data collected includes three clast fabrics. The ice-flow direction was undetermined from one clast fabric since it has a spread bimodal modality, but the two other fabrics are interpreted to have formed by W- to WSW-trending ice-flow (265°, 258°; Appendix D, Table S1-1). Unit 11 contains above average proportions of carbonate (75th percentile of 75.1 ct. % versus 68.6 ct. % for dataset; Figure 5.7) and Kenogami clasts (75th percentile of 15.4 ct. % versus 10.3 ct. % for dataset; Figure 5.7). Detrital hornblende $^{40}Ar/^{39}Ar$ ages from one sample has a variable distribution and contains six grains with a Superior-source age range (Figure 5.8). Together, ice-flow data and composition provide supporting evidence for an eastern provenance. In particular, the high proportion of Kenogami clasts in Unit 11 till along the Nelson River Estuary provides robust evidence of west-trending dispersal (c.f., Figure 5.2). The lower contact of Unit 11 is with Unit 6 (one section), Unit 8 (one sections), Unit 9 (one sections) or Unit 10 (two sections). The upper contact is with Unit 12 (two sections) or Unit 13 (three sections).

5.5.1.12 Unit 12: Till deposited by southwest-trending ice-flow

Unit 12 consists of massive, matrix-supported till that is overconsolidated but less than underlying tills (where observed) and has a minor blocky appearance or no blocky appearance. The matrix

colour is variable, but typically a brown or light olive brown (Appendix D, Table S1-2) and has a silty sand to sandy silt matrix, which places in a relatively 'sand-rich' till group for the study area (Figure 5.6). Ice-flow data collected from Unit 12 includes four clast fabrics that are interpreted to have formed by SW- to WSW-trending ice-flow (215–257°; Appendix D, Table S1-1). Unfortunately, due to time constraints in the field, no clast fabrics were measured from the uppermost till exposed along the Nelson River Estuary. Thus, the correlation of these sections to Unit 12 till defined at sections on the Machichi and Kaskattama rivers relies on till sedimentology observations, composition (clast-lithology and texture) and stratigraphic relationships. Unit 12 till contains a relatively high proportion of carbonate and granitoid clasts (Figure 5.7). Given the SW-trending ice flow indicators, the high granitoid proportion is not what would be expected (c.f., Figure 5.2). Therefore, the ice-flow event that deposited Unit 12 either eroded a previously deposited granitoid-rich till in Hudson Bay or has a mainland Nunavut provenance, which would require long-distance transport as part of a curvilinear transport direction. Minor intertill, organic-barren, sorted sediments (sand, gravel) were recognized at sections and are tentatively grouped with Unit 12. The significance of these sediments is uncertain, but they are likely subglacially deposited sorted sediments associated with Unit 12 till. The lower contact of Unit 12 till occurs with Unit 6 (two sections), Unit 8 (five sections), Unit 9 (two sections) or Unit 11 (two sections). The upper contact of Unit 12 till occurs with Unit 13 (eleven sections).

5.5.1.13 Unit 13: Marine and fluvial deposits

Unit 13 consists of massive to bedded clay, silt, sand and gravel that was deposited during the Holocene Epoch (MIS 1) following retreat of the LIS from northeastern Manitoba. These sediments are interpreted to have been deposited in marine (Unit 13a) or fluvial (Unit 13b) environments based on fossil content and facies. Marine sediments are ubiquitous across the study area at surface and typically form thin (<1–4m) deposits draping underlying till (e.g., Figure 5.4). Shell radiocarbon ages from these sediments provide a minimum limiting age for marine incursion of 7948–8345 cal. yr. BP (2 sigma probability; UOC-10981; Table 5.3), in agreement with previous regional studies (Gauthier et al., 2020). At section 19-616, directly overlying 0.15 m of marine sand that contains

whole valves of *Hiatella arctica* is a bed of organic-rich material that includes leaf litter and wood. A large (10 cm length) piece of wood sampled directly above this bed within fluvial sands yielded an age of 5730–5899 cal yr. BP (2 sigma probability; UOC-10977), which provides a minimum limiting age for beginning of Holocene fluvial processes and the growth of trees along the Kaskattama River. This timing roughly aligns with regional land emergence, which resulted in a shift from marine to freshwater ecosystems across the Hudson Bay Lowlands and was possibly a warmer and wetter time in the Holocene (Hargan et al., 2020).

The optical age of Unit 13a marine sands at section 19-610 was investigated (Figure 5.4b). The observed marine facies consists of bedded sand and gravel containing whole valves of *Macoma calcarea*. The bed sampled for optical dating consisted of moderately to well sorted, medium to coarse sand. The optical age of the sand was determined to be 6.2 ± 0.3 ka [MAM, 1σ (sample 112-19-610-OSL005)] or 6.3 ± 0.2 ka [CAM, 1σ (sample 112-19-610-OSL005). This optical age is in close approximation to the radiocarbon age of a *Macoma calcarea* whole valve of 6.9 cal ka (median probability; 6693–7154 cal yr BP, 2 sigma probability; 6609 ± 26 ^{14}C yr BP; UOC-10982; Table 5.3) from the same bed.

5.5.2 Till geochemistry

Principal components (PC) 1, 2, 3 and 4 account for 45%, 14%, 10% and 8%, respectively, of the observed variance within the dataset (Appendix D, Figure S5-4) and biplots of PC1, 2 and 3 are provided in Figure 5.14). Not surprisingly, there is variability within, and overlap across all units identified which is typically seen within glacial sediments in HBL (Wang, 2018). Despite this variability, certain units have discernible geochemical-to-lithological relationships, yet some units are highly scattered or have spatially-defined relationships. For example, most of Unit 3 samples plot within the same (-)PC1 and (+)PC2 area of the biplot (Figure 5.14A) and is the end-member unit for the Al-Ti-Cr-LREE assemblage. The unit also contains a higher proportion of UGG clasts relative to other units, and this is consistent with the geochemical signature of the matrix. In contrast, PC scores for Unit 6 and 8 are more scattered, although there is a noticeable spatial influence (Figure 5.14). For instance, almost all Unit 8 samples from the Nelson River Estuary plot in (+)PC1 space and

along a narrow PC2 range (close to zero), whereas most Machichi River and Kaskattama River samples from Unit 8 plot in (-)PC1, with most Machichi samples falling in (-)PC2 space. This corresponds to a noticeable difference observed in the granitoid proportions within till from the Nelson River Estuary compared to the Machichi and Kaskattama River areas (Figure S5-2). This highlights compositional differences within Unit 8 across the study area both in terms of matrix geochemistry and clast composition. Specifically, in the Nelson River Estuary area, Unit 8 seems to be more of a granitoid/carbonate blend, whereas in the Machichi and Kaskattama regions appear to be more influenced by the mixture of Kenogami and carbonate. This could be the result of a relatively higher input of granitoid rocks from mainland Nunavut that were deposited in Nelson River Estuary area during this ice-flow event as a result of an ~east-west oriented ice divide situated in northern Hudson Bay and mainland Nunavut. The influence of Kenogami detritus is further exemplified with Unit 10a and 10b, which are well-separated in PC space (Figure 5.14), with 10a being characterized by its K and HREE content, whereas 10b has more blended or average composition (i.e., plots near the centre). The relatively high K content of Unit 10a is consistent with the relatively greater proportion of Kenogami clasts (Figure 5.7), reflecting input from the local bedrock. Multivariate analysis thus provides useful insights for provenance interpretation, although heterogeneities within certain units show the limit of a strictly compositional-based approach to till identification, as demonstrated in other studies in the western HBL (Wang, 2018; Hodder et al., 2024b; Chapter 4).

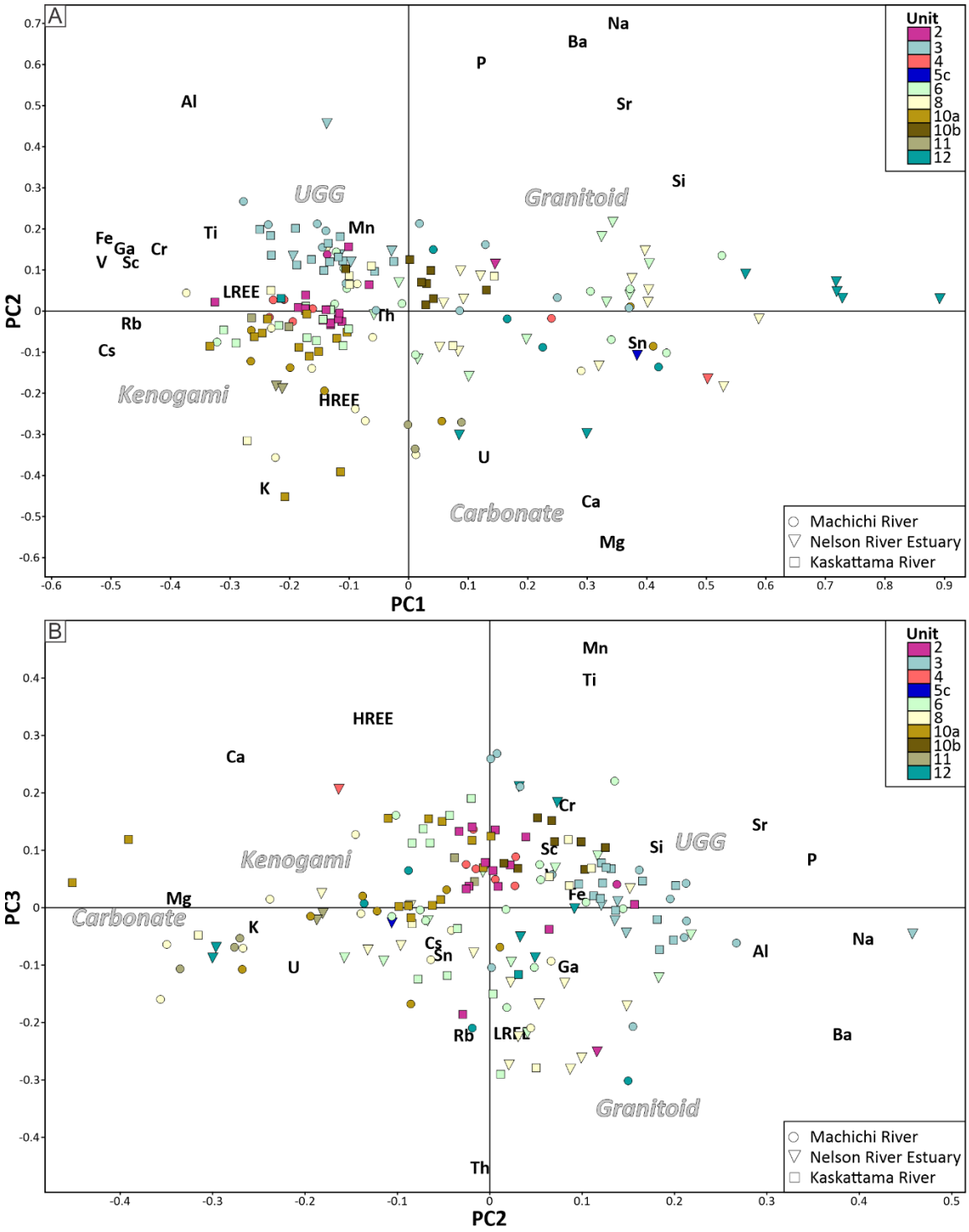

Figure 5.14: Principal component analysis classified according to each area studied and stratigraphic unit: A) PC2 vs. PC1 and B) PC3 vs. PC2.

5.6 Discussion

The Quaternary stratigraphic framework presented herein recognizes eight tills that were deposited across at least three separate glaciations and three pre-Holocene interglacial beds (Figure 5.15). We first discuss the glacial dynamics from the Late Pleistocene (Glaciation I; ~MIS 5-1), the penultimate glacial cycle (Glaciation II; ~ MIS 6) and then earlier ice advances (Glaciation(s) III; ~MIS 8 or older). Next, we discuss the likely timing of past interglacials and correlation of interglacial deposits in region based on geochronological and stratigraphic constraints.

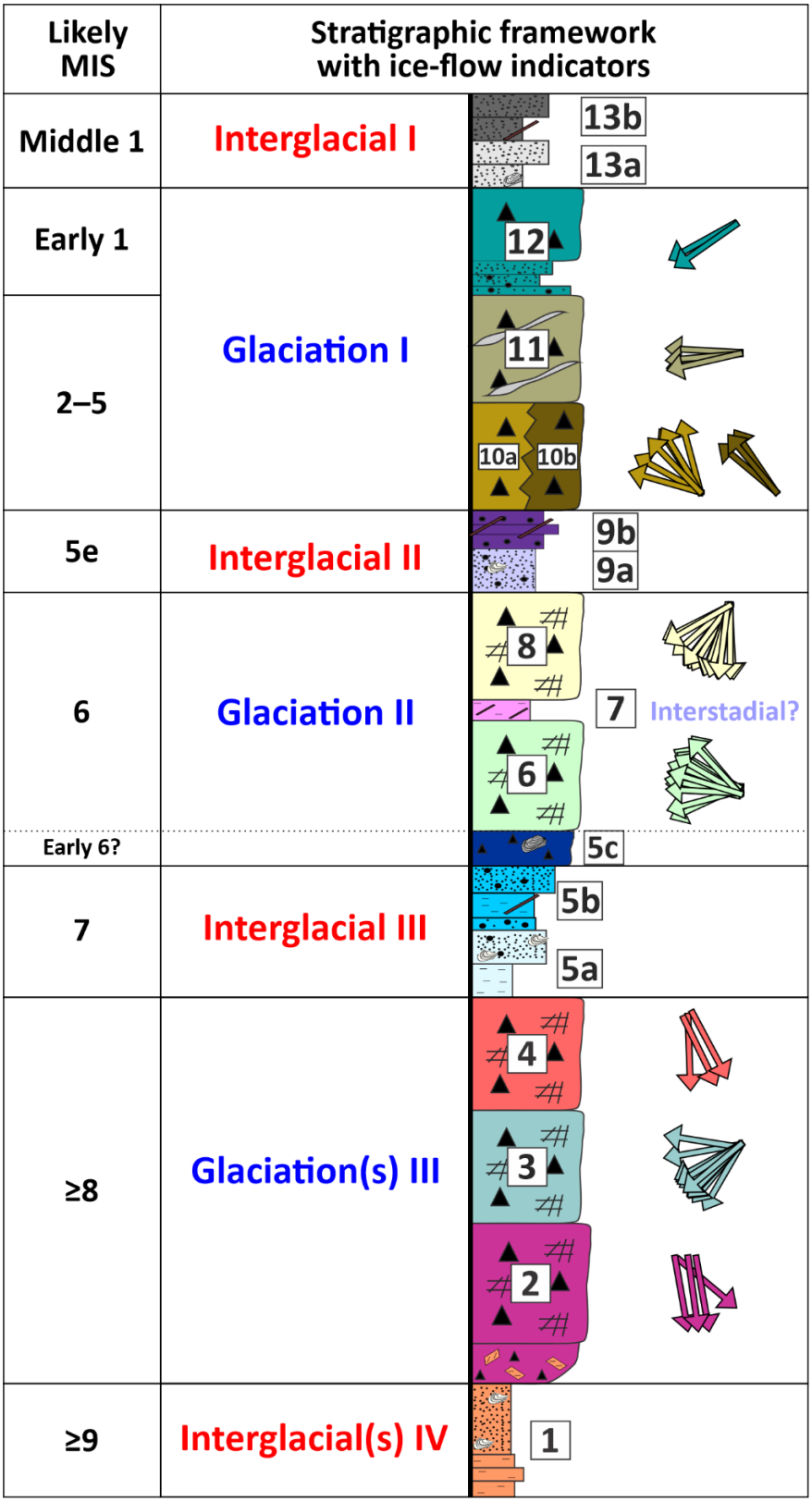

Figure 5.15: Quaternary stratigraphic framework for the Nelson River Estuary to Kaskattama River region of the western Hudson Bay Lowland. All ice-flow indicators from each identified unit are plotted along the right side of the figure.

5.6.1 Glacial dynamics

5.6.1.1 Glaciation I (~MIS 5–1)

At the start of the last glaciation (Glaciation I), the study area was over-run by ice-flowing towards the northwest. Till deposited by this ice-flow event has a distal eastern (Unit 10b) or local bedrock (Unit 10a) provenance signature. This ice-flow event has now been recognized across the western HBL (Chapter 3, 4) and is interpreted to reflect an expansion of the Q-L dome at the start of the last glacial cycle. Next, there is a switch to W-trending ice flow (Unit 11), which could correspond to a documented northward migration of the Q-L dome in Quebec related to a pre-LGM ice-flow phase (Parent et al., 1995; Veillette et al., 1999). This ice-flow event was not recognized in the Kaskattama highland area to the south of this study ('H' on Figure 5.1b), where NNW-trending streamlined landforms are preserved at surface (Hodder et al., 2024b). However, this ice-flow event is recognized in the stratigraphic record of the Churchill River area ('C' on Figure 5.1b) and at surface where W-trending landforms are preserved (Chapter 4). This indicates that the imprint of this ice-flow event on landscape is spatially constrained and that the Kaskattama highland was possibly a large-scale subglacial 'sticky spot' (Trommelen et al., 2012) during this ice-flow event. Following these relatively early Q-L sourced ice-flow events, there is a shift to SW-trending ice-flow (Figure 5.15). This SW-trending ice-flow is interpreted to have been deposited by a late-glacial event that was associated with the Hayes Lobe ice stream (Dredge and Cowan, 1989; Margold et al., 2018; Gauthier et al., 2019; Gauthier et al., 2022). Interestingly, till deposited by the ice-flow event has a relatively elevated proportion of granitoid detritus and Dubawnt erratics (this study; Hodder et al., 2024b). This requires that ice-flowing from a saddle or dome in Hudson Bay, which is typically shown in late-glacial reconstruction of the LIS (Dyke et al., 1982; Dredge and Cowan, 1989), eroded a previously deposited till in Hudson Bay that had high granitoid content (mainland Nunavut provenance). Alternatively, the provenance of this till could reflect long-distance transport from mainland Nunavut as part of late-glacial ice-streaming. This would require that late-glacial ice-streaming into northeastern Manitoba was sourced from the Keewatin Dome and not a saddle situated in Hudson Bay, which could have occurred after weakening of the Hudson Strait ice stream (HSIS). Reconstructions of the Hudson Strait indicate that retreat of the LIS from the strait likely

occurred by ~9.4–9.5 ka BP (MacLean et al., 2001; Dalton et al., 2023). Around this time, ice-streaming was active in northeastern Manitoba, with construction of the Hudwin-Hargrave moraine by the Hayes Lobe in central Manitoba at ~9.55 ka BP (Gauthier et al, 2022).

5.6.1.2 Glaciation II (~MIS 6)

At the start of Glaciation II, there are both SW- and NW-trending ice-flow indicators identified within the stratigraphic record (Unit 6). The relative age-relationship between these ice-flow directions is limited to one section (20-705; Appendix D, Figure S1-1), where a striated boulder pavement suggests WSW-trending (245°) ice-flow may have occurred prior to W-trending (273°) ice-flow. In the Churchill River area ('C' on Figure 5.1b), more robust stratigraphic relationships indicate that SW-trending ice-flow first advanced into the western HBL, followed by a switch to NW-trending ice-flow and it is possible that a similar situation occurred in the study area. Following these initial ice-flow phases from the Q-L dome, there is a switch to S- to SW-trending ice-flow (Unit 8). The timing of this ice-flow (and provenance) change is uncertain and it is possible that there was a retreat of the LIS from the region between these distinctly different ice-flow events. Nonetheless, this documented change in ice-flow during Glaciation II (~MIS 6) is interpreted to reflect a switch to a dome situated in northern Hudson Bay and eastern mainland Nunavut.

5.6.1.3 Glaciation III (~MIS 8 or older)

Ice-flow events assigned to Glaciation III were possibly deposited across multiple glaciations of the western HBL. The timing of these ice-flow events is less certain owing to the fragmented stratigraphic record, that becomes increasingly difficult to reconcile with relatively older sediments that lack confident correlation to dated nonglacial sediments. Nonetheless, there is widespread evidence of at least three glacial events. The oldest recognized ice-flow event recognized is a S- to SSE-trending ice-flow (Unit 2) that is recognized across the study area and reached at least to the Kaskattama River, where it is well-documented underlying Unit 3. Unit 3 is a SW-trending ice-flow event that is recognized across the study area. The till has a provenance indicating dispersal of detritus from east of Hudson Bay into the region and the till has a distinct clay-rich matrix. The clay-rich matrix possibly reflects an increased incorporation of marine sediments from Hudson Bay.

Following this, Unit 4 was deposited by S- to SSE-trending ice-flow and is recognized in the Nelson River Estuary and Machichi River areas but was not recognized in the Kaskattama River area. It is uncertain if this reflects an eastern limit of this ice-flow event, a lack of preservation (eroded) or non-deposition (e.g., sticky spot). While the timing of these ice-flow events is uncertain, units 2 and 4 represent the only occurrences of SE- to SSE-trending ice-flow recognized within the stratigraphic record of the study area (Figure 5.15), which suggest an increased role of ice-flowing from mainland Nunavut at times during previous glaciation(s) compared to the last two glacial cycles.

5.6.2 Reconciling the timing and correlation of nonglacial deposits

Subtill nonglacial deposits are found throughout the western HBL (Dredge and McMartin, 2011); however, there remains considerable debate about the timing of ice-free conditions which is primarily due to inherent difficulties dating Late Quaternary sediments beyond the limit of radiocarbon dating (Miller and Andrews, 2019). Furthermore, regional correlations are complicated by the fragmented nature of the stratigraphic record, which needs to be considered when comparing stratigraphic records across the western HBL (Hodder et al., 2024b; Gauthier et al., 2025). For example, recent geochronology and stratigraphy studies in the Gillam area have uncovered that the 'Nelson River Sediments', previously assumed to have been deposited during the Sangamonian Interglacial (~MIS 5e), were likely deposited during the prior interglacial (~MIS 7; Gauthier et al., 2024, 2025). Similarly, the uppermost intertill organic-bearing sediments along the Echoing River are now interpreted to have been deposited during a prior interglacial (~MIS 7) based on recent geochronology and stratigraphic investigations (Hodder et al., 2024b). These recent studies used a hybrid lithostratigraphic-allostratigraphic approach to better understand the fragmented nature of the stratigraphic record and this same methodology was applied to sections investigated as part of this study and this has proven to be a very useful approach for correlating nonglacial beds across the area, which is discussed below for each nonglacial unit recognized.

5.6.2.1 Interglacial II (Sangamonian; ~MIS 5e)

In this study, the penultimate interglacial is recorded by Unit 9 sediments, which are interpreted to have been deposited in marine (Unit 9a) or terrestrial (Unit 9b) depositional environments. The

pollen and radiocarbon record of Unit 9b sediments indicate deposition during an interglacial climate that occurred prior to the upper limit of radiocarbon dating (~55 ka) at a time when relative sea level was similar to the present day or lower. The marine sediments (Unit 9a) have one MAM optical age that suggests deposition around 138 ± 13 ka, which is within 1σ of the start of MIS 5e at 130 ka and a time period when marine incursion would be expected into the western HBL following the MIS 6 glaciation (Lisiecki and Raymo, 2005). The interpreted marine transgression and regression over the study area that was followed by an interglacial period provides robust evidence that Unit 9 sediments were most likely deposited during the Sangamonian Interglacial (~MIS 5e).

5.6.2.1.1 Correlation of previous studies

Along the Nelson River, the interglacial sediments previously recognized at Flamborough Head are correlated to Unit 9b in this study, based on descriptions of the bounding tills (Dredge and Nixon, 1992). At Flamborough Head, the interglacial sediments have a sharp upper contact with an 'unoxidized, crumbly, brown fissile till with sand seams' that contains 81% carbonate granules and is underlain by a 'compact, fissile, grey-brown oxidized till with red staining' (Dredge and Nixon, 1992). The upper crumbly brown till is correlated to Unit 12 till and the underlying compact grey-brown till is correlated to Unit 6 or 8 based on qualitative characteristics, stratigraphic positions and comparisons to sections investigated nearby as part of this study. Similarly, organic-bearing sediments deposited during climatic conditions similar to the present day have also been documented along the Black Duck River (Figure 5.1a; Dalton et al., 2016; Dalton et al., 2022a). The interglacial sediments at the reported site were not overlain by glacial sediments, making it hard to place in context with the stratigraphic framework established during this study. However, nearby observations [within 1 km of the Dalton et al. (2016) section] by Hodder et al. (2023) noted interglacial sediments overlain by a brown to dark greyish-brown, massive, matrix-supported diamicton containing 5% clasts that had a minor blocky structure with minor oxidation rind on the joint surfaces. The till has a strong (S_1=0.76) W-trending (273°) clast fabric and a sandy clayey-silt matrix (24% sand, 51% silt, and 25% clay). As such, the overlying Black Duck River till is correlated with Unit 11 herein; based on the stratigraphic position and interpreted ice-flow direction. If our

correlation is correct, the Black Duck River interglacial sediments belong to Unit 9b herein. An optical age of 150 ± 22 ka (MAM) or 191 ± 15 (CAM; Hodder et al., 2023) was obtained for the underlying sands on the Black Duck River. The MAM optical age is within 1σ of the MAM optical age determined on Unit 9a sediments during this study, which supports the interpretation that these sediments were likely deposited during the Sangamonian Interglacial (~MIS 5e).

5.6.2.2 Interglacial III (~MIS 7)

Unit 5 is the next (older) unit that is confidently assigned to an interglacial recognized in the stratigraphic record (Figure 5.15). Similar to Unit 9, in order to deposit terrestrial sediments with in-situ peat beds that are situated at 26.3–30.0 m above the current sea level (Unit 5b) requires relative sea level close to, or lower than present day. Paleo-climate reconstructions using pollen support the interpretation of deposition during an interglacial with mean summer temperature and precipitation similar to the present day or wetter. Furthermore, this interglacial was also preceded by a marine incursion (Unit 5a), which requires a higher relative sea level than present day conditions; either under conditions of higher eustatic sea level or increased glacio-isostatic depression. Considering that Unit 9 sediments are interpreted to have been deposited during the Sangamonian (~MIS 5e) interglacial, and that units 9 and 5 are separated by a glaciation, the timing of Unit 5 is likely one of the MIS 7c or 7e warm peaks (Lisiecki and Raymo, 2005). Optical ages from the marine beds (Unit 5a) range from ~112–158 ka (MAM) or ~159–213 ka (CAM; Table 5.2, Figure 5.4). The upper range of two CAM ages is within agreement with MIS 7 (191–243 ka; Lisiecki and Raymo, 2005), but there is clear variability in age determinations. The optical ages from terrestrial beds (Unit 5b) range from ~57–97 ka (MAM) or ~89–107 (CAM; Table 5.2, Figure 5.4). These ages suggest deposition during MIS 3 or MIS 5 and contradict ages the determined from marine sediments (Unit 5a). At this time, the preferred interpretation is that at least some of the quartz optical ages are underestimated since they are not in agreement with conclusions drawn from stratigraphic framework which is supported by paleoenvironmental analyses and indicates that Unit 5 was likely deposited during MIS 7.

Along the Machichi River there are two subtill beds that contain very similar facies assemblages (sand or clay) that are interpreted to have been deposited in marine environments (Unit 5a and Unit 1; Figure 5.4b). Since the upper contact of these sorted sediment units is erosional, there is an alternative interpretation that the marine sediments at 20-705 and sections 19-620/19-621 could be correlative. While this remains a possibility, the till correlations across the Machichi River indicate that there are two different marine beds preserved in the stratigraphic record as evidenced by the lowermost sediments exposed at section 19-624 (Figure 5.4b). Based on the tills that overlie the marine bed at section 20-705, which are in sharp contact and have contrasting ice-flow and till compositional data (Appendix D, Figure S1-1), the preferred interpretation at this time is that the marine sediments at section 20-705 are correlative to Unit 1. This highlights the importance of understanding the till record to better understand the fragmented record and inform the relative age of interglacial beds.

5.6.2.2.1 Correlation of previous studies

The intertill interglacial sediments previously recognized at the Port Nelson section along the Nelson River Estuary are overlain by three till beds (Dredge and Nixon, 1992). Dredge and Nixon (1992) described the uppermost till as an unoxidized, loose, brown till with stringers of sand. This description is similar to units 11 or 12 defined by this study at sections on the Nelson River Estuary at a similar stratigraphic position. The middle till, underlying a layer of imbricated cobbles, is an oxidized brown till and the lowermost till overlying the interglacial sediments is an olive-brown till. It is unclear what till this would be correlated to in this study, but likely Unit 6 or 8 based on stratigraphic position. The third till bed is olive-brown till that is separated from the middle till by 0.5 m of sand and underlain by sediments interpreted to have been deposited during an interglacial period. The sediments near the Port Nelson section were investigated (section 20-702, Figure 5.4c; Hodder et al., 2023), and the tills exposed overlying nonglacial sediments are similar to uppermost and middle tills described by Dredge and Nixon (1992). Based on stratigraphy observed along the Nelson River Estuary (Figure 5.4c) and across the region (Figure 5.15), it is interpreted that ‘Port Nelson’ interglacial sediments (Dredge et al., 1990) are likely correlative to Unit 5a (~MIS 7).

5.6.2.3 Interglacial IV (~MIS 9 or earlier interglacial period?)

Unit 1 marine sediments are situated at ≤19.0–30.5 asl, which means they must have been deposited during a time period when relative sea level was higher than the present day. The stratigraphic framework herein establishes that these marine sediments are succeeded by at least two pre-Holocene ice-free periods with interglacial climates (units 5 and 9; Figure 5.15). Comparing this with the marine isotope record, it would suggest that these sediments could have been deposited during MIS 9 or possibly an older ice-free period, such as MIS 11 (Lisiecki and Raymo, 2005). Unit 1 optical ages agree at 1σ, indicating good precision among the optical dating results. However, these optical ages are the only geochronology constraint available for this unit and there are no independent ages that can be used to assess the accuracy of these optical ages. If the Unit 1 optical ages are accurate, then this indicates deposition of this marine bed at ~177–209 ka (MAM) or ~211–225 ka (CAM), which is in agreement with the MIS 7a interglacial period. However, it must be noted that this would require two succeeding interglacial periods (units 5 and 9) separated by glacial periods following MIS 7 which is not evident in the marine $\delta^{18}O$ record. For this reason, the current preferred interpretation is that the optical ages are underestimations which has been interpreted from similar studies in the Churchill River area of the western HBL and elsewhere (see discussion in Chapter 4). Thus, Unit 1 marine sediments were likely deposited during the MIS 9 interglacial period or a prior interglaciation.

5.6.2.4 Enigmatic Unit 7 – possible interstadial period?

The regional stratigraphic record indicates that there are at least three interglacial periods that are recognized at multiple sections across the region (units 1, 5 and 9; Figure 5.15). At this time, Unit 7 is considered an enigma because it was only recognized as a thin bed at one section (19-613; Figure 5.11). This organic-rich peaty interval appears to have been deposited in-situ; there is no sedimentological evidence to suggest this is a glacially thrusted bed. Interestingly, stratigraphic observations along the Churchill River (Chapter 4) indicate that there is a bed of sorted sediments at the same stratigraphic position providing some supporting evidence for an ice-free period between the deposition of Unit 6 and Unit 8 tills, likely during MIS 6 (Figure 5.15). However, based on the

marine isotope record, MIS 6 was a time of widespread continental glaciation, so it is difficult to reconcile ice-free conditions in this region at that time. More investigation is needed to confirm the depositional setting and timing of Unit 7, which will inform the regional significance of this depositional event. Unfortunately, pollen was of insufficient concentration at this interval to offer any in-depth paleoclimate insights, other than to suggest a deposition within a Boreal peatland.

5.6.3 Correlation of nonglacial beds across the Hudson Bay Lowland

There is increasing evidence from studies in the western HBL that sediments deposited during the penultimate (~MIS 5e) interglacial period are poorly preserved in the stratigraphic record compared to sediments deposited during the preceding interglacial period (~MIS 7; Hodder et al., 2024b; Gauthier et al., 2025). Similar conclusions can be drawn from the stratigraphic record in this study where there is robust evidence that sediments deposited during the penultimate interglacial period (Unit 9) exists; however, most sites are organic-barren and only one section contained an in-situ peat bed with detrital wood (section 19-601). Yet, sediments that were likely deposited during MIS 7 (Unit 5) are wide-spread, commonly organic-bearing or contain well-preserved marine records. This unequal preservation of interglacial sediments is interesting, yet hard to explain whether deposition or erosion had the greater influence on the stratigraphic record that we observe today. For example, the stratigraphic record could be a result of a higher degree of glacial erosion at the start of the last glacial cycle compared to the previous glacial cycle. Nonetheless, the relative increased preservation of interpreted MIS 7 sediments across the western HBL does have important implications for correlations and reinforces that subtill organic-bearing beds should not be correlated without supporting till datasets or lumped into lithostratigraphic units such as “Nelson River Sediments” or “Missinaibi Formation” since this provides a false sense of correlation certainty that could lead to misleading interpretations. Lastly, the age of identified interglacial beds needs to be confirmed, ideally using multiple age determinations methods similar to the approach used by Möller et al. (2019). The stratigraphic framework presented herein did not rely on geochronology constraints to anchor correlations and the age of identified interglacial beds (Figure 5.15) can be further tested to confirm the age of interglacial beds.

5.7 Conclusions

This study developed a stratigraphic framework for the Nelson River Estuary–Kaskattama rivers area of the western HBL that consists of eight glacial (till) units that were deposited across at least three separate glaciations along with at least three pre-Holocene interglacial units and possibly a fourth recognized. This study confirmed the effectiveness of using the hybrid allostratigraphic-lithostratigraphic approach with an emphasis on till characterization in unstudied areas of the western HBL to advance our understanding of the Quaternary record. Several important findings from this stratigraphic record are:

- The ice-flow phases recognized during the last glaciation support recent findings in the western HBL that NW-trending ice-flow advanced into the region, which was followed by W-trending ice-flow and finally late-glacial SW-trending ice-flow, likely associated with ice-streaming.
- Likewise, WSW- to NW-trending ice-flow first advance into the study area during the penultimate glacial cycle (~MIS 6), which was followed by an ice-flow change to S- and SW-trending ice-flow with a possible interstadial occurring between deposition of these ice-flow events.
- The Quaternary stratigraphy along the Machichi River contains a previously unknown rich archive of past nonglacial events. These sediments were likely deposited during the MIS 7 interglacial period with climatic conditions similar to the present day when the region experienced deposition within marine and fluvial/floodplain environments.
- The interglacial sediments previously documented on the Nelson River Estuary are now confirmed to have been deposited by separate nonglacial periods based on the revised stratigraphy of the area, with the previously described ‘Flamborough Head’ sediments

likely deposited during MIS 5e and the 'Port Nelson' sediments likely deposited during MIS 7.

- The stratigraphic record contains thick, organic-bearing exposures, that are interpreted to have been deposited during MIS 7 interglacial conditions, yet sediments correlated to the MIS 5e interglacial period are comparatively less well preserved and often occur as thin intertill, organic-barren sorted sediments.
- Due to the fragmented nature of the stratigraphic record, subtill organic-bearing beds should not be correlated without supporting till datasets or lumped into lithostratigraphic units such as "Nelson River Sediments" or "Missinaibi Formation" since this provides a false sense of correlation certainty that could lead to misleading correlations
- The stratigraphic framework constructed for this region likely extends to at least MIS 9 and additional geochronology studies are encouraged to confirm the age of nonglacial beds.

5.8 References

Andrews, J.T. and Smith, D.I. 1969. Statistical analysis of till fabric: methodology, local and regional variability (with particular reference to the north Yorkshire till cliffs). Quarterly Journal of the Geological Society, 125(1-4): 503–542. doi:10.1144/gsjgs.125.1.0503.

Benn, D.I. 1994. Fabric shape and the interpretation of sedimentary fabric data. Journal of Sedimentary Research, 64: 910–915.

Catto, N.R. 1998. Comparative study of striations and basal till clast fabrics, Malpeque-Bedeque region, Prince Edward Island. Boreas, 27:259–274. doi:10.1111/j.1502-3885.1998.tb01420.x.

Campbell, J.F.E., Fletcher, W.J., Hughes, P.D., and Shuttleworth, E.L. 2016. A comparison of pollen extraction methods confirms dense-media separation as a reliable method of pollen preparation. Journal of Quaternary Science, 31: 631–640. doi:10.1002/jqs.2886.

Crann, C.A., Murseli, S., St-Jean, G., Zhao, X., Clark, I.D. and Kieser, W.E. 2017. First status report on radiocarbon sample preparation techniques at the A.E. Lalonde AMS laboratory (Ottawa, Canada). Radiocarbon 59, 695–704. doi:10.1017/RDC.2016.55.

Dalton, A.S., Finkelstein, S.A., Barnett, P.J. and Forman, S.L. 2016. Constraining the Late Pleistocene history of the Laurentide Ice Sheet by dating the Missinaibi Formation, Hudson Bay Lowlands, Canada. Quaternary Science Reviews, 146: 288–299. doi:10.1016/j.quascirev.2016.06.015.

Dalton, A.S., Väliranta, M., Barnett, P.J., and Finkelstein, S.A. 2017. Pollen and macrofossil-inferred paleoclimate at the Ridge Site, Hudson Bay Lowlands, Canada: evidence for a dry climate and significant recession of the Laurentide Ice Sheet during Marine Isotope Stage 3. Boreas, 46: 388–401. doi:10.1111/bor.12218.

Dalton, A.S., Finkelstein, S.A., Hodder, T.J. and Gauthier, M.S. 2022a. Palynological analyses of subtill sediments from four sites in the western Hudson Bay Lowland region (parts of NTS 53O, 54A, C, D). Manitoba Geological Survey, Open File OF2022-1, 13 p.

Dalton, A.S., Stokes, C.R. and Batchelor, C.L. 2022b. Evolution of the Laurentide and Innuitian ice sheets prior to the Last Glacial Maximum (115 ka to 25 ka). Earth Science Reviews 224: 103875. doi:10.1016/j.earscirev.2021.103875.

Dalton, A.S., Dulfer, H., Margold, M., Heyman, J., Clague, J., Froese, D., et al. 2023. Deglaciation of the North American Ice Sheet Complex in calendar years based on a new comprehensive database of chronological data: NADI-1. Quaternary Science Reviews, 321: 108345. doi:10.1016/j.quascirev.2023.108345.

Dalton, A.S., Finkelstein, S.A., Hodder, T.J. and Gauthier, M.S. 2024. Palynological analyses of subtill sediments from eleven sites in the western Hudson Bay Lowland region of Manitoba (parts of NTS 54B, 54C, 54E, 54F). Manitoba Geological Survey, Open File OF2024-5, 6p.

Dredge, L.A. and Cowan, W.R. 1989. Quaternary geology of the southwestern Canadian Shield. *In* Quaternary Geology of Canada and Greenland. *Edited by* R.J. Fulton. Geological Survey of Canada, Geology of Canada Series, No. 1: 214–248.

Dredge, L.A. and Dyke, L.D. 2020. Landscapes and Landforms of the Hudson Bay Lowlands. I*n* Landscapes and Landforms of Eastern Canada. *Edited by* O. Slaymaker and N. Catto. Springer International Publishing: 211–227. doi:10.1007/978-3-030-35137-3_8.

Dredge, L.A. and McMartin, I. 2011. Glacial stratigraphy of northern and central Manitoba. Geological Survey of Canada, Bulletin 600, 27 p. doi:10.4095/288561.

Dredge, L.A., Morgan, A.V., and Nielsen, E. 1990. Sangamon and pre-Sangamon interglaciations in the Hudson Bay Lowlands of Manitoba. Géographie Physique et Quaternaire, 44(3): 319–336. doi:10.7202/032833ar.

Dredge, L.A. and Nixon, F.M. 1992. Glacial and environmental geology of northeastern Manitoba. Geological Survey of Canada, Memoir 432, 80 p.

Dyke, A.S. and Prest, V.K., 1987. Late Wisconsinan and Holocene history of the Laurentide Ice Sheet. Geographie physique et Quaternaire 41: 237–263.

Dyke, A.S., Dredge, L.A., and Vincent, J.S. 1982. Configuration and dynamics of the Laurentide Ice Sheet during the Late Wisconsinan Maximum. Geographie physique et Quaternaire, 36(1–2): 5–14. doi:10.7202/032467ar.

Dyke, A.S., Andrews, J.T., Clark, P.U., England, J.H., Miller, G.H., Shaw, J., Veillette, J.J., 2002. The Laurentide and Innuitian ice sheets during the Last Glacial Maximum. Quaternary Science Reviews, 21: 9–31.

Evans. 2018. Till: a glacial process sedimentology. Wiley-Blackwell, Chichester.

Evans, D.J.A., Phillips, E.R., Hiemstra, J.F., and Auton, C.A. 2006. Subglacial till: formation, sedimentary characteristics and classification. Earth-Science Reviews, 78(1–2): 115–176. doi:10.1016/j.earscirev.

Faegri, K., and Iversen, J. 1975. Textbook of pollen analysis. 3rd ed. Munksgaard, Copenhagen and Denmark.

Farley-Gill, L.D. 1980. Contemporary pollen spectra in the James Bay Lowland, Canada, and comparison with other forest-tundra assemblages. Géographie physique et Quaternaire, 34(3): 321–334. doi:10.7202/1000415ar.

Galbraith, R.F., Roberts, R.G., Laslett, G.M., Yoshida, H. and Olley, J.M. 1999. Optical dating of single and multiple grains of quartz from Jinmium rock shelter, northern Australia: part i, experimental design and statistical models. Archaeometry, 41: 339–364. doi:10.1111/j.1475-4754.1999.tb00987.x.

Gao, C., Huot, S., McDonald, A.M., Crabtree, D.C. and Turton, C.L. 2020. Subtill nonglacial deposits and their climatic implications for the Last Interglacial (MIS 5e), Hudson Bay Lowlands, Canada. Quaternary Science Reviews, 248: 106590. doi:10.1016/j.quascirev.2020.106590.

Gauthier, M.S., Hodder, T.J., Ross, M., Kelley, S.E., Rochester, A., and McCausland, P. 2019. The subglacial mosaic of the Laurentide Ice Sheet; a study of the interior region of southwestern Hudson Bay. Quaternary Science Reviews, 214: 1–27. doi:10.1016/j.quascirev.2019.04.015.

Gauthier, M.S., Kelley, S.E. and Hodder, T.J. 2020. Lake Agassiz drainage bracketed Holocene Hudson Bay Ice Saddle collapse. Earth and Planetary Science Letters, 544: 116372. doi:10.1016/j.epsl.2020.116372.

Gauthier, M.S., Breckenridge, A. and Hodder, T.J. 2022. Patterns of ice recession and ice stream activity for the MIS 2 Laurentide Ice Sheet in Manitoba, Canada. Boreas, 51: 274–298. doi:10.1111/bor.12571.

Gauthier, M.S., Hodder, T.J., Dalton, A.S., Lian, O.B., Schaarschmidt, M., Ross, M., Väliranta, M. and Finkelstein, S.A. 2024. Preservation of MIS 7 deglacial and nonglacial deposits near the edge of the Hudson Bay Lowland in Manitoba, Canada. Canadian Journal of Earth Sciences, 61(11): 1184–1211. doi:10.1139/cjes-2024-0019.

Gauthier, M.S., Hodder, T.J., Hathaway, J., Ross, M., Schaarschmidt, M., Lian, O.B., Finkelstein, S.A. and Kelley, S.E. 2025. Extending the western Hudson Bay Lowland Quaternary stratigraphy, in Manitoba Canada, to at least Marine Isotope Stage 10. Canadian Journal of Earth Sciences, *in press*. doi:10.1139/cjes-2025-0027.

Hargan, K. E., Finkelstein, S.A., Rühland, K.M., Packalen, M.S., Dalton, A.S., Paterson, A.M., Keller, W. and Smol, J.P. 2020. Post-glacial lake development and paleoclimate in the central Hudson Bay Lowlands inferred from sediment records. Journal of Paleolimnology, 64: 25–46. doi:10.1007/s10933-020-00119-z.

Heaton, T.J., Köhler, P., Butzin, M., Bard, E., Reimer, R.W., Austin, W.E.N., Ramsey, C.B., Grootes, P.M., Hughen, K. A., Kromer, B., Reimer, P.J., Adkins, J., Burke, A., Cook, M.S., Olsen, J. and Skinner, L.C. 2020. Marine20—The Marine Radiocarbon Age Calibration Curve (0–55,000 cal BP). Radiocarbon, 62(4): 779–820. doi:10.1017/RDC.2020.68.

Hicock, S.R., Goff, J.R., Lian, O.B. and Little, E.C. 1996. On the interpretation of subglacial till fabric. Journal of Sedimentary Research, 66(5): 928–934. doi:10.1306/D4268441-2B26-11D7-8648000102C1865D.

Hodder, T.J. and Gauthier, M.S. 2025. Quaternary site, till composition and ice-flow indicator datasets in the Nelson River Estuary–Black Duck River area, northeastern Manitoba (parts of NTS 54A, B, C, F). Manitoba Geological Survey, Open File OF2025-2, 6 p., 8 appendices.

Hodder, T.J., Gauthier, M.S. and Nielsen, E. 2017. Quaternary stratigraphy and till composition along the Hayes, Gods, Nelson, Fox, Stupart, Yakaw, Angling and Pennycutaway rivers, northeast Manitoba (parts of NTS 53 N, 54C, 54D, 54F). Manitoba Geological Survey, Open File OF2017-4, 20 p.

Hodder, T.J., Gauthier, M.S., Ross, M. and Lian, O.B. 2023. Was there a nonglacial episode in the western Hudson Bay Lowland during Marine Isotope Stage 3? Quaternary Research, 116: 148–161. doi:10.1017/qua.2023.35.

Hodder, T.J., Gauthier, M.S., Kelley, S.E. and Ross, M. 2024a: Quaternary site, till composition and ice-flow indicator datasets in the Kaskattama highland area, northeastern Manitoba (parts of NTS 53N, O, 54B, C). Manitoba Geological Survey, Open File OF2024-1, 20 p., 9 appendices.

Hodder, T.J., Gauthier, M.S., Ross, M., Kelley, S.E., Lian, O.B., Dalton, A.S. and Finkelstein, S.A. 2024b. Unravelling the fragmented sediment-landform assemblage in an area of thick Quaternary sediment, western Hudson Bay Lowland, Canada. Canadian Journal of Earth Sciences, 61(11): 1156–1183. doi:10.1139/cjes-2024-0018.

Juggins, S. 2015. rioja: Analysis of Quaternary science data. R package version (0.9-5). Available from http://cran.r-project.org/package=rioja [accessed November 2023].

Juggins, S., Simpson, G.L., and Telford, R.J. 2015. Taxon selection using statistical learning techniques to improve transfer function prediction. The Holocene, 25(1): 130–136. doi:10.1177/095968361455638.

Kitaba, I., and Nakagawa, T. 2017. Black ceramic spheres asmarker grains for microfossil analyses, with improved chemical, physical, and optical properties. Quaternary International, 455: 166–169. doi:10.1016/j.quaint.2017.08.052.

Kleman, J., Jansson, K.N., De Angelis, H., Stroeven, A., Hättestrand, C., Alm, G. and Glasser, N.F., 2010. North American Ice Sheet build-up during the last glacial cycle, 115–21 kyr. Quaternary Science Reviews, 29(17–18): 2036-2051. doi:10.1016/j.quascirev.2010.04.021.

Larsen, N.K. and Piotrowski, J.A. 2003. Fabric pattern in a basal till succession and its significance for reconstructing subglacial processes. Journal of Sedimentary Research, 73(5): 727–734. doi:10.1306/021303730725.

Lian, O.B. and Hicock, S.R. 2000. Thermal conditions beneath parts of the last Cordilleran Ice Sheet near its centre as inferred from subglacial till, associated sediments, and bedrock. Quaternary International, 68–71: 147–162. doi:10.1016/S1040-6182(00)00040-9.

Lisiecki, L.E., and Raymo, M.E. 2005. A Pliocene–Pleistocene stack of 57 globally distributed benthic d18O records. Paleoceanography, 20: PA1003. doi:10.1029/2004PA001071.

MacLean, B., Andrews, J.T., Gray, J.T., Hall, F.R., Hardy, I., Jennings, A.E., Manley, W.F, Pfeffer, W.T. and Vilks, G. 2001. Hudson Strait Quaternary sediments and late glacial and deglaciation history: a discussion and summary. *In* Marine Geology of Hudson Strait and Ungava Bay, Eastern Arctic Canada: Late Quaternary Sediments, Depositional Environments, and Late Glacial–Deglacial history derived from marine and terrestrial studies. *Edited by* B. MacLean. Geological Survey of Canada, Bulletin 566: 181–191.

Margold, M., Stokes, C.R. and Clark, C.D. 2018. Reconciling records of ice streaming and ice margin retreat to produce a palaeogeographic reconstruction of the deglaciation of the Laurentide Ice Sheet. Quaternary Science Reviews, 189: 1–30. doi:10.1016/j.quascirev.2018.03.013.

Mark, D.M. 1973. Analysis of axial orientation data, including till fabrics. Geological Society of America Bulletin, 84: 1369–1374. doi:10.1130/0016-7606(1973)84%3c1369:AOAODI%3e2.0.CO;2.

McDonald, B. and Partin, C. 2024. Paleoproterozoic Rocks of the Belcher Islands, Nunavut: A Review of Their Remarkable Geology and Relevance to Inuit-led Conservation Efforts. Geoscience Canada 51(2): 7–42. doi:10.12789/geocanj.2024.51.207.

McDonald, B.C. 1969. Glacial and interglacial stratigraphy, Hudson Bay Lowland. *In* Earth Sciences Symposium on Hudson Bay. *Edited by* P.J. Hood. GSC Paper 68-53: 78–99.

McDonald, B.S. and Partin, C.A. 2025. Sedimentary provenance analysis by coupled detrital zircon U-Pb, Hf isotopes of the Paleoproterozoic Belcher Group, Nunavut, Canada and implications for sedimentation during the opening and closure of the Manikewan Ocean. Gondwana Research, 140: 17–33. doi:10.1016/j.gr.2025.01.004.

McMartin, I., and Paulen, R.C. 2009. Ice-flow indicators and the importance of ice-flow mapping for drift prospecting. *In* Application of till and stream sediment heavy mineral and geochemical methods to mineral exploration in Western and Northern Canada. GAC Short Course Notes 18. *Edited by* R.C. Paulen and I. McMartin. Geological Association of Canada: 15–34.

Medialdea, A., Thomsen, K.J., Murray, A.S. and Benito, G. 2014. Reliability of equivalent-dose determination and age-models in the OSL dating of historical and modern palaeoflood sediments. Quaternary Geochronology, 22: 11–24. doi:10.1016/j.quageo.2014.01.004.

Mesich, L.N. 2025. The Quaternary stratigraphy of the Gods and Yakaw rivers area, northeastern Manitoba. Master of Science thesis, University of Waterloo, Waterloo, Canada, 511 p.

Miller, G.H. and Andrews, J.T. 2019. Hudson Bay was not deglaciated during MIS-3. Quaternary Science Reviews, 225: 105944. doi:10.1016/j.quascirev.2019.105944.

Möller, P., Benediktsson, I. O., Anjar, J., Bennike, O., Bernhardson, M., Funder, S., Håkansson, L. M., Lemdahl, G., Licciardi, J. M., Murray, A. S. and Seidenkrantz, M. 2019. Glacial history and palaeo-environmental change of southern Taimyr Peninsula, Arctic Russia, during the Middle and Late Pleistocene. Earth Science Reviews, 196: 102832. doi:10.1016/j.earscirev.2019.04.004.

Murray, A.S., and Wintle, A.G. 2000. Luminescence dating of quartz using an improved single-aliquot regenerative-dose protocol. Radiation Measurements, 32: 57–73. doi:10.1016/S1350-4487(99)00253-X.

Murray, A.S., and Wintle, A.G. 2003. The single aliquot regenerative dose protocol: potential for improvements in reliability. Radiation Measurements, 37: 377–381. doi:10.1016/S1350-4487(03)00053-2.

Nielsen, E. 2002. Quaternary stratigraphy and ice-flow history along the Lower Nelson, Hayes, Gods and Pennycutaway rivers and implications for diamond exploration in northeastern Manitoba; *in* Report of Activities 2002, Manitoba Geological Survey: 209–215.

Nielsen, E., Morgan, A.V., Morgan, A., Mott, R.J., Rutter, N.W., and Causse, C. 1986. Stratigraphy, paleoecology and glacial history of the Gillam area, Manitoba. Canadian Journal of Earth Sciences, 23: 1641–1661. doi:10.1139/e86-153.

Overpeck, J.T., Webb, T., and Prentice, I.C. 1985. Quantitative interpretation of fossil pollen spectra: dissimilarity coefficients and the method of modern analogs. Quaternary Research, 23: 87–108. doi:10.1016/0033-5894(85)90074-2.

Parent, M., Paradis, S.J. and Boisvert, E. 1995. Ice-flow patterns and glacial transport in the eastern Hudson Bay region: implications for the late Quaternary dynamics of the Laurentide Ice Sheet. Canadian Journal of Earth Sciences, 32(12): 2057–2070. doi:10.1139/e95-159.

Pieńkowski, A.J., Coulthard, R.D. and Furze, M.F.A. 2023. Revised marine reservoir offset (ΔR) values for molluscs and marine mammals from Arctic North America. Boreas, 52(2): 145–167. doi:10.1111/bor.12606.

Piercey, S.J., 2014. Modern Analytical Facilities 2. A Review of Quality Assurance and Quality Control (QA/QC) Procedures for Lithogeochemical Data. Geoscience Canada 41(1): 75–88. doi:10.12789/geocanj.2014.41.035.

Prest, V.K. 1990. Laurentide ice-flow patterns: a historical review, and implications of the dispersal of Belcher Islands Erratics. Geographie physique et Quaternaire, 44: 113–136. doi:10.7202/032812ar.

Prest, V.K., Donaldson, J.A., and Mooers, H.D. 2000. The Omar story: the role of Omars in assessing glacial history of west–central North America. Geographie Physique et Quaternaire, 54: 257–270. doi:10.7202/005654ar.

Rainbird, R.H., Hadlari, T., Aspler, L.B., Donaldson, J.A., LeCheminant, A.N., and Peterson, T.D. 2003. Sequence stratigraphy and evolution of the Paleoproterozoic intracontinental Baker Lake and Thelon basins, western Churchill Province, Nunavut, Canada. Precambrian Research, 125: 21–53. doi:10.1016/S0301-9268(03)00076-7.

R.D Fecteau and Associates 2024. Identification of wood samples from sites in Manitoba. Rodolphe D. Fecteau and Associates, unpublished report prepared for Dr. M.S. Gauthier, Quaternary Geologist, Manitoba Geological Survey, Government of Manitoba. p. 10.

Reimer, P. J., Austin, W. E. N., Bard, E., Bayliss, A., Blackwell, P. G., Ramsey, C. B., Butzin, M., Cheng, H., Edwards, R. L., Friederich, M., Grootes, P., Guilderson, T. P., Hajdas, I., Heaton, T. J., Hogg, A. G., Hughen, K. A., Kromer, B., Manning, S. W., Muscheler, R., Palmer, J. G., Pearson, C., van der Plicht, J., Reimer, R. W., Richards, D. A., Scott, E. M., Southon, J. R., Turney, C. S. M., Wacker, L., Adolphi, F., Büntgen, U., Capano, M., Fahrni, S. M., Fogtmann-Schulz, A., Friedrich, R., Köhler, P., Kudsk, S., Miyake, F., Olsen, J., Reinig, F., Sakamoto, M., Sookdeo, A. and Talamo, S. 2020. The IntCal20 Northern Hemisphere Radiocarbon Age Calibration Curve (0–55 cal kBP). Radiocarbon, 62(4): 725–757. doi 10.1017/RDC.2020.41.

Roy, M., Clark, P.U., Duncan, R.A., and Hemming, S.R. 2007. Insights into the late Cenozoic configuration of the Laurentide Ice Sheet from 40Ar/39Ar dating of glacially transported minerals in midcontinent tills. Geochemistry, Geophysics, Geosystems, 8(9): doi:10.1029/2006GC001572.

Saarnisto, M. and Peltoniemi, H. 1984. Glacial stratigraphy and compositional properties of till in Kainuu, eastern Finland. Fennia, 162: 163–199.

Schaen, A.J., Jicha, B.R., Hodges, K.V., Vermeesch, P., Stelten, M.E.,Mercer, C.M., et al. 2021. Interpreting and reporting $^{40}Ar/^{39}Ar$ geochronologic data. GSA Bulletin, 133(3–4): 461–487. doi:10.1130/B35560.1.

Shepard, F.P. 1954: Nomenclature based on sand-silt-clay ratios. Journal of Sediment, 24(3): 151–158. doi:10.1306/D4269774-2B26-11D7-8648000102C1865D.

Shilts, W.W. 1980. Flow patterns in the central North American ice sheet. Nature, 286: 213–218. doi:10.1038/286213a0.

Skinner, R.G. 1973. Quaternary stratigraphy of the Moose River Basin, Ontario. Geological Survey of Canada, Bulletin 225, 77 p.

Stokes, C.R., Tarasov, L. and Dyke, A.S. 2012. Dynamics of the North American Ice Sheet Complex during its inception and build-up to the Last Glacial Maximum. Quaternary Science Reviews, 50: 86–104. doi:10.1016/j.quascirev.2012.07.009.

Stott, G.M., Buse, S., Davis, D.W., and Hamilton, M.A. 2010. The Sutton inliers——a Paleoproterozoic succession in the Hudson Bay Lowland. *In* Summary of Field Work and Other Activities 2010, Ontario Geological Survey, Open File Report 6260: 19-1–19-14.

Stuiver, M. and Reimer, P. J. 1993. Extended ^{14}C Data Base and Revised CALIB 3.0 ^{14}C Age Calibration Program. Radiocarbon, 35(1): 215–230. doi:10.1017/S0033822200013904.

Thorleifson, L.H., Wyatt, P.H., Shilts, W.W., and Nielsen, E. 1992. Hudson Bay Lowland Quaternary Stratigraphy: evidence for early Wisconsinan glaciation centred in Quebec. *In* Geological Society of America Special Papers 270: 207–222. doi:10.1130/SPE270-p207.

Thorleifson, L.H., Wyatt, P.H. and Warman, T.A. 1993. Quaternary stratigraphy of the Severn and Winisk drainage basins, northern Ontario. Geological Survey of Canada Bulletin 442, 65 p.

Trefethen, J.M. 1950. Classification of sediments. American Journal of Science, 48: 55–62.

Trommelen, M.S., Ross, M. and Campbell, J.E. 2012. Glacial terrain zone analysis of a fragmented paleoglaciological record, southeast Keewatin sector of the Laurentide Ice Sheet. Quaternary Science Reviews, 40: 1–20. doi:10.1016/j.quascirev.2012.02.015.

Tyrrell, J.B. 1916. Notes on the geology of Nelson and Hayes rivers. Proceedings and Transactions of the Royal Society of Canada, 10, sec. IV: 1–27.

Van Gosen, B.S., Verplanck, P.L., Seal II, R.R., Long, K.R. and Gambogi, J. 2017. Rare-earth elements. *In* Critical mineral resources of the United States—Economic and environmental geology and prospects for future supply. *Edited by* K.K. Schulz, J.H. DeYoung Jr., R.R. Seal II and D. Bradley. United States Geological Survey Professional Paper 1802: 01–031. doi:10.3133/pp1802O.

Veillette, J.J., Dyke, A.S. and Roy, M. 1999. Ice-flow evolution of the Labrador Sector of the Laurentide Ice Sheet: a review, with new evidence from northern Quebec. Quaternary Science Reviews, 18: 993–1019. doi:10.1016/S0277-3791(98)00076-6.

Vermeesch, P. 2018. IsoplotR: A free and open toolbox for geochronology. Geoscience Frontiers, 9(5): 1479–1493. doi:10.1016/j.gsf.2018.04.001.

Wheeler, J.O., Hoffman, P.F., Card, K.D., Davidson, A., Sanford, B.V., Okulitch, A.V. and Roest, W.R. 1996. Geological Map of Canada, Geological Survey of Canada Map 1860A. doi:10.4095/208175.

Whitmore, J., Gajewski, K., Sawada, M., Williams, J.W., Shuman, B., Bartlein, P.J., et al. 2005. North American and Greenland modern pollen data for multi-scale paleoecological and paleoclimatic applications. Quaternary Science Reviews, 24: 1828–1848. doi:10.1016/j.quascirev.2005.03.005.

Zabenskie, S. 2006. Postglacial climatic change on Boothia Peninsula, Nunavut, Canada. Master of Science thesis, University of Ottawa, Ottawa, Ontario, Canada, 98p.

Chapter 6

Long-term evolution of the Laurentide Ice Sheet: insights from stratigraphic records of western Hudson Bay Lowland, central Canada

6.1 Overview

Understanding the terrestrial Quaternary stratigraphic record is necessary to reconstruct regional- to continental-scale ice sheet fluctuations and compare how these events relate to oxygen isotope proxies derived from marine sediments and contemporary ice sheets. In particular, regions that contain an extensive stratigraphic record beyond the last glacial maximum are key to understanding the long-term behaviour of ice sheets. The Hudson Bay Lowland (HBL) is one of these key regions that contains a fragmented stratigraphic record of at least the last four Laurentide Ice Sheet (LIS) glaciations. The HBL is centrally located within the LIS and was affected by ice-flowing from both major domes (Quebec-Labrador and Keewatin) at different times, which allows for insight into the spatial-temporal evolution of ice flowing from these domes during glaciations. This study synthesizes recent investigations in the western HBL and proposes a new stratigraphic framework for the area, which provides better constrains to model the long-term evolution of the LIS in central Canada.

6.2 Introduction

The Laurentide Ice Sheet (LIS) waxed and waned over the North American continent throughout the Pleistocene Epoch (Batchelor et al., 2019; Jennings et al., 2025) and was responsible for a significant proportion of global eustatic sea level fluctuations of the Quaternary (Stokes et al., 2012; Gowan et al., 2021). Despite this importance for understanding global sea level change, there is limited field-based knowledge about the extent and glacial dynamics of the LIS prior to the Last Glacial Maximum (LGM) (Dalton et al., 2022b), including during previous glaciations (Batchelor et al., 2019). To advance our understanding of the spatial-temporal evolution of the LIS across multiple glaciations and provide field-based constraints to ice-sheet reconstruction and modelling efforts, it is necessary to document and better understand the terrestrial Quaternary stratigraphic record. The Hudson Bay Lowland (HBL) in central Canada is one important region that contains a stratigraphic record beyond the LGM (e.g., Skinner, 1973; Nielsen et al., 1986; Thorleifson et al., 1992), and is situated between the two largest ice spreading centres of the LIS (Quebec-Labrador and Keewatin domes) — an ideal location to understand the growth and evolution of ice cover in North America (Figure 6.1).

Initial investigations of the Quaternary sediments exposed along deeply incised fluvial valleys in the western HBL indicated the presence of at least four tills and two pre-Holocene interglacial beds (Netterville, 1974; Klassen, 1986; Nielsen et al., 1986; Dredge et al., 1990; Dredge and Nixon, 1992; Roy, 1998; Dredge and McMartin, 2011). A recent investigation combined the erosional and depositional record of northeastern Manitoba (Gauthier et al., 2019) and identified at least 10 ice-flow phases indicating that the stratigraphic record is much more complex and fragmented than previously realized. To better understand the HBL paleo-glaciology, multiple field campaigns worked to unravel the fragmented Quaternary stratigraphy across a large region of the western HBL (Figure 6.1; Chapters 2–5; Gauthier et al., 2024, 2025). This study uses those individual stratigraphic frameworks constructed to propose an updated synthesis of the Quaternary record in the western HBL. We then focus on the paleo–glaciological implications of this long and complex record and how this informs our understanding of the LIS across multiple glaciations.

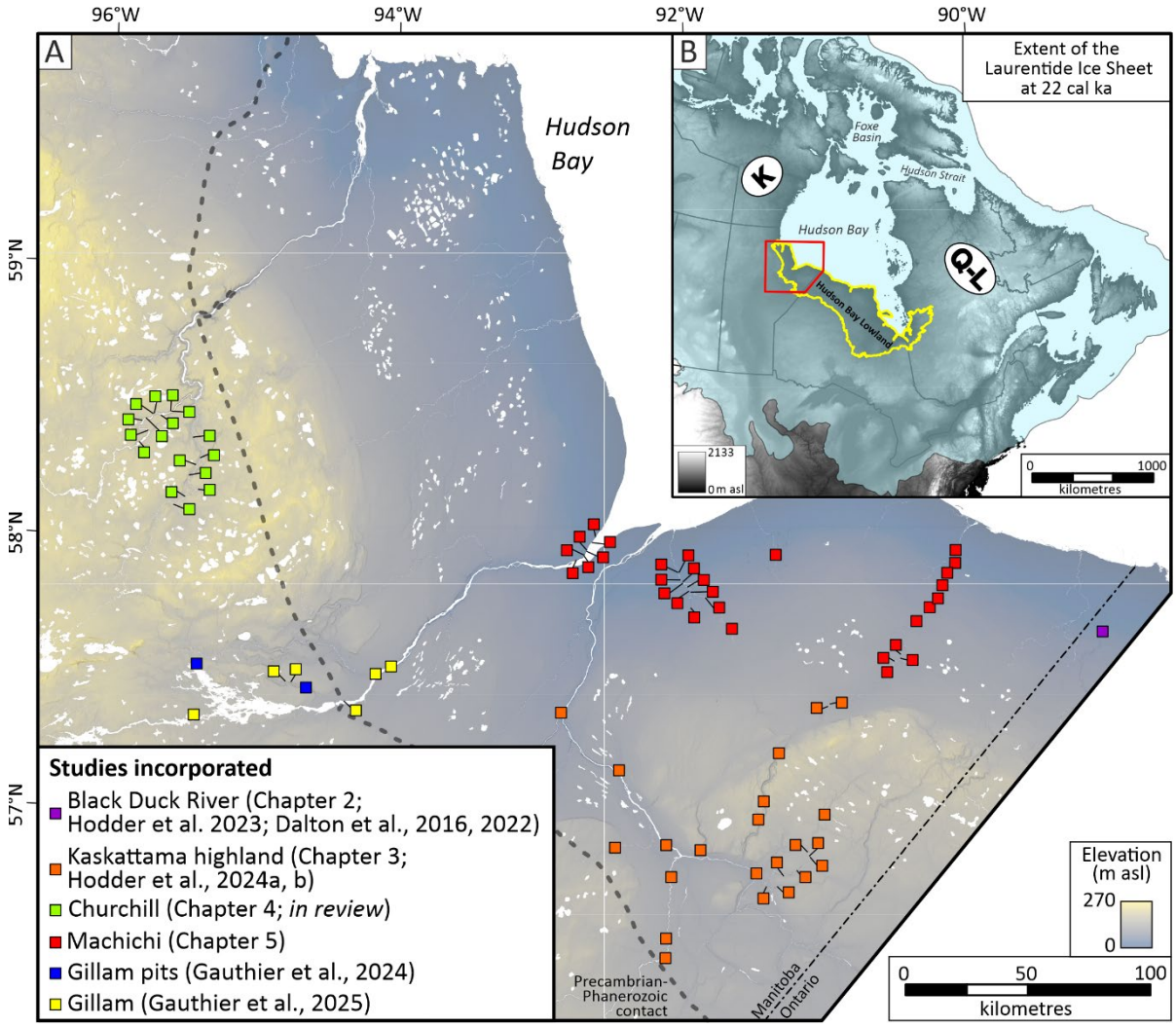

Figure 6.1: Location of sections investigated in the western Hudson Bay Lowland, central Canada (A) and the context of the study area to the Laurentide Ice Sheet at 22 cal. ka (B) based on the reconstruction by Dalton et al. (2023). Abbreviations: K, Keewatin dome; Q-L, Quebec-Labrador dome.

6.3 Stratigraphic correlations and nomenclature

The oxygen isotopic records from deep sea marine sediments and contemporary ice sheets have proven to be crucial to understand long-term global-scale climatic fluctuations throughout the Quaternary (Grootes et al., 1993; Lisiecki and Raymo, 2005; Rasmussen et al., 2014; Spratt and Lisiecki, 2016). The marine oxygen isotope stratigraphic record mostly reflects continental ice-sheet volume changes (Shackleton and Opdyke, 1973) and its breakdown into Marine Isotope Stages (MIS)

provide a common framework for Quaternary scientists including those working with terrestrial stratigraphic records. However, since this is a global record, regional- to continental-scale ice sheet fluctuations may not be reflected or in sync with marine oxygen isotope stratigraphic record and this needs to be carefully considered when making comparisons with the terrestrial record (Gibbard and Hughes, 2021). The North American chronostratigraphic framework previously consisted of glacial and interglacial stages that were defined along the southern margin of the LIS where the most recent glaciation has been termed the Wisconsinan (e.g., Flint, 1963); however, subsequent detailed stratigraphic investigations of the pre-Wisconsinan sediments, supported by age dating of volcanic beds and paleomagnetic measurements, indicated that the pre-Wisconsinan stratigraphic framework was largely an oversimplification (Boellstorff, 1978; Hallberg, 1986; Roy et al., 2004). The penultimate glaciation is still referred to as the Illinoian Stage, but other Early- to Mid-Pleistocene Glacial Stages are currently referred to as 'pre-Illinoian A' through to 'pre-Illinoian K' and there are currently no defined stages for pre-Sangamonian Stage interglacial sediments (Cohen and Gibbard, 2019). The North American Stratigraphic Code (North American Commission on Stratigraphic Nomenclature, 2021) recommends defining informal units when the extent and significance of units beyond the study area are still undetermined and/or when units are defined using innovative techniques. For this reason, we first identify a regional chronostratigraphic framework for the western HBL consisting of informal 'Glacial' and 'Interglacial' stages and then compare this record to the MIS record and North American chronostratigraphic framework. The stages are numbered from youngest to oldest to allow for easier revisions of the relatively older stages recognized.

The Quaternary stratigraphic record is intrinsically fragmented (Gibbard and Hughes, 2021). Considering the fragmented architecture of the Quaternary stratigraphic record and the current limitations of dating methods, 'interglacial sediments' cannot be used as marker beds without the support of the glacial-sediment correlations between studies (Hodder et al., 2023, 2024; Gauthier et al., 2025). To unravel this fragmented record, a hybrid lithostratigraphy-allostratigraphy method was generated that focuses on field stratigraphy and interpreted ice-flow orientation, combined with multi-parameter characterization of glacial and nonglacial sediments across numerous sections to document the Quaternary stratigraphic record (Chapter 3; Hodder et al., 2024). This method was

then successfully applied to other regions across the western HBL (Figure 6.1; Chapters 4, 5; Gauthier et al., 2025). Using this same method, it is now possible to construct a western HBL stratigraphic framework.

6.4 Western Hudson Bay Lowland Glaciations

6.4.1 HBL Glacial Stage I (~MIS 5–1)

There is wide-spread evidence across the western HBL for NW-trending ice advance at the onset of the last glaciation (Figure 6.2; Phase I-A, Figure 6.3). The northwestern extent of this ice-advance is unknown, but a minimum advance limit is provided by the Trout Lake flowset in north-central Manitoba, which is supported by the dispersal of carbonate detritus towards the west/northwest from the Hudson Bay Basin (Gauthier, 2023). The composition of till deposited by this ice-flow event requires a dome situated east of James Bay (Chapters 3, 4; Hodder et al., 2024). This is consistent with observations in Quebec that indicate a relatively early NW-trending ice-flow event (Parent et al., 1995; Veillette et al., 1999), with possible glacial inception in the highlands north of the St. Lawrence River (LGM 1 ice flow of Veillette et al., 1999). Following this initial advance, there is a switch in ice-flow direction to W-trending ice-flow (Phase I-B, Figure 6.3), as evidence by stacked tills in the stratigraphic record (Figure 6.2, units M11, C13). This W-trending ice-flow event does not cross-cut the Kaskattama or Trout Lake streamlined-landform flowsets (Figure 6.3), implying sluggish ice-flow or the presence of cold-based ‘sticky spots’ over areas of the HBL during this time period. Streamlined landforms formed during this W-trending ice-flow event are preserved in the Churchill area (Chapter 4). Near the core region of the Q-L dome, there is evidence for northward migration of the ice-divide following an initial NW-trending ice-flow (Parent et al., 1995; Veillette et al., 1999) and it is likely that this migration resulted in the W-trending ice-flow event observed in the western HBL.

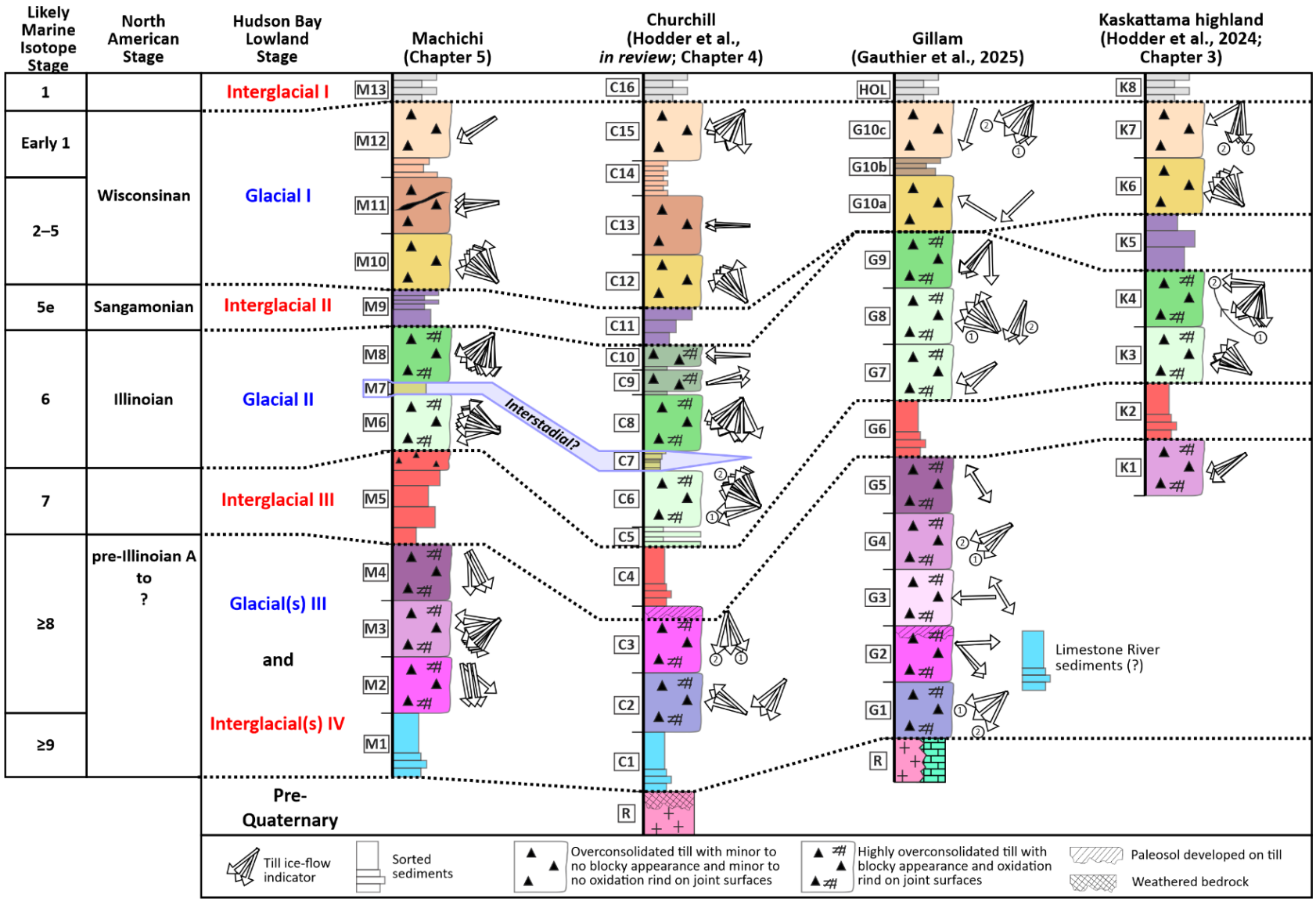

Figure 6.2: Quaternary stratigraphy correlations across the western Hudson Bay Lowland. Numbered stratigraphic units recognized have been given a letter modifier according to their study (M, for Machichi [Chapter 5]; K, for Kaskattama highland [Chapter 3; Hodder et al., 2024]; C, for Churchill [Chapter 4; *In review*] and G, for Gillam [Gauthier et al., 2025]).

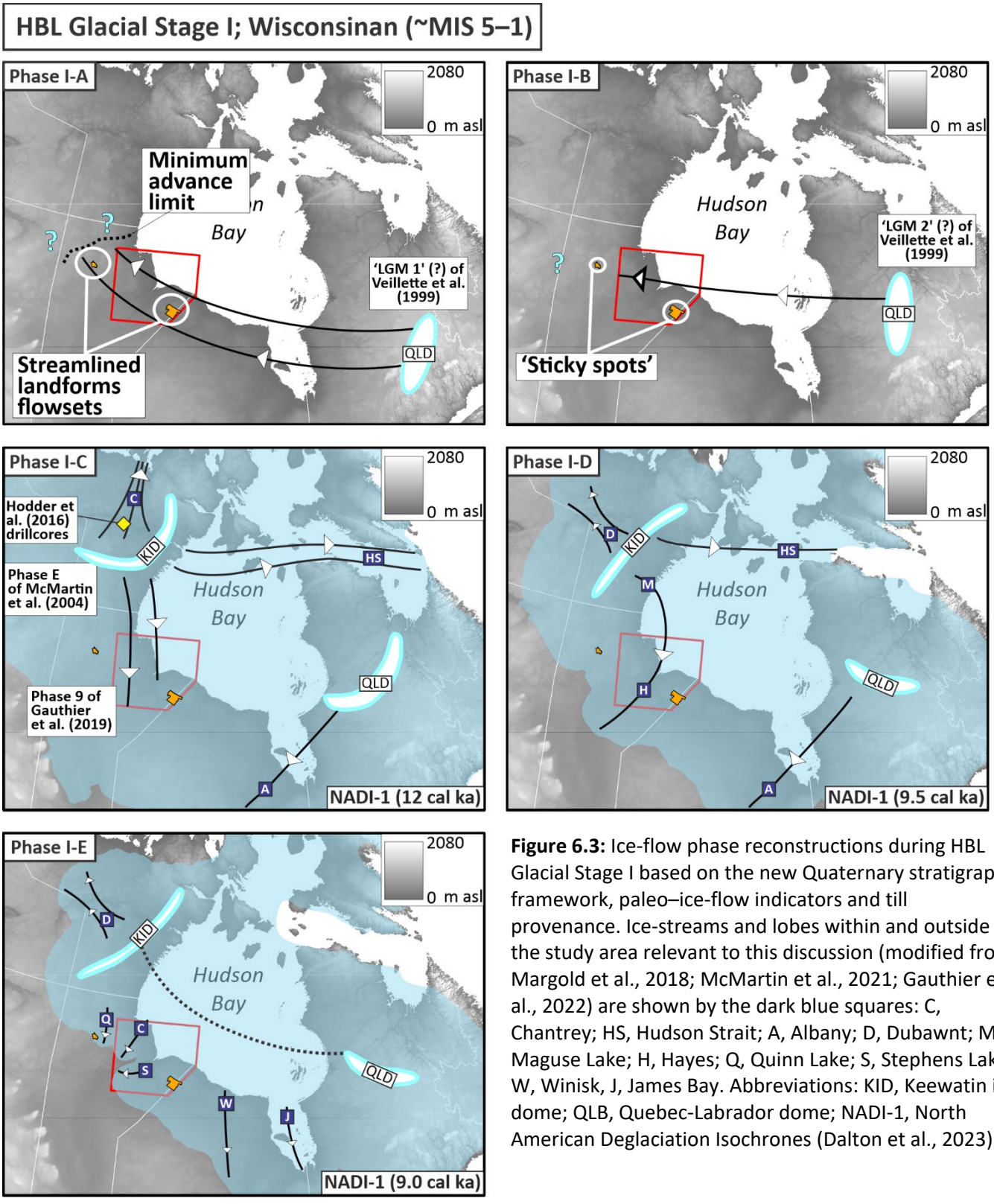

Figure 6.3: Ice-flow phase reconstructions during HBL Glacial Stage I based on the new Quaternary stratigraphic framework, paleo–ice-flow indicators and till provenance. Ice-streams and lobes within and outside of the study area relevant to this discussion (modified from Margold et al., 2018; McMartin et al., 2021; Gauthier et al., 2022) are shown by the dark blue squares: C, Chantrey; HS, Hudson Strait; A, Albany; D, Dubawnt; M, Maguse Lake; H, Hayes; Q, Quinn Lake; S, Stephens Lake; W, Winisk, J, James Bay. Abbreviations: KID, Keewatin ice dome; QLB, Quebec-Labrador dome; NADI-1, North American Deglaciation Isochrones (Dalton et al., 2023).

Following these relatively early ice-flow events, the next ice-flow event within the depositional record is S- to SW-trending ice-flow (Phase I-C, Figure 6.3), which indicates a significant shift in glacial dynamics and the first incursion of ice originating from the Keewatin dome flowing over the region during the last glaciation. The timing of the S-trending ice-flow event is not known precisely, but the eastward migration of the Keewatin ice divide toward Hudson Bay is well documented and sufficiently constrained to post-LGM time (McMartin and Henderson, 2004) to link S-trending ice-flow events in the study area to the late-stage position of the Keewatin ice divide. HBL Glacial Phase I-C is possibly linked to Phase E of McMartin and Henderson (2004), when part of the ice divide was likely situated in southern mainland Nunavut. During that time of LIS retreat, warm-based basal conditions would have been more prevalent across the western HBL (Marshall and Clark, 2002) which, together with ice sheet drawdown (and no subsequent major increase in effective stress), would produce a softer till (i.e., less overconsolidated) relative to older tills. The till deposited by this southward ice flow event is one of the post-LGM softer tills which are all interpreted as late-glacial event(s) based on regional ice-flow reconstructions (Gauthier et al., 2019, 2022). The S-trending ice-flow event then transitions into a SW- to SSW-trending ice-flow event (Phase I-D, Figure 6.3) as ice-streaming initiates in the western HBL as part of the Hayes Lobe (Gauthier et al., 2022). Till deposited by the Hayes Lobe in the Machichi and Kaskattama highland areas has an elevated proportion of granitoid and Dubawnt erratics relative to the underlying till (Chapters 3, 5). This does not align with erosion and deposition of the Hudson Bay Basin, which is dominated by carbonate bedrock and instead indicates a provenance signature indicative of mainland Nunavut. This suggests that either till being deposited by the Hayes Lobe eroded and remobilized a previously deposited till in Hudson Bay that had high granitoid content (mainland Nunavut provenance) or the till provenance could reflect long-distance transport from mainland Nunavut due to late-glacial ice-streaming as shown in Figure 6.3 (Phase I-D).

Robust stratigraphic evidence, including buried proglacial sediments at multiple locations in the Churchill area, indicates a retreat of the ice-sheet prior to SSW-trending ice-flow and it is interpreted that this was a late-glacial ice-flow event (Chapter 4). This lobe, herein referred to as the Churchill Lobe, formed the Etawney moraine likely around 9.49–9.04 cal ka (Gauthier et al., 2022). This late-glacial ice-flow event is coeval with the Quinn Lake ice stream since this ice stream was deflected by

the Churchill Lobe (Trommelen, 2015). The Quinn Lake ice stream also re-advanced into proglacial Lake Agassiz (Trommelen, 2015). In the central HBL, a retreat and re-advance of the LIS during this time period is well documented in the Winisk and James Bay ice streams (Dredge and Cowan, 1989; Veillette et al., 2017), indicating dynamic late-glacial behaviour of this southern margin of the LIS in central Canada. This resurgence of ice streaming into the HBL could have occurred after weakening of the Hudson Strait ice stream (HSIS). Reconstructions of the Hudson Strait indicate that retreat of the LIS from the strait was likely well underway by 9.5 ka cal. BP (Dalton et al., 2023). Around this time, ice-streaming was active in northeastern Manitoba, with construction of the Hudwin-Hargrave moraine by the Hayes Lobe in central Manitoba at ~9.55 cal ka BP (Gauthier et al, 2022).

6.4.2 HBL Glacial Stage II (~MIS 6)

Similar to the start of the HBL Glacial Stage I, there is widespread evidence that ice first advanced from the Q-L dome into the western HBL during the onset of Glacial Stage II (Figure 6.2; Phase II-A, Figure 6.4). Stratigraphic evidence in the Churchill area suggests that a proglacial lake possibly developed in front of the advancing SW-trending LIS. Following this initial SW-trending ice-flow, there is a shift to NW-trending ice-flow which is more predominant in the stratigraphic record and the till provenance indicates significant input from rocks lying east of Hudson/James Bay region. Despite the similar ice-flow direction, there are noticeable differences in till provenance between this NW-trending ice-flow event and the Glacial I NW-trending ice-flow event (Hodder et al., 2024), with the Glacial Stage II event (Phase II-A) sediments containing a higher proportion of Hudson Bay Basin detritus.

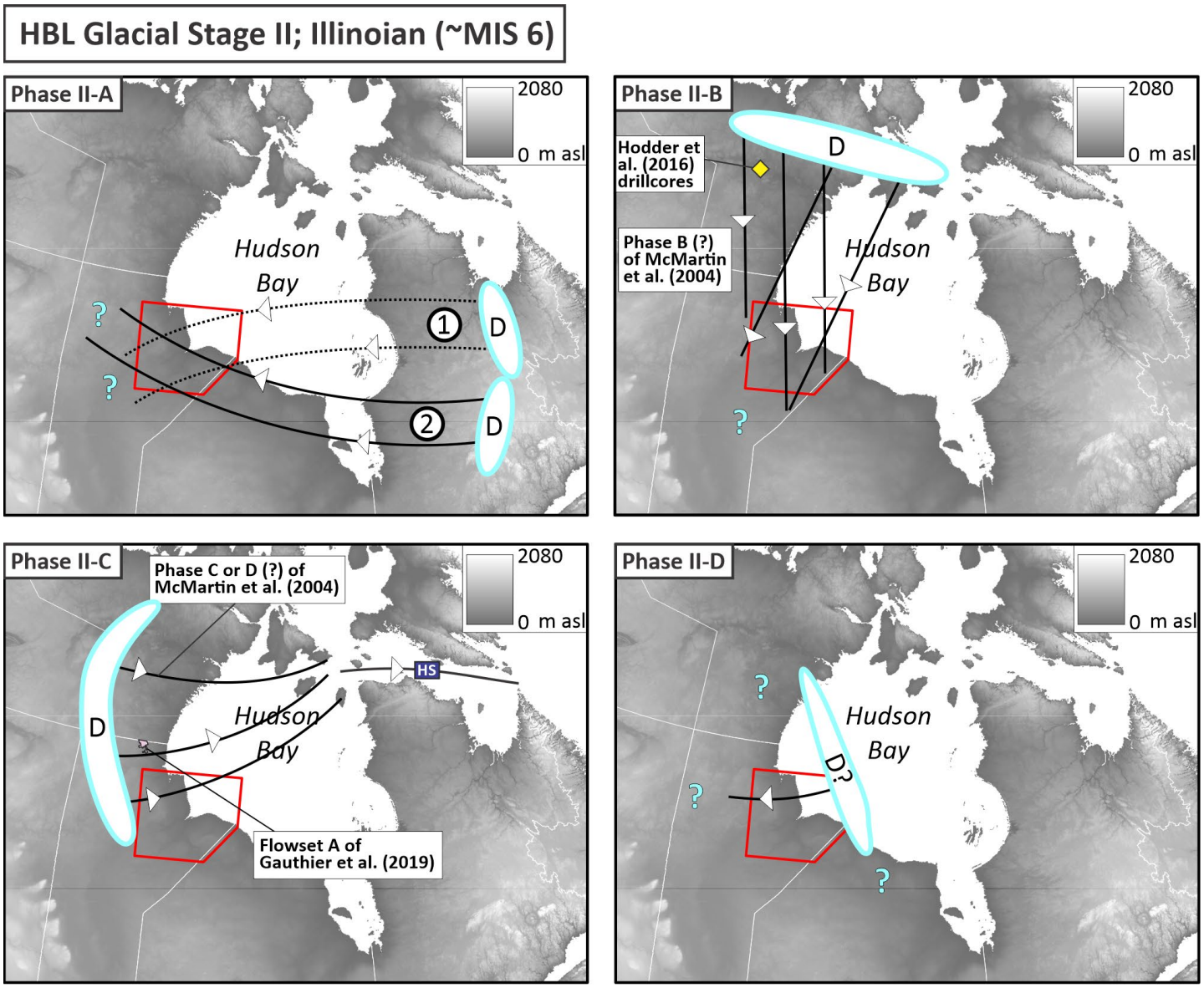

Figure 6.4: Ice-flow phase reconstructions during HBL Glacial Stage II based on the new Quaternary stratigraphic framework, paleo–ice-flow indicators and till provenance. Abbreviations: HS, Hudson Strait ice stream.

During HBL Glacial Stage II there is a shift from NW-trending to a S- and/or SW-trending ice-flow that is observed across the western HBL (Phase II-B, Figure 6.4). Considering the high sediment production and large spatial footprint of this ice-flow event, it is interpreted that this was not a late-glacial ice streaming event but rather one of the main ice-flow events that occurred during Glacial Stage II. Similarly, in the Aberdeen Lake area the stratigraphic record indicates deposition of till by a relatively early S-trending ice flow event (Regional Unit C of Hodder et al., 2016), which could be possibly linked to Phase B identified in McMartin and Henderson (2004) and constrain the ice divide/dome to northern mainland Nunavut.

A question that remains is whether or not there was a retreat of the LIS from the western HBL during the transition between these two distinct ice-flow events. In the Churchill area, an interpreted proglacial deposit is situated between these two ice-flow events and in the Machichi area there is a 0.3 m thick organic-rich bed that contains wood situated between the tills that record these two ice-flow events at one section. These organic-rich beds provide scant evidence for a retreat of the ice sheet during these events and needs to be investigated further to confirm a reduction in the LIS during Glacial Stage II. Tills interpreted to belong to late Glacial Stage II ice-flow events have been identified in the Churchill area and indicate a dynamic LIS in the western HBL during this time period (Chapter 4). Here, the stratigraphic record indicates that an E-trending ice-flow event occurred, which is correlated to the oldest streamlined landforms recognized in northeastern Manitoba (Gauthier et al., 2019; Figure 6.4) and was likely an onset zone for the Hudson Strait ice stream during this time period. Following this ice-flow event, there is a switch to W-trending ice-flow, which suggest a migration of an ice-divide across northeastern Manitoba late in Glacial Stage II, possibly with a dome situated over western HBL during this time period.

6.4.3 HBL Glacial Stage(s) III (~MIS 8 or older glaciations)

There are at least four distinct phases of ice-flow recognized that occurred prior the HBL Interglacial Stage III (Figure 6.2; Figure 6.5). Reconciling the correlation of these ice-flow phases between regions within the western HBL is difficult due to the fragmented stratigraphic record and relatively lower number of observations. For example, there is one relatively old till across the region has elevated proportions of granitoid detritus (units M2, C3 and G2) but has different relative-age

relationships determined between regions studied. The composition of this till suggest a Precambrian Shield provenance, and when combined with ice-flow indicators, indicate deposition by SSE- to SE- to E- trending ice-flow (Figure 6.2; Phase II-B, Figure 6.5). Interestingly, this is the only till in the western HBL where a paleosol at the upper contact of the till has been observed in the Churchill and Gillam areas. It is unclear if this was a unique occurrence and the result of a more intense interglacial period or if ice-flow events succeeding deposition of this till were relatively less erosive, leading to higher preservation of the paleosol. Nonetheless, the paleosol indicates a period of subaerial exposure, although the timing of this paleosol development remains uncertain. In the Churchill area, the paleosol development has been interpreted to be associated with Interglacial Stage III. Yet in the Gillam area, the paleosol is interpreted to have formed during the MIS 9 interglacial. Hence, either current stratigraphic correlations are incorrect or there is two separate granitoid rich tills that were deposited by SE-trending ice-flow events with a paleosol developed on the till. This is one example of inconsistencies in the stratigraphic record beyond Interglacial Stage III that needs to be reconciled through additional field study.

Prior to the deposition of this Precambrian-rich till, there is evidence of a SW-trending ice-flow event in the Gillam and Churchill River area and a NW-trending ice-flow event in the Churchill River area (Figure 6.2; Phase III-A, Figure 6.5). Following deposition of the Precambrian-rich till (Phase III-B, Figure 6.5), there is evidence for a widespread W- to SW-trending ice-flow event (units K1, M3, G3, G4, Figure 6.2; Phase III-C, Figure 6.5) and a spatially restricted SSE-trending ice-flow event (units M4 and G5, Figure 6.2; Phase III-D, Figure 6.5). Tills assigned to Glacial Stage III were likely deposited across multiple glaciations.

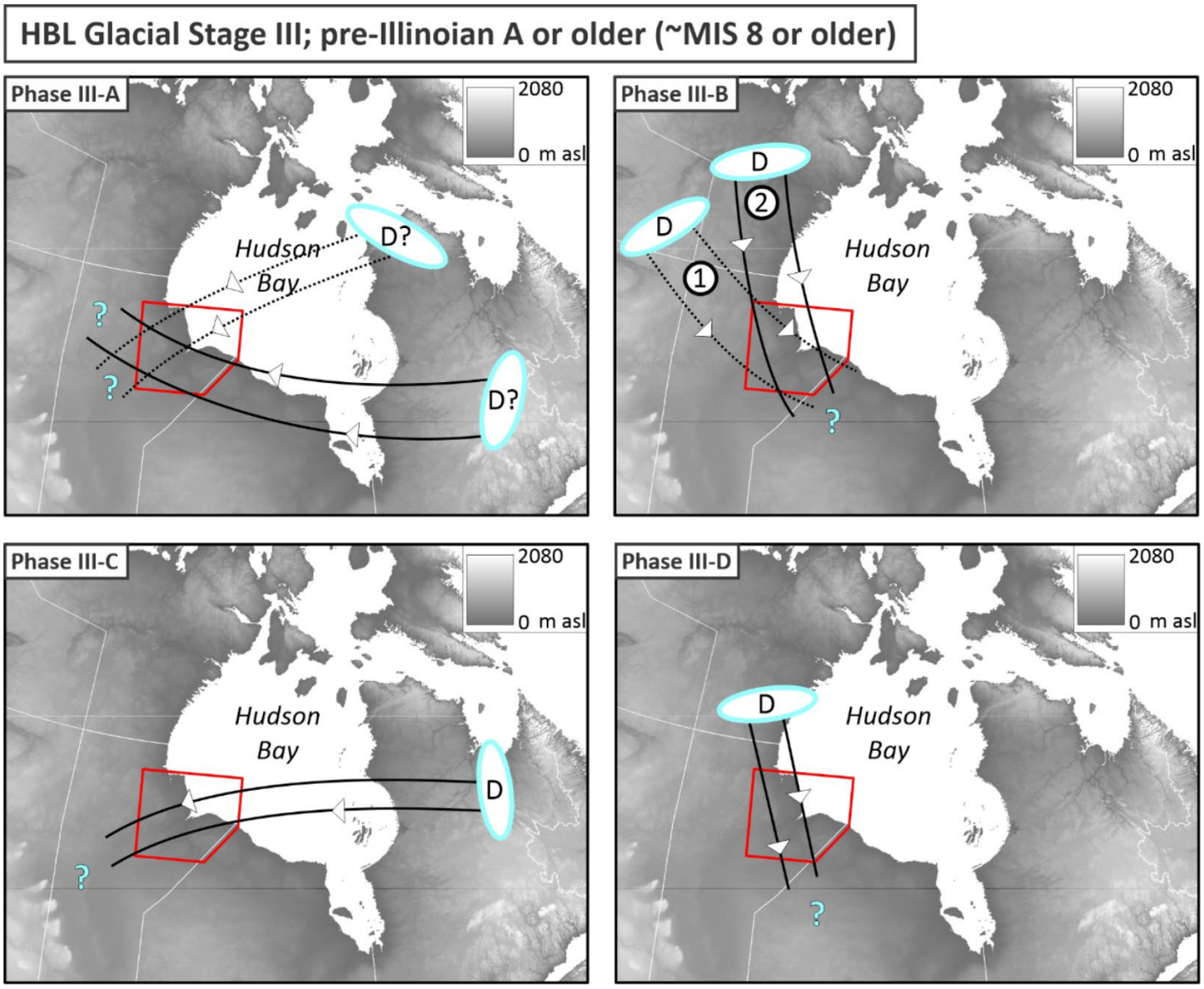

Figure 6.5: Ice flow phase reconstructions during HBL Glacial Stage III based on the new Quaternary stratigraphic framework, paleo–ice-flow indicators and till provenance.

6.5 Laurentide Ice Sheet evolution across the last two glaciations

The final deglacial position of the Keewatin and Q-L domes of the LIS are recognized based on the position and orientation of mapped streamlined landforms, eskers and moraines (e.g., Dyke and Preset, 1987; Dalton et al., 2023). However, these domes were highly mobile throughout glaciations and in order to understand their previous positions the erosional paleo–ice-flow record and Quaternary stratigraphic record near these core regions need to be unravelled by documenting ice-flow reversals and sediment provenance (Veillette et al., 1999; McMartin and Henderson, 2004; Hodder et al., 2016; Rice et al., 2019). The western HBL is situated at the heart of LIS at times of extensive ice, i.e., when a multi-dome configuration was fully developed, and the Quaternary stratigraphic records provide important constraints for the positions of LIS domes through time and the relative strength of ice-flow events emanating from these domes. A discussion of the relatively early and deglacial ice-flow patterns observed across the last two glaciations is presented below.

6.5.1 Initial ice-sheet growth and evolution

There is robust evidence that early in Glacial Stage 1 (~MIS 5–1) and 2 (~MIS 6) the growth of the Q-L dome outpaced that of the Keewatin dome. The western extent of the LIS during these initial expansions of the Q-L dome is currently unknown, but the presence of Omar erratics across central Canada and into Alberta indicates long-distance transport of detritus derived from eastern Hudson Bay over time (Prest et al., 2000). Similarly, calcareous till across the Saskatchewan prairies is palimpsest evidence of old phases of west-trending ice flow that brought material from carbonate bedrock sources located in Manitoba (Ross et al. 2009), and evidence of west-trending ice-flow is observed in the erosional ice-flow record of southeastern Manitoba (Henderson, 1994; Hodder and Lian, 2024). Following these early ice-flow events originating from east of the Hudson Bay/James Bay region, there is a dramatic shift to S- and or SW-trending ice-flow(s), which is interpreted to indicate that growth of the Keewatin Dome becomes more dominant relatively later during both glaciations. Thus, the stratigraphic record indicates a similar evolution of the LIS across the last two glaciations with asynchronous growth rates of the two major domes as evidence by early expansion Q-L dome, which is important for modelling spatial-temporal evolution of the LIS. Current models of LIS evolution depict a very different evolution pattern. A common theme among LIS models is arctic-

driven ice sheet expansion (Stokes et al., 2012; Geng et al., 2025) and reconstructions typically show synchronous growth of the two major domes of the LIS throughout MIS 4 and again in MIS 2 (Dalton et al., 2022b). This is not in agreement with the stratigraphic record in the western HBL, which clearly indicate an accelerated expansion of the Q-L dome at the start of the last two glaciations.

The question that remains is when does this switch in ice sheet configuration occur during the glacial stages? During HBL Glacial Stage I, it is suspected that following the initial ice-flow events from the Q-L dome that cold-based conditions persisted for much of the last glacial cycle and that ice-flowing from the Keewatin Dome did not occur until after the LGM as S-trending ice-flow transitioned into SW-trending ice-flow associated with late-glacial ice streaming events. If this interpretation holds true, then this would indicate that, during the last glaciation, a large build-up of Keewatin Dome likely did not occur until MIS 2. During HBL Glacial Stage II, it is less certain when the shift to Keewatin dominated ice-flow occurred but till production from Keewatin-dominant phases was significantly greater compared to during HBL Glacial Stage I (e.g., Chapter 4) and is possibly correlated to till deposited by S-trending ice-flow in central mainland Nunavut (Hodder et al., 2016). Thus, ice-flowing from the Keewatin Dome may have played a relatively more important role during MIS 6, with the dome possibly being situated in northeastern mainland Nunavut/northern Hudson Bay (Phase II-B, Figure 6.4). The Glacial Stage II record is also complicated by the possibility of an interstadial in the record (Figure 6.2), which is hard to reconcile with the oxygen isotope stage record for MIS 6 (Lisiecki and Raymo, 2005).

6.5.2 Late-glacial dynamics in the HBL

During deglaciation of the LIS at the end of Glacial Stage II, there is evidence in the geological record of stacked tills with near opposite ice-flow directions (constrained by till provenance) which is interpreted to indicate a late glacial ice-flow reversal occurred in the western HBL (Figure 6.4, Phase II-C to Phase II-D). Stratigraphic evidence suggests that E- and ENE-trending ice flowed towards Hudson Bay late in Glacial Stage II. This may indicate the position of an onset region for the HSIS, which would suggest a different configuration of the catchment zone compared to Glacial Stage I. Following this ice-flow event, W-trending ice-flow occurred which implies that an ice divide crossed

the area (Figure 6.4, Phase II-D), possibly as a result of significant drawdown of ice through the Hudon Strait. The presence of an ice-divide in the area suggests that the Keewatin Dome could have been situated in a more southerly position during Glacial Stage II deglaciation. At the southern margin of the LIS, the penultimate glaciation extended further south into north-central USA compared to the last glacial cycle (e.g., Curry et al., 2011), which could partly have been a result of the Keewatin Dome being situated in a more southern position during the latter part of this glaciation as evidenced in the western HBL. Furthermore, the presence of a thicker mass of ice in northeastern Manitoba during HBL Glacial Stage II is supported by the relatively higher incursion of marine waters following Termination II in the Churchill River area (Chapter 4). Although there is evidence for a divide and possibly a dome situated in the western HBL during Glacial Stage II, there is no evidence that the same LIS configuration existed during Glacial Stage I deglaciation. Instead, there is evidence that the region was over-ridden by S-trending ice-flow (Phase I-C, Figure 6.3), which transitioned to SSW-trending ice-flow as part of late-glacial ice streaming (Phase I-D and Phase I-E, Figure 6.3). Thus, the common depiction of an ice-divide over the western HBL that persists until deglaciation (e.g., Margold et al., 2018) lacks stratigraphic support.

6.6 Conclusions

This study provides an updated stratigraphic framework for the western HBL region of central Canada, a key region for understanding the late Quaternary dynamics of the LIS. This stratigraphic framework provides significant insight into growth, evolution and retreat of the LIS during the past two glaciations and a starting point for better understanding the glacial dynamics of pre-Illinoian ice-flow events. In particular, there is robust stratigraphic evidence for:

1. Asynchronous growth of the two major domes of the LIS during the last two glaciations, with the Q-L dome expansion dominant early in the glaciation and Keewatin dome buildup later in the glaciation.
2. Occurrence of an ice-divide and possible dome in the western HBL during Glacial Stage II deglaciation, which is supported by a higher marine limit during Termination II (end of MIS 6) deglaciation compared to Termination I (Holocene Tyrrell Sea).

3. The presence of weathered bedrock in places suggests that areas within central Canada experienced negligible glacial bedrock erosion during the Quaternary period.
4. The Quaternary stratigraphic record is highly fragmented, which reflects patchy erosion and deposition over multiple glacial-interglacial cycles.

6.7 Future work

The stratigraphic record beyond Glacial Stage II (pre-Illinoian) requires additional studies to understand the relative timing of glacial and nonglacial events. The timing of ice-free periods remains the largest uncertainty in the Quaternary stratigraphic record of the western HBL. Recent studies in the western HBL have been testing the limits of optical dating using quartz in this geological setting and while this work has provided excellent insights into age estimations for identified interglacial periods, there are numerous cases where the optical ages are possibly age underestimations because they are inconsistent with stratigraphic observations. As such, additional geochronological studies using multiple dating methods (e.g., cosmogenic burial, electron spin resonance and/or single-grain optical dating) is a necessary step to better understand the exact timing of ice-free periods. Robust dating of identified ~MIS 9 or older nonglacial sediments (HBL Interglacial Stage IV) will be imperative to understanding the extent of the Quaternary stratigraphic record in the HBL. The stratigraphic frameworks presented within this study did not rely on geochronology constraints to anchor any correlations, thus the age of identified interglacial beds presented within stratigraphic frameworks can be further tested.

6.8 References

Batchelor, C.L., Margold, M., Krapp, M., Murton, D. K., Dalton, A.S., Gibbard, P.L., Stokes, C.R., Murton, J.B. and Manica, A. 2019. The configuration of Northern Hemisphere ice sheets through the Quaternary. Nature Communications, 10:3713. doi:10.1038/s41467-019-11601-2.

Boellstorff, J. 1978. North American Pleistocene Stages Reconsidered in Light of Probable Pliocene-Pleistocene Continental Glaciation. Science, 202(4365): 305–307. doi:10.1126/science.202.4365.305.

Cohen, K.M. and Gibbard, P.L. 2019. Global chronostratigraphical correlation table for the last 2.7 million years, version 2019 QI-500. Quaternary International, 500: 20–31. doi:10.1016/j.quaint.2019.03.009.

Curry, B.B., Grimley, D.A. and McKay III, E.D. 2011. Chapter 36 – Quaternary Glaciations in Illinois. In Quaternary Glaciations – Extent and Chronology: a closer look. Developments in Quaternary Science 15. Edited by J. Ehlers, P.L. Gibbard and P.D. Hughes. Elsevier, Amsterdam. pp. 467–487. doi:10.1016/B978-0-444-53447-7.00036-2.

Dalton, A.S., Finkelstein, S.A., Barnett, P.J. and Forman, S.L. 2016. Constraining the Late Pleistocene history of the Laurentide Ice Sheet by dating the Missinaibi Formation, Hudson Bay Lowlands, Canada. Quaternary Science Reviews, 146: 288–299. doi: 10.1016/j.quascirev.2016.06.015.

Dalton, A.S., Finkelstein, S.A., Hodder, T.J. and Gauthier, M.S. 2022a. Palynological analyses of subtill sediments from four sites in the western Hudson Bay Lowland region (parts of NTS 53O, 54A, C, D). Manitoba Geological Survey, Open File OF2022-1, 13 p.

Dalton, A.S., Stokes, C.R. and Batchelor, C.L. 2022b. Evolution of the Laurentide and Innuitian ice sheets prior to the Last Glacial Maximum (115 ka to 25 ka). Earth Science Reviews, 224:103875. doi:10.1016/j.earscirev.2021.103875.

Dredge, L.A. and Cowan, W.R. 1989. Quaternary geology of the southwestern Canadian Shield. *In* Quaternary Geology of Canada and Greenland. *Edited by* R.J. Fulton. Geological Survey of Canada, Geology of Canada Series, No. 1: 214–248.

Dredge, L.A. and McMartin, I. 2011. Glacial stratigraphy of northern and central Manitoba. Geological Survey of Canada Bulletin 600, 27 p. doi:10.4095/288561.

Dredge, L.A. and Nixon, F.M. 1992. Glacial and environmental geology of northeastern Manitoba. Geological Survey of Canada Memoir 432, 80 p.

Dredge, L.A., Morgan, A.V., and Nielsen, E. 1990. Sangamon and pre-Sangamon interglaciations in the Hudson Bay Lowlands of Manitoba. Géographie Physique et Quaternaire, 44(3): 319–336. doi:10.7202/032833ar.

Dyke, A.S. and Prest, V.K., 1987. Late Wisconsinan and Holocene history of the Laurentide Ice Sheet. Geographie physique et Quaternaire 41: 237–263.

Flint, R.F. 1963. Status of the Pleistocene Wisconsin Stage in Central North America. Science, 139(3553): 402–404. doi: 10.1126/science.139.3553.40.

Gauthier, M.S. 2023: Manitoba till-matrix geochemistry compilation: total carbonate of the silt plus clay (<63 µm) size-fraction. Manitoba Geological Survey, GeoFile 7-2023.

Gauthier, M.S., Hodder, T.J., Ross, M., Kelley, S.E., Rochester, A., and McCausland, P. 2019. The subglacial mosaic of the Laurentide Ice Sheet; a study of the interior region of southwestern Hudson Bay. Quaternary Science Reviews, 214: 1–27. doi:10.1016/j.quascirev.2019.04.015.

Gauthier, M.S., Kelley, S.E. and Hodder, T.J. 2020. Lake Agassiz drainage bracketed Holocene Hudson Bay Ice Saddle collapse. Earth and Planetary Science Letters, 544: 116372. doi:10.1016/j.epsl.2020.116372.

Gauthier, M.S., Breckenridge, A. and Hodder, T.J. 2022. Patterns of ice recession and ice stream activity for the MIS 2 Laurentide Ice Sheet in Manitoba, Canada. Boreas, 51: 274–298. doi:10.1111/bor.12571.

Gauthier, M.S., Hodder, T.J., Dalton, A.S., Lian, O.B., Schaarschmidt, M., Ross, M., Väliranta, M. and Finkelstein, S.A. 2024. Preservation of MIS 7 deglacial and nonglacial deposits near the edge of the Hudson Bay Lowland in Manitoba, Canada. Canadian Journal of Earth Sciences, 61(11): 1184–1211. doi:10.1139/cjes-2024-0019.

Gauthier, M.S., Hodder, T.J., Hathaway, J., Ross, M., Schaarschmidt, M., Lian, O.B., Finkelstein, S.A. and Kelley, S.E. 2025. Extending the western Hudson Bay Lowland Quaternary stratigraphy, in Manitoba Canada, to at least Marine Isotope Stage 10. Canadian Journal of Earth Sciences, *in press*. doi:10.1139/cjes-2025-0027.

Geng, M.S., Tarasov, L. and Dalton, A.S. 2025. A comparison of the last two glacial inceptions (MIS 7/5) via fully coupled transient ice and climate modeling. EGUsphere [preprint]. doi:10.5194/egusphere-2025-495.

Gibbard, P.L. and Hughes, P.D. 2021. Terrestrial stratigraphical division in the Quaternary and its correlation. Journal of the Geological Society 178(2): jgs2020-2134. doi:10.1144/jgs2020-134.

Gowan, E.J., Zhang, X., Khosravi, S., Rovere, A., Stocchi, P., Hughes, A.L.C., et al. 2021. A new global ice sheet reconstruction for the past 80 000 years. Nature Communications, 12: 1199. doi:10.1038/s41467-021-21469-w.

Grootes, P. M., Stuiver, M., White, J. W. C., Johnsen, S. and Jouzel, J. 1993. Comparison of oxygen isotope records from the GISP2 and GRIP Greenland ice cores. Nature, 366: 552–554.

Hallberg, G.R. 1986. Pre-Wisconsin glacial stratigraphy of the central plaines region in Iowa, Nebraska, Kansas, and Misouri. Quaternary Science Reviews, 5: 11–15. doi:10.1016/0277-3791(86)90169-1.

Hodder, T.J., Ross, M. and Menzies, J. 2016. Sedimentary record of ice divide migration and ice streams in the Keewatin core region of the Laurentide Ice Sheet. Sedimentary Geology, 338: 97–114. doi:10.1016/j.sedgeo.2016.01.001

Hodder, T.J., Gauthier, M.S., Ross, M. and Lian, O.B. 2023. Was there a nonglacial episode in the western Hudson Bay Lowland during Marine Isotope Stage 3? Quaternary Research, 116: 148–161. doi:10.1017/qua.2023.35

Hodder, T.J., Gauthier, M.S., Ross, M., Kelley, S.E., Lian, O.B., Dalton, A.S. and Finkelstein, S.A. 2024. Unravelling the fragmented sediment-landform assemblage in an area of thick Quaternary sediment, western Hudson Bay Lowland, Canada. Canadian Journal of Earth Sciences, 61(11): 1156–1183. doi:10.1139/cjes-2024-0018.

Jennings, C.E., Aber, J.S. Barendregt, R., Bierman, P.R., Rovery, C.W., Roy, M., Thorleifson, H. 2025. Middle Pleistocene glaciations in North America. *In* Encyclopedia of Quaternary Science (Third edition). *Edited by* Elias, S. Elsevier, Amsterdam. pp. 647-655. doi:10.1016/B978-0-323-99931-1.00123-9.

Klassen, R.W. 1986. Surficial geology of north-central Manitoba. Geological Survey of Canada, Memoir 419, 57 p.

Lisiecki, L.E., and Raymo, M.E. 2005. A Pliocene–Pleistocene stack of 57 globally distributed benthic $\delta^{18}O$ records. Paleoceanography, 20: PA1003. doi:10.1029/2004PA001071.

Margold, M., Stokes, C.R. and Clark, C.D. 2018. Reconciling records of ice streaming and ice margin retreat to produce a palaeogeographic reconstruction of the deglaciation of the Laurentide Ice Sheet. Quaternary Science Reviews, 189: 1–30. doi: 10.1016/j.quascirev.2018.03.013.

Marshall, S.J. and Clark, P.U. 2002. Basal temperature evolution of North American ice sheets and implications for the 100-kyr cycle. Geophysical Research Letters, 29(24): 67-1–67-4. doi:10.1029/2002GL015192.

McMartin, I., and Henderson, P. 2004. Evidence from Keewatin (central Nunavut) for paleo-ice divide migration. Geographie physique et Quaternaire, 58(2–3): 163–186. doi:10.7202/013137ar.

McMartin, I., Godbout, P.-M., Campbell, J.E., Tremblay, T., Behnia, P., 2021. A new map of glacigenic features and glacial landsystems in central mainland Nunavut, Canada. Boreas, 50(1): 51–75. doi:10.1111/bor.12479.

Netterville, J.A. 1974. Quaternary stratigraphy of the lower Gods River region, Hudson Bay Lowlands, Manitoba. Master of Science thesis, University of Calgary, Calgary, Canada, 79 p.

Nielsen, E., Morgan, A.V., Morgan, A., Mott, R.J., Rutter, N.W., and Causse, C. 1986. Stratigraphy, paleoecology and glacial history of the Gillam area, Manitoba. Canadian Journal of Earth Sciences, 23: 1641–1661. doi:10.1139/e86-153.

North American Commission on Stratigraphic Nomenclature. 2021. Stratigraphy, 18(3): 153–204. doi:10.29041/strat.18.3.01.

Parent, M., Paradis, S.J. and Boisvert, E. 1995. Ice-flow patterns and glacial transport in the eastern Hudson Bay region: implications for the late Quaternary dynamics of the Laurentide Ice Sheet. Canadian Journal of Earth Sciences, 32(12): 2057–2070. doi:10.1139/e95-159.

Prest, V.K., Donaldson, J.A., and Mooers, H.D. 2000. The Omar story: the role of Omars in assessing glacial history of west–central North America. Geographie Physique et Quaternaire, 54: 257–270. doi:10.7202/005654ar.

Rasmussen, S.O., Bigler, M., Blockley, S.P., Blunier, T., Buchardt, S.L., Clausen, H.B., Cvijanovic, I., Dahl-Jensen, D., et al. 2014. A stratigraphic framework for abrupt climatic changes during the Last Glacial period based on three synchronized Greenland ice-core records: refining and extending the INTIMATE event stratigraphy. Quaternary Science Reviews, 106: 14–28. doi: 10.1016/j.quascirev.2014.09.007.

Rice, J.M., Ross, M., Paulen, R.C., Kelley, S.E., Briner, J.P., Neudorf, C.A. and Lian, O.B. 2019. Refining the ice flow chronology and subglacial dynamics across the migrating Labrador Divide of the Laurentide Ice Sheet with age constraints on deglaciation. Journal of Quaternary Science, 34(7): 519–535. doi:10.1002/jqs.3138.

Ross, M., Campbell, J.E., Parent, M. and Adams, R.S. 2009. Paleo-ice streams and the subglacial landscape mosaic of the North American mid-continental prairies. Boreas 38(3): 421–439. doi:10.1111/j.1502-3885.2009.00082.x.

Roy, M. 1998. Pleistocene stratigraphy of the lower Nelson River area—implications for the evolution of the Hudson Bay lowland of Manitoba, Canada. Master of Science thesis, University of Quebec, Montreal, Canada, 220 p.

Roy, M., Clark, P.U., Barendregt, R.W., Glasmann, J.R. and Enkin, R. J. 2004. Glacial stratigraphy and paleomagnetism of late Cenozoic deposits of the north-central United States. GSA Bulletin, 116(1-2): 30–41. doi: 10.1130/B25325.1.

Shackleton, N.J. and Opdyke, N.D. 1973. Oxygen isotope and palaeomagnetic stratigraphy of Equatorial Pacific core V28-238: Oxygen isotope temperatures and ice volumes on a 10^5 year and 10^6 year scale. Quaternary Research 3(1): 39–55, doi: 10.1016/0033-5894(73)90052-5.

Skinner, R.G. 1973. Quaternary stratigraphy of the Moose River Basin, Ontario. Geological Survey of Canada, Bulletin 225, 77 p.

Spratt, R.M. and Lisiecki, L.E. 2016. A Late Pleistocene sea level stack. Climate of the Past, 12(4): 1079–1092. doi: 10.5194/cp-12-1079-2016.

Stokes, C.R., Tarasov, L. and Dyke, A.S. 2012. Dynamics of the North American Ice Sheet Complex during its inception and build-up to the Last Glacial Maximum. Quaternary Science Reviews, 50: 86–104. doi:10.1016/j.quascirev.2012.07.009.

Thorleifson, L.H., Wyatt, P.H., Shilts, W.W., and Nielsen, E. 1992. Hudson Bay Lowland Quaternary Stratigraphy: evidence for early Wisconsinan glaciation centred in Quebec. *In* Geological Society of America Special Papers 270. pp. 207–222. doi:10.1130/SPE270-p207.

Trommelen, M. S. 2015. Till composition and glacial history, Gauer Lake – Wishart Lake, Manitoba (NTS 64H4, 5, 12, 13). Manitoba Geological Survey, Geoscientific Paper 2014-1, 32 p.

Veillette, J.J., Dyke, A.S., and Roy, M. 1999. Ice-flow evolution of the Labrador Sector of the Laurentide Ice Sheet: a review, with new evidence from northern Quebec. Quaternary Science Reviews, 18: 993–1019. doi:10.1016/S0277-3791(98)00076-6.

Veillette, J.J., Roy, M., Paulen, R.C., Ménard, M. and St-Jacques, G. 2017. Uncovering the hidden part of a large ice stream of the Laurentide Ice Sheet, northern Ontario, Canada. Quaternary Science Reviews, 155: 136–158. doi: 10.1016/j.quascirev.2016.11.008.

Chapter 7

Main contributions and future work

This thesis combined detailed field observations of Quaternary sediments with analytical data (till composition, geochronology) to better understand the Quaternary stratigraphy in the western Hudson Bay Lowland (HBL). This thesis has provided an increased understanding of glacial and nonglacial events that have occurred over at least the last three glacial-interglacial cycles, including additional insight into the timing and climatic conditions of past ice-free periods (interstadial or interglacial). The main contributions of which are summarized herein.

7.1 Western Hudson Bay Lowland Quaternary Stratigraphy advances

Prior to this thesis, the Quaternary stratigraphic framework of the western HBL was reliant on detailed investigations of sections on the Nelson River, near the town of Gillam, Manitoba (Figure 1.2; Nielsen et al., 1986; Roy, 1998). Additional sections across the western HBL had been investigated and interglacial sediments characterized (Dredge et al., 1990), but these sites were placed within the context of the stratigraphic framework first established in the Gillam area (Dredge and McMartin, 2011). Furthermore, there was the assumption that the first encountered interglacial bed in the subsurface was deposited during the penultimate ice-free period and these sediments ("Nelson River Sediments") were used as a tool to correlate between points of stratigraphic observations.

This thesis investigated three areas to gain a better understanding of the regional Quaternary stratigraphic record of the western HBL (Chapters 3–5), while also contributing to a better understanding of the Quaternary stratigraphy of the Gillam region (Gauthier et al., 2024, 2025b). The extensive collection of ice-flow data across the region has proven to be the most important parameter for the characterization of till units, which was necessary to construct stratigraphic frameworks using a hybrid lithostratigraphy-allostratigraphy approach for each region investigated. In particular, this study emphasized the importance of collecting a-axis clast fabric data from tills while paying attention to A/B plane dip of clasts being measured. Previous work in the HBL documented numerous tills with a NW-SE oriented ice-flow direction in the stratigraphic record,

which could not be confidently assigned direction (Gauthier et al., 2019). One objective of this thesis was to further investigate the composition of these tills using multiple parameters to confirm whether they were deposited by NW- or SE-trending ice-flow. By confirming the direction of ice-flow that deposited these tills, important observations could then be deduced about the history of the Laurentide Ice Sheet (LIS).

7.2 Laurentide Ice Sheet reconstructions

The Quaternary stratigraphic frameworks developed during this thesis have provided important insights into the growth, evolution and retreat of the LIS during the past two glaciations and provided documentation of ice-flow events that occurred during pre-Illinoian glaciations.

During the last glaciation (Wisconsinan glaciation; HBL Glacial Stage I), there is widespread evidence that the LIS first advanced into the study area from the Quebec-Labrador dome. Evidence of this NW-trending ice-flow event is preserved at surface (Kaskattama and Trout Lake flowsets), indicating significant landscape preservation in places during the remainder of the glaciation. This NW-trending ice-flow is followed by W-trending ice-flow, which likely reflects a migration of the Quebec-Labrador Dome northwards and streamlined landforms belonging to this event are preserved in the Churchill River area. Following these relatively early ice-flow events, the western HBL was likely situated in a cold-based ice or sluggish ice environment for much of the last glaciation and S-trending ice flowing from the Keewatin Dome likely did not occur until MIS 2, which transitions into SW-trending late-glacial ice streams.

This thesis is not the first to suggest that NW-trending ice flowing from the Quebec-Labrador Dome first advanced into the HBL during the last glaciation. Thorleifson et al. (1992) came to a similar conclusion based on the identification of relatively old till deposited by NW-trending ice-flow, called the ‘Rocksand Till’. The timing of this ice-flow event was interpreted to be either the start of the last glaciation (MIS 5) or the penultimate glaciation (MIS 6) and was dependent on thermoluminescence (TL) age estimations of the overlying sorted sediments. These TL ages are now interpreted to be age underestimations in the western HBL and the ‘alternative framework’ proposed by Thorleifson et al. (1992) is supported by correlations and age estimations within this thesis, which has important

ramifications for our understanding of the Quaternary stratigraphy in the central HBL. For example, the alternative framework presented in Thorleifson et al. (1992) assigns the Missinaibi Formation, including the Bell Sea sediments, to the MIS 7 interglacial period (HBL Interglacial Stage III of western HBL). Therefore, this ice-flow event should no longer be used as evidence for westward expansion of the Quebec-Labrador Dome during the last glaciation (e.g., Kleman et al., 2010; Dalton et al., 2022b) but instead is an important regional-scale ice-flow event to be considered in reconstructions of the MIS 6 glaciation in the central HBL and is now observed across the western HBL.

Similar to the last glaciation, at the start of the penultimate glaciation (Illinoian glaciation; HBL Glacial Stage II) ice-flowing from the Quebec-Labrador dome first advance into the study area, although initial ice-flow may have been towards the SW instead of the NW (Phase II-A). However, evidence of this early SW-trending ice-flow is scant, and instead NW-trending ice-flow is the dominant ice-flow direction that deposited till at beginning of the Illinoian glaciation across most of the sections investigated. This suggests that initial SW-trending ice-flow direction may have been a short-lived ice advance and/or was mostly overprinted by later NW-trending ice-flow across much of the western HBL. Following this early expansion of the Quebec-Labrador Dome, there is a significant build-up of the Keewatin Dome and the western HBL is over-run by S- to SW-trending ice that is pervasive across sections investigated.

The Quaternary stratigraphic record in the Churchill River area provides important constraints on the late-glacial ice dynamics of the LIS in the western HBL during the Illinoian glaciation. Here, ice first flowed towards the east, which is interpreted as a possible onset region for the Hudson Strait ice stream and indicates an ice-divide and/or ice dome likely existed west of the Churchill River in north-central Manitoba. This ice-divide later crossed the study area and ice flowed towards the west providing an important field-based constraint for a late-glacial ice divide during the Illinoian glaciation.

The correlation of ice-flow events that pre-date the Illinoian glaciation is less certain between regions studied. Nonetheless, these identified tills provide important information about glacier

dynamics during prior glaciations and reconciling these records is an important avenue of future research. Currently, the western HBL Quaternary stratigraphic record likely extends to at least the MIS 10 glaciation (Gauthier et al., 2025b) and this is likely a conservative estimate based on recent studies along the Gods River (Mesich, 2025).

7.3 Previous interglacials

This thesis documented that there are at least three (and likely more) separate interglacial periods recognized within the stratigraphic record of the western HBL (Figure 6.2). Fieldwork uncovered many new interglacial exposures and by using a hybrid lithostratigraphy-allostratigraphy approach clarified that numerous subtill organic-bearing beds previously interpreted to have been deposited during the last interglacial period (MIS 5e), likely were deposited during the MIS 7 interglacial period instead. A summary of interglacial sites recognized, and their interpreted relative age is provided in Appendix E, Supplemental material 1.

Intertill sorted sediments interpreted to have been deposited during the penultimate interglacial period (Interglacial Stage II) are recognized across the western HBL (Figure 7.1a) but noticeably absent from the stratigraphic record in the Gillam area (Gauthier et al., 2025b). Paleobotanical datasets derived from these sediments typically indicate a climate similar to the present day. Key organic-bearing exposures include the Black Duck River sites (Dalton et al., 2016; Dalton et al., 2022a; Hodder et al., 2023) and exposures along the Nelson River Estuary (Chapter 5; Figure 7.1a). However, many of the interpreted Interglacial Stage II sediments do not contain organic material and consist of sorted planar- to cross-bedded sand and gravel that are stratigraphically constrained by different bounding tills. While these sedimentary facies could have been deposited in glacial environments, they are situated between tills that are correlated to different glaciations based on stratigraphic relationships at other organic-bearing exposures; thus, it is reasonable to interpret them as interglacial deposits (fluvial or lacustrine) or deposited subaerially during or shortly after HBL Glacial Stage II deglaciation (marine, glaciofluvial outwash). Indeed, in the Churchill River area, thick exposures of sand and gravel have been interpreted to record marine inundation following Termination II (Chapter 4).

Intertill sorted sediments interpreted to have been deposited during an earlier interglacial period (Interglacial Stage III), which likely corresponds to MIS 7, are recognized across the western HBL (Figure 7.1b). These sorted sediments have been associated to various depositional environments including fluvial, glaciofluvial, marine and lacustrine. The preservation of Interglacial Stage III sites is excellent and contains more organic-bearing exposed sediments compared to Interglacial Stage II sites. Paleo–climate reconstructions from across the western HBL indicate an environment and climate similar to the present day. Interpreted marine sediments are situated within the Churchill and Machichi areas (Figure 7.1b). In the Churchill area, these marine sediments provide a minimum limit on the marine incursion during Termination III (~243 ka) of 161 m above current sea level, which is at a greater elevation compared to the marine limit the region experienced during Termination I of 140–150 m above current sea level.

There is at least one occurrence in the stratigraphic record of sediments deposited during an interglacial that preceded Glacial Stage III (units M1 and C1, Figure 6.2). As acknowledged during previous work on these units (Chapter 4), the correlation of these identified interglacial beds within an individual study is tentative and there is a strong possibility that sediments deposited during separate interglacial periods that have been grouped as one unit due to the relative scarcity of observations and uncertainty in correlations between sections investigated. Thus, correlating identified units between studies must be done cautiously. There are also previously identified interglacial sediments, such as the Limestone River Sediments (Roy, 1998), where it is currently uncertain what their stratigraphic relationship is with identified bounding glacial sediments and this is reflected in the updated stratigraphic framework for that region (Gauthier et al., 2025b). The age of these sediments is currently unknown, but nonetheless they provide an important archive of past interglacial conditions. Interestingly, occurrences of weathered bedrock at several localities in northeastern Manitoba (Chapter 4; Dredge and Nixon, 1992), indicate that glacial erosion of bedrock was likely minimal in parts of central Canada during the Quaternary Period. This also hints at the possibility that some of the Interglacial Stage IV sediments are older than we might think (early- to mid-Quaternary?). This concept is supported by the presence of unconsolidated sediments with a reversed remnant magnetism from a drillcore within the Kaskattama highland region (Su, 2022),

which provides evidence for the preservation of early-mid Quaternary deposits within the western HBL stratigraphic record in central Canada.

7.3.1 Marine Isotope Stage 3

This thesis reviewed data interpreted to support the hypothesis of a deglaciation of the western HBL during the MIS 3 interstadial (Dalton et al., 2019). This data review was supplemented by new geochronology results from the uppermost intertill nonglacial sediments in the region that were suspected to have been deposited during the penultimate ice-free period, including one region with previously reported near finite radiocarbon ages from wood (Black Duck River; Dalton et al., 2016). This thesis emphasized the importance of understanding field-based stratigraphic relationships, which is necessary to unravel the fragmented record and establish the relative age of intertill sorted sediments. New radiocarbon and optical age constraints for the stratigraphically youngest intertill sorted sediments identified within the Quaternary stratigraphic record concluded that the western HBL was likely glaciated during the MIS 3 interstadial (Chapter 2; Hodder et al., 2023).

This research spurred an interest to better understand where the MIS 3 ice margin was situated in central Canada during this interstadial. As a result, an area in southeastern Manitoba which had previously been interpreted to possibly contain MIS 3 deposits was investigated (Gauthier et al., 2025a). While this research is not presented in this thesis, this study determined that fluvial deposits were deposited in the region and that the area was inundated by a proglacial lake (Lake Vita) during MIS 3. This indicates that the MIS 3 ice margin was likely situated somewhere between southeastern Manitoba and the Hudson Bay Lowland during this time period, probably similar to the ‘Hypothesis I’ ice limits proposed by Dredge and Thorleifson (1987).

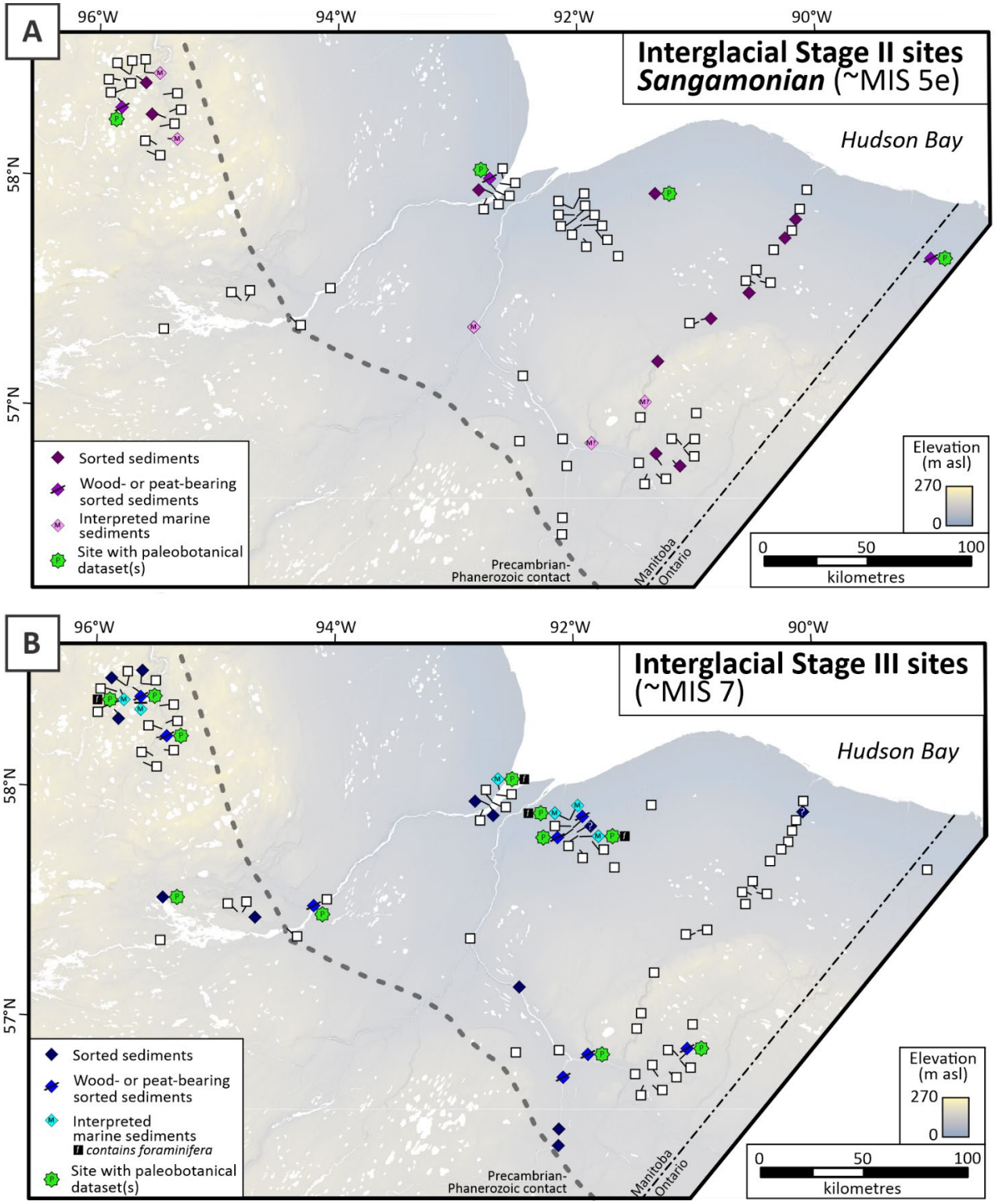

Figure 7.1: Inventory of interpreted interglacial deposits: A) Interglacial Stage II sites (Sangamonian; ~MIS 5e) and B) Interglacial stage III sites (~MIS 7). These sites are tabulated in Appendix E, Supplemental materials 1.

7.4 Future work

Quaternary stratigraphic studies must acknowledge the highly fragmented geological record and incorporate detailed characterization of glacial deposits to fully understand the stratigraphic context of intertill nonglacial deposits. This thesis incorporated a hybrid lithostratigraphy-allostratigraphy that proved to be a useful approach to unravelling the fragmented record and this type of investigation is recommend for future endeavors into the HBL Quaternary stratigraphy. Regions with a higher concentration of preserved nonglacial deposits are worthy of additional investigations to clarify stratigraphic relationships and advance our understanding of relatively old ice-flow events. This includes the Nelson River Estuary area that was investigated as part of this study. Due to time constraints in the field and curious on-lookers (Polar Bears), this study was not able to obtain the ideal amount of ice-flow data for tills investigated. Furthermore, this is one of the rare regions where both MIS 5e and MIS 7 sediments are well preserved in the stratigraphic record. During the writing of this thesis, stratigraphic studies in the Gods River area have supported the notion that there is still much to be gleaned from the stratigraphic record of the HBL (Mesich, 2025).

This thesis highlighted several relict streamlined landforms and/or flowsets at surface based on correlations with the Quaternary stratigraphic record. These landforms are crosscut by late-glacial meltwater corridors and/or glaciofluvial sediments aligned SW-NE, similar to the direction of late-glacial ice-flow events in surrounding areas. This includes preserved W-trending streamlined landforms in the Churchill River area where the surficial record is relatively poorly understood. As new elevation models become available, additional investigation could provide important information on late-glacial LIS dynamics.

The LIS underwent a significant late-glacial retreat in the HBL that was followed by an ice advance that likely deposited the Etawney moraine around 9.49–9.04 cal ka (Gauthier et al., 2022), which possibly coincides with re-advances documented in Greenland and Baffin Island at 9.2 cal ka (Young et al., 2020). The margin of the LIS in the western HBL prior to this re-advance is unknown but is constrained to somewhere northeast of the Kaskattama highland based on presence of iceberg scours at height of land on the highland, indicating inundation by glacial Lake Agassiz at some point in time prior to collapse of LIS and subsequent marine incursion. Understanding the timing and

extent of this retreat has important implications for understanding both Lake Agassiz and LIS dynamics in the early Holocene (early MIS 1).

It is a monumental task to assemble a regional stratigraphic framework that identifies all ice-flow events, and the correct order of events, over an area of ~50 000 km^2 that contains thick sequences of Quaternary sediments and has experienced a complex ice-flow history. As such, the revised stratigraphic framework presented in Chapter 6 will need revision as new data are acquired. This is especially true for glacial events beyond the last two Glacial Stages (pre-Illinoian), which are more difficult to unravel due to a lower number of observations (deeper in subsurface) and lower preservation of landforms and sediment due to erosion from successive ice-flow events.

This thesis used radiocarbon and optical dating methods to attempt to understand the age of identified nonglacial units in the stratigraphic record. All of the wood radiocarbon ages were nonfinite and finite shell radiocarbon ages near the upper limit of this geochronometer are interpreted to be nonfinite ages as well owing to the possibilities of contamination by younger carbon (e.g., Miller and Andrews, 2019). Optical dating methods have provided the first age estimations for many of the beds investigated during this study. At many sites, these ages appear to be reasonable estimations when compared to pollen records and regional stratigraphic frameworks. However, at some sections there are age reversals documented (decreasing ages with depth; e.g., section 21-812, Chapter 4) or the ages appear to be an underestimation of true depositional age when compared to the stratigraphic frameworks constructed. Thus, additional geochronological studies incorporating complementary age dating techniques and/or the application of single-grain optical dating would be beneficial to assess the ages assigned to interglacial beds identified and is recommended as geochronological methods improve. This could include cosmogenic burial dating, electron spin resonance dating or perhaps the establishment of a cryptotephra framework. The stratigraphic frameworks presented within this thesis did not rely on geochronology constraints to anchor any correlations, thus the age of identified interglacial beds presented within stratigraphic frameworks can be further tested.

References

Aitchison, J. 1984. The statistical analysis of geochemical compositions. Mathematical Geology, 16 (6): 531–564.

Aitchison, J. 1986. The Statistical Analysis of Compositional Data. Methuen Inc.

Andrews, J.T. and Smith, D.I. 1969. Statistical analysis of till fabric: methodology, local and regional variability (with particular reference to the north Yorkshire till cliffs). Quarterly Journal of the Geological Society, 125(1-4): 503–542. doi:10.1144/gsjgs.125.1.0503.

Andrews, J.T., Shilts, W.W., Miller, G.H., 1983. Multiple deglaciations of the Hudson Bay Lowlands, Canada, since deposition of the Missinaibi (last interglacial?) Formation. Quaternary Research, 19: 18–37. doi:10.1016/0033-5894(83)90025-X.

Batchelor, C.L., Margold, M., Krapp, M., Murton, D. K., Dalton, A.S., Gibbard, P.L., Stokes, C.R., Murton, J.B. and Manica, A. 2019. The configuration of Northern Hemisphere ice sheets through the Quaternary. Nature Communications, 10:3713. doi:10.1038/s41467-019-11601-2.

Bell, R. 1880. Report of explorations on the Churchill and Nelson rivers and around God's and Island Lakes, 1879. Geological Survey of Canada Report of Progress for 1878–1879, part C, 72 p.

Benn, D.I. 1994. Fabric shape and the interpretation of sedimentary fabric data. Journal of Sedimentary Research, 64: 910–915.

Berger, G.W. and Nielsen, E., 1991. Evidence from thermoluminescence dating for Middle Wisconsinan deglaciation in the Hudson Bay Lowland of Manitoba. Canadian Journal of Earth Sciences, 28: 240–249. doi:10.1139/e91-023.

Boellstorff, J. 1978. North American Pleistocene Stages Reconsidered in Light of Probable Pliocene-Pleistocene Continental Glaciation. Science, 202(4365): 305–307. doi:10.1126/science.202.4365.305.

Briner, J., Kaufman, D. and Bennike, O. 2025. The size of the Greenland Ice Sheet during Marine Isotope Stage 3. Quaternary Research, 127: 59–68. doi:10.1017/qua.2025.21.

Clayton, L. and Moran, S.R. 1982. Chronology of Late Wisconsinan glaciation in middle North America. Quaternary Science Reviews, 1(1): 55–82. doi:10.1016/0277-3791(82)90019-1.

Cohen, K.M. and Gibbard, P.L. 2019. Global chronostratigraphical correlation table for the last 2.7 million years, version 2019 QI-500. Quaternary International, 500: 20–31. doi:10.1016/j.quaint.2019.03.009.

Dalton, A.S., Finkelstein, S.A., Barnett, P.J., Forman, S.L. 2016. Constraining the Late Pleistocene history of the Laurentide Ice Sheet by dating the Missinaibi Formation, Hudson Bay Lowlands, Canada. Quaternary Science Reviews, 146: 288–299. doi:10.1016/j.quascirev.2016.06.015.

Dalton, A.S., Finkelstein, S.A., Barnett, P.J., Väliranta, M., Forman, S.L. 2018. Late Pleistocene chronology, palaeoecology and stratigraphy at a suite of sites along the Albany River, Hudson Bay Lowlands, Canada. Palaeogeography, Palaeoclimatology, Palaeoecology, 492: 50–63. doi:10.1016/j.palaeo.2017.12.011

Dalton, A.S., Finkelstein, S.A., Forman, S.L., Barnett, P.J., Pico, T. and Mitrovica, J.X., 2019. Was the Laurentide Ice Sheet significantly reduced during Marine Isotope Stage 3? Geology, 47: 111–114. doi:10.1130/G45335.1.

Dalton, A.S., Finkelstein, S.A., Hodder, T.J. and Gauthier, M.S. 2022a. Palynological analyses of subtill sediments from four sites in the western Hudson Bay Lowland region (parts of NTS 53O, 54A, C, D). Manitoba Geological Survey, Open File OF2022-1, 13 p.

Dalton, A.S., Stokes, C.R. and Batchelor, C.L. 2022b. Evolution of the Laurentide and Innuitian ice sheets prior to the Last Glacial Maximum (115 ka to 25 ka). Earth Science Reviews, 224:103875. doi:10.1016/j.earscirev.2021.103875.

Dalton, A.S., Dulfer, H., Margold, M., Heyman, J., Clague, J., Froese, D., et al. 2023. Deglaciation of the North American Ice Sheet Complex in calendar years based on a new comprehensive database of chronological data: NADI-1. Quaternary Science Reviews, 321: 108345. doi:10.1016/j.quascirev.2023.108345.

Davis, J.C. 2002: Statistics and data analysis in geology, third edition; John Wiley and Sons, New York.

Dredge, L.A. and Thorleifson, L.H. 1987. The Middle Wisconsinan history of the Laurentide Ice Sheet. Geographie physique et Quaternaire, 41: 215–235. doi:10.7202/032680ar.

Dredge, L.A. and McMartin, I., 2011. Glacial stratigraphy of northern and central Manitoba. Geological Survey of Canada, Bulletin 600, 27 p. doi:10.4095/288561.

Dredge, L.A. and Nixon, F.M. 1992. Glacial and environmental geology of northeastern Manitoba. Geological Survey of Canada Memoir 432, 80 p.

Dredge, L.A., Morgan, A.V. and Nielsen, E. 1990. Sangamon and pre-Sangamon interglaciations in the Hudson Bay Lowlands of Manitoba. Géographie Physique et Quaternaire, 44(3) : 319–336. doi:10.7202/032833ar.

Dube-Loubert, H., Roy, M., Allard, G. and Veillette, J.J. 2013. Glacial and nonglacial events in the eastern James Bay lowlands, Canada. Canadian Journal of Earth Science, 50: 379–396. doi:10.1139/cjes-2012-0065.

Flint, R.F. 1963. Status of the Pleistocene Wisconsin Stage in Central North America. Science, 139(3553): 402–404. doi:10.1126/science.139.3553.40.

Forman, S.L., Wintle, A.G., Thorleifson, L.H. and Wyatt, P.H. 1987. Thermoluminescence properties and age estimates for Quaternary raised marine sediments, Hudson Bay Lowland, Canada. Canadian Journal of Earth Sciences, 24: 2405–2411. doi:10.1139/e87-226.

Gauthier, M.S., Hodder, T.J., Ross, M., Kelley, S.E., Rochester, A., and McCausland, P. 2019. The subglacial mosaic of the Laurentide Ice Sheet; a study of the interior region of southwestern Hudson Bay. Quaternary Science Reviews, 214: 1–27. doi:10.1016/j.quascirev.2019.04.015.

Gauthier, M.S., Hodder, T.J., Dalton, A.S., Lian, O.B., Schaarschmidt, M., Ross, M., Väliranta, M. and Finkelstein, S.A. 2024. Preservation of MIS 7 deglacial and nonglacial deposits near the edge of the Hudson Bay Lowland in Manitoba, Canada. Canadian Journal of Earth Sciences, 61(11): 1184–1211. doi:10.1139/cjes-2024-0019.

Gauthier M.S., Hodder T.J., Dalton A.S., Brewer, V., Lian, O.B., Finkelstein, S.F. Schaarschmidt, M. and Mereghetti, A. 2025a. South-central Laurentide Ice Sheet dynamics and the formation of proglacial Lake Vita during MIS 3. Quaternary Research, 123: 83–105. doi:10.1017/qua.2024.34.

Gauthier, M.S., Hodder, T.J., Hathaway, J., Ross, M., Schaarschmidt, M., Lian, O.B., Finkelstein, S.A. and Kelley, S.E. 2025b. Extending the western Hudson Bay Lowland Quaternary stratigraphy, in Manitoba Canada, to at least Marine Isotope Stage 10. Canadian Journal of Earth Sciences, *in press*. doi:10.1139/cjes-2025-0027.

Gowan, E.J., Zhang, X., Khosravi, S., Rovere, A., Stocchi, P., Hughes, A.L.C., Gyllencreutz, R., Mangerud, J., Svendsen, J.-I. and Lohmann, G. 2021. A new global ice sheet reconstruction for the past 80 000 years. Nature Communications, 12:1199. doi:10.1038/s41467-021-21469-w.

Grunsky, E. 2010. The interpretation of geochemical survey data. Geochemistry, Exploration, Environment, Analysis 10, 27–74. doi:10.1144/1467-7873/09-210.

Hallberg, G.R. 1986. Pre-Wisconsin glacial stratigraphy of the central plaines region in Iowa, Nebraska, Kansas, and Misouri. Quaternary Science Reviews, 5: 11–15. doi:10.1016/0277-3791(86)90169-1.

Hemming, S.R. 2004. Heinrich events: massive late Pleistocene detritus layers of the North Atlantic and their global climate imprint. Review of Geophysics 42 (1), Paper number 2003RG000128. doi:10.1029/2003RG000128.

Hemmings, S.R. and Hajdas, I. 2003: Ice–rafted detritus evidence from $^{40}Ar/^{39}Ar$ ages of individual hornblende grains for evolution of the eastern margin of the Laurentide ice sheet since 43 ^{14}C ky; Quaternary International.

Henderson, P.J. 1990. Provenance and depositional facies of surficial sediments in Hudson Bay, a glaciated epeiric sea. Doctor of Philosophy thesis, University of Ottawa, Ottawa, Canada, 288 p.

Henderson, P.J. 1994. Surficial geology and drift composition of the Bissett-English Brook area, Rice Lake Greenstone Belt, southeastern Manitoba. Geological Survey of Canada Open File 2910, 190 p.

Hodder, T.J. and Gauthier, M.S. 2025a. Quaternary site, till composition and ice-flow indicator data for the Little Churchill to Churchill rivers area, northeastern Manitoba (part of NTS 54E). Manitoba Geological Survey Open File OF2025-1, 5 p., 6 appendices.

Hodder, T.J. and Gauthier, M.S. 2025b. Quaternary site, till composition and ice-flow indicator datasets in the Nelson River Estuary–Black Duck River area, northeastern Manitoba (parts of NTS 54A, B, C, F). Manitoba Geological Survey Open File OF2025-2, 6 p., 8 appendices.

Hodder, T.J. and Lian, O.B. 2024. Reconnaissance-scale Quaternary geology investigations to support lithium exploration in southeastern Manitoba (parts of NTS 52L, M, 62P, 63A); *in* Report of Activities 2024, Manitoba Geological Survey, p. 200–208.

Hodder, T.J., Ross, M. and Menzies, J. 2016. Sedimentary record of ice divide migration and ice streams in the Keewatin core region of the Laurentide Ice Sheet. Sedimentary Geology, 338: 97–114. doi:10.1016/j.sedgeo.2016.01.001.

Hodder, T.J., Gauthier, M.S., Ross, M. and Lian, O.B. 2023. Was there a nonglacial episode in the western Hudson Bay Lowland during Marine Isotope Stage 3? Quaternary Research, 116: 148–161. doi:10.1017/qua.2023.35.

Hodder, T.J., Gauthier, M.S., Ross, M., Kelley, S.E., Lian, O.B., Dalton, A.S. and Finkelstein, S.A. 2024a. Unravelling the fragmented sediment-landform assemblage in an area of thick Quaternary sediment,

western Hudson Bay Lowland, Canada. Canadian Journal of Earth Sciences, 61(11): 1156–1183. doi:10.1139/cjes-2024-0018.

Hodder, T.J., Gauthier, M.S., Kelley, S.E. and Ross, M. 2024b. Quaternary site, till composition and ice-flow indicator datasets in the Kaskattama highland area, northeastern Manitoba (parts of NTS 53N, O, 54B, C). Manitoba Geological Survey Open File OF2024-1, 20 p.

Holmes, C.D. 1941. Till fabric. Bulletin of the Geological Society of America, 52: 1299–1354

Hicock, S.R., Goff, J.R., Lian, O.B., Little, E.C. 1996. On the interpretation of subglacial till fabric. Journal of Sedimentary Research 66, 928–934. doi:10.1306/D4268441-2B26-11D7-8648000102C1865D.

Kleman, J., Hättestrand, C., Borgström, I. and Stroeven, A. 1997. Fennoscandian palaeoglaciology reconstructed using a glacial geological inversion model. Journal of Glaciology, 43: 283-299. doi:10.3189/S0022143000003233.

Kleman, J., Jansson, K.N., De Angelis, H., Stroeven, A., Hättestrand, C., Alm, G. and Glasser, N.F., 2010. North American Ice Sheet build-up during the last glacial cycle, 115–21 kyr. Quaternary Science Reviews, 29(17–18): 2036-2051. doi:10.1016/j.quascirev.2010.04.021.

Kleman, J., Hättestrand, C., Borgström, I., Fabel, D. and Preusser, F. 2021. Age and duration of a MIS 3 interstadial in the Fennoscandian Ice Sheet core area - Implications for ice sheet dynamics. Quaternary Science Reviews, 264: 107011. doi:10.1016/j.quascirev.2021.107011.

Lisiecki, L.E. and Raymo, M.E. 2005. A Pliocene-Pleistocene stack of 57 globally distributed benthic $\delta^{18}O$ records. Paleoceanography, 20: PA1003. doi:10.1029/2004PA001071.

Mangerud, J., Alexanderson, H., Birks, H.H., Paus, A., Perić, Z.M. and Svendsen, J.I. 2023. Did the Eurasian ice sheets melt completely in early Marine Isotope Stage 3? New evidence from Norway and a synthesis for Eurasia. Quaternary Science Reviews, 311: 108136. doi:10.1016/j.quascirev.2023.108136.

Mark, D.M. 1973. Analysis of axial orientation data, including till fabrics. Geological Society of America Bulletin 84, 1369–1374. doi:10.1130/0016-7606(1973)84<1369:AOAODI>2.0.CO;2.

McDonald, B.C. 1969. Glacial and interglacial stratigraphy, Hudson Bay Lowland. *In* Earth Sciences Symposium on Hudson Bay. *Edited by* P.J. Hood. GSC Paper 68-53: 78–99.

McMartin, I. and McClenaghan, M.B. 2001: Till geochemistry and sampling techniques in glaciated shield terrain: a review; *in* Drift Exploration in Glaciated Terrain. *Edited by* M.B. McClenaghan, P.T. Bobrowsky, G.E.M. Hall and S.J. Cook. Geological Society, Special Publications, 185: 19–43.

McMartin, I. and Paulen, R.C. 2009. Ice-flow indicators and the importance of ice-flow mapping for drift prospecting; *in* Application of Till and Stream Sediment Heavy Mineral and Geochemical Methods to Mineral Exploration in Western and Northern Canada. *Edited by* R.C. Paulen and I. McMartin. Geological Association of Canada, GAC Short Course Notes 18: 15–34.

McMartin, I., and Henderson, P. 2004. Evidence from Keewatin (central Nunavut) for paleo-ice divide migration. Geographie physique et Quaternaire, 58(2–3): 163–186. doi:10.7202/013137ar.

McMartin, I., Godbout, P.-M., Campbell, J.E., Tremblay, T. and Behnia, P. 2021. A new map of glacigenic features and glacial landsystems in central mainland Nunavut, Canada. Boreas, 50(1): 51–75. doi:10.1111/bor.12479.

McQueen, J. 1967. Some methods for classification of and analysis of multivariate observations. 5th Berkeley Symposium on Mathematics, Statistics and probability, 1: 281–298.

Mesich, L.N. 2025. The Quaternary stratigraphy of the Gods and Yakaw rivers area, northeastern Manitoba. Master of Science thesis, University of Waterloo, Waterloo, Canada, 511 p.

Miller, G.H. and Andrews, J.T. 2019. Hudson Bay was not deglaciated during MIS-3. Quaternary Science Reviews, 225: 105944. doi:10.1016/j.quascirev.2019.105944.

Netterville, J. A. 1974. Quaternary stratigraphy of the lower Gods River region, Hudson Bay lowlands, Manitoba. Master of Science thesis, The University of Calgary, Calgary, Alberta, Canada, 79 p.

Nielsen, E., Morgan, A.V., Morgan, A., Mott, R.J., Rutter, N.W., and Causse, C. 1986. Stratigraphy, paleoecology and glacial history of the Gillam area, Manitoba. Canadian Journal of Earth Sciences, 23: 1641–1661. doi:10.1139/e86-153.

North American Commission on Stratigraphic Nomenclature. 2021. Stratigraphy, 18(3): 153–204. doi:10.29041/strat.18.3.01.

Ovtos, E.G. 2015. The Last Interglacial Stage: Definitions and marine highstand, North America and Eurasia. Quaternary International 383, 158–173. doi:10.1016/j.quaint.2014.05.010.

Pico, T., Birch, L., Weisenberg, J. and Mitrovica, J.X. 2018. Refining the Laurentide Ice Sheet at Marine Isotope Stage 3: A data-based approach combining glacial isostatic simulations with a dynamic ice model. Quaternary Science Reviews, 195: 171–179. doi:10.1016/j.quascirev.2018.07.023.

Pigati, J.S., Quade, J., Wilson, J., Timothy Jull, A.J. and Lifton, N.A. 2007. Development of low-background vacuum extraction and graphitization systems for ^{14}C dating of old (40–60 ka) samples. Quaternary International, 166(1): 4–14. doi:10.1016/j.quaint.2006.12.006.

Prest, V.K., Donaldson, J.A., and Mooers, H.D. 2000. The Omar story: the role of Omars in assessing glacial history of west–central North America. Geographie Physique et Quaternaire, 54: 257–270. doi:10.7202/005654ar.

Rhodes, E.J. 2011. Optically stimulated luminescence dating of sediments over the past 200 00 years. Annual Review of Earth and Planetary Sciences, 39: 461–488. doi: 10.1146/annurev-earth-040610-133425.

Rice, J.M., Ross, M., Paulen, R.C., Kelley, S.E., Briner, J.P., Neudorf, C.A. and Lian, O.B. 2019. Refining the ice flow chronology and subglacial dynamics across the migrating Labrador Divide of the Laurentide Ice Sheet with age constraints on deglaciation. Journal of Quaternary Science, 34(7): 519–535. doi:10.1002/jqs.3138.

Roy, M. 1998. Pleistocene stratigraphy of the lower Nelson River area—implications for the evolution of the Hudson Bay lowland of Manitoba, Canada. Master of Science thesis, University of Quebec, Montreal, Canada, 220 p.

Hallberg, G.R. 1986. Pre-Wisconsin glacial stratigraphy of the central plaines region in Iowa, Nebraska, Kansas, and Misouri. Quaternary Science Reviews, 5: 11–15. doi: 10.1016/0277-3791(86)90169-1.

Roy, M., Clark, P.U., Duncan, R.A. and Hemming, S.R. 2007. Insights into the late Cenozoic configuration of the Laurentide Ice Sheet from $^{40}Ar/^{39}Ar$ dating of glacially transported minerals in midcontinent tills. Geochemistry, Geophysics, Geosystems, 8(9): Q09006. doi:10.1029/2006GC001572.

Roy, M., Hemmings, S. and Parent, M. 2009. Sediment sources of northern Quebec and Labrador glacial deposits and the northeastern sector of the Laurentide Ice Sheet during ice-rafting events of the last glacial cycle. Quaternary Science Reviews, 28: 3236–3245. doi:10.1016/j.quascirev.2009.08.008.

Ross, M., Campbell, J.E., Parent, M. and Adams, R.S. 2009. Paleo-ice streams and the subglacial landscape mosaic of the North American mid-continental prairies. Boreas 38 (3): 421–439. 10.1111/j.1502-3885.2009.00082.x

Schaen, A.J., Jicha, B.R., Hodges, K.V., Vermeesch, P., Stelten, M.E., Mercer, C.M., et al. 2021. Interpreting and reporting $^{40}Ar/^{39}Ar$ geochronologic data. GSA Bulletin, 133(3–4): 461–487. doi:10.1130/B35560.1.

Shilts, W.W. 1980. Flow patterns in the central North American ice sheet. Nature, 286: 213–218. doi:10.1038/286213a0.

Shilts, W.W. 1982: Quaternary evolution of the Hudson/James Bay region. Le Naturaliste Canadien, 109: 309–332.

Stirling, C.H., Esat, T.M., Lambeck., K. and McCulloch, M.T. 1998. Timing and duration of the Last Interglacial: evidence for a restricted interval of widespread coral reef growth. Earth and Planetary Science Letters, 160(3–4): 745–762. doi:10.1016/S0012-821X(98)00125-3.

Stuiver, M. and Polach, H.A. 1977. Discussion Reporting of ^{14}C Data. Radiocarbon, 19(3):355–363. doi:10.1017/S0033822200003672

Skinner, R.G. 1973. Quaternary stratigraphy of the Moose River Basin, Ontario. Geological Survey of Canada, Bulletin 225, 77 p.

Stea, R.R. and Finck, P.W. 2001. An evolutionary model of glacial dispersal and till genesis in Maritime Canada. *In* Drift Exploration in Glaciated Terrain. *Edited by* M. B. McClenaghan, P. T. Bobrowsky, G.E.M. Hall and S. J. Cook. The Geological Society of London, Special Publications 185: 237–265. doi:10.1144/GSL.SP.2001.185.01.11.

Stokes, C.R., Tarasov, L., Dyke, A.S. 2012. Dynamics of the North American Ice Sheet Complex during its inception and build-up to the Last Glacial Maximum. Quaternary Science Reviews, 50: 86–104. doi: 10.1016/j.quascirev.2012.07.009.

Su, Y. 2022. Using Paleomagnetism to Date Quaternary Sediments in the Hudson Bay Lowlands, Northeastern Manitoba. University of Waterloo, B. Sc. thesis, 27 p.

Thorleifson, L.H., Wyatt, P.H., Shilts, W.W., and Nielsen, E. 1992. Hudson Bay Lowland Quaternary Stratigraphy: evidence for early Wisconsinan glaciation centred in Quebec. *In* Geological Society of America Special Papers 270. pp. 207–222. doi:10.1130/SPE270-p207.

Trommelen, M.S. and Ross, M. 2014. Distribution and type of sticky spots at the centre of a deglacial streamlined lobe in northeastern Manitoba, Canada. Boreas, 43: 557–576. doi:10.1111/bor.12064

Trommelen, M.S., Ross, M. and Campbell, J.E. 2012. Glacial terrain zone analysis of a fragmented paleoglaciological record, southeast Keewatin sector of the Laurentide Ice Sheet. Quaternary Science Reviews, 40: 1–20. doi:10.1016/j.quascirev.2012.02.015.

Trommelen, M.S., Ross, M. and Campbell, J.E. 2013. Inherited clast dispersal patterns: implications for paleoglaciology of the southeast Keewatin Sector of the Laurentide Ice Sheet. Boreas, 42: 693–713. doi: 10.1111/j.1502-3885.2012.00308.x.

Trumbore, S.E. 2000. Radiocarbon geochronology. *In* Quaternary Geochronology: methods and applications. *Edited by* Noller, J.S., Sowers, J.M. and Lettis, W.T. doi: 10.1029/RF004p0041.

Tyrrell, J.B. 1913. Hudson Bay exploring expedition. *in* 22nd report of the Ontario Bureau of Mines. pp. 161–209.

Veillette, J.J., Dyke, A.S. and Roy, M. 1999. Ice-flow evolution of the Labrador Sector of the Laurentide Ice Sheet: a review, with new evidence from northern Quebec. Quaternary Science Reviews, 18: 993–1019. doi:10.1016/S0277-3791(98)00076-6.

Wang, Y. 2018. Statistical analysis of till geochemistry in the Nelson River area, northeastern Manitoba: implications for Quaternary glacial stratigraphy. Master of Science thesis, University of Waterloo, Waterloo, Canada, 162 p.

Young, N.E., Briner, J.P., Miller, G.H., Lesnek, A.J., Crump, S.E., Thomas, E.K., Pendleton, S.L., Cuzzone, J., Lamp, J., Zimmerman, S., Caffee, M. and Schaefer, J.M. 2020. Deglaciation of the Greenland and Laurentide ice sheets interrupted by glacier advance during abrupt coolings. Quaternary Science Reviews, 229: 106091.

Appendix A

Supplemental materials for Chapter 2

Chapter 2 supplemental material is published in Hodder et al. (2023).

Supplemental material 1: Geochronology dataset of Quaternary intertill sediments in western Hudson Bay Lowland.

Supplemental material 2: Till fabric statistics and measurements.

Supplemental material 3: Till composition to support stratigraphic correlations in the Lower Nelson River area (sites 3 and 4).

Supplemental 1: Geochronology dataset of Quaternary intertill sediments in western Hudson Bay Lowland

Site_Reference	Latitude (DD)	Longitude (DD)	Published_Section_ID	Informal_Name	Age_Method*	Material_dated†	Age‡	error (1σ)	Lab_ID	Reference
1	56.418	-94.224	Leslie Creek	Leslie Creek	Luminescence (TL)	alkali feldspar	34000	5000	EKN-3	Berger and Nielsen (1991)
2	56.492	-94.128	Henday	Henday	Luminescence (TL)	alkali feldspar	32000	2000	EKN-5	Berger and Nielsen (1991)
2	56.492	-94.128	Henday	Henday	^{14}C (conv)	wood	>49000		GSC-4420HP	Dredge et al. (1990)
3	56.975	-92.697	112-19-601	Flamborough	^{14}C (AMS)	wood	>55000		UOC-10974	This study
3	56.975	-92.697	112-19-601	Flamborough	^{14}C (AMS)	wood	>55000		UOC-10975	This study
3	56.975	-92.697	Flamborough	Flamborough	Luminescence (TL)	alkali feldspar	46000	4000	EKN-8	Berger and Nielsen (1991)
4	57.023	-92.637	Port Nelson	Port Nelson	Luminescence (TL)	alkali feldspar	38000	3000	EKN-7	Berger and Nielsen (1991)
5	56.61	-89.29	11-PJB-186	Black Duck River	^{14}C (AMS)	wood	50100	3300	ISGS A1995	Dalton et al. (2016)
5	56.61	-89.29	11-PJB-186	Black Duck River	^{14}C (AMS)	wood	49586	949	UOC-0587	Dalton et al. (2016)
5	56.61	-89.29	11-PJB-186	Black Duck River	^{14}C (AMS)	wood	45700	1300	ISGS A1656	Dalton et al. (2016)
5	56.61	-89.29	11-PJB-186	Black Duck River	^{14}C (AMS)	wood	>48000		UOC-0839	Dalton et al. (2016)
6	55.92	-88.32	Beaver River	Beaver River	^{14}C (AMS)	wood	>50 800		ISGS A1658	Dalton et al. (2016)
7	55.43	-88.20	Severn River Marine	Severn River Marine	Luminescence (TL)	polymineral	73000	10000	CTHL2; CTHL3	Forman et al. (1987)
7	55.43	-88.20	Severn River Marine	Severn River Marine	Luminescence (OSL)	quartz	52480	5050	BG3807	Dalton et al. (2016)
7	55.43	-88.20	Severn River Marine	Severn River Marine	Luminescence (OSL)	quartz	42190	4010	BG3808	Dalton et al. (2016)
8	57.346	-95.736	Mountain Rapids	Mountain Rapids	^{14}C (conv)	wood	>32000		GSC-3074	Dredge et al. (1990)
8	57.346	-95.736	112-21-812	Mountain Rapids	^{14}C (AMS)	wood	>50000		UOC-16584	This study
11	56.537	-95.295	115-20-200	-	^{14}C (AMS)	wood	>50000		UOC-13391	This study
12	56.525	-94.122	Limestone	Limestone	Luminescence (TL)	alkali feldspar	119000	18000	EKN-2	Berger and Nielsen (1991)
13	56.512	-94.088	Moondance	Moondance	^{14}C (conv)	wood	>37000		GSC-6011	Roy (1998)
13	56.512	-94.088	13115MT281	Moondance	^{14}C (AMS)	wood	>51200		UCIAMS-184562	This study
13	56.512	-94.088	Moondance	Moondance	Luminescence (IRSL)	alkali feldspar	121000	16000	MOON 2C	Roy (1998)
14	55.997	-93.409	Stupart	Stupart	^{14}C (conv)	wood	>37000		GSC-2481	Dredge et al. (1990)
15	56.378	-92.872	112-19-629	-	Luminescence (OSL)	quartz	146000	20000	112-19-629-024	This study
16	56.173	-92.527	Section 7	Gods River	^{14}C (conv)	wood	>41000		GSC-1736	Netterville (1974)
17	56.157	-92.491	Gods River	Gods River	^{14}C (conv HP)	wood	>49000		GSC-4471HP	Dredge et al. (1990)
18	56.854	-92.054	112-19-613	-	^{14}C (AMS)	wood	>55000		UOC-10976	This study
18	56.854	-92.054	112-19-613	-	^{14}C (AMS)	wood	>55000		UOC-10978	This study
19	55.868	-91.963	112-16-416	Shamattawa	^{14}C (AMS)	wood	>56000		UOC-9641	This study
20	56.043	-91.543	112-16-407	-	Luminescence (OSL)	quartz	166000	12000	112-16-407-019	This study
21	55.838	-91.254	Echoing River	Echoing River	^{14}C (conv)	wood	>37000		GSC-892	Dredge et al. (1990)
21	55.838	-91.254	Echoing River	Echoing River	^{14}C (conv HP)	wood	>51000		GSC-4444HP	Dredge et al. (1990)
23	56.621	-89.262	112-19-605	Black Duck River	Luminescence (OSL)	quartz	150000	22000	112-19-605-004	This study
25	55.22	-88.44	11-PJB-187	-	^{14}C (AMS)	wood	>50400		ISGS A2459	Dalton et al. (2016)
25	55.22	-88.44	11-PJB-187	-	^{14}C (AMS)	wood	>50800		ISGS A1996	Dalton et al. (2016)
4	*57.023*	*-92.637*	*112-20-702*	*Port Nelson*	*^{14}C (AMS)*	*shell*	*49928*	*1040*	*UOC-13465*	*This study*
5	*56.621*	*-89.262*	*112-19-605*	*Black Duck River*	*^{14}C (AMS)*	*shell*	*42658*	*558*	*UOC-10978*	*This study*
6	55.92	-88.32	*Beaver River*	*Beaver River*	^{14}C (conv)	*bulk organics*	*37040*	*1660*	*WAT-1378*	*Wyatt (1990)*
6	55.92	-88.32	*Beaver River*	*Beaver River*	^{14}C (conv)	*bulk organics*	*>38000*		*GSC-4146*	*Wyatt (1990)*
6	55.92	-88.32	*Beaver River*	*Beaver River*	^{14}C (conv)	*bulk organics*	*>51000*		*GSC-4423*	*Wyatt (1990)*
6	55.92	-88.32	*Beaver River*	*Beaver River*	^{14}C (conv)	*bulk organics*	*>43000*		*GSC-4154*	*Dalton et al. (2016)*
6	55.92	-88.32	*Beaver River*	*Beaver River*	^{14}C (conv)	*bulk organics*	*>51000*		*GSC-4423HP*	*Dalton et al. (2016)*
9	*57.434*	*-95.696*	*112-21-807*	*-*	^{14}C (AMS)	*shell*	*46153*	*1150*	*UOC-16662*	*This study*
10	*57.462*	*-95.524*	*112-21-828*	*-*	^{14}C (AMS)	*shell*	*44460*	*853*	*UOC-16663*	*This study*
22	*56.818*	*-90.315*	*112-19-607*	*-*	*^{14}C (AMS)*	*shell*	*>50000*		*UOC-11389*	*This study*
24	*55.399*	*-88.382*	*Severn River*	*Severn River*	^{14}C (conv)	*bulk organics*	*>41000*		*GSC-1011*	*McDonald (1969); Thorleifson et al. (1993)*

* Abbreviations: 14C (conv), radiocabon age determing using conventional counting method; 14C (AMS), radiocarbon age determined using accelerator mass spectrometry; Lumisence (TL), thermoluminescence; Luminescence (OSL), optical stimulated luminescence age; Luminescence (IRSL), infrared stimulated luminescence age

† Radiocarbon ages that that were removed from the dataset during the vetting process are italicized with red text colour. See main text for criteria used.

‡ Radiocarbon ages are provided in uncalibrated ^{14}C yr BP and luminescence ages are given in years

Table Supplemental 2-a: Till fabric ice-flow indicator statistics and interpretations.

Site_ID	Section_ID	Fabric_ID	Easting (UTM Zone 15N)	Northing (UTM Zone 15N)	Latitude	Longitude	Depth_top (m)	Fabric type	Number of clasts measured	V_1 azimuth (degrees)	V_1 dip (degrees)	S_1	S_2	S_3	Interpreted ice-flow (azimuth degrees)	Interpreted ice-flow (direction)
15	112-19-629	W9765	507925	6248129	56.3777	-92.8717	15.1	a-axis	30	348	6	0.67	0.27	0.05	348	NNW
15	112-19-629	112-19-629-X01	507925	6248129	56.3777	-92.8717	15.1	a-axis	38	133	8	0.63	0.30	0.07	313	NW
15	112-19-629	112-19-629-Y01	507925	6248129	56.3777	-92.8717	18.0	a-axis	30	220	9	0.79	0.14	0.07	220	SW
15	112-19-629	W9769	507925	6248129	56.3777	-92.8717	21.0	a-axis	30	314	6	0.63	0.30	0.07	314	NW
15	112-19-629	W9771	507925	6248129	56.3777	-92.8717	23.5	a-axis	30	327	11	0.62	0.26	0.12	327	NNW
20	112-16-407	112-16-407-X01	590752	6211820	56.0430	-91.5432	1.5	a-axis	40	147	16	0.63	0.34	0.03	327	NNW
20	112-16-407	112-16-407-X03	590752	6211820	56.0430	-91.5432	8.6	a-axis	30	145	20	0.66	0.27	0.06	325	NW
20	112-16-407	112-16-407-Y01	590752	6211820	56.0430	-91.5432	10.3	a-axis	30	141	0	0.76	0.13	0.12	321	NW
23	112-19-605	112-19-605-C01	729339	6281395	56.6205	-89.2617	2.7	a-axis	31	273	5	0.76	0.14	0.10	273	W

Table Supplemental 2-b: Till fabric measurement data.

Site_ID	Section_ID	Fabric_ID	a-axis dip direction	a-axis dip	a-axis length	b-axis length	c-axis length	a:b
15	112-19-629	112-19-629-X01	145	17	20	10	3	2.0
15	112-19-629	112-19-629-X01	205	33	25	15	5	1.7
15	112-19-629	112-19-629-X01	15	24	25	12	8	2.1
15	112-19-629	112-19-629-X01	110	3	10	5	4	2.0
15	112-19-629	112-19-629-X01	150	22	12	7	4	1.7
15	112-19-629	112-19-629-X01	165	24	20	8	7	2.5
15	112-19-629	112-19-629-X01	335	33	16	10	5	1.6
15	112-19-629	112-19-629-X01	148	28	20	11	7	1.8
15	112-19-629	112-19-629-X01	172	18	21	14	6	1.5
15	112-19-629	112-19-629-X01	145	20	40	25	11	1.6
15	112-19-629	112-19-629-X01	112	5	20	10	8	2.0
15	112-19-629	112-19-629-X01	130	6	15	10	5	1.5
15	112-19-629	112-19-629-X01	140	5	21	14	9	1.5
15	112-19-629	112-19-629-X01	120	15	30	20	12	1.5
15	112-19-629	112-19-629-X01	131	10	15	8	5	1.9
15	112-19-629	112-19-629-X01	315	5	30	13	10	2.3
15	112-19-629	112-19-629-X01	110	10	10	5	4	2.0
15	112-19-629	112-19-629-X01	128	37	18	12	2	1.5
15	112-19-629	112-19-629-X01	122	30	16	8	6	2.0
15	112-19-629	112-19-629-X01	15	5	28	16	10	1.8
15	112-19-629	112-19-629-X01	180	16	11	6	4	1.8
15	112-19-629	112-19-629-X01	318	16	22	11	6	2.0
15	112-19-629	112-19-629-X01	142	10	8	4	2	2.0
15	112-19-629	112-19-629-X01	252	11	18	10	4	1.8
15	112-19-629	112-19-629-X01	104	4	8	5	5	1.6
15	112-19-629	112-19-629-X01	120	2	17	7	6	2.4
15	112-19-629	112-19-629-X01	168	10	20	9	6	2.2
15	112-19-629	112-19-629-X01	152	14	32	12	8	2.7
15	112-19-629	112-19-629-X01	242	4	15	8	2	1.9
15	112-19-629	112-19-629-X01	270	6	8	3	3	2.7
15	112-19-629	112-19-629-X01	200	22	26	14	12	1.9
15	112-19-629	112-19-629-X01	80	22	14	7	3	2.0
15	112-19-629	112-19-629-X01	300	6	55	25	14	2.2
15	112-19-629	112-19-629-X01	302	20	8	5	2	1.6
15	112-19-629	112-19-629-X01	230	16	37	18	10	2.1
15	112-19-629	112-19-629-X01	222	14	62	35	8	1.8
15	112-19-629	112-19-629-X01	240	16	17	10	7	1.7
15	112-19-629	112-19-629-X01	280	24	17	9	6	1.9
15	112-19-629	112-19-629-Y01	58	22	14	6	4	2.3
15	112-19-629	112-19-629-Y01	62	2	17	6	5	2.8
15	112-19-629	112-19-629-Y01	238	30	6	3	3	2.0
15	112-19-629	112-19-629-Y01	208	2	7	3	2	2.3
15	112-19-629	112-19-629-Y01	232	18	15	7	5	2.1
15	112-19-629	112-19-629-Y01	45	24	14	8	4	1.8
15	112-19-629	112-19-629-Y01	255	32	13	6	5	2.2
15	112-19-629	112-19-629-Y01	85	12	12	5	3	2.4
15	112-19-629	112-19-629-Y01	238	5	6	3	2	2.0
15	112-19-629	112-19-629-Y01	228	42	13	6	6	2.2
15	112-19-629	112-19-629-Y01	222	2	21	6	4	3.5
15	112-19-629	112-19-629-Y01	212	28	4	2	1	2.0
15	112-19-629	112-19-629-Y01	208	30	6	2	2	3.0
15	112-19-629	112-19-629-Y01	212	8	18	6	3	3.0
15	112-19-629	112-19-629-Y01	212	8	12	6	5	2.0
15	112-19-629	112-19-629-Y01	242	8	17	11	3	1.5
15	112-19-629	112-19-629-Y01	220	10	8	4	3	2.0
15	112-19-629	112-19-629-Y01	0	50	9	5	3	1.8
15	112-19-629	112-19-629-Y01	218	16	12	6	2	2.0
15	112-19-629	112-19-629-Y01	216	8	30	20	8	1.5
15	112-19-629	112-19-629-Y01	38	16	35	20	10	1.8
15	112-19-629	112-19-629-Y01	222	28	15	8	6	1.9
15	112-19-629	112-19-629-Y01	28	42	10	6	2	1.7
15	112-19-629	112-19-629-Y01	208	16	11	6	4	1.8

15	112-19-629	112-19-629-Y01	216	6	14	8	6	1.8
15	112-19-629	112-19-629-Y01	196	20	31	15	14	2.1
15	112-19-629	112-19-629-Y01	208	14	10	6	2	1.7
15	112-19-629	112-19-629-Y01	208	36	5	2	2	2.5
15	112-19-629	112-19-629-Y01	2	44	14	8	6	1.8
15	112-19-629	112-19-629-Y01	196	18	8	4	4	2.0
15	112-19-629	W9765[1]	332	36	-	-	-	-
15	112-19-629	W9765[1]	50	5	-	-	-	-
15	112-19-629	W9765[1]	330	15	-	-	-	-
15	112-19-629	W9765[1]	104	21	-	-	-	-
15	112-19-629	W9765[1]	21	6	-	-	-	-
15	112-19-629	W9765[1]	63	19	-	-	-	-
15	112-19-629	W9765[1]	12	21	-	-	-	-
15	112-19-629	W9765[1]	350	26	-	-	-	-
15	112-19-629	W9765[1]	3	2	-	-	-	-
15	112-19-629	W9765[1]	18	16	-	-	-	-
15	112-19-629	W9765[1]	188	7	-	-	-	-
15	112-19-629	W9765[1]	337	1	-	-	-	-
15	112-19-629	W9765[1]	110	16	-	-	-	-
15	112-19-629	W9765[1]	120	13	-	-	-	-
15	112-19-629	W9765[1]	3	9	-	-	-	-
15	112-19-629	W9765[1]	356	4	-	-	-	-
15	112-19-629	W9765[1]	325	6	-	-	-	-
15	112-19-629	W9765[1]	162	10	-	-	-	-
15	112-19-629	W9765[1]	166	10	-	-	-	-
15	112-19-629	W9765[1]	244	9	-	-	-	-
15	112-19-629	W9765[1]	10	1	-	-	-	-
15	112-19-629	W9765[1]	312	38	-	-	-	-
15	112-19-629	W9765[1]	11	10	-	-	-	-
15	112-19-629	W9765[1]	294	4	-	-	-	-
15	112-19-629	W9765[1]	310	15	-	-	-	-
15	112-19-629	W9765[1]	13	10	-	-	-	-
15	112-19-629	W9765[1]	143	8	-	-	-	-
15	112-19-629	W9765[1]	129	11	-	-	-	-
15	112-19-629	W9765[1]	167	12	-	-	-	-
15	112-19-629	W9765[1]	5	7	-	-	-	-
15	112-19-629	W9769[1]	120	8	-	-	-	-
15	112-19-629	W9769[1]	297	18	-	-	-	-
15	112-19-629	W9769[1]	353	6	-	-	-	-
15	112-19-629	W9769[1]	297	15	-	-	-	-
15	112-19-629	W9769[1]	101	20	-	-	-	-
15	112-19-629	W9769[1]	110	9	-	-	-	-
15	112-19-629	W9769[1]	141	10	-	-	-	-
15	112-19-629	W9769[1]	305	16	-	-	-	-
15	112-19-629	W9769[1]	357	23	-	-	-	-
15	112-19-629	W9769[1]	171	1	-	-	-	-
15	112-19-629	W9769[1]	104	21	-	-	-	-
15	112-19-629	W9769[1]	116	9	-	-	-	-
15	112-19-629	W9769[1]	340	19	-	-	-	-
15	112-19-629	W9769[1]	160	2	-	-	-	-
15	112-19-629	W9769[1]	91	7	-	-	-	-
15	112-19-629	W9769[1]	109	25	-	-	-	-
15	112-19-629	W9769[1]	212	28	-	-	-	-
15	112-19-629	W9769[1]	310	26	-	-	-	-
15	112-19-629	W9769[1]	267	18	-	-	-	-
15	112-19-629	W9769[1]	36	26	-	-	-	-
15	112-19-629	W9769[1]	330	14	-	-	-	-
15	112-19-629	W9769[1]	45	22	-	-	-	-
15	112-19-629	W9769[1]	344	15	-	-	-	-
15	112-19-629	W9769[1]	327	10	-	-	-	-
15	112-19-629	W9769[1]	322	41	-	-	-	-

15	112-19-629	W9769[1]	74	22	-	-	-	-
15	112-19-629	W9769[1]	316	1	-	-	-	-
15	112-19-629	W9769[1]	312	18	-	-	-	-
15	112-19-629	W9769[1]	5	2	-	-	-	-
15	112-19-629	W9769[1]	226	7	-	-	-	-
15	112-19-629	W9771[1]	220	27	-	-	-	-
15	112-19-629	W9771[1]	355	1	-	-	-	-
15	112-19-629	W9771[1]	201	25	-	-	-	-
15	112-19-629	W9771[1]	332	37	-	-	-	-
15	112-19-629	W9771[1]	352	2	-	-	-	-
15	112-19-629	W9771[1]	333	40	-	-	-	-
15	112-19-629	W9771[1]	351	25	-	-	-	-
15	112-19-629	W9771[1]	109	10	-	-	-	-
15	112-19-629	W9771[1]	303	22	-	-	-	-
15	112-19-629	W9771[1]	340	16	-	-	-	-
15	112-19-629	W9771[1]	326	11	-	-	-	-
15	112-19-629	W9771[1]	256	3	-	-	-	-
15	112-19-629	W9771[1]	333	22	-	-	-	-
15	112-19-629	W9771[1]	243	40	-	-	-	-
15	112-19-629	W9771[1]	311	22	-	-	-	-
15	112-19-629	W9771[1]	268	1	-	-	-	-
15	112-19-629	W9771[1]	15	21	-	-	-	-
15	112-19-629	W9771[1]	297	25	-	-	-	-
15	112-19-629	W9771[1]	162	18	-	-	-	-
15	112-19-629	W9771[1]	122	25	-	-	-	-
15	112-19-629	W9771[1]	148	18	-	-	-	-
15	112-19-629	W9771[1]	141	33	-	-	-	-
15	112-19-629	W9771[1]	291	9	-	-	-	-
15	112-19-629	W9771[1]	338	9	-	-	-	-
15	112-19-629	W9771[1]	92	11	-	-	-	-
15	112-19-629	W9771[1]	329	10	-	-	-	-
15	112-19-629	W9771[1]	2	1	-	-	-	-
15	112-19-629	W9771[1]	47	32	-	-	-	-
15	112-19-629	W9771[1]	348	37	-	-	-	-
15	112-19-629	W9771[1]	311	19	-	-	-	-
20	112-16-407	112-16-407-Y01	335	25	1.2	0.6	0.2	2.0
20	112-16-407	112-16-407-Y01	302	12	1.1	0.5	0.2	2.2
20	112-16-407	112-16-407-Y01	336	17	1.3	0.8	0.3	1.6
20	112-16-407	112-16-407-Y01	342	38	1.5	0.9	0.8	1.7
20	112-16-407	112-16-407-Y01	136	8	1.2	0.8	0.5	1.5
20	112-16-407	112-16-407-Y01	319	12	2.5	1	0.9	2.5
20	112-16-407	112-16-407-Y01	309	42	2	1.2	0.9	1.7
20	112-16-407	112-16-407-Y01	314	17	0.7	0.4	0.3	1.8
20	112-16-407	112-16-407-Y01	325	9	1.8	1.2	1	1.5
20	112-16-407	112-16-407-Y01	89	10	0.8	0.4	0.3	2.0
20	112-16-407	112-16-407-Y01	325	15	1.5	1	0.9	1.5
20	112-16-407	112-16-407-Y01	314	42	3	1.8	1.2	1.7
20	112-16-407	112-16-407-Y01	144	27	0.8	0.4	0.4	2.0
20	112-16-407	112-16-407-Y01	133	12	1.2	0.8	0.3	1.5
20	112-16-407	112-16-407-Y01	132	24	0.7	0.3	0.2	2.3
20	112-16-407	112-16-407-Y01	145	24	1.2	0.6	0.4	2.0
20	112-16-407	112-16-407-Y01	135	9	1.1	0.5	0.3	2.2
20	112-16-407	112-16-407-Y01	96	2	1.9	1.1	0.9	1.7
20	112-16-407	112-16-407-Y01	143	12	1.2	0.7	0.2	1.7
20	112-16-407	112-16-407-Y01	98	6	0.5	0.2	0.1	2.5
20	112-16-407	112-16-407-Y01	342	28	1.5	0.9	0.7	1.7
20	112-16-407	112-16-407-Y01	326	22	1	0.5	0.3	2.0
20	112-16-407	112-16-407-Y01	168	12	1	0.4	0.2	2.5
20	112-16-407	112-16-407-Y01	184	14	0.8	0.4	0.4	2.0
20	112-16-407	112-16-407-Y01	158	16	2.5	1.2	1	2.1
20	112-16-407	112-16-407-Y01	142	10	1	0.6	0.5	1.7
20	112-16-407	112-16-407-Y01	120	19	1	0.6	0.4	1.7

20	112-16-407	112-16-407-Y01	118	14	1.2	0.6	0.5	2.0
20	112-16-407	112-16-407-Y01	175	34	0.8	0.4	0.4	2.0
20	112-16-407	112-16-407-Y01	170	25	0.8	0.5	0.4	1.6
20	112-16-407	112-16-407-X01	298	8	9.0	4	3	2.3
20	112-16-407	112-16-407-X01	152	28	3.2	1.5	1	2.1
20	112-16-407	112-16-407-X01	248	10	4.5	2.9	2.2	1.6
20	112-16-407	112-16-407-X01	245	10	1.8	1	0.7	1.8
20	112-16-407	112-16-407-X01	107	14	1.7	0.9	0.4	1.9
20	112-16-407	112-16-407-X01	152	19	2.2	1.4	1	1.6
20	112-16-407	112-16-407-X01	80	14	3.9	2	1	2.0
20	112-16-407	112-16-407-X01	135	4	2	1.1	1	1.8
20	112-16-407	112-16-407-X01	116	12	1.5	1	0.3	1.5
20	112-16-407	112-16-407-X01	184	20	1.9	0.9	0.7	2.1
20	112-16-407	112-16-407-X01	232	4	1	0.5	0.3	2.0
20	112-16-407	112-16-407-X01	236	14	4.8	2.8	1.8	1.7
20	112-16-407	112-16-407-X01	170	18	1.2	0.6	0.6	2.0
20	112-16-407	112-16-407-X01	64	2	0.9	0.5	0.2	1.8
20	112-16-407	112-16-407-X01	204	25	1	0.6	0.4	1.7
20	112-16-407	112-16-407-X01	322	3	1.2	0.7	0.3	1.7
20	112-16-407	112-16-407-X01	194	24	1.3	0.7	0.3	1.9
20	112-16-407	112-16-407-X01	158	6	2.3	1.3	1.3	1.8
20	112-16-407	112-16-407-X01	140	19	1.4	0.7	0.4	2.0
20	112-16-407	112-16-407-X01	270	6	1.3	0.8	0.3	1.6
20	112-16-407	112-16-407-X01	116	4	2	1.2	0.9	1.7
20	112-16-407	112-16-407-X01	150	10	0.8	0.4	0.3	2.0
20	112-16-407	112-16-407-X01	109	20	1.8	1.2	1.2	1.5
20	112-16-407	112-16-407-X01	165	16	1.5	0.9	0.4	1.7
20	112-16-407	112-16-407-X01	100	6	1	0.6	0.4	1.7
20	112-16-407	112-16-407-X01	107	20	1.3	0.3	0.3	4.3
20	112-16-407	112-16-407-X01	175	28	1.2	0.6	0.2	2.0
20	112-16-407	112-16-407-X01	160	14	1.5	1	0.6	1.5
20	112-16-407	112-16-407-X01	178	12	1	0.5	0.3	2.0
20	112-16-407	112-16-407-X01	124	8	1.3	0.6	0.6	2.2
20	112-16-407	112-16-407-X01	188	8	1	0.5	0.3	2.0
20	112-16-407	112-16-407-X01	148	32	1.7	0.9	0.3	1.9
20	112-16-407	112-16-407-X01	102	18	1.7	0.9	0.9	1.9
20	112-16-407	112-16-407-X01	186	10	1	0.5	0.2	2.0
20	112-16-407	112-16-407-X01	189	22	2	0.9	0.7	2.2
20	112-16-407	112-16-407-X01	158	6	1.4	0.9	0.4	1.6
20	112-16-407	112-16-407-X01	184	25	1	0.5	0.4	2.0
20	112-16-407	112-16-407-X01	312	12	1.4	0.9	0.3	1.6
20	112-16-407	112-16-407-X01	178	22	2.4	1	0.6	2.4
20	112-16-407	112-16-407-X01	130	22	1.4	0.9	0.7	1.6
20	112-16-407	112-16-407-X03	158	40	4.7	2.4	1.3	2.0
20	112-16-407	112-16-407-X03	174	35	3	1.7	1.2	1.8
20	112-16-407	112-16-407-X03	94	22	3.7	2.3	1.5	1.6
20	112-16-407	112-16-407-X03	184	14	2.6	1.2	0.8	2.2
20	112-16-407	112-16-407-X03	186	24	1.0	0.6	0.4	1.7
20	112-16-407	112-16-407-X03	132	42	1.8	1.1	0.9	1.6
20	112-16-407	112-16-407-X03	122	29	3	2	1.5	1.5
20	112-16-407	112-16-407-X03	152	28	5.4	3.6	1.6	1.5
20	112-16-407	112-16-407-X03	152	18	3	1.4	1.4	2.1
20	112-16-407	112-16-407-X03	168	26	3.1	1.5	1.3	2.1
20	112-16-407	112-16-407-X03	110	28	3.3	1.6	1.5	2.1
20	112-16-407	112-16-407-X03	172	10	2.5	1.5	1.3	1.7
20	112-16-407	112-16-407-X03	119	24	2	1.3	0.9	1.5
20	112-16-407	112-16-407-X03	170	12	5.5	3	1.9	1.8
20	112-16-407	112-16-407-X03	5	6	2.7	1.1	1.1	2.5
20	112-16-407	112-16-407-X03	10	20	2.3	1	0.8	2.3
20	112-16-407	112-16-407-X03	171	16	1.1	0.7	0.4	1.6
20	112-16-407	112-16-407-X03	130	22	1.5	0.6	0.4	2.5
20	112-16-407	112-16-407-X03	320	18	0.9	0.4	0.2	2.3
20	112-16-407	112-16-407-X03	250	18	4	2.2	1.3	1.8
20	112-16-407	112-16-407-X03	114	8	1	0.4	0.4	2.5

20	112-16-407	112-16-407-X03	80	16	1	0.6	0.6	1.7
20	112-16-407	112-16-407-X03	165	4	1.4	0.9	0.3	1.6
20	112-16-407	112-16-407-X03	84	10	1	0.6	0.5	1.7
20	112-16-407	112-16-407-X03	132	14	1.5	0.7	0.6	2.1
20	112-16-407	112-16-407-X03	74	22	1.2	0.7	0.5	1.7
20	112-16-407	112-16-407-X03	120	18	1.6	1	0.5	1.6
20	112-16-407	112-16-407-X03	170	16	1.9	1	0.5	1.9
20	112-16-407	112-16-407-X03	106	28	0.9	0.6	0.3	1.5
20	112-16-407	112-16-407-X03	355	22	2.5	1.5	0.9	1.7
23	112-19-605	112-19-605-C01	272	22	1.4	0.9	0.4	1.6
23	112-19-605	112-19-605-C01	74	14	1.5	0.7	0.7	2.1
23	112-19-605	112-19-605-C01	250	22	2.8	1.8	1.7	1.6
23	112-19-605	112-19-605-C01	96	8	1.0	0.4	0.3	2.5
23	112-19-605	112-19-605-C01	262	2	1.7	0.9	0.3	1.9
23	112-19-605	112-19-605-C01	274	38	0.6	0.3	0.3	2.0
23	112-19-605	112-19-605-C01	96	12	1.0	0.4	0.4	2.5
23	112-19-605	112-19-605-C01	90	14	1.1	0.7	0.2	1.6
23	112-19-605	112-19-605-C01	234	20	0.7	0.3	0.1	2.3
23	112-19-605	112-19-605-C01	262	55	0.7	0.4	0.4	1.8
23	112-19-605	112-19-605-C01	290	30	1.9	1.2	0.9	1.6
23	112-19-605	112-19-605-C01	288	8	1.8	1.1	0.7	1.6
23	112-19-605	112-19-605-C01	290	12	2.6	1.6	1.5	1.6
23	112-19-605	112-19-605-C01	276	20	1.2	0.7	0.6	1.7
23	112-19-605	112-19-605-C01	118	16	3.1	1.8	0.8	1.7
23	112-19-605	112-19-605-C01	140	6	3.3	2.0	0.7	1.7
23	112-19-605	112-19-605-C01	108	32	0.8	0.4	0.2	2.0
23	112-19-605	112-19-605-C01	92	4	0.9	0.6	0.4	1.5
23	112-19-605	112-19-605-C01	230	25	0.7	0.3	0.2	2.3
23	112-19-605	112-19-605-C01	76	2	0.6	0.3	0.3	2.0
23	112-19-605	112-19-605-C01	276	12	1.6	1.0	0.5	1.6
23	112-19-605	112-19-605-C01	308	30	0.9	0.4	0.3	2.3
23	112-19-605	112-19-605-C01	246	8	1.2	0.7	0.4	1.7
23	112-19-605	112-19-605-C01	82	10	0.9	0.3	0.2	3.0
23	112-19-605	112-19-605-C01	118	6	1.1	0.6	0.4	1.8
23	112-19-605	112-19-605-C01	108	8	2.7	1.6	1.5	1.7
23	112-19-605	112-19-605-C01	310	22	2.0	1.0	0.5	2.0
23	112-19-605	112-19-605-C01	124	12	0.9	0.5	0.4	1.8
23	112-19-605	112-19-605-C01	84	14	0.9	0.5	0.3	1.8
23	112-19-605	112-19-605-C01	242	4	1.2	0.6	0.3	2.0
23	112-19-605	112-19-605-C01	34	6	0.6	0.4	0.1	1.5

1. This fabric measurement is from a legacy dataset. The authors gathering these measurments stated that they only measured clasts with an a:b axis ratio >1.5, but they did not record these observations.

Supplemental 3: Till compositional data analysis for site 3 and 4 in the Lower Nelson River area to support till stratigraphy correlations.

The till-matrix (<63 µm size-fraction) geochemistry was determined by total digestion (lithium metaborate/tetraborate fusion) and ICP-MS and ICP-OES analysis (Hodder and Gauthier, 2021). The major elements (Al, K, Fe, Ti, Mn, Na, Si, Ca, Mg) from this dataset were then transformed using a centred log ratio (CLR) transformation and analysed using principal component analysis (Figure Supplemental 3-a). Till samples are classified according to their stratigraphic section and interpreted stratigraphic bed that they were collected from. The first principal components account for 52.4% of the variance within the dataset and best describes the compositional difference between Bed B and D (Figure Supplemental 3-a). Positive PC1 values are associated with Bed B and are defined by elements Ca and Mg, which are most prevalent in local carbonate bearing rocks of the Hudson Bay Basin. Negative PC1 values are associated with Bed D and are defined by Al, Fe, Ti and K, elements most commonly associated with igneous sources rocks that were transported into the region from the Precambrian shield. This interpretation is supported by the till clast-lithology data, where Bed D and Bed E have higher proportions of Precambrian clasts (Figure Supplemental 3-b). Bed B has a significantly higher proportion of sand in the matrix compared to beds D and E (Figure Supplemental 3-c). This compositional analysis supports the correlation of Bed B and Bed D between sites 3 and 4, which reinforces that uppermost intertill nonglacial sediments (Bed C) are missing from site 4.

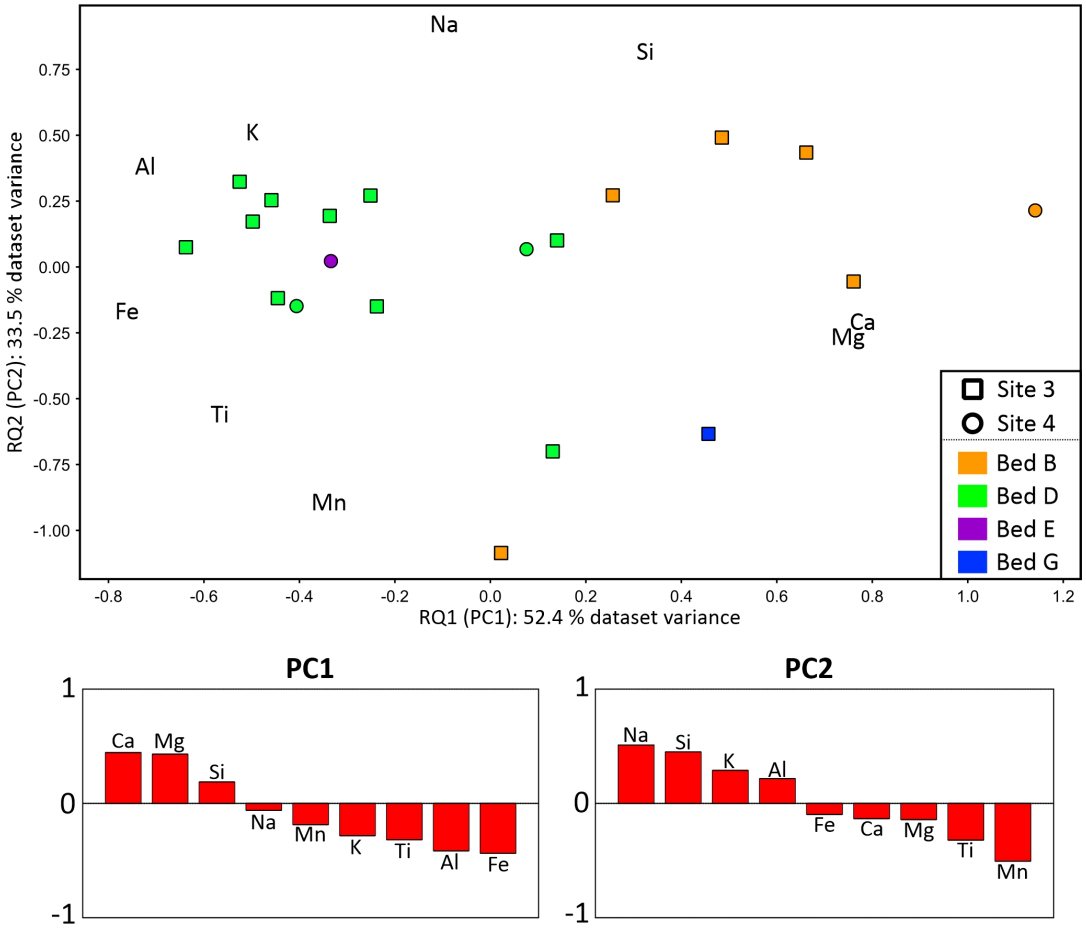

Figure Supplemental 3-a: *Scatterplot of PC2 vs. PC1 and elemental loadings for till samples from site 3 and 4.*

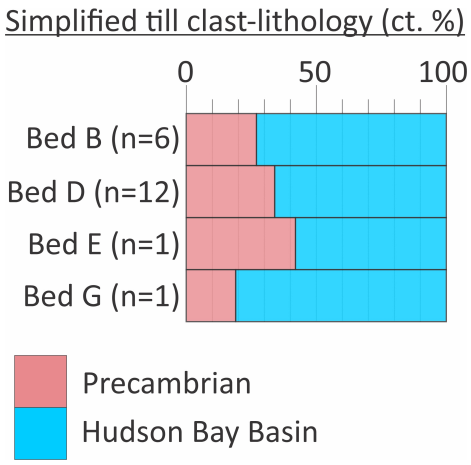

Figure Supplemental 3-b: *Average values for the proportion of Precambrian and Hudson Bay Basin clasts in each interpreted till unit. An average of 398 clasts in the 2–8 mm size-fraction were counted for each till sample.*

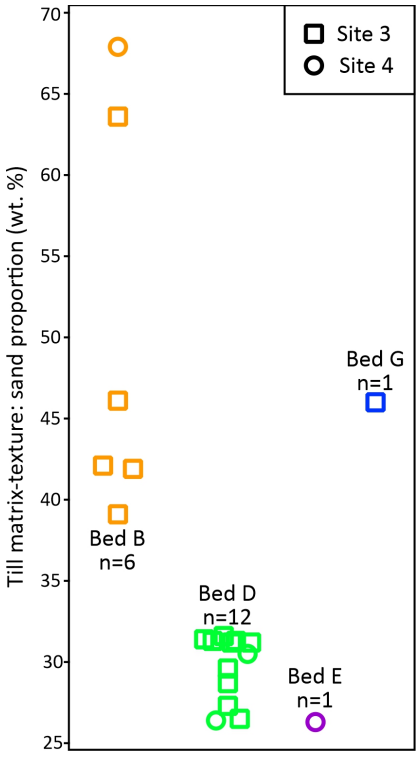

Figure Supplemental 3-c: *Proportion of sand in the till-matrix of each interpreted till unit.*

References:

Hodder, T.J., Gauthier, M.S. 2021. Till-matrix geochemistry data, Machichi–Kettle rivers area, far northeastern Manitoba (parts of NTS 54A–C). Manitoba Agriculture and Resource Development, Manitoba Geological Survey, Data Repository Item DRI2021007, Microsoft® Excel® file.

Appendix B

Supplemental materials for Chapter 3

Chapter 3 supplemental material is published in Hodder et al. (2024).

Supplemental material 1: Additional key Quaternary sections in the Kaskattama highland area.

Supplemental material 2: Detrital hornblende $^{40}Ar/^{39}Ar$ age dataset.

Supplemental material 3: Till-matrix geochemistry levelling and outlier analysis.

Supplemental material 4: Biplot of PC2 vs. PC1. Samples have been coloured according to the stratigraphic unit they were sampled from. Surficial and subsurface (section) samples are differentiated by shape.

Supplemental material 1: Additional Quaternary stratigraphic columns of sections in the Kaskattama highland area.

Figure SA1: Cross-section of the Quaternary stratigraphy in the Echoing River area.

Figure SA2: Quaternary stratigraphic column and photos for section 112-16-416 / 112-17-505 (composite).

Figure SA3: Quaternary stratigraphic column and photos for section 112-16-407.

Figure SA4: Quaternary stratigraphic column and photos for section 112-17-519.

Figure SA5: Quaternary stratigraphic column and photos for section 112-17-542.

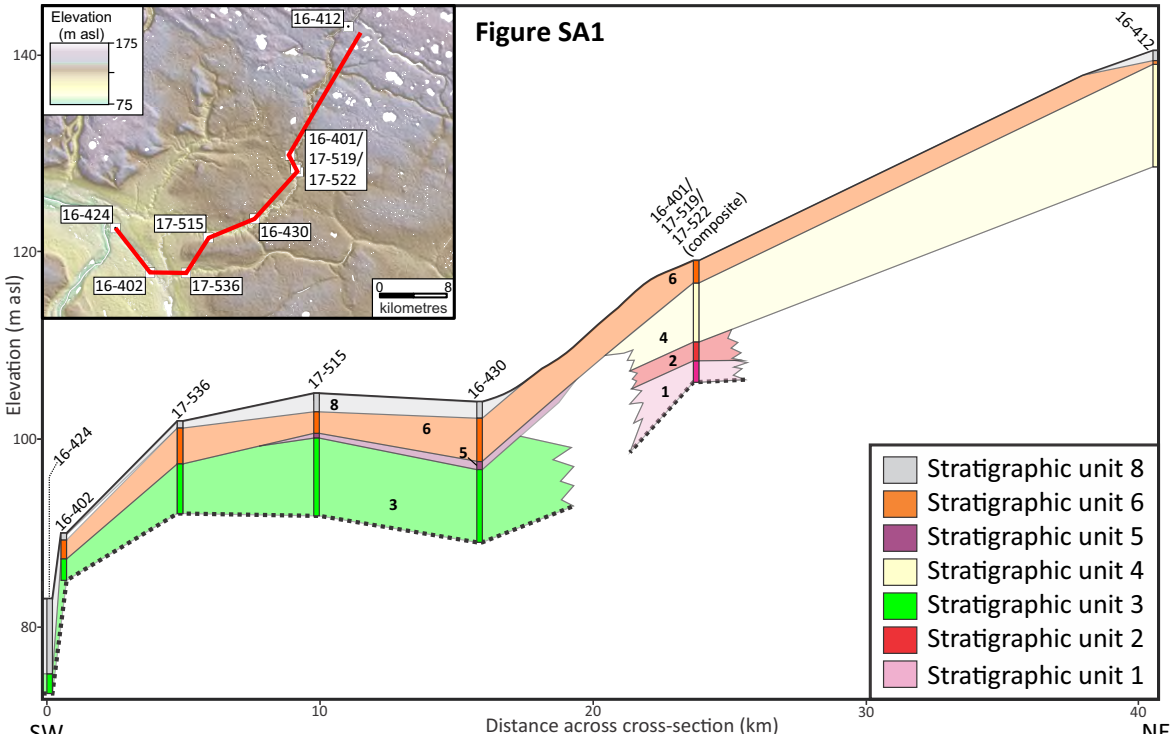
Figure SA1
Elevation (m asl)
175
75
16-412
16-401/
17-519/
17-522
16-424
17-515
16-430
16-402
17-536
0
8
kilometres
16-401/
17-519/
17-522
(composite)
16-412
16-424
16-402
17-536
17-515
16-430
6
4
2
1
8
6
5
3
Elevation (m asl)
140
120
100
80
0
10
20
30
40
Distance across cross-section (km)
SW
NE
Stratigraphic unit 8
Stratigraphic unit 6
Stratigraphic unit 5
Stratigraphic unit 4
Stratigraphic unit 3
Stratigraphic unit 2
Stratigraphic unit 1

Figure SA2

Ice-flow data

Unit 7 fabric
[5.2 m depth]

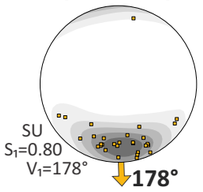

Unit 4 fabric
[12.5 m depth]

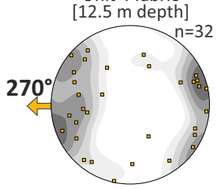

SU; S_1=0.56; V_1=270°

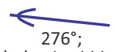

276°;
lodged cobble;
19.0 m depth

Unit 4 fabric
[30.5 m depth]

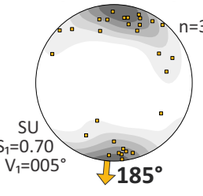

Stratigraphic unit [thickness]

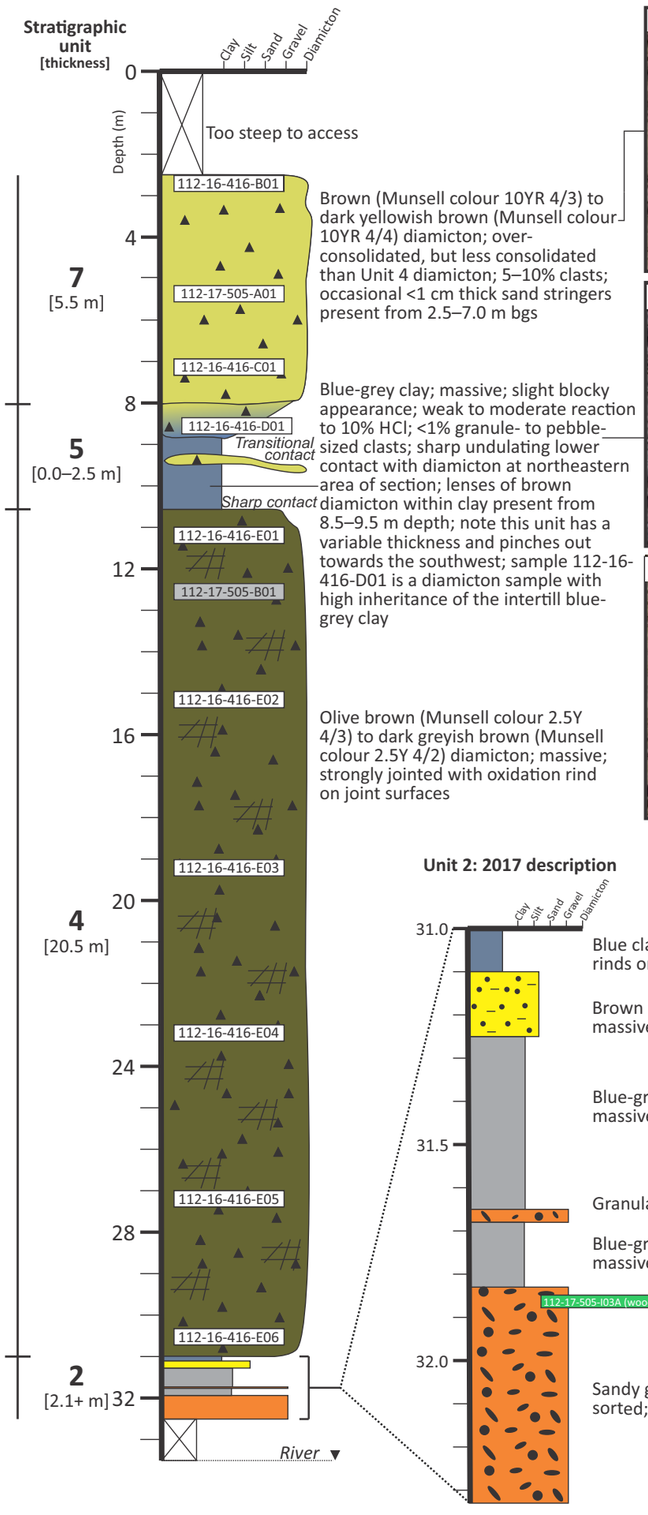

Brown (Munsell colour 10YR 4/3) to dark yellowish brown (Munsell colour 10YR 4/4) diamicton; over-consolidated, but less consolidated than Unit 4 diamicton; 5–10% clasts; occasional <1 cm thick sand stringers present from 2.5–7.0 m bgs

Blue-grey clay; massive; slight blocky appearance; weak to moderate reaction to 10% HCl; <1% granule- to pebble-sized clasts; sharp undulating lower contact with diamicton at northeastern area of section; lenses of brown diamicton within clay present from 8.5–9.5 m depth; note this unit has a variable thickness and pinches out towards the southwest; sample 112-16-416-D01 is a diamicton sample with high inheritance of the intertill blue-grey clay

Olive brown (Munsell colour 2.5Y 4/3) to dark greyish brown (Munsell colour 2.5Y 4/2) diamicton; massive; strongly jointed with oxidation rind on joint surfaces





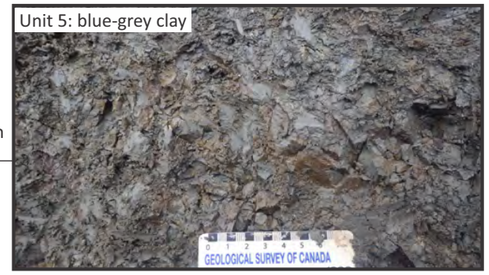



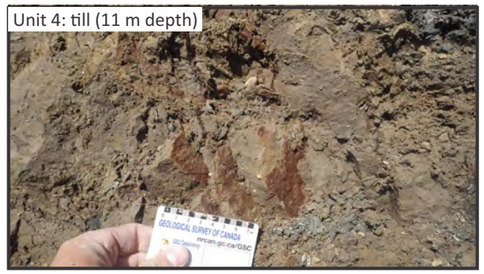



Section 112-16-416 / 112-17-505 (composite)
Unnamed tributary of the Echoing River
Elevation (top): 114 m asl
NAD83 UTM 15N: 6191871N, 564895E

Simplified till clast-lithology (ct. %)

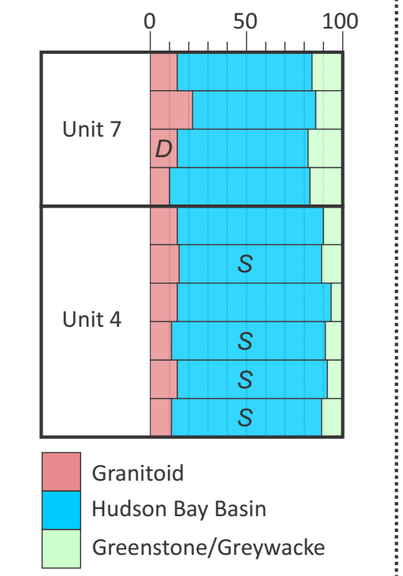

Unit 2: 2017 description

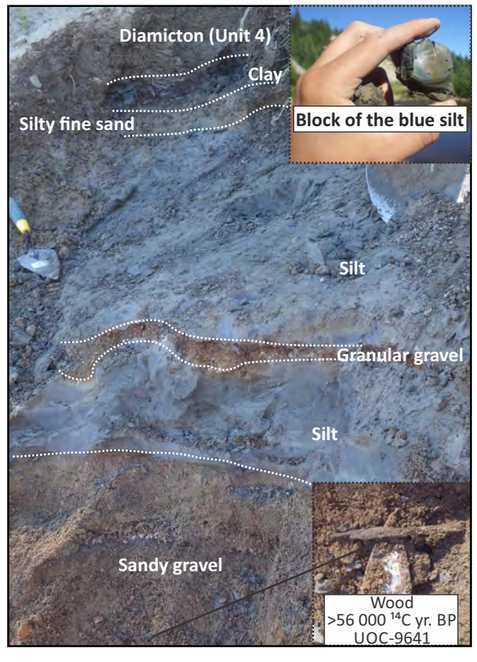

Unit 2: 2019 description and pollen sampling

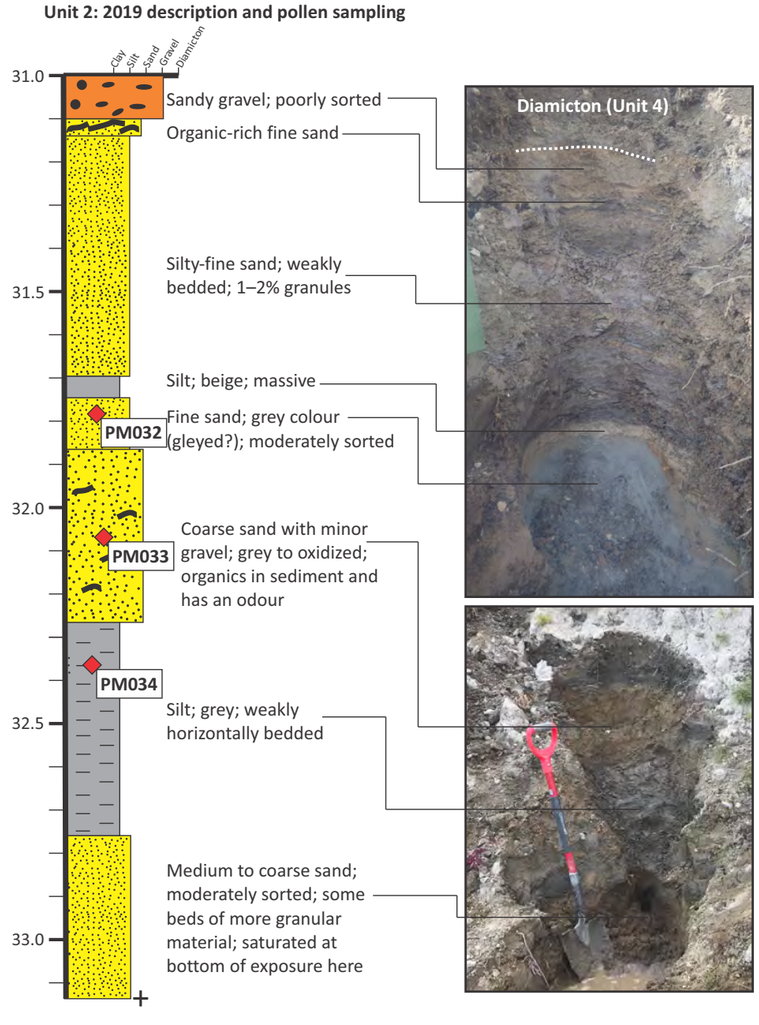

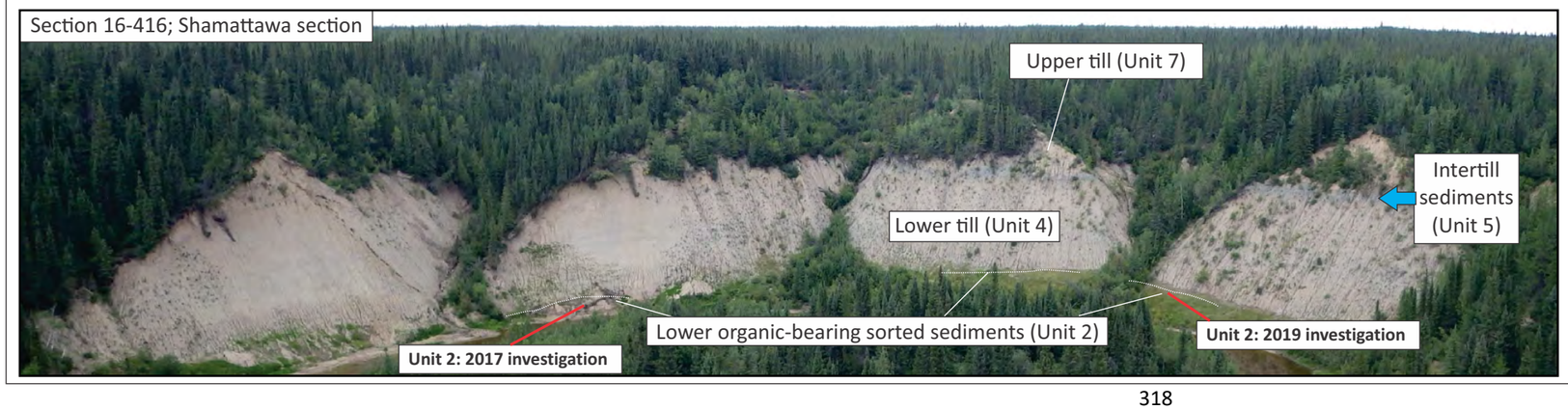

Figure SA3

Section 112-16-407
Edge of a meltwater corridor
Elevation (top): 168 m asl
UTM Zone 15, NAD83: 590752E, 6211820N

Ice-flow data

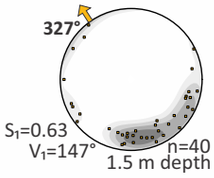

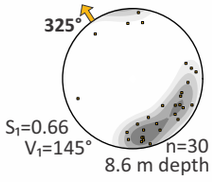

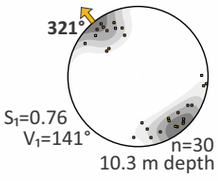

Interpretation

Lake Agassiz (postglacial)

Till (glaciation)

Till (glacial advance)

Cross-bedded sands (nonglacial)

Stratigraphic Unit [thickness]

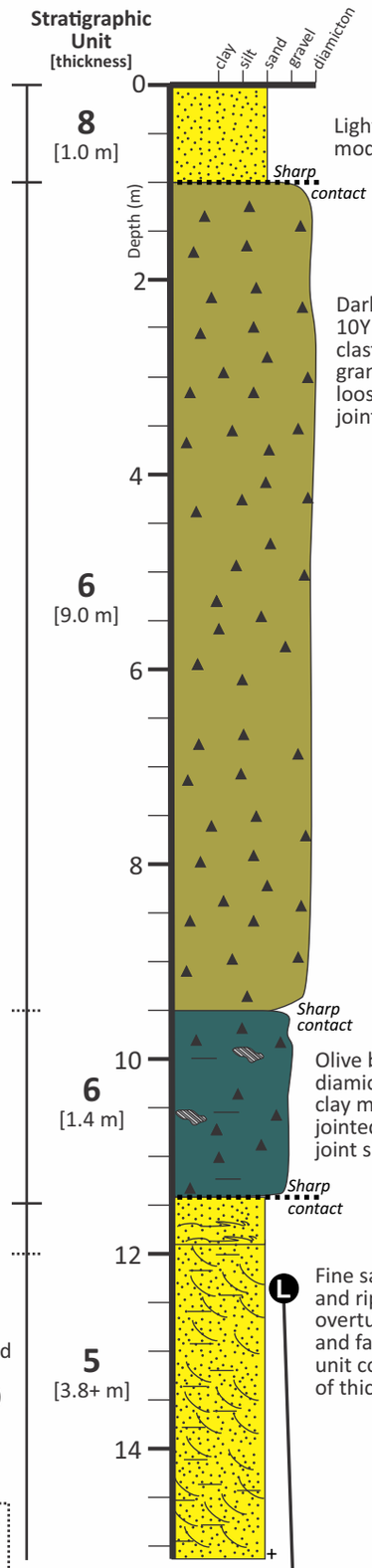

Light brown medium sand; moderately- to well-sorted; massive

Dark yellowish brown (Munsell colour 10YR 4/4) diamicton; massive; 10% clasts; sandy clayey-silt matrix; granule- to large pebble-sized clasts; loose and not compact; becomes jointed at 8.2 m depth

Olive brown (Munsell colour 2.5Y 4/3) diamicton; massive; 10% clasts, silty-clay matrix; clay-rich mud rip-up clasts; jointed with minor oxidation rinds on joint surfaces

Fine sand; well sorted; cross-bedded and ripple cross-laminated; overturned beds, convolute bedding and faulting within upper 1 m of unit; unit continues past 15.2 m bgs; ~4 m of thick colluvium to base of gully

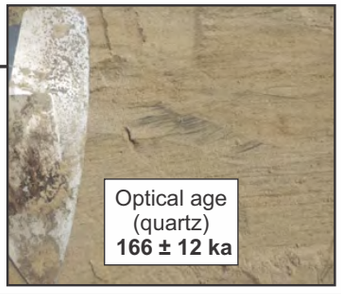

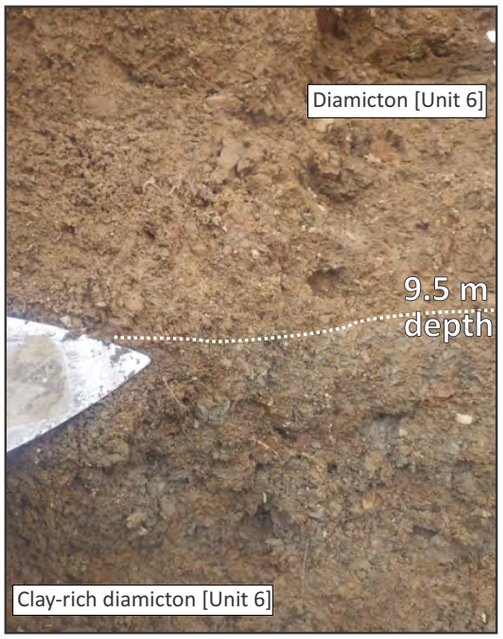

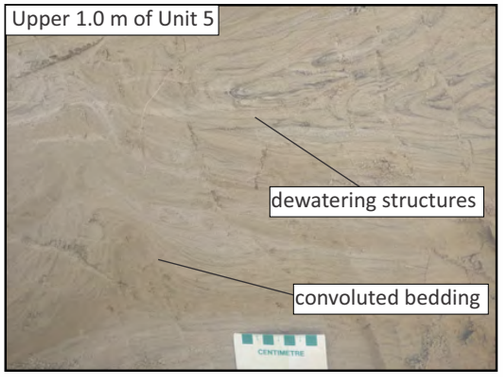

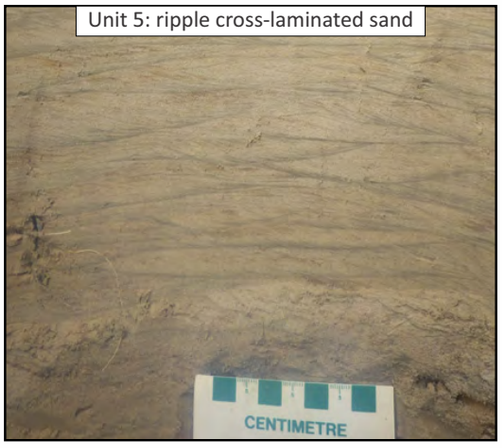

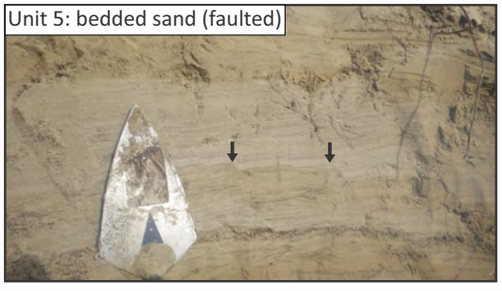

Simplified till clast-lithology (ct. %)

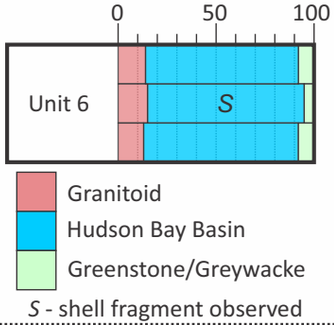

Figure SA4

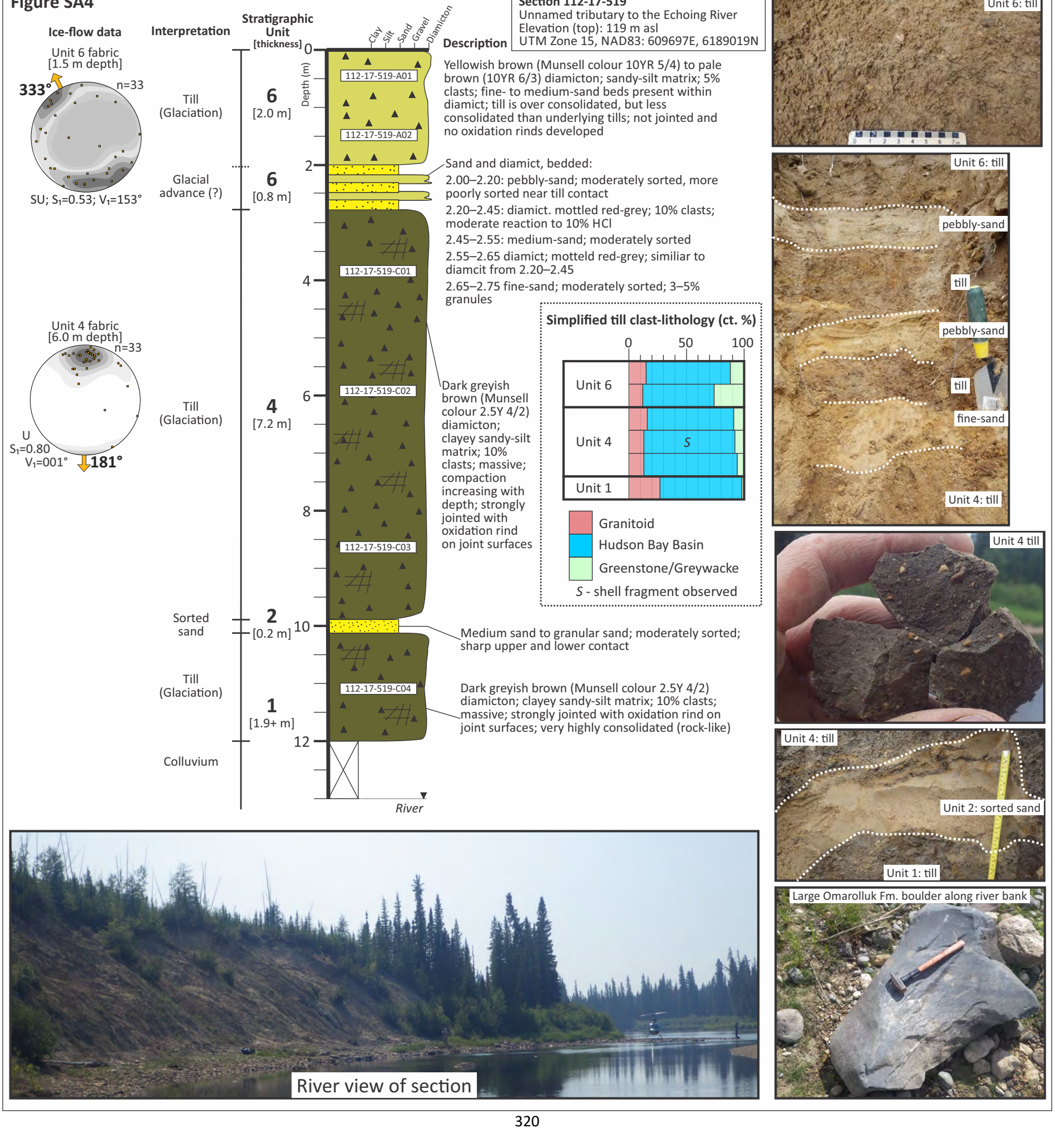
Ice-flow data
Interpretation
Stratigraphic Unit [thickness]
Description
Clay
Silt
Sand
Gravel
Diamicton
Depth (m)
Section 112-17-519
Unnamed tributary to the Echoing River
Elevation (top): 119 m asl
UTM Zone 15, NAD83: 609697E, 6189019N
Unit 6 fabric [1.5 m depth]
333°
n=33
SU; S1=0.53; V1=153°
Till (Glaciation)
6 [2.0 m]
112-17-519-A01
112-17-519-A02
Yellowish brown (Munsell colour 10YR 5/4) to pale brown (10YR 6/3) diamicton; sandy-silt matrix; 5% clasts; fine- to medium-sand beds present within diamict; till is over consolidated, but less consolidated than underlying tills; not jointed and no oxidation rinds developed
Glacial advance (?)
6 [0.8 m]
Sand and diamict, bedded:
2.00–2.20: pebbly-sand; moderately sorted, more poorly sorted near till contact
2.20–2.45: diamict. mottled red-grey; 10% clasts; moderate reaction to 10% HCl
2.45–2.55: medium-sand; moderately sorted
2.55–2.65 diamict; motteld red-grey; similiar to diamcit from 2.20–2.45
2.65–2.75 fine-sand; moderately sorted; 3–5% granules
Unit 4 fabric [6.0 m depth]
n=33
U
S1=0.80
V1=001°
181°
Till (Glaciation)
4 [7.2 m]
112-17-519-C01
112-17-519-C02
Dark greyish brown (Munsell colour 2.5Y 4/2) diamicton; clayey sandy-silt matrix; 10% clasts; massive; compaction increasing with depth; strongly jointed with oxidation rind on joint surfaces
112-17-519-C03
Simplified till clast-lithology (ct. %)
0
50
100
Unit 6
Unit 4
Unit 1
S
Granitoid
Hudson Bay Basin
Greenstone/Greywacke
S - shell fragment observed
Sorted sand
2 [0.2 m]
Medium sand to granular sand; moderately sorted; sharp upper and lower contact
Till (Glaciation)
1 [1.9+ m]
112-17-519-C04
Dark greyish brown (Munsell colour 2.5Y 4/2) diamicton; clayey sandy-silt matrix; 10% clasts; massive; strongly jointed with oxidation rind on joint surfaces; very highly consolidated (rock-like)
Colluvium
River
Unit 6: till
Unit 6: till
pebbly-sand
till
pebbly-sand
till
fine-sand
Unit 4: till
Unit 4 till
Unit 4: till
Unit 2: sorted sand
Unit 1: till
Large Omarolluk Fm. boulder along river bank
River view of section

Figure SA5

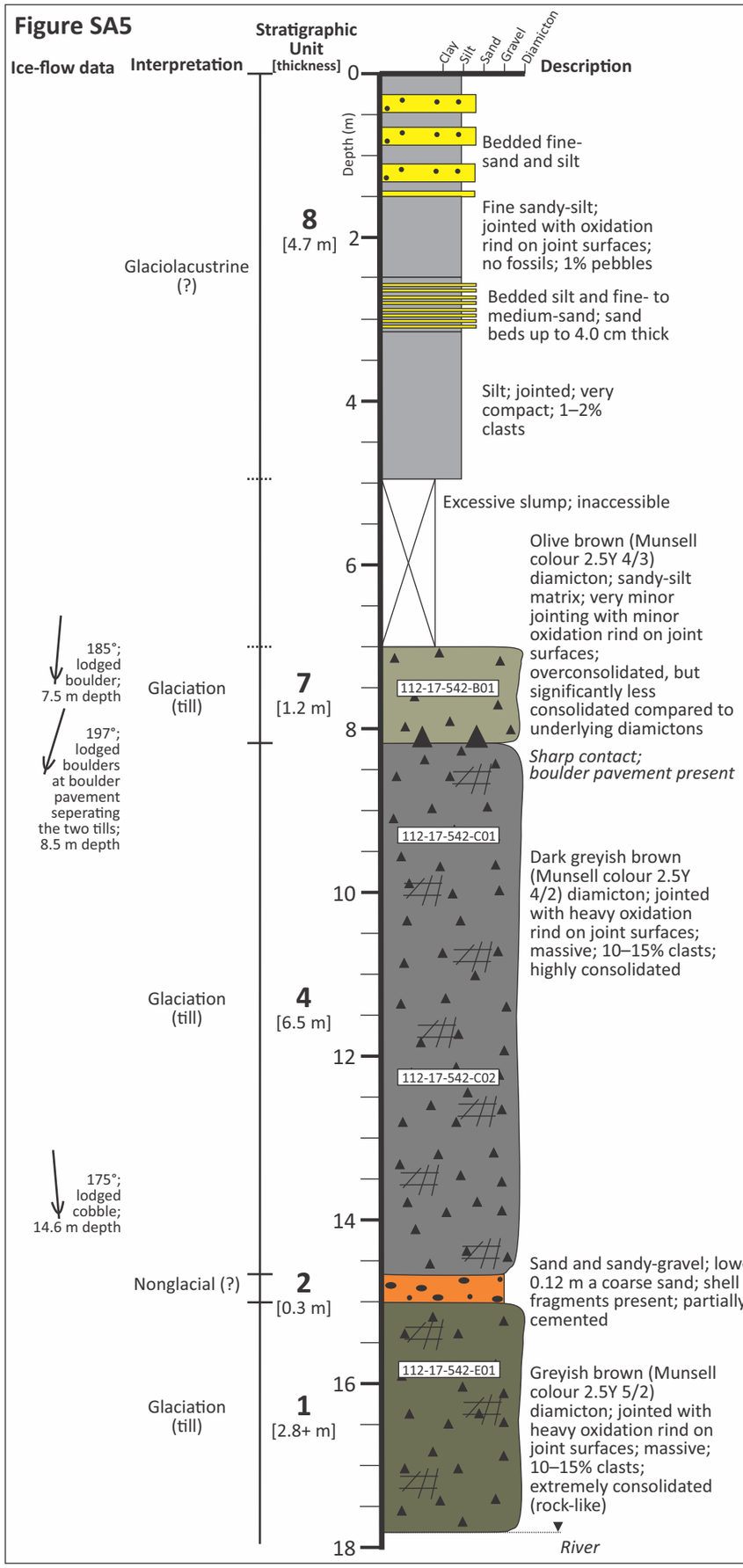









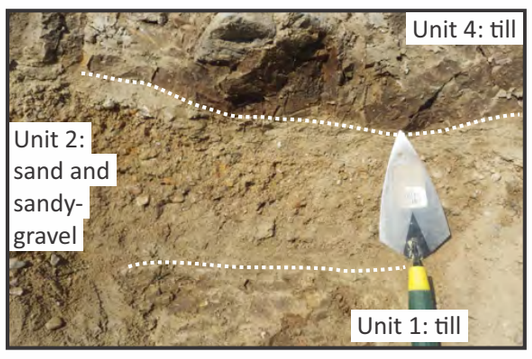

Section 112-17-542
Tributary of the Gods River
Elevation (top): 90 m asl
UTM Zone 15, NAD83: 550811E, 6155660N

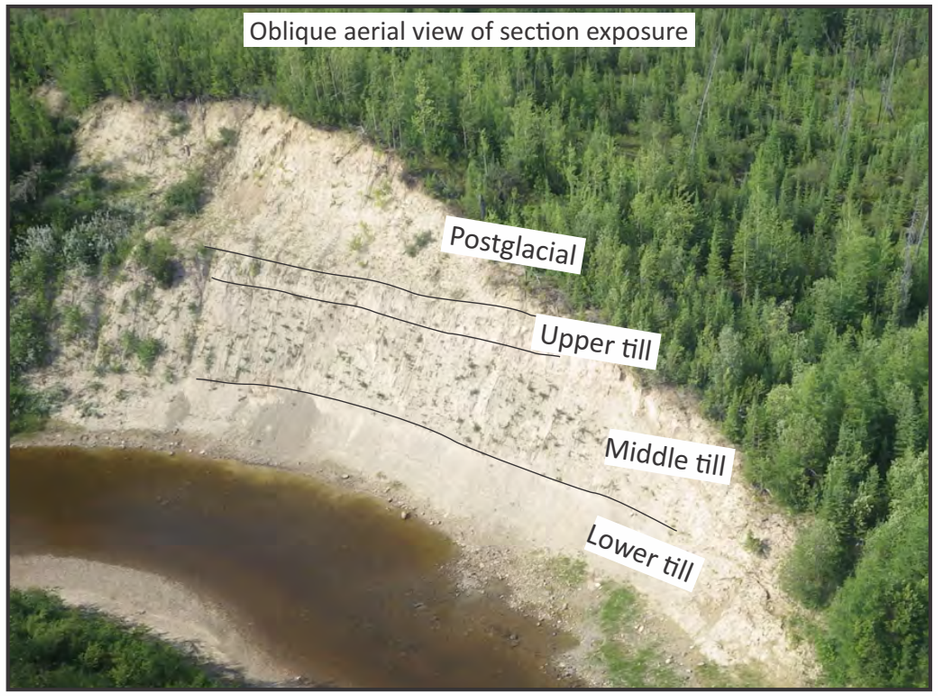

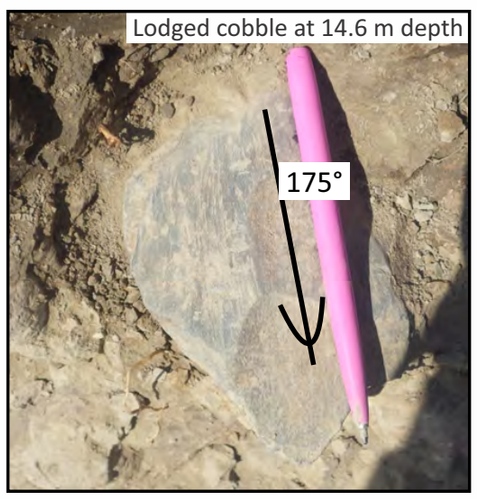

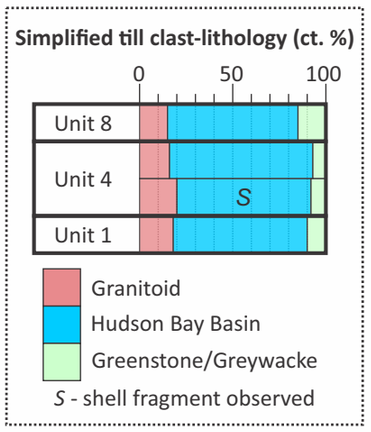



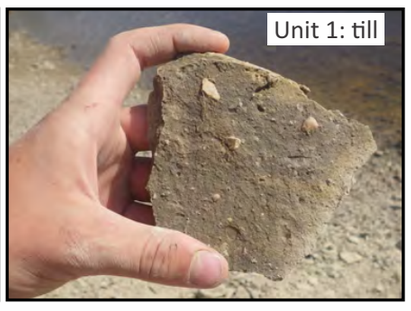

Supplemental material 2: Ar-Ar analytical data.

Ar/Ar analytical data.

Sample: 112-16-414-A01 **Identifier:** Unit 7, surficial sample 112-16-414-A01
Material: Hornblende **Location:** Kaskattama highland

N	Power W	Age (Ma)	±1σ (Ma)	Ca/K	±1σ	Cl/K	±1σ	%^{40}Ar	^{40}Ar*/^{39}Ar$_K$	±1σ	Corrected[1] ^{40}Ar (fA)	±1σ	^{39}Ar (fA)	±1σ	^{38}Ar (fA)	±1σ	^{37}Ar (fA)	±1σ	^{36}Ar (fA)	±1σ	Blanks ^{40}Ar (fA)	±1σ	^{39}Ar (fA)	±1σ	^{38}Ar (fA)	±1σ	^{37}Ar (fA)	±1σ	^{36}Ar (fA)	±1σ	IC^{m1}	±1σ	IC^{m2}	±1σ	IC^{13}	±1σ	IC^{12}	±1σ	IC^{CDD}	±1σ	Δt[2] (days)	J	±1σ	^{39}Ar Decay	^{37}Ar Decay	LambdaK
01A	TF	1782.3	1.5	7.85	0.01	0.02	0.00	99.73	176.690	0.240	1755.2425	0.1021	9.9318	0.0134	0.2050	0.0153	15.7634	0.0141	0.0265	0.0004	0.6791	0.0223	0.0287	0.0089	0.0125	0.0110	-0.0162	0.0092	0.0023	0.0001	1.0000	0	1.0726	0.000248	1.0594	0.000488	1.0483	0.000856	1.0251	0.0034	49.0978125	0.0093	8.29768E-05	1.0003	2.5176	5.463E-10
01B	TF	1764.9	1.1	7.16	0.01	0.01	0.00	99.75	174.007	0.172	2480.9727	0.1239	14.2540	0.0140	0.2002	0.0156	20.6216	0.0153	0.0347	0.0005	0.5810	0.0196	0.0012	0.0092	-0.0329	0.0116	-0.0037	0.0091	0.0020	0.0001	1.0000	0	1.0726	0.000248	1.0594	0.000488	1.0483	0.000856	1.0251	0.0034	49.13070602	0.0093	8.29768E-05	1.0003	2.5192	5.463E-10
01C	TF	1970.5	0.7	4.79	0.00	0.02	0.00	99.93	207.437	0.124	4826.4259	0.2058	23.2819	0.0139	0.4706	0.0169	22.5298	0.0143	0.0269	0.0005	1.3667	0.0223	0.0157	0.0081	0.0051	0.0120	-0.0166	0.0091	0.0047	0.0002	1.0000	0	1.0726	0.000248	1.0594	0.000488	1.0483	0.000856	1.0251	0.0034	49.16577546	0.0093	8.29768E-05	1.0003	2.5210	5.463E-10
01D	TF	1856.7	15.8	4.82	0.10	0.00	0.04	99.95	188.467	2.554	178.3238	0.0421	0.9470	0.0128	0.0109	0.0143	0.9206	0.0132	0.0009	0.0002	1.4466	0.0233	-0.0151	0.0094	0.0155	0.0101	-0.0140	0.0093	0.0048	0.0002	1.0000	0	1.0726	0.000248	1.0594	0.000488	1.0483	0.000856	1.0251	0.0034	49.23631944	0.0093	8.29768E-05	1.0003	2.5245	5.463E-10
01E	TF	2640.4	1.5	8.60	0.01	0.05	0.00	99.92	346.491	0.375	4871.6717	0.1938	14.0867	0.0152	0.4017	0.0153	24.3900	0.0142	0.0302	0.0006	1.3407	0.0232	-0.0163	0.0096	-0.0296	0.0108	0.0305	0.0098	0.0047	0.0002	1.0000	0	1.0726	0.000248	1.0594	0.000488	1.0483	0.000856	1.0251	0.0034	49.27090278	0.0093	8.29768E-05	1.0003	2.5262	5.463E-10
01F	TF	1862.0	1.1	6.15	0.01	0.01	0.00	99.94	189.335	0.182	2664.2656	0.1336	14.0902	0.0135	0.2207	0.0152	17.4658	0.0155	0.0166	0.0004	1.2893	0.0238	0.0069	0.0092	0.0094	0.0104	0.0022	0.0106	0.0043	0.0002	1.0000	0	1.0726	0.000248	1.0594	0.000488	1.0483	0.000856	1.0251	0.0034	49.3056713	0.0093	8.29768E-05	1.0003	2.5280	5.463E-10
01G	TF	1876.2	2.2	14.04	0.03	0.00	0.01	99.38	191.644	0.355	1364.1384	0.0906	7.1070	0.0130	0.0926	0.0155	20.0195	0.0149	0.0422	0.0005	1.4376	0.0261	0.0231	0.0093	0.0295	0.0112	-0.0068	0.0090	0.0048	0.0002	1.0000	0	1.0726	0.000248	1.0594	0.000488	1.0483	0.000856	1.0251	0.0034	49.37618056	0.0093	8.29768E-05	1.0003	2.5315	5.463E-10
01H	TF	1785.0	0.8	6.72	0.01	0.01	0.00	99.91	177.115	0.119	4144.4241	0.1840	23.4281	0.0156	0.3948	0.0148	31.6243	0.0150	0.0330	0.0006	1.4807	0.0214	0.0131	0.0086	-0.0072	0.0101	0.0083	0.0097	0.0048	0.0002	1.0000	0	1.0726	0.000248	1.0594	0.000488	1.0483	0.000856	1.0251	0.0034	49.41085648	0.0093	8.29768E-05	1.0003	2.5332	5.463E-10
01I	TF	1734.1	0.7	6.36	0.01	0.02	0.00	99.90	169.316	0.106	4344.2420	0.1726	25.6817	0.0160	0.5258	0.0155	32.8150	0.0159	0.0366	0.0006	1.4190	0.0214	0.0302	0.0097	0.0048	0.0108	-0.0034	0.0093	0.0047	0.0002	1.0000	0	1.0726	0.000248	1.0594	0.000488	1.0483	0.000856	1.0251	0.0034	49.44561343	0.0093	8.29768E-05	1.0003	2.5350	5.463E-10
01J	TF	1931.8	0.9	4.67	0.01	0.02	0.00	99.93	200.856	0.143	4235.3528	0.1629	21.0992	0.0150	0.4044	0.0164	19.7992	0.0159	0.0236	0.0005	1.4137	0.0227	0.0225	0.0092	-0.0080	0.0110	0.0164	0.0099	0.0048	0.0002	1.0000	0	1.0726	0.000248	1.0594	0.000488	1.0483	0.000856	1.0251	0.0034	49.51627315	0.0093	8.29768E-05	1.0003	2.5385	5.463E-10
01K	TF	1762.8	0.7	6.52	0.01	0.01	0.00	99.81	173.681	0.109	4091.9379	0.1572	23.5618	0.0147	0.3382	0.0158	30.7915	0.0166	0.0472	0.0006	1.2966	0.0257	0.0285	0.0093	-0.0027	0.0115	0.0001	0.0095	0.0044	0.0002	1.0000	0	1.0726	0.000248	1.0594	0.000488	1.0483	0.000856	1.0251	0.0034	49.5509375	0.0093	8.29768E-05	1.0003	2.5402	5.463E-10
01P	TF	1777.7	1.3	7.12	0.01	0.01	0.00	99.81	175.983	0.197	2330.0301	0.1260	13.2612	0.0147	0.2218	0.0151	18.7414	0.0141	0.0277	0.0005	1.2633	0.0206	0.0020	0.0093	0.0130	0.0095	0.0116	0.0090	0.0037	0.0002	1.0000	0	1.0726	0.000248	1.0594	0.000488	1.0483	0.000856	1.0239	0.0009	50.04711806	0.0093	8.29768E-05	1.0003	2.5653	5.463E-10
01Q	TF	1767.8	1.5	6.61	0.01	0.02	0.00	99.90	174.449	0.234	2074.8605	0.1019	11.9059	0.0159	0.2348	0.0143	15.6060	0.0146	0.0176	0.0004	1.2954	0.0228	-0.0089	0.0099	0.0156	0.0104	-0.0021	0.0095	0.0040	0.0002	1.0000	0	1.0726	0.000248	1.0594	0.000488	1.0483	0.000856	1.0239	0.0009	50.08202546	0.0093	8.29768E-05	1.0003	2.5670	5.463E-10
01R	TF	1758.0	1.3	9.11	0.01	0.03	0.00	99.95	172.949	0.201	2137.7621	0.0999	12.3906	0.0143	0.2661	0.0145	22.3467	0.0161	0.0188	0.0005	1.2851	0.0218	0.0349	0.0099	0.0186	0.0106	-0.0150	0.0092	0.0038	0.0002	1.0000	0	1.0726	0.000248	1.0594	0.000488	1.0483	0.000856	1.0239	0.0009	50.11665509	0.0093	8.29768E-05	1.0003	2.5688	5.463E-10
01S	TF	2661.3	1.9	10.56	0.02	0.01	0.00	99.90	351.714	0.465	3791.6693	0.1618	10.8068	0.0142	0.1833	0.0148	22.5537	0.0154	0.0283	0.0005	1.3032	0.0215	0.0066	0.0083	-0.0004	0.0107	-0.0055	0.0087	0.0042	0.0002	1.0000	0	1.0726	0.000248	1.0594	0.000488	1.0483	0.000856	1.0239	0.0009	50.18734481	0.0093	8.29768E-05	1.0003	2.5724	5.463E-10
01T	TF	1775.6	0.7	5.99	0.01	0.03	0.00	99.78	175.660	0.112	4140.9559	0.1615	23.5647	0.0149	0.4930	0.0160	27.9165	0.0160	0.0494	0.0007	1.3520	0.0205	0.0083	0.0091	-0.0012	0.0108	-0.0159	0.0096	0.0043	0.0001	1.0000	0	1.0726	0.000248	1.0594	0.000488	1.0483	0.000856	1.0239	0.0009	50.22212963	0.0093	8.29768E-05	1.0003	2.5741	5.463E-10

Sample: 112-17-534-A01 **Identifier:** Unit 6, surficial sample 112-17-534-A01
Material: Hornblende **Location:** Kaskattama highland

N	Power W	Age (Ma)	±1σ (Ma)	Ca/K	±1σ	Cl/K	±1σ	%^{40}Ar	^{40}Ar*/^{39}Ar$_K$	±1σ	Corrected ^{40}Ar (fA)	±1σ	^{39}Ar (fA)	±1σ	^{38}Ar (fA)	±1σ	^{37}Ar (fA)	±1σ	^{36}Ar (fA)	±1σ	Blanks ^{40}Ar (fA)	±1σ	^{39}Ar (fA)	±1σ	^{38}Ar (fA)	±1σ	^{37}Ar (fA)	±1σ	^{36}Ar (fA)	±1σ	IC^{m1}	±1σ	IC^{m2}	±1σ	IC^{13}	±1σ	IC^{12}	±1σ	IC^{CDD}	±1σ	Δt[2] (days)	J	±1σ	^{39}Ar Decay	^{37}Ar Decay	LambdaK
01U	TF	1778.4	0.7	9.29	0.01	0.03	0.00	99.74	174.479	0.101	4676.5542	0.1730	26.8142	0.0153	0.5778	0.0171	48.5141	0.0175	0.0741	0.0007	1.2576	0.0212	0.0002	0.0096	0.0227	0.0117	0.0143	0.0114	0.0043	0.0002	1.0000	0	1.0726	0.000248	1.0594	0.000488	1.0483	0.000856	1.0239	0.0024	50.96762731	0.0094	8.29768E-05	1.0003	2.6123	5.463E-10
01V	TF	1747.6	0.6	7.69	0.00	0.06	0.00	99.78	169.803	0.089	5345.6480	0.2047	31.4869	0.0162	0.9913	0.0156	47.1362	0.0172	0.0718	0.0007	1.2541	0.0237	0.0343	0.0095	0.0052	0.0114	0.0186	0.0102	0.0040	0.0002	1.0000	0	1.0726	0.000248	1.0594	0.000488	1.0483	0.000856	1.0239	0.0024	51.0027662	0.0094	8.29768E-05	1.0003	2.6141	5.463E-10
01W	TF	2656.2	0.7	9.78	0.01	0.01	0.00	99.91	347.241	0.166	10461.6253	0.3871	30.1945	0.0142	0.4924	0.0139	58.3046	0.0179	0.0734	0.0008	1.3457	0.0232	0.0093	0.0078	0.0045	0.0091	-0.0118	0.0095	0.0043	0.0002	1.0000	0	1.0726	0.000248	1.0594	0.000488	1.0483	0.000856	1.0239	0.0009	50.2568287	0.0094	8.29768E-05	1.0003	2.5759	5.463E-10
01B	TF	1809.8	1.1	13.62	0.01	0.02	0.00	99.93	179.344	0.173	2733.2796	0.1117	15.2990	0.0146	0.2669	0.0152	41.0419	0.0174	0.0346	0.0005	1.3765	0.0207	0.0437	0.0089	-0.0202	0.0108	0.0083	0.0101	0.0044	0.0002	1.0000	0	1.0726	0.000248	1.0594	0.000488	1.0483	0.000856	1.0239	0.0009	50.3274537	0.0094	8.29768E-05	1.0003	2.5795	5.463E-10
01C	TF (Biotite)	1861.4	0.3	0.03	0.00	0.00	0.00	96.71	119.743	0.040	7419.7924	0.3326	60.3886	0.0188	0.8746	0.0161	0.3853	0.0142	0.8325	0.0022	1.2972	0.0240	0.0360	0.0090	-0.0026	0.0113	-0.0061	0.0101	0.0042	0.0001	1.0000	0	1.0726	0.000248	1.0594	0.000488	1.0483	0.000856	1.0239	0.0009	50.36211806	0.0094	8.29768E-05	1.0003	2.5813	5.463E-10
01D	TF	2660.5	1.8	14.03	0.02	0.01	0.00	99.53	348.286	0.442	3736.3076	0.1694	10.6703	0.0134	0.1712	0.0152	29.4240	0.0179	0.0789	0.0008	1.4688	0.0215	0.0319	0.0090	-0.0122	0.0100	0.0023	0.0101	0.0043	0.0002	1.0000	0	1.0726	0.000248	1.0594	0.000488	1.0483	0.000856	1.0239	0.0009	50.39703704	0.0094	8.29768E-05	1.0003	2.5830	5.463E-10
01E	TF	2618.9	0.6	7.58	0.00	0.03	0.00	99.73	338.072	0.134	15947.1394	0.5867	47.1542	0.0184	1.1166	0.0159	70.3336	0.0186	0.1949	0.0012	1.4601	0.0218	0.0262	0.0093	-0.0128	0.0111	0.0064	0.0098	0.0045	0.0002	1.0000	0	1.0726	0.000248	1.0594	0.000488	1.0483	0.000856	1.0239	0.0009	50.46775463	0.0094	8.29768E-05	1.0003	2.5867	5.463E-10
01F	TF	2644.4	1.2	9.78	0.01	0.01	0.00	99.97	344.323	0.284	7008.7825	0.2770	20.4164	0.0167	0.2900	0.0163	39.3447	0.0179	0.0941	0.0006	1.4058	0.0268	0.0469	0.0096	0.0008	0.0123	-0.0128	0.0102	0.0045	0.0002	1.0000	0	1.0726	0.000248	1.0594	0.000488	1.0483	0.000856	1.0239	0.0009	50.50263889	0.0094	8.29768E-05	1.0003	2.5884	5.463E-10
01G	TF	2657.8	1.0	10.30	0.01	0.01	0.00	99.90	347.629	0.244	7620.5068	0.3465	21.9729	0.0153	0.3264	0.0137	44.4370	0.0171	0.0562	0.0007	1.3995	0.0242	0.0279	0.0084	-0.0125	0.0096	0.0086	0.0089	0.0039	0.0002	1.0000	0	1.0726	0.000248	1.0594	0.000488	1.0483	0.000856	1.0239	0.0009	50.53748843	0.0094	8.29768E-05	1.0003	2.5902	5.463E-10
01K	TF	2650.8	0.8	11.23	0.01	0.01	0.00	99.78	345.905	0.207	8102.1522	0.3428	23.4581	0.0138	0.3484	0.0174	51.1337	0.0209	0.0951	0.0009	1.3042	0.0253	0.0166	0.0077	-0.0052	0.0118	0.0288	0.0097	0.0041	0.0001	1.0000	0	1.0726	0.000248	1.0594	0.000488	1.0483	0.000856	1.0239	0.0024	51.08164352	0.0094	8.29768E-05	1.0003	2.6182	5.463E-10
01L	TF	2658.4	1.3	17.11	0.02	0.01	0.00	99.96	347.781	0.332	5392.4050	0.1866	15.5892	0.0147	0.2229	0.0150	51.6476	0.0176	0.0428	0.0006	1.3144	0.0290	0.0243	0.0094	0.0067	0.0105	-0.0113	0.0098	0.0045	0.0002	1.0000	0	1.0726	0.000248	1.0594	0.000488	1.0483	0.000856	1.0239	0.0024	51.15818056	0.0094	8.29768E-05	1.0003	2.6200	5.463E-10
01M	TF	2667.6	0.7	8.78	0.01	0.06	0.00	99.88	350.064	0.169	12759.8753	0.4984	36.5088	0.0174	1.1856	0.0140	62.2162	0.0194	0.0945	0.0010	1.2988	0.0250	0.0251	0.0091	0.0092	0.0087	0.0041	0.0099	0.0043	0.0002	1.0000	0	1.0726	0.000248	1.0594	0.000488	1.0483	0.000856	1.0239	0.0024	51.15083333	0.0094	8.29768E-05	1.0003	2.6218	5.463E-10
01N	TF	2679.0	0.5	9.29	0.00	0.02	0.00	99.92	352.912	0.132	16383.4484	0.6246	46.5239	0.0170	0.9101	0.0150	83.7527	0.0213	0.1036	0.0010	1.2878	0.0249	0.0031	0.0087	0.0090	0.0111	-0.0163	0.0098	0.0040	0.0002	1.0000	0	1.0726	0.000248	1.0594	0.000488	1.0483	0.000856	1.0239	0.0024	51.2202662	0.0094	8.29768E-05	1.0003	2.6254	5.463E-10
01O	TF	2642.2	0.6	8.81	0.00	0.06	0.00	99.64	343.770	0.151	12778.9817	0.4927	37.1450	0.0161	1.2216	0.0150	63.4003	0.0187	0.1979	0.0012	1.3238	0.0257	0.0477	0.0097	0.0144	0.0097	0.0010	0.0092	0.0042	0.0002	1.0000	0	1.0726	0.000248	1.0594	0.000488	1.0483	0.000856	1.0239	0.0024	51.24481481	0.0094	8.29768E-05	1.0003	2.6272	5.463E-10
01P	TF	1864.2	0.7	15.82	0.01	0.11	0.00	99.71	187.956	0.106	5529.8133	0.2483	29.4914	0.0162	1.4904	0.0155	90.0874	0.0215	0.1177	0.0009	1.6231	0.0255	0.0293	0.0080	0.0092	0.0100	0.0062	0.0106	0.0054	0.0002	1.0000	0	1.0726	0.000248	1.0594	0.000488	1.0483	0.000856	1.0239	0.0024	51.28914352	0.0094	8.29768E-05	1.0003	2.6290	5.463E-10

Sample: 112-16-402-C01 **Identifier:** Unit 3, section 16-402
Material: Hornblende **Location:** Kaskattama highland

N	Power W	Age (Ma)	±1σ (Ma)	Ca/K	±1σ	Cl/K	±1σ	%^{40}Ar	^{40}Ar*/^{39}Ar$_K$	±1σ	Corrected ^{40}Ar (fA)	±1σ	^{39}Ar (fA)	±1σ	^{38}Ar (fA)	±1σ	^{37}Ar (fA)	±1σ	^{36}Ar (fA)	±1σ	Blanks ^{40}Ar (fA)	±1σ	^{39}Ar (fA)	±1σ	^{38}Ar (fA)	±1σ	^{37}Ar (fA)	±1σ	^{36}Ar (fA)	±1σ	IC^{m1}	±1σ	IC^{m2}	±1σ	IC^{13}	±1σ	IC^{12}	±1σ	IC^{CDD}	±1σ	Δt[2] (days)	J	±1σ	^{39}Ar Decay	^{37}Ar Decay	LambdaK
01A	TF	1803.8	1.6	7.84	0.01	0.02	0.00	99.84	177.751	0.254	1692.6349	0.0921	9.5310	0.0135	0.1829	0.0139	14.4519	0.0148	0.0190	0.0004	1.3394	0.0218	0.0190	0.0089	-0.0056	0.0105	-0.0086	0.0092	0.0042	0.0002	1.0000	0	1.0726	0.000248	1.0594	0.000488	1.0483	0.000856	1.0239	0.0024	51.35862269	0.0094	8.28992E-05	1.0003	2.6326	5.463E-10
01B	TF	2693.6	1.4	13.52	0.02	0.01	0.00	99.90	355.295	0.365	4698.3671	0.2206	13.2700	0.0135	0.1952	0.0151	34.5883	0.0169	0.0402	0.0006	1.2716	0.0221	0.0258	0.0093	-0.0019	0.0106	0.0190	0.0105	0.0042	0.0002	1.0000	0	1.0726	0.000248	1.0594	0.000488	1.0483	0.000856	1.0239	0.0024	51.39390028	0.0094	8.28992E-05	1.0003	2.6344	5.463E-10
01C	TF	2638.0	1.6	11.14	0.01	0.02	0.00	99.92	341.506	0.396	4308.2296	0.1912	12.6518	0.0146	0.2240	0.0151	27.1809	0.0147	0.0301	0.0005	1.2472	0.0266	0.0140	0.0104	0.0013	0.0109	-0.0086	0.0095	0.0039	0.0002	1.0000	0	1.0726	0.000248	1.0594	0.000488	1.0483	0.000856	1.0239	0.0024	51.47975787	0.0094	8.28992E-05	1.0003	2.6362	5.463E-10
01D	TF	2608.5	1.7	8.53	0.01	0.02	0.00	99.94	334.357	0.410	3846.7437	0.1694	11.5289	0.0141	0.2064	0.0160	18.9517	0.0151	0.0213	0.0005	1.3127	0.0217	0.0059	0.0083	0.0001	0.0117	-0.0076	0.0099	0.0045	0.0002	1.0000	0	1.0726	0.000248	1.0594	0.000488	1.0483	0.000856	1.0246	0.0019	51.53143519	0.0094	8.28992E-05	1.0003	2.6416	5.463E-10
01E	TF	2562.3	1.8	9.12	0.01	0.01	0.00	99.86	323.372	0.417	3650.5517	0.1571	11.3063	0.0145	0.1614	0.0137	19.8463	0.0151	0.0310	0.0005	1.4065	0.0235	0.0186	0.0095	-0.0038	0.0105	0.0009	0.0091	0.0045	0.0002	1.0000	0	1.0726	0.000248	1.0594	0.000488	1.0483	0.000856	1.0246	0.0019	51.56596065	0.0094	8.28992E-05	1.0003	2.6434	5.463E-10
01F	TF	2658.6	1.6	7.91	0.01	0.02	0.00	99.98	346.569	0.402	4226.7533	0.1922	12.5137	0.0141	0.2212	0.0158	18.9396	0.0148	0.0160	0.0004	1.2547	0.0235	0.0277	0.0093	0.0129	0.0114	0.0048	0.0093	0.0037	0.0002	1.0000	0	1.0726	0.000248	1.0594	0.000488	1.0483	0.000856	1.0246	0.0019	51.60451389	0.0094	8.28992E-05	1.0003	2.6452	5.463E-10
01G	TF	1769.6	2.1	7.39	0.02	0.01	0.01	99.68	172.515	0.327	1264.2694	0.0914	7.3216	0.0138	0.1219	0.0157	10.3935	0.0142	0.0210	0.0004	1.2772	0.0236	0.0035	0.0092	0.0151	0.0112	-0.0031	0.0092	0.0043	0.0002	1.0000	0	1.0726	0.000248	1.0594	0.000488	1.0483	0.000856	1.0246	0.0019	51.6696875	0.0094	8.28992E-05	1.0003	2.6488	5.463E-10
01H	TF	2699.1	2.3	9.23	0.02	0.02	0.01	99.92	356.698	0.589	2689.1328	0.1402	7.5555	0.0124	0.1504	0.0150	13.3914	0.0145	0.0163	0.0004	1.2454	0.0234	0.0182	0.0084	-0.0083	0.0100	-0.0038	0.0095	0.0037	0.0002	1.0000	0	1.0726	0.000248	1.0594	0.000488	1.0483	0.000856	1.0246	0.0019	51.70417824	0.0094	8.28992E-05	1.0003	2.6506	5.463E-10
01I	TF	2757.4	3.6	13.10	0.04	0.02	0.01	99.82	371.662	0.950	2125.1130	0.1233	5.7303	0.0133	0.1133	0.0146	15.8817	0.0146	0.0230	0.0005	1.2047	0.0219	0.0151	0.0098	0.0018	0.0115	-0.0132	0.0094	0.0036	0.0001	1.0000	0	1.0726	0.000248	1.0594	0.000488	1.0483	0.000856	1.0246	0.0019	51.73844838	0.0094	8.28992E-05	1.0003	2.6524	5.463E-10
01J	TF	2992.1	12.0	9.48	0.09	0.05	0.03	99.33	436.993	3.563	687.8091	0.0591	1.5682	0.0127	0.0497	0.0148	2.8485	0.0147	0.0176	0.0003	1.3748	0.0256	0.0000	0.0085	0.0001	0.0107	0.0057	0.0101	0.0041	0.0002	1.0000	0	1.0726	0.000248	1.0594	0.000488	1.0483	0.000856	1.0246	0.0019	51.80787037	0.0094	8.28992E-05	1.0003	2.6560	5.463E-10
01K	TF	2667.2	1.4	11.04	0.01	0.03	0.00	99.97	348.708	0.357	4877.4119	0.2124	14.0340	0.0143	0.3038	0.0159	29.6468	0.0163	0.0251	0.0005	1.2471	0.0229	0.0212	0.0093	-0.0121	0.0114	-0.0141	0.0105	0.0041	0.0001	1.0000	0	1.0726	0.000248	1.0594	0.000488	1.0483	0.000856	1.0246	0.0019	51.84234954	0.0094	8.28992E-05	1.0003	2.6578	5.463E-10
01L	TF	2665.6	1.7	9.32	0.01	0.02	0.00	99.98	348.304	0.411	4263.4945	0.1575	12.2749	0.0144	0.2346	0.0153	21.8748	0.0146	0.0182	0.0004	1.2104	0.0222	0.0199	0.0090	-0.0214	0.0118	-0.0042	0.0095	0.0037	0.0002	1.0000	0	1.0726	0.000248	1.0594	0.000488	1.0483	0.000856	1.0264	0.0020	52.56564352	0.0094	8.28992E-05	1.0004	2.6596	5.463E-10
01M	TF	2641.8	1.1	10.20	0.01	0.02	0.00	99.88	342.428	0.275	6545.8657	0.2820	19.1562	0.0153	0.3491	0.0151	37.2398	0.0170	0.0529	0.0006	1.2326	0.0279	0.0010	0.0101	0.0105	0.0104	-0.0112	0.0108	0.0042	0.0002	1.0000	0	1.0726	0.000248	1.0594	0.000488	1.0483	0.000856	1.0264	0.0019	52.04665509	0.0094	8.28992E-05	1.0004	2.6686	5.463E-10
01N	TF	2687.7	0.8	9.54	0.01	0.02	0.00	99.91	353.826	0.201	8546.0574	0.3210

Supplemental material 3: Till-matrix geochemistry levelling and outlier analysis

Exploratory data analysis of the near-total digestion dataset indicated significant variation between the 2016 and 2017 dataset (**Figure Supplemental 3-1**). The observations herein cannot be explained by geological field variability, as the 2017 survey increased the density of sampling, but did not expand the spatial bounds of the 2016 survey. Normal probability plots for four elements comprising both major and trace elements (K, Al, Ga, Zn; near total digestion [Ultratrace 4 package]) are displayed in **Figure Supplemental 3-1**). These elements demonstrate the variability between analyses in 2016 and 2017 that is observed between the datasets. In some cases, such as with Ga, the range in the datasets between the two years barely overlap. To correct for this the 2017 dataset was levelled to 2016 data. A linear regression-based leveling approach was used (as described in Grunsky 2007), correcting the 2017 data with respect to the 2016 data following our assumption about incomplete digestion. Leveling was performed using a linear regression equation derived from the comparison of every 5th percentile (e.g., 5th, 10th, 15th up to the 95th).

Exploratory data analysis of the clast-lithology datasets indicated that two surficial till samples within the dataset have an anomalous proportion of Precambrian clasts (**Figure Supplemental 3-2**). These two samples are interpreted as outliers and possibly reflect erosion of an unknown, locally Precambrian bedrock source, as discussed in Hodder et al. (2024). Therefore, these surficial till samples are not reflective of the regional-scale provenance trends within till units identified and were removed from the dataset prior to provenance analysis.

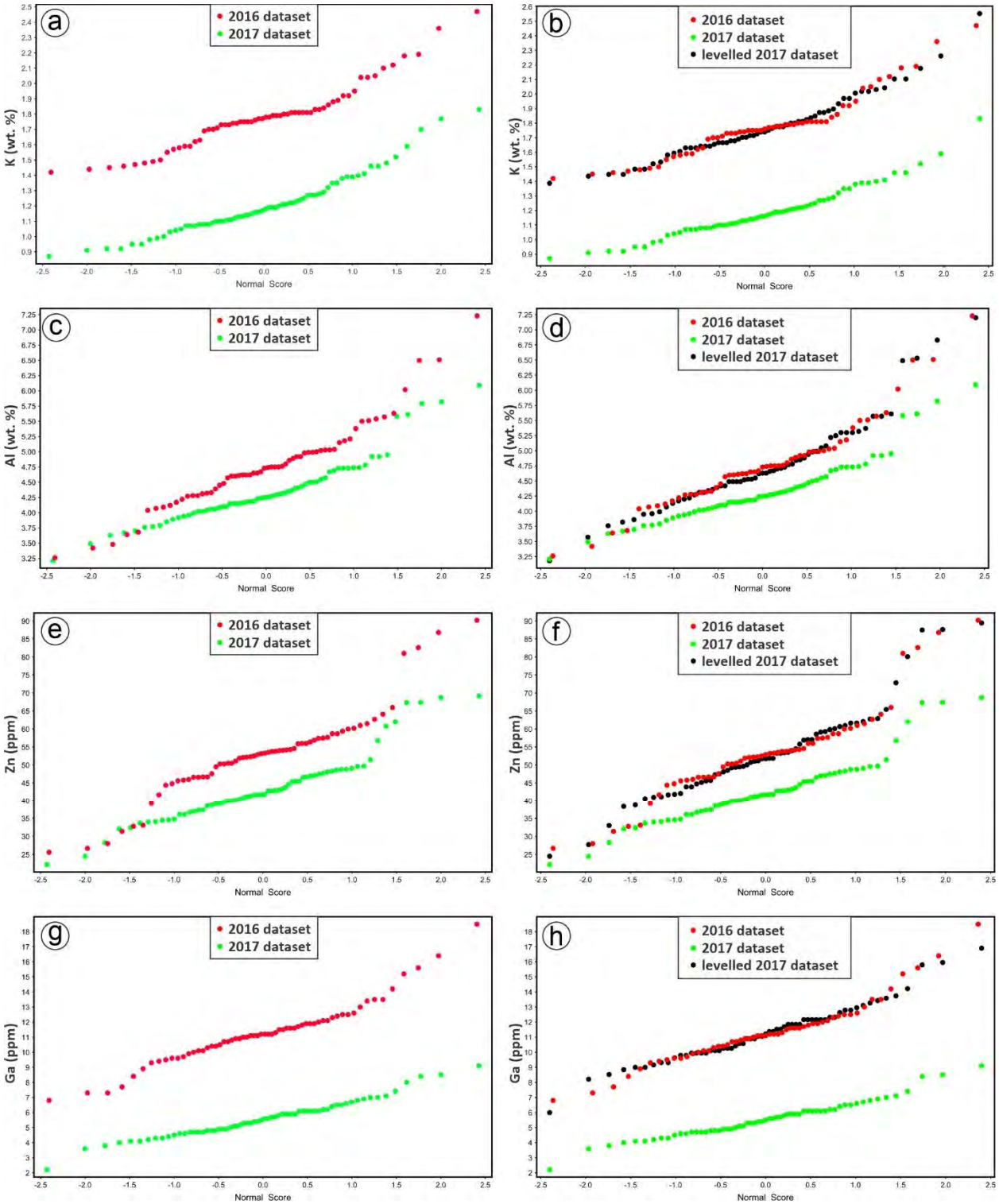

Figure Supplemental 3-1: *Normal probability plots comparting the near-total digestion dataset from 2016, 2017 and the levelled 2017 data for selected elements: a, b) K; c, d) Al; e, f,) Zn; and g, h) Ga.*

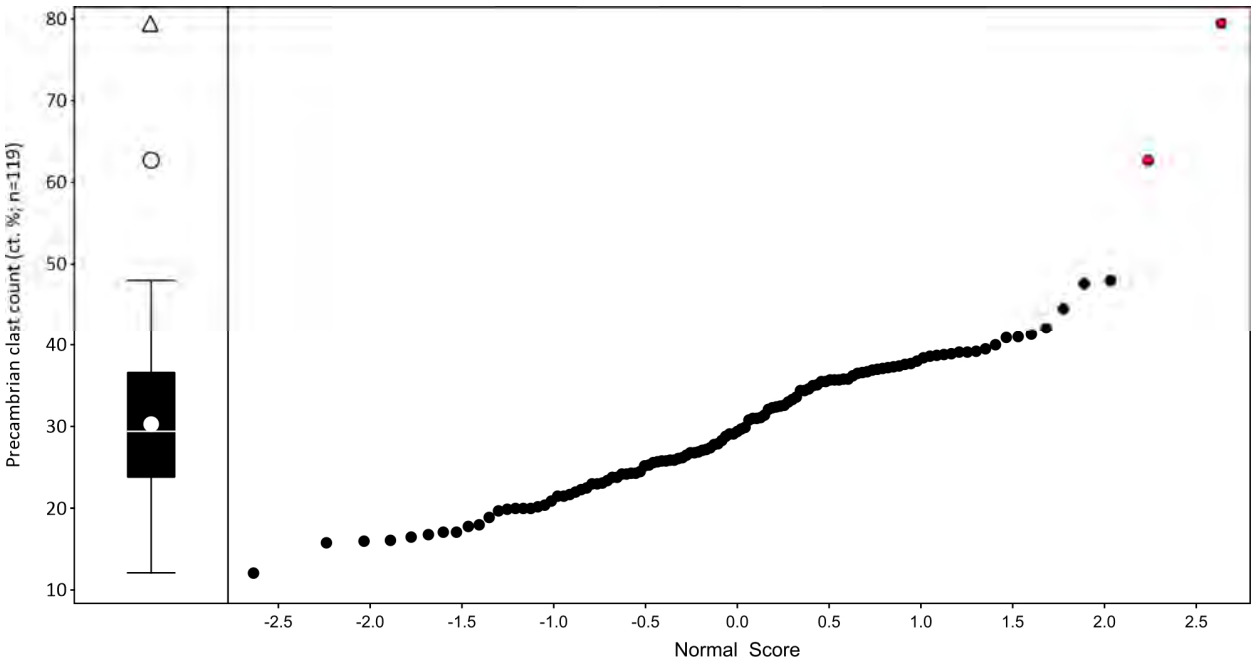

Figure Supplemental 3-2: *Box plot and normal probability plot showing the distribution of Precambrian clasts within till sampled in the Kaskattama highland area. Two surficial till samples, highlighted by the red circles, have anomalous concentrations of Precambrian clasts.*

References:

Hodder, T.J., M.S. Gauthier, Kelley, S.E. and Ross, M. 2024. Quaternary site, till composition and ice-flow indicator datasets in the Kaskattama highland area, northeastern Manitoba (parts of NTS 53N, O, 54B, C). Manitoba Geological Survey, Open File OF2024-1, 20 p.

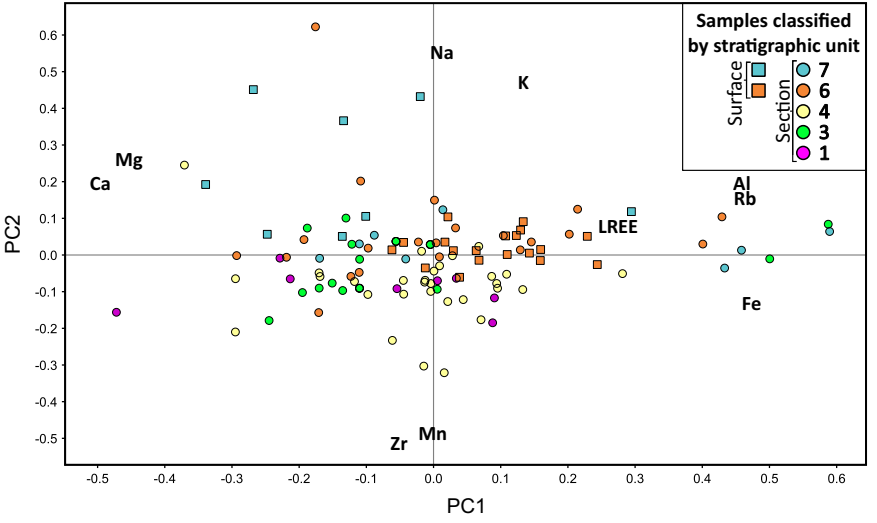

Supplemental material 4: Biplot of PC2 vs. PC1. Samples have been coloured according to the stratigraphic unit they were sampled from. Surficial and subsurface (section) samples are differentiated by shape.

Appendix C

Supplemental materials for Chapter 4

Chapter 4 supplemental material has been submitted alongside the Chapter 4 manuscript to the Canadian Journal of Earth Sciences.

Supplemental material 1: Additional stratigraphic data.

Supplemental material 2: Spatial distribution of stratigraphic units and sediment photos.

Supplemental material 3: Till-matrix geochemistry multivariate analysis.

Supplemental material 4: Optical age data.

Laurentide ice sheet dynamics across multiple glacial-interglacial cycles, from Quaternary stratigraphic records in central Canada by Hodder et al., Canadian Journal of Earth Sciences.

Supplemental material 1: Additional stratigraphic data.

Figure S1-1: Quaternary stratigraphy exposed at section 21-811 on the Little Churchill River. Till sample numbers are labelled within the white boxes. Simplified clast-lithology counts, <63 µm carbonate values and matrix texture data are provided for these samples in the top right panel. Till clast-fabric data are plotted on equal area, lower hemisphere projection stereonets. The value of the principal eigenvalue (S_1) and direction of the principal eigenvector (V_1) are provided, and an interpretation of the ice-flow direction is indicated (orange arrow).

Figure S1-2: Quaternary stratigraphy exposed at section 21-812 on the Churchill River. Till sample numbers are labelled within the white boxes. Simplified clast-lithology counts, <63 µm carbonate values and matrix texture data are provided for these samples in the top right panel. Till clast-fabric data are plotted on equal area, lower hemisphere projection stereonets. The value of the principal eigenvalue (S_1) and direction of the principal eigenvector (V_1) are provided, and an interpretation of the ice-flow direction is indicated (orange arrow).

Figure S1-3: Till-matrix grainsize proportions for identified till units: A) Tukey box plot of sand (wt. %); B) Tukey box plot of silt (wt. %); C) Tukey box plot of clay (wt. %); and D) sand-silt-clay ternary plot, textural fields plotted are modified from Trefethen (1950) and Shepard (1954).

Table S1-1: Lithofacies codes used in this study (modified from Möller et al. (2019b).

Table S1-2: Till-matrix Munsell colours for each stratigraphic unit.

Table S1-3: Ice-flow data summary for each stratigraphic unit.

Section 112-21-811
Little Churchill River
Elevation (top): 188 m asl
UTM Zone 15, NAD83: 359402E, 6339572N

Figure S1-1

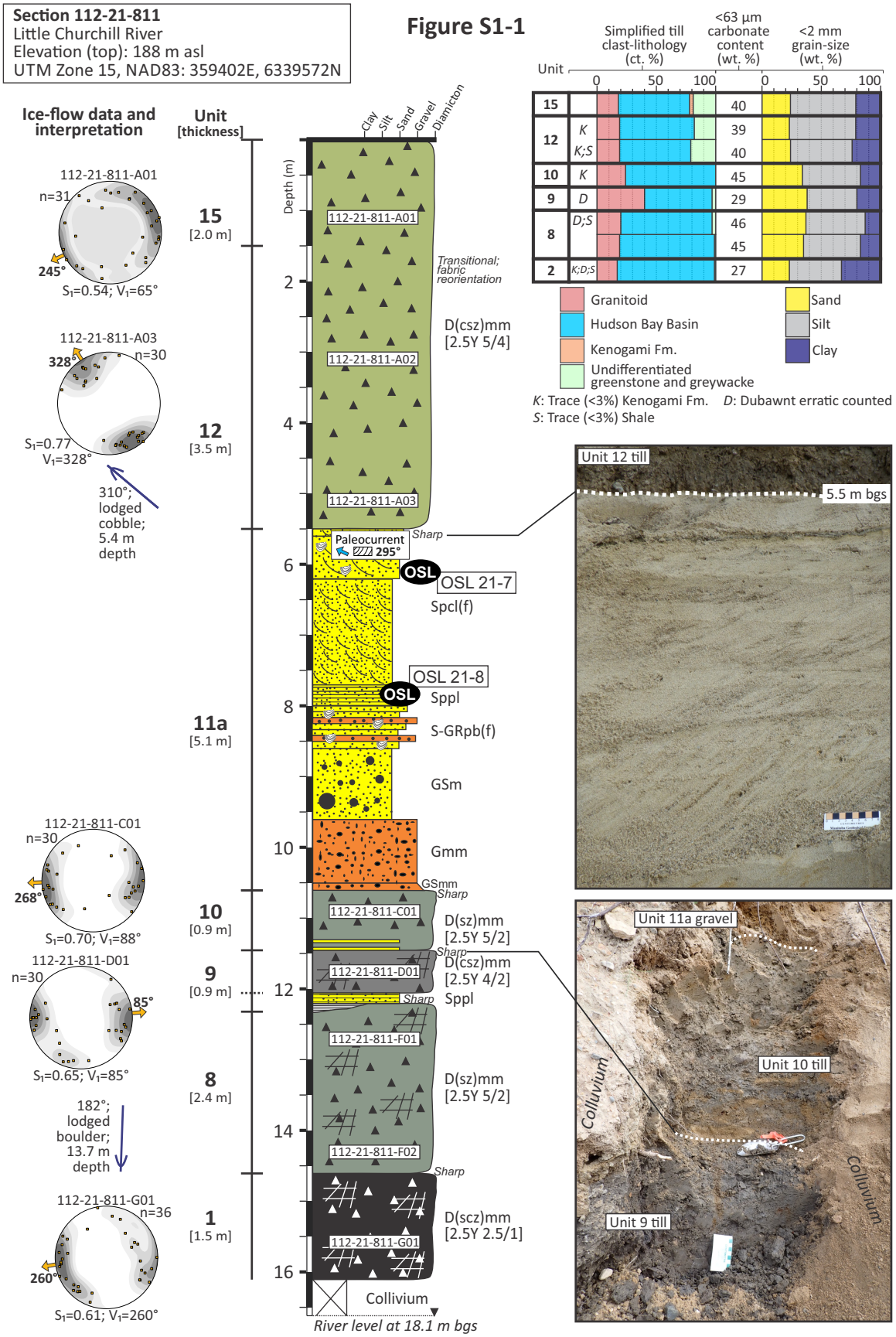

Figure S1-2

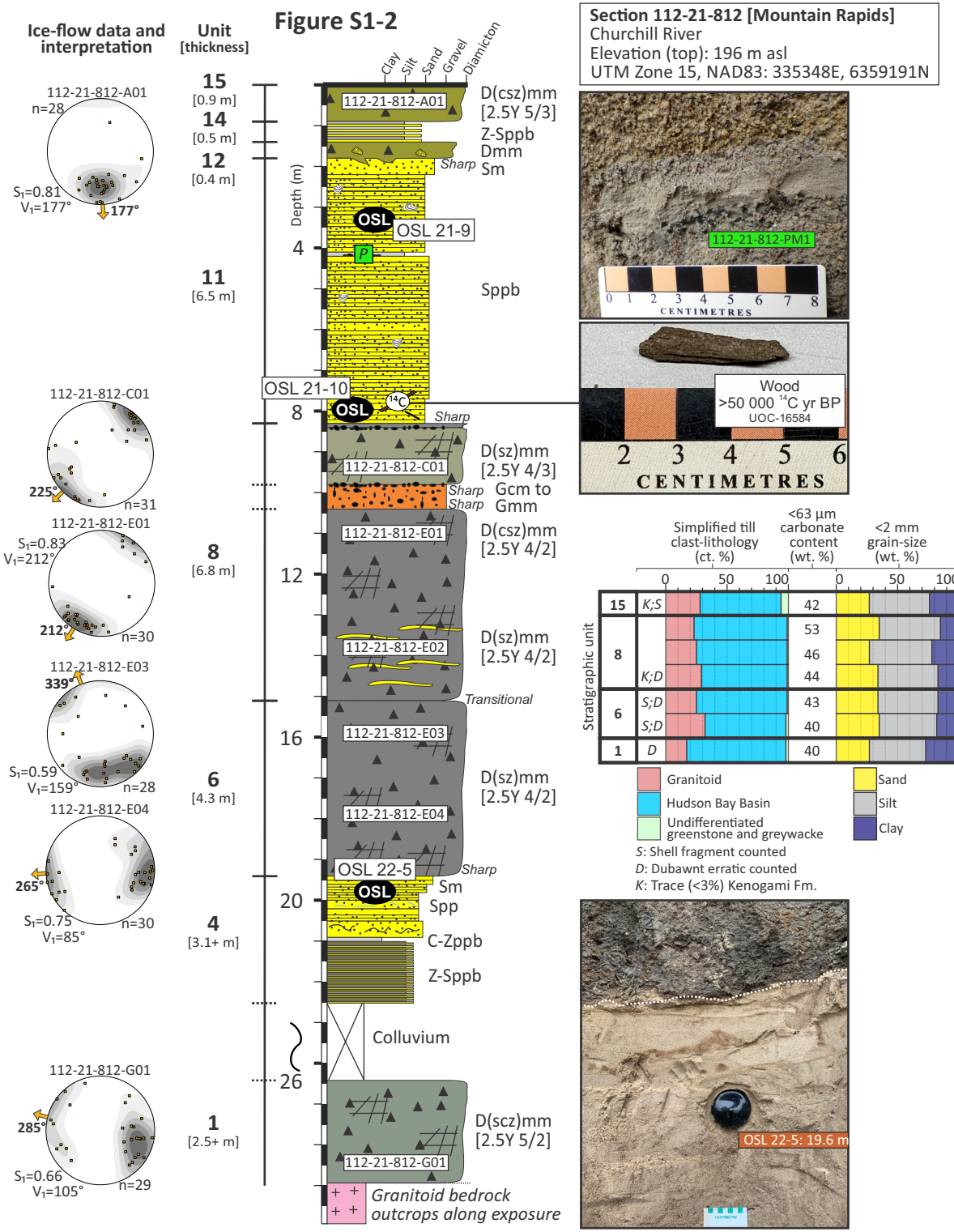
Ice-flow data and interpretation
Unit [thickness]
Clay
Silt
Sand
Gravel
Diamicton
Depth (m)
112-21-812-A01
n=28
S1=0.81
V1=177°
177°
15 [0.9 m]
14 [0.5 m]
12 [0.4 m]
11 [6.5 m]
112-21-812-A01
D(csz)mm [2.5Y 5/3]
Z-Sppb
Dmm
Sharp
Sm
OSL
OSL 21-9
P
Sppb
OSL 21-10
OSL
14C
Sharp
112-21-812-C01
225°
n=31
D(sz)mm [2.5Y 4/3]
Sharp
Gcm to Gmm
Sharp
112-21-812-E01
S1=0.83
V1=212°
212°
n=30
8 [6.8 m]
112-21-812-E01
D(csz)mm [2.5Y 4/2]
112-21-812-E02
D(sz)mm [2.5Y 4/2]
112-21-812-E03
339°
S1=0.59
V1=159°
n=28
6 [4.3 m]
Transitional
112-21-812-E03
D(sz)mm [2.5Y 4/2]
112-21-812-E04
265°
S1=0.75
V1=85°
n=30
4 [3.1+ m]
OSL 22-5
OSL
Sharp
Sm
Spp
C-Zppb
Z-Sppb
Colluvium
112-21-812-G01
285°
S1=0.66
V1=105°
n=29
1 [2.5+ m]
D(scz)mm [2.5Y 5/2]
112-21-812-G01
Granitoid bedrock outcrops along exposure
Section 112-21-812 [Mountain Rapids]
Churchill River
Elevation (top): 196 m asl
UTM Zone 15, NAD83: 335348E, 6359191N
112-21-812-PM1
CENTIMETRES
Wood
>50 000 14C yr BP
UOC-16584
CENTIMETRES
Simplified till clast-lithology (ct, %)
<63 µm carbonate content (wt. %)
<2 mm grain-size (wt. %)
Stratigraphic unit
15 K;S 42
8 53
8 46
K;D 44
6 S;D 43
S;D 40
1 D 40
Granitoid
Hudson Bay Basin
Undifferentiated greenstone and greywacke
Sand
Silt
Clay
S: Shell fragment counted
D: Dubawnt erratic counted
K: Trace (<3%) Kenogami Fm.
OSL 22-5: 19.6 m

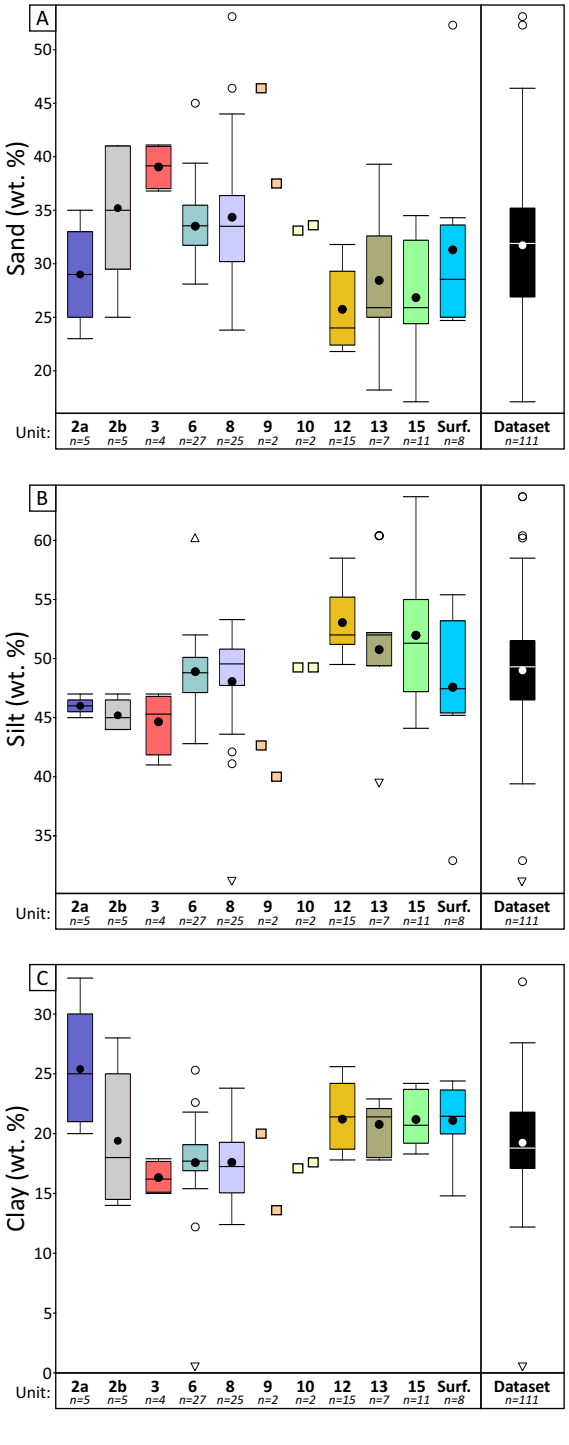
A
Sand (wt. %)
50
45
40
35
30
25
20
Unit:
2a n=5
2b n=5
3 n=4
6 n=27
8 n=25
9 n=2
10 n=2
12 n=15
13 n=7
15 n=11
Surf. n=8
Dataset n=111
B
Silt (wt. %)
60
55
50
45
40
35
C
Clay (wt. %)
30
25
20
15
10
5
0

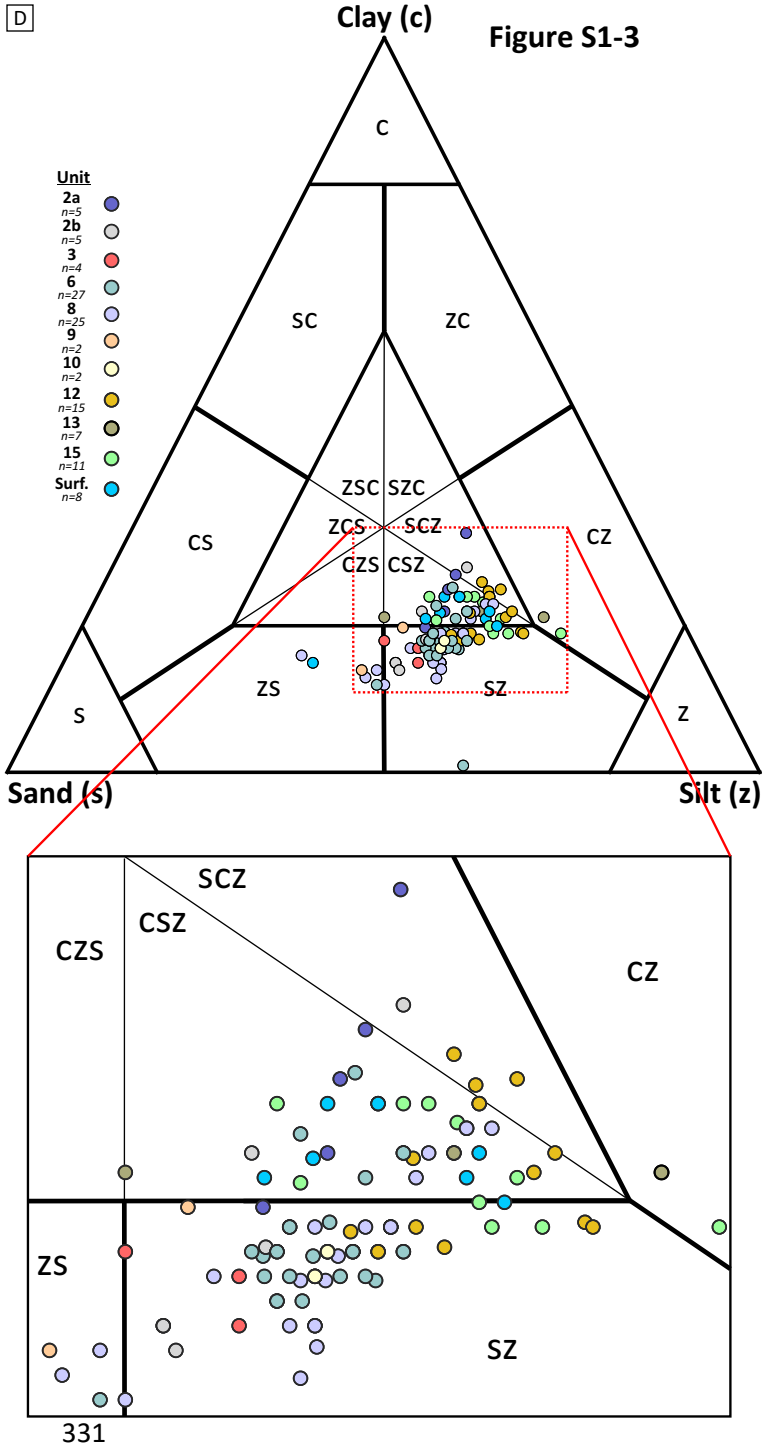
D
Clay (c)
C
SC
ZC
CS
CZ
ZSC SZC
ZCS SCZ
CZS CSZ
ZS
SZ
S
Z
Sand (s)
Silt (z)
Unit
2a n=5
2b n=5
3 n=4
6 n=27
8 n=25
9 n=2
10 n=2
12 n=15
13 n=7
15 n=11
Surf. n=8
SCZ
CSZ
CZS
CZ
ZS
SZ

Figure S1-3

Table S1-1: lithofacies code (1st, 2nd and 3rd order code system) and their description as used in this study.[a]

Lithofacies code:	Lithofacies type description: Grain size, grain support system, internal structures
Diamictons	
D(s/z/c) [colour]	Diamicton, with matrix grainsize (sand, silt and clay listed by increasing proportions, e.g., scz is sandy clayey-silt matrix; texture classes with <20 wt.% are not listed) and colour [Munsell colour code[b]].
D( )mm [ ]	Diamicton, matrix-supported, massive
D( )ms [ ]	Diamicton, matrix-supported, stratified
D( )mm/ms(s) [ ]	Diamicton, …., sheared
D( )mm(ng) [ ]	Diamicton, matrix-supported, massive, normally graded
D( )mm(ig) [ ]	Diamicton, matrix-supported, massive, inversely graded
Sorted sediment facies, 1st code on grain size:	
B, Co, G, CoG, G, SG, GS, S, ZS, SZ, Z, ZC, CZ, C	Boulder, Cobble, Cobble-gravel, Gravel, Gravelly-sandy, Sand, Silty-sand, Sandy-silt, Silt, Silty-clay, Clayey-silt, Clay facies. A dash indicates two grain sizes with the first listed more dominant than the second and is often listed for bedded or laminated sediments, e.g., S-SZppb = sand and sandy silt, planar parallel bedded.
Sorted sediment facies, 2nd code on clast support system and internal lamination:	
-cm	Clast-supported, massive
-mm	Matrix-supported, massive
-m	Massive
-ppl	Planar parallel-laminated (≤1 cm thickness)
-ppb	Planar parallel-bedded (>1 cm thickness)
-l	Laminated (silt, clay)
-dpl	Delta planar-laminated (≤1 cm thickness)
-dpb	Delta planar-bedded (>1 cm thickness)
-tcl	Trough cross-laminated (≤1 cm thickness)
-tcb	Trough cross-bedded (>1 cm thickness)
-pcl	Planar cross-laminated (≤1 cm thickness)
-pcb	Planar cross-bedded (>1 cm thickness)
-r	Ripple
-r(A), r(B)	Type A, type B ripple laminated
-r(d)	Draped ripple
-lg	Stringer, lag, erosion remnant
Sorted sediment facies, 3rd code:	
(o)	Contains detrital or disseminated organics
(f)	Contains fossil shell fragments
(fv)	Contains fossil wholve valve shells
(w)	Contains fossil wood
(rft)	Contains sediment rafts
(ic)	Intra-clasts (e.g., silt, clay in sand)
(bi)	Bimodal composition
(im)	Imbricated clast axes
(ng), (ig)	Normally graded, inversely graded
(b)	Burrows, bioturbated
(def)	Deformed
(dr)	Drop clast (IRD)
Organic sediment, 1st code:	
O	Organic matter, unspecified
P	Peat
2nd code:	
Cd	Coarse detritus
Fd	Fine detritus

[a]Lithofacies code system original defined by Eyles et al. (1983) and this current systems is modified from Möller et al (2019).

[b]Munsell code from Munsell Color–X-Rite (2015).

Table S1-2: Till-matrix Munsell colours for each stratigraphic unit.

		10YR 5/3	10YR 5/4	10YR 4/3	2.5Y 5/4	2.5Y 5/3	2.5Y 4/3	2.5Y 4/4	5Y 3/2	2.5Y 5/2	2.5Y 4/2	2.5Y 4/1	2.5Y 5/1	2.5Y 2.5/1	5Y 2.5/2	10YR 2/1
Strat Unit	**n**	Brown	Yellowish brown	Brown	Light olive brown	Light olive brown	Olive brown	Olive brown	Dark olive grey	Greyish brown	Dark greyish brown	Dark grey	Grey	Black	Black	Black
2a	5									1		2		1		1
2b	5							1			3			1		
3	4								1	1	1	1				
6	27						5			1	20		1			
8	25					1	9			2	10				3	
9	2									1	1					
10	2						1			1						
12	15			2	2	4	6				1					
13	7	2			1	1	3									
15	11	2			7	2										
15_Surface	8		3		3	2										

Table S1-3: Till clast fabric and lodged clast data.

Section	Stratigraphic unit	depth	n	V_1 azimuth degrees	V_1 dip degrees	S_1	S_2	S_3	Interpreted ice-flow azimuth degrees
112-21-806	2a	14.8	40	122	19	0.70	0.24	0.06	302 (WNW)
112-21-811	2a	15.5	36	260	0	0.61	0.26	0.12	260 (W)
112-21-812	2a	28.0	29	105	18	0.66	0.19	0.15	285 (WNW)
112-21-832	2a	40.7	31	132	11	0.68	0.25	0.07	312 (NW)
112-21-807	2b	24.9	36	34	12	0.65	0.28	0.06	214 (SW)
112-21-826	2b	14.7	30	52	16	0.84	0.09	0.06	232 (SW)
112-21-833	2b	13.4	30	200	8	0.80	0.11	0.09	200 (SSW)
112-21-805	3	8.6	31	194	1	0.80	0.13	0.07	194 (SSW)
112-21-805	3	10.6	--			Lodged clast			174 (S)
112-21-806	3	11.7	30	154	1	0.78	0.13	0.09	154 (SSE)
112-21-807	3	19.7	30	158	1	0.69	0.22	0.09	158 (SSE)
112-21-806	6	8.5	31	138	13	0.68	0.17	0.15	318 (NW)
112-21-807	6	9.0	30	121	9	0.83	0.14	0.03	301 (WNW)
112-21-807	6	15.1	32	123	6	0.76	0.18	0.06	303 (WNW)
112-21-812	6	15.9	28	159	19	0.59	0.28	0.13	339 (NNW)
112-21-812	6	17.9	30	85	14	0.75	0.15	0.10	265 (W)
112-21-814	6	13.7	30	299	10	0.73	0.14	0.13	299 (WNW)
112-21-814	6	18.7	30	111	20	0.74	0.16	0.10	291 (WNW)
112-21-819	6	14.2	30	121	5	0.79	0.15	0.06	301 (WNW)
112-21-820	6	18.5	31	162	17	0.66	0.29	0.04	335 (NNW)
112-21-826	6	1.0	30	110	20	0.79	0.12	0.09	290 (WNW)
112-21-826	6	9.5	31	70	0	0.66	0.23	0.11	250 (WSW)
112-21-832	6	5.9	30	133	12	0.60	0.35	0.05	313 (WNW)
112-21-832	6	12.4	30	118	2	0.79	0.14	0.07	298 (WNW)
112-21-832	6	23.2	31	327	4	0.59	0.25	0.15	327 (NNW)
112-21-832	6	33.0	35	327	26	0.70	0.19	0.12	327 (NNW)
112-21-833	6	1.5	31	117	3	0.77	0.14	0.09	297 (WNW)
112-21-833	6	1.5	--			Lodged clast			285 (W)
112-21-804	8	9.9	30	190	8	0.83	0.12	0.05	190 (S)
112-21-805	8	4.5	30	188	5	0.75	0.15	0.10	188 (S)
112-21-806	8	4.1	--			Lodged clast			155 (SSE)
112-21-806	8	4.8	--			Lodged clast			185 (S)
112-21-807	8	5.0	31	188	12	0.62	0.32	0.05	188 (S)
112-21-811	8	13.7	--			Lodged clast			182 (S)
112-21-812	8	9.2	31	45	1	0.75	0.15	0.10	225 (SW)
112-21-812	8	10.9	30	212	11	0.83	0.12	0.05	212 (SSW)
112-21-814	8	11.5	30	227	10	0.69	0.18	0.13	227 (SW)
112-21-819	8	8.5	30	60	16	0.75	0.14	0.11	240 (WSW)
112-21-823	8	3.5	31	234	6	0.77	0.16	0.07	234 (SW)
112-21-823	8	5.3	--			Lodged clast			190 (S)
112-21-823	8	8.0	--			Lodged clast			210 (SSW)
112-21-828	8	13.2	30	174	14	0.68	0.27	0.05	174 (S)
112-21-828	8	25.6	30	358	2	0.69	0.23	0.08	178 (S)
112-21-804	8	6.0	30	190	19	0.66	0.18	0.16	190 (S)
112-21-811	9	11.8	30	85	1	0.65	0.25	0.10	85 (E)
112-21-832	9	4.5	29	73	2	0.53	0.40	0.06	88 (E)
112-21-806	10	2.3	30	85	12	0.64	0.27	0.10	265 (W)
112-21-811	10	10.9	30	88	2	0.70	0.18	0.12	268 (W)
112-21-804	12	3.5	30	230	25	0.72	0.22	0.07	230 (SW)
112-21-805	12	3.6	30	136	13	0.81	0.12	0.07	316 (NW)
112-21-811	12	5.0	30	328	0	0.77	0.15	0.08	328 (NNW)
112-21-811	12	5.4	--			Lodged clast			310 (NW)
112-21-814	12	7.5	39	311	5	0.58	0.32	0.09	311 (NW)
112-21-819	12	1.5	32	317	4	0.63	0.23	0.15	317 (NW)
112-21-819	12	6.5	30	323	8	0.63	0.21	0.16	323 (NW)
112-21-820	12	1.0	30	143	5	0.79	0.15	0.07	323 (NW)
112-21-820	12	7.0	31	144	4	0.65	0.25	0.10	324 (NW)
112-21-832	12	1.5	30	348	5	0.70	0.21	0.09	348 (NW)
112-21-804	13	1.0	30	108	16	0.56	0.33	0.12	275 (W)
112-21-805	13	2.8	31	265	9	0.85	0.10	0.05	265 (W)
112-21-806	13	1.3	30	118	6	0.68	0.24	0.08	298 (WNW)
112-21-807	13	2.0	31	274	7	0.73	0.18	0.09	274 (W)
112-21-814	13	4.0	30	87	4	0.64	0.24	0.12	267 (W)
112-21-828	13	3.5	40	261	4	0.73	0.23	0.04	261 (W)
112-21-802	15	2.7	28	200	3	0.76	0.19	0.05	200 (SSW)
112-21-802	15	5.7	31	222	11	0.84	0.08	0.08	222 (SW)
112-21-811	15	1.0	31	65	9	0.54	0.35	0.11	245 (WSW)
112-21-812	15	0.4	28	177	30	0.81	0.11	0.08	177 (S)
112-21-814	15	1.0	--			Lodged clast			220 (SW)
112-21-823	15	1.0	30	237	7	0.61	0.24	0.14	237 (WSW)
112-21-823	15	2.5	30	238	12	0.72	0.25	0.03	238 (WSW)
112-21-827	15	1.2	31	239	5	0.79	0.13	0.07	239 (WSW)
112-21-828	15	0.6	29	202	8	0.71	0.18	0.11	202 (SSW)

Laurentide ice sheet dynamics across multiple glacial-interglacial cycles, from Quaternary stratigraphic records in central Canada by Hodder et al., Canadian Journal of Earth Sciences.

Supplemental material 2: Spatial distribution of stratigraphic units and sediment photos

This supplemental file contains the spatial location and thickness of each identified unit in the study area, along with additional photos of the sediment at these locations. For till units, the ice-flow datasets are shown for each section.

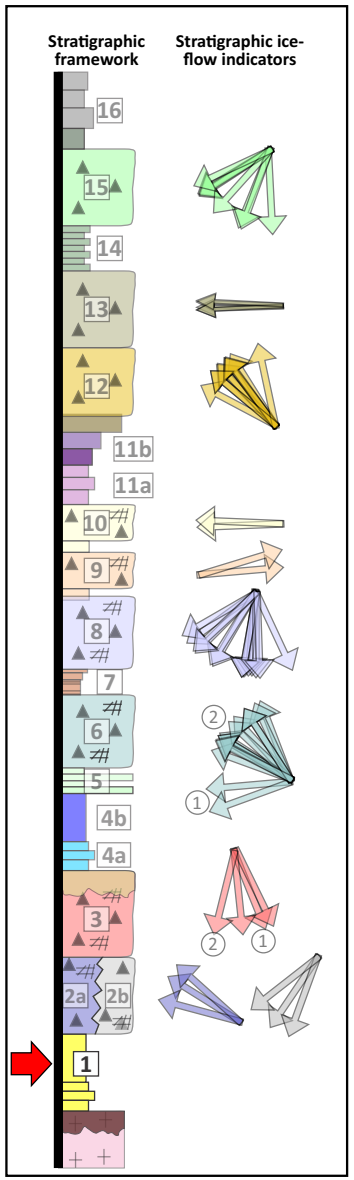

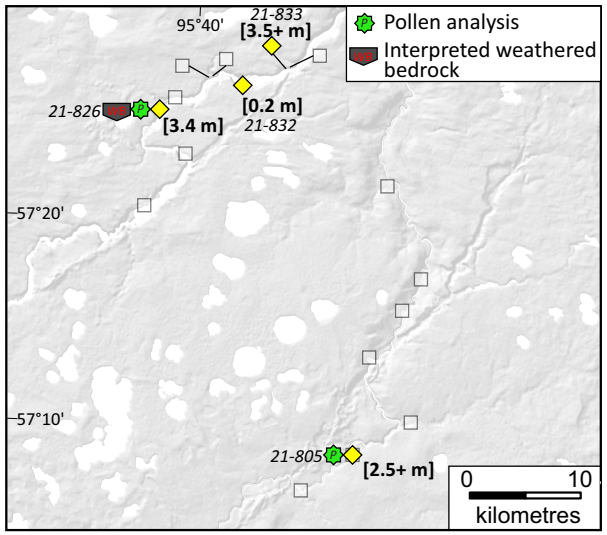

Unit 1 sediments
Key section(s): 21-826; 21-833

Notes:
-Unit 1 at section 21-826 has likely incorporated a lot of the weathered bedrock, which gives it colourful hue; this sediment could be very old.
-Unit 1 sediments were likely deposited during different time periods and additional stratigraphic work may be able to expand on the documentation of these old sediments. More work along the Churchill River northeast of section 21-833 is recommended.

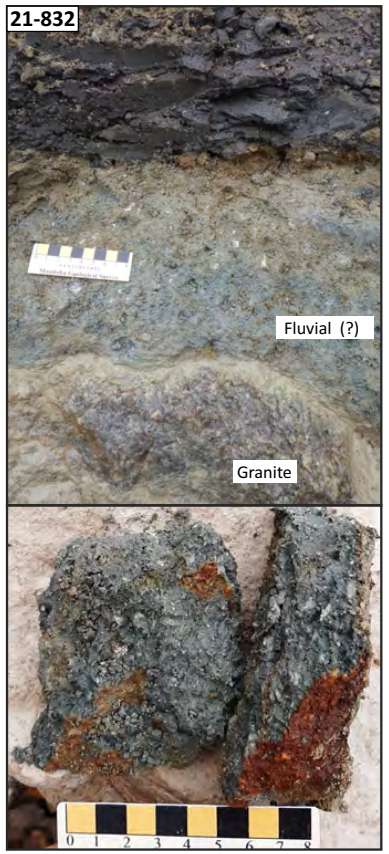



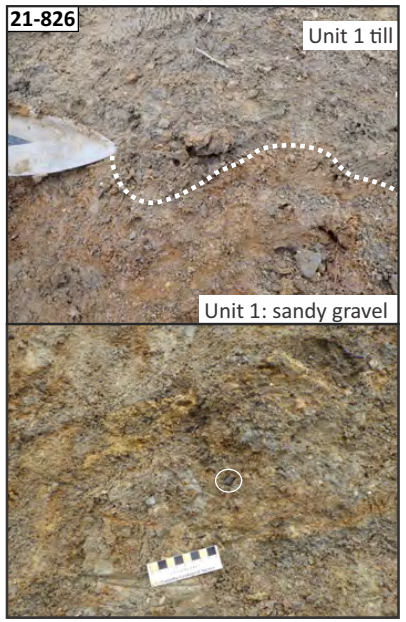

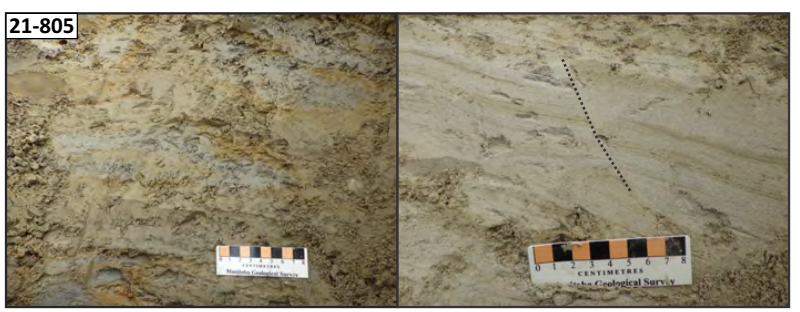

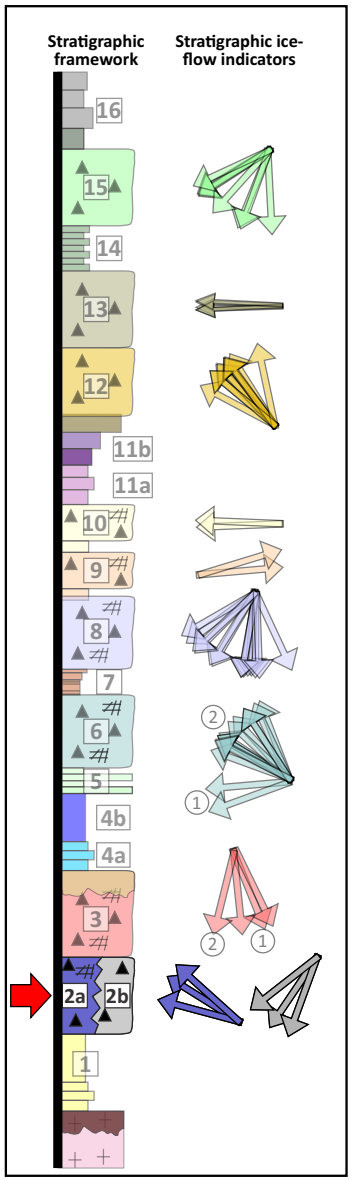

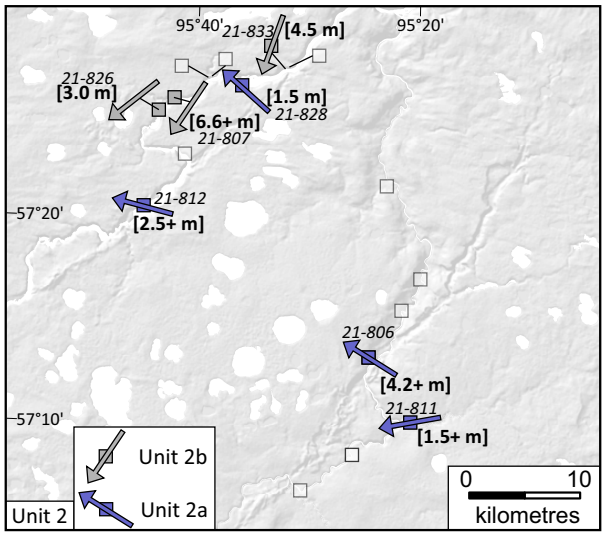

Unit 2 sediments
Key section(s): 21-807; 21-806

Notes:
-No relative-age relationship between ice-flow events and more stratigraphic work should attempt to unravel this history. Additional investigations on the Churchill River near the junction with the Little Churchill River is recommended.
-All but one of the black till occurrences have been correlated to Unit 2.
-Black tills were deposited by both NW- and SW-trending ice-flow (e.g., 21-832 and 21-833) and there is no known bedrock source for this bedrock. Completely eroded or buried?









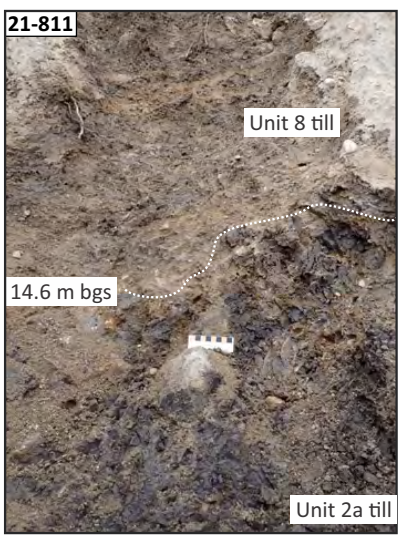

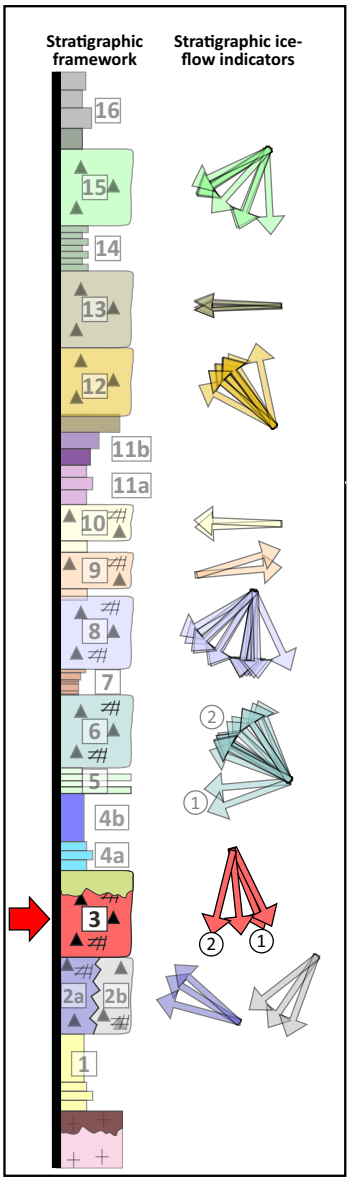

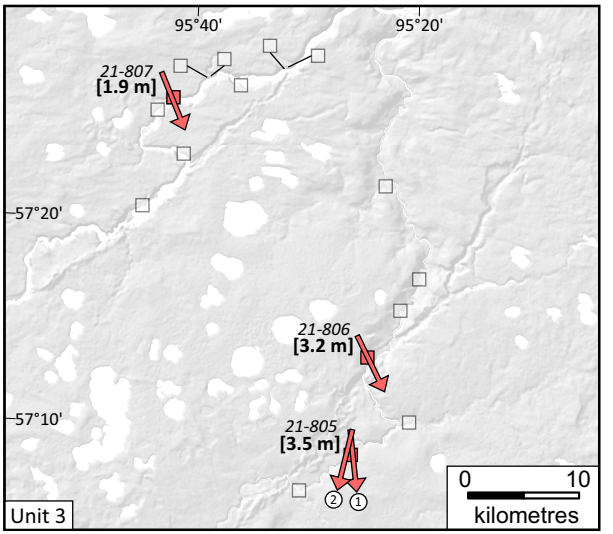

Unit 3 sediments
Key section(s): 21-806; 21-807

Notes:
-This till is not distinguishable in the field from other dark greyish brown till.
-Fabrics combined with till composition are necessary to identify this old SSE-trending ice-flow event.
-The paleosol development on this old till needs to be investigated more. Confirming the dates of the overlying interglacial periods is needed in the future to constrain the timing of paleosol development.







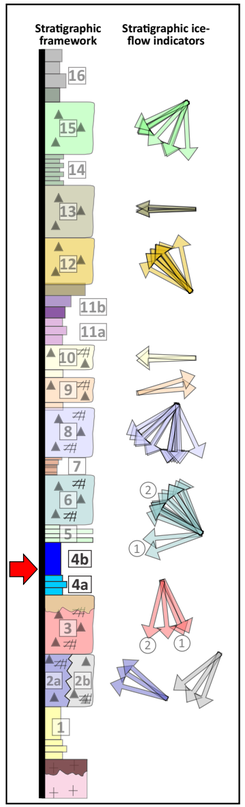

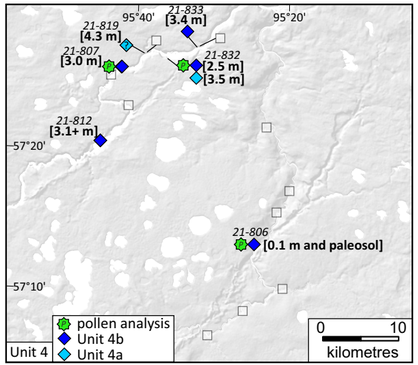

Unit 4 sediments
Key section(s): 21-832; 21-807

Notes:
-Marine sediments at 21-807 and 21-832; possibly at 21-819 too.
-21-832 has terrestrial sediments overlying the marine sediments and the most robust optical age too indicating possible deposition during MIS 7; requires further geochronology studies to confirm.

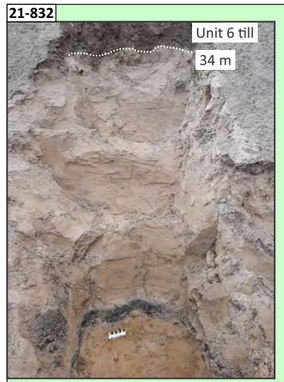

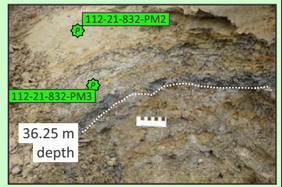



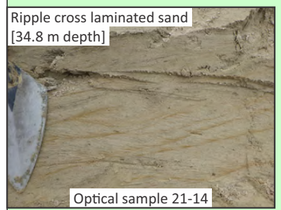

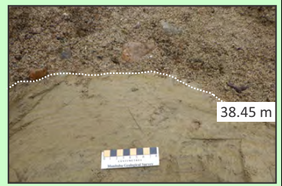



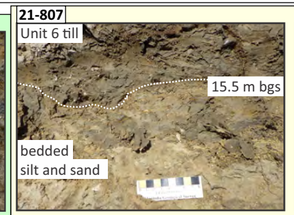

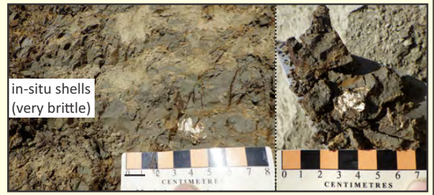

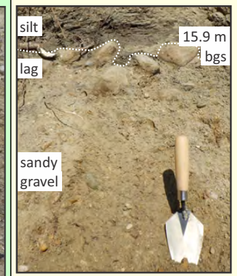

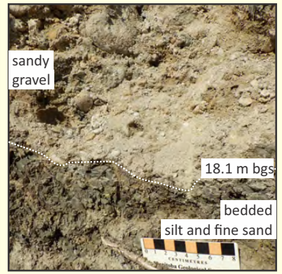





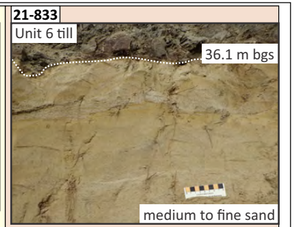

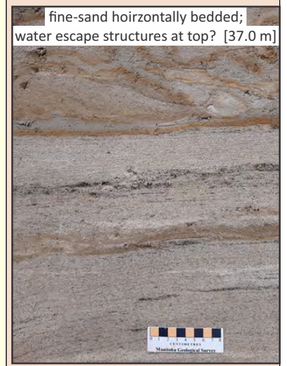



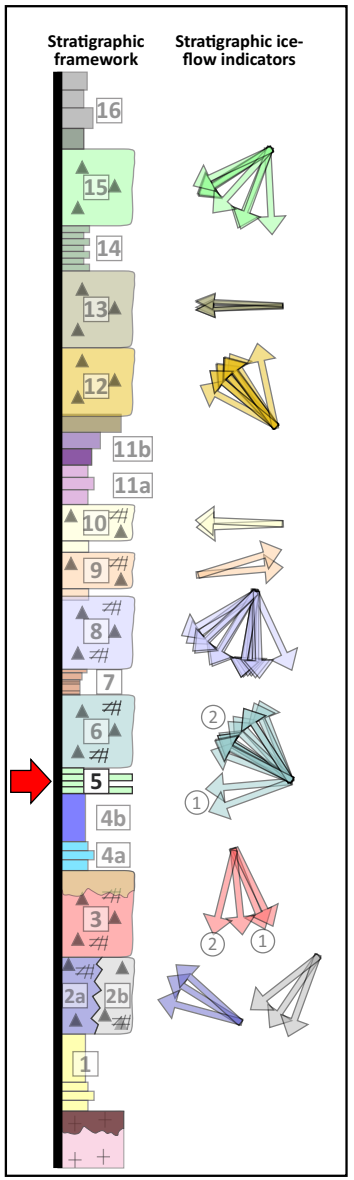

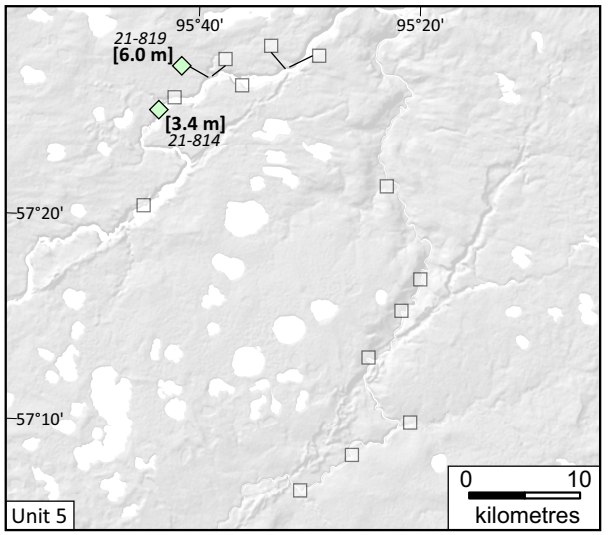

Unit 5 sediments
Key section(s): 21-819

Notes:
-Thick occurrences of bedded diamicton, sand and gravel.
-Interpreted to have occurred during advance of an ice sheet that blocked the natural northeastern drainage routes.
-An identical sequence of sediments were observed in 2022 at the junction of the Hayes and Gods rivers where the overlying till was also deposited by NW-trending ice-flow (Hodder and Gauthier, 2022; MGS report of activities 2022, p. 110–120).

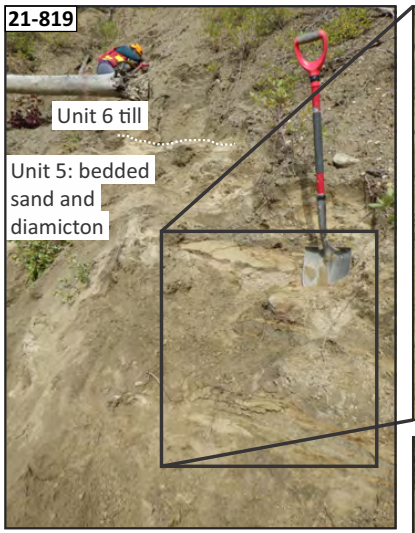

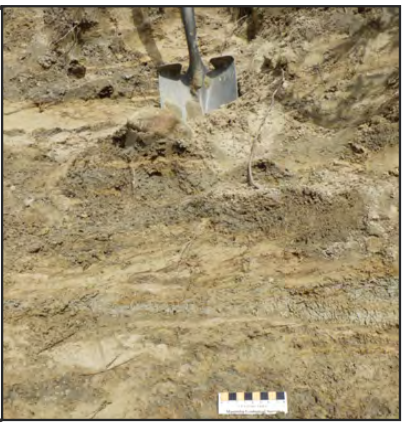





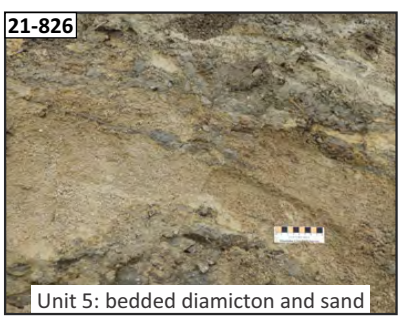

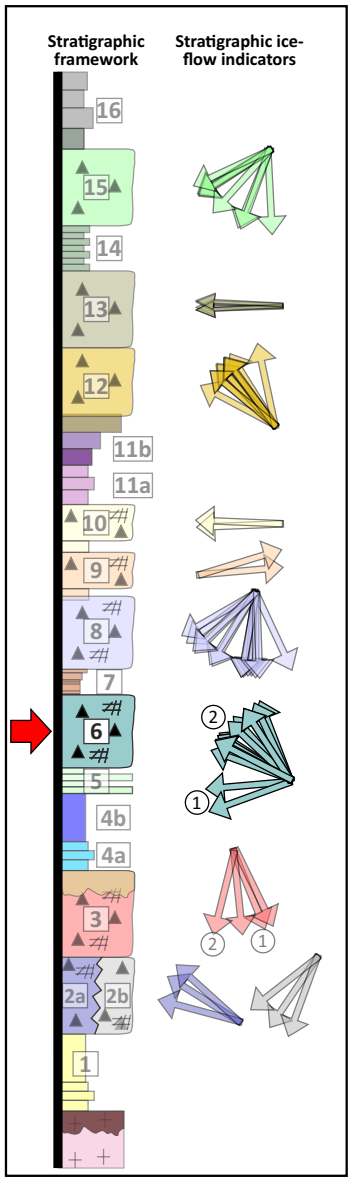

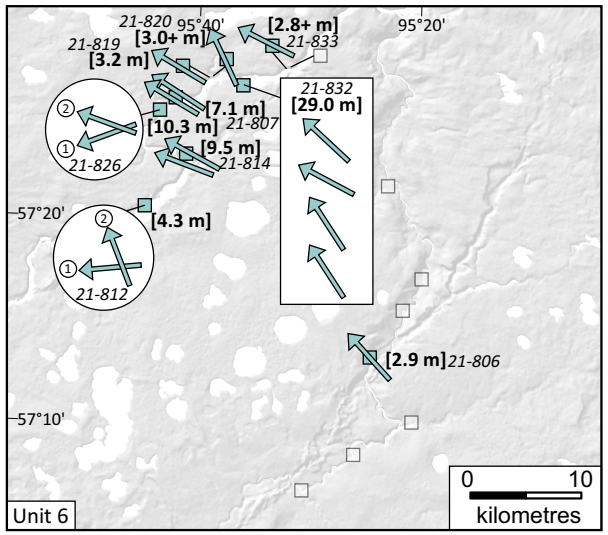

Unit 6 sediments
Key section(s): 21-832; most Churchill R. sections

Notes:
-The till often had a distinguishable fissile appearance in field (e.g., 21-814), but not always and other tills showed similiar characteristics (e.g., Unit 3)
-Fabrics combined with till composition are necessary to differentiate this till from Unit 3 and 8 tills
-The till reaches impressive thicknesses at 21-832. This section was logged in detail and no changes were noticeable throughout the entire interval, except in the lower parts of the till which contains rafts of Unit 4 sediments.



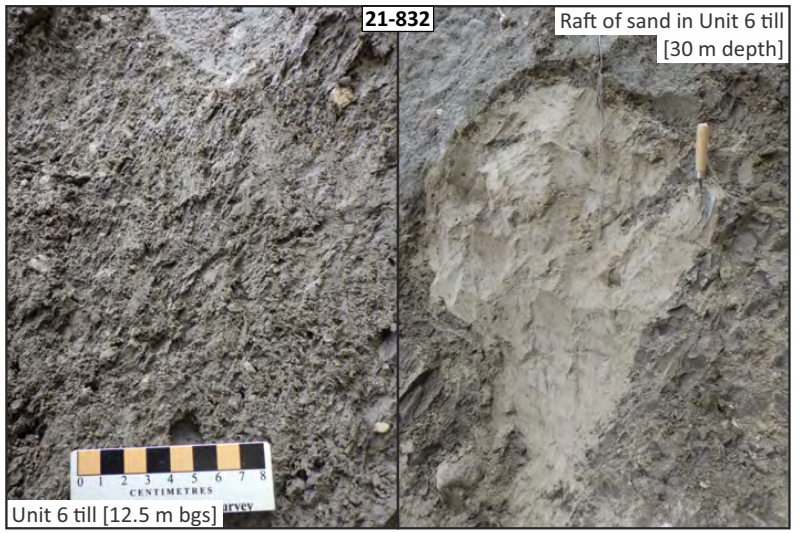

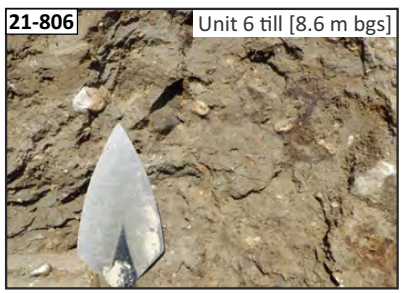









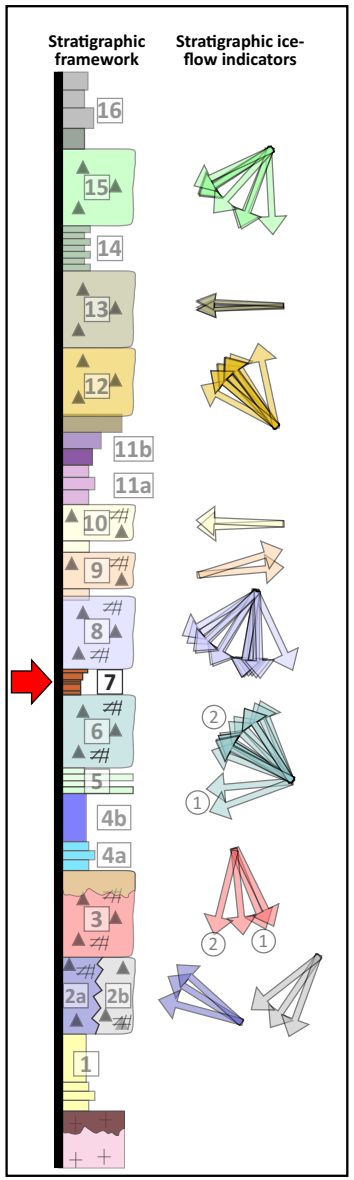

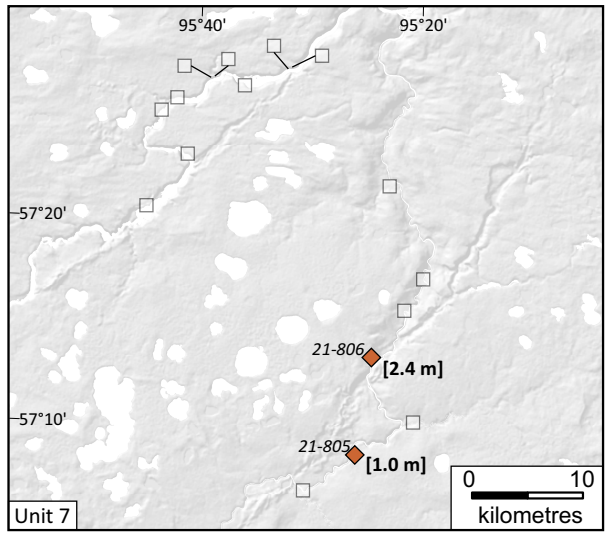

Unit 7 sediments
Key section(s): 21-806

Notes:
-Unit is defined at section 21-806 where it is 2.4 m thick and bounded by two tills deposited by very different ice-flow directions.
-The main question remaining is what do these sediments represent? Interstadial? Or subglacial deposition? The preferred interpretation at this time is proglacial deposition during a brief pull back of the ice sheet; additional investigations required to confirm the significance of these deposits.

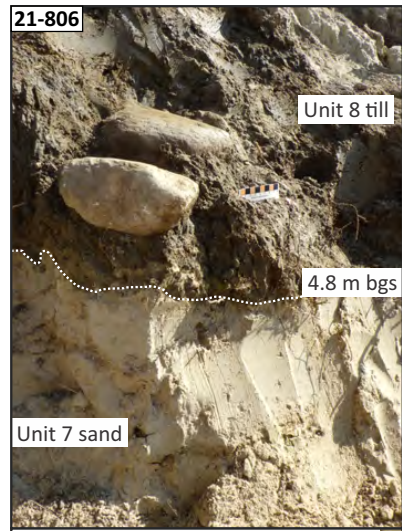



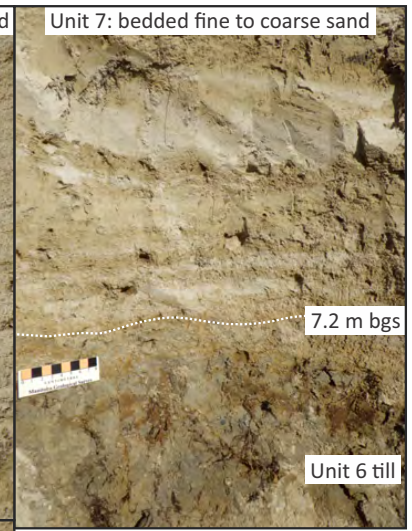

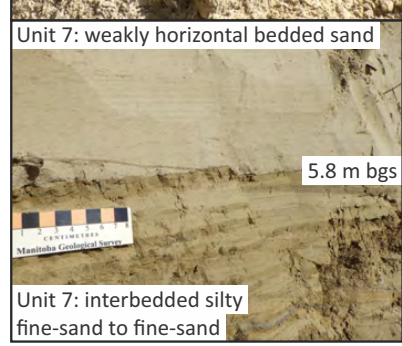

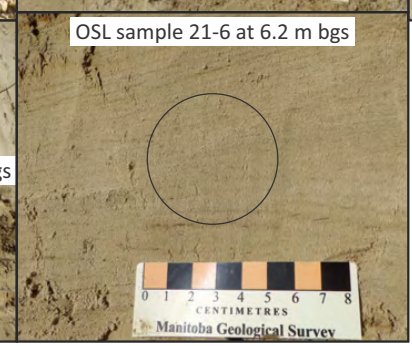





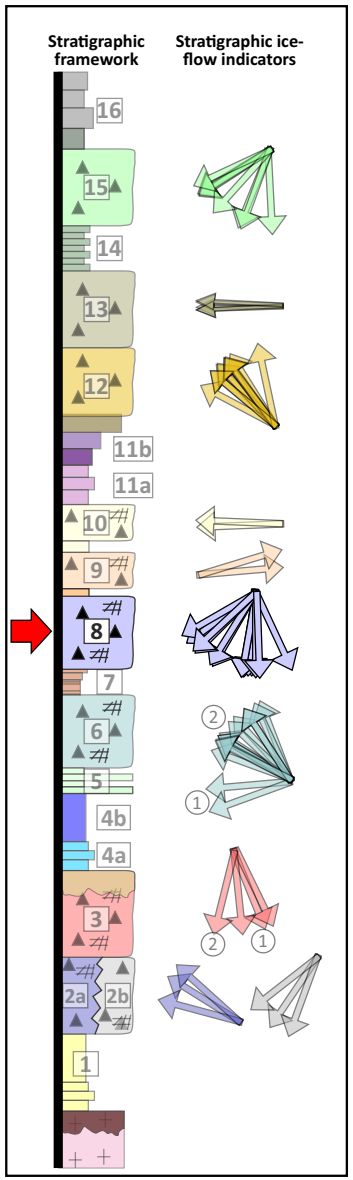

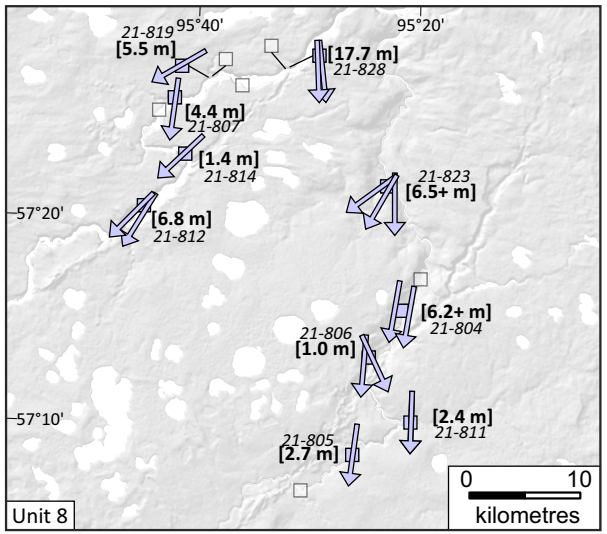

Unit 8 sediments

Key section(s): 21-807; 21-828

Notes:

-Easily identified in the field from the younger tills (e.g., 21-805), but fabrics and composition is needed to differentiate this till from other older tills.

-Unit 8 is exceptionally thick at section 21-828. Unlike Unit 6 at section 21-832, this thick till does contain intertill organic-barren sorted sediments. There's possible more to the story here, but we had limited time at this section and could not obtain more clast fabrics or look for lateral facies variations.

-Likewise, there is 0.6 m of gravel separating two beds of Unit 8 till at section 21-812. What are the implication of these intertill sorted sediments? Ice-marginal oscillations? Subglacial?

-One occurrence of black till correlated to Unit 8 (21-23); no lower bounding surface to constrain this interpretation (could be Unit 1).



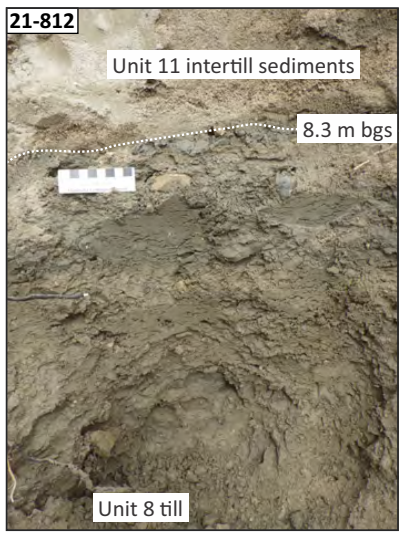

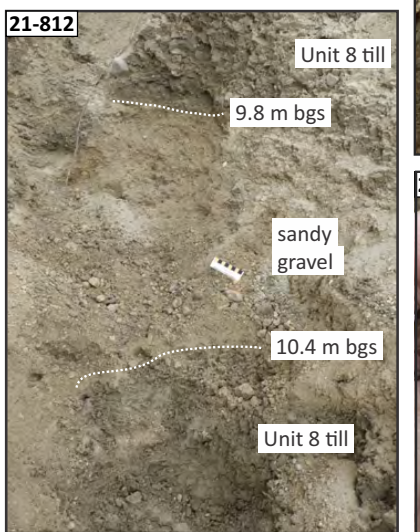

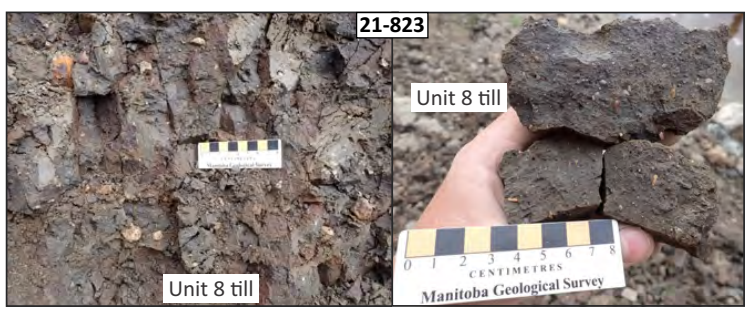





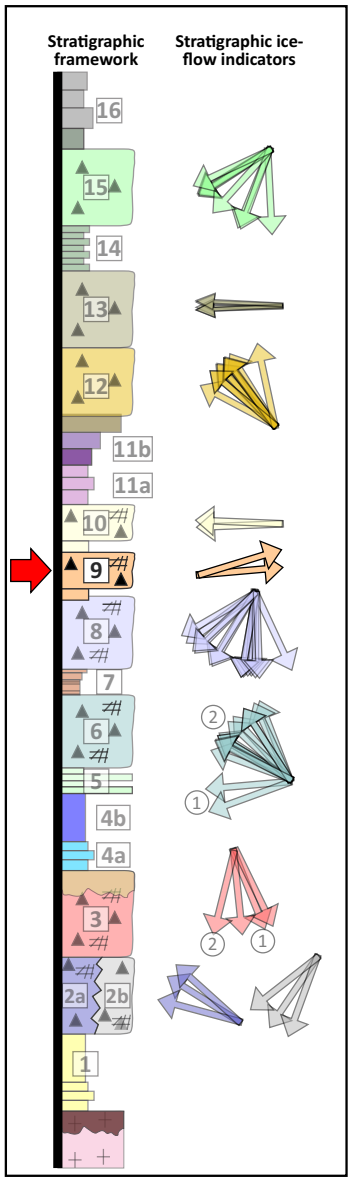

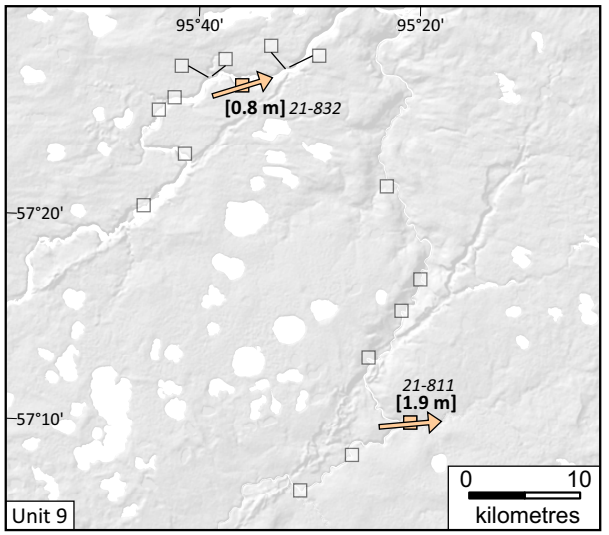

Unit 9 sediments
Key section(s): 21-811

Notes:
-Unit 9 and 10 are defined at section 21-811, where they are in contact.
-An important late-glacial ice-flow event. It would be great to track this down in more sections within the region.

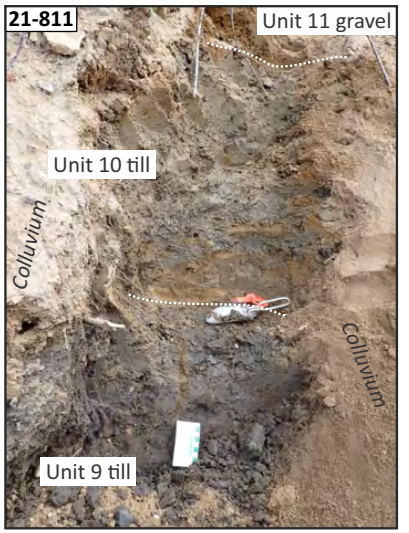

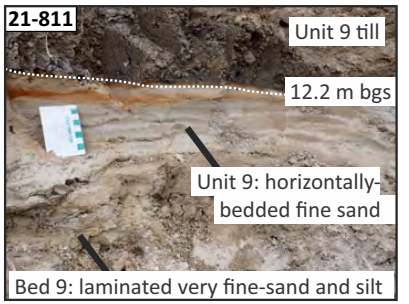





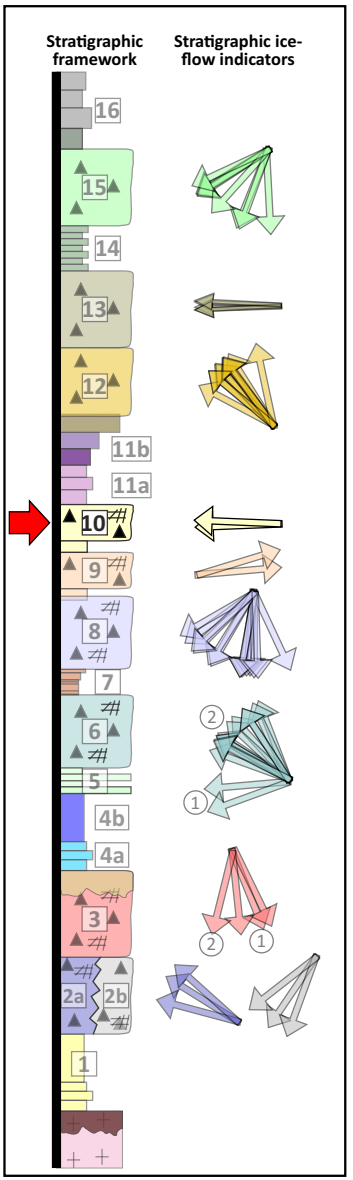

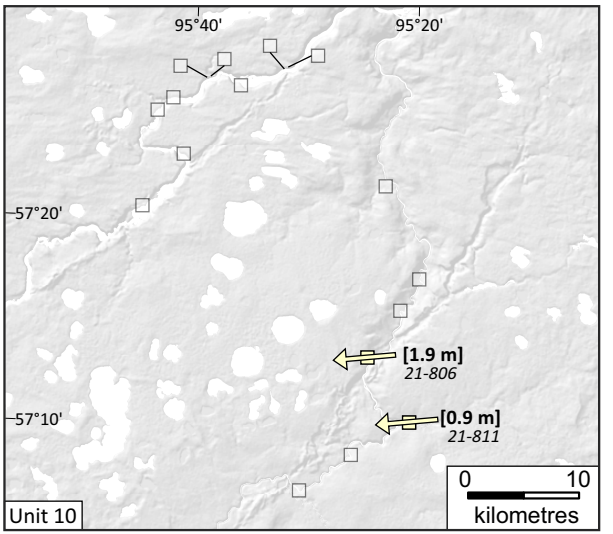

Unit 10 sediments
Key section(s): 21-811

Notes:
-Unit 9 and 10 are defined at section 21-811, where they are in contact.
-More work needs to be done to document these important ice-flow events that are relatively thin within the stratigraphic record.

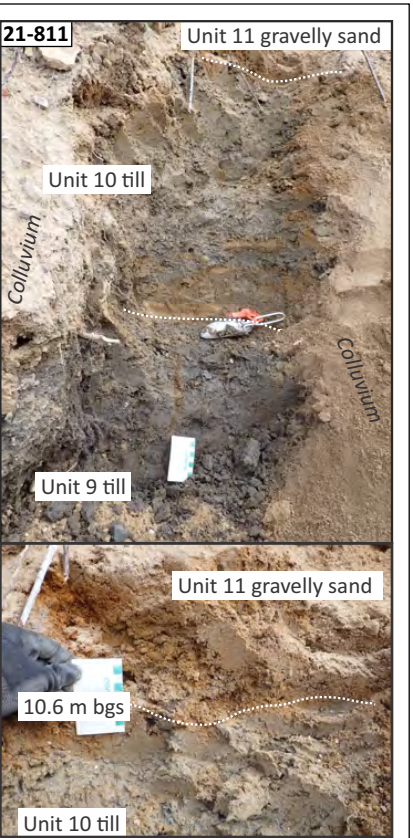

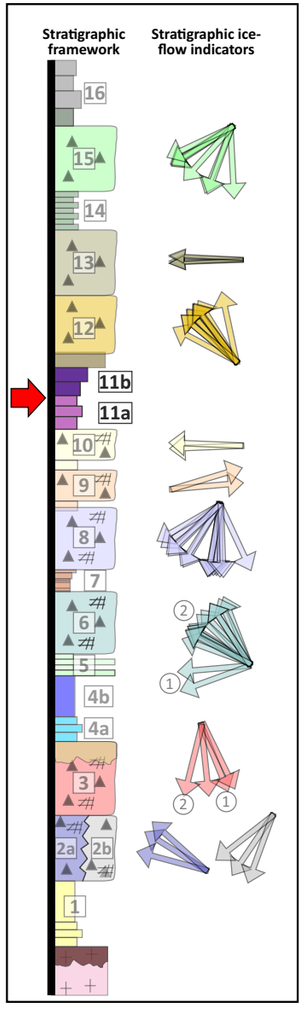

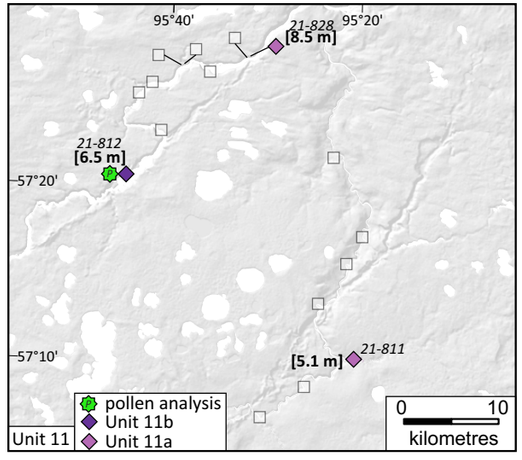

Unit 11 sediments
Key section(s): 21-828; 21-812

Notes:
-Intertill sediments defined by their till bounding surfaces (allostratigraphy)



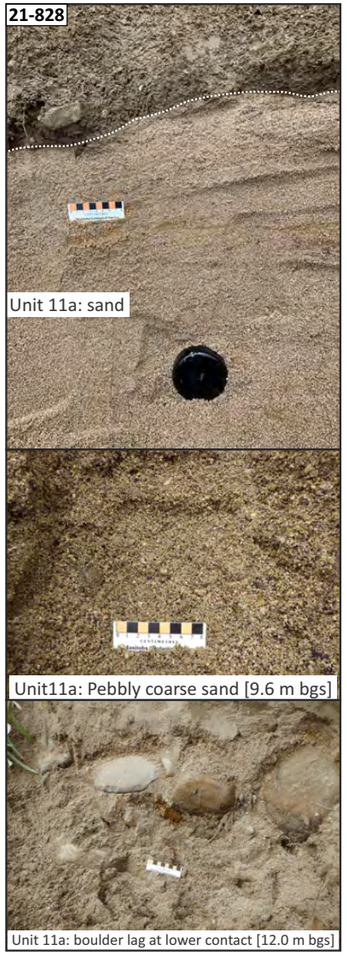



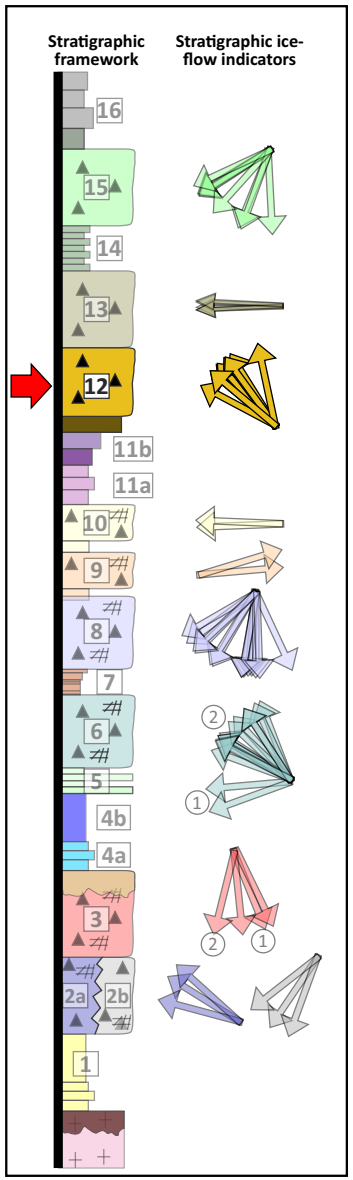

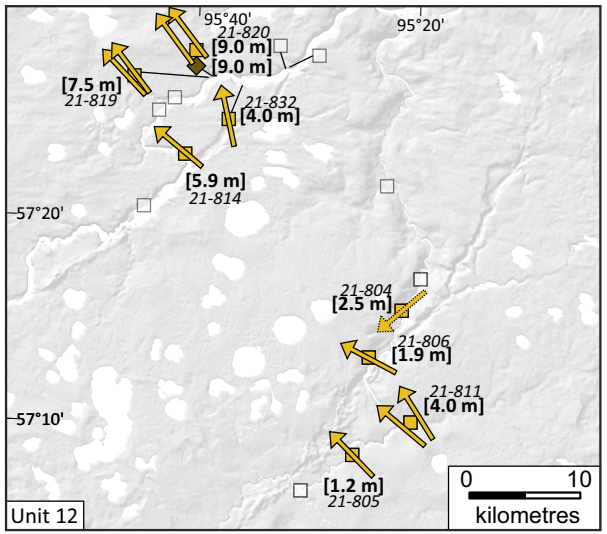

Unit 12 sediments
Key section(s): 21-811; 21-805, 21-819/21-820

Notes:
-Key stratigraphic relationships established with Unit 13 till at sections 21-805 and 21-814.
-Light brown to yellowish brown appearance in field and is significantly less consolidated relative to the older tills in section and has a minor blocky appearance or no blocky appearance
-The subtill gravel at section 21-820 was interpreted to be related to this glacial event (see text); an alternative interpretation is that the gravel was deposited during the preceding nonglacial event (Unit 11).

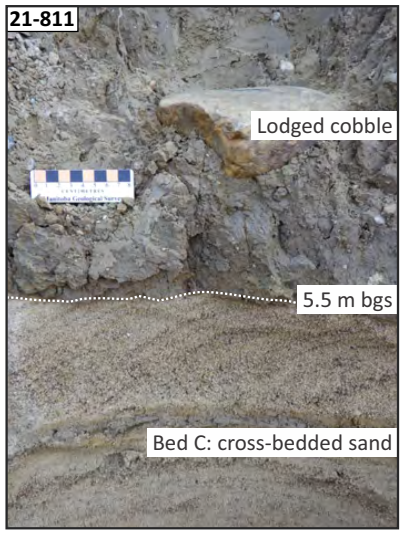





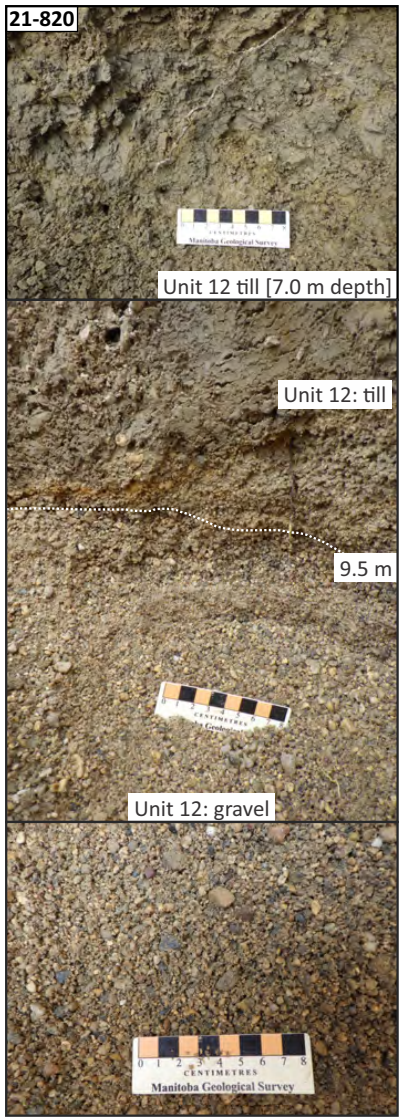

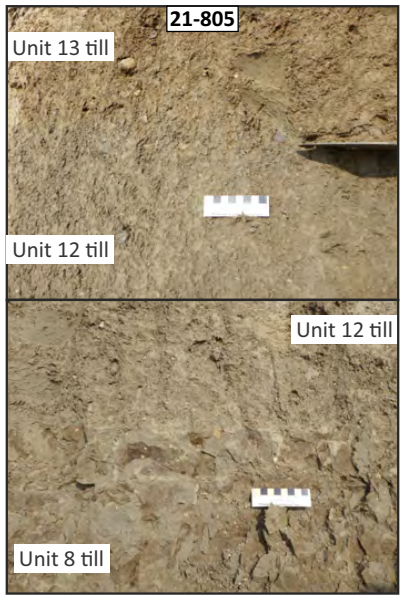

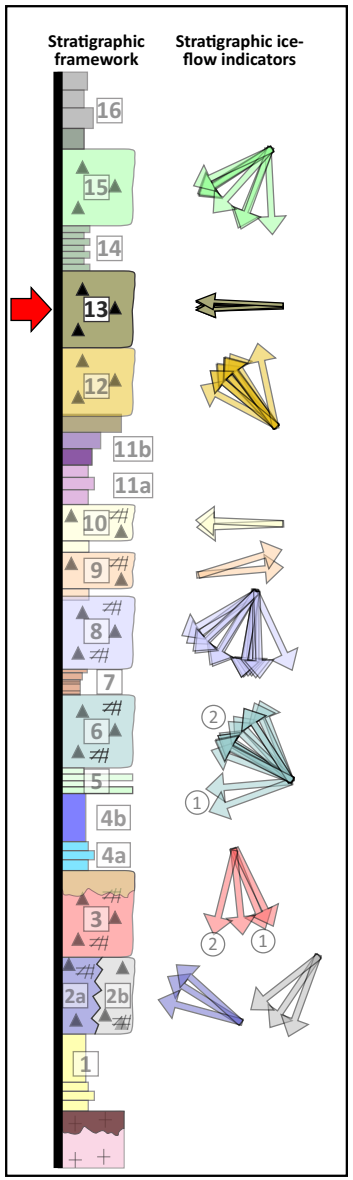

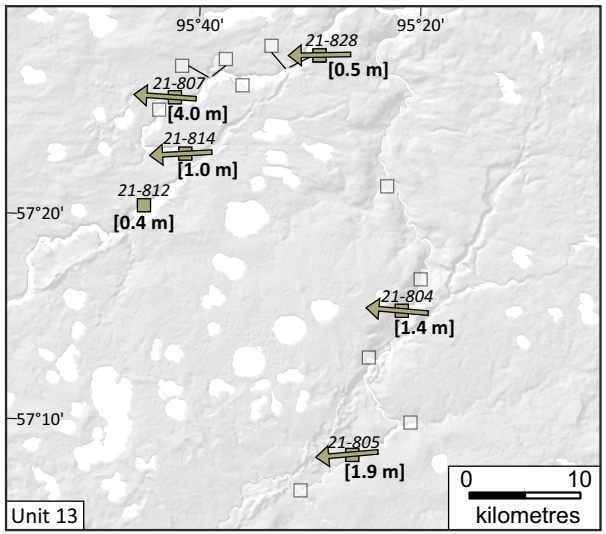

Unit 13 sediments
Key section(s): 21-805, 21-814; 21-828

Notes:
-Key stratigraphic relationships established with Unit 12 till at sections 21-805 and 21-814.

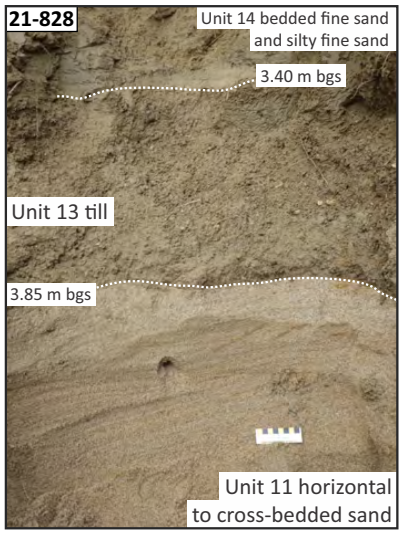

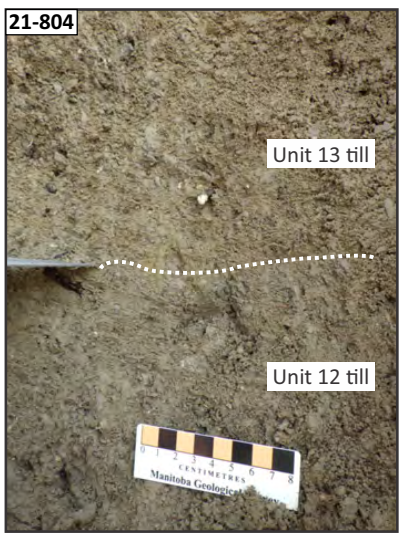



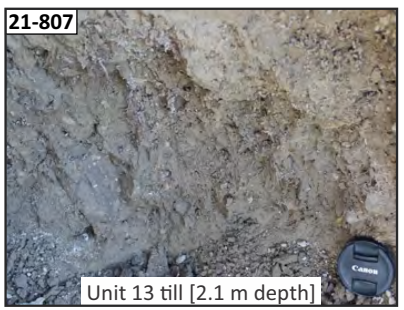

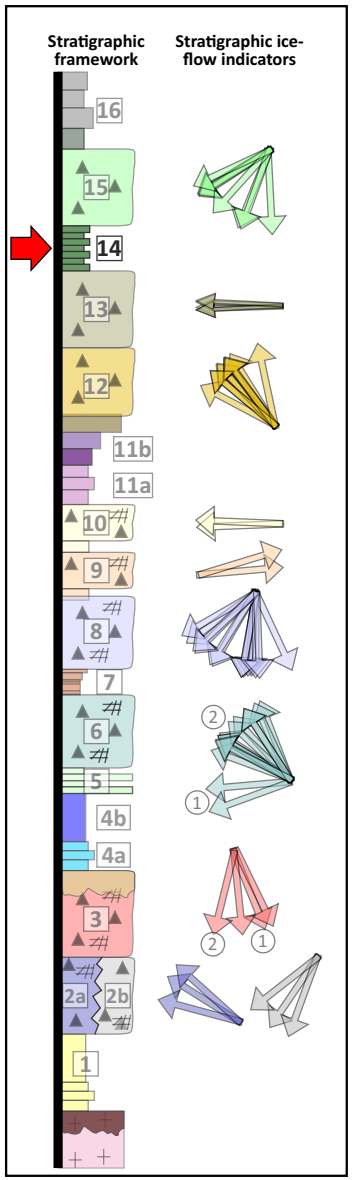

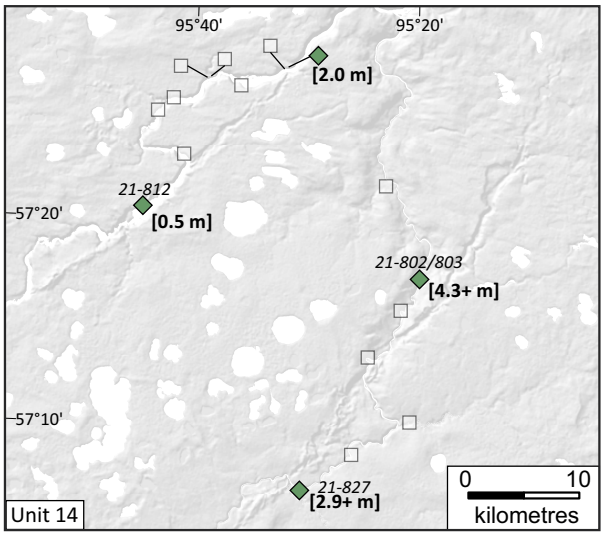

Unit 14 sediments
Key section(s): 21-827; 21-828

Notes:
-Sediments are best exposed at section 21-827 and this section highlights a sharp contact with the overlying Unit 15 till
-Section 21-828 provides key relationships with Unit Unit 13 till.
-The timing of this retreat is unknown but likely late-glacial.

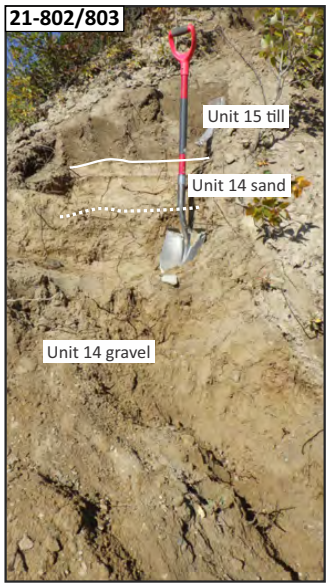

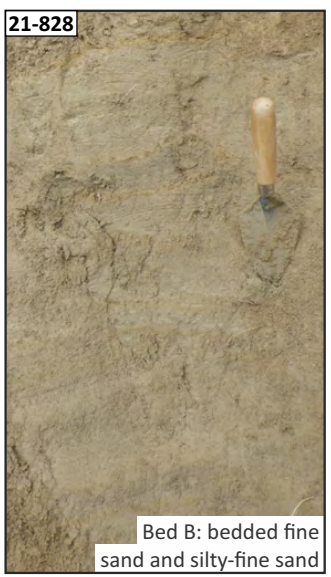



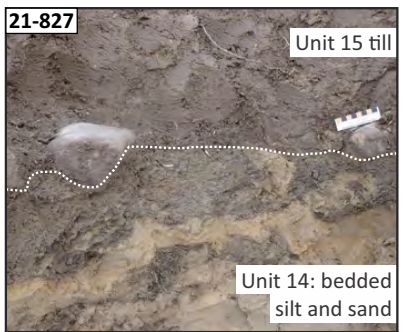



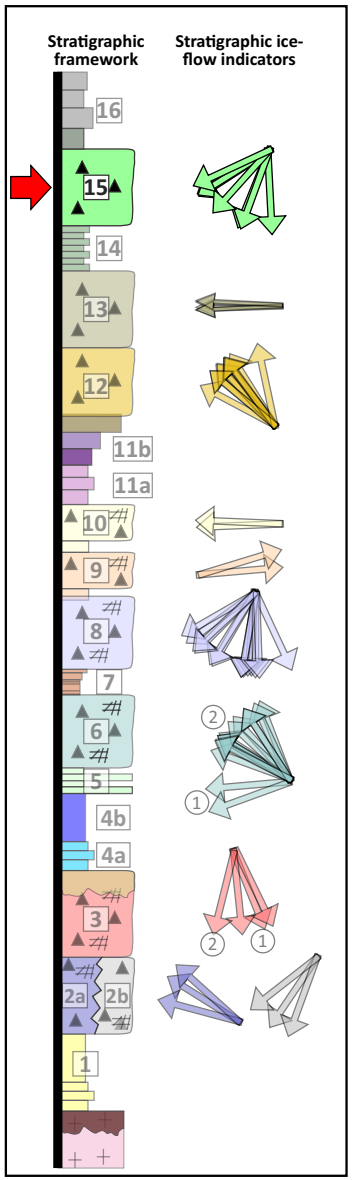

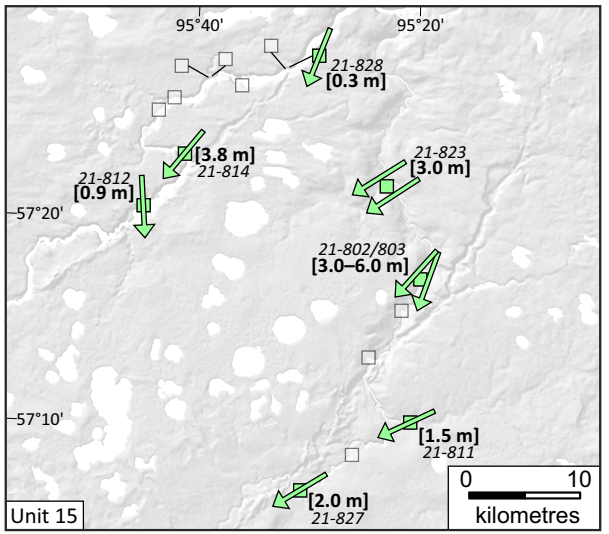

Unit 15 sediments

Key section(s): 21-827; 21-802/803; 21-828

Notes:

-Youngest till in the study area. The till is not blocky and noticeably less consolidated than older tills.

-Ice-flow indicators generally align with eskers, which supports a late-glacial timing of this ice-flow re-advance, which also aligns with the pattern of moraines.

-



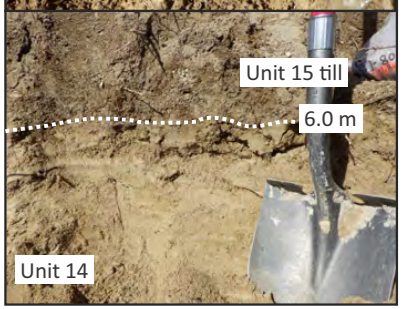

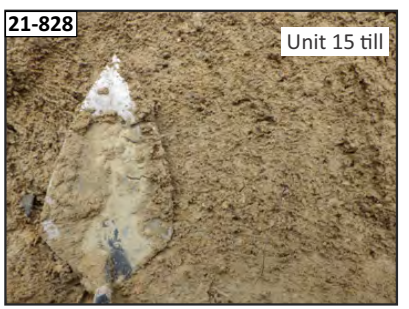



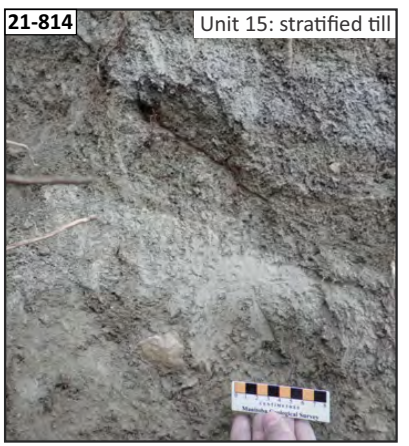

Laurentide ice sheet dynamics across multiple glacial-interglacial cycles, from Quaternary stratigraphic records in central Canada by Hodder et al., Canadian Journal of Earth Sciences.

Supplemental material 3: Till-matrix geochemistry multivariate analysis

First iteration of principal component analysis

Till with a black-coloured matrix (e.g., Figure S2-1) was observed at four sections (21-811; 21-823; 21-832; 21-833) where it is the lowermost exposed till bed at each site. These beds were observed to contain shale cobbles in the field, and this was confirmed by clast counts that indicated a relatively high proportions of black shale or light brown shale and siltstone (BSS). These BSS lithologies are significantly softer compared to other Paleozoic and Precambrian rocks, thus much easier to comminute. The clast counts are not an accurate reflection of the proportion of BSS detritus within till samples and this is reflected in a comparison between the proportion of carbonate clasts and till-matrix (<63 μm size-fraction) carbonate content (Fig. S2-2), which shows that till with a black-coloured matrix have decreased proportions of carbonate content in till-matrix, which is interpreted to be as a result of higher proportions of BSS detritus in the till-matrix (<63 μm size-fraction). The bedrock source of the siltstone/shale detritus is an enigma, since there is no known bedrock source in the region (Dredge and Nixon, 1992). Paleo–ice-flow indicators from these tills (W-, NW- and SSW-trending) indicates that there is likely not a single point source.

An initial iteration of principal component analysis (PCA) was completed using all of the till samples collected during this study. This analysis indicated that the majority of the variance within the dataset was attributed to till that had a black till-matrix colour. The black tills have a strong geochemical association with LREE, HREE, Ti and Mn and plots separately from other samples in PC2-PC1 space (Figure S2-3). Additionally, a single till sample with a grey-coloured matrix plots separately in PC2-PC1 space (Fig. S2-3) and this sample contains a highly elevated proportion of granitoid clasts (81 ct. %), which is an outlier within the dataset (manuscript Figure 10).



Figure S2-1: *Tills with a black-coloured matrix and clast count example: a) contact between Unit 15 and Unit 8 (black-coloured till) at section 21-823; b) Unit 2b black-coloured till at section 21-833; c, d) Unit 2a black-coloured till at section 21-832; e) contact between Unit 8 and Unit 2a (black-coloured till) at section 21-811; and f) example of a clast count (4-8 mm size-fraction) from the black till exposed at section 21-823 with black shale clasts and sulphides associated with shale highlighted by the red dotted ellipse.*

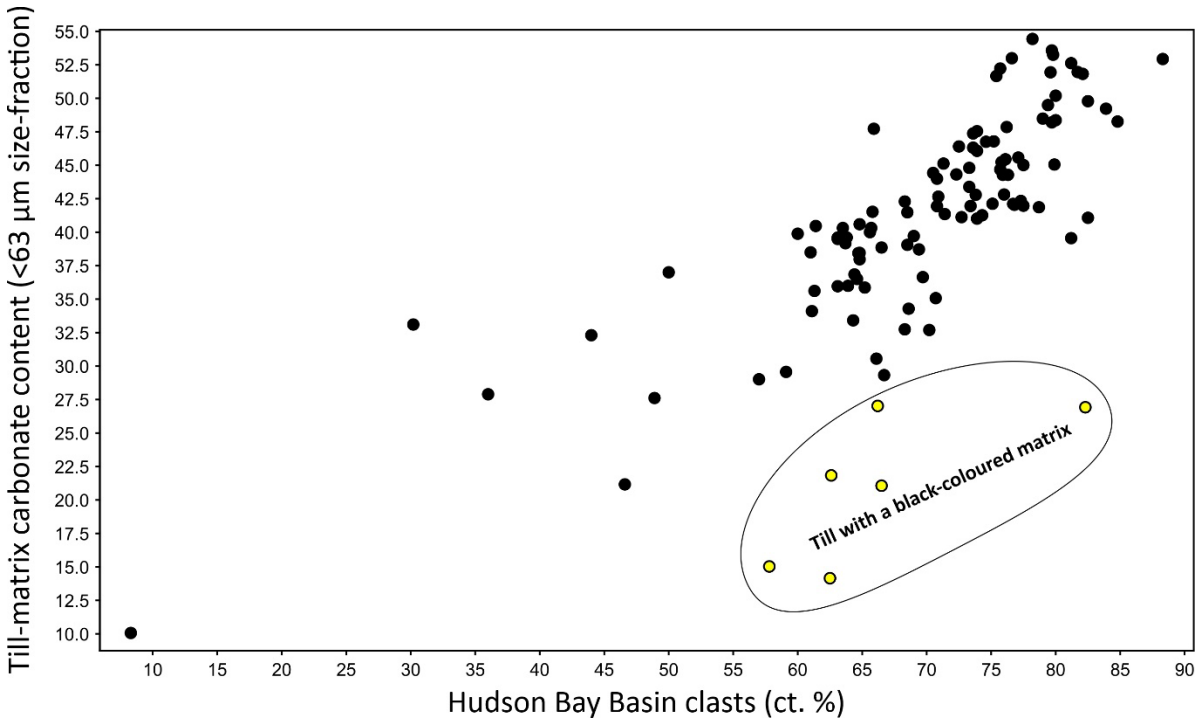

Figure S2-2: *Till-matrix (<63 µm) carbonate content vs. proportion of Hudson Bay Basin clasts (2–8 mm size-fraction).*

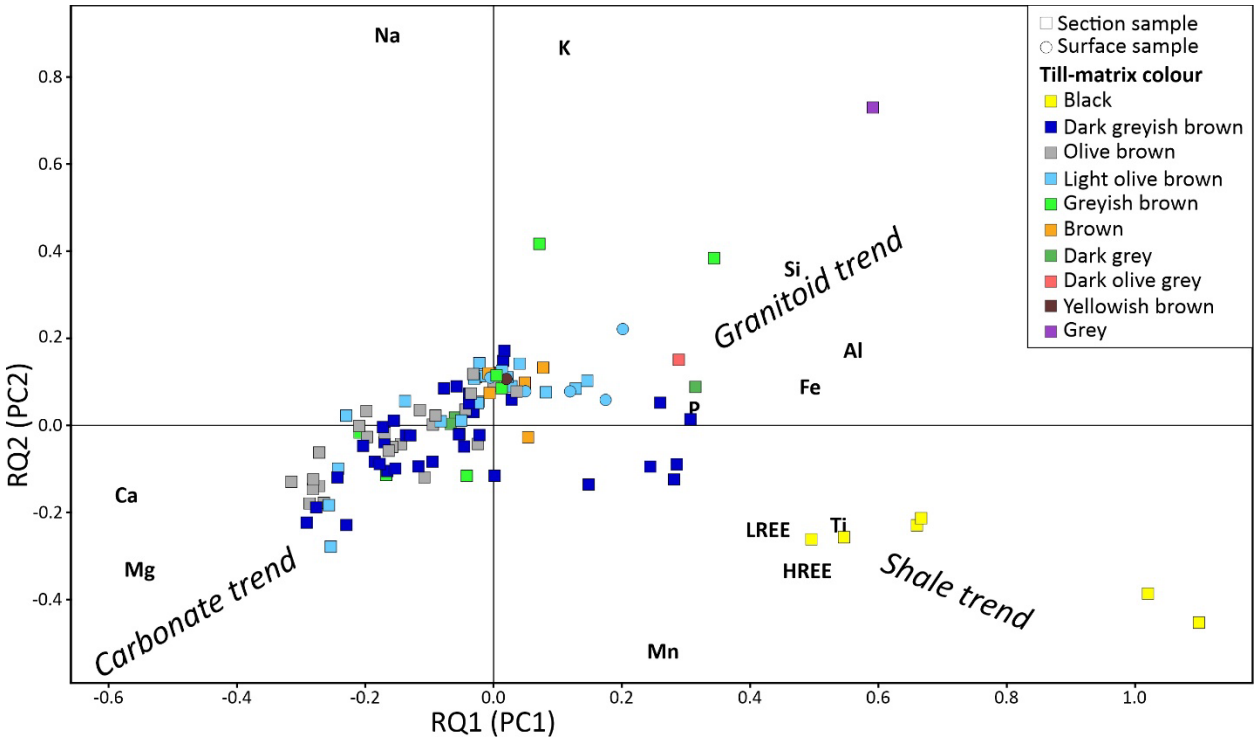

Figure S2-3: *Initial principal component analysis (PC2 vs. PC1 shown) highlighting the distinct black- and grey-coloured tills.*

Second iteration of principal component analysis and k-means clustering – additional plots.

To better understand relationship within the dataset, tills with a black-coloured matrix (high BSS component) and grey-coloured matrix (anomalous granitoid) were removed from the dataset and second iteration of principal component analysis and k-means clustering analysis was completed. The findings of this analysis are presented in the main text of the manuscript and additional plots are provided below (Figures S3-4, S3-5 and S3-6).

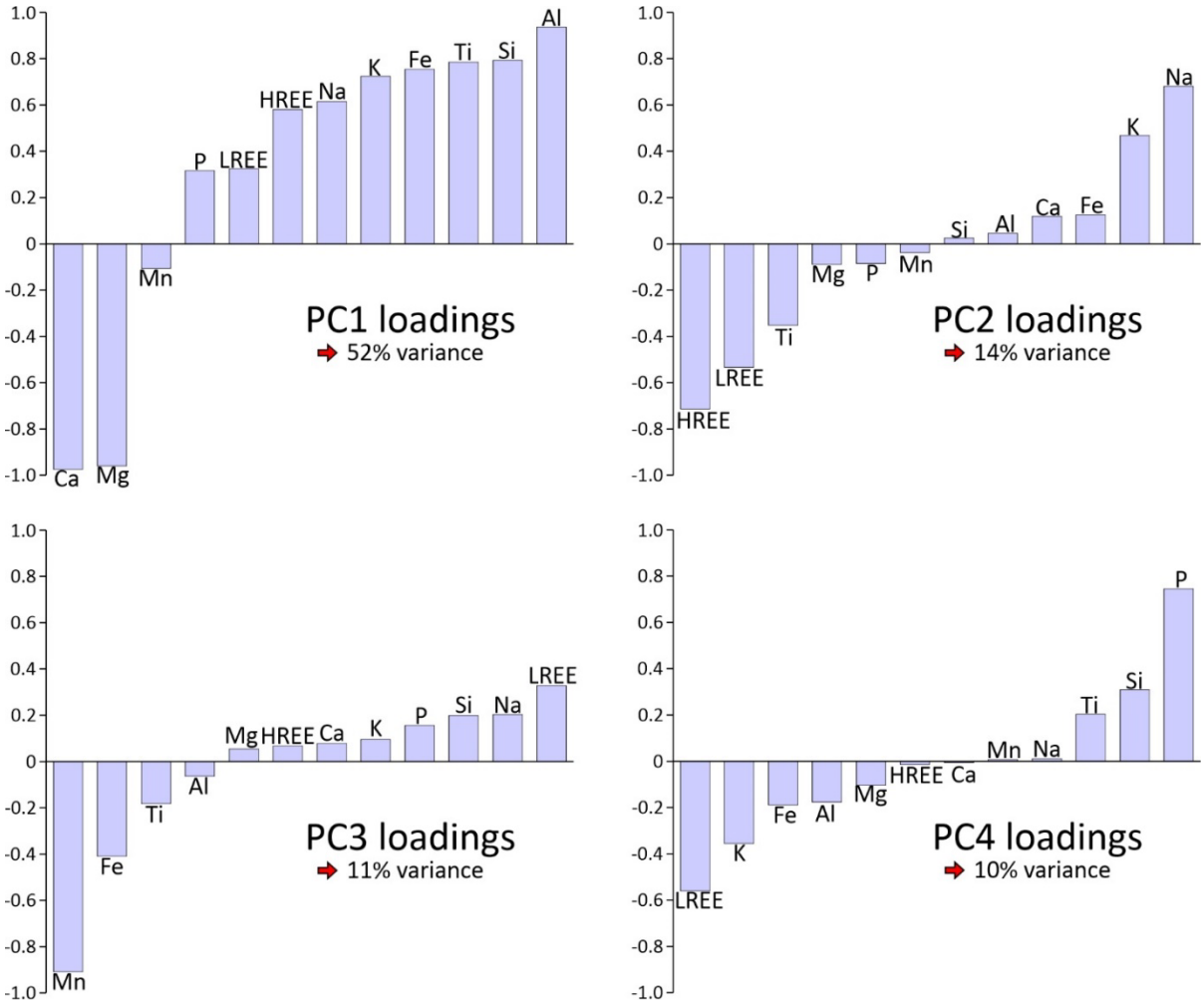

Figure S3-4: *Principal components 1–4 loadings.*

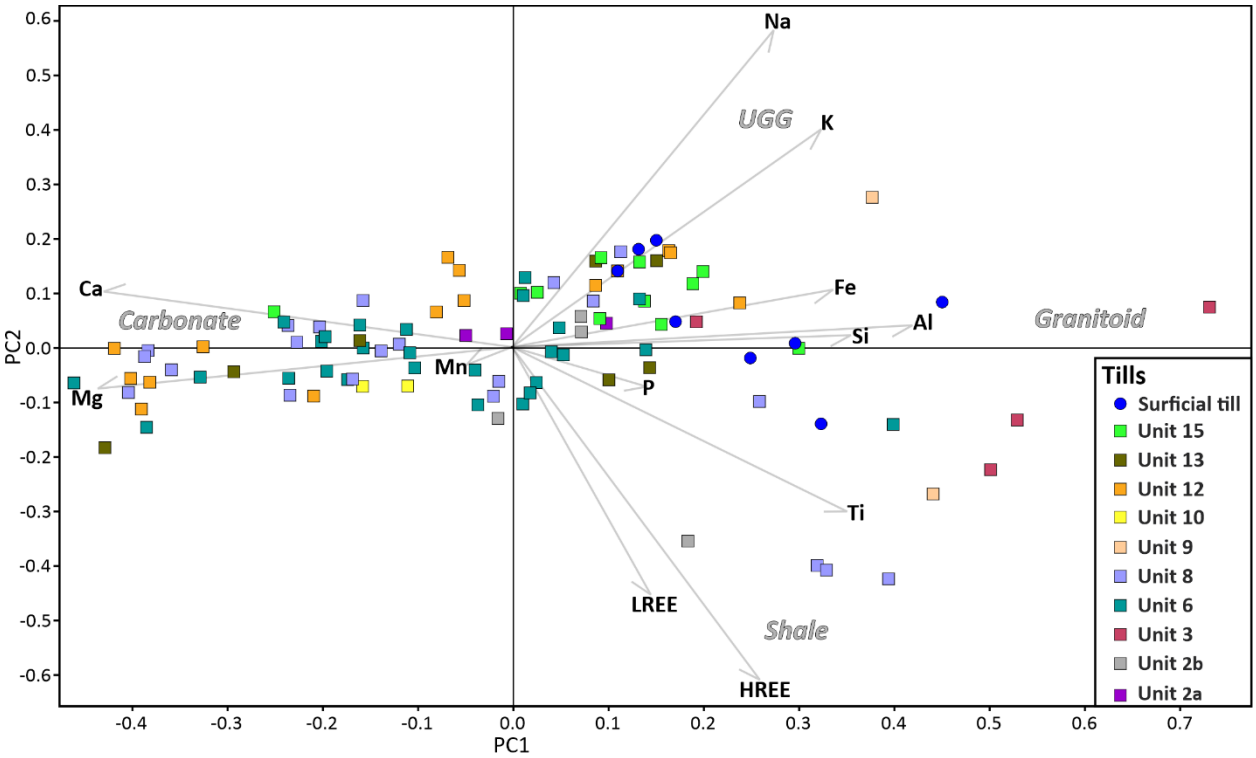

Figure S3-5: *Principal component analysis (PC2 vs. PC1 shown) classified by stratigraphic unit.*

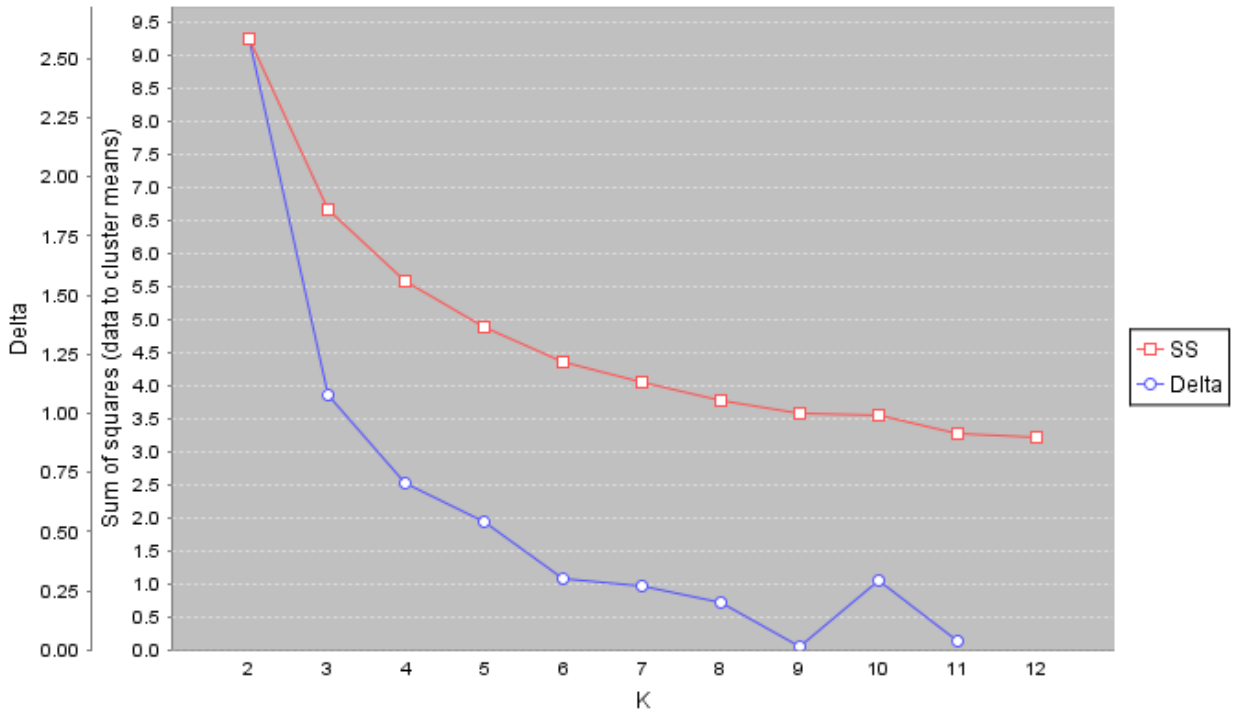

Figure S3-6: *Scree plot of the sum of squares distances of samples to their closest cluster center.*

Laurentide ice sheet dynamics across multiple glacial-interglacial cycles, from Quaternary stratigraphic records in central Canada by Hodder et al., Canadian Journal of Earth Sciences.

Supplemental material 4: Optical age data

This supplemental file contains additional information about the optical dating procedures used including the SAR protocol (Table S3-1), radial plots for dose recovery tests (Figure S3-1), dose rate calculations (Table S3-2), radial plots for samples analyzed (Figure S3-2) and examples of decay curves and dose response curves for aliquots analyzed (Figure S3-3).

Sample measurements

All luminescence measurements were made on a Risø TL/OSL DA-20 reader containing a $^{90}Sr/^{90}Y$ source (the dose rate over measurements period was 4.32–4.52 Gy/min). Luminescence was detected by an Electron Tube PDM 9107Q-AP-TTL-03 photomultiplier tube mounted behind a combination of 5 mm and 2.5 mm-thick Hoya U-340 optical filters, or by an Electron Tubes Ltd. 9235QB placed behind a 7.5-mm-thick Hoya U-340 optical filter. Aliquots were stimulated by blue light at 56 mW/cm^2 for 100 s while being held at 125°C.

Equivalent dose (D_e) values for each aliquot (50-100 quartz grains of 180-250 µm diameter per aliquot) was determined by repeatedly measuring and dosing them using the single aliquot regenerative-dose (SAR) protocol (Murray and Wintle 2000, 2003). Quality assurance tests are built into the measurement sequence (i.e., tests to check for sensitivity changes and recuperation (Murray and Wintle 2000; Wintle and Murray 2006). Table S1 shows the SAR protocol used to determine D_e values for all samples in this study, including an IR wash before each blue stimulation to reduce signals from potential feldspar contamination. For each aliquot the first 0.1 seconds of the signal, with the last 20 s subtracted, was used to construct dose-response curves onto which the natural signal was interpolated to find the D_e value.

Table S4-1: SAR protocol for Hudson Bay Lowland quartz samples. All steps of the protocol constitute one SAR cycle. Ln = natural signal, Lx= regenerative dose signal. Tn = test dose signal measured after Ln, Tx = test dose signal measured after Lx. The first SAR cycle measures the sensitivity corrected natural signal, and subsequent SAR cycles measure the Lx/Tx value after a series of successively increasing laboratory radiation doses (regeneration doses) administered to the sample. The regeneration doses are used to generate a dose-response curve onto which the natural signal (Ln/Tn) is plotted to calculate the De value. Regeneration doses include: 1) one "zero-dose" point where no radiation dose is given to check for recuperation and 2) one "repeat-dose" point, where a previous regeneration dose is given a second time to perform a recycling ratio test.

Step	Procedure	Measured	
1	Natural/Regenerative dose	~45–528 Gy	
2	Preheat (220º C, 10 s)		
3	IR stimulation (50ºC, 100 s at 130 mW/cm^3)		IR wash
4	Blue stimulation (125º C, 100 s at 56 mW/cm^2)	L_n or L_x	

5	Test dose	~5 Gy	
6	Preheat (160º C, 10 s)		
7	IR stimulation (50º C, 100 s at 130 mW/cm^3)		IR wash
8	Blue stimulation (125 ºC, 100 s at 56 mW/cm^2)	T_n or T_x	
9	Return to step 1		

The suitability of the protocol and measurement conditions were tested in a pilot study where 10 aliquots were measured using the protocol shown in Table S3-2. Analysis of the data showed the presence of the desired 'fast component' in all samples, i.e., bright, fast-decaying luminescence signals (Figure S3-2).

To ensure the sample can reproduce a given dose using the chosen SAR protocol, a dose recovery test was performed on 10 aliquots. Aliquots (50–100 grains per aliquots) were bleached in natural direct sunlight for 30 min and then given a laboratory dose close to the expected natural dose (90-330 Gy, depending on the sample). All dose response curves were fitted with a saturating exponential plus linear function, and routine screening criteria were applied. Aliquots were excluded from further analysis if (Wintle and Murray 2006):

- Luminescence signal counts were less than three times the background signal.
- Significant IR signals indicated feldspar contamination that could not be removed using the IR wash (steps 3 and 7 in Table S3-2).
- Failure to produce, to within 10%, the same sensitivity-corrected signal from identical regeneration doses given at the beginning and end of the SAR sequence, which suggests inaccurate sensitivity correction (recycling test).
- The test dose error was >10%.
- The recuperation (thermal transfer) value (i.e., the L_x/T_x value measured after the "zero-dose" point regenerative dose) exceeded 10 % of the sensitivity-corrected natural signal (L_n/T_n) indicating This 10 % tolerance value was set higher than the typical 5 % to be able to accept more aliquots for D_e (age) determination.
- The L_n/T_n signal was extrapolated onto the dose response curve beyond the highest given dose point.

A sample is deemed suitable for dating if the dose recovery ratio (ratio of given dose to measured equivalent dose) does not exceed ±10 % of unity (at 1σ) (Murray and Wintle 2003). Dose recovery ratios (DRR) between 0.80 ± 0.06 and 1.12 ± 0.04 were calculated which suggests that any given dose can be sufficiently and accurately recovered using the chosen SAR protocol with a preheat of 220 º C for 10 s (Table 4). For sample HBL21-13, the DRR is slightly lower than the desired ±10 % of unity at 1σ. Overdispersion (OD) for dose recovery tests range 2 ± 14 % to 15 ± 7 %. The dose recovery overdispersion for sample HBL21-9 is 0 ± 0 % which is unusual, as is the OD value (0 ± 3%) for the fraction of this sample that was dated (Table 4).

OD is the spread in the aliquot D_e values that is above and beyond that associated with analytical uncertainties (Lian and Roberts 2006; Roberts et al. 2015), beyond the spread that might come from incomplete bleaching (inherited signal/age). The causes of OD are unknown. But some of it is likely due to variations in luminescence characteristics of individual grains and microdosimetry effects (Galbraith

and Roberts 2012). Even for samples that have been bleached and dosed in the laboratory, where microdosimetry is not present, as is done for dose recovery tests, OD can be as high as 15% or more. But for most dose recovery experiments OD is typically only a few percent (Galbraith and Roberts 2012). For sample HBL21-9 it is possible (likely?) that its unusually low OD indicates that it consists of grains that were well bleached in the environment with uniform luminescence characteristics.

Supplemental 4 references

Galbraith, R.F., and Roberts, R.G., 2012. Statistical aspects of equivalent dose and error calculation and display in OSL dating: an overview and some recommendations. Quaternary Geochronology 11, 1-27.

Lian, O.B., Roberts, R.G., 2006. Dating the Quaternary: progress in luminescence dating of sediments. Quaternary Science Reviews 25, 2449–2468.

Murray, A.S., and Wintle, A.G. 2000. Luminescence dating of quartz using an improved single-aliquot regenerative-dose protocol. Radiation Measurements, 32: 57–73. doi:10.1016/S1350-4487(99)00253-X.

Murray, A.S., and Wintle, A.G. 2003. The single aliquot regenerative dose protocol: potential for improvements in reliability. Radiation Measurements, 37: 377–381. doi:10.1016/S1350-4487(03)00053-2.

Roberts, R.G., Jacobs, Z., Bo, Li, Jankowski, N.R., Cunningham, A.C, and Rosenfeld, A.B. 2015. Optical dating in archaeology: thirty years in retrospect and grand challenges for the future. Journal of Archaeological Science 56: 41–60

Wintle, A.G., Murray, A.S., 2006. A review of quartz optically stimulated luminescence characteristics and their relevance in single-aliquot regeneration dating protocols. Radiation Measurements 4:1 396–391.

Figure S3-1: Radial plots for each sample of the dose recovery ratios for single aliquots of quartz from the Hudson Bay Lowland. The grey lines indicate the weighted mean for the dose recovery ratios (CAM), and the grey bar should capture 95% of all measured aliquots if they are statistically consistent at 2σ with a common value, which is the CAM of the dose recovery ratios in these plots.

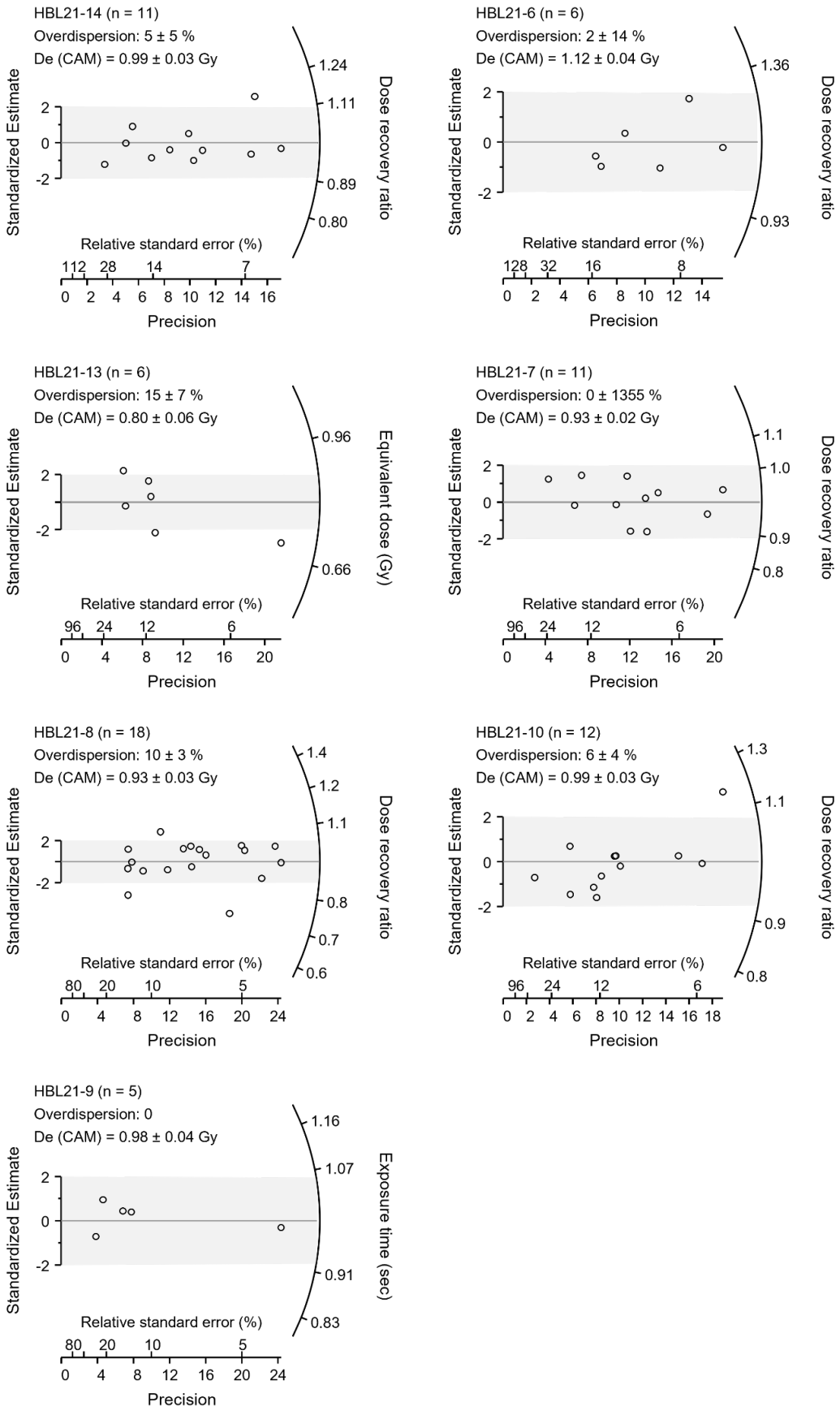

Table S3-2: Optical age sample water content, radioisotopes concentrations, sample depths, and calculated dose rates.

SectionID	Unit	Interpreted depositional environment	Lab ID	Latitude	Longitude	d^a (m)	$\Delta^{w\,b}$	K (%)	U (μg·g^{-1})	Th (μg·g^{-1})	$\dot{D}_C$ (Gy/ka)[c]	$\dot{D}_T$ (Gy/ka)[c]
112-21-832	4a	nearshore marine	HBL21-14	57.4461	-95.5957	34.8	0.111	1.40 ± 0.04	1.12 ± 0.06	5.37 ± 0.14	0.018 ± 0.002	1.79 ± 0.05
112-21-819	4a	nearshore marine	HBL21-11	57.4501	-95.6473	23.1	0.029	1.24 ± 0.09	0.520 ± 0.131	3.43 ± 0.19	0.032 ± 0.003	1.55 ± 0.09
112-21-812	4b	fluvial or lacustrine	HBL22-5	57.3458	-95.7363	19.6	0.302	1.57 ± 0.10	0.610 ± 0.129	3.70 ± 0.20	0.040 ± 0.004	1.91 ± 0.10
112-21-806	7	proglacial lacustrine	HBL21-6	57.2293	-95.3912	6.2	0.120	1.26 ± 0.09	1.11 ± 0.16	6.47 ± 0.34	0.112 ± 0.011	1.81 ± 0.09
112-21-828	11a	nearshore marine	HBL21-13	57.4621	-95.5241	4.1	0.013	1.10 ± 0.06	0.689 ± 0.088	2.79 ± 0.14	0.140 ± 0.010	1.55 ± 0.07
112-21-811	11a	nearshore marine	HBL21-7	57.1778	-95.3258	6.1	0.012	1.56 ± 0.12	0.560 ± 0.125	3.08 ± 0.17	0.113 ± 0.011	1.96 ± 0.11
112-21-811	11a	nearshore marine	HBL21-8	57.1778	-95.3258	7.8	0.113	1.36 ± 0.08	0.510 ± 0.102	3.15 ± 0.16	0.100 ± 0.010	1.57 ± 0.07
112-21-812	11b	fluvial or lacustrine	HBL21-10	57.3458	-95.7363	8.0	0.061	1.31 ± 0.07	1.05 ± 0.10	4.08 ± 0.20	0.100 ± 0.010	1.79 ± 0.08
112-21-812	11b	fluvial or lacustrine	HBL21-9	57.3458	-95.7363	3.3	0.010	1.18 ± 0.10	0.710 ± 0.127	3.30 ± 0.18	0.150 ± 0.015	1.68 ± 0.08

[a] d = sample depth beneath the ground surface, measured from the centre of the collection tube (5 cm diameter).

[b] Δ^w = water content (mass water/mass dry sediment). For the dose rate calculations each Δ^w value included an uncertainty of ±10% (1s) to account for fluctuations in water content over time.

[c] $\dot{D}_C$ = cosmic ray dose rate; $\dot{D}_T$ = total dose rate (that due to cosmic rays plus that due to β and γ radiation).

Figure S3-2: Radial plots showing the distribution of aliquot D_e values for each sample and estimations of representative D_e values (weighed mean) used for dating, using either the CAM (dotted line that intersects the curved axis) or the MAM (solid line that intersects the curved axis). Values that plot in the shaded zones fall within 2σ of the weighted mean value.

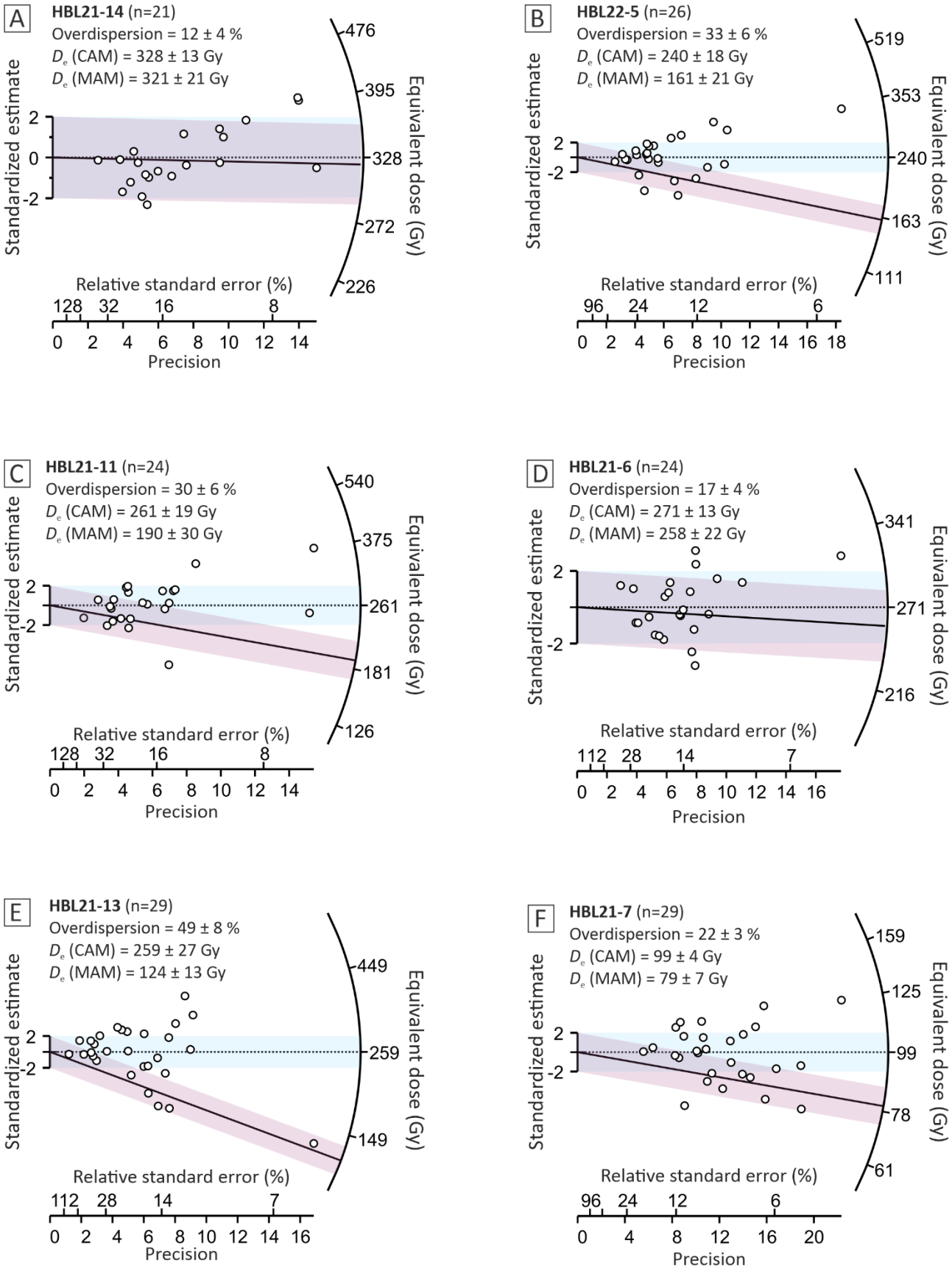

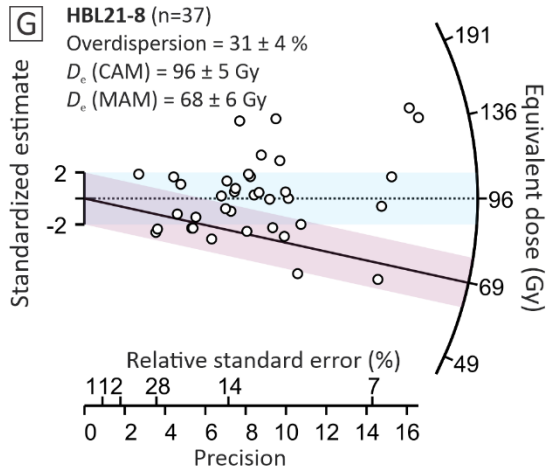

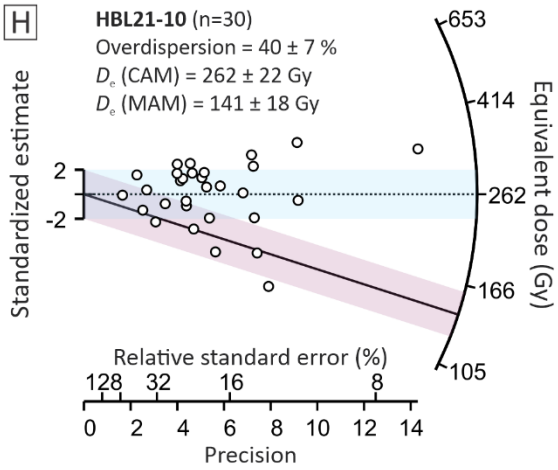

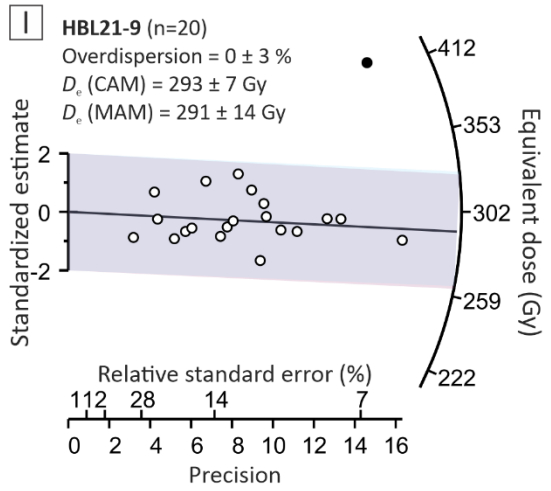

CAM and MAM values shown with the outlier (black solid circle) removed from the dataset.

Figure S3-3: Luminescence decay curves (main graph) showing the "natural" signal and dose response curves (inset) for each optical sample analyzed (A–I). These curves are typical for aliquots measured for each sample and show a clear exponential plus linear dose response. Note, that the initial part of the decay curve is dominated by the desired 'fast' component for each sample. In each case, the final 20 s of the signal was subtracted from the initial 0.1 s and this value (L_i) was divided by the value measured from a subsequent test dose (T_i) to produce the sensitivity-corrected signal (L_i/T_i), which is plotted on the y-axis of the dose response curve.

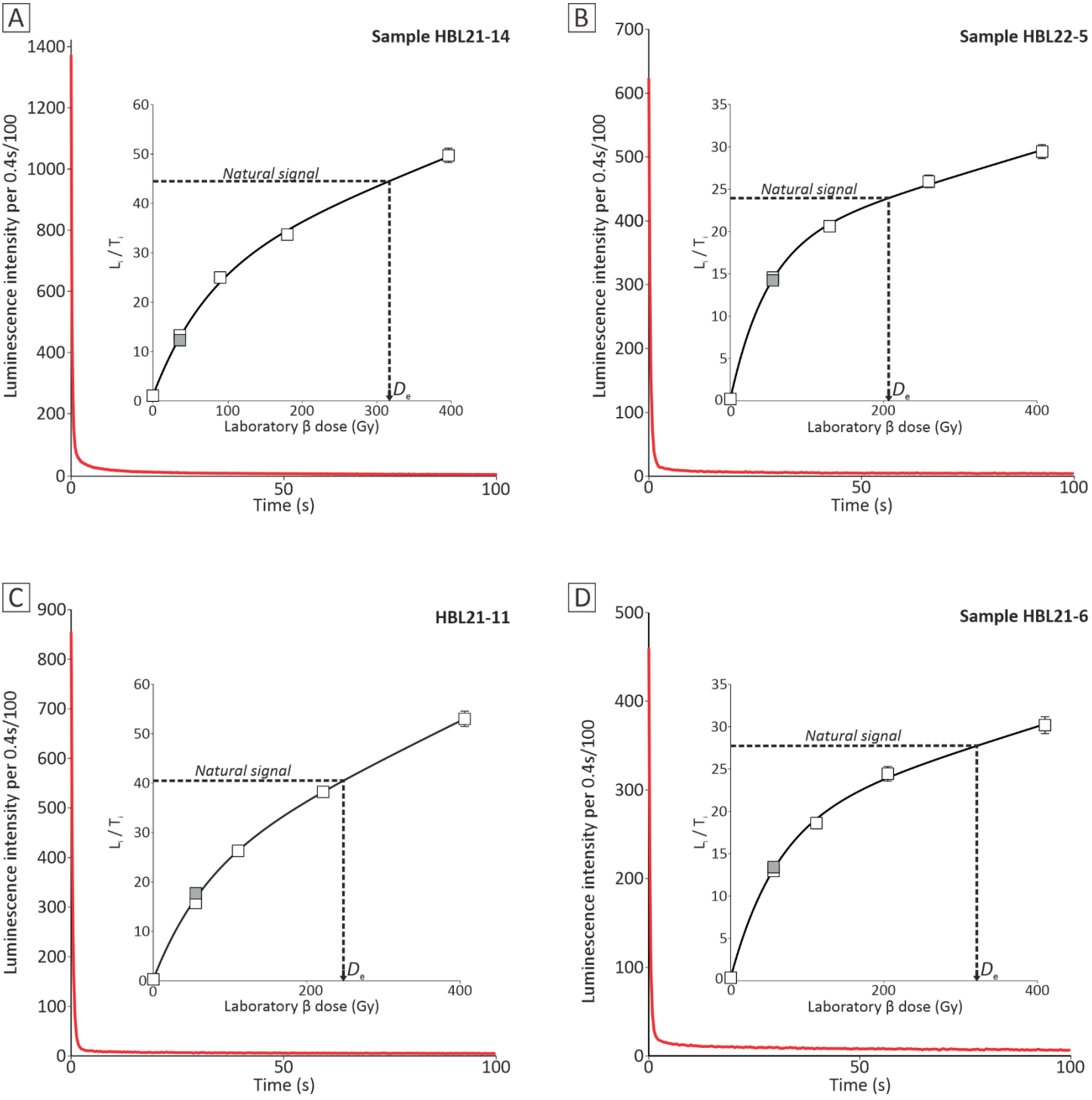

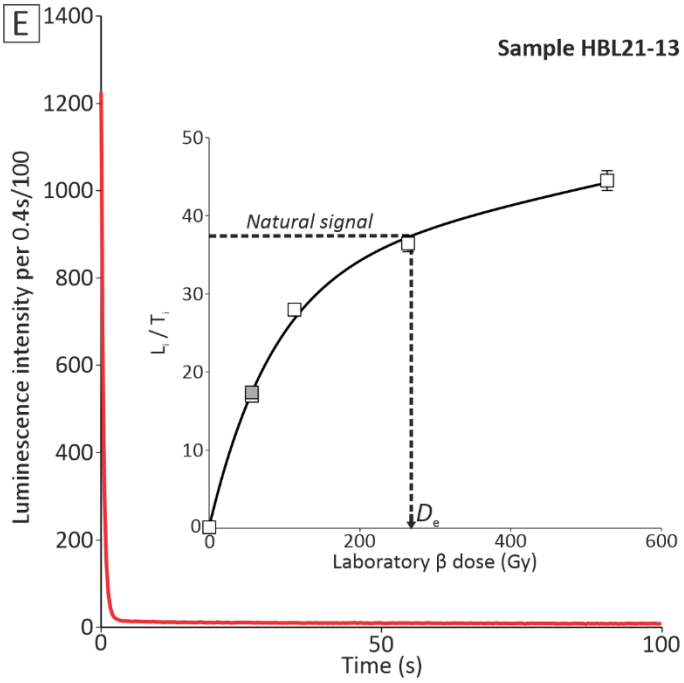
E
Sample HBL21-13
Luminescence intensity per 0.4s/100
Time (s)
Natural signal
L_i / T_i
D_e
Laboratory β dose (Gy)

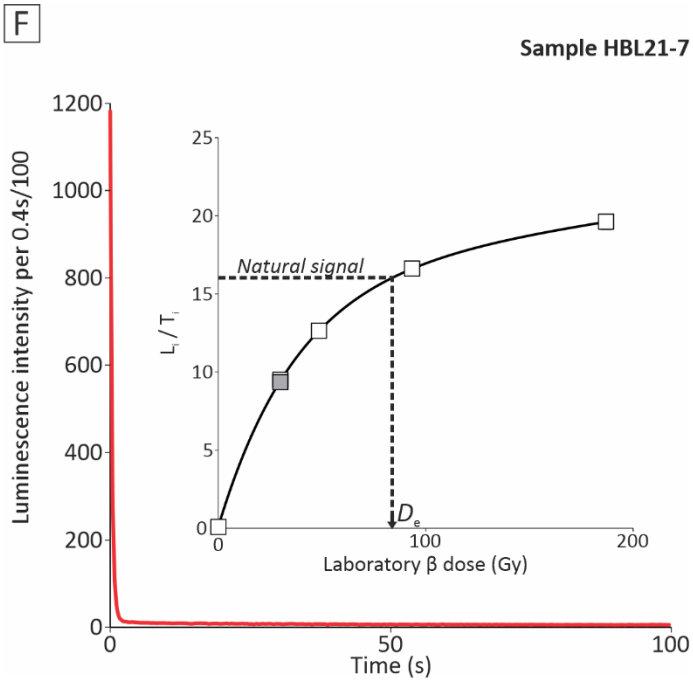
F
Sample HBL21-7
Luminescence intensity per 0.4s/100
Time (s)
Natural signal
L_i / T_i
D_e
Laboratory β dose (Gy)

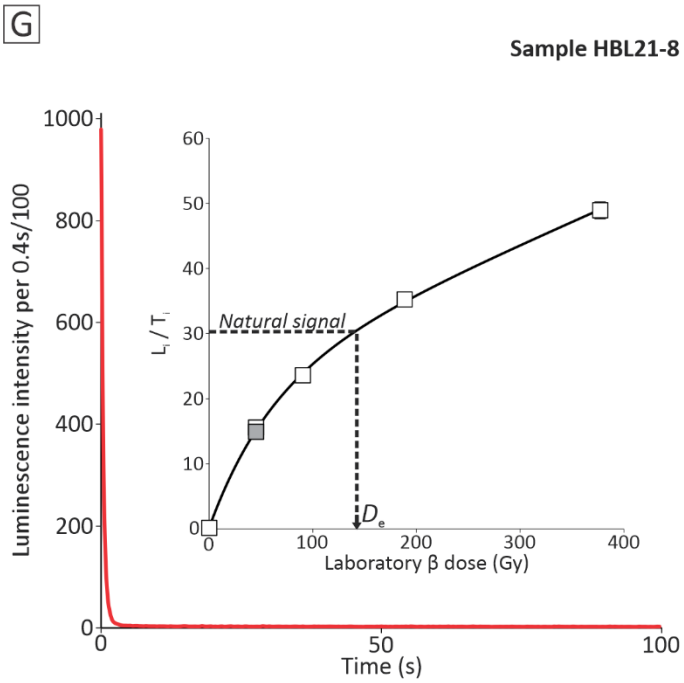
G
Sample HBL21-8
Luminescence intensity per 0.4s/100
Time (s)
Natural signal
L_i / T_i
D_e
Laboratory β dose (Gy)

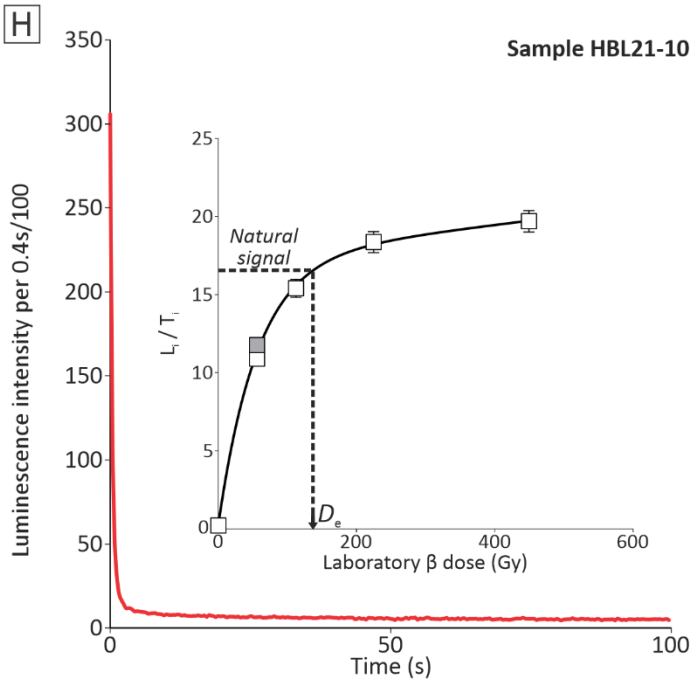
H
Sample HBL21-10
Luminescence intensity per 0.4s/100
Time (s)
Natural signal
L_i / T_i
D_e
Laboratory β dose (Gy)

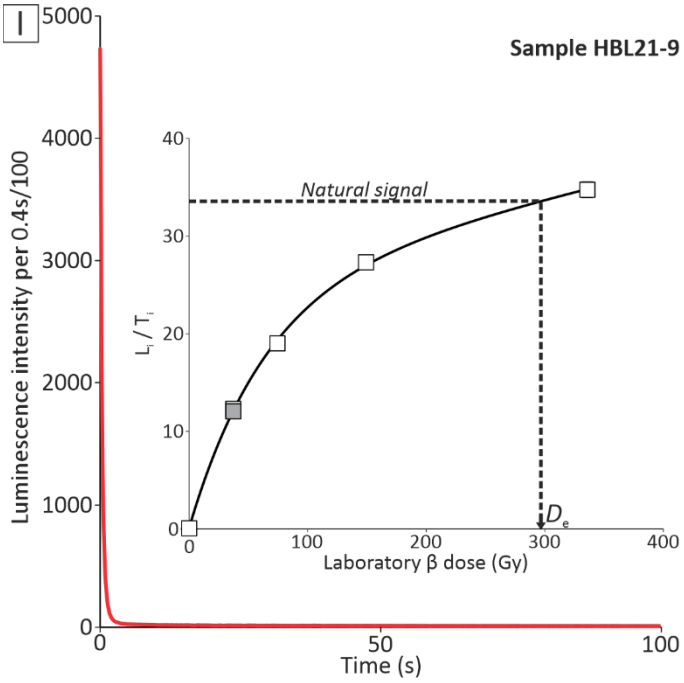
I
Sample HBL21-9
Luminescence intensity per 0.4s/100
5000
4000
3000
2000
1000
0
0
50
100
Time (s)
Natural signal
L_i / T_i
40
30
20
10
0
0
100
200
300
400
D_e
Laboratory β dose (Gy)

Appendix D

Supplemental materials for Chapter 5

Chapter 5 supplemental material has not been submitted to an academic journal yet.

Supplemental material 1: Additional stratigraphic data.

Supplemental material 2: Detailed cross-sections for each region investigated.

Supplemental material 3: Spatial distribution of stratigraphic units and sediment photos.

Supplemental material 4: Optical age data.

Supplemental material 5: Supporting till composition analysis and figures.

Glacial-interglacial cycles: insights from the stratigraphic record of western Hudson Bay Lowland
by Hodder et al., Supplemental Materials

Supplemental material 1: Additional stratigraphic data.

Figure S1-1: Quaternary stratigraphy exposed at section 20-705 on the Machichi River. Till sample numbers are labelled within the white boxes. Simplified clast-lithology counts, <63 µm carbonate values and matrix texture data are provided for these samples in the bottom right panel. Till clast-fabric data are plotted on equal area, lower hemisphere projection stereonets. The value of the principal eigenvalue (S_1) and direction of the principal eigenvector (V_1) are provided, and an interpretation of the ice-flow direction is indicated (orange arrow).

Table S1-1: Summary of ice-flow indicators for each identified unit.

Table S1-2: Till-matrix colours for each identified unit.

Chap. 5, Figure S1-1

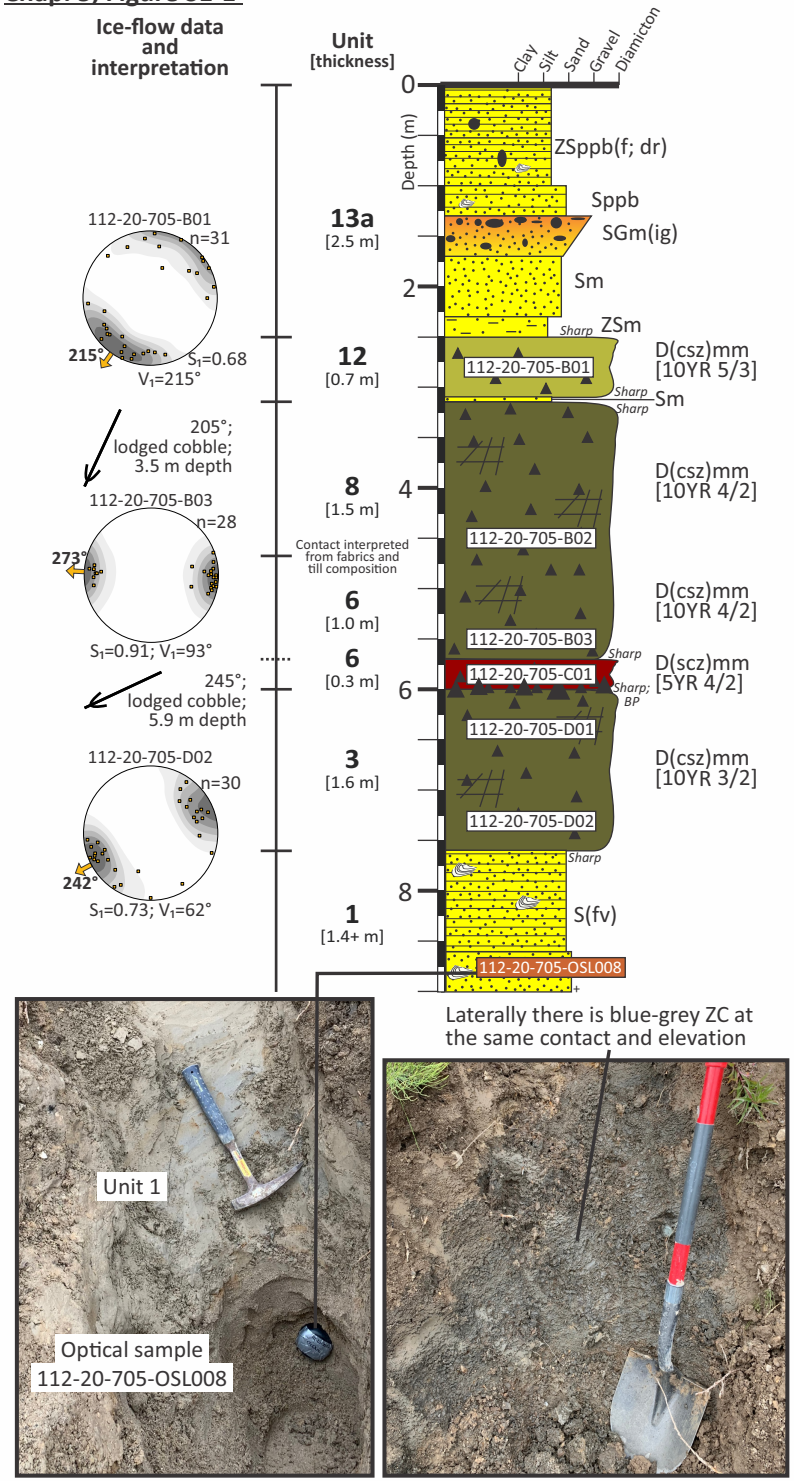

Section 112-20-705
Machichi River
Elevation (top): 28 m asl
UTM Zone 15, NAD83: 556773E, 6302504N



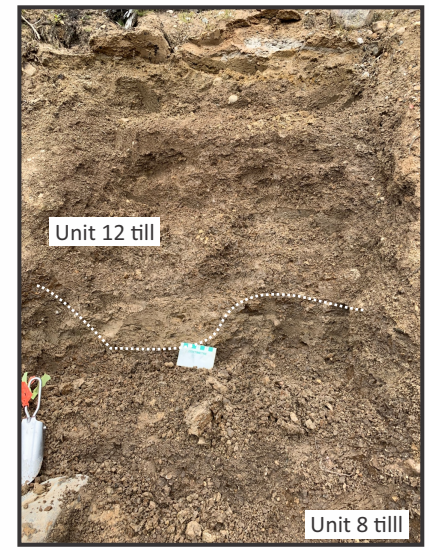



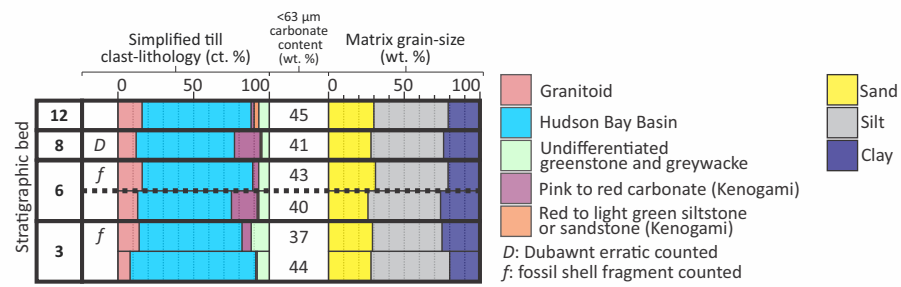

Table S1-1

Section	depth (m)	Stratigraphic unit	Ice-flow indicator	n	V_1 azimuth degrees	V_1 dip degrees	S_1	S_2	S_3	Modality	Interpreted ice-flow[1] azimuth degrees
Till clast fabric											
112-19-607	11.9	2	a-axis fabric	29	310	15	0.64	0.28	0.08	SU	132 (SE)
112-19-624	11.1	2	a-axis fabric	34	353	7	0.71	0.17	0.12	SU	173 (S)
112-21-810	19.2	2	a-axis fabric	30	172	3	0.71	0.19	0.10	SU	172 (S)
112-19-607	5.9	3	a-axis fabric	31	251	7	0.64	0.28	0.08	SU	240 (WSW)
112-19-608	8.8	3	a-axis fabric	31	190	10	0.56	0.38	0.07	BC	SB; 165/235
112-19-614	8.7	3	a-axis fabric	30	99	9	0.73	0.20	0.07	SU	279 (W)
112-19-620	9.8	3	a-axis fabric	32	58	0	0.69	0.26	0.05	SU	238 (WSW)
112-19-626	8.5	3	a-axis fabric	35	46	36	0.64	0.28	0.08	SU	226 (SW)
112-19-627	10.5	3	a-axis fabric	30	50	9	0.70	0.17	0.13	SU	230 (SW)
112-20-704	11.7	3	a-axis fabric	31	347	3	0.51	0.34	0.14	PM	PM; no interpretation
112-20-705	7.3	3	a-axis fabric	30	62	2	0.73	0.16	0.11	SU	242 (WSW)
112-21-810	11.4	3	a-axis fabric	30	219	12	0.78	0.17	0.05	SU	219 (SW)
112-21-810	13.0	3	a-axis fabric	30	80	2	0.58	0.32	0.10	SU	260 (W)
112-21-810	16.0	3	a-axis fabric	31	30	17	0.64	0.22	0.14	SU	210 (SSW)
112-19-613	8.6	4	a-axis fabric	30	7	2	0.69	0.23	0.09	SU	178 (S)
112-19-627	7.4	4	a-axis fabric	30	154	14	0.73	0.22	0.05	SU	154 (SSE)
112-20-704	10.5	4	a-axis fabric	29	142	12	0.72	0.21	0.07	SU	142 (SE)
112-19-601	6.7	6	a-axis fabric	34	287	7	0.56	0.37	0.07	SB	287 (W)
112-19-608	5.9	6	a-axis fabric	29	304	0	0.76	0.13	0.11	SU	304 (NW)
112-19-613	2.9	6	a-axis fabric	32	208	8	0.59	0.32	0.09	SB	SB; 208/280
112-19-614	7.5	6	a-axis fabric	30	91	20	0.59	0.23	0.18	SU	273 (W)
112-19-616	5.9	6	a-axis fabric	29	140	8	0.74	0.17	0.09	SU	320 (NW)
112-19-621	4.9	6	a-axis fabric	33	255	11	0.64	0.31	0.05	SU	255 (WSW)
112-19-626	7.5	6	a-axis fabric	35	123	21	0.67	0.21	0.12	SU	303 (WNW)
112-20-704	3.5	6	a-axis fabric	30	111	10	0.80	0.12	0.08	SU	283 (WNW)
112-20-704	9.1	6	a-axis fabric	30	102	14	0.92	0.06	0.02	U	282 (WNW)
112-20-705	5.5	6	a-axis fabric	28	93	3	0.91	0.07	0.02	U	273 (W)
112-21-809	7.2	6	a-axis fabric	30	52	8	0.56	0.35	0.09	SU	317 (NW)
112-19-602	7.7	8	a-axis fabric	30	63	22	0.74	0.14	0.12	SU	243 (WSW)
112-19-607	5.0	8	a-axis fabric	30	217	5	0.73	0.18	0.09	SU	217 (SW)
112-19-608	4.0	8	a-axis fabric	29	213	7	0.77	0.17	0.06	SU	213 (SSW)
112-19-609	3.8	8	a-axis fabric	29	37	31	0.83	0.10	0.07	UC	217 (SW)
112-19-610	4.4	8	a-axis fabric	30	21	2	0.83	0.10	0.07	SU	201 (SSW)
112-19-611	5.6	8	a-axis fabric	32	210	8	0.76	0.18	0.05	SU	210 (SSW)
112-19-613	1.9	8	a-axis fabric	32	214	12	0.74	0.15	0.11	SU	214 (SW)
112-19-618	11.8	8	a-axis fabric	30	218	2	0.57	0.37	0.07	SB	218 (SW)
112-19-622	7.6	8	a-axis fabric	32	190	5	0.64	0.26	0.10	SU	183 (S)
112-19-623	9.7	8	a-axis fabric	30	49	17	0.82	0.10	0.08	SU	229 (SW)
112-19-627	4.1	8	a-axis fabric	30	189	7	0.65	0.23	0.13	SU	189 (S)
112-20-701	4.0	8	a-axis fabric	33	177	11	0.80	0.13	0.07	SU	177 (S)
112-21-809	2.4	8	a-axis fabric	30	317	24	0.56	0.38	0.06	SB	240 (WSW)
112-21-810	6.6	8	a-axis fabric	30	16	10	0.23	0.27	0.10	SU	196 (SSW)
112-21-810	10.6	8	a-axis fabric	30	187	15	0.73	0.20	0.08	SU	187 (S)
112-19-607	3.2	11	a-axis fabric	29	78	6	0.71	0.20	0.09	SU	258 (WSW)
112-19-611	1.5	11	a-axis fabric	29	265	1	0.78	0.15	0.07	SU	265 (W)
112-19-619	2.5	11	a-axis fabric	30	335	15	0.53	0.40	0.07	SB	SB; 170/275
112-19-610	0.9	12	a-axis fabric	35	55	2	0.78	0.15	0.07	SU	235 (SW)
112-19-616	2.8	12	a-axis fabric	32	241	12	0.73	0.20	0.07	SU	241 (WSW)
112-19-627	1.9	12	a-axis fabric	30	77	12	0.56	0.36	0.08	SU	257 (WSW)
112-20-705	2.8	12	a-axis fabric	31	215	5	0.68	0.23	0.09	SU	215 (SW)
112-19-609	2.0	10a	a-axis fabric	31	149	4	0.73	0.17	0.10	SU	329 (NNW)
112-19-614	2.5	10a	a-axis fabric	30	147	17	0.78	0.15	0.07	SU	327 (NNW)
112-19-619	6.2	10a	a-axis fabric	29	106	3	0.71	0.20	0.09	SU	286 (WNW)
112-19-622	2.3	10a	a-axis fabric	30	185	11	0.63	0.28	0.09	SB	SB; 220/340
112-19-622	6.0	10a	a-axis fabric	31	130	6	0.72	0.23	0.05	SU	310 (NW)
112-19-623	9.0	10a	a-axis fabric	30	358	10	0.82	0.15	0.03	SU	178 (S)
112-19-626	2.0	10a	a-axis fabric	32	136	10	0.62	0.23	0.14	SB	310 (NW)
112-20-704	1.1	10a	a-axis fabric	30	119	38	0.76	0.20	0.05	SU	299 (NW)
112-19-602	4.2	10b	a-axis fabric	32	146	2	0.85	0.11	0.04	SU	326 (NW)
Lodged clast ice-flow indicator data											
112-19-607	9.4	2	Lodged boulder	--	--	--	--	--	--	--	170 (S)
112-19-626	10.6	2	Lodged boulder	--	--	--	--	--	--	--	174 (S)
112-19-616	9.6	3	Lodged boulder	--	--	--	--	--	--	--	235 (SW)
112-19-616	9.6	3	Lodged boulder	--	--	--	--	--	--	--	242 (WSW)
112-19-616	9.9	3	Lodged boulder	--	--	--	--	--	--	--	224 (SW)
112-19-621	5.4	3	Lodged cobble	--	--	--	--	--	--	--	253 (WSW)
112-19-621	5.4	3	Lodged cobble	--	--	--	--	--	--	--	257 (WSW)
112-19-621	5.4	3	Lodged cobble	--	--	--	--	--	--	--	272 (W)
112-19-625	15.6	3	Lodged boulder	--	--	--	--	--	--	--	230 (SW)
112-20-705	5.9	3	Lodged cobble	--	--	--	--	--	--	--	245 (WSW)
112-19-608	5.9	6	Lodged cobble	--	--	--	--	--	--	--	285 (W)
112-20-703	8.0	6	Lodged cobble	--	--	--	--	--	--	--	300 (NW)
112-20-704	5.3	6	Lodged boulder	--	--	--	--	--	--	--	300 (NW)
112-20-704	7.1	6	Lodged cobble	--	--	--	--	--	--	--	290 (WNW)
112-20-703	4.0	8	Lodged boulder	--	--	--	--	--	--	--	190 (S)
112-20-705	3.5	8	Lodged cobble	--	--	--	--	--	--	--	205 (SSW)
112-19-618	4.6	10b	Lodged boulder	--	--	--	--	--	--	--	320 (NW)
112-19-625	6.8	10b	Lodged cobble	--	--	--	--	--	--	--	335 (NNW)

Table S2-2		10YR 4/2	2.5Y 4/2	10YR 4/3	7.5YR 4/2	2.5Y 4/3	7.5YR 4/3	7.5YR 5/3	5YR 4/2	2.5Y 5/3	7.5YR 4/1	2.5Y 6/3	10YR 3/2	10YR 4/1	10YR 4/4	10YR 5/3	10YR 5/4
Strat Unit	**n**	Dark greyish brown	Dark greyish brown	Brown	Brown	Olive brown	Brown	Brown	Dark reddish grey	Light olive brown	Dark grey	Light yellow brown	Brown	Dark grey	Dark yellowish brown	Brown	Yellowish brown
2	15	4	3	6	2												
3	31	13	10	2		2			1				1	2			
4	7	1		3	2											1	
5c	1										1						
6	32	16	3	1	1	8		1	2								
8	31	6	12	7	2	3	1										
10a	20				14		2		1						1	2	
10b	8			4	3		1										
11	7			2	2		1	2									
12	12			1	1	1				3		2				3	1

Supplemental material 2: Detailed cross-sections for each region investigated.

This supplemental file contains detailed cross-sections of sections investigated in the study area.

Figure S2-1: Quaternary sediment observations at sections investigated in the Kaskattama River area.

Figure S2-2: Quaternary sediment observations at sections investigated in the Machichi River area.

Figure S2-3: Quaternary sediment observations at sections investigated in the Nelson River Estuary area.

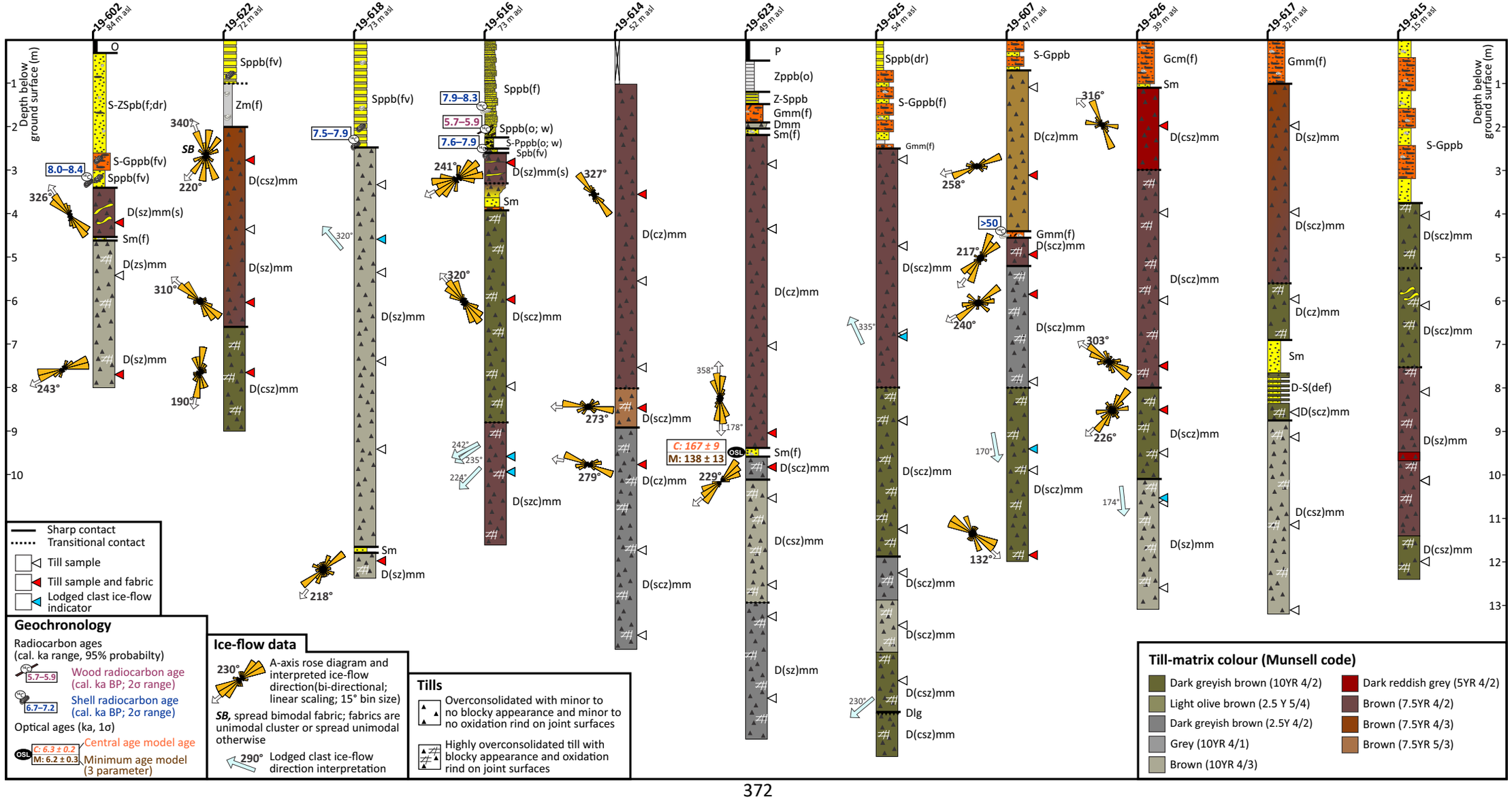
19-602 84 m asl
19-622 72 m asl
19-618 73 m asl
19-616 73 m asl
19-614 52 m asl
19-623 49 m asl
19-625 54 m asl
19-607 47 m asl
19-626 39 m asl
19-617 32 m asl
19-615 15 m asl
Depth below ground surface (m)
O
S-ZSpb(f;dr)
S-Gppb(fv)
Sppb(fv)
D(sz)mm(s)
Sm(f)
D(zs)mm
D(sz)mm
8.0–8.4
326°
340°
220°
SB
243°
310°
190°
Zm(f)
D(csz)mm
D(sz)mm
D(csz)mm
7.5–7.9
320°
218°
Sm
7.9–8.3
5.7–5.9
7.6–7.9
Sppb(o; w)
S-Pppb(o; w)
Spb(fv)
D(sz)mm(s)
241°
320°
242°
235°
224°
D(szc)mm
327°
273°
279°
358°
178°
C: 167 ± 9
M: 138 ± 13
229°
P
Zppb(o)
Z-Sppb
Gmm(f)
Dmm
Sm(f)
D(cz)mm
D(scz)mm
D(cz)mm
D(csz)mm
D(scz)mm
D(sz)mm
Sppb(dr)
S-Gppb(f)
Gmm(f)
335°
D(scz)mm
D(csz)mm
D(scz)mm
Dlg
D(csz)mm
230°
258°
>50
217°
240°
S-Gppb
316°
D(cz)mm
Gmm(f)
D(scz)mm
D(scz)mm
170°
303°
226°
132°
174°
Gcm(f)
Sm
D(csz)mm
D(scz)mm
D(sz)mm
Gmm(f)
D(sz)mm
D(scz)mm
D(cz)mm
Sm
D-S(def)
D(scz)mm
D(csz)mm
S-Gppb
D(scz)mm
D(sz)mm
D(csz)mm
Sharp contact
Transitional contact
Till sample
Till sample and fabric
Lodged clast ice-flow indicator
Geochronology
Radiocarbon ages (cal. ka range, 95% probabilty)
5.7–5.9
Wood radiocarbon age (cal. ka BP; 2σ range)
6.7–7.2
Shell radiocarbon age (cal. ka BP; 2σ range)
Optical ages (ka, 1σ)
C: 6.3 ± 0.2
M: 6.2 ± 0.3
Central age model age
Minimum age model (3 parameter)
Ice-flow data
230°
A-axis rose diagram and interpreted ice-flow direction(bi-directional; linear scaling; 15° bin size)
SB, spread bimodal fabric; fabrics are unimodal cluster or spread unimodal otherwise
290°
Lodged clast ice-flow direction interpretation
Tills
Overconsolidated with minor to no blocky appearance and minor to no oxidation rind on joint surfaces
Highly overconsolidated till with blocky appearance and oxidation rind on joint surfaces
Till-matrix colour (Munsell code)
Dark greyish brown (10YR 4/2)
Light olive brown (2.5 Y 5/4)
Dark greyish brown (2.5Y 4/2)
Grey (10YR 4/1)
Brown (10YR 4/3)
Dark reddish grey (5YR 4/2)
Brown (7.5YR 4/2)
Brown (7.5YR 4/3)
Brown (7.5YR 5/3)

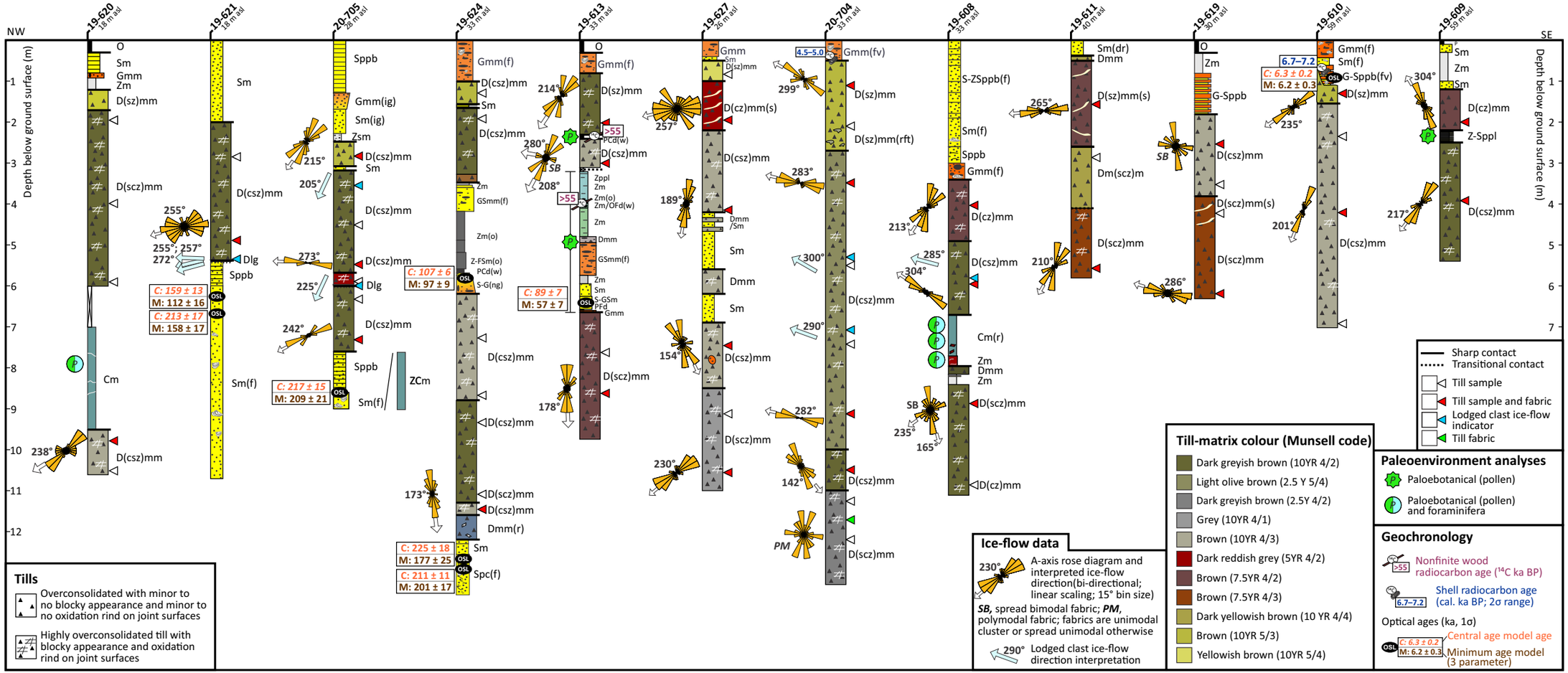
NW
SE
Depth below ground surface (m)
19-620 18 m asl
19-621 18 m asl
20-705 28 m asl
19-624 33 m asl
19-613 33 m asl
19-627 26 m asl
20-704 33 m asl
19-608 33 m asl
19-611 40 m asl
19-619 30 m asl
19-610 59 m asl
19-609 59 m asl
O
Sm
Gmm
Zm
D(sz)mm
D(scz)mm
Cm
D(csz)mm
Dlg
Sppb
Sm(f)
Gmm(ig)
Sm(ig)
Zsm
Dlg
ZCm
Gmm(f)
Zm
GSmm(f)
Zm(o)
Z-FSm(o)
PCd(w)
S-G(ng)
Dmm(r)
Spc(f)
Zppl
Zm(o)
Zm/OFd(w)
Dmm
Sm
S-GSm
PFd
Gmm(fv)
D(cz)mm
Dmm/Sm
S-ZSppb(f)
Cm(r)
Sm(dr)
Dmm
Dm(scz)m
G-Sppb
G-Sppb(fv)
Z-Sppl
C: 159 ± 13
M: 112 ± 16
C: 213 ± 17
M: 158 ± 17
C: 217 ± 15
M: 209 ± 21
C: 107 ± 6
M: 97 ± 9
C: 89 ± 7
M: 57 ± 7
C: 225 ± 18
M: 177 ± 25
C: 211 ± 11
M: 201 ± 17
C: 6.3 ± 0.2
M: 6.2 ± 0.3
>55
6.7–7.2
4.5–5.0
PCd(w)
SB
PM
Sharp contact
Transitional contact
Till sample
Till sample and fabric
Lodged clast ice-flow indicator
Till fabric
Tills
Overconsolidated with minor to no blocky appearance and minor to no oxidation rind on joint surfaces
Highly overconsolidated till with blocky appearance and oxidation rind on joint surfaces
Ice-flow data
A-axis rose diagram and interpreted ice-flow direction(bi-directional; linear scaling; 15° bin size)
SB, spread bimodal fabric; PM, polymodal fabric; fabrics are unimodal cluster or spread unimodal otherwise
Lodged clast ice-flow direction interpretation
Till-matrix colour (Munsell code)
Dark greyish brown (10YR 4/2)
Light olive brown (2.5 Y 5/4)
Dark greyish brown (2.5Y 4/2)
Grey (10YR 4/1)
Brown (10YR 4/3)
Dark reddish grey (5YR 4/2)
Brown (7.5YR 4/2)
Brown (7.5YR 4/3)
Dark yellowish brown (10 YR 4/4)
Brown (10YR 5/3)
Yellowish brown (10YR 5/4)
Paleoenvironment analyses
Paloebotanical (pollen)
Paloebotanical (pollen) and foraminifera
Geochronology
Nonfinite wood radiocarbon age (14C ka BP)
Shell radiocarbon age (cal. ka BP; 2σ range)
Optical ages (ka, 1σ)
Central age model age
Minimum age model (3 parameter)

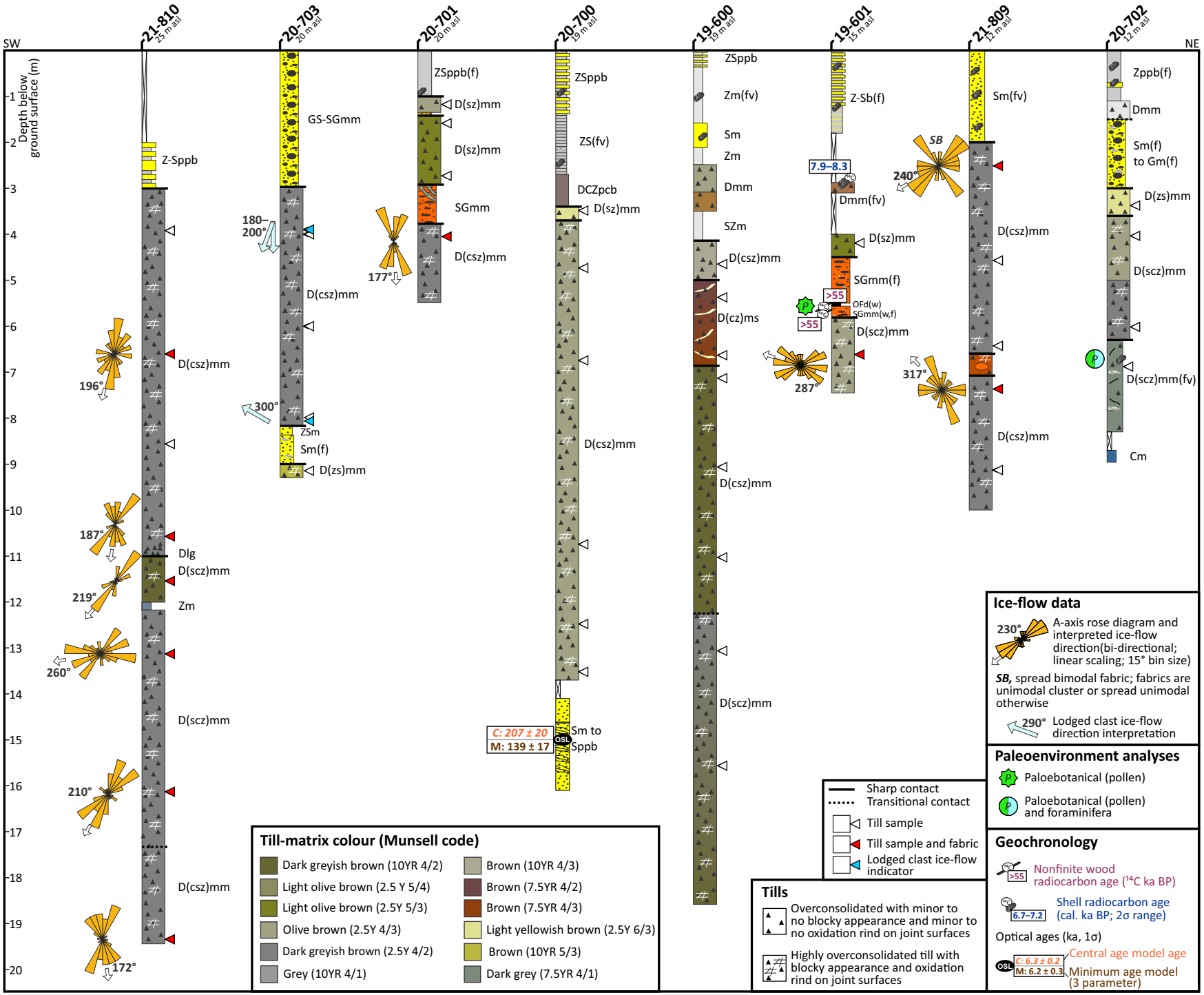
SW
NE
Depth below ground surface (m)
21-810
25 m asl
20-703
20 m asl
20-701
20 m asl
20-700
19 m asl
19-600
19 m asl
19-601
15 m asl
21-809
12 m asl
20-702
12 m asl
Z-Sppb
D(csz)mm
196°
187°
Dlg
D(scz)mm
219°
Zm
260°
D(scz)mm
210°
D(csz)mm
172°
GS-SGmm
180–200°
D(csz)mm
300°
ZSm
Sm(f)
D(zs)mm
ZSppb(f)
D(sz)mm
D(sz)mm
SGmm
D(csz)mm
177°
ZSppb
ZS(fv)
DCZpcb
D(sz)mm
D(csz)mm
C: 207 ± 20
M: 139 ± 17
OSL
Sm to Sppb
ZSppb
Zm(fv)
Sm
Zm
Dmm
SZm
D(csz)mm
D(cz)ms
D(csz)mm
D(scz)mm
Z-Sb(f)
7.9–8.3
Dmm(fv)
D(sz)mm
SGmm(f)
>55
OFd(w)
SGmm(w,f)
>55
D(scz)mm
287°
SB
240°
Sm(fv)
D(csz)mm
317°
D(csz)mm
Zppb(f)
Dmm
Sm(f) to Gm(f)
D(zs)mm
D(scz)mm
D(scz)mm(fv)
Cm
Till-matrix colour (Munsell code)
Dark greyish brown (10YR 4/2)
Light olive brown (2.5 Y 5/4)
Light olive brown (2.5Y 5/3)
Olive brown (2.5Y 4/3)
Dark greyish brown (2.5Y 4/2)
Grey (10YR 4/1)
Brown (10YR 4/3)
Brown (7.5YR 4/2)
Brown (7.5YR 4/3)
Light yellowish brown (2.5Y 6/3)
Brown (10YR 5/3)
Dark grey (7.5YR 4/1)
Sharp contact
Transitional contact
Till sample
Till sample and fabric
Lodged clast ice-flow indicator
Tills
Overconsolidated with minor to no blocky appearance and minor to no oxidation rind on joint surfaces
Highly overconsolidated till with blocky appearance and oxidation rind on joint surfaces
Ice-flow data
230°
A-axis rose diagram and interpreted ice-flow direction(bi-directional; linear scaling; 15° bin size)
SB, spread bimodal fabric; fabrics are unimodal cluster or spread unimodal otherwise
290°
Lodged clast ice-flow direction interpretation
Paleoenvironment analyses
Paloebotanical (pollen)
Paloebotanical (pollen) and foraminifera
Geochronology
>55
Nonfinite wood radiocarbon age (14C ka BP)
6.7–7.2
Shell radiocarbon age (cal. ka BP; 2σ range)
Optical ages (ka, 1σ)
OSL
C: 6.3 ± 0.2
M: 6.2 ± 0.3
Central age model age
Minimum age model (3 parameter)

Supplemental material 3: Spatial distribution of stratigraphic units and sediment photos.

This supplemental file contains the spatial location and thickness of each identified unit in the study area, along with additional photos of the sediment at these locations. For till units, the iceflow datasets are shown for each section.

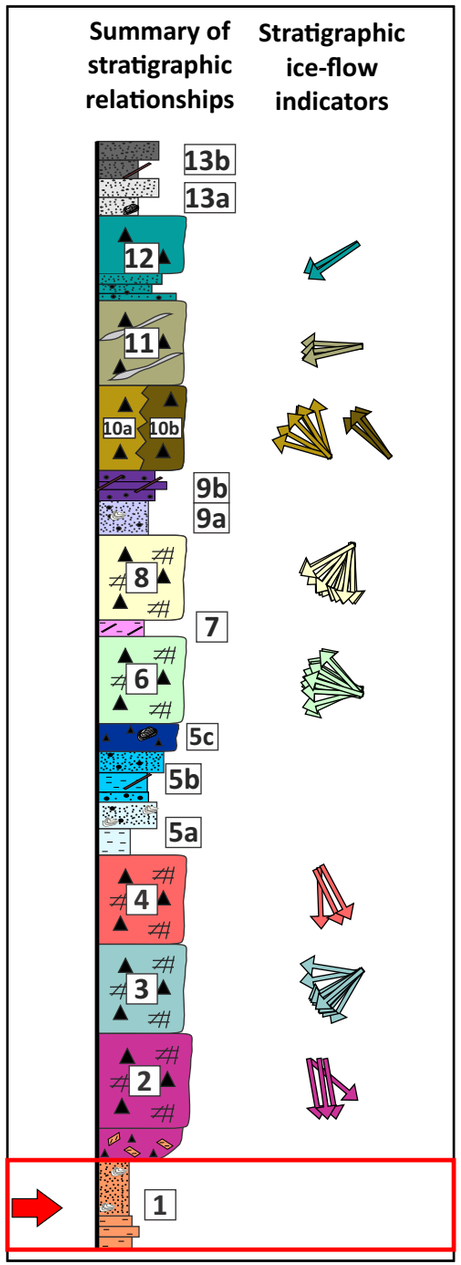

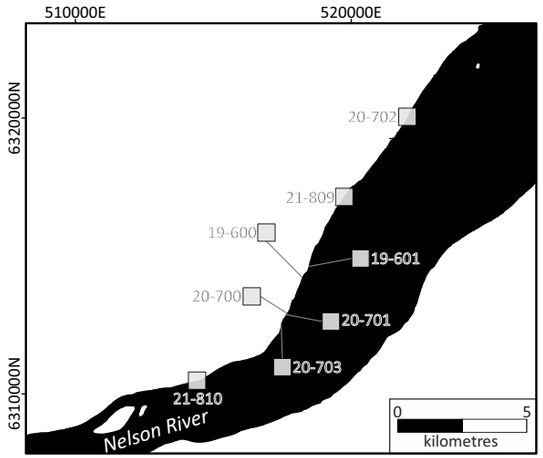

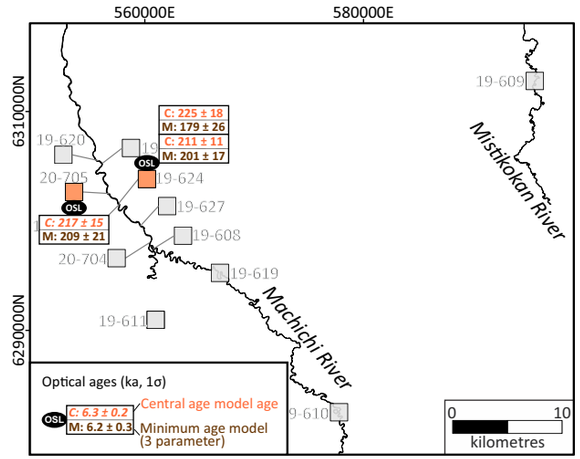

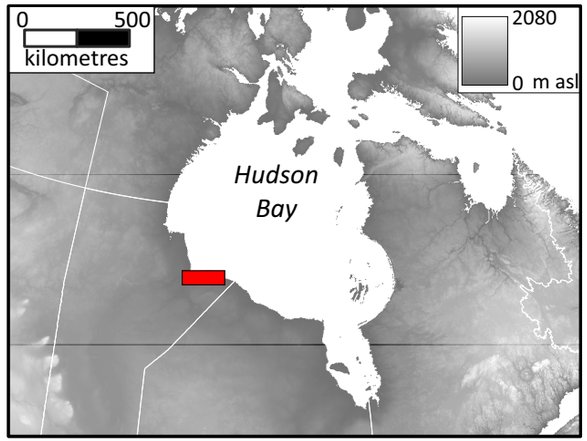

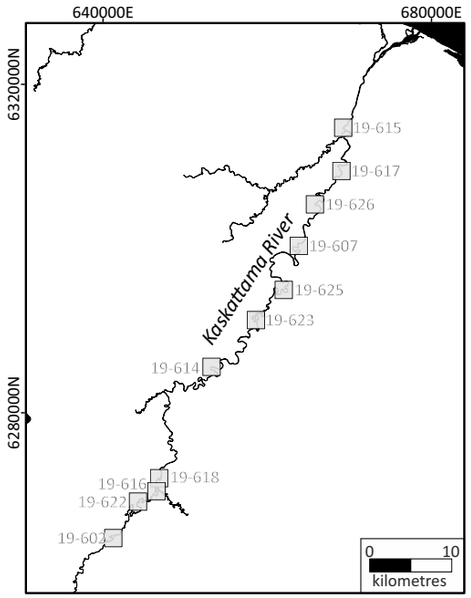





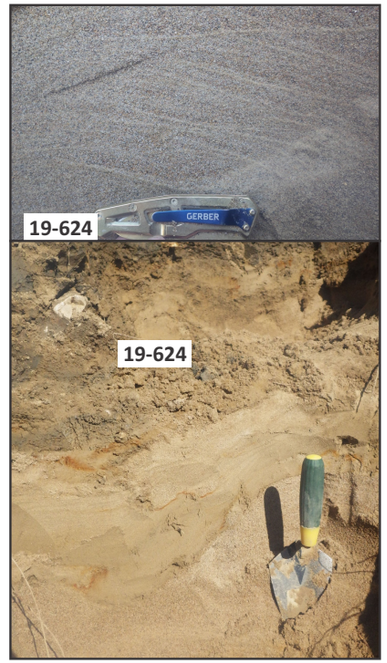

Unit 1 sediments: 20-705, 19-624

Notes:

- There are two well documented occurrences of Unit 2 sediments. Additional geochronology constrains are needed to confirm OSL age estimations.

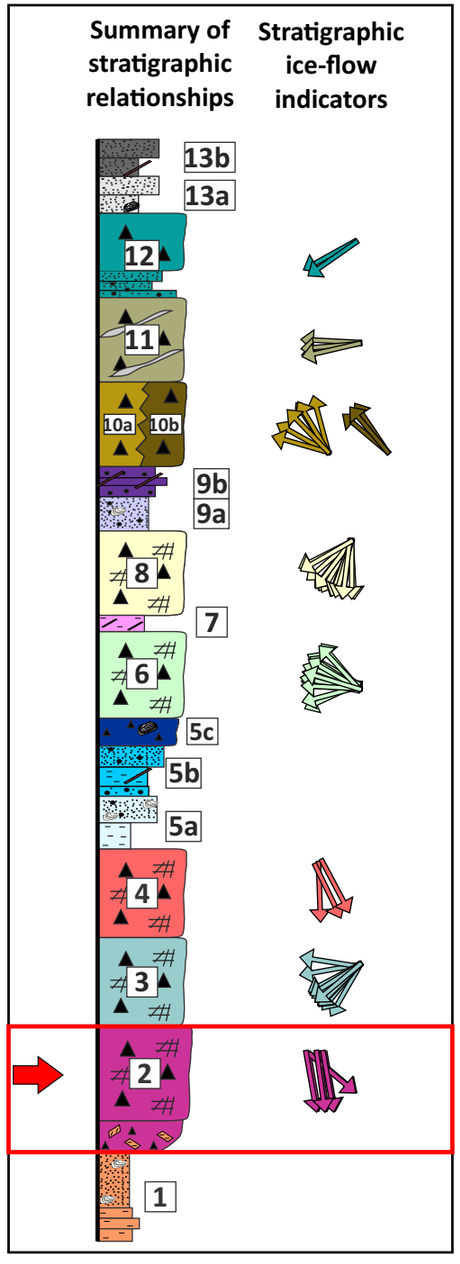

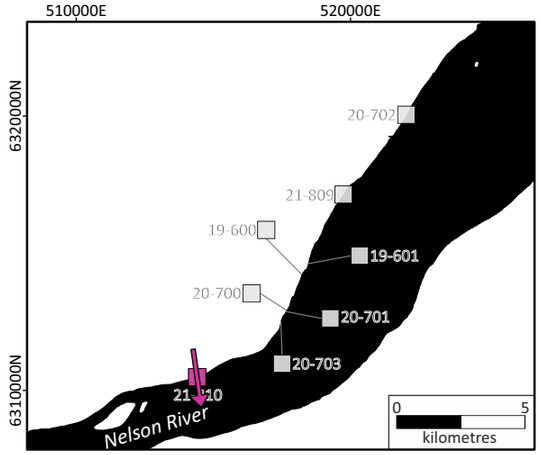

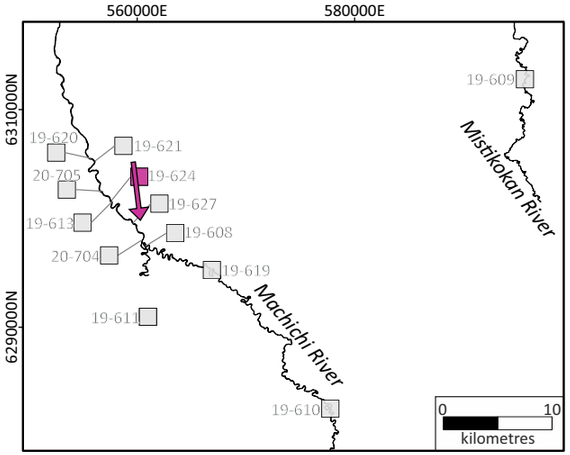

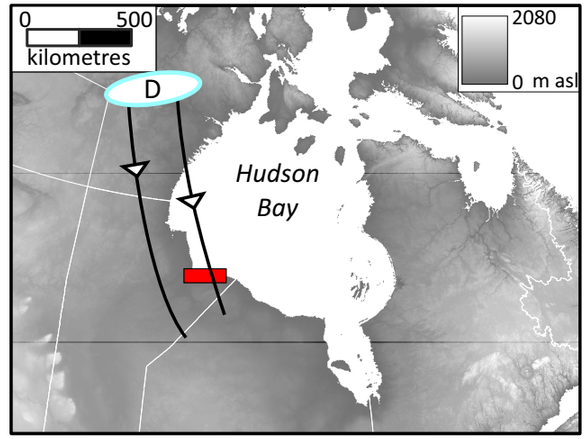

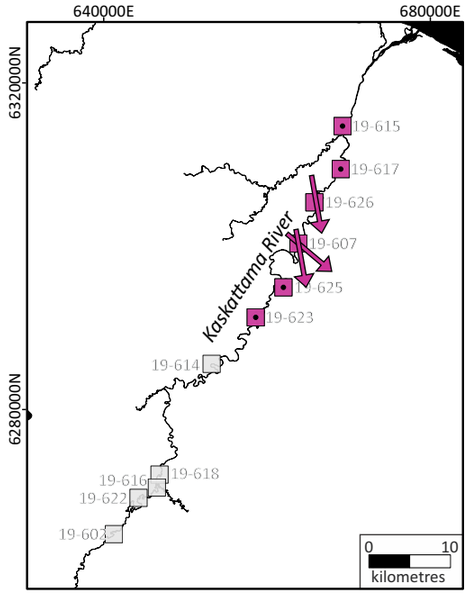

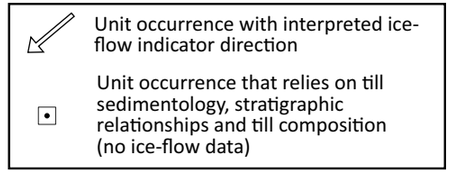

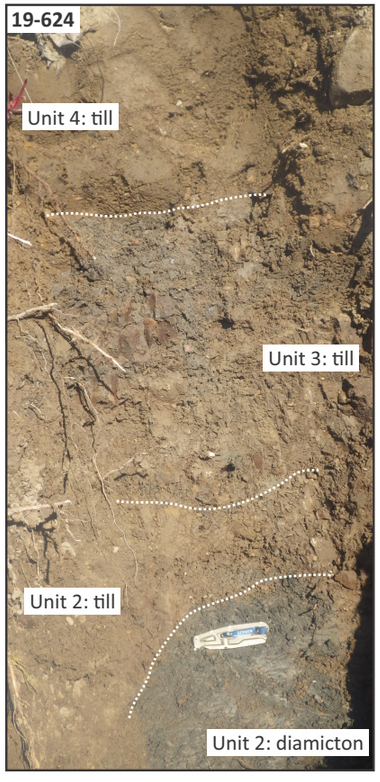

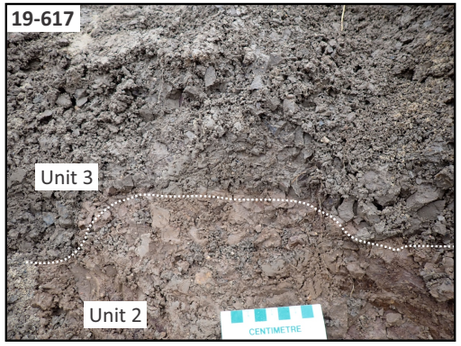







Unit 2 sediments, key sections: 21-810, 19-607, 19-613

Notes:

- The till appears brown in the field and is blocky with oxidation rind on joint surfaces with clast fabrics are primarily oriented towards the south-southeast.
- Direct stratigraphic relationship with an upper contact at multiple locations with the Unit 3 grey till.
- On the Machichi River, there is only one occurrence is at section 19-624. Here, Unit 2 is a very thin (0.3 m) bed of diamicton that directly overlies a blue-grey diamicton with rafted laminated sediments which is included as part of this unit and interpreted to represent advance into the area. Further investigations should seek to find more stratigraphic evidence between Unit 2 and Unit 1.

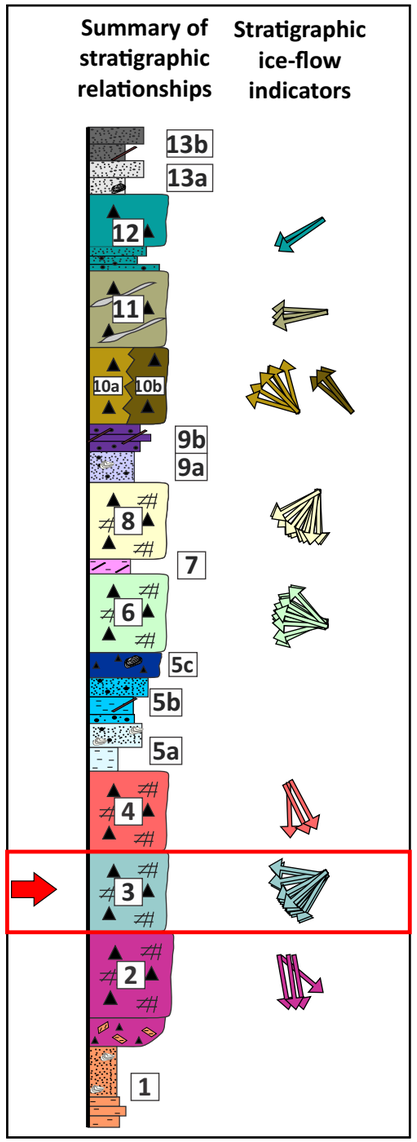

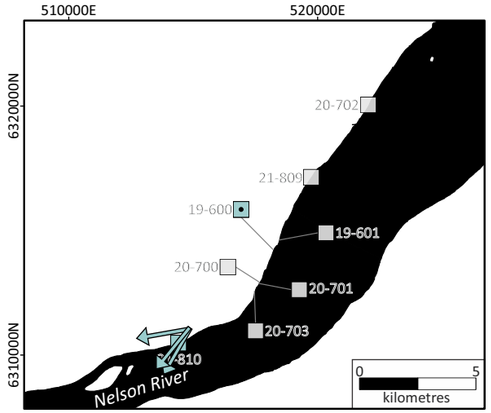

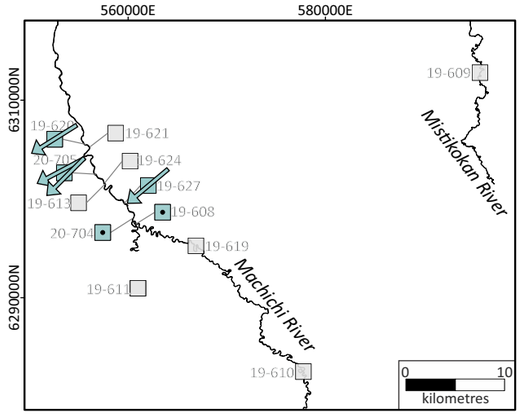

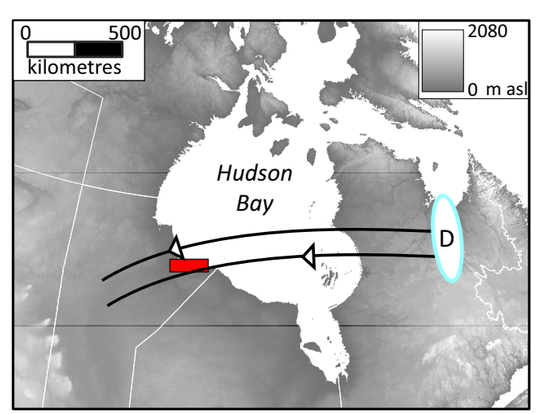

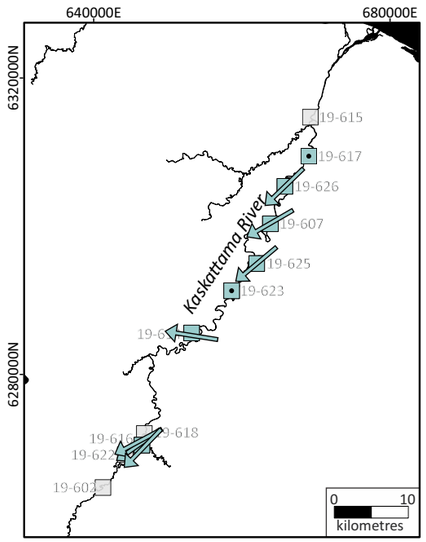

Unit occurrence with interpreted ice-flow indicator direction

Unit occurrence that relies on till sedimentology, stratigraphic relationships and till composition (no ice-flow data)









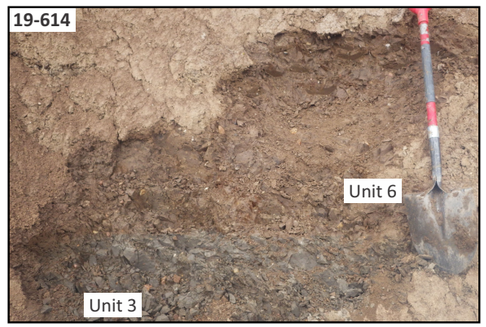

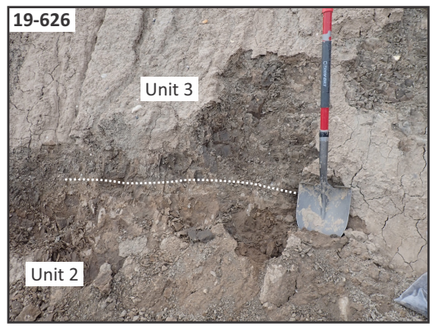

Unit 3 sediments, key sections: 19-607, 19-626, 19-627, 20-705

Notes:

- Unit 3 till appears very grey in the field at most sections and the colour is a sharp contrast to the greyish brown tills that dominant the stratigraphic record. This till is typically in sharp contact with these tills (see examples).
- Clast fabrics are primarily oriented towards the southwest with a west orientation indicated at a couple of sections; several weak or bimodal fabrics from this till as well.
- Clay-rich relative to other tills in the region.
- The till has a high undifferentiated greenstone and greywacke content; therefore, it is interpreted that the Q-L dome may have been situated in a more northern position in Quebec to significantly erode the Belcher Group rocks. This would line up with having more clay in the matrix (incorporation of Hudson Bay Marine sediments)

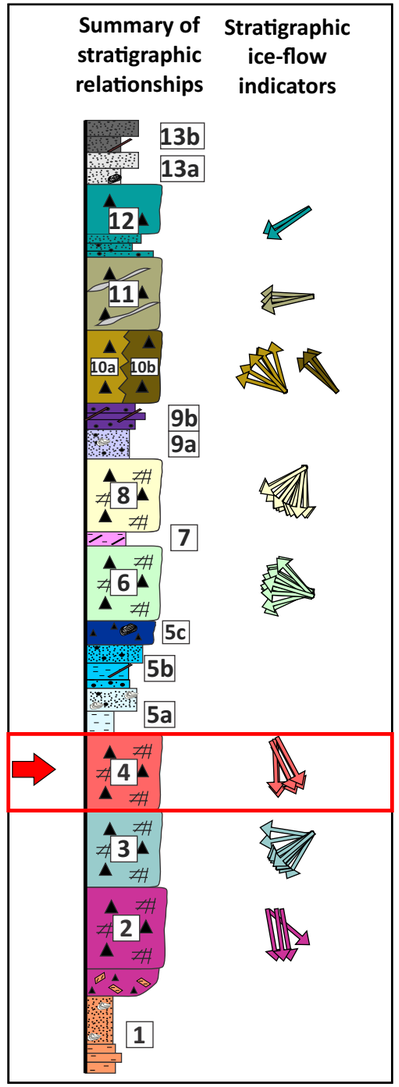

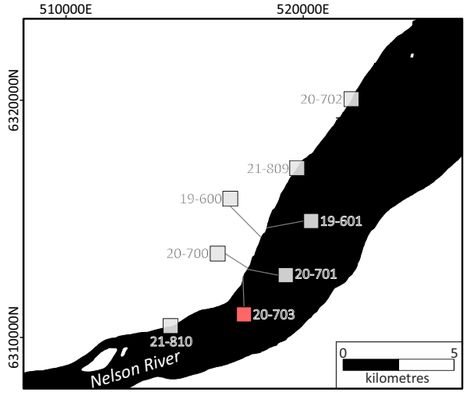

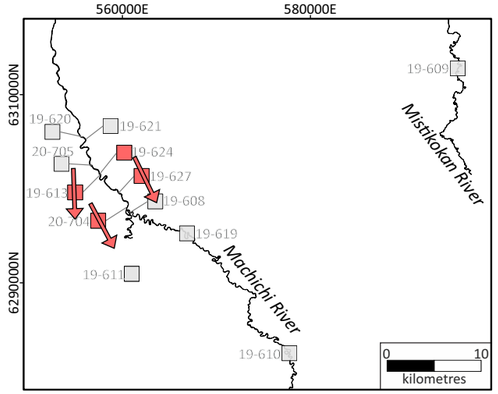

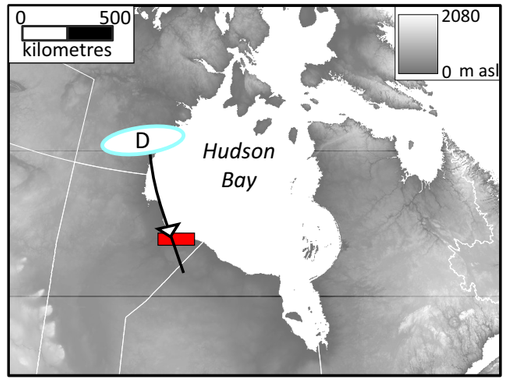

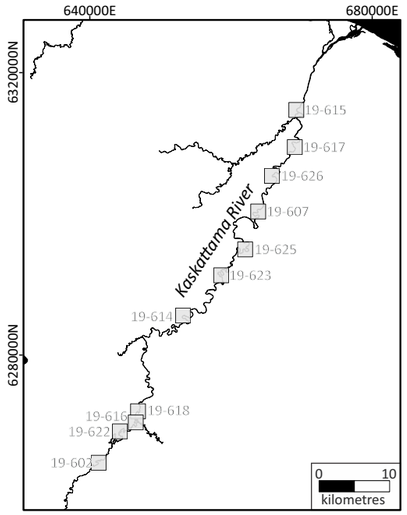

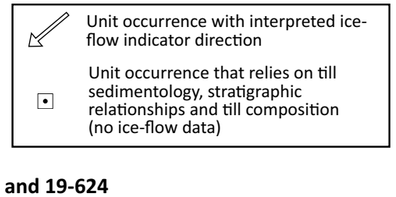



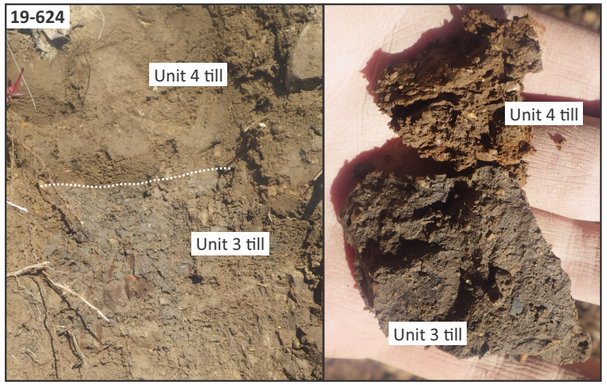



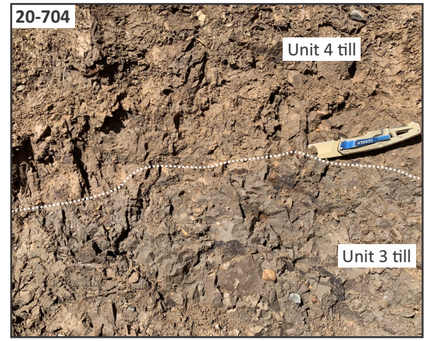

Unit 4 sediments, key sections: 19-627, 20-704 and 19-624

Notes:

- Unit 4 till has a reddish-brown appearance in section. In sharp contact with grey till of Unit 3 along Machichi River.
- The till has average proportions of Precambrian clasts, but a higher proportion of Kenogami Formation clasts. This is interesting because it is a nearly identical ice-flow direction as Unit 2. This could be the result of a late-glacial ice-flow event originating in the southern portion of mainland Nunavut.

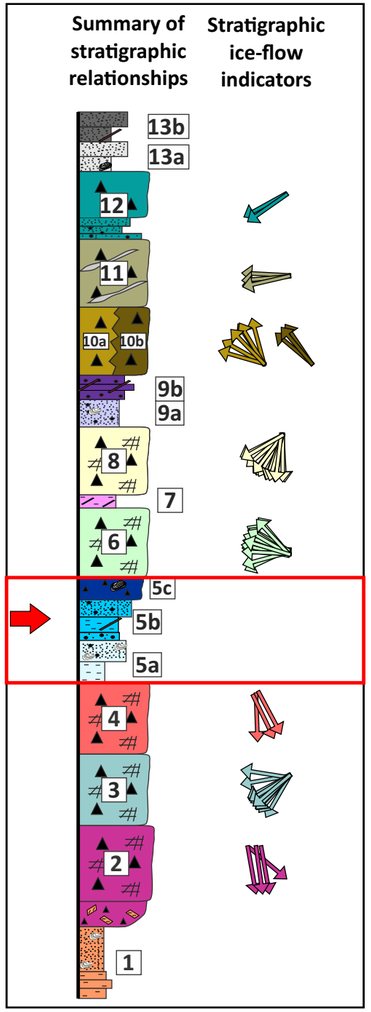

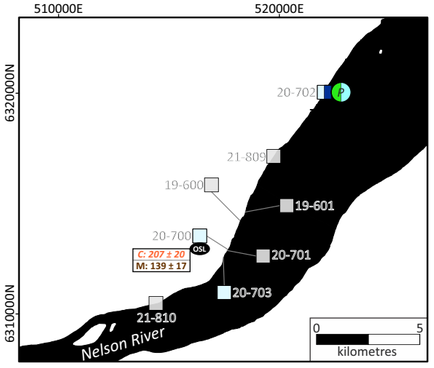

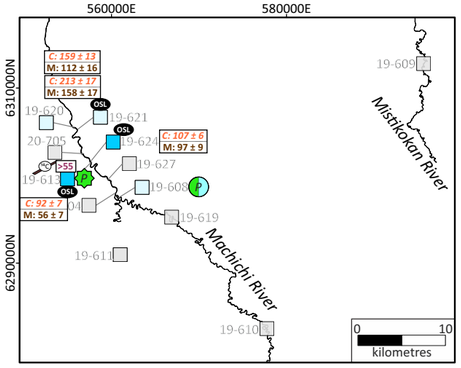

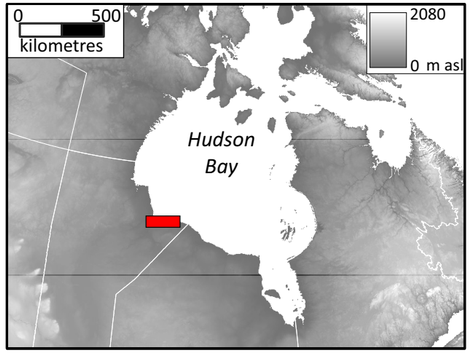



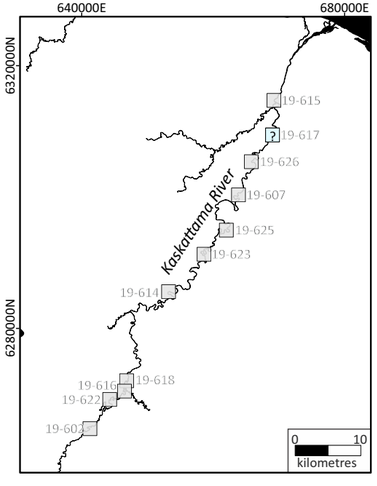

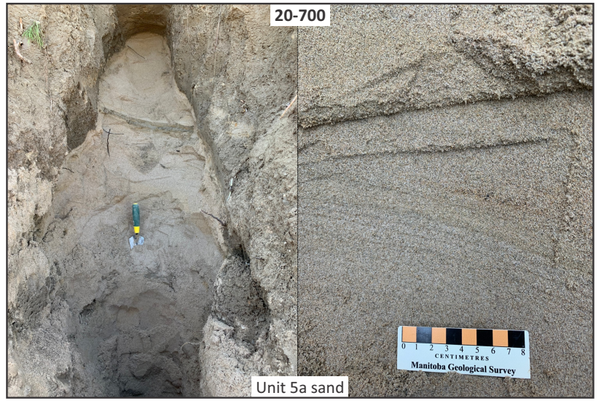



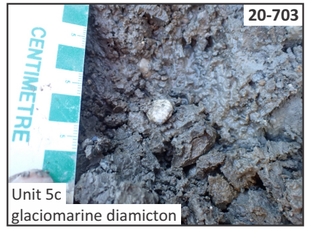

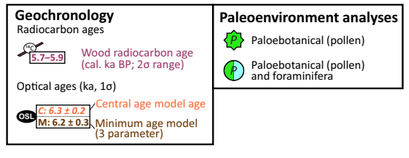

Unit 5 sediments, key sections: 19-613, 20-700, 19-608, 19-621

Notes:

- Additional geochronology constrains are needed to confirm OSL age estimations; additional photos in figures 11 and 12 of manuscript.

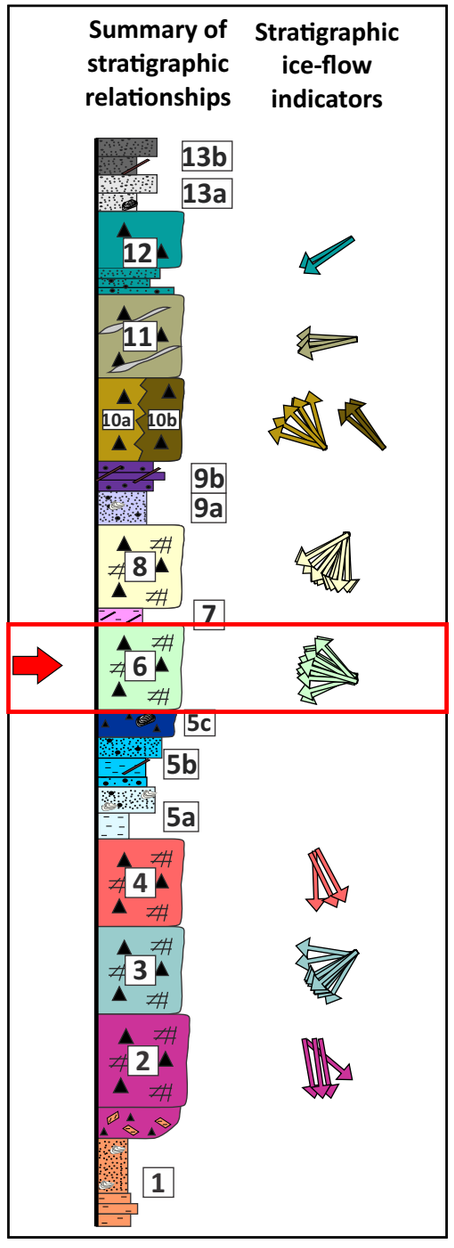

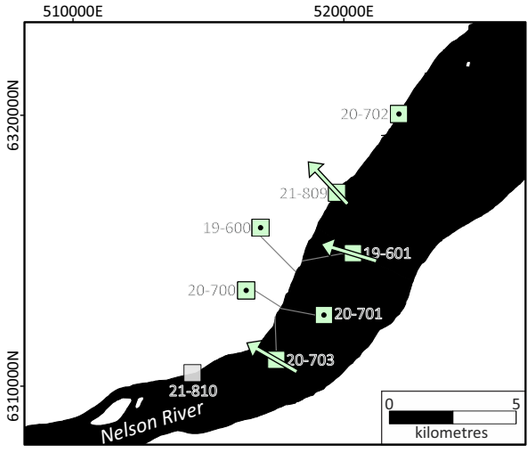

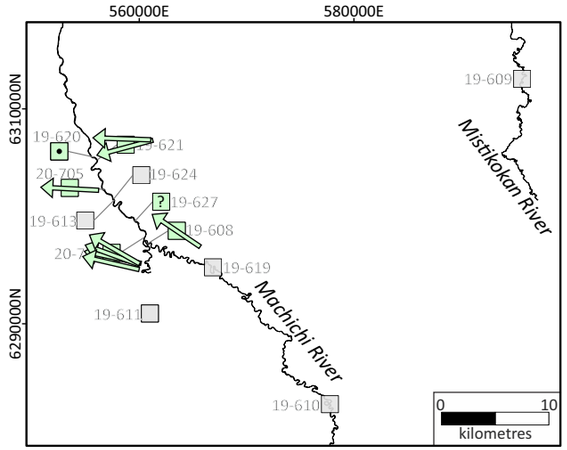

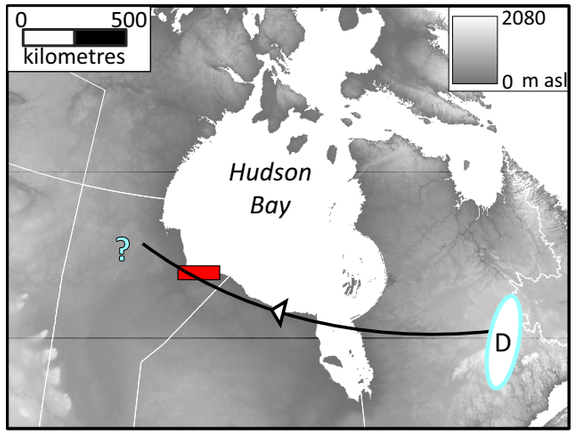

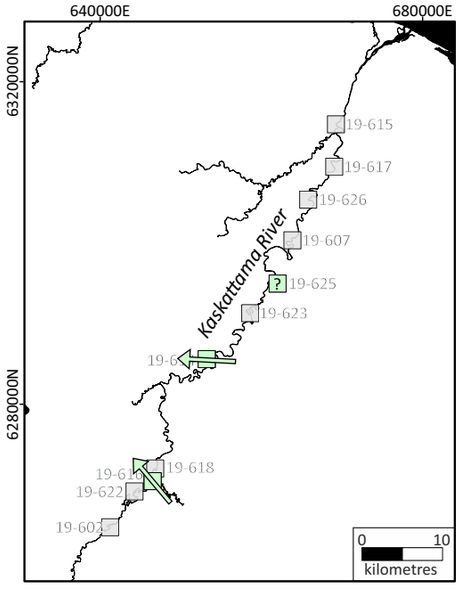

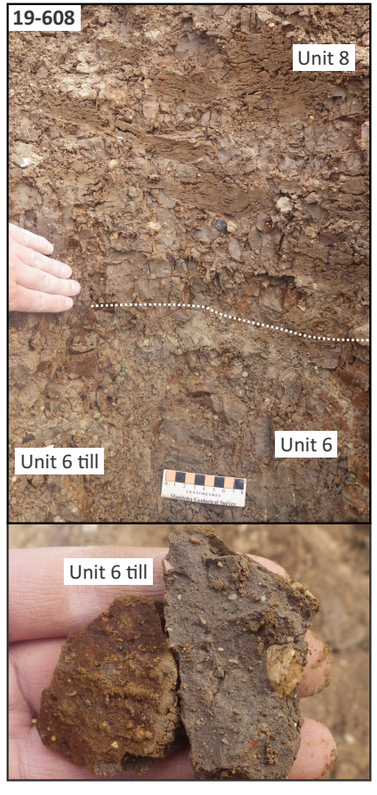









Unit occurrence with interpreted ice-flow indicator direction

Unit occurrence that relies on till sedimentology, stratigraphic relationships and till composition (no ice-flow data)

Unit 6 sediments, key sections: 19-608, 20-704

Notes:

- Unit 6 till is typically greyish brown and appears similar to Unit 8 till at most sections in the field but is differentiated by till fabrics and composition. In places there is a sharp contact between units 6 and 8, such as at section 19-608

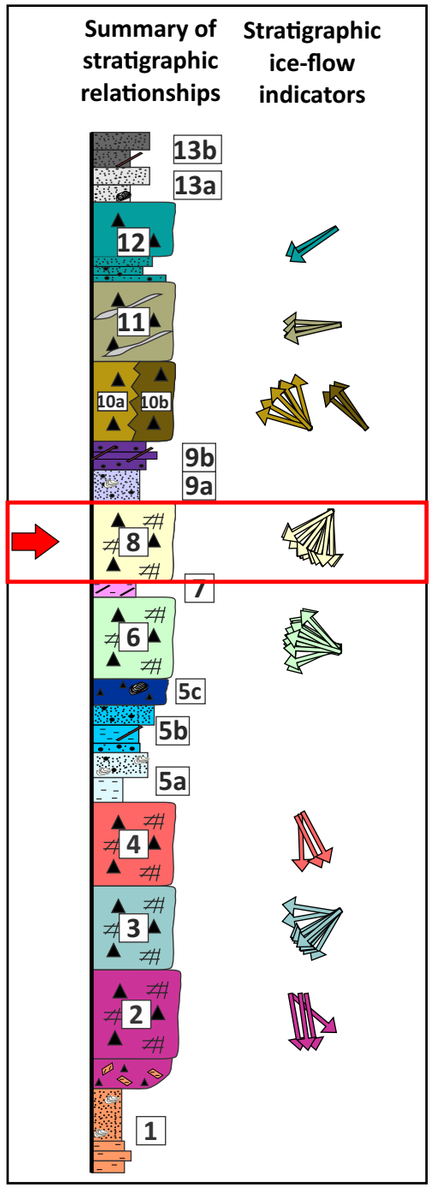

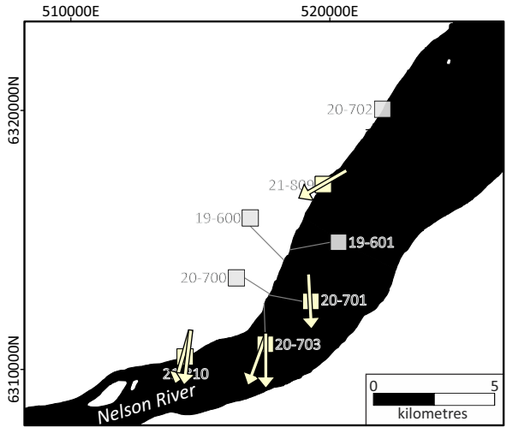

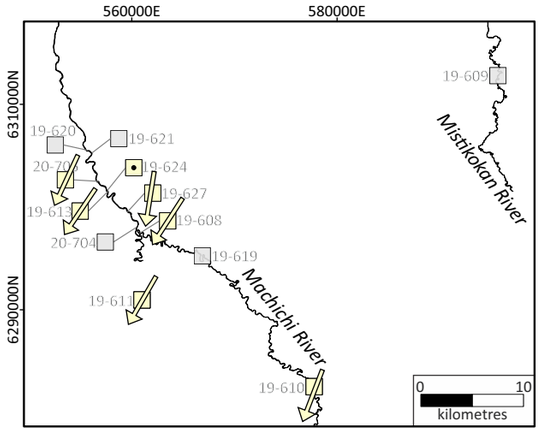

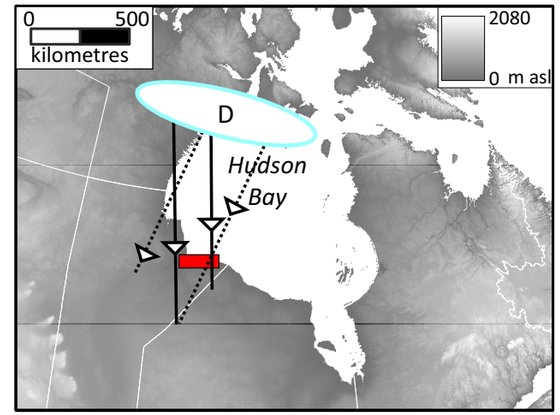

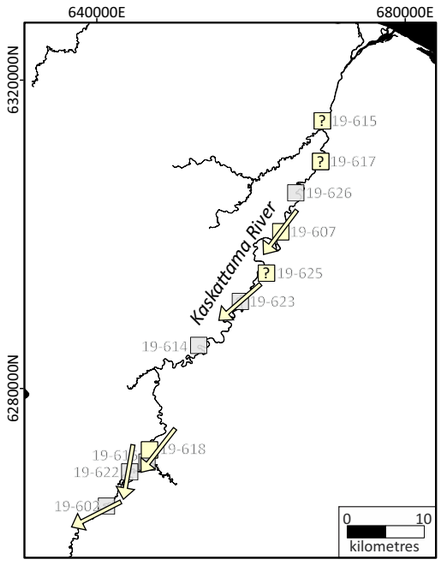

Unit occurrence with interpreted ice-flow indicator direction

Unit occurrence that relies on till sedimentology, stratigraphic relationships and till composition (no ice-flow data)











Unit 8 sediments, key sections: 19-608, 20-704

Notes:

- Unit 8 till is typically greyish brown and appears similar to Unit 6 till at most sections in the field but is differentiated by till fabrics and composition.

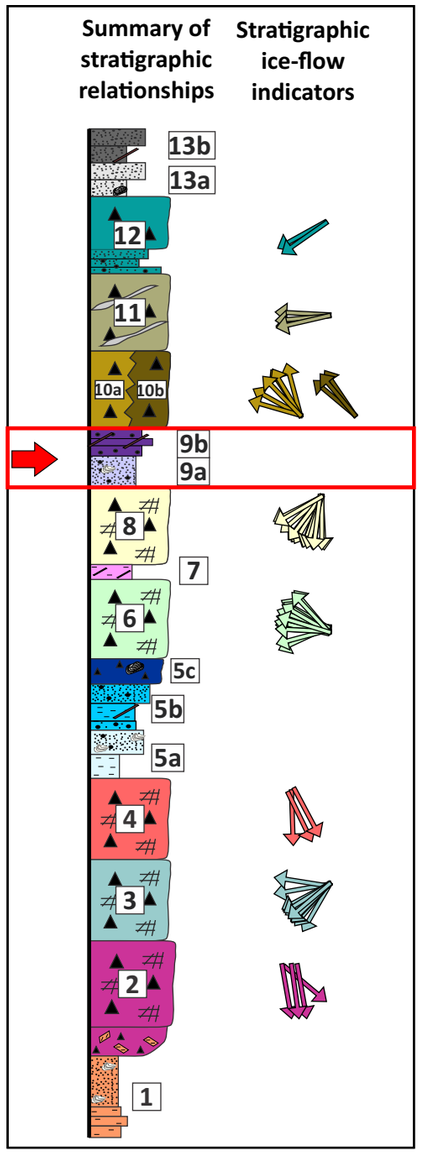

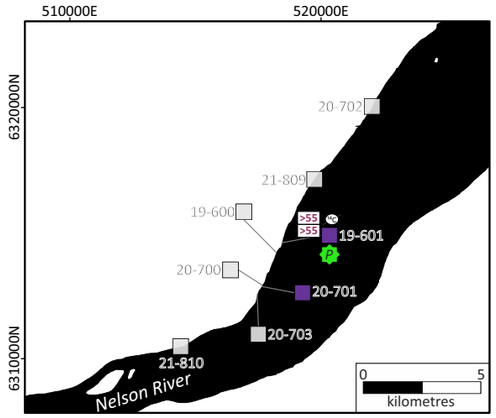

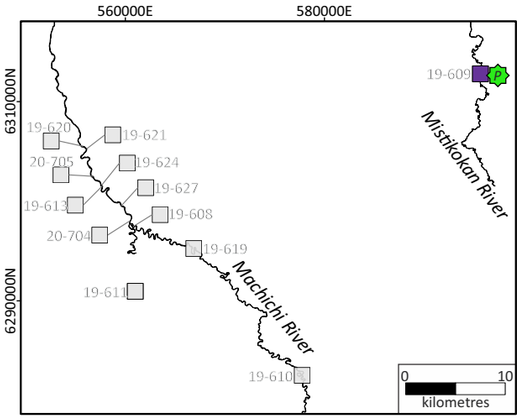

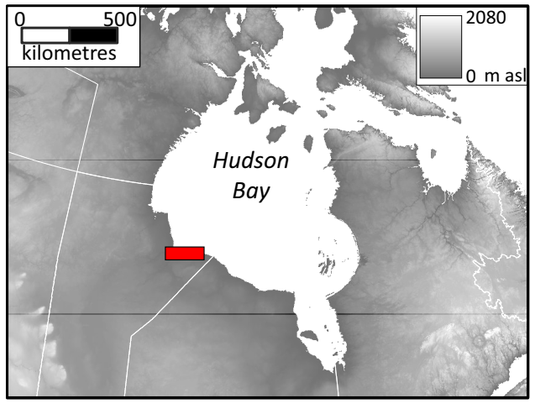

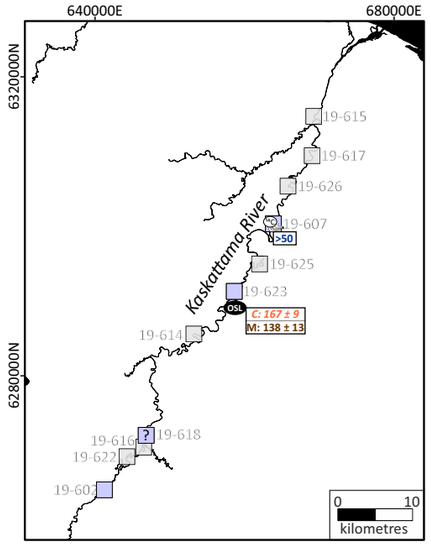

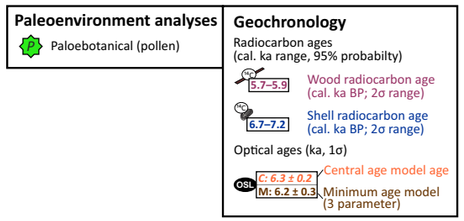



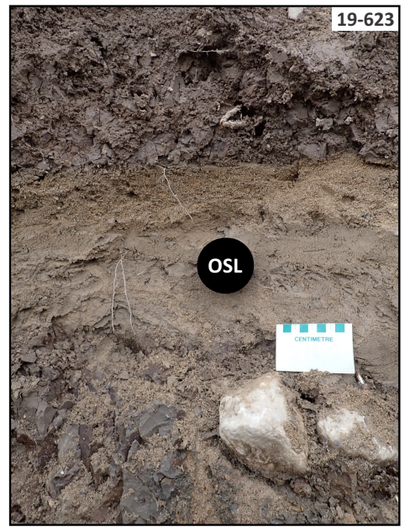

Unit 9 sediments, key sections: 19-601, 19-607, 19-609

Notes:

- Additional geochronology constrains are needed to confirm OSL age estimations; additional photos in Figure 13 of manuscript.

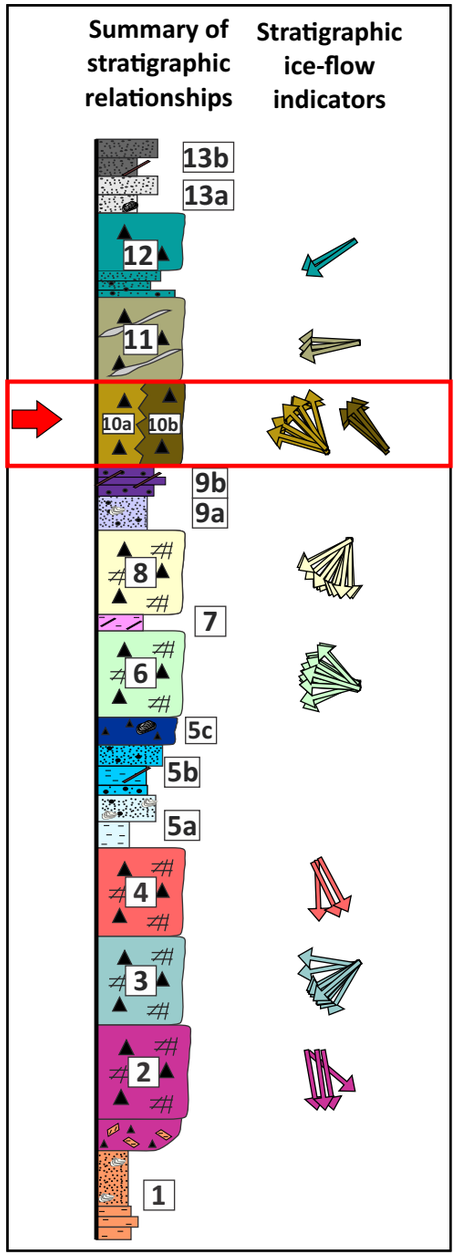

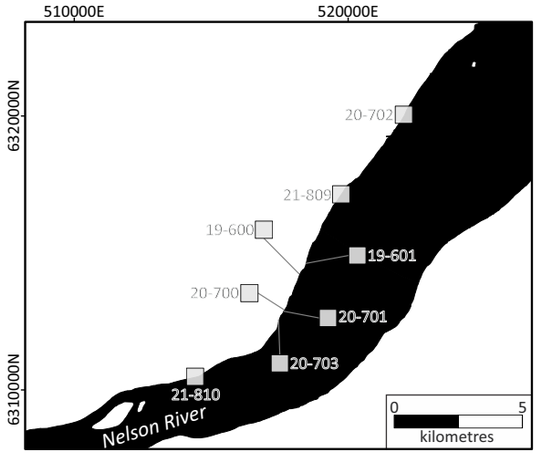

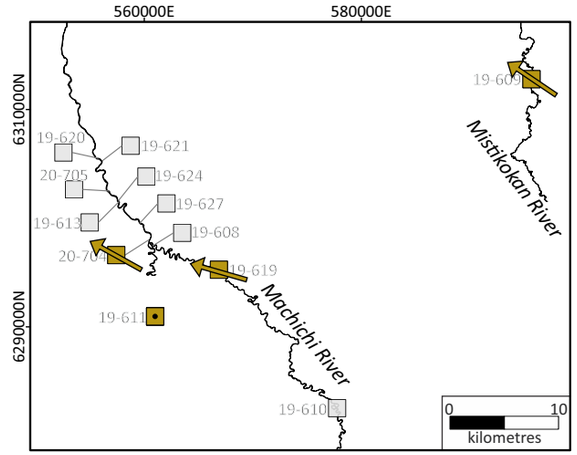

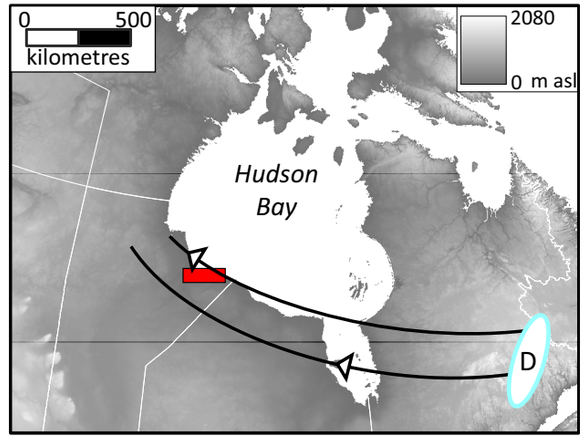

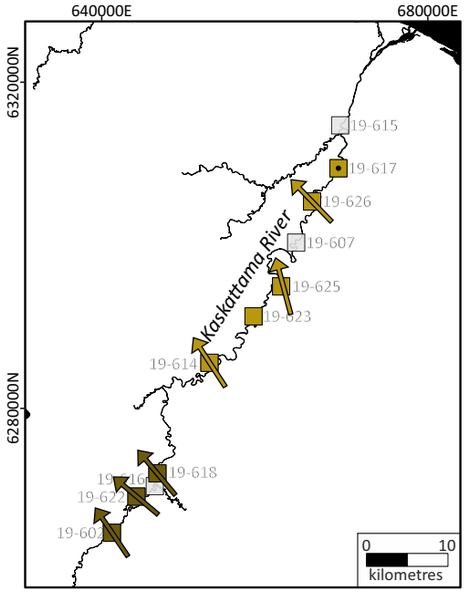

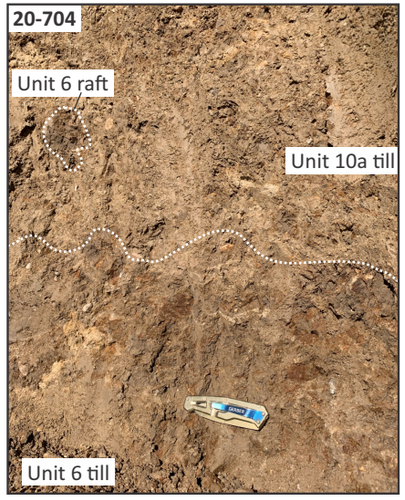

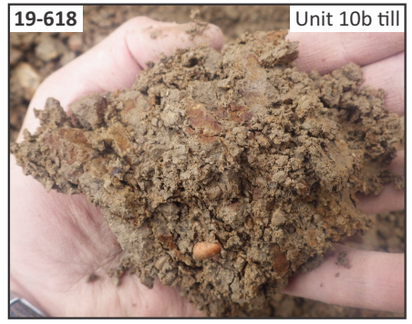

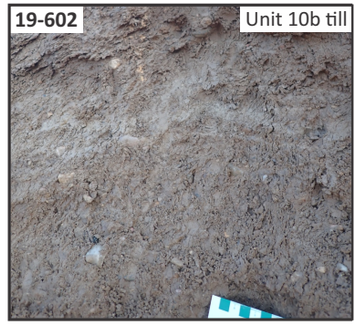



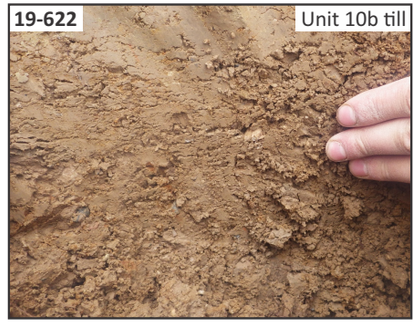

Unit occurrence with interpreted ice-flow indicator direction

Unit occurrence that relies on till sedimentology, stratigraphic relationships and till composition (no ice-flow data)

Unit 10 sediments, key sections: 20-704, 19-609, 19-626, 19-602

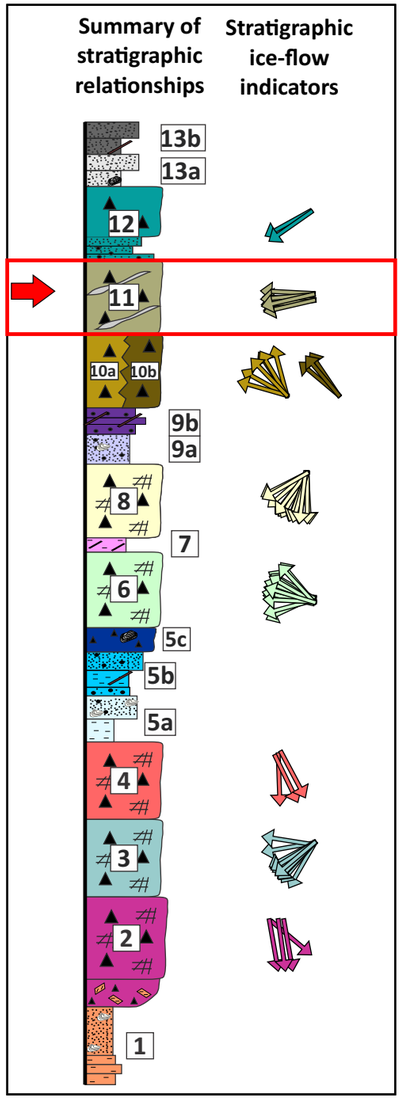

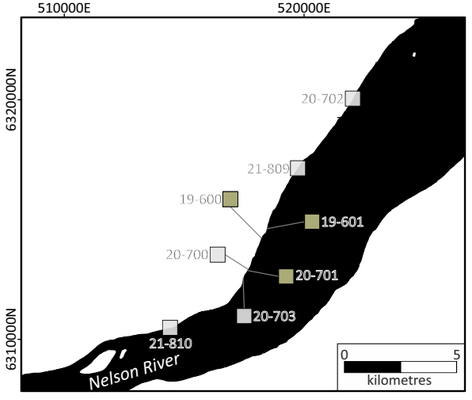

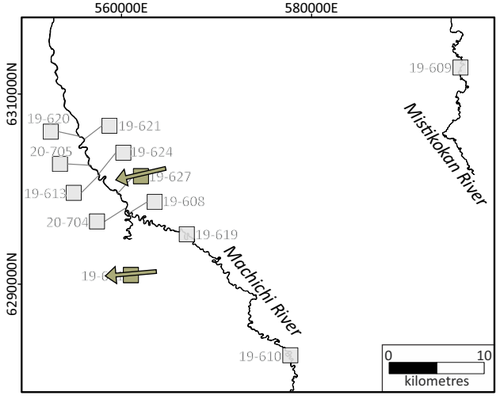

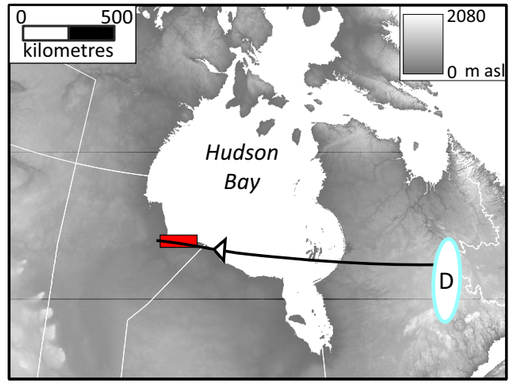

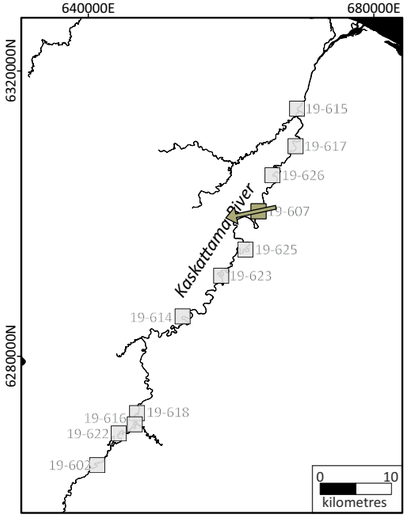

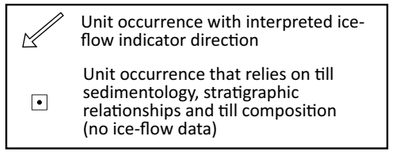









Unit 11 sediments, key sections: 19-627, 19-600

Notes:

- Unit 11 till is typically reddish brown and often contains silt and/or sand stringers.

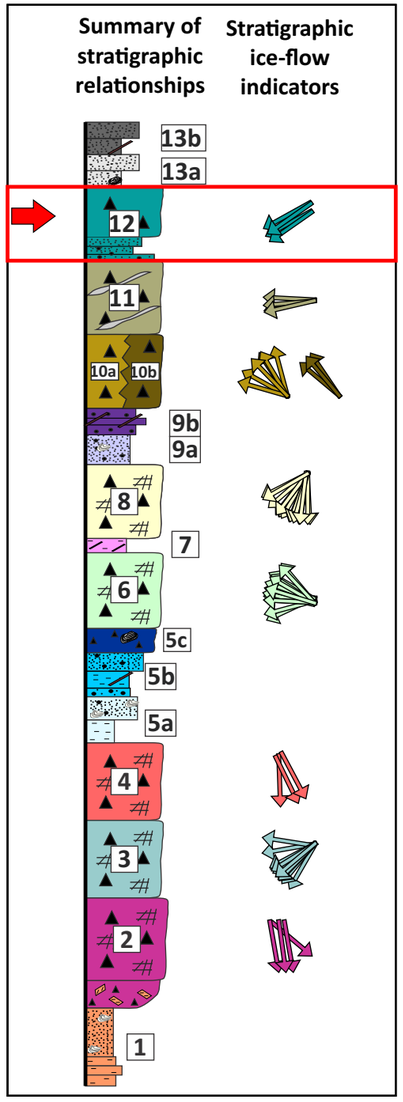

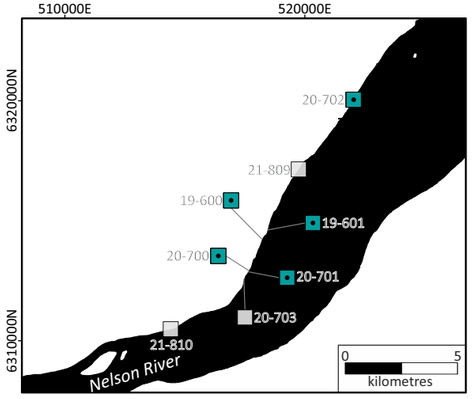

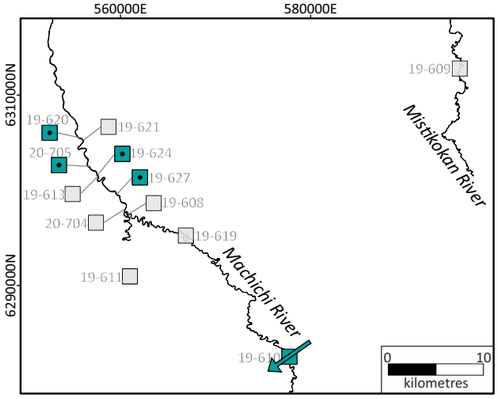

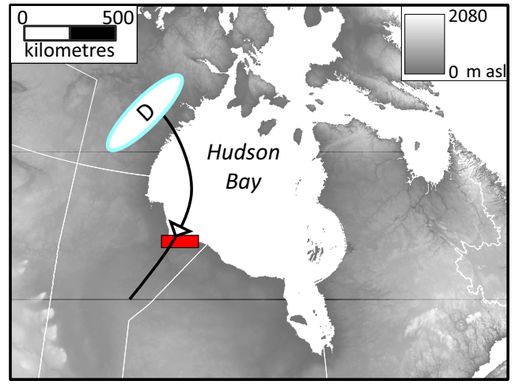



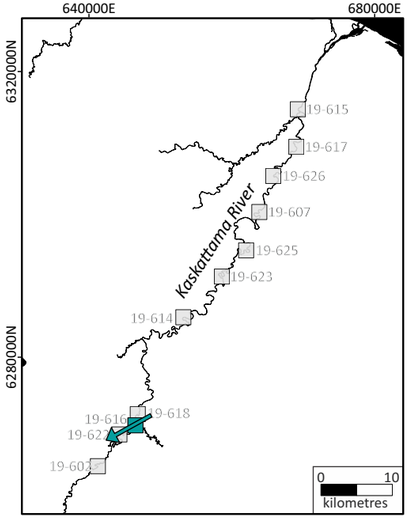

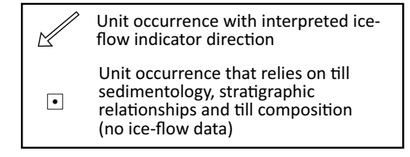

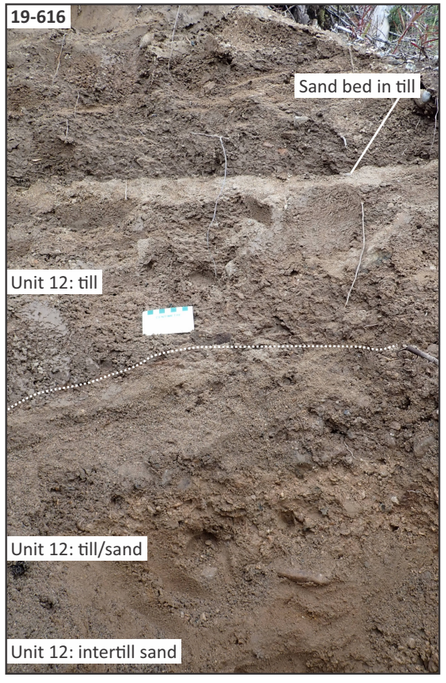





Unit 12 sediments, key sections: 19-627, 19-600

Notes:

- Unit 12 till is typically reddish brown and often contains silt and/or sand stringers.
- Additional ice-flow data needs to be collected to confirm interpretations along the Nelson River Estuary.

Supplemental material 4: Optical age data.

This supplemental file contains additional optical age datasets and plots including dose rate calculations (Table S4-1), radial plots for samples analyzed (Figure S4-1), examples of decay curves and dose response curves for aliquots analyzed (Figure S4-2) and radial plots for dose recovery tests (Figure S4-3).

Table S4-1: Optical age sample water content, radioisotopes concentrations, sample depths, and calculated dose rates.

Section_ID	Unit	Interpreted depositional environment	Lab ID	Latitude	Longitude	*d* (m) [a]	Δw [b]	K (%)	U (µg·g-1)	Th (µg·g-1)	$\dot{D}_C$ (Gy/ka)[c]	$\dot{D}_T$ (Gy/ka)[c]
112-19-610	13a	nearshore marine	112-19-610-OSL005	56.6802	-91.7308	1.1	0.125	1.27 ± 0.04	1.020 ± 0.049	5.96 ± 0.15	0.186 ± 0.019	1.83 ± 0.05
112-19-623	9a	nearshore marine	112-19-623-OSL015	56.7387	-90.4066	9.6	0.102	1.18 ± 0.03	1.020 ± 0.058	4.09 ± 0.11	0.081 ± 0.008	1.57 ± 0.04
112-19-613	5b	fluvial	112-19-613-OSL007	56.8540	-92.0541	6.3	0.085	1.02 ± 0.03	0.870 ± 0.037	4.20 ± 0.11	0.108 ± 0.011	1.46 ± 0.04
112-19-624	5b	fluvial	112-19-624-OSL300	56.8547	-92.0552	6	0.077	0.99 ± 0.05	0.559 ± 0.100	3.10 ± 0.16	0.078 ± 0.008	1.28 ± 0.05
112-20-700	5a	nearshore marine	112-20-700-OSL004	56.9597	-92.7097	15	0.346	0.97 ± 0.06	0.721 ± 0.129	3.24 ± 0.17	0.053 ± 0.005	1.00 ± 0.05
112-19-621	5a	nearshore marine	112-19-621-OSL016	56.8876	-92.0786	6.2	0.042	1.20 ± 0.04	0.700 ± 0.031	3.32 ± 0.08	0.109 ± 0.011	1.60 ± 0.04
112-19-621	5a	nearshore marine	112-19-621-OSL012	56.8876	-92.0786	6.7	0.670	1.11 ± 0.07	0.600 ± 0.070	2.82 ± 0.15	0.104 ± 0.010	1.55 ± 0.07
112-20-705	1	nearshore marine	112-20-705-OSL008	56.8628	-92.0688	8.7	0.073	0.91 ± 0.05	0.752 ± 0.109	3.59 ± 0.18	0.087 ± 0.009	1.30 ± 0.06
112-19-624	1	nearshore marine	112-19-624-OSL100	56.8547	-92.0552	13.1	0.086	1.20 ± 0.07	0.551 ± 0.110	3.44 ± 0.18	0.105 ± 0.010	1.50 ± 0.07
112-19-624	1	nearshore marine	112-19-624-OSL018	56.8547	-92.0552	13.1	0.045	1.15 ± 0.04	0.580 ± 0.028	2.36 ± 0.06	0.061 ± 0.006	1.41 ± 0.04

[a] *d* = sample depth beneath the ground surface, measured from the centre of the collection tube (5 cm diameter).

[b] Δ^w = water content (mass water/mass dry sediment). For the dose rate calculations each Δ^w value included an uncertainty of ±10% (1σ) to account for fluctuations in water content over time.

[c] $\dot{D}_C$ = cosmic ray dose rate; $\dot{D}_T$ = total dose rate (that due to cosmic rays plus that due to β and γ radiation).

Figure S4-1: Radial plots showing the distribution of aliquot D_e values for each sample and estimations of representative D_e values (weighed mean) used for dating, using either the CAM (dotted line that intersects the curved axis) or the MAM (solid line that intersects the curved axis). Values that plot in the shaded zones fall within 2σ of the weighted mean value.

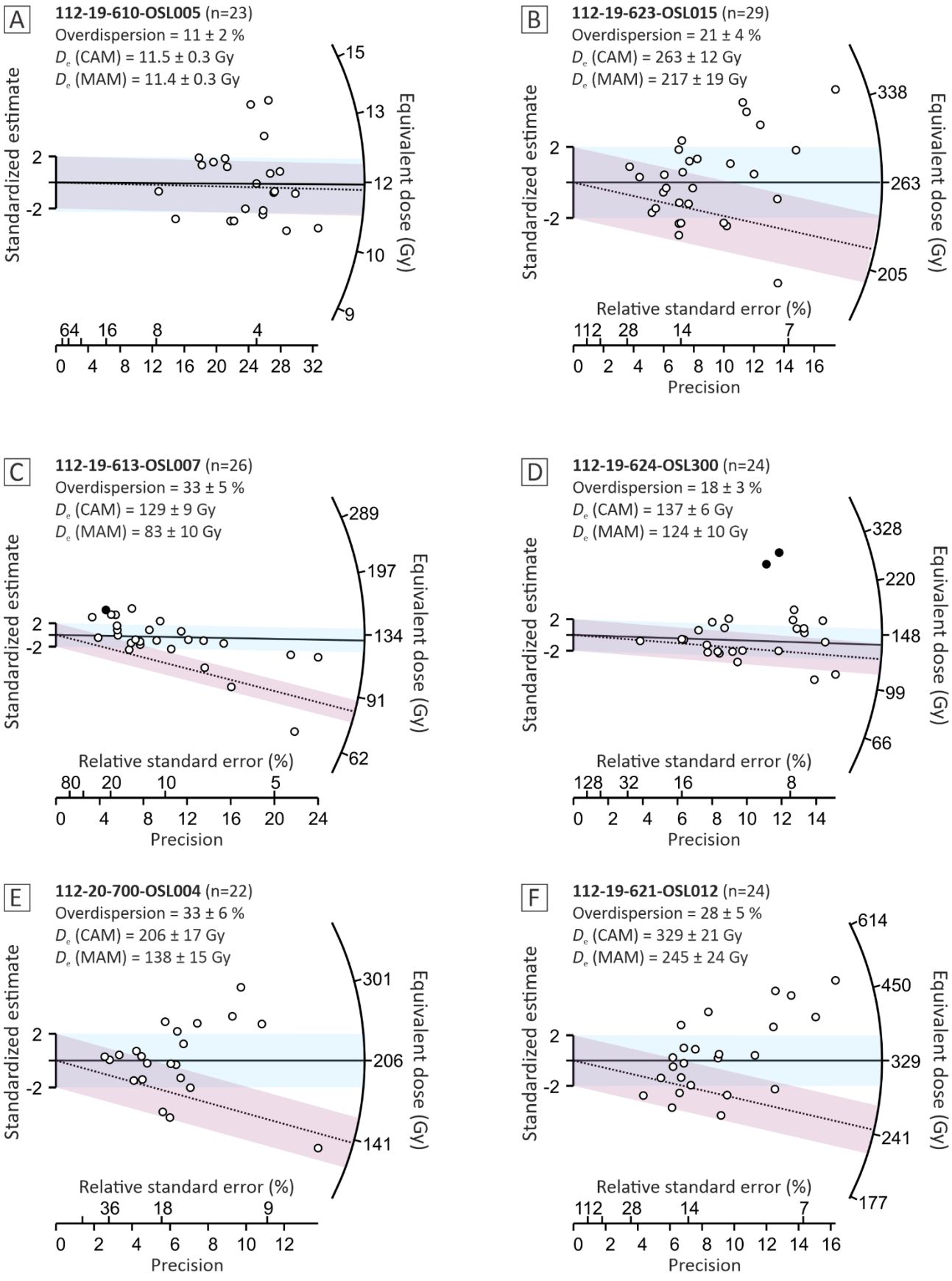

G **112-19-621-OSL016** (n=23)
Overdispersion = 31 ± 6 %
D_e (CAM) = 254 ± 20 Gy
D_e (MAM) = 180 ± 25 Gy

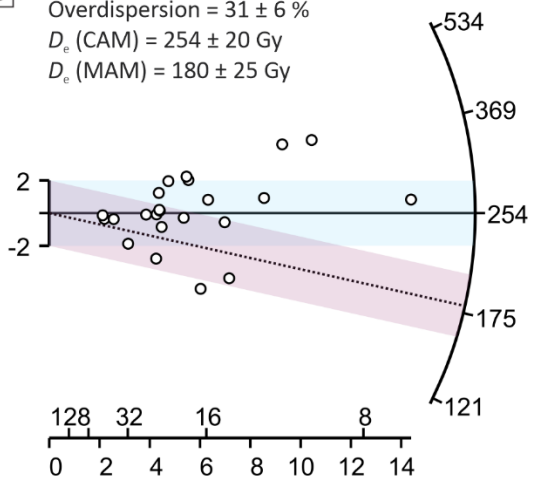

H **112-20-705-OSL0008** (n=24)
Overdispersion = 18 ± 5 %
D_e (CAM) = 282 ± 15 Gy
D_e (MAM) = 272 ± 25 Gy

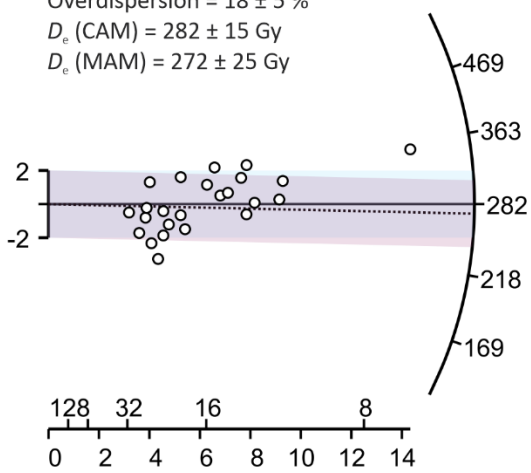

I **112-19-624-OSL100** (n=21)
Overdispersion = 26 ± 5 %
D_e (CAM) = 339 ± 22 Gy
D_e (MAM) = 266 ± 35 Gy

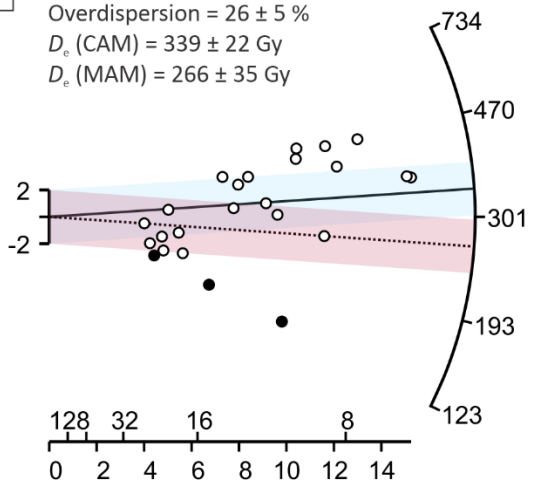

J **112-19-624-OSL018** (n=21)
Overdispersion = 14 ± 5 %
D_e (CAM) = 297 ± 14 Gy
D_e (MAM) = 283 ± 22 Gy

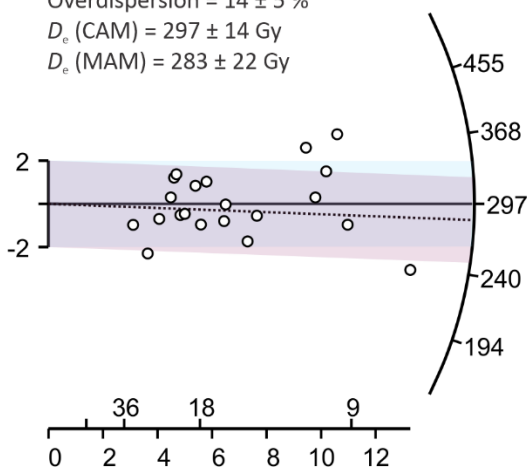

Figure S4-2: Luminescence decay curves (main graph) showing the "natural" signal and dose response curves (inset) for each optical sample analyzed (A–I). These curves are typical for aliquots measured for each sample. Note, that the initial part of the decay curve is dominated by the desired 'fast' component for each sample. In each case, the final 20 s of the signal was subtracted from the initial 0.2 or 0.4 s and this value (L_i) was divided by the value measured from a subsequent test dose (T_i) to produce the sensitivity-corrected signal (L_i/T_i), which is plotted on the y-axis of the dose response curve.

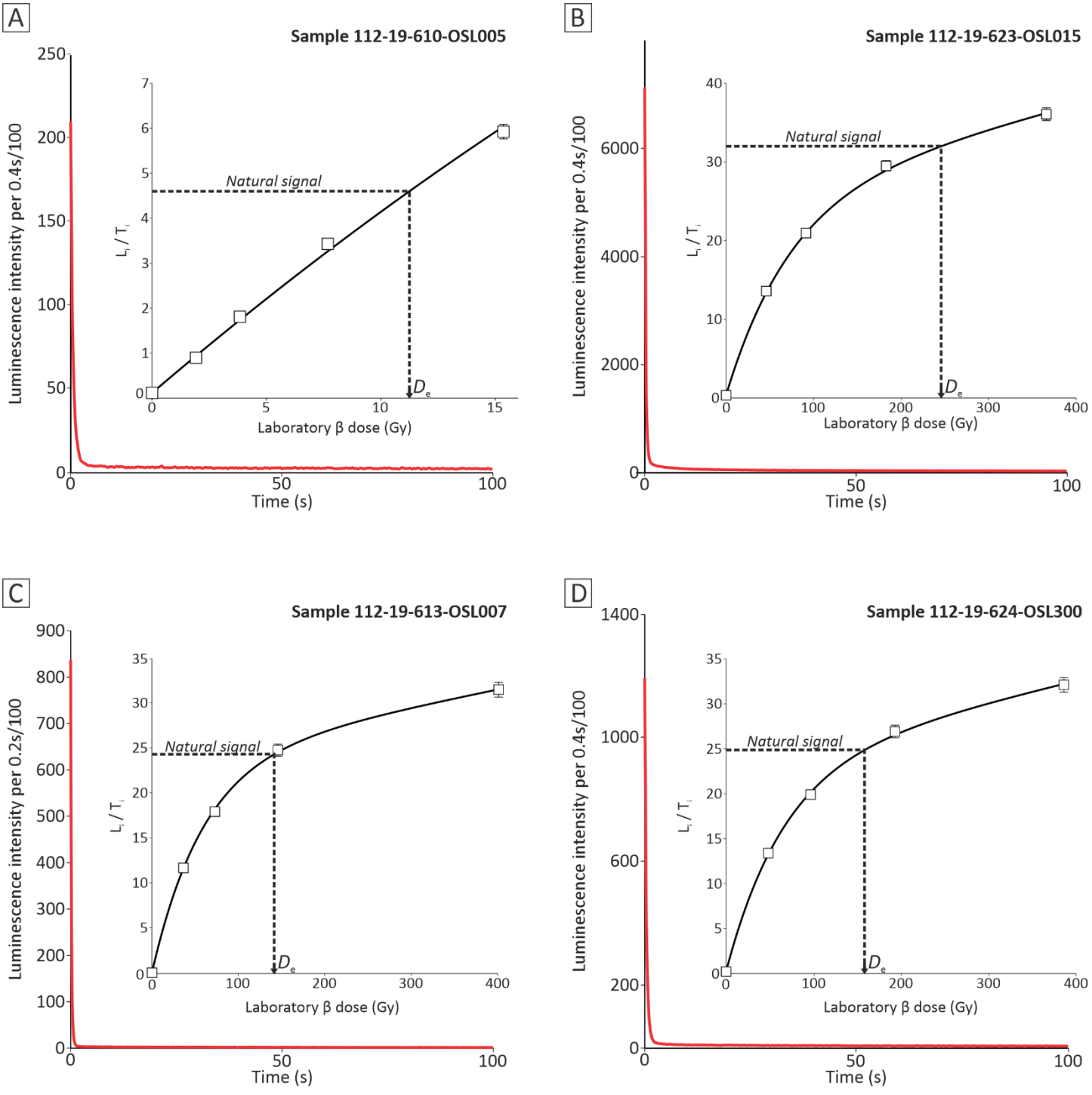

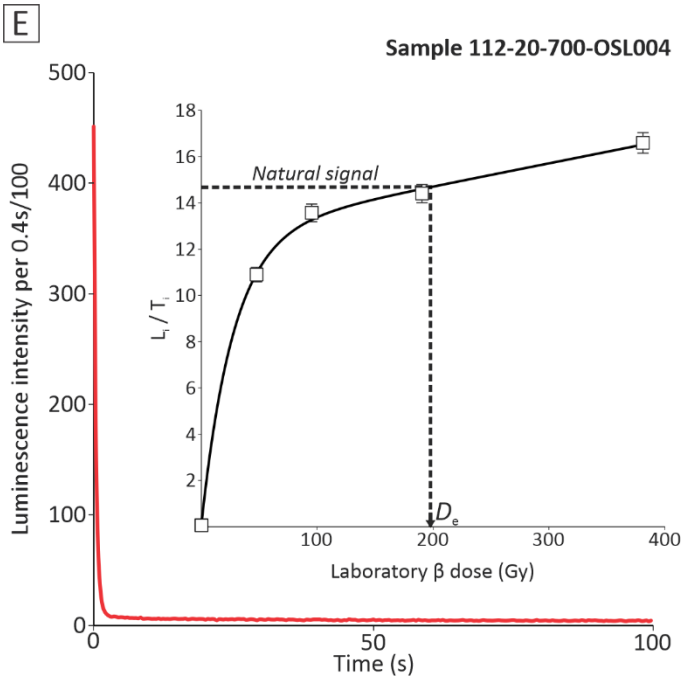
E
Sample 112-20-700-OSL004
Luminescence intensity per 0.4s/100
Time (s)
Natural signal
L_i / T_i
D_e
Laboratory β dose (Gy)

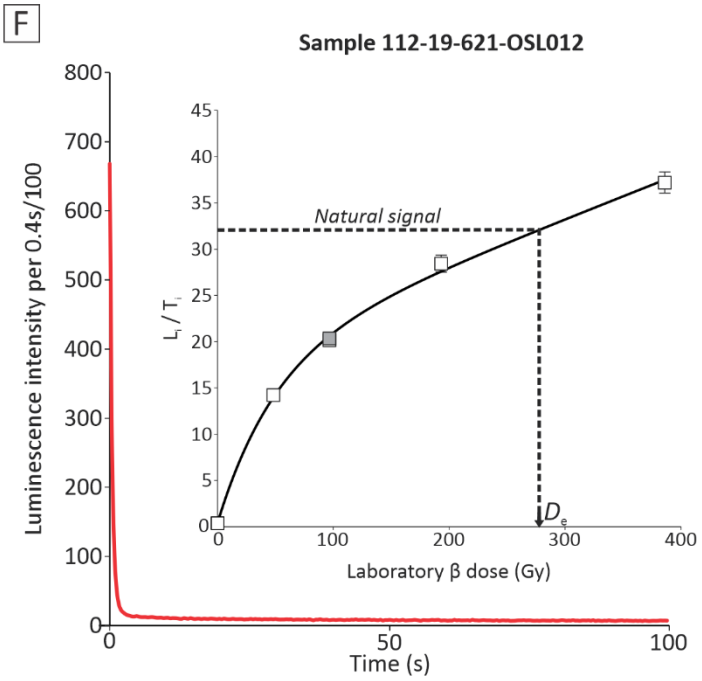
F
Sample 112-19-621-OSL012
Luminescence intensity per 0.4s/100
Time (s)
Natural signal
L_i / T_i
D_e
Laboratory β dose (Gy)

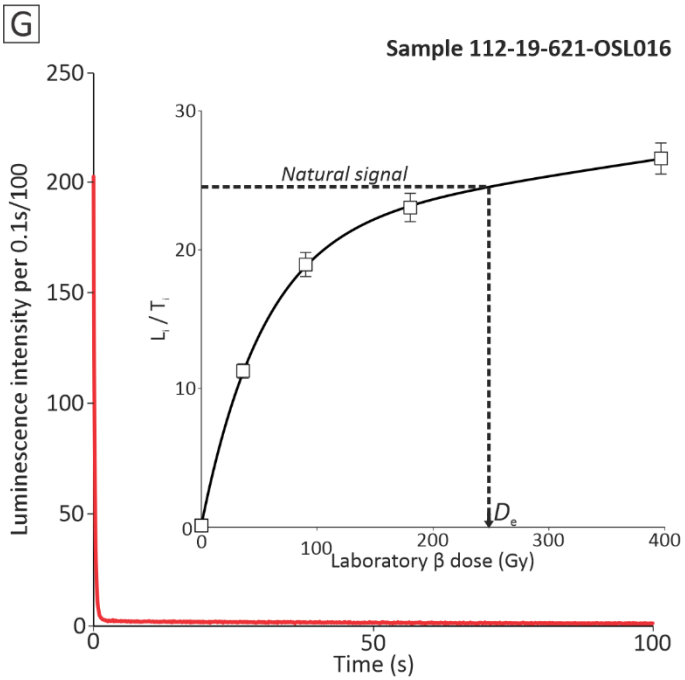
G
Sample 112-19-621-OSL016
Luminescence intensity per 0.1s/100
Time (s)
Natural signal
L_i / T_i
D_e
Laboratory β dose (Gy)

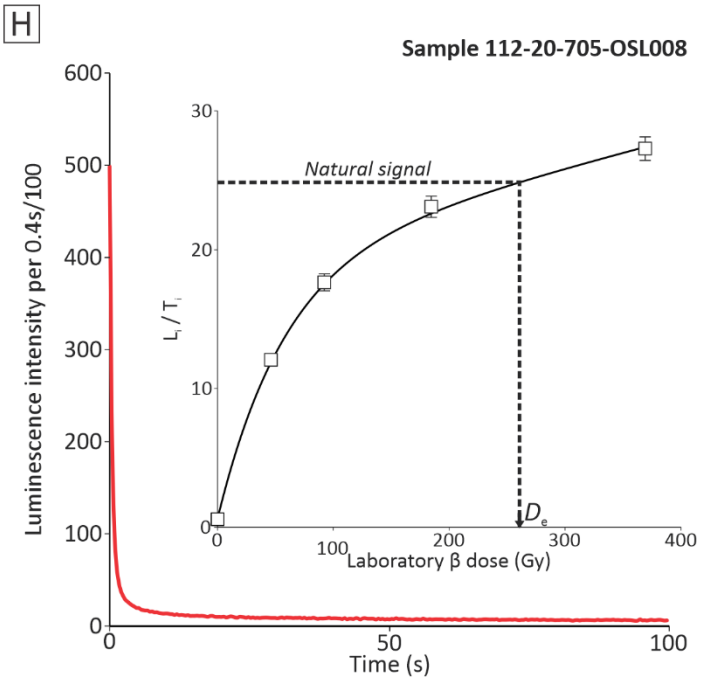
H
Sample 112-20-705-OSL008
Luminescence intensity per 0.4s/100
Time (s)
Natural signal
L_i / T_i
D_e
Laboratory β dose (Gy)

I

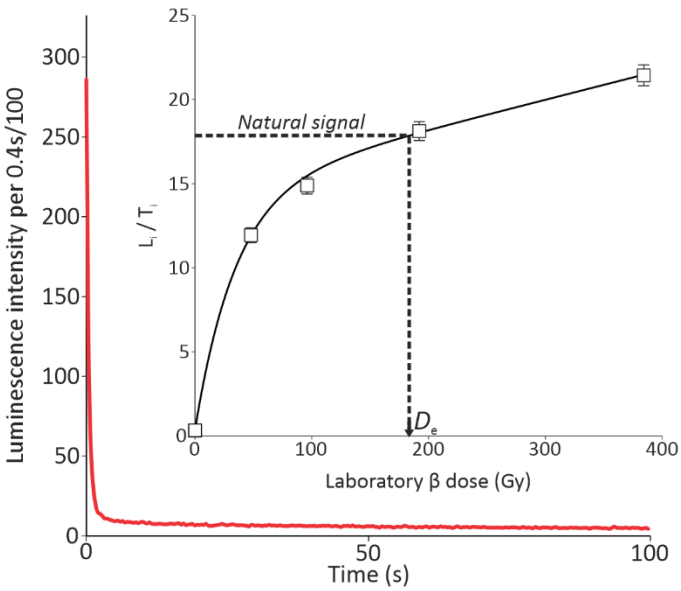
Sample 112-19-624-OSL100
Luminescence intensity per 0.4s/100
Time (s)
Natural signal
L_i / T_i
D_e
Laboratory β dose (Gy)

J

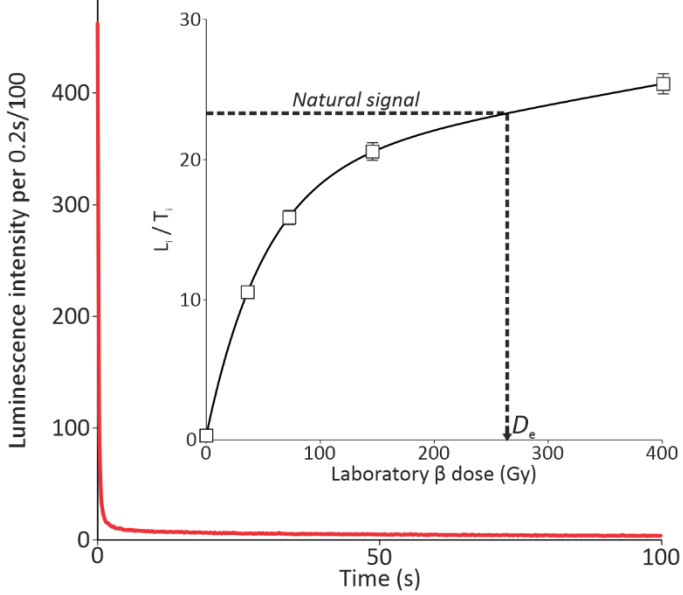
Sample 112-19-624-OSL018
Luminescence intensity per 0.2s/100
Time (s)
Natural signal
L_i / T_i
D_e
Laboratory β dose (Gy)

Figure S4-3: Radial plots for each sample of the dose recovery ratios for single aliquots of quartz from the Hudson Bay Lowland. The grey lines indicate the weighted mean for the dose recovery ratios (CAM), and the grey bar should capture 95% of all measured aliquots if they are statistically consistent at 2σ with a common value, which is the CAM of the dose recovery ratios in these plots.

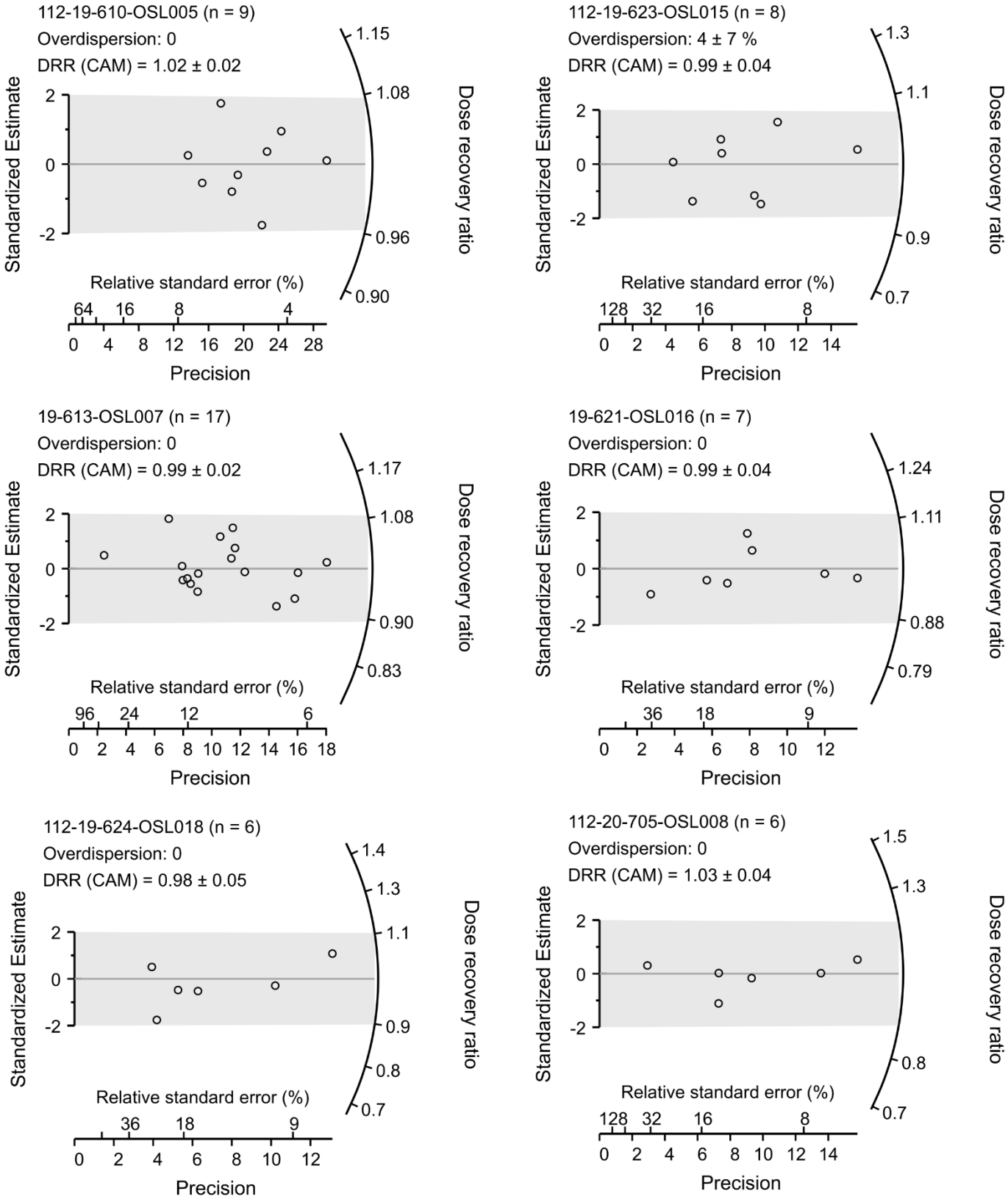

Supplemental material 5: Supporting till composition analysis and figures.

This supplemental file contains supporting till compositional figures.

Figure S5-1: Till-matrix grainsize proportions for identified till units separated by region investigated: A) Tukey box plot of sand (wt. %); B) Tukey box plot of silt (wt. %) and C) Tukey box plot of clay (wt. %). Abbreviations: N, Nelson River Estuary area; M, Machichi River area; K, Kaskattama River area.

Figure S5-2: Till clast-lithology proportions for identified till units separated by region investigated: A) undifferentiated greenstone and greywacke (UGG) clasts; B) granitoid clasts; C) Kenogami River Formation clasts; and D) Kenogami River Formation carbonate clasts.

Figure S5-3: Till detrital hornblende ages summed for each identified till unit displayed on kernel density estimation plots.

Figure S5-4: Principal components 1–4 loadings.

Figure S5-5: Principal component results classified by the proportion of undifferentiated greywacke and greenstone (UGG) clasts (2–8mm size fraction; ct. %) and plotted on PC2 vs. PC1 (A) and PC3 vs. PC2 (B) biplots.

Figure S5-6: Principal component results classified by the proportion of granitoid (2–8mm size fraction; ct. %) and plotted on PC2 vs. PC1 (A) and PC3 vs. PC2 (B) biplots.

Figure S5-7: Principal component results classified by the proportion of Kenogami River Formation clasts (2–8mm size fraction; ct. %) and plotted on PC2 vs. PC1 (A) and PC3 vs. PC2 (B) biplots.

Figure S5-8: Principal component results classified by the proportion of carbonate clasts (2–8mm size fraction; ct. %) and plotted on PC2 vs. PC1 (A) and PC3 vs. PC2 (B) biplots.

Figure S5-1: Till-matrix grainsize proportions for identified till units separated by region investigated: A) Tukey box plot of sand (wt. %); B) Tukey box plot of silt (wt. %) and C) Tukey box plot of clay (wt. %). Abbreviations: N, Nelson River Estuary area; M, Machichi River area; K, Kaskattama River area.

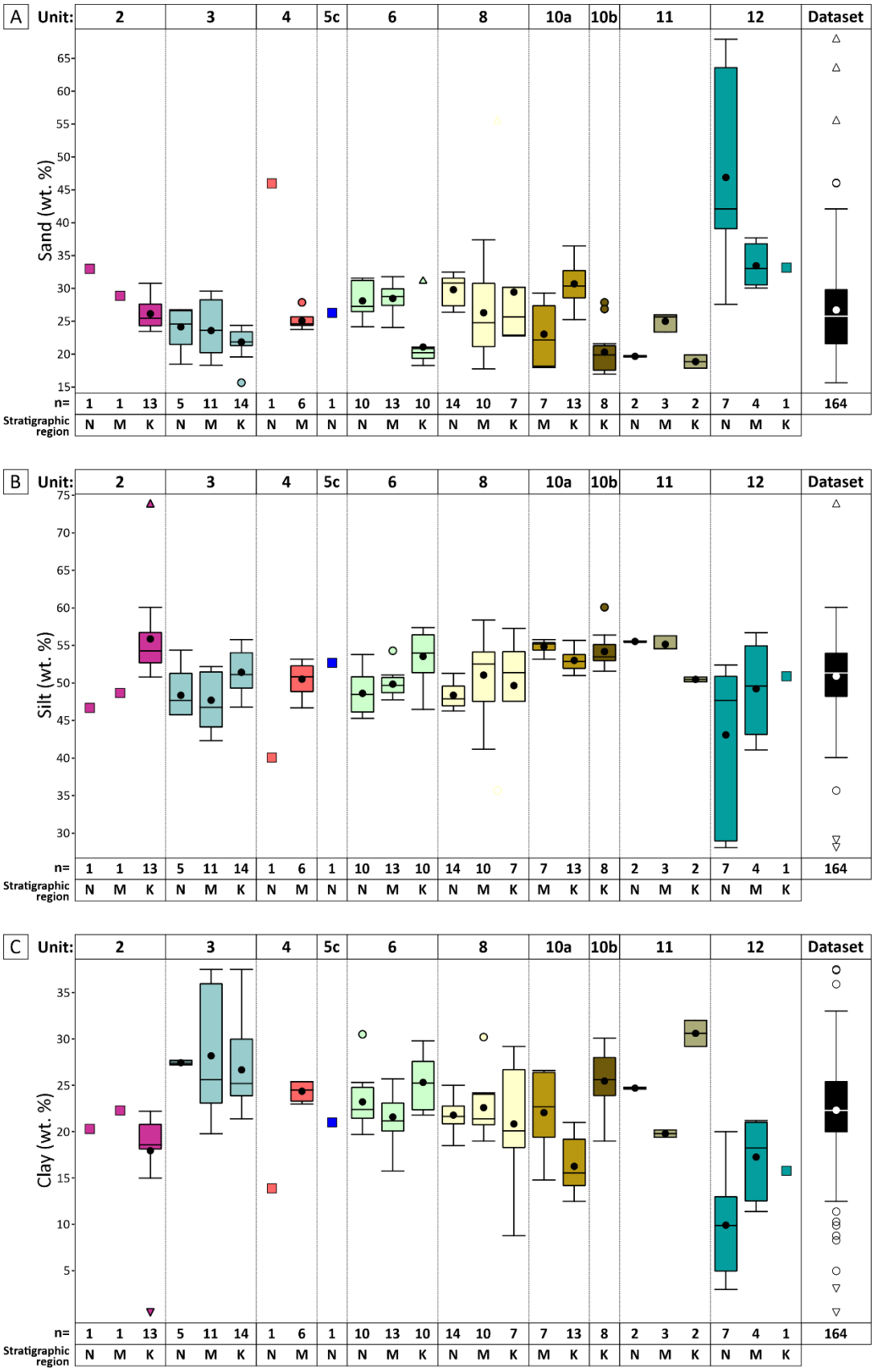

Figure S5-2: Till clast-lithology proportions for identified till units separated by region investigated: A) undifferentiated greenstone and greywacke (UGG) clasts; B) granitoid clasts; C) Kenogami River Formation clasts; and D) Kenogami River Formation carbonate clasts.

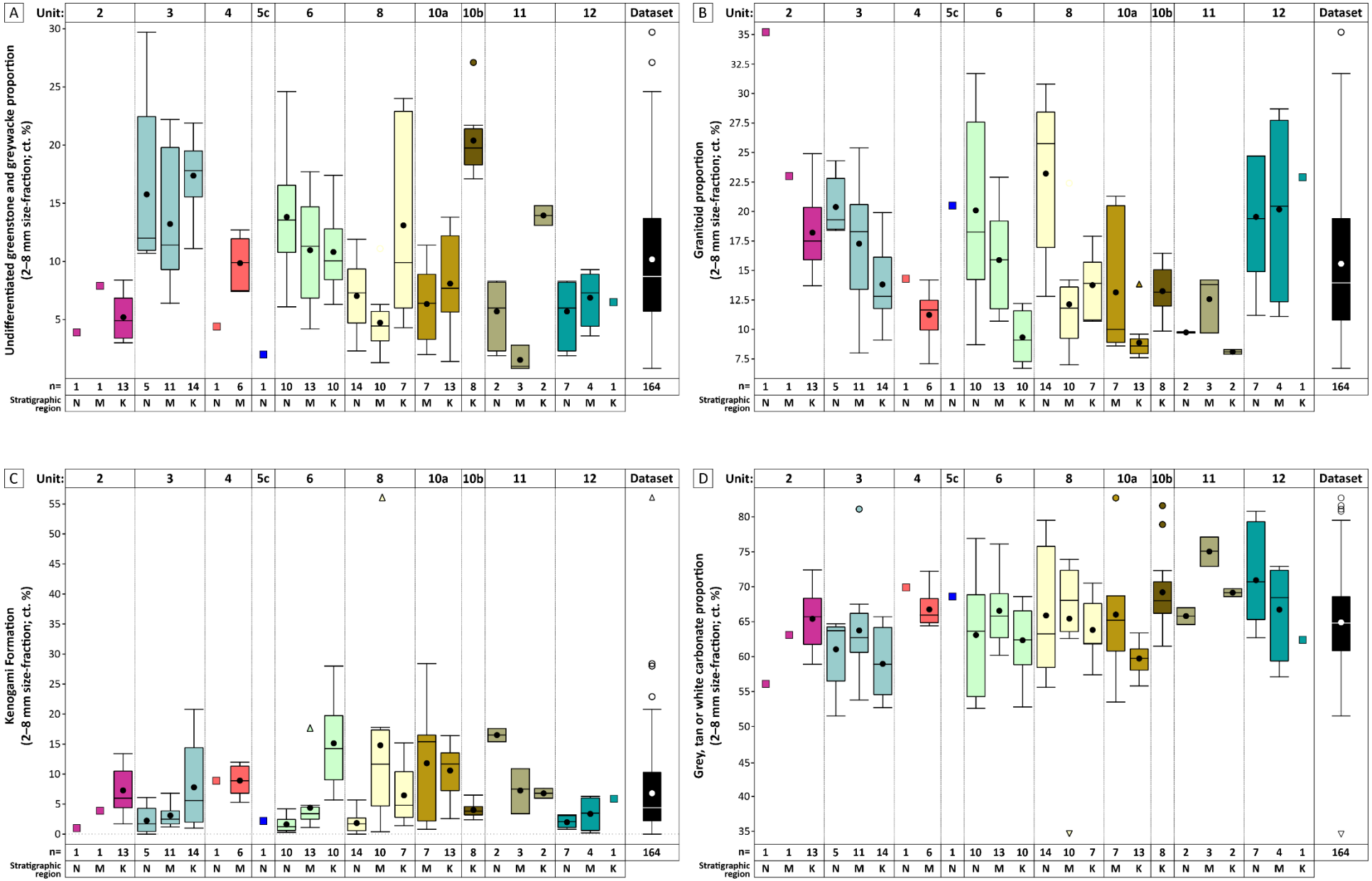

Figure S5-3: Till detrital hornblende ages summed for each identified till unit displayed on kernel density estimation plots.

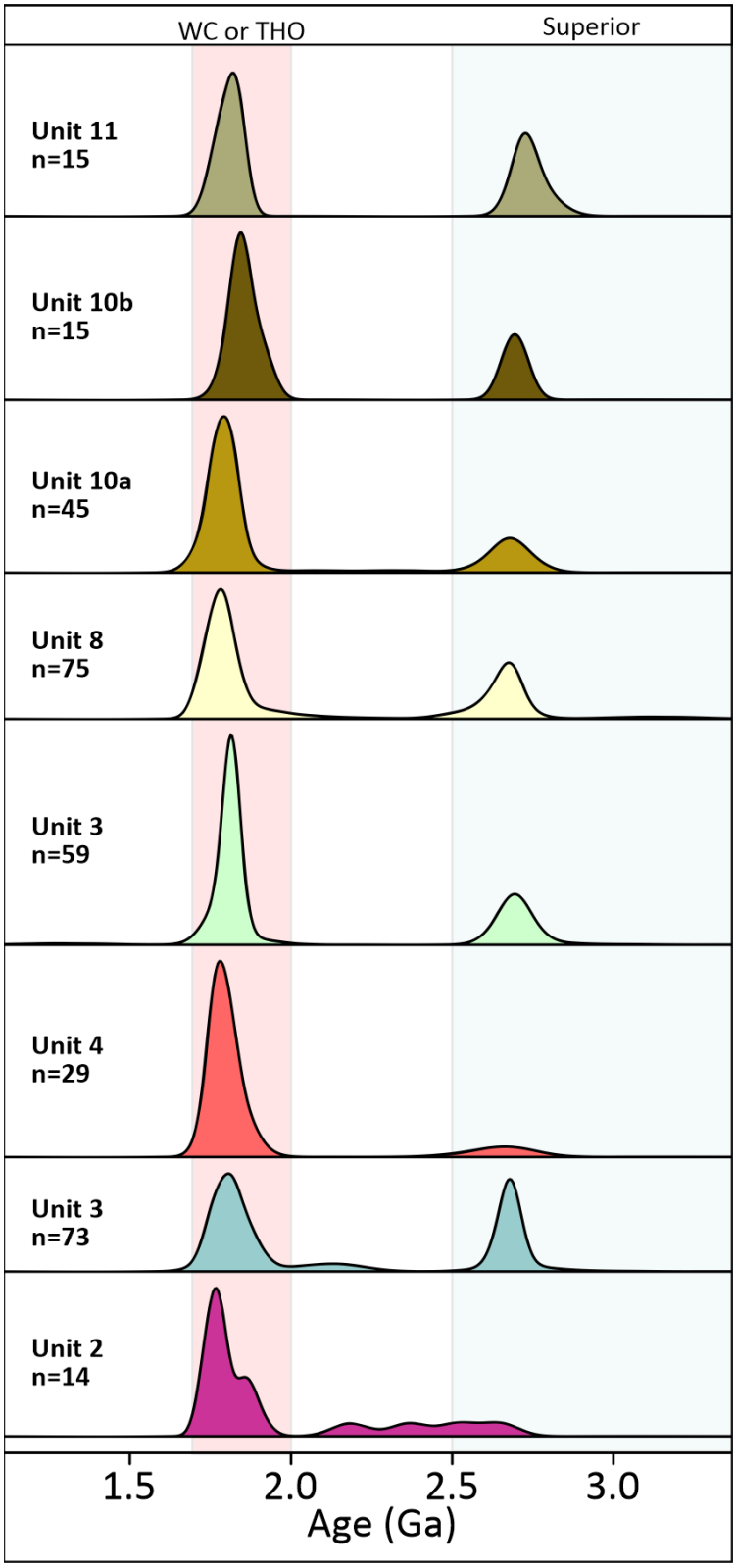

Figure S5-4: Principal components 1–4 loadings.

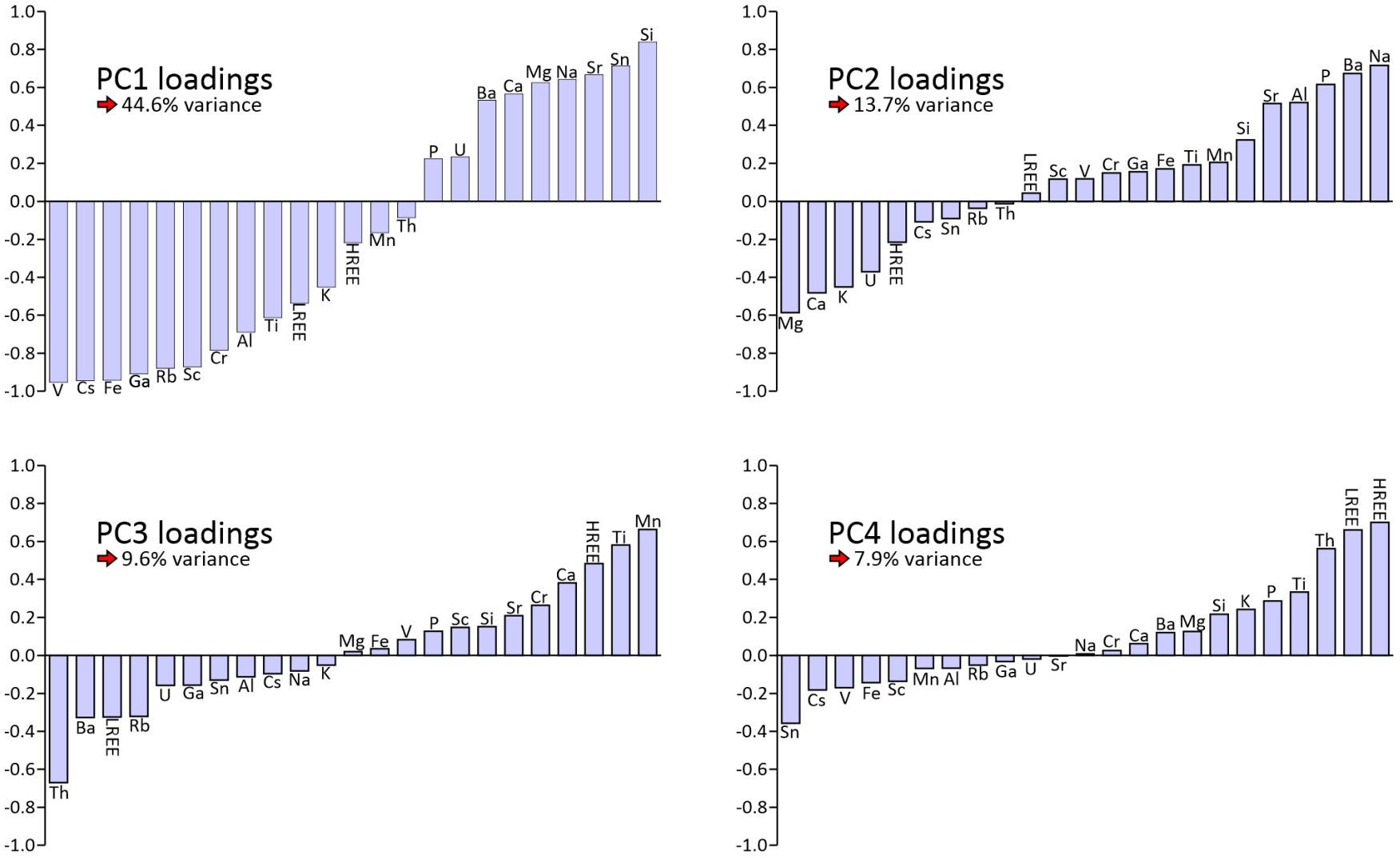

Figure S5-5: Principal component results classified by the proportion of undifferentiated greywacke and greenstone (UGG) clasts (2–8mm size fraction; ct. %) and plotted on PC2 vs. PC1 (A) and PC3 vs. PC2 (B) biplots.

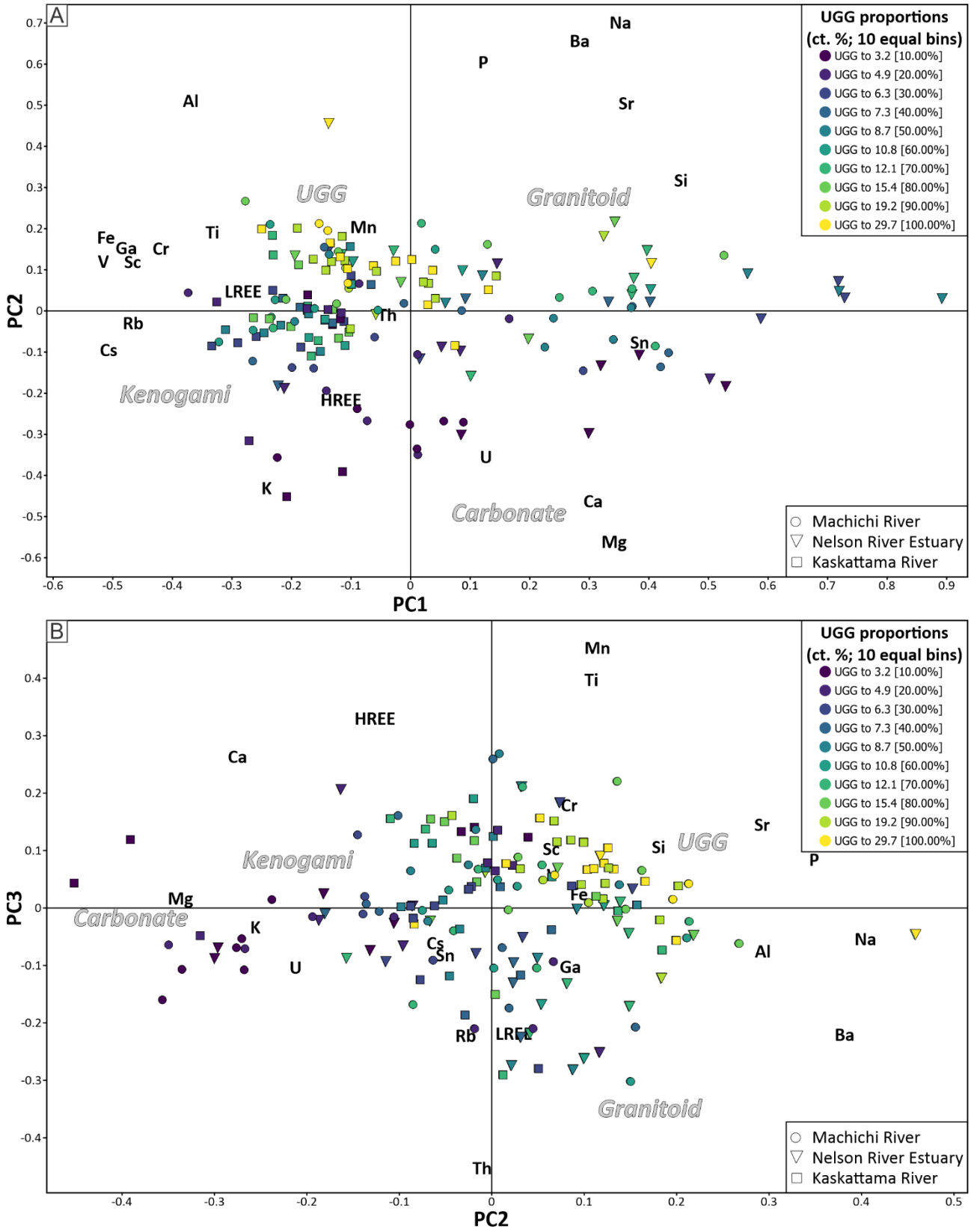

Figure S5-6: Principal component results classified by the proportion of granitoid (2–8mm size fraction; ct. %) and plotted on PC2 vs. PC1 (A) and PC3 vs. PC2 (B) biplots.

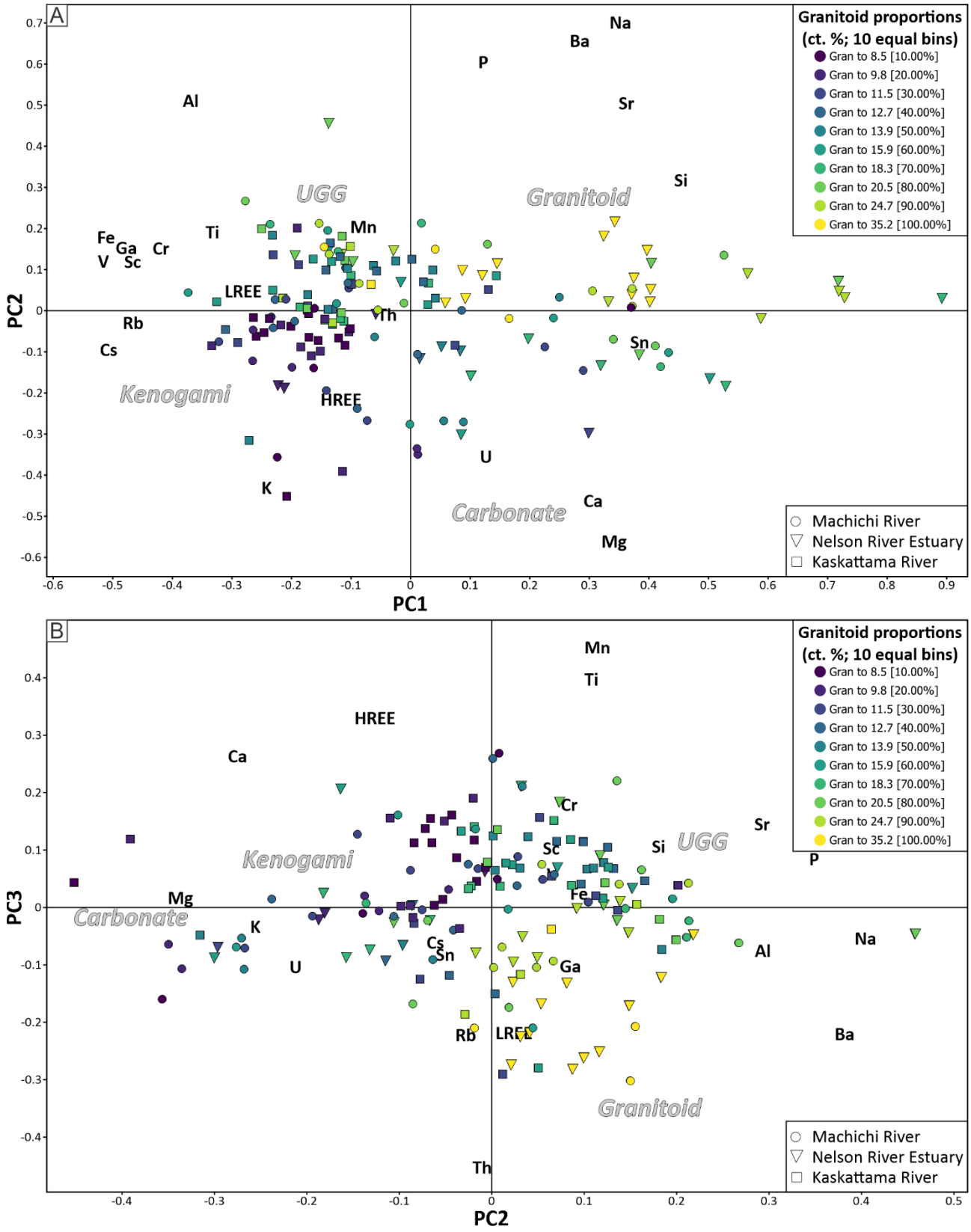

Figure S5-7: Principal component results classified by the proportion of Kenogami River Formation clasts (2–8mm size fraction; ct. %) and plotted on PC2 vs. PC1 (A) and PC3 vs. PC2 (B) biplots.

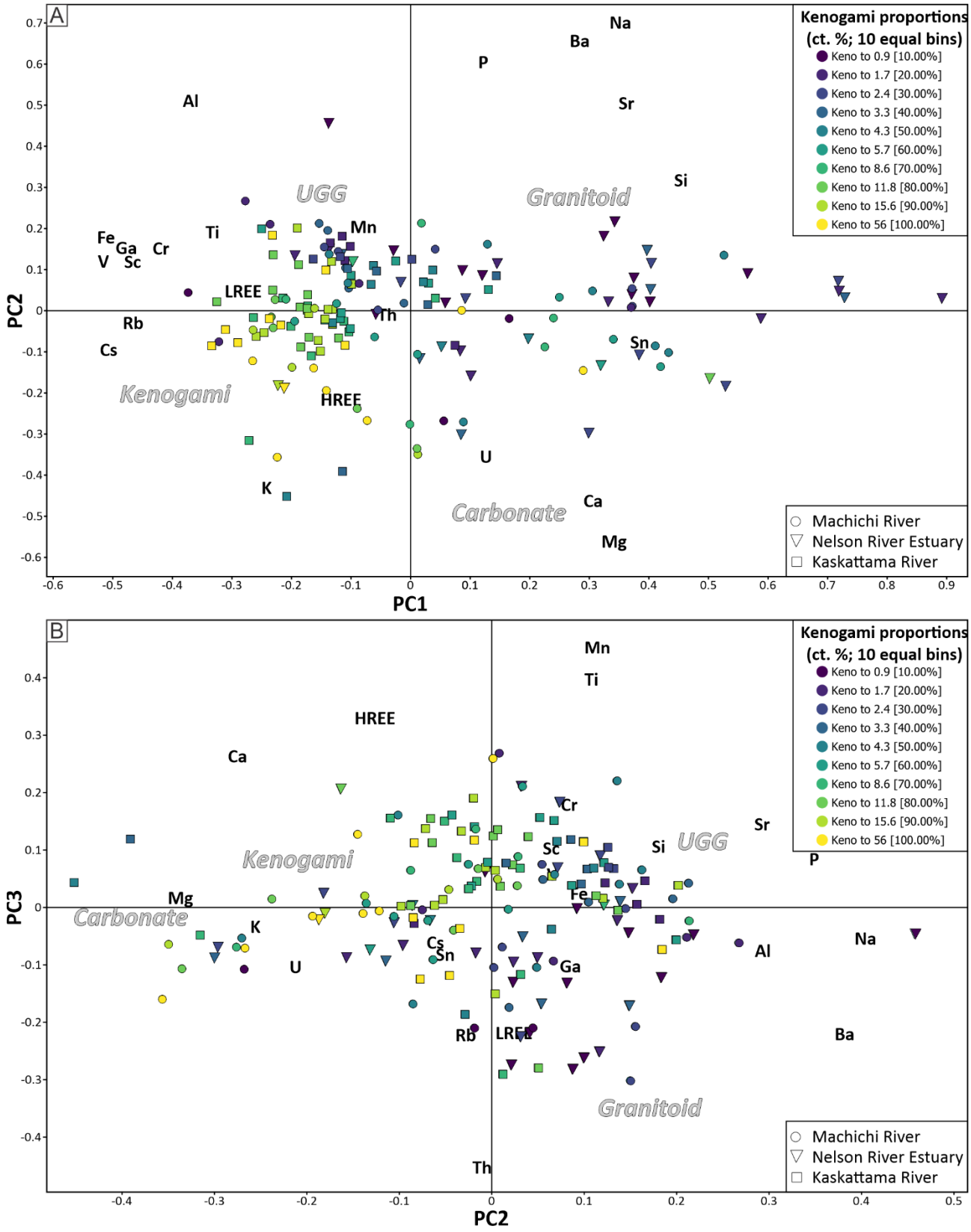

Figure S5-8: Principal component results classified by the proportion of carbonate clasts (2–8mm size fraction; ct. %) and plotted on PC2 vs. PC1 (A) and PC3 vs. PC2 (B) biplots.

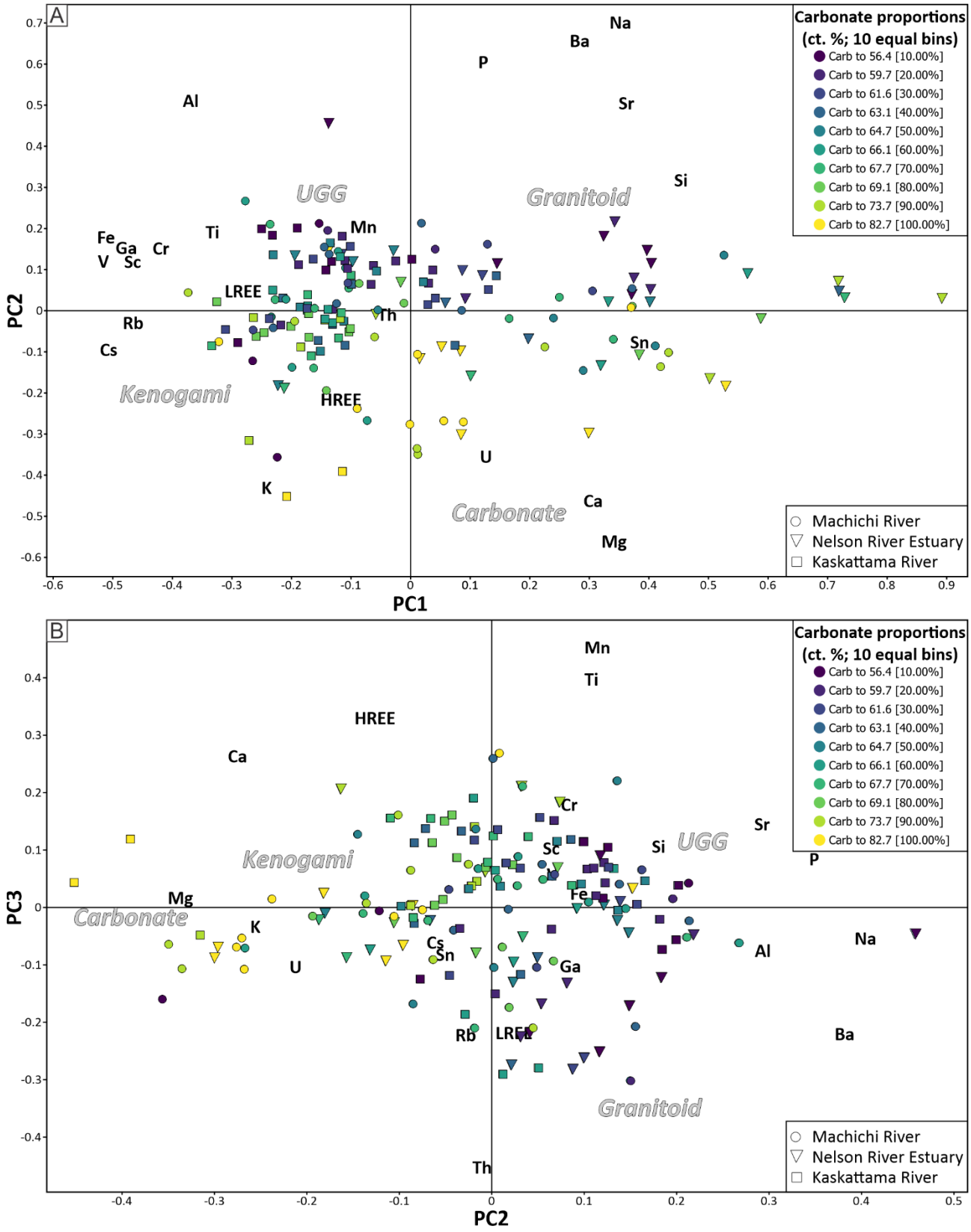

Appendix E

Supplemental materials for Chapter 7

Supplemental material 1: Inventory of intertill sorted nonglacial sediments in the western Hudson Bay Lowland.

Supplemental Materials 1. Inventory of intertill sorted nonglacial sediments in the western Hudson Bay Lowland.

This supplemental file contains an inventory of intertill nonglacial deposits documented during this study in the western HBL and their assigned interglacial stage based on the updated stratigraphic framework (Table S1-1). At this time, the inventory does not include all sections documented by previous researchers such as McDonald (1969), Netterville (1974) and Dredge et al. (1990, 1992).

Supplemental Materials 1 references:

Dalton, A.S., Finkelstein, S.A., Barnett, P.J. and Forman, S.L. 2016. Constraining the Late Pleistocene history of the Laurentide Ice Sheet by dating the Missinaibi Formation, Hudson Bay Lowlands, Canada. Quaternary Science Reviews, 146, 288–299. doi:10.1016/j.quascirev.2016.06.015.

Dalton, A.S., Finkelstein, S.A., Hodder, T.J. and Gauthier, M.S. 2022. Palynological analyses of subtill sediments from four sites in the western Hudson Bay Lowland region (parts of NTS 53O, 54A, C, D). Manitoba Geological Survey Open File OF2022-1, 13 p.

Dalton, A.S., Finkelstein, S.A., Hodder, T.J. and Gauthier, M.S. 2024. Palynological analyses of subtill sediments from eleven sites in the western Hudson Bay Lowland region of Manitoba (parts of NTS 54B, 54C, 54E, 54F). Manitoba Geological Survey Open File OF2024-5, 6 p.

Dredge, L.A. and Nixon, F.M. 1992. Glacial and environmental geology of northeastern Manitoba. Geological Survey of Canada Memoir 432, 80 p.

Dredge, L.A., Morgan, A.V., and Nielsen, E. 1990. Sangamon and pre-Sangamon interglaciations in the Hudson Bay Lowlands of Manitoba. Géographie Physique et Quaternaire, 44(3): 319–336. doi:10.7202/032833ar.

Gauthier, M.S., Hodder, T.J., Dalton, A.S., Lian, O.B., Schaarschmidt, M., Ross, M., and Valiranta, M. 2024. Preservation of probable MIS 7 deglacial and nonglacial deposits near the edge of the Hudson Bay Lowland in Manitoba, Canada. Canadian Journal of Earth Sciences, 61(11): 1184–1211. doi:10.1139/cjes-2024-0019.

Gauthier, M.S., Hodder, T.J., Hathaway, J., Ross, M., Schaarschmidt, M., Lian, O.B., Finkelstein, S.A. and Kelley, S.E., 2025. Extending the western Hudson Bay Lowland Quaternary stratigraphy, in Manitoba Canada, to at least Marine Isotope Stage 10. Canadian Journal of Earth Sciences, in press. doi: 10.1139/cjes-2025-0027.

Hodder, T.J. and Gauthier, M.S. 2025a. Quaternary site, till composition and ice-flow indicator data for the Little Churchill to Churchill rivers area, northeastern Manitoba (part of NTS 54E). Manitoba Geological Survey Open File OF2025-1, 5 p., 6 appendices.

Hodder, T.J. and Gauthier, M.S. 2025b. Quaternary site, till composition and ice-flow indicator datasets in the Nelson River Estuary–Black Duck River area, northeastern Manitoba (parts of NTS 54A, B, C, F). Manitoba Geological Survey, Open File OF2025-2, 6 p., 8 appendices.

Hodder, T.J., Gauthier, M.S., Ross, M. and Lian, O.B. 2023. Was there a nonglacial episode in the western Hudson Bay Lowland during Marine Isotope Stage 3? Quaternary Research, 116: 148–161. doi:10.1017/qua.2023.35

Hodder, T.J., Gauthier, M.S., Kelley, S.E. and Ross, M. 2024a. Quaternary site, till composition and ice-flow indicator datasets in the Kaskattama highland area, northeastern Manitoba (parts of NTS 53N, O, 54B, C). Manitoba Geological Survey Open File OF2024-1, 20 p., 9 appendices.

Hodder, T.J., Gauthier, M.S., Ross, M., Kelley, S.E., Lian, O.B., Dalton, A.S. and Finkelstein, S.A. 2024b. Unravelling the fragmented sediment-landform assemblage in an area of thick Quaternary sediment, western Hudson Bay Lowland, Canada. Canadian Journal of Earth Sciences, 61(11), 1156–1183. doi:10.1139/cjes-2024-0018

McDonald, B.C. 1969. Glacial and interglacial stratigraphy, Hudson Bay Lowland. *In* Earth Sciences Symposium on Hudson Bay. *Edited by* P.J. Hood. GSC Paper 68-53: 78–99.

Netterville, J. A. 1974. Quaternary stratigraphy of the lower Gods River region, Hudson Bay lowlands, Manitoba. Master of Science thesis, The University of Calgary, Calgary, Alberta, Canada, 79 p.

Table S1-1. Subtill intertill sorted nonglacial sediments documented by this study in the western Hudson Bay Lowland.

Unique_section_ID	Informal_name	Easting (NAD83, UTM15N)	Northing (NAD83, UTM15N)	Stage	Likely MIS	Interpreted depositional setting†	Paleoenvironment analyses‡	Geochronology§	Reference(s)	Notes
19-605	Black Duck River	729339	6281395	HBL Interglacial Stage II	MIS 5e	Fluvial?		OSL; 14C(AMS)	Hodder et al. 2023	
11-PJB-186	Black Duck River	727628	6280097	HBL Interglacial Stage II	MIS 5e	Fluvial?	P	14C(AMS)	Dalton et al. 2016; Dalton et al. 2022	The location of this site is not absolute since lat/long provided only has two decimal places listed.
19-601	Flamborough Head	518443	6314617	HBL Interglacial Stage II	MIS 5e	Terrestrial; fluvial	P	14C(AMS)	Dredge et al. 1990; Hodder and Gauthier 2025b; Chapter 5	
20-701	--	517616	6312880	HBL Interglacial Stage II	MIS 5e	Sorted sediments; unknown			Hodder and Gauthier 2025b; Chapter 5	
19-609	--	595656	6312799	HBL Interglacial Stage II	MIS 5e	Sorted sediments; unknown	P		Hodder and Gauthier 2025b; Chapter 5	Contains pollen
19-607	--	663862	6300336	HBL Interglacial Stage II	MIS 5e	Sorted sediments; unknown		14C(AMS)	Hodder and Gauthier 2025b; Chapter 5	Possible marine
19-623	--	658626	6291297	HBL Interglacial Stage II	MIS 5e	Sorted sediments; unknown		OSL	Hodder and Gauthier 2025b; Chapter 5	
19-602	--	641256	6264744	HBL Interglacial Stage II	MIS 5e	Sorted sediments; unknown			Hodder and Gauthier 2025b; Chapter 5	
17-529	--	617819	6251678	HBL Interglacial Stage II	MIS 5e	Sorted sediments; unknown			Hodder et al. 2024a; Hodder et al. 2024b	
16-413	--	596981	6231508	HBL Interglacial Stage II	MIS 5e	Sorted sediments; unknown			Hodder et al. 2024a; Hodder et al. 2024b	
16-407	--	590752	6211820	HBL Interglacial Stage II	MIS 5e	Sorted sediments; marine?		OSL	Hodder et al. 2024a; Hodder et al. 2024b	Possible marine
17-515	--	598923	6181172	HBL Interglacial Stage II	MIS 5e	Sorted sediments; unknown			Hodder et al. 2024a; Hodder et al. 2024b	
16-430	--	604456	6183453	HBL Interglacial Stage II	MIS 5e	Sorted sediments; unknown			Hodder et al. 2024a; Hodder et al. 2024b	
16-416/17-505	Shamattawa	564895	6191871	HBL Interglacial Stage II	MIS 5e	Sorted sediments; marine?		14C(AMS)	Hodder et al. 2024a; Hodder et al. 2024b	Possible marine based on chemistry of sample 112-16-416-D01
19-629	--	507894	6248114	HBL Interglacial Stage II	MIS 5e	Marine		OSL	Hodder et al. 2023; Hodder et al. 2024a; Hodder et al. 2024b	
21-811	--	359402	6339572	HBL Interglacial Stage II	MIS 5e	Sorted sediments; marine?		OSL	Hodder and Gauthier 2025a; Chapter 4	
21-812	--	335348	6359191	HBL Interglacial Stage II	MIS 5e	Terrestrial; fluvial	P	14C(AMS); OSL	Hodder and Gauthier 2025a; Chapter 4	
21-828	--	348592	6371636	HBL Interglacial Stage II	MIS 5e	Marine		14C(AMS); OSL	Hodder and Gauthier 2025a; Chapter 4	
19-621	--	556143	6305252	HBL Interglacial Stage III	MIS 7	Marine	P	OSL	Hodder and Gauthier 2025b; Chapter 5	Interpreted to be marine based on section 19-620
19-620	--	555762	6305517	HBL Interglacial Stage III	MIS 7	Marine	F		Hodder and Gauthier 2025b; Chapter 5	Confirmed marine
19-624	--	557616	6301610	HBL Interglacial Stage III	MIS 7	Terrestrial; fluvial		OSL	Hodder and Gauthier 2025b; Chapter 5	
19-613	--	557686	6301533	HBL Interglacial Stage III	MIS 7	Terrestrial; fluvial	P	14C(AMS); OSL	Hodder and Gauthier 2025b; Chapter 5	
19-627	--	559577	6299526	HBL Interglacial Stage III	MIS 7	Sorted sediments; unknown			Hodder and Gauthier 2025b; Chapter 5	Tentative correlation; possible subglacial sorted sediments
19-608	--	560763	6297445	HBL Interglacial Stage III	MIS 7	Marine			Hodder and Gauthier 2025b; Chapter 5	Confirmed marine
20-702	Port Nelson	522038	6320049	HBL Interglacial Stage III	MIS 7	Marine	P; F	14C(AMS)	Dredge et al. 1990; Hodder et al. 2023; Hodder and Gauthier 2025b; Chapter 5	Marine diamicton
20-700	--	517654	6312932	HBL Interglacial Stage III	MIS 7	Sorted sediments; unknown		OSL	Hodder and Gauthier 2025b; Chapter 5	Possible marine
20-703	--	517459	6312571	HBL Interglacial Stage III	MIS 7	Sorted sediments; unknown			Hodder and Gauthier 2025b; Chapter 5	Possible marine
19-617	--	669046	6309459	HBL Interglacial Stage III	MIS 7	Sorted sediments; unknown			Hodder and Gauthier 2025b; Chapter 5	Tentative correlation; possible subglacial sorted sediments
21-832	--	344230	6370022	HBL Interglacial Stage III	MIS 7	Terrestrial over marine	P	OSL	Hodder and Gauthier 2025a; Chapter 4	
21-833	--	348238	6371554	HBL Interglacial Stage III	MIS 7	Sorted sediments; unknown			Hodder and Gauthier 2025a; Chapter 4	
21-819	--	341151	6370586	HBL Interglacial Stage III	MIS 7	Sorted sediments; unknown		OSL	Hodder and Gauthier 2025a; Chapter 4	Possible marine
21-807	--	338134	6368948	HBL Interglacial Stage III	MIS 7	Marine	P; F	14C(AMS)	Hodder and Gauthier 2025a; Chapter 4	
21-812	Mountain Rapids	335348	6359191	HBL Interglacial Stage III	MIS 7	Sorted sediments; unknown		OSL	Hodder and Gauthier 2025a; Chapter 4; Dredge et. al 1990	
21-806	--	355651	6345441	HBL Interglacial Stage III	MIS 7	Terrestrial; fluvial?	P		Hodder and Gauthier 2025a; Chapter 4	Thin organic-rich sediment bed over a paleosol developed on till
17-522/19-630	Echoing River	609350	6189408	HBL Interglacial Stage III	MIS 7	Sorted sediments; unknown	P	OSL	Hodder et al. 2024a; Hodder et al. 2024b; Dredge et. al 1990	
16-416/17-505	Shamattawa	564895	6191871	HBL Interglacial Stage III	MIS 7	Terrestrial; fluvial	P		Hodder et al. 2024a; Hodder et al. 2024b	
17-531	--	552925	6180782	HBL Interglacial Stage III	MIS 7	Terrestrial; fluvial?			Hodder et al. 2024a; Hodder et al. 2024b	Discontinous organic-rich bed
17-542	--	550811	6155660	HBL Interglacial Stage III	MIS 7	Sorted sediments; unknown			Hodder et al. 2024a; Hodder et al. 2024b	
17-540	--	550600	6147652	HBL Interglacial Stage III	MIS 7	Sorted sediments; unknown			Hodder et al. 2024a; Hodder et al. 2024b	
19-628	--	531614	6224516	HBL Interglacial Stage III	MIS 7	Sorted sediments; unknown			Hodder et al. 2024a; Hodder et al. 2024b	
115-20-200	Pit 1	358939	6268244	HBL Interglacial Stage III	MIS 7	;trial; floodplain or pond over glacio	P; M	14C(AMS); OSL	Gauthier et al. 2024	
115-20-320	Pit 2	403592	6258431	HBL Interglacial Stage III	MIS 7	Sorted sediments; glaciofluvial		OSL	Gauthier et al. 2024	
Limestone dam area	Moondance; Limestone; Sundance; Birds Island	432012	6264217	HBL Interglacial Stage III	MIS 7	Terrestrial; fluvial	P; DNA	14C(AMS); OSL	Gauthier et al. 2025; Dredge et al. 1992; Roy 1998; Hodder et al. 2017	See Gauthier et al. 2025 for map and coordinates for sections in this area.
19-624		557616	6301610	HBL Interglacial Stage IV	MIS 9 or older	Sorted sediments; marine?		OSL	Hodder and Gauthier 2025b; Chapter 5	
20-705		556773	6302504	HBL Interglacial Stage IV	MIS 9 or older	Sorted sediments; marine?		OSL	Hodder and Gauthier 2025b; Chapter 5	
21-805		354158	6336643	HBL Interglacial Stage IV	MIS 9 or older	Sorted sediments; marine?			Hodder and Gauthier 2025a; Chapter 4	
21-826		336718	6367842	HBL Interglacial Stage IV	MIS 9 or older	Terrestrial; fluvial?			Hodder and Gauthier 2025a; Chapter 4	
21-832		344230	6370022	HBL Interglacial Stage IV	MIS 9 or older	Terrestrial; fluvial?			Hodder and Gauthier 2025a; Chapter 4	
21-833		348238	6371554	HBL Interglacial Stage IV	MIS 9 or older	Terrestrial; fluvial?			Hodder and Gauthier 2025a; Chapter 4	
21-806		355651	6345441	Interstadial of Glacial Stage II?	Unknown	Sorted sediments; unknown		OSL	Hodder and Gauthier 2025a; Chapter 4	
21-805		354158	6336643	Interstadial of Glacial Stage II?	Unknown	Sorted sediments; unknown			Hodder and Gauthier 2025a; Chapter 4	
19-613		557686	6301533	Interstadial of Glacial Stage II?	Unknown	Terrestrial; floodplain?	P	14C	Hodder and Gauthier 2025b; Chapter 5	

† Please refer to published materials for additional information regarding the sediments exposed at these sections and their depositional environment interpretations

‡ Please refer to published materials for pollen, macrofossil or foraminifera data associated with these nonglacial deposits. Abbreviations: P, pollen analysis; F, foraminifera analysis; M, macrofossil analysis; DNA, ancient DNA

§ Please refer to published materials for geochronology data associated with these nonglacial deposits. Abbreviations: 14C(AMS), radiocarbon age determined using accelerator mass spectrometry; OSL, optically stimulated luminescence age.